RGT - RETE GEOTERMICA TOSCANA s.r.l.

VIA ERNESTO ROSSI N°9 - 52100, AREZZO

P.I. - 03263030540 C.S. 120.000.00 i.v.

PEC: retegeotermicatoscana@pec.it

Impianto Geotermico Pilota Castelnuovo

REV	DATA	OGGETTO	PREPARATO	VERIFICATO	APPROVATO
01	19/07/2017	Emissione	Golder Associates	Magma Energy Italia	Rete Geotermica Toscana
00	06/03/2017	Emissione	Golder Associates	Magma Energy Italia	Rete Geotermica Toscana

MAGMA ENERGY ITALIA SRL
Via E.Rossi n. 9/A Arezzo 52100
Tel 0575 32641 - Fax 0575 326457
magmaenergy@legalmail.it
C.F. 06059240488

RGT-RETE GEOTERMICA TOSCANA SRL
VIA E. ROSSI N. 9 - 52100 AREZZO
C.F. 03263030540

Golder Associates

ORDINE GEOLOGI REGIONE PIEMONTE * ALBO PROFESSIONALE *
LIVIA VANZONE GEOLOGO N. 672

TITOLO:

Approfondimenti relativi all'abbattimento delle emissioni aeriformi

NOTE:

IDENTIFICAZIONE ELABORATO

ARGOMENTO	PROGETTO	LIVELLO	AREA	TIPO	PROGRESSIVO
CAS	02	DE	GE	R	076

FOGLIO	FORMATO
1 di 217	A4

1. Premessa

Il progetto geotermico "Castelnuovo" è stato sviluppato in seno alla normativa nazionale di riferimento del settore geotermico (Decreto Legislativo 11 febbraio 2010, n. 22, modificato dal Decreto Legislativo 3 marzo 2011, n. 28 e dall'articolo 28 del Decreto Legge 18 ottobre 2012, n. 179), che ha previsto, al fine di promuovere la ricerca e lo sviluppo di nuove centrali geotermoelettriche a ridotto impatto ambientale, di considerare di interesse nazionale i fluidi geotermici a media ed alta entalpia finalizzati alla sperimentazione, su tutto il territorio nazionale, di impianti pilota con reiniezione del fluido geotermico nelle stesse formazioni di provenienza, e comunque con emissioni di processo nulle.

1.1 Caratteristiche del fluido

Il progetto geotermico "Castelnuovo" è improntato alla ricerca di risorse geotermiche finalizzata alla sperimentazione di Impianti Pilota in quanto il proponente dispone dei dati geotermici necessari per stimare con accuratezza le caratteristiche del fluido geotermico.

Il potenziale geotermico dell'area dove verrà realizzato l'impianto è stato valutato attraverso la ricostruzione di un modello geologico 3D utilizzando dati geologici di superficie, dati geofisici e dati di pozzo. Tale modello, che tiene conto delle caratteristiche geologiche e termiche del serbatoio e delle formazioni di copertura, ha permesso di constatare l'area meridionale del P.R. Castelnuovo come fortemente promettente, permettendo di stimare che nel sottosuolo del progetto "Castelnuovo" siano presenti fluidi geotermici con temperatura superiore a 150 °C all'interno di due tipi di rocce serbatoio:

- il primo in rocce evaporitiche mesozoiche a profondità comprese tra 1200-1600 m;
- il secondo in rocce metamorfiche all'interno delle quali sono presenti zone permeabili, a profondità compresa tra 2500-4000 m, nelle quali la capacità di produrre fluidi è già stata accertata in aree limitrofe. I fluidi geotermici sono costituiti prevalentemente da vapore con pressioni di strato superiori a 50 bar e temperature che raggiungono circa 300°C a 3500 m di profondità.

Il fluido che alimenterà la centrale avrà, nelle condizioni peggiori stimate, temperatura di 180 °C e pressione di 10 bar alla bocca pozzo, ovvero il circuito primario downstream sarà alimentato da vapore saturo.

I dati disponibili sul chimismo dei fluidi reperiti nel campo limitrofo di Sesta indicano la presenza di vapore con gas incondensabili, che rappresentano circa l'8% in peso del fluido geotermico, di cui circa

il 97,5% in peso di anidride carbonica, il 2% in peso di idrogeno solforato e il restante 0,5% di metano, azoto e idrogeno, oltre altre specie chimiche volatili quali mercurio, boro, arsenico e ammoniaca. **Dunque il fluido che alimenterà l'impianto è catalogabile**, secondo la classificazione proposta nell'art. 1 comma 2 del D.Lgs. 22/2010, che definisce il livello di entalpia sulla base della temperatura del fluido, **come una risorsa geotermica ad alta entalpia (temperatura del fluido > 150°C) in condizioni di vapore saturo.**

Lo studio di "Caratterizzazione e accertamento delle risorse geotermiche" è riportato nell'Allegato 1.

1.2 Caratteristiche dell'impianto

Il sistema tecnologico garantisce l'assenza di emissioni aeriformi di processo attraverso una soluzione progettuale innovativa "a ciclo chiuso" seppur operante con un fluido geotermico ad alta entalpia in stato di vapore saturo, risorsa fino ad oggi sfruttata con impianti di tipo flash che operano con emissioni in atmosfera e reiniezione solo parziale dei fluidi

L'innovazione tecnologica dell'impianto sta nel fatto che la reiniezione totale viene garantita attraverso la gestione separata della frazione liquida e di quella gassosa e cioè, dopo la separazione dalla frazione liquida, attraverso la compressione e iniezione dei gas incondensabili nelle stesse formazioni rocciose di provenienza del fluido geotermico estratto attraverso una condotta dedicata (3)

Gli impianti a ciclo binario sono invece solitamente alimentati con un fluido geotermico in fase liquida, in cui i gas non condensabili restano disciolti nel liquido, spesso mantenuto in pressione, e cedono il proprio calore senza cambiare stato. In questi casi la reiniezione prevede un'unica condotta per la sola fase liquida.

L'analisi modellistica del sistema di reiniezione nel sottosuolo è riportata nell'Allegato 2.

La configurazione dell'impianto è rappresentata in Figura 1.

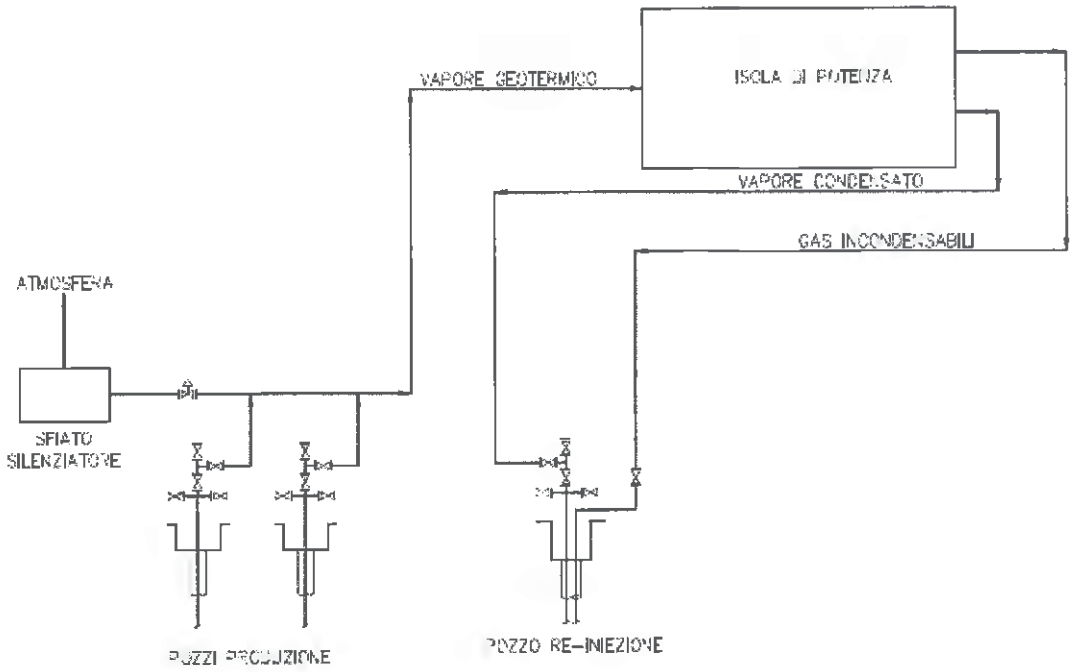

Figura 1

Il fluido geotermico nel circuito primario proveniente dai pozzi di produzione, dopo aver ceduto il proprio calore al fluido ORC tramite lo scambiatore di calore, condensa e viene raccolto in un accumulatore.

Il fluido organico bassobollente dell'isola di potenza (circuito secondario) riscaldato passa dalle condizioni di liquido saturo a quelle di vapore surriscaldato, ed espandendo in turbina, permette la produzione di elettricità. Lo stesso fluido, dopo essere passato attraverso un recuperatore in grado di sfruttare il calore ancora disponibile nel fluido allo scarico della turbina, viene condensato e, raggiunto lo stato di liquido saturo, pompato alla pressione massima per re-iniziare il ciclo termodinamico, **senza contatto con l'esterno**.

La frazione di risorsa geotermica non condensata[1], unita ai gas incondensabili (NCG), passa attraverso il separatore dove avviene la separazione secondaria delle condense: il flusso risultante di gas incondensabili è reso disponibile per la reiniezione attraverso una specifica condotta e iniettato mediante un compressore, mentre le condense vengono inviate all'accumulatore da dove prelevano

[1] Può esserci una frazione minima di fluido geotermico che dopo essere passata nello scambiatore resta vapore miscelato ai gas, e quindi c'è un separatore che serve per separare questa minima frazione, che condensa, e i gas non condensabili. Questa piccolissima frazione di condensa si unisce al fluido geotermico già condensato e va alla pompa per la reiniezione.

le pompe di reinezione con una condotta separata. Le due tubazioni arrivano separatamente alla bocca pozzo dove la reineizione in serbatoio avviene impiegando un unico pozzo di reiniezione, nel quale i due fluidi {condensato e gas incondensabili) verranno immessi attraverso due tubazioni concentriche calate in pozzo, come rappresentato in Figura 2.

(OMISSIS AI SENSI DEL DPR 184/2006 ART.3 COMMA 2)

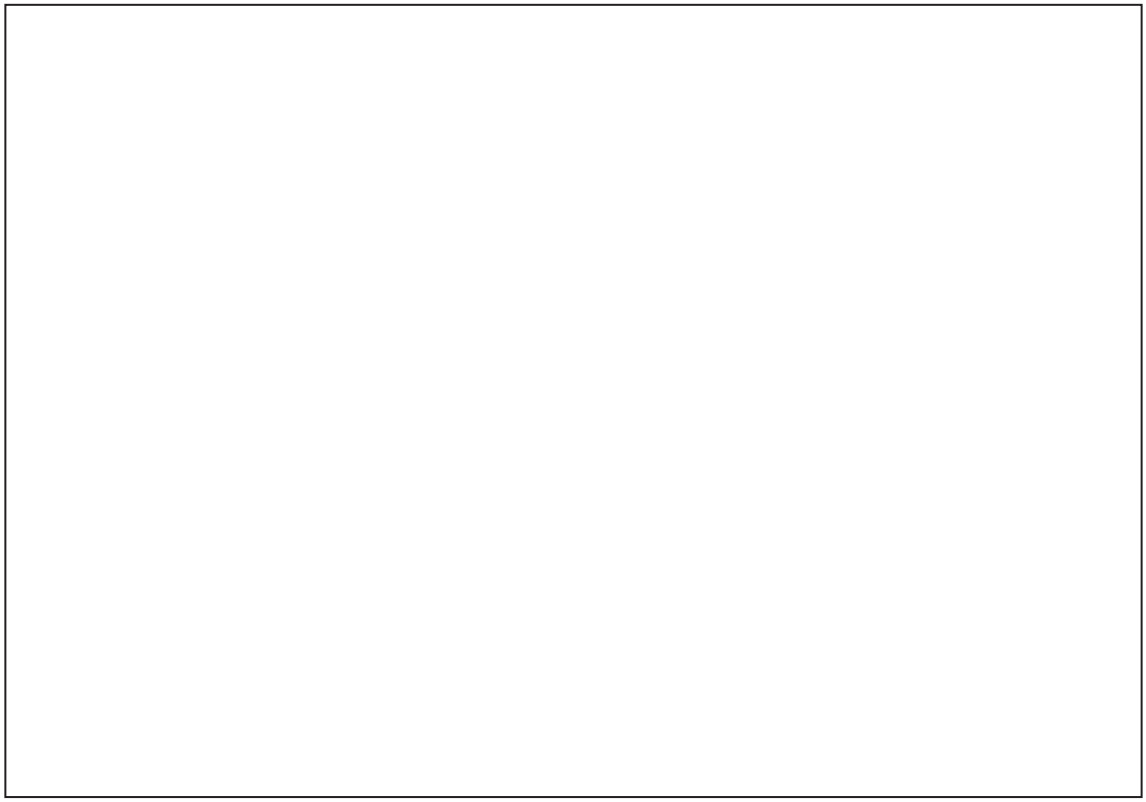

Figura 2 OMISSIS AI SENSI DEL DPR 184/2006 ART.3 COMMA 2

Le condense saranno reimmesse per caduta o con pressione di poche unità di bar a testa pozzo, mentre i NCG saranno rilasciati in profondità nel flusso liquido discendente mediante un tubing concentrico. Il punto di rilascio, dove sarà posizionato un gas sparger, verrà stabilito in modo tale che la velocità di flusso e la pressione idrostatica consentano il miscelamento in un'unica corrente e il rilascio del fluido all'interno delle stesse formazioni che costituiscono il serbatoio di estrazione.

Nel caso specifico il processo prevede l'iniezione della totalità degli NCG (anidride carbonica, idrogeno solforato, frazioni di metano, azoto e idrogeno) ed altre specie chimiche volatili (mercurio, boro, arsenico, ammoniaca) contenuti nel fluido geotermico evitando la dispersione delle emissioni all'esterno del sistema. A garanzia della validità e idoneità dell'applicazione di tale metodologia nel campo specifico è stata eseguita una simulazione numerica del pozzo in collaborazione con GeothermEx-Schlumberger, utilizzando il software di modellazione di flussi multifase OLGA

"Compositional Tracking", in grado di modellare l'iniezione di gas incondensabili (prevalentemente anidride carbonica) nella corrente liquida (Allegato 2)

L'analisi è stata condotta valutando l'impatto di alcune variabili sul sistema, tra cui la profondità di mixing per le due correnti fluide, in diverse condizioni di iniettività. Sono state valutate le pressioni necessarie per l'iniezione dei fluidi per profondità di mixing comprese tra 0 m e 1.250 m.

In generale si assiste a una maggiore spesa energetica per la compressione del gas abbassando il punto di mixing e, al contrario un aumento della potenza richiesta per comprimere il condensato se il punto si alza verso la superficie. L'intervallo ritenuto più favorevole per unire le due correnti, tra 250 e 500 m, consente di reiniettare il vapore condensato a pressioni prossime a quella atmosferica e i gas a pressioni inferiori a 60 bar a boccapozzo.

Dai risultati del modello, la reiniezione attraverso un solo pozzo appare sempre fattibile, avendo l'accortezza di gestire le fasi transitorie in modo opportuno: ad esempio, durante le operazioni di messa in esercizio dell'impianto, sarà avviata l'iniezione del condensato prima di quella dei gas, in modo da consentire all'acqua di raggiungere una velocità tale da trasportare i gas verso il basso consentendo il loro ingresso in serbatoio. In nessuno degli scenari simulati si è assistito ad un ritorno dei gas in superficie, né ad un accumulo sotto il punto di mixing.

1.3 Processo di abbattimento delle emissioni aeriformi

La soluzione innovativa, adottata nel progetto Castelnuovo, di reiniettare anche la parte non condensabile del fluido geotermico, opportunatamente separata, è assimilabile all'applicazione, in campo geotermico, delle tecnologie CCS (*Carbon Capture and Storage)*, sistemi che permettono di abbattere le emissioni di CO_2 in atmosfera, attraverso un vero e proprio processo di cattura e stoccaggio della CO_2, con la differenza vantaggiosa di poter attuare tale processo in prossimità dello stesso sito dal quale i gas non condensabili vengono estratti.

La soluzione più matura nel settore delle tecnologie CCS è il confinamento nel sottosuolo in formazioni geologiche a profondità superiori agli 800 metri, secondo diverse modalità, tra le quali l'iniezione in acquiferi salini profondi (1).

Di seguito una tabella esplicativa delle varie metodologie impiegabili per lo stoccaggio della CO_2, dalla quale si evince come l'impiego di depositi geologici, e in particolare l'iniezione in acquiferi salini, rappresenti una tecnologia già ampiamente realizzata (2), in quanto l'iniezione di CO_2 nelle

formazioni geologiche profonde comporta l'adozione di tecnologie già pienamente sviluppate ed utilizzate per l'esplorazione e produzione di gas e petrolio.

Componenti CCS	Tecnologia CCS	Fase di ricerca*	Fase dimostrativa*	Economicamente realizzabile*	Matura per il mercato
Cattura	Post-combustione			X	
	Precombustione			X	
	Combustione di ossigeno		X		
	Separazione industriale				X
Trasporto	Gasdotto				X
	Trasporto navale			X	
Deposito geologico	Recupero di petrolio (EOR)*				X*
	Campi di gas e petrolio			X	
	Formazioni saline			X	
	Recupero di metano da giacimenti di carbone		X		
Deposito marino	Iniezione diretta (dissoluzione)	X			
	Iniezione diretta (formazione di laghi)	X			
Fissazione in carbonati	Silicati naturali	X			
	Materiali di scarto		X		
Utilizzo industriale					X

Tabella 1

L'abbattimento dei gas incondensabili durante il funzionamento dell'impianto è garantito, permettendo, oltre la totale reiniezione, la sostenibilità e la rinnovabilità della risorsa ed evitando inoltre alcuni indesiderabili effetti associabili ad un eventuale depauperamento dei fluidi e alla depressurizzazione del serbatoio. Inoltre un ulteriore vantaggio è rappresentato dal fatto che la reiniezione dei gas non condensabili è realizzata in prossimità dello stesso sito dal quale vengono estratti.

L'impianto pertanto è in grado di soddisfare i requisiti di cui al D.M. 23 Giugno 2016 art. 10 comma 3, lettera e) punti *i e ii.*

2. Conclusioni

Il progetto Castelnuovo prevede la realizzazione di un impianto a ciclo chiuso con emissioni di processo nulle, capace di generare energia elettrica a partire da una risorsa rinnovabile, così come definita nella Direttiva CEE 2001/77/CE recepita dalla 2009/38/CE, con l'abbattimento attraverso il confinamento della CO_2 e degli altri NCG, con un processo assimilabile all'applicazione, in campo geotermico, delle tecnologie CCS.

Il progetto risulta pienamente coerente con la definizione di impianto pilota, così come dettato dalla normativa nazionale di riferimento, e con gli obiettivi e le strategie dell'attuale politica energetica internazionale, rappresentando le tecnologie CCS una valida soluzione energetica ambientalmente sostenibile. Tali tecnologie sono infatti presenti nel portfolio di provvedimenti per il raggiungimento dell'obiettivo 20-20-20 con cui l'UE conferma la volontà di sviluppare strumenti programmatici di indirizzo e coordinamento degli Stati membri, basati sulla sostenibilità ambientale e finalizzati a realizzare un significativo risparmio energetico e una lotta ai cambiamenti climatici.

Si rimarca infine quanto già evidenziato nello Studio di Impatto Ambientale nel documento CAS.02.DE.AM.R.005-Q_Progettuale, par. 3.1.3 Criteri tecnologici e scelta finale: la reiniezione totale dei fluidi estratti (fluido condensato in centrale e gas non condensabili NCG) all'interno delle stesse formazioni di estrazione consente di evitare la depressurizzazione del serbatoio e l'emissione degli NCG e altre specie chimiche volatili in atmosfera.

L'approfondimento proposto chiarisce pertanto aspetti progettuali già valutati nello Studio di Impatto Ambientale, consegnato in data 17 dicembre 2015, avvalorando le considerazioni ivi riportate.

Bibliografia

(1) A cura di G. Girardi - Tecnologie di cattura e sequestrazione della CO_2 2011, ENEA (http://www.enea.it/it/comunicare-la-ricerca/documenti/quaderni-energia/catturaco2.pdf)

(2) A. Rossi- Il ruolo della tecnologia CCS per l'abbattimento delle emissioni di CO2, 2011 (www.isprambiente.gov.it/contentfiles/00004900/4962-rossi.zip/at_download/file)

(3) Esteban Rodríguez, William Scott Harvey, Einar Jón Ásbjörnsson - Review of H2S Abatement Methods in Geothermal Plants, Reykjavík University, School of Science and Engineering, April 2015.

TOSCOGEO
geothermal energy
Società del gruppo GRAZIELLA green power

magma ENERGY ITALIA

RETE GEOTERMICA TOSCANA

C/O TOSCOGEO S.R.L.
VIA ERNESTO ROSSI N° 9 - 52100, AREZZO
TEL. 0575 32641 - FAX. 0575 326464

PROGETTO GEOTERMICO PILOTA CASTELNUOVO

CARATTERIZZAZIONE E ACCERTAMENTO DELLE RISORSE GEOTERMICHE

Rev.	Data	Oggetto	Autore	Approv.
00	22.07.2016	Emissione	Magma Energy	F.Batini

1. Caratterizzazione della risorsa a Castelnuovo Val Di Cecina

1. Premessa

La presente relazione è stata redatta in conformità alla Circolare esplicativa dei criteri di valutazione per il riconoscimento del carattere nazionale o locale della risorsa geotermica ai fini dell'iscrizione al registro ex decreto interministeriale 23.6.2016 - *Incentivazione dell'energia elettrica prodotta da fonti rinnovabili diverse dal fotovoltaico.*

2. Introduzione

Con istanza presentata in data 29 aprile 2013, prot. n. 8771 del 30 aprile 2013 - pubblicazione BUIG anno LVIII, n. 1, la società TOSCO GEO s.r.l., rappresentante unico della costituenda Rete Geotermica Toscana, ha chiesto il rilascio del permesso di ricerca per risorse geotermiche finalizzato alla sperimentazione di impianto pilota, denominato "CASTELNUOVO", ricadente nel territorio delle province di Pisa (comune di Castelnuovo Val di Cecina) e Siena (comune di Radicondoli), ai sensi del D. Lgs. 22/2010, come modificato dal D.Lgs. 28/2011 e s.mm.ii.

Nella seduta del 27 novembre 2014 la CIRM (Commissione per gli Idrocarburi e Ie Risorse Minerarie) ha espresso parere favorevole al prosieguo istruttorio dell'istanza, compatibilmente con il limite di potenza autorizzabile dalla normativa vigente. Tale esito e stato trasmesso alla scrivente Società e, per conoscenza, al Ministero dell'ambiente e della tutela del territorio e del mare (MATTM) e alla Regione Toscana con nota n. 1128 del 21 gennaio 2015.

Con nota prot. 17608 del 28 luglio 2015, la Direzione Generale (già Direzione Generale per Ie Risorse Minerarie ed Energetiche) comunicava che il progetto denominato "CASTELNUOVO", relativo all'immissione di 5 MWe nel sistema elettrico, risultava compatibile con iI quadro della potenza autorizzabile e disponibile in base alla normativa vigente.

Con istanza inviata a mezzo pec il 20 ottobre 2015, acquisita in pari data agli atti della citata Direzione Generale con prot. 25532, la scrivente società, con riferimento all'istanza di permesso di ricerca ha comunicato che, a seguito di affinamenti del modello termo-fluido-dinamico del serbatoio geotermico e di nuove simulazioni numeriche sulle modalità di produzione e reiniezione dei fluidi, riteneva opportuno riconsiderare l'ubicazione dei pozzi già indicata nel Programma dei Lavori allegato all'istanza originariamente presentata, volendo procedere quindi ad una ottimizzazione progettuale che migliori ulteriormente la sostenibilità ambientale del progetto.

La Direzione Generale ha provveduto quindi ad acquisire iI previsto parere della CIRM nella seduta del 27 novembre 2015 durante la quale la CIRM ha espresso pare e favorevole all'accoglimento dell'istanza di variazione del programma lavori del progetto "CASTELNUOVO".

Con note del 10/12/2015 e del 11/12/2015, rispettivamente acquisite dal Ministero dell'Ambiente e della Tutela del territorio e del Mare con prot. DVA-2015-0031354 e prot. DVA-2015-0031371 del 17/12/2015, successivamente integrate con le note del 20/01/2016, rispettivamente acquisite al prot. DVA-0001293 e

prot. 0001324 del 20/01/2016, la Soc. Tosco Geo S.r.l. in qualità di unico rappresentante della "Rete Geotermica Toscana" ha presentato, ai sensi dell'art. 23 del D.Lgs. n. 152/2006 e ss.mm.ii., istanza di valutazione di impatto ambientale relativa al progetto "Impianto pilota geotermico Castelnuovo" finalizzato alla produzione di energia elettrica mediante l'utilizzo di fluidi geotermici.

La documentazione depositata, alla quale si fa riferimento nella presente relazione, è consultabile sul sito web del Ministero dell'Ambiente e della Tutela del Territorio e del Mare all'indirizzo http://www.va.minambiente.it/ .

3. Caratterizzazione e classificazione delle risorse geotermiche

La caratterizzazione delle risorse/riserve geotermiche è richiesta sulla base dei seguenti riferimenti normativi:

- D.P.R 395 del 27-5-1991, Articolo 22 *" Riconoscimento del carattere nazionale e locale" che riporta al comma 1: "Ai fini del riconoscimento del carattere nazionale o locale delle risorse geotermiche rinvenute, il permissionario deve trasmettere all'Ufficio nazionale minerario per gli idrocarburi e la geotermia ed alla Sezione competente la documentazione completa delle prospezioni effettuate nell'ambito del permesso e dei risultati ottenuti, nonché i risultati di prove di strato e di produzione effettuate nei pozzi, le conclusioni sulle caratteristiche produttive dei pozzi stessi e sulle caratteristiche chimiche-fisiche dei fluidi geotermici, la stima delle risorse geotermiche rinvenute, delle riserve recuperabili in relazione alla loro eventuale utilizzazione per la realizzazione di un progetto geotermico tecnicamente ed economicamente valido."*

- La Direttiva Direttoriale del 1 luglio 2011 emessa dal MISE, riguardante la prima attuazione delle modifiche introdotte dal Decreto Legislativo 28/2011 al Decreto Legislativo 22/2010 di riassetto della normativa in materia di ricerca e coltivazione delle risorse geotermiche per gli aspetti di competenza del MiSE-DGRME afferma che:
  "Il comma 2 bis dell'articolo 3 indica chiaramente che la sperimentazione di impianti pilota sia da concedere mediante un permesso di ricerca nel quale vengono stabilite le modalità di coltivazione dei fluidi geotermici. Le attività di ricerca mineraria sono rappresentate in tali casi esclusivamente dalla sperimentazione dell'impianto pilota, nel cui contesto ricadono anche le specifiche operazioni minerarie di realizzazione dello stesso (geofisica di dettaglio e pozzi di accertamento e di reiniezione) per cui verranno accettate utilmente solo le istanze per cui il proponente disponga dei dati geotermici necessari per avviare un impianto pilota (esistenza di un pozzo esplorativo o di conoscenze sufficienti della situazione geotermica del sottosuolo) già nel primo periodo di vigenza del permesso."

2. Descrizione del progetto

Il Progetto geotermico pilota Castelnuovo, ricadente nell'area del Permesso di Ricerca "Castelnuovo", è localizzato in Toscana nelle province di Pisa e Siena (Figura 1), ha una superficie di 7.52 km^2 e ha riserve geotermiche sufficienti a sostenere una potenza di generazione di energia elettrica netta di 5MWe per almeno e/o minimo 30 anni. È adiacente alla concessione "Larderello" e il vertice sud-ovest confina con la concessione "Travale".
Il progetto prevede la realizzazione di una centrale geotermoelettrica a "ciclo chiuso" (ciclo binario), con reimmissione totale del fluido geotermico nelle formazioni di provenienza, compresi i gas non condensabili, evitando pertanto emissioni aeriformi, al fine di assicurare la massima sostenibilità sia della risorsa geotermica sia quella ambientale.

La centrale sarà alimentata da fluidi geotermici ad alta entalpia presenti nelle rocce serbatoio all'interno del complesso metamorfico. Tali rocce serbatoio, situate a profondità comprese tra 2500 e 4000 m, contengono fluidi geotermici caratterizzati da temperatura compresa tra 250 - 300 °C e pressione tra 60-80 bar.
Da un'unica postazione di perforazione saranno perforati un pozzo verticale (CAS-P1 produttore)e due pozzi deviati (CAS-P2 produttore e CAS-I reiniettore). Per ulteriori approfondimenti è possibile consultare la documentazione sopracitata nella premessa, oppure la relazione CAS.02.DE.GR.R.058 - RELAZIONE GEOLOGICO-MINERARIA_SECRETATO, non disponibile al pubblico.

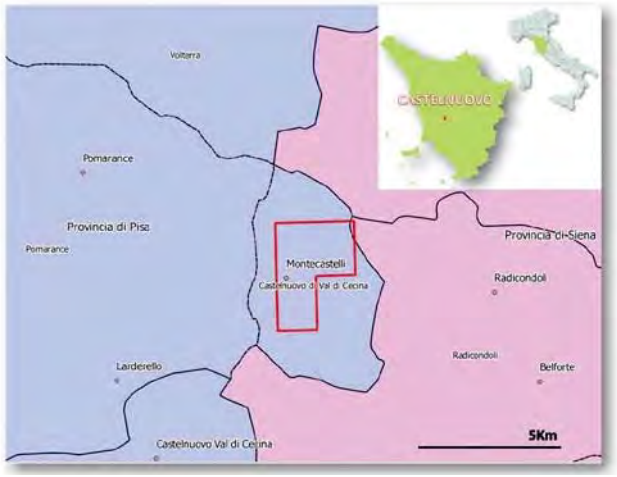

Figura 1 - Localizzazione del Permesso di Ricerca "Castelnuovo"

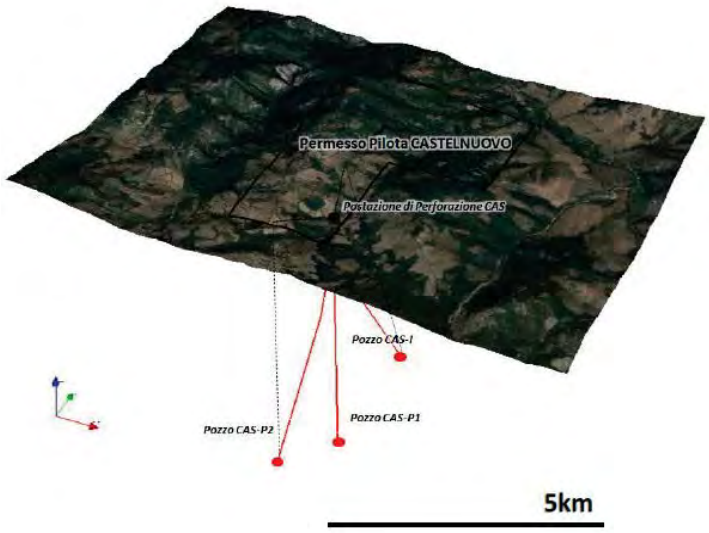

Figura 2- Vista in tre dimensioni dei profili dei pozzi

Figura 3 – Inserimento ambientale della centrale del Progetto Pilota Castelnuovo

3. Quadro delle conoscenze geotermiche

1. Esplorazione geotermica nell'area del permesso

L'area del Progetto geotermico pilota Castelnuovo è adiacente all'area di Sesta,(Figura 4), dove è installata una centrale geotermoelettrica da 20 MW dal 2002 ed è adiacente ad altri Permessi di Ricerca per risorse geotermiche ("Mensano" di Magma Energy Italia e Montegemoli di Enel Green Power) e alla Concessione di coltivazione Travale di Enel Green Power; è inoltre nelle immediate vicinanze della Concessione Larderello di Enel Green Power.

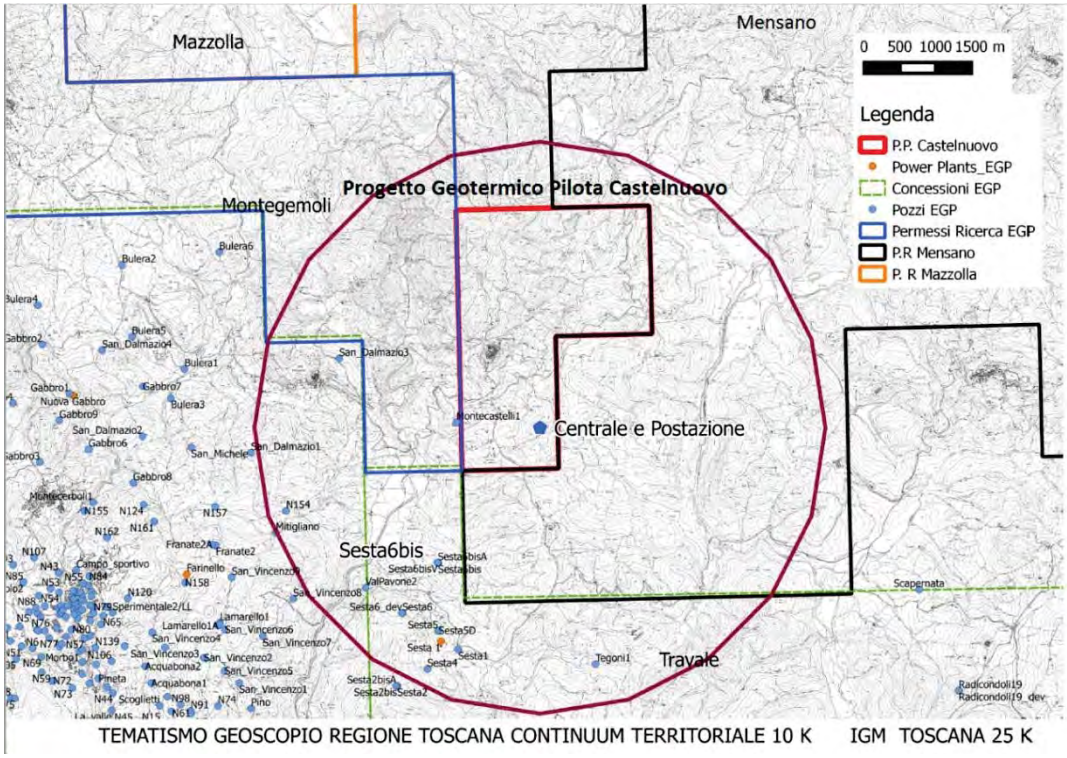

Figura 4- Centrali e pozzi Enel nel raggio di 4 km, concessioni e permessi confinanti

In tale area sono state eseguite **numerose prospezioni** e perforati **numerosi pozzi**, i cui dati sono disponibili in database pubblici e in pubblicazioni scientifiche (allegate alla presente).

Prospezioni sismiche:
- 1978: sismica a riflessione 2D (**Batini et al.1978**)
- 2003: Sismica a riflessione 3D (**Casini et. al 2010**)

Ulteriori prospezioni sono state eseguite recentemente da Magma Energy Italia s.r.l. nell'adiacente Permesso di Ricerca per risorse geotermiche "Mensano "

- rilevamenti geologici di dettaglio;
- nuova carta dell'assetto geostrutturale
- prospezioni geochimiche;
- prospezioni gravimetriche;
- prospezioni magnetiche;
- prospezioni magnetotelluriche;

I risultati di tali prospezioni sono illustrati nell'appendice della relazione "Integrazioni alla Relazione Mineraria" relativa al Procedimento di valutazione di impatto ambientale per il Progetto di realizzazione di due postazioni di perforazione, perforazione di due pozzi esplorativi e delle relative opere a rete nell'ambito del permesso di ricerca di risorse geotermiche "Mensano" nel Comune di Castelnuovo di val di Cecina (PI) - (Magma Energy Italia S.r.l.), consultabile online sul sito http://www.regione.toscana.it/-/progetti-sottoposti-a-procedura-di-valutazione-di-impatto-ambientale.
Copia di tale appendice è allegata alla presente.

Nell'ambito delle indagini realizzate nell'ambito del P.R "Mensano " è stata inoltre realizzata una nuova carta del gradiente geotermico, ottenuta dall'integrazione di tutti i dati di temperatura e/o gradiente pubblicati dagli anni '60 ad oggi, che ricopre anche l'area del Progetto Pilota Castelnuovo.

Pozzi nel primo serbatoio:
- 1961: "N 154" (esplorativo, 2500 m ad ovest-sudovest del bordo del progetto);
http://unmig.mise.gov.it/deposito/geotermia/inventario/p_pi_1.pdf

- 1963: "S.Dalmazio 1" (esplorativo, 2900 m ad ovest);
http://unmig.mise.gov.it/deposito/geotermia/inventario/p_pi_1.pdf

- 1964: "Bulera 1" (produttivo, 3800 m ad ovest);
http://unmig.mise.gov.it/deposito/geotermia/inventario/p_pi_6.pdf

- 1965: "S.Dalmazio 3" (esplorativo, 1700 m ad ovest);
http://unmig.mise.gov.it/deposito/geotermia/inventario/p_pi_9.pdf

- 1967: "S.Michele" (produttivo, 3700 m ad ovest);
http://unmig.mise.gov.it/deposito/geotermia/inventario/p_pi_9.pdf

- 1967: "Montecastelli 1" (esplorativo, 60 m ad ovest);
http://unmig.mise.gov.it/deposito/geotermia/inventario/p_pi_3.pdf

- 1968: "Sesta 1" (produttivo, 2500 m a sud);
http://unmig.mise.gov.it/deposito/geotermia/inventario/p_si_4.pdf

- 1970: "Bulera 3" (produttivo, 4000 m ad ovest);
http://unmig.mise.gov.it/deposito/geotermia/inventario/p_pi_6.pdf

- 1979: "Val Pavone 2"(esplorativo, 2100 m a sud);
http://unmig.mise.gov.it/deposito/geotermia/inventario/p_si_1.pdf

- 1981: "Sesta 5" (produttivo, 2400 m a sud).
http://unmig.mise.gov.it/deposito/geotermia/inventario/p_si_4.pdf

Pozzi nel serbatoio profondo:
- 1997: "Sesta 6bis" (produttivo, 1300 m a sud); (**Barelli et. al 2000**)
- 2000: "Sesta 6bisA" (produttivo, 1300 m a sud), (**Batini et. al 2002**) attualmente impiegato come reiniettore.

2. Risultati ottenuti dalle prospezioni

L'area del Progetto geotermico pilota Castelnuovo è stata interessata da varie prospezioni geofisiche:

- **Modello 3D tomografico**

Vanorio et al. (2004) hanno proposto un modello 3D tomografico ad alta risoluzione del sistema geotermico Larderello-Travale da registrazione di micro-terremoti. L'area di "Castelnuovo" ricade parzialmente all'interno del modello tomografico, ed in particolare nella sua parte nord-occidentale in prossimità del pozzo S.Dalmazio (SDAL, Figura *5*). La figura indica che nella porzione superficiale della suddetta area (ossia fino a circa 2 km) sono presenti corpi geologici con velocità delle onde di compressione (VP) relativamente basse (circa 3.6 km/s). A seguire, sono state misurate VP pari a circa 5.2 km/s fino alla profondità di circa 5 km, profondità alla quale si assume sia presente l'orizzonte K (**Batini & Nicolich, 1985**).

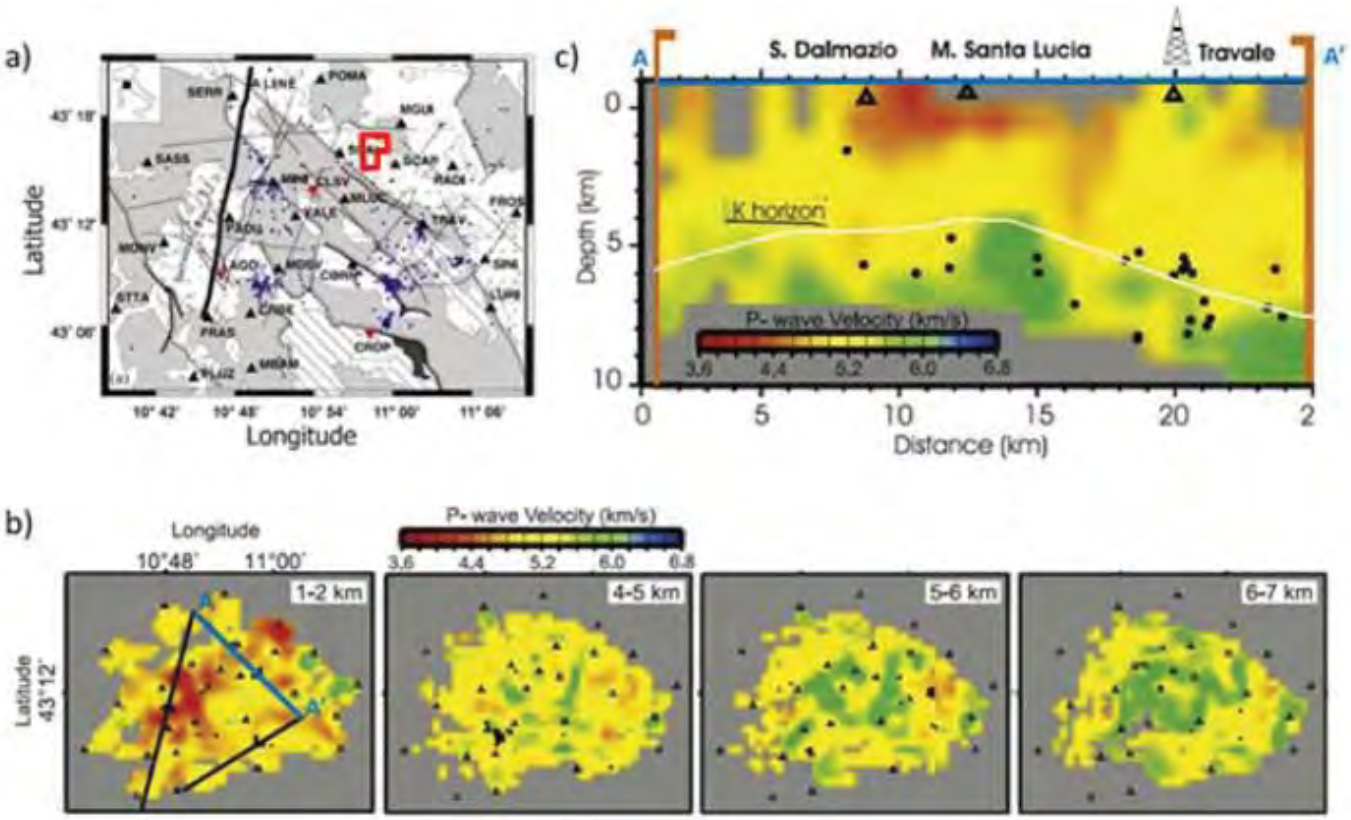

Figura 5 -Mappa dell'area geotermica Larderello-Travale in cui sono raffigurate le stazioni sismiche (triangoli) e la localizzazione dei micro-terremoti (punti). b) Mappa delle velocità VP per varie profondità di riferimento. Profilo A-A' usato per la rappresentazione della sezione 2D in VP (linea blu). c) Sezione sismica 2D in VP. Ipocentri dei micro-terremoti (punti), orizzonte K (linea bianca) e stazioni sismiche (triangoli). (modificata da ***Vanorio et al., 2004****).*

- **Prospezioni sismiche**

Durante l'esplorazione geotermica condotta da ENEL sono state realizzate una serie di prospezioni di sismica a riflessione 2D e 3D al fine di localizzare le porzioni del serbatoio potenzialmente più produttive, alcune di esse fino al limite sud del Progetto Pilota Castelnuovo. Alcuni di questi dati pubblicati hanno permesso di ricostruire la geometria dei principali corpi geologici con notevole dettaglio (**Batini et al.1978**; **Batini & Nicolich 1985**) .

La prospezione sismica 3D per l'area di Gabbro-Sesta (**Casini et. al 2010**) (Figura 6), interessa parzialmente l'area del progetto.

La prospezione ha messo in evidenza alcuni riflettori sismici di potenziale interesse geotermico (Figura 7) . Alcune perforazioni (es. Sesta 6 bis, **Barelli et al.2000**) in prossimità dell'area del Progetto geotermico pilota Castelnuovo hanno raggiunto tali obiettivi ottenendo produzione di fluidi geotermici per generazione geotermoelettrica.

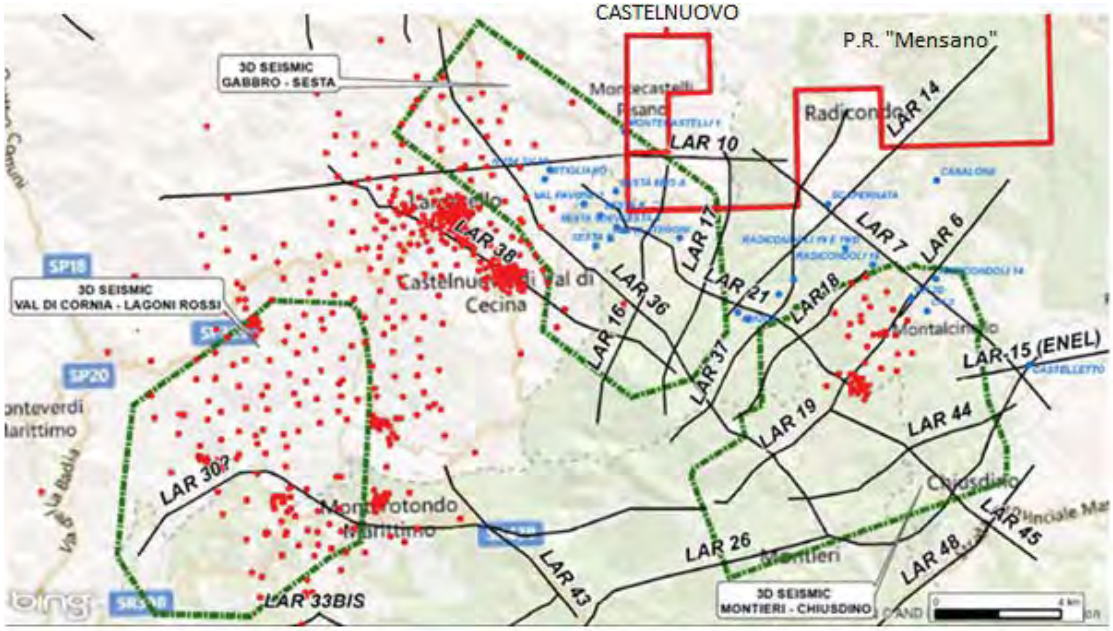

Figura 6: Mappa dei dati sismici 2D (in nero) e 3D (in verde) acquisiti nelle vicinanze ed all'interno della parte Sud del permesso pilota "Castelnuovo" Punti rossi e blu con etichette = pozzi geotermici.

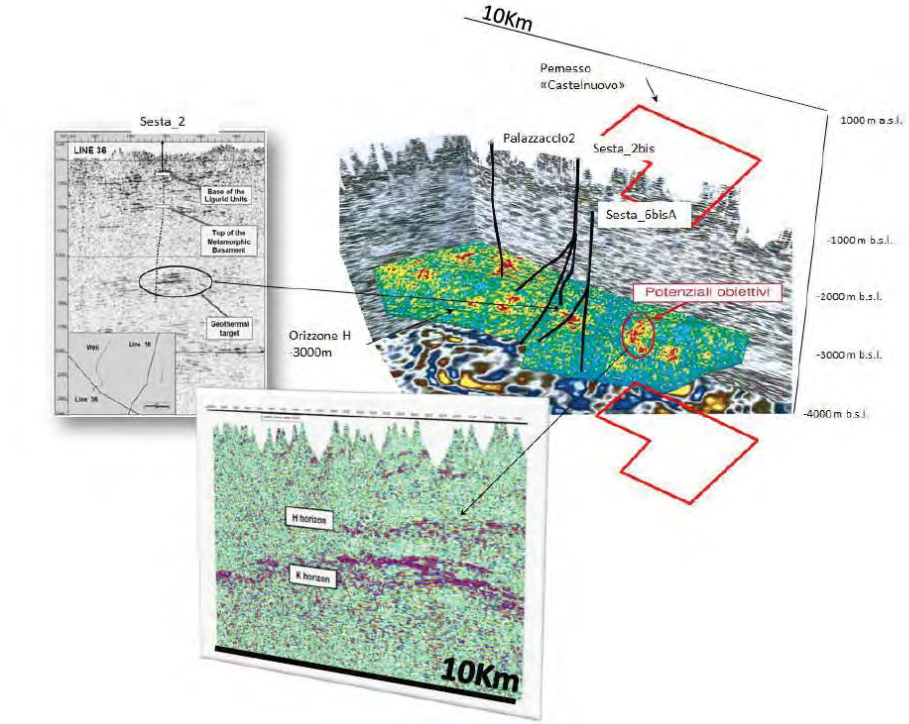

Figura 7 - Ricostruzione dei risultati della prospezione sismica 3D per l'area di "Castelnuovo"

3. Modello geologico

La disponibilità di dati geologici di superficie e di dati geofisici in parte inediti, integrati con i dati litostratigrafici dei pozzi ha permesso di realizzare un modello geologico tridimensionale per il Progetto geotermico pilota Castelnuovo.

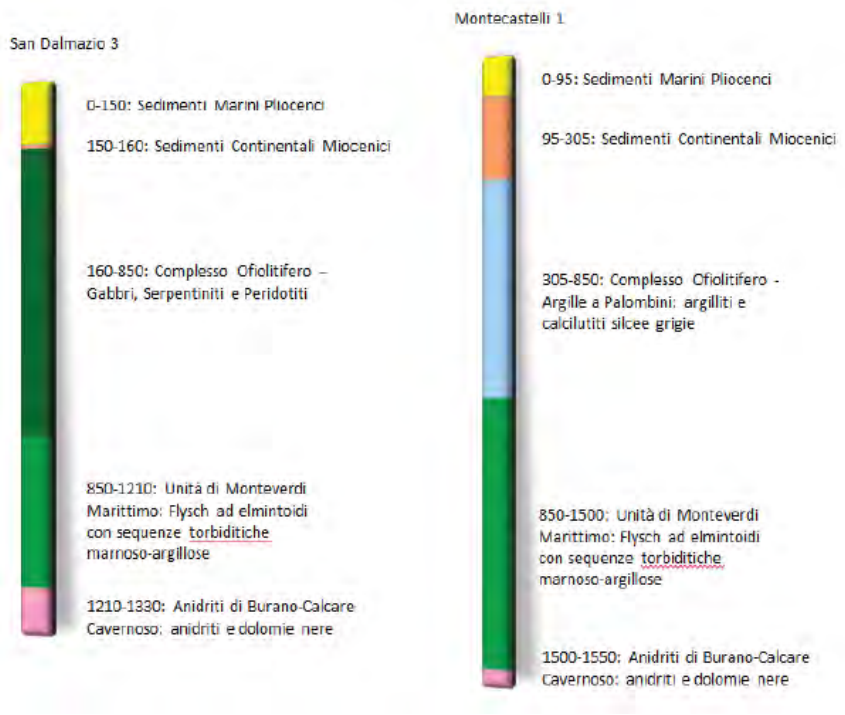

Figura 8 -Stratigrafie dei pozzi San Dalmazio 3 e Montecastelli 1 (mod. da da UNMIG - Inventario delle risorse geotermiche nazionali)

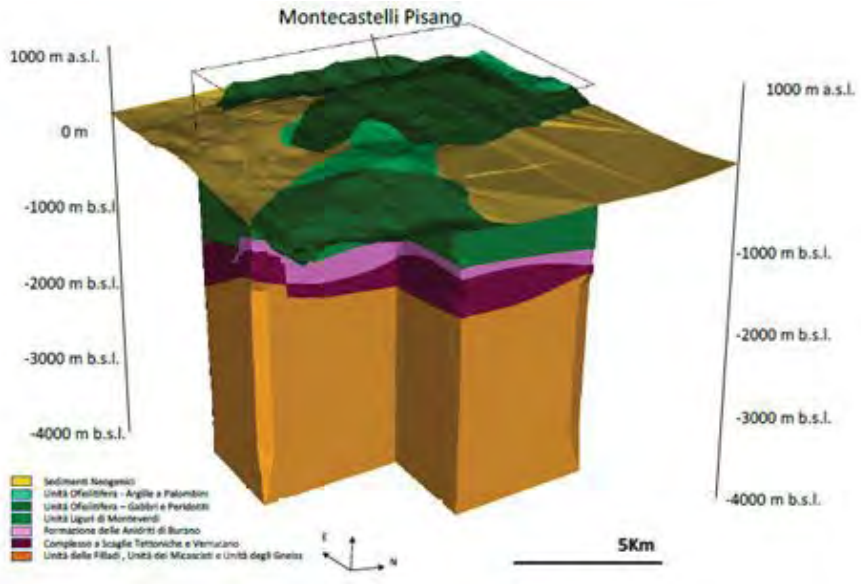

Figura 9 modellizzazione geologica tridimensionale del permesso "Castelnuovo"

Il modello ha consentito di ricostruire le geometrie delle strutture geologiche e la distribuzione delle proprietà petrofisiche (e.g. densità, conducibilità termica, porosità, ecc.) necessarie per la realizzazione di un modello termofluidodinamico del serbatoio geotermico.

4. Modello di temperatura

La **disponibilità di dati di numerosi pozzi** ha permesso di ricostruire la distribuzione di temperatura all'interno del sistema geotermico di Castelnuovo. In Figura 10 è riportata la carta del gradiente geotermico calcolato anche sulla base dei pozzi geotermici che hanno raggiunto il basamento metamorfico. Si può osservare come la superficie del Progetto geotermico pilota Castelnuovo sia caratterizzata da un gradiente geotermico compreso tra 0.7 e 1.3°C/10 m. Il gradiente mostra un trend crescente da NE verso SW con valori che superano 1°C/10m nella maggior parte dell'area .

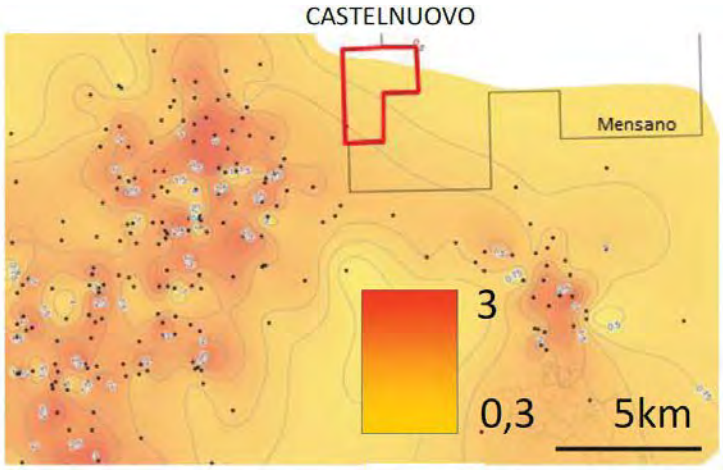

Figura 10 Mappa del gradiente geotermico realizzata sulla base dei dati di pozzi geotermici che hanno raggiunto il basamento metamorfico ad una profondità maggiore di 750 m. Il gradiente è espresso in °C/10m; i punti neri rappresentano i pozzi analizzati (elaborazione Magma Energy Italia).

Tale carta ha permesso di stimare la distribuzione della temperatura a differenti profondità e in Figura 12 sono riportate le temperature alle profondità di -1000, -2000 e -3000. È possibile osservare che il permesso già alla profondità di -2000m presenta condizioni di temperature superiori a 250°C nell'angolo SO. Temperature superiori sono previste a partire da -3000m dove i 300°C sono stati stimati ipotizzando un gradiente pari a 1°C/10 m come attestato dalle misure nel pozzo Montecastelli 1 che presentava una temperatura di circa 150 °C a 1500 m .

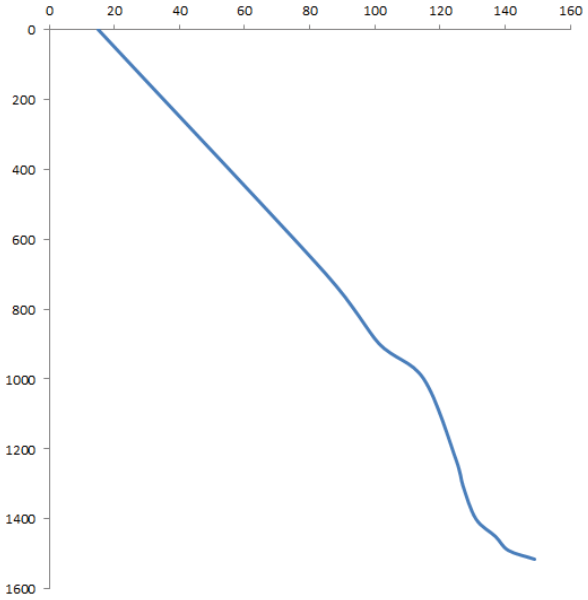

Figura 11 - Profilo termico del pozzo Montecastelli1

Indicazioni dirette della temperatura a profondità maggiori possono essere ottenute dai pozzi che raggiungono il complesso metamorfico, ad esempio il Sesta 6 bis (**Barelli et. al 2000**). (Figura 13).

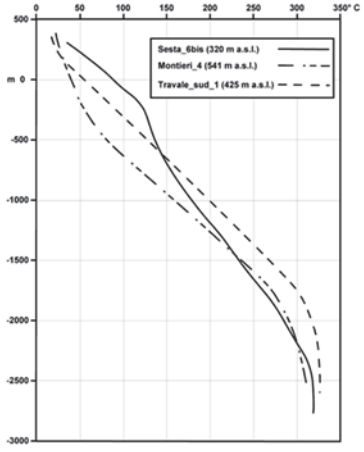

*Figura 13 - Profilo termico del pozzo Sesta_6bis (da **Barelli et al. 2000**).*

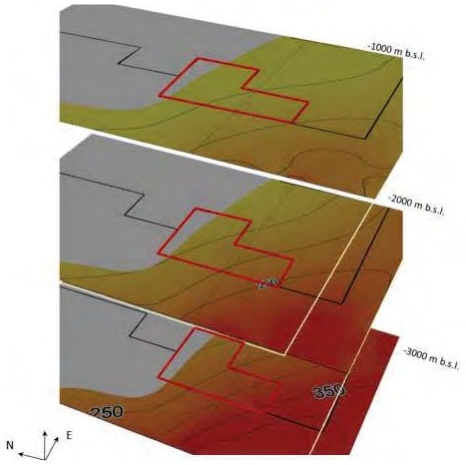

Figura 12- Distribuzione delle temperature alle profondità di -1000, - 2000 e -3000 m - elaborazione Magma Energy Italia

La ricostruzione dell'andamento del flusso di calore ricostruito per l'intera area di Larderello-Travale (**Bellani et. al., 2004**) mette in evidenza come l'area di Montecastelli, rappresentata dal riquadro rosso, sia caratterizzata da valori compresi, mediamente, tra 100 e 300 mW/m^2 (Figura 14).

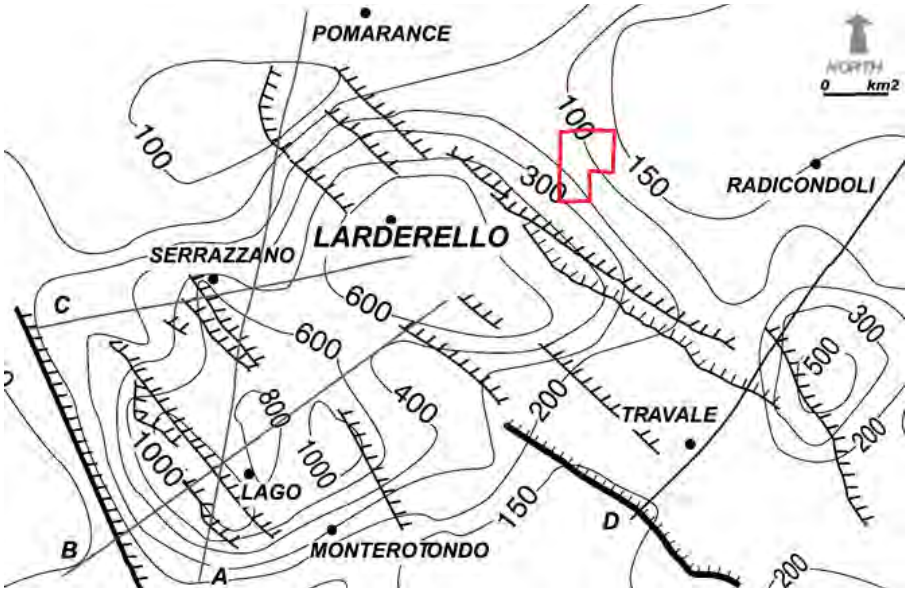

*Figura 14- Schema tettonico con riportate le principali faglie dirette ad alto angolo e distribuzione del flusso di calore espresso in mW/m2 (da **Bellani et al., 2004**).*

5. Prove di produzione dei pozzi

Nell'immediate vicinanze del Progetto geotermico pilota Castelnuovo, come già mostrato nella Figura 4 sono stati perforati numerosi pozzi, alcuni profondi oltre 3000 m ed in alcuni di essi sono state eseguite prove di produzione o di iniezione.

In particolare:

- Il pozzo Sesta_6bis, profondo 3921 m e situato a circa 1300 m dal bordo SW Progetto Geotermico Pilota Castelnuovo, ha intercettato varie zone produttive, come riportato nella pubblicazione di **Barelli et al. (2000)** ,alle seguenti profondità:
    - 2363 m , con un'iniettività di 5-6 m^3/h/bar e con una pressione del vapore di circa 50 bar.
    - 3120 m , 3375 m, 3600 - 3720 m, con un valore di iniettività di 2,5 m^3/h/bar, temperatura di 300 °C e pressione di circa 70 bar.

  Le prove di produzione hanno mostrato che questo pozzo poteva sostenere una produzione di circa 35 t/h di vapore "secco" (titolo di vapore=1) con una percentuale dell' 8, 5% di incondensabili in peso.

- Il pozzo Sesta 6 bis A (**Batini et. al. 2002**), profondo circa 4000 m e ubicato nella stessa postazione del Sesta6 bis, ha intercettato alcune zone produttive come riportato nel log di temperatura (Figura 15) . In Figura 16 è riportata la lista delle fratture e la produzione cumulativa, mentre un test finale di buildup sulla pressione ha premesso di risalire al valore di 0,7 mD come valore di permeabilità della formazione, assumendo per il serbatoio uno spessore di 1000 m.

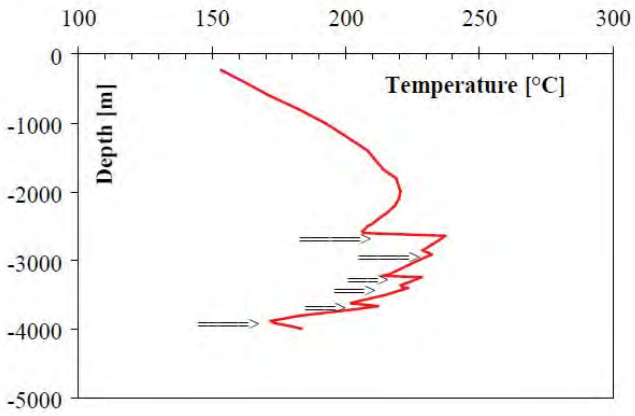

Figura 15- Log di temperatura dopo i test di produzione, le zone fratturate sono visibili in corrispondenza della variazione della pendenza del gradiente di temperatura

Depth (m)	First T&P Flow rate (kg/s)	Second T&P Flow rate (kg/s)
2640	2.08	1.77
2910	1.11	0.14
3240	N/A	0.33
3400	N/A	0.14
3660	N/A	0.33
3880	2.31	1.44
TOTAL	**5.50**	**4.15**

Figura 16- fratture rinvenute con i log di temperatura e pressione (T & P) durante il test di produzione)

6. Caratteristiche chimico- fisiche dei fluidi

Le caratteristiche dei fluidi che si prevede di reperire per il Progetto geotermico pilota Castelnuovo sono simili a quelle dei fluidi che alimentano la centrale di Sesta, non solo per quanto riguarda temperatura e pressione , ma anche dal punto di vista della composizione chimica.

Sulla base dei dati Arpat [(1)], il fluido che alimenta la centrale di Sesta aveva nel 2003 la composizione del fluido riportata in Tabella 1.

Centrale Sesta					
Centrale	Carico al momento dei controlli	Portata fluido alimentazione:	Portata torre	Prelievo da	Date prelievi
Sesta1	12,5 MW	91,5 t/h	7020000 Nm3	torre	24-26.02.2003

Flusso di massa in g/h						
CO_2	H_2S	NH_3	As *	Sb*	Se*	Hg*
$6,2 \times 10^{6}$	128100	26700	1,3	< 0,28	< 0,28	5,37
Cd*	Cr*	Mn*	Ni*	Pb*	Cu*	V*
< 0,0003	< 0,0008	0,023	0,004	<0,003	0,004	< 0,0003
Concentrazione in mg/Nm³						
CO_2	H_2S	NH_3	As*	Sb*	Se*	Hg*
885,9	18,2	3,8	$1,8 \times 10^{-4}$	4×10^{-5}	4×10^{-5}	$7,7 \times 10^{-4}$
Cd*	Cr*	Mn*	Ni*	Pb*	Cu*	V*
$5,6 \times 10^{-8}$	$1,1 \times 10^{-7}$	$3,3 \times 10^{-6}$	$5,5 \times 10^{-7}$	$4,4 \times 10^{-7}$	$5,5 \times 10^{-7}$	$5,5 \times 10^{-8}$

*Tabella 1: esiti delle analisi effettuate sulle emissioni: con * si intendono anche i composti dell'elemento*

La centrale prevista per il Progetto geotermico pilota Castelnuovo dista circa 3 km dalla centrale in esercizio Sesta 1 e circa 2,4 km dalla postazione Sesta 6 bis.

7. Modellistica di serbatoio

Sulla base dei dati delle prospezioni e dei pozzi è stato ricostruito il modello termofluidodinamico del serbatoio oggetto di interesse per il Progetto geotermico pilota Castelnuovo. Con un lavoro svolto

1 http://sira.arpat.toscana.it/sira/Efesto/cg_13.htm

congiuntamente tra Magma Energy Italia e Schlumberger-Geothermex è stato costruito e calibrato sulla base dei dati esistenti un modello geotermico di serbatoio, sul quale sono state svolte simulazioni volte a valutare la fattibilità di un impianto binario per l'area di Castelnuovo.

Il modello sviluppato da Geothermex copre un'area di 9,5 x 13 km; l'ampiezza della superficie oggetto della simulazione è stata scelta per rappresentare il quadro geologico generale e per ridurre l'impatto dei possibili effetti di bordo sui risultati del modello. Il modello geometrico si estende in direzione verticale fino a una profondità massima di circa 7000 m, ed è suddiviso in 18 strati di vario spessore .Ogni strato del modello è suddiviso a sua volta in 28 x 21 celle. La suddivisione è stata realizzata in modo tale da avere una discretizzazione più dettagliata del reservoir principale e della zona di produzione, dove le celle hanno dimensioni di 200m x 200m x 300m. La griglia di base si compone di 10594 celle, ma il numero è incrementato dall'utilizzo della formulazione dual porosity fino a un valore complessivo di 21168 blocchi, dando origine a un modello elaborato che richiede sforzi computazionali notevoli per ogni simulazione. La base del modello è definita dal top dell'orizzonte K ottenuto da articoli e da dati sismici pubblicati relativamente alla zona di interesse.
L' orizzonte K", è un riflettore sismico, che caratterizza Toscana Meridionale e si colloca a profondità variabile da 3 km (zona di Larderello) a 8-10 km (zona dell'Amiata) ed è considerato la base del sistema geotermico.

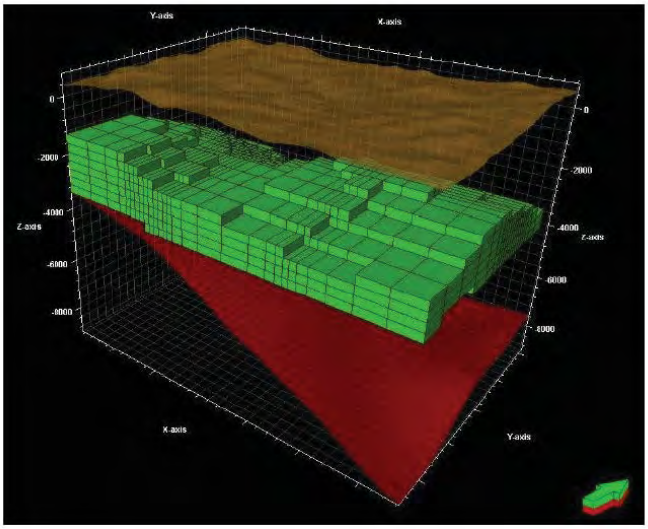

Figura 17 - In verde le celle che rappresentano l'orizzonte produttivo. Come riferimenti sono indicate la superficie topografica e il top dell'orizzonte K

a) Modello indisturbato

Definito il layout della griglia di simulazione, la prima parte della modellistica è stata incentrata sulla riproduzione delle condizioni termodinamiche del modello imperturbato, che rappresenta il punto di partenza per le simulazioni successive. Per il modello iniziale si sono considerati valori di permeabilità presenti in letteratura come dati di partenza (Tabella 2). Questi dati includono i valori misurati per il pozzo Sesta 6 bis A durante le prove di pozzo (**Batini et al., 2002**) e i range di valori impiegati in modelli precedentemente realizzati in letteratura (**Barelli et al., 2010**; **Della Vedova et al., 2007**; **Ebigbo et al., 2015** e **Romagnoli et al., 2010**).

Alle celle appartenenti alla stessa formazione geologica sono stati assegnati inizialmente gli stessi valori di permeabilità, mentre durante il processo di calibrazione del modello , i valori sono stati modificati localmente per riprodurre un buon accordo con i dati di temperatura misurati nei pozzi profondi (Barelli et. al. 2000)e il trend generale delle pressioni.

	Permeabilità		
Unità geologica	Della Vedova 2008	Ebigbo 2015	Romagnoli 2010
Serbatoio carbonatico	$5x10^{-15}$-$5x10^{-16}$	10^{-14}-10^{-15}	10^{-13}-10^{-16}
Serbatoio metamorfico	$5x10^{-16}$-$5x10^{-17}$	$6x10^{-16}$	
Faglie	10^{-13}-10^{-14}		

Tabella 2 - Valori di permeabilità usati in precedenti simulazioni numeriche

Il valore di permeabilità assegnato alle fratture della porzione di reservoir più permeabile è pari a 18 mD, mentre per i blocchi di matrice è stato assunto un valore uniforme di 0,01 mD. Per quanto riguarda la porosità è stato assegnato un valore del 3% per tutto il serbatoio, in analogia con studi precedenti che assumono valori compresi tra il 2 e il 5. I valori di permeabilità, porosità, e altri parametri utilizzati nella simulazione sono riportati nella Tabella 3.

Proprietà	**Matrice**	**Fratture**
Porosità	0,03	0,03
Permeabilità (mD)	0,01	0,0001-18
Densità (kg/m^3)	2650	
Calore specifico (kJ/kgK)	0,82	

Tabella 3 - Parametri usati per la simulazione

Le fasi principali della modellizzazione sono state (Figura 18):

- Ricostruzione della distribuzione delle temperature iniziali attraverso l'interpolazione di dati dei pozzi geotermici esistenti nelle zone circostanti l'area di studio.
- Ricostruzione della distribuzione delle pressioni attraverso l'interpolazione di dati dei pozzi geotermici esistenti nelle zone circostanti l'area di studio.
- Ricostruzione della concentrazione in gas incondensabili in serbatoio

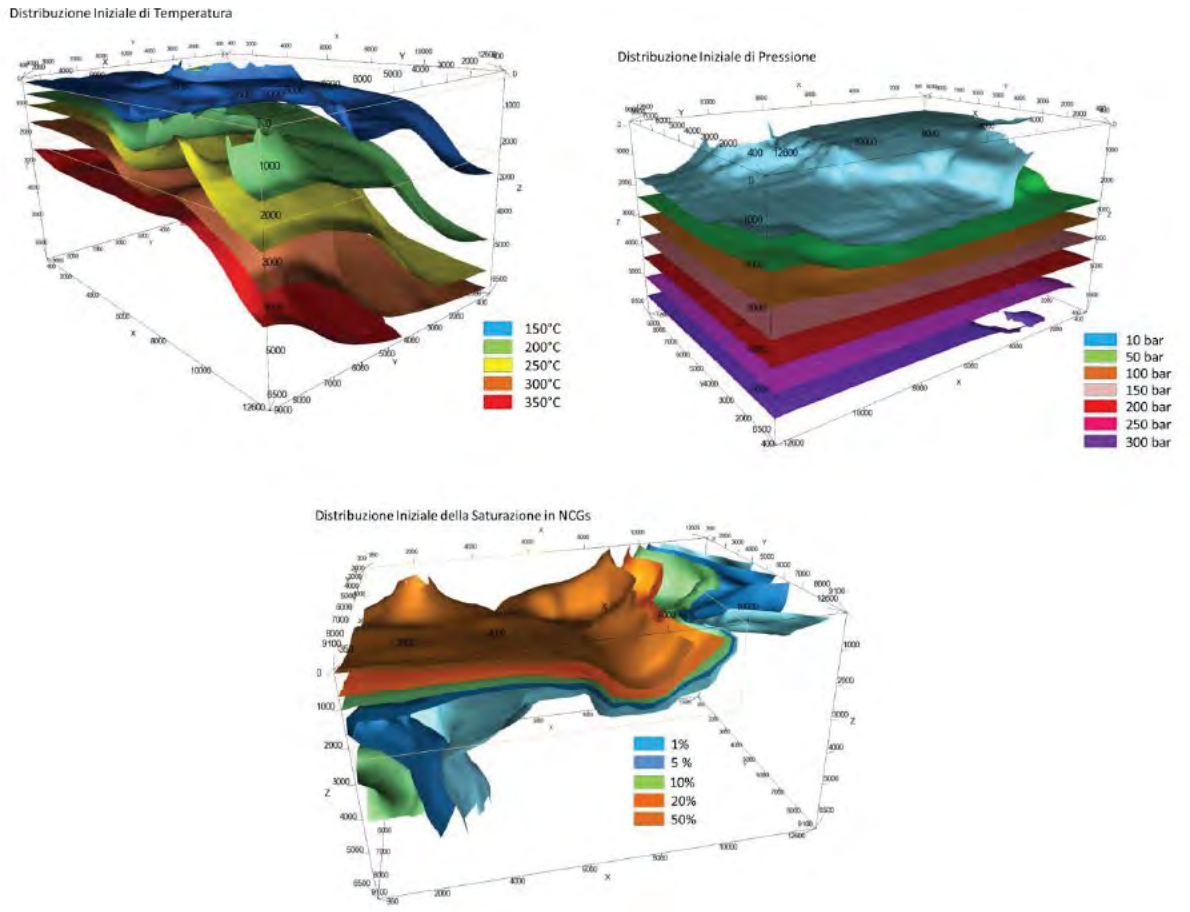

Figura 18 - Modello di serbatoio iniziale imperturbato

Il modello imperturbato è stato ottenuto mediante simulazioni eseguite su scala temporale di 200.000 anni, in modo da garantire che l'evoluzione della pressione e della temperatura in serbatoio sia trascurabile rispetto ai cambiamenti indotti dalla simulazione della coltivazione (decine di anni).

b) Simulazioni di coltivazione

Il risultato dello stato stazionario rappresenta il punto di partenza per un'analisi più specifica del serbatoio, valutando la risposta del sistema alla coltivazione in termini di abbassamento della temperatura e della pressione su un periodo di 30 anni, che coincide con la vita utile di un impianto geotermico.

Al modello sono stati aggiunti i pozzi di estrazione e reiniezione previsti dal progetto, per valutare la sostenibilità dello stesso.

Per la simulazione della coltivazione del campo si sono considerati due pozzi di estrazione e un pozzo per la reiniezione totale del fluido. Al fine di simulare i pozzi di estrazione sono state considerate come vincoli le seguenti condizioni a boccapozzo: pressione minima = 15 bar; portata totale del campo pozzi = 70 t/h. Per il pozzo di reiniezione è stato considerato di reimmettere la stessa portata estratta ad una temperatura di 85-90 °C. La modellistica di serbatoio ha tenuto in considerazione gli effetti cumulativi sul serbatoio legati non solo al Progetto geotermico pilota Castelnuovo, ma anche alla presenza della centrale di Sesta già in esercizio dal 2002 e di un eventuale centrale da realizzare nell'adiacente P.R. Mensano, qualora l'attività esplorativa in corso all'interno dello stesso dia esito positivo.

Il progetto prevede di reimmettere il condensato insieme ai gas incondensabili presenti nel fluido geotermico e il modello di coltivazione simula il comportamento e la propagazione dei gas nel serbatoio.

Tutti i pozzi sono posizionati nella stessa postazione di perforazione: il primo produttore (CAS-P1) è ipotizzato verticale, il secondo produttore CAS-P2 è ipotizzato deviato verso sud ovest , con uno scostamento dalla verticale a fondo pozzo di 800 m, Il pozzo di reiniezione è deviato a nord-ovest e ha uno scostamento di 1000 m dalla verticale. I pozzi saranno in Open Hole tra 2200 e circa 3500 m, profondità che interseca la zona dove è maggiore la probabilità di incontrare le fratture produttive nella formazione metamorfica.

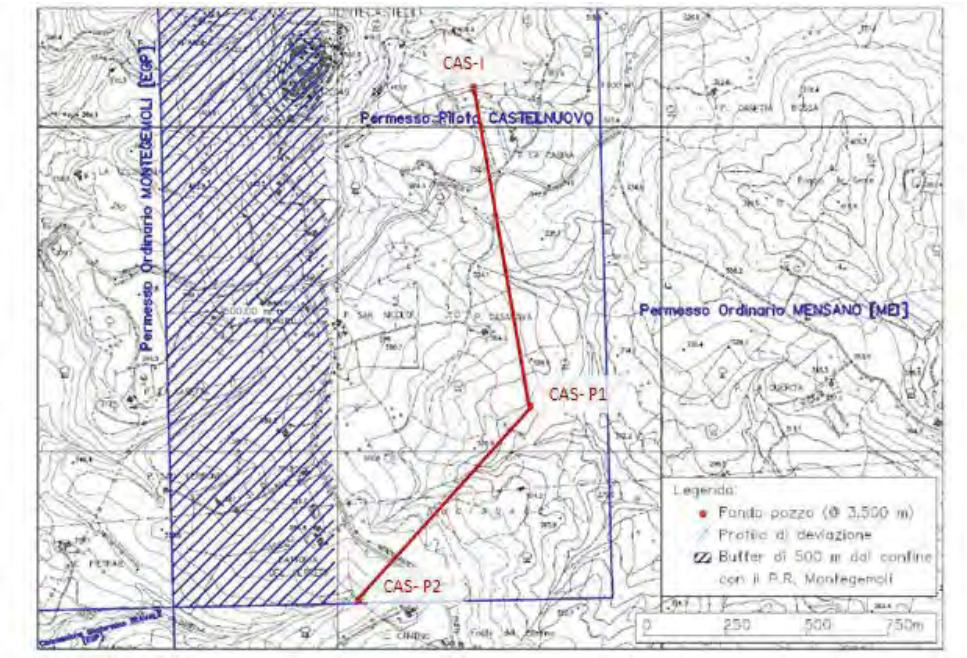

Figura 19 - Localizzazione del fondo pozzo per i pozzi del permesso pilota "Castelnuovo"

La scelta della localizzazione della reiniezione è stata determinata dall'esigenza di ridurre il rischio di eventuali ritorni di gas ai pozzi di produzione.

Il serbatoio appare dalle simulazioni in grado di sostenere l'estrazione e la reiniezione di 70 t/h di fluido geotermico, in condizioni tali da garantire il funzionamento dell'impianto per tutta la sua vita utile, mantenendo livelli di temperatura e pressione superiori a quelli minimi di progetto.

In 30 anni, risultano dal modello una diminuzione di temperatura ai produttori non superiore a 8°C (Figura 20) e una diminuzione di pressione inferiore a 6 bar.

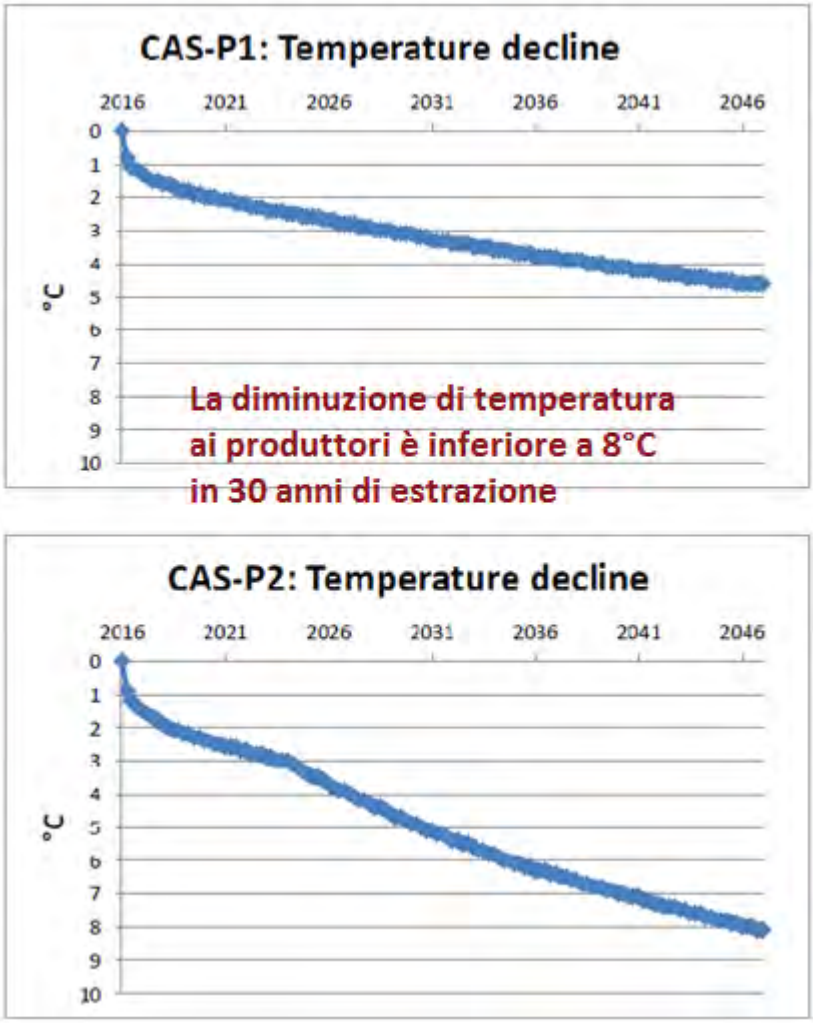

Figura 20 - Variazione di temperatura per i pozzi di produzione

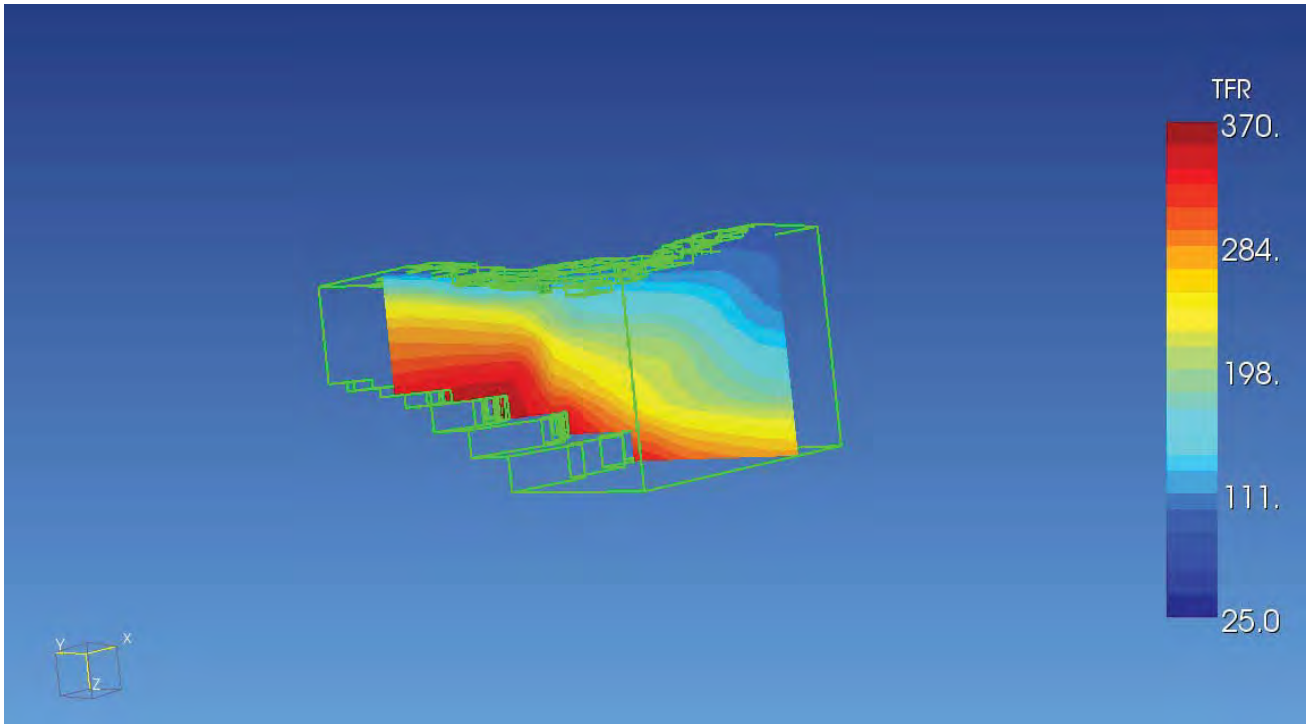

Figura 21- Temperatura a inizio periodo (sezione sul pozzo di reiniezione)

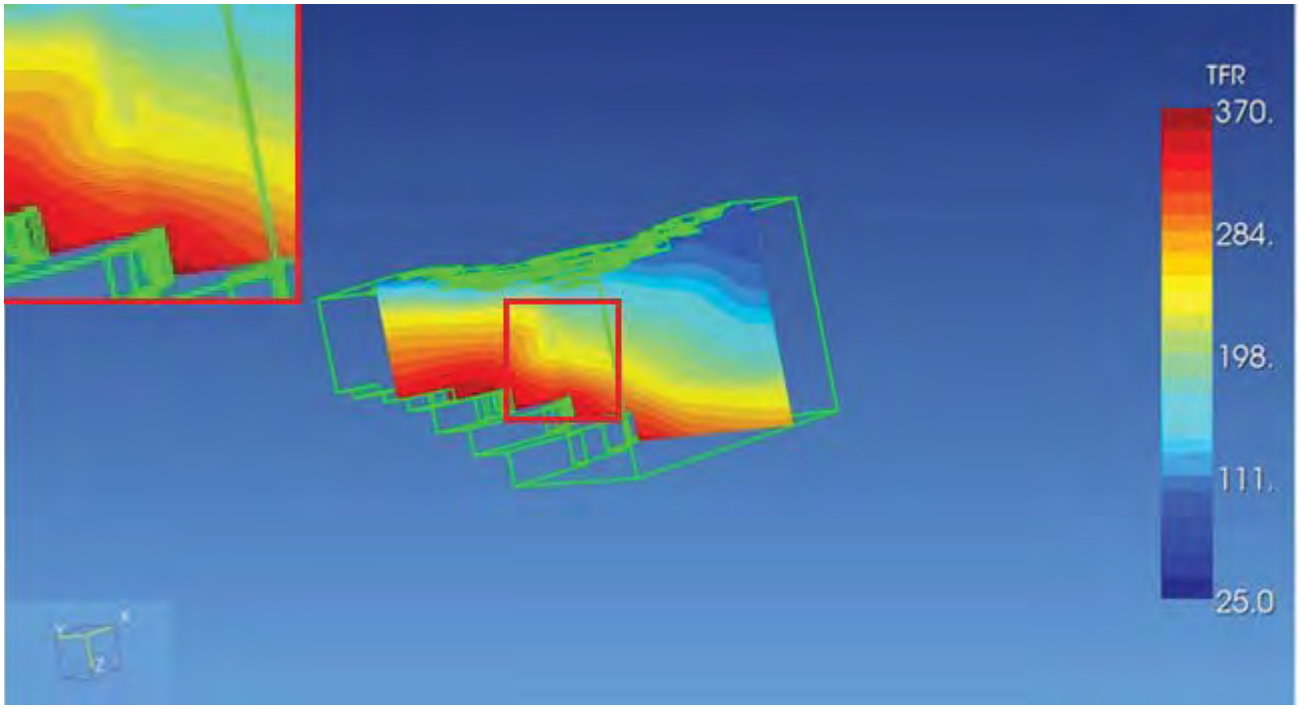

Figura 22- Temperatura dopo 30 anni di coltivazione (sezione sul pozzo di reiniezione)

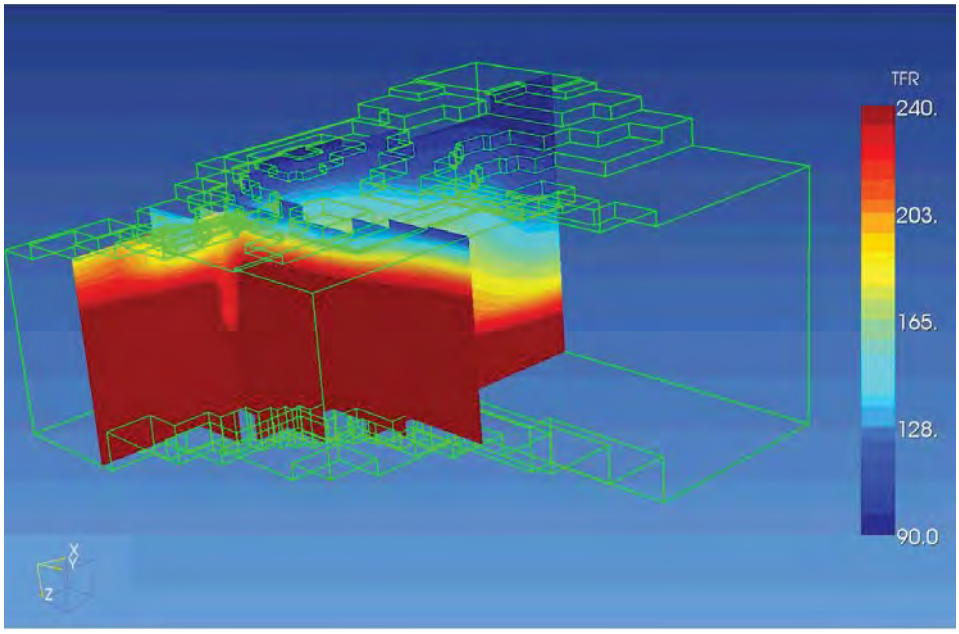

Figura 23- Temperatura dopo 30 anni di coltivazione; la riduzione di temperatura appare confinata al reiniettore (sezione sul pozzo di reiniezione; il range di valori di temperatura visualizzati è stato modificato per rendere l'immagine più comprensibile.)

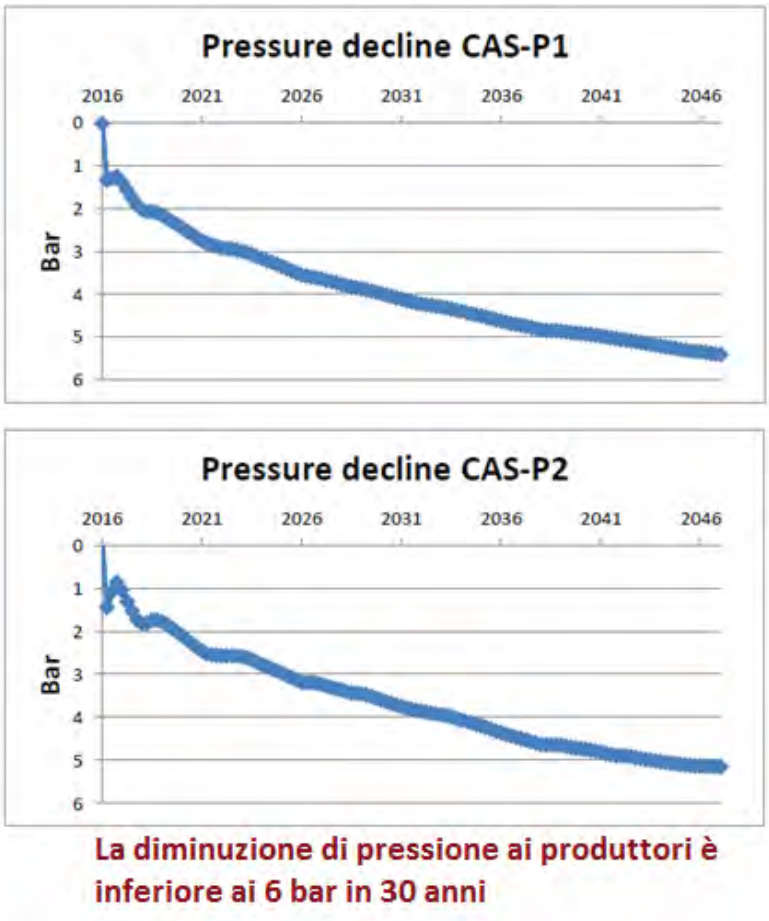

Figura 24 - Variazione di pressione per i pozzi di produzione

Dalle simulazioni appare (Figura 25) come la reiniezione non comporti alcun effetto di disturbo sui pozzi produttivi, né per quanto riguarda l'eventuale propagazione di un "fronte freddo" dal reiniettore ai produttori (la perturbazione termica generata è confinata attorno al reiniettore e non raggiunge mai i pozzi di produzione), né per un' eventuale propagazione dei gas incondensabili reiniettati; in particolare, questi ultimi rimangono confinati nella zona del pozzo reiniettore senza influenzare la composizione del fluido estratto e senza raggiungere i pozzi produttori. Per quanto riguarda la sovrapressione al reiniettore ottenuta per un periodo di coltivazione di 30 anni essa si attesta attorno ai 15 bar e appare confinata per lo più in un'area di circa 400 m di raggio (Figura 25).

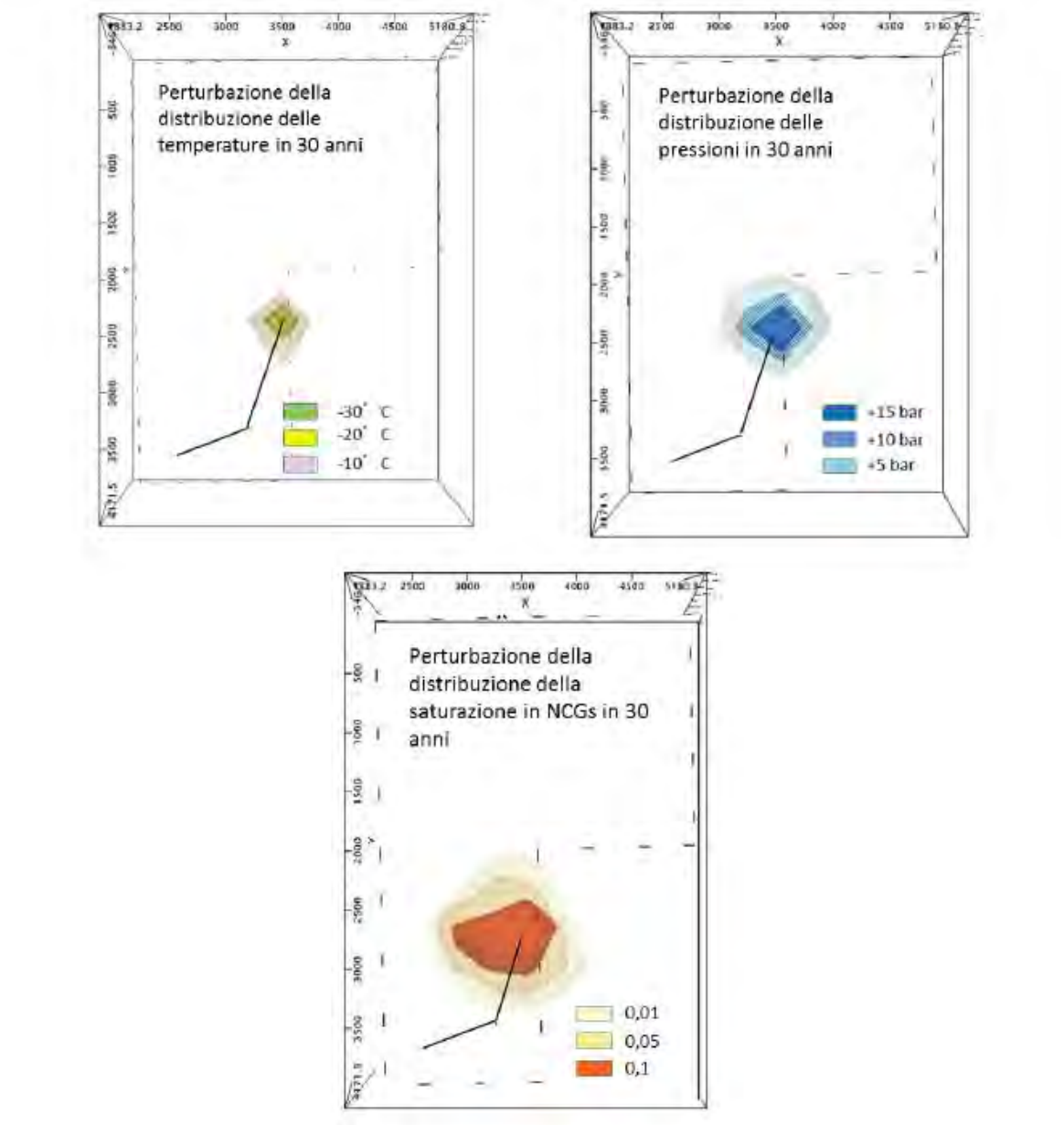

Figura 25- Risultati della modellistica di serbatoio dopo 30 anni di simulazione della coltivazione

4. Conclusioni

I risultati ottenuti dalle prospezioni, dai dati di pozzo e relative prove di produzione , delle caratteristiche chimiche-fisiche dei fluidi geotermici e delle simulazioni numeriche eseguite per la stima delle riserve

geotermiche recuperabili, hanno consentito di accertare la presenza di riserve geotermiche ad alta entalpia di interesse nazionale sufficienti ad alimentare la centrale geotermoelettrica a ciclo binario da 5 MWe netti per almeno 30 anni del Progetto geotermico pilota Castelnuovo.

La presenza delle riserve geotermiche nell'area del Progetto geotermico pilota Castelnuovo è confermata anche da Enel Green Power, che nell'osservazione presentata alle Integrazioni al procedimento di Valutazione di Impatto Ambientale di due pozzi esplorativi da realizzarsi sulla stessa postazione di perforazione nel margine sud ovest del Permesso di Ricerca "Mensano" di titolarità di Magma Energy Italia S.r.l. (Allegato 1 - Osservazione n° 114 del 15/3/2016), afferma che :

"Il progetto Mensano si trova a poco più di un chilometro a nord est dal campo geotermico di Sesta esercito da EGP dal 2002 con la centrale omonima da 20 MW e utilizzerebbe il fluido geotermico proveniente dallo stesso serbatoio."

Pertanto anche il progetto Castelnuovo, che è adiacente al P.R Mensano ed alla Concessione di coltivazione Travale, fa parte dello stesso sistema geotermico Sesta-Mensano.

Nell'ottica di evitare eventuali interferenze tra le varie zone produttive, il proponente intende pianificare una strategia di estrazione - reiniezione mirata ad evitare il depauperamento della risorsa in accordo con Enel Green Power e Magma Energy Italia con l'obbiettivo comune di garantire la sostenibilità della coltivazione delle riserve geotermiche a lungo termine.

5. Bibliografia

Casini, M., Ciuffi, S., Fiordalisi, A. & Mazzotti, A. (2010). 3D Seismic Surveys and Deep Target Detection in the Larderello-Travale Geothermal Field (Italy). Proceedings World Geothermal Congress 2010 Bali, Indonesia, 25-30 April 2010

Barelli , A., Bertini, G., Buonasorte, G., Cappetti, G. & Fiordalisi, A. (2000). Recent deep exploration results at the margins of the Larderello Travale geothermal system. Proceedings World Geothermal Congress 2000, Kyushu –Tohoku Japan, may 28 – June 10, 2000.

Batini, F., Bertani, R. , Ciulli , B., Fiordelisi, A. & Valenti, P. (2002). Geophysical well logging- a contribution to the fractures characterization. PROCEEDINGS, Twenty-Seventh Workshop on Geothermal Reservoir Engineering Stanford University, Stanford, California, January 28-30, 2002 SGP-TR-171

http://sira.arpat.toscana.it/sira/Efesto/cg_13.htm

http://unmig.mise.gov.it/unmig/geotermia/pozzi/irg_pozzi.asp

Barelli ,A., Cei ,M., Lovari ,F.& Romagnoli, P.(2010). Numerical Modeling for the Larderello-Travale Geothermal System (Italy). Proceedings World Geothermal Congress 2010 Bali, Indonesia, 25-29 April 2010.

Della Vedova, B., Vecellio, C., Bellani , S. & Tinivella, U.(2007). Thermal modelling of the Larderello geothermal field (Tuscany, Italy), Int J Earth Sci (Geol Rundsch) (2007) 97:317–332 DOI 10.1007/s00531-007-0249-0

Ebigbo, A., Niederau, J., Thorwart, M., Riedel, M., Alexandrakis, C., Marquart, G. , Pechnig, R., Dini, I. & R. Bertani, R.. (2015). Simulation of Flow and Heat Transport in a High-Enthalpy Reservoir in Tuscany, Italy. Proceedings World Geothermal Congress 2015 Melbourne, Australia, 19-25 April 2015

Romagnoli P., Arias A., Barelli A., Cei M. & Casini M. (2010). An updated numerical model of the Larderello–Travale geothermal system, Italy. Geothermics 39 (2010) 292–313

Bellani, S., Brogi, A., Lazzarotto, A., Liotta, D., Ranalli, G., 2004. Heat flow, deep temperatures and extensional structures in the Larderello geothermal field (Italy): constraints on geothermal fluid flow. J. Volcanol. Geotherm.Res. 132, 15– 29.

Vanorio, T., De Matteis, R., Zollo, A., Batini, F., Fiordalisi, A., & Ciulli, B. (2004). The deep structure of the Larderello-Travale geothermal field fom 3D microearthquake traveltime tomoraphy. Geopysical Research Letters, 31, L07613.

Batini, F. & Nicolich, R. (1985). P and S reflection seismic profiling and well logging in the Travale geothermal field. Geothermics, 14, 731-747.

Batini, F., Burgassi, P.D., Cameli, G.M., Nicolich, R. & Squarci, P. 1978. Contribution to the study of the deep lithospheric profiles: Deep reflecting horizons in Larderello-Travale. Geothermal field. Mem. Soc. Geol. It., 19 (1978) 477-484.

Green Power

AREA EUROPA
OPERATION & MAINTENANCE ITALIA GEOTERMICO
56122 Pisa, via Andrea Pisano 120
ITALIA
T +39 0506185801 - F +39 050533290
enelgreenpower@pec.enel.it

Prot. AC_1006/16
del 15.03.2016

Spett.li
REGIONE TOSCANA
Settore Valutazione di Impatto Ambientale –
Valutazione ambientale strategica –
Opere pubbliche di interesse strategico regionale
P.zza Unità D'Italia, 1
50127 FIRENZE
PEC:
regionetoscana@postacert.toscana.it

Regione Toscana
Direzione Ambiente ed Energia
Settore Miniere e monitoraggio Acque minerali e termali
Piazza Baccarini,1
58100 Grosseto (GR)
PEC:
regionetoscana@postacert.toscana.it

Oggetto: Procedimento di Valutazione di impatto ambientale - Artt. 52 e seguenti della L.R.10/2010 - Proponente MAGMA ENERGY ITALIA S.r.l. – Invio Osservazioni al Progetto di realizzazione di due postazioni di perforazione, perforazione di due pozzi esplorativi e delle relative opere a rete (condutture interrate per il trasporto del fluido geotermico, nuovi tratti e/o adeguamento delle viabilità di accesso) nell'ambito del permesso di ricerca di risorse geotermiche "Mensano", nel comune di Castelnuovo Val di Cecina (PI)

In riferimento al procedimento di valutazione d'impatto ambientale per il conseguimento del Permesso di Ricerca Mensano, nel comune di Castelnuovo val di Cecina (PI) presentato dalla Società Magma Energy Italia S.r.l., facendo seguito alle precedenti osservazioni che la scrivente Società ha già inoltrato in data 3/2/2015 Prot. EGP 0001916 e valutate le controdeduzioni fornite dall'azienda Magma Energy Italia S.r.l. **con la presente si ribadisce la richiesta che non vengano perforati pozzi a distanze inferiori ai 2000 m. dal confine di concessione e, in ogni caso, dalla postazione Sesta 6bis.**
A supporto di tale richiesta si inviano le seguenti considerazioni:

- Il progetto Mensano si trova poco più di un chilometro a nord est dal campo geotermico di Sesta esercito da EGP dal 2002 con la centrale omonima da 20 MW e utilizzerebbe il fluido geotermico proveniente dallo stesso serbatoio.

EMAS
GESTIONE AMBIENTALE VERIFICATA
Reg. n. IT-001333

RINA

- Sperimentalmente (grafico sottostante) risulta che il sistema geotermico di Sesta ha un declino di pressione molto più accentuato rispetto al vicino campo di Larderello ed a quello modellato da Magma per il progetto Mensano (circa 1 bar/y con una sostanziale parità tra massa estratta e re iniettata). La depressurizzazione modellata da Magma a seguito della produzione prevista nel progetto Mensano (1-3.5 bar in 30 anni), risulta pertanto ampiamente sottostimata.

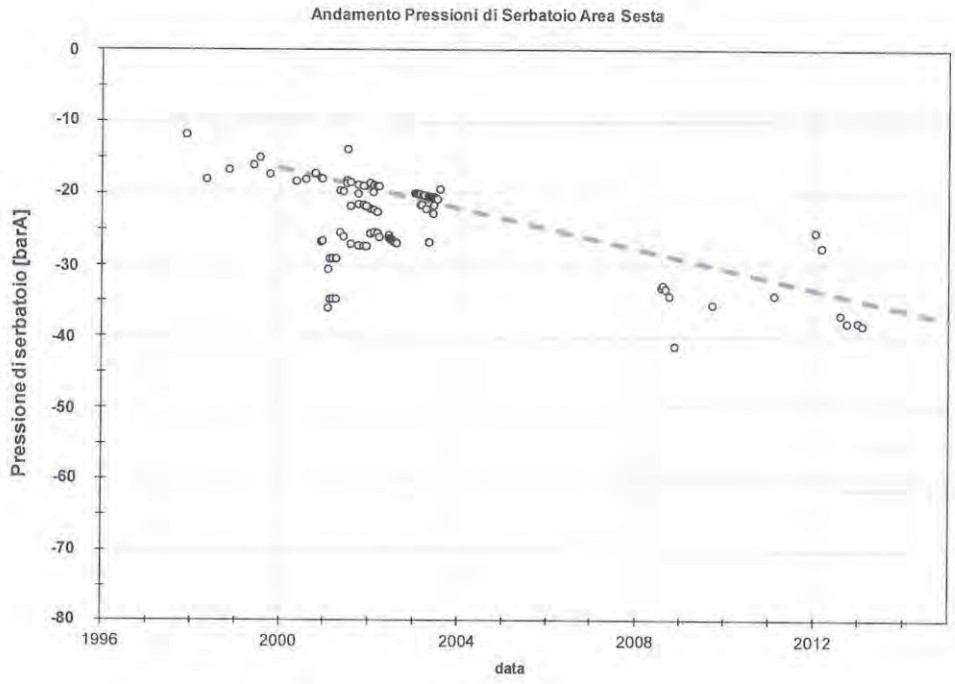

- I nostri dubbi sulla possibile interferenza tra i nostri pozzi di produzione e quelli previsti nel nuovo permesso di ricerca non sono inoltre legati solo all'abbassamento di pressione nel serbatoio, ma anche, e soprattutto, al possibile effetto termico della reiniezione. È infatti noto ed evidente dai dati sperimentali, che pozzi distanti anche alcuni chilometri rispetto ad un polo reiniettivo, possono direttamente risentirne con conseguente raffreddamento del fluido e possibile "affogamento" del pozzo stesso (interruzione dell'erogazione spontanea di vapore). Ciò è evidenziato dalle analisi chimico-fisiche ed isotopiche condotte durante il periodo di coltivazione dei sistemi geotermici. Nel sistema geotermico di Sesta l'interferenza è stata sperimentalmente verificata tra la reiniezione nella postazione SESTA_6BIS e i pozzi produttivi nella postazione SESTA_2BIS distanti quasi due chilometri.
  In questa situazione è fondamentale poter gestire la reiniezione, variando, se necessario, la distribuzione dei flussi di iniezione nei diversi pozzi disponibili, con lo scopo di ridurre il rischio di "affogamento" dei pozzi di produzione e la conseguente perdita di produzione. L'eventualità di avere una produzione/reiniezione **non gestibile** a distanza inferiore ai due chilometri rispetto ad una postazione di produzione esistente, potrebbe pertanto comportare fenomeni di interferenza con conseguente perdita di produttività dei pozzi in esercizio.

Green Power

- La criticità dell'interferenza tra reiniezione e produzione del campo in esercizio di Sesta è documentata dall'analisi del rapporto gas/vapore sul collettore di centrale (grafico seguente) che diminuisce nel tempo in relazione alla portata di acqua reiniettata.

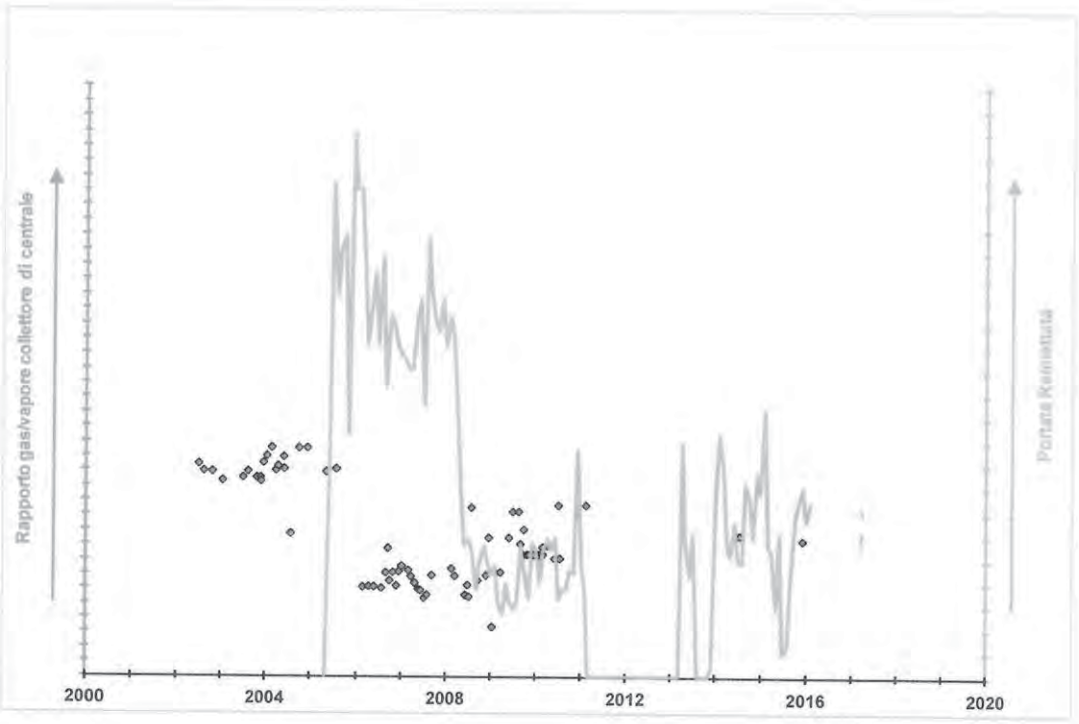

A disposizione per qualsiasi ulteriore chiarimento si rendesse necessario porgiamo,
Distinti Saluti

Massimo Montemaggi
IL RESPONSABILE

APPENDICE (INTEGRAZIONI ALLA RELAZIONE MINERARIA PERMESSO DI RICERCA DI "MENSANO")

1. RILIEVI GEOLOGICI DI CAMPAGNA

1.1. Metodi di acquisizione ed elaborazione dati

L'attività di carattere geologico svolta si è sviluppata secondo le seguenti fasi:

- Revisione dei dati esistenti per la creazione di una carta geologica di base alla scala 1:50.000 corredata da opportune sezioni geologiche;
- Attività di campagna legata alla raccolta di dati geologico-strutturali e cinematici delle strutture geologiche osservate. Questa fase ha permesso di integrare i dati esistenti con quelli raccolti direttamente dallo staff Magma Energy Italia in collaborazione con l'Università di Siena e ha prodotto una carta geologica originale alla scala 1:25.000.

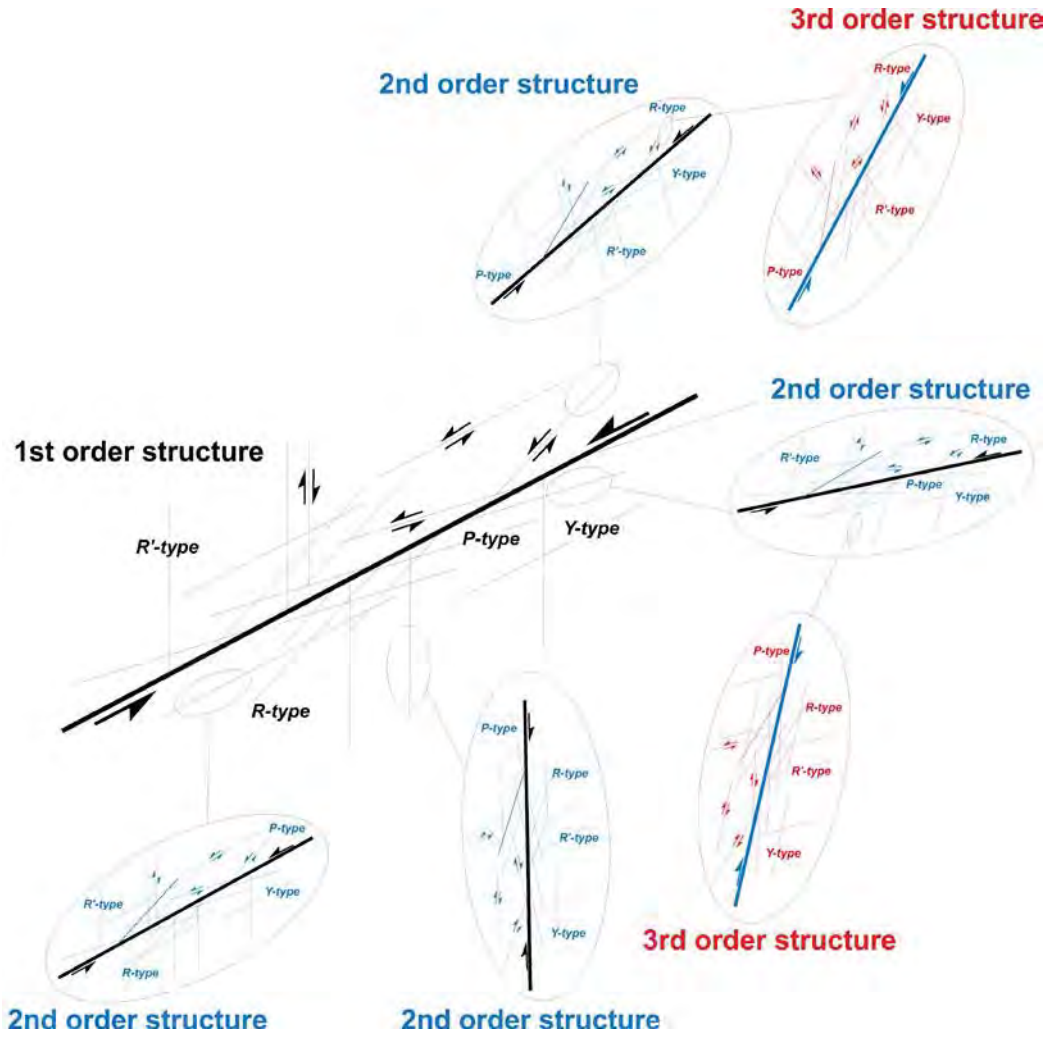

Fig. 1 – Analisi cinematica delle strutture geologiche osservate in campagna.

L'analisi cinematica è stata svolta categorizzando in un database apposito i diversi indicatori cinematici di movimento e analizzandoli con il software FaultKinWin 5.0 nel quale sono stati riportati i seguenti parametri cinematici:

- Codice stazione di misura:
- Numero stazione di misura
- Azimuth del piano d faglia
- Inclinazione del piano di faglia
- Pitch del piano di faglia
- Tipo di cinematica
- Offset
- Presenza di mineralizzazione
- Nome del rilevatore
- Località
- Descrizione
- Coordinate
- Quota

1.2. Analisi Morfologica

L'area del P.R. Mensano è caratterizzata da un'alternanza di bacini neogenici e di alti strutturali orientati NO-SE che compongono una complessa rete di allineamenti morfologici orientati NE-SO, NNO-SSE e E-O definiti da allineamenti di creste e di corsi d'acqua.

È stata svolta un'attività di analisi da 91 foto aeree fornite dal Dipartimento di Scienze della Terra dell'Università di Siena, da immagini satellitari Landsat e da modelli digitali del terreno.

In Fig. 14 è riportata la mappa delle strutture evidenziate dall'anilisi morfologica e il diagramma mostra la distribuzione statistica dei principali lineamenti morfo-tettonici.

La carta mostra come siano presenti due allineamenti principali:

- NE-SO associato ai corsi d'acqua principali
- ONO-ESE come ad esempio nel caso del Fiume Cecina.

Questi due lineamenti interessano anche i bacini Neogenico-Quaternari suggerendo un probabile controllo delle morfostrutture da parte di strutture tettoniche fragili.

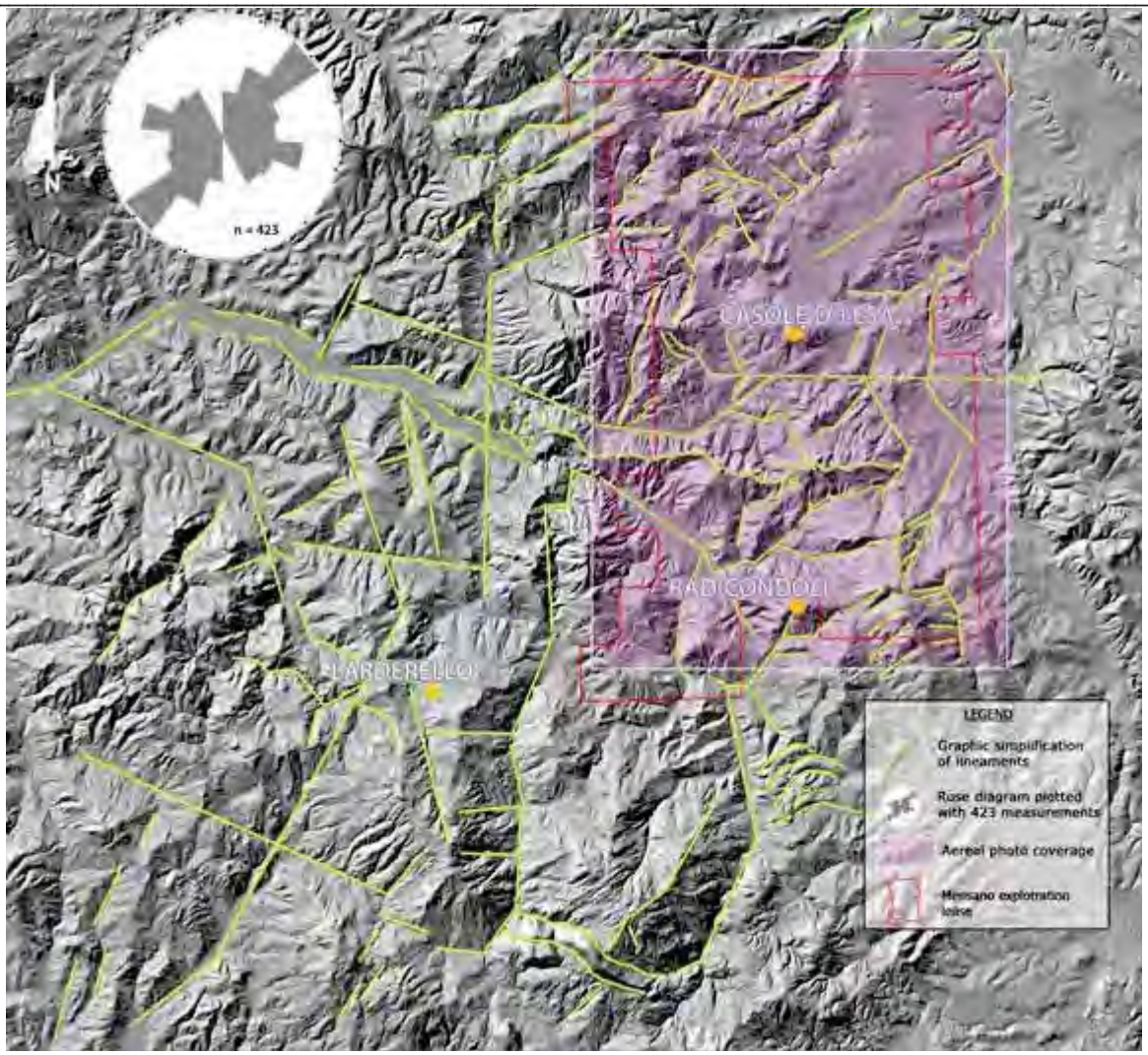

Fig. 2 – Principali allineamenti morfotettonici nel P.R: Mensano.

1.3. **Assetto Geologico del P.R. Mensano**

L'attività di rilevamento e ricostruzione geologica è stata svolta congiuntamente con l'Università di Siena e si è sviluppata nell'arco del 2012. La campagna di raccolta e interpretazione dati è stata resa possibile da una collaborazione scientifica del Dipartimento di Scienze della Terra dell'Università di Siena e lo staff Magma Energy Italia. I rilevamenti e le analisi sono state svolte tra ottobre 2011 e Dicembre 2012 ed hanno visto il lavoro congiunto in campo di 2 Professori Associati, un Ricercatore ed un dottorando dell'Università e di 5 geologi Magma Energy/Alterra Power, coordinati dall'exploration manager Magma Energy.

L'attività è consistita in una raccolta di dati di carattere geologico strutturale in tutto il P.R. Mensano coprendo un'area di circa 300km^2 raccogliendo oltre 500 misure cinematico strutturali su oltre 50 stazioni di misura

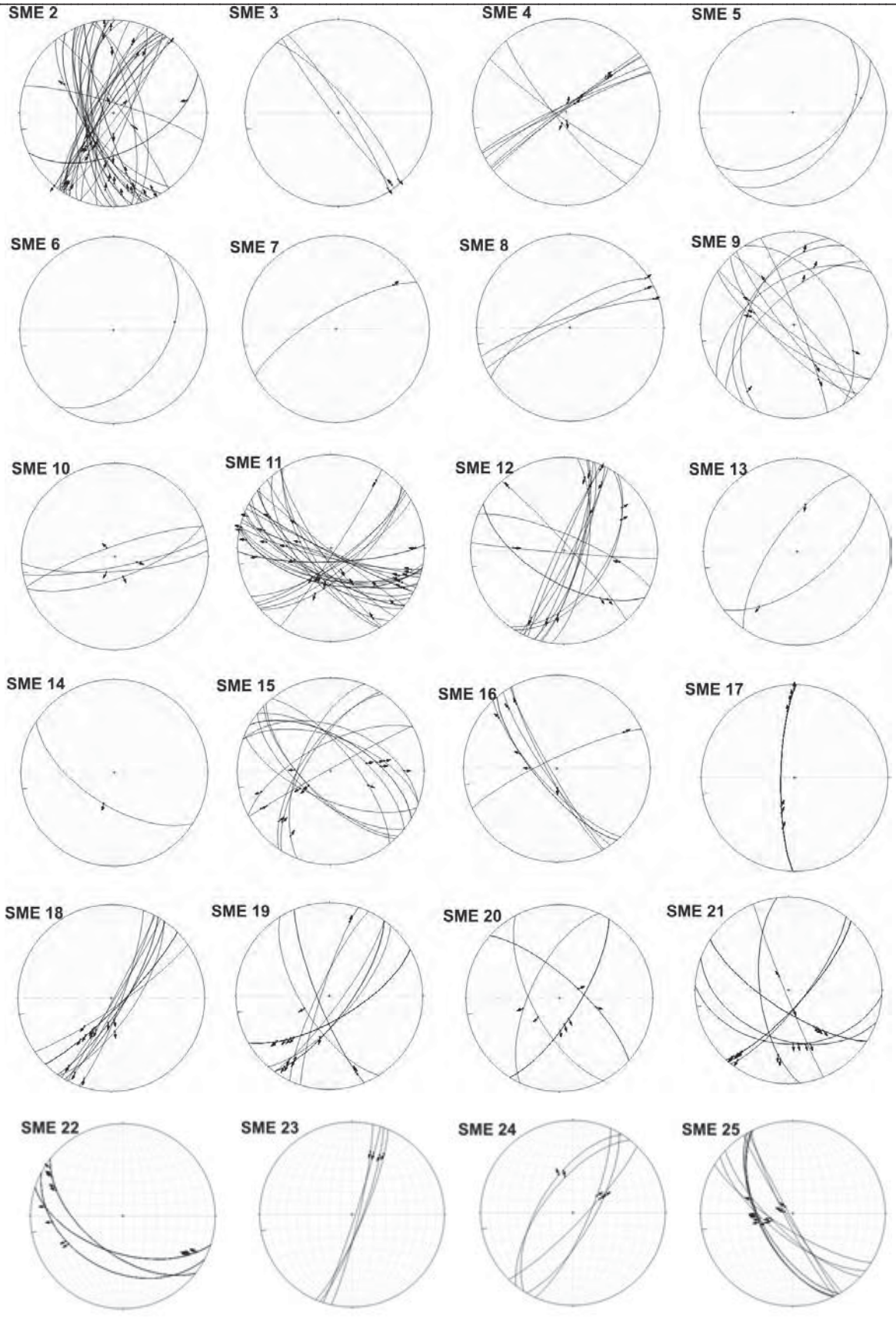

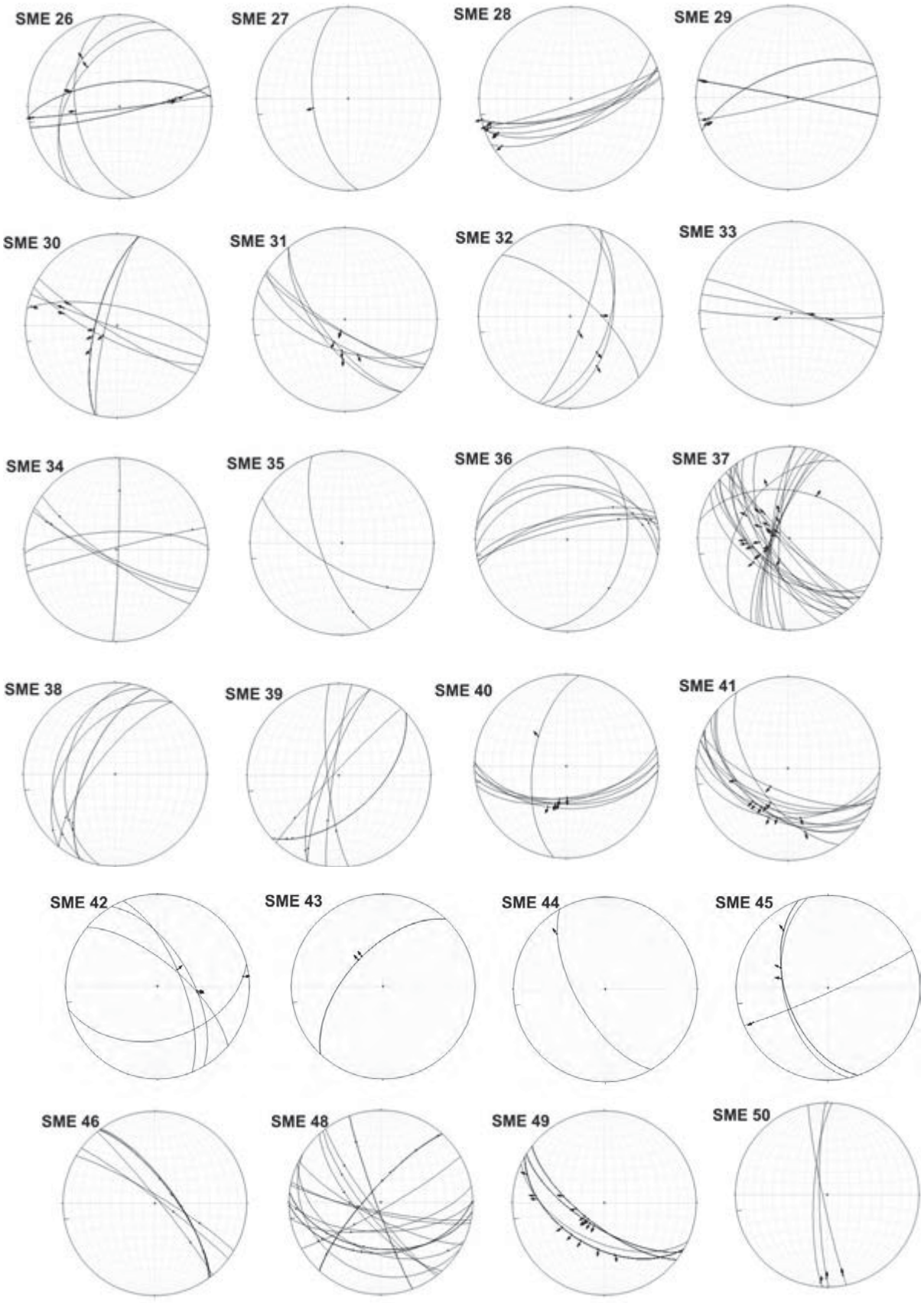

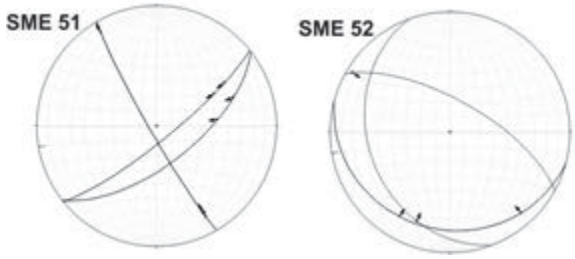

Fig. 3 – Proiezioni stereografiche delle stazioni di misura strutturale raccolte nel P.R. Mensano.

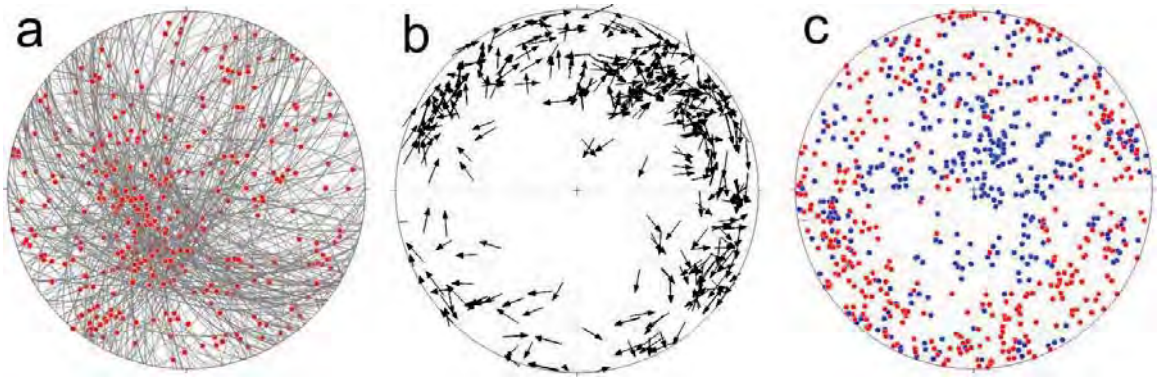

Fig. 4 – Proiezioni stereografiche delle stazioni di misura strutturale raccolte nel P.R. Mensano a: faglie e strie ; b :lineazioni; c: diagramma P-T diagram.

In Fig. 16 gli stereogrammi mostrano la cinematica delle strutture misurate che si possono dividere in due grandi gruppi a orientazione N130° and N50°. Le strutture afferenti al primo gruppo sono caratterizzate da un predominante cinematismo normale mentre le strutture appartenenti al secondo gruppo mostrano una cinematica di carattere transtensivo con componente sia destra sia sinistra.

L'assetto geologico del P.R. Mensano è strutturato da una successione stratigrafica composta da:

- *Unità neoautoctone*, comprendenti i sedimenti post-orogenici di età Mio-Pliocenica e i sedimenti recenti;
- *Unità alloctone*, comprendenti le varie formazioni liguri, sub-liguri e toscane, con età variabili dal Trias al Paleocene, sovrascorse sul substrato e accavallatesi l'una all'altra durante l'orogenesi appenninica, ivi incluso il cosiddetto "complesso a scaglie";
- *Unità autoctone*, comprendenti le rocce metamorfiche Paleozoiche, considerate come il basamento originario della pila tettonica.

La messa in posto delle unità tettoniche in fase compressiva e quindi l'edificazione della catena appenninica settentrionale, è stata seguita da un'evoluzione tettonica che si è sviluppata in regime distensivo, con assottigliamento litosferico (secondo un modello inzialmente proposto da Carmignani e Kligfield, 1990[1]), dando origine alle depressioni strutturali in cui si sono depositate le unità stratigrafico-sedimentarie del Miocene. Lo

[1] *Carmignani, L and Kligfield, R. - Crustal extension in the northern Apennines: The transition from compression to extension in the Alpi Apuane Core Complex. Tectonics, Volume 9, Issue 6, pages 1275–1303, December 1990*

spazio di accomodamento per i sedimenti miocenici, principalmente rappresentato dal Bacino di Radicondoli che si colloca nel settore centrale del P.R: Mensano, è dato dai settori che alcuni Autori hanno interpretato come più intensamente assottigliati e compresi tra corpi costituiti dal Gruppo del Verrucano (es. Brogi & Liotta, 2008)[2].

La tettonica distensiva pliocenico-quaternaria è caratterizzata dallo sviluppo di faglie dirette ed oblique ad alto angolo, che definiscono le depressioni strutturali entro le quali si sono depositati i sedimenti marini del Pliocene Inferiore-Medio. Queste strutture sono caratterizzate per lo sviluppo contemporaneo di zone di deformazione ortogonali alle faglie dirette, a prevalente rigetto orizzontale (faglie transtensive), che hanno svolto la funzione cinematica di trasferire l'entità di distensione tra un settore di bacino e l'altro, differenziando ambiti con stili deformativi diversi ma riferibili allo stesso contesto tettonico.

All'interno del P.R: Mensano, grazie alle osservazioni di campagna e all'analisi cinematica condotta, sono state osservate due tipologie di strutture principali:

- Strutture orientate NO-SE, a cinematismo normale che delimitano le depressioni strutturali.
- Strutture orientate SO-NE a cinematismo di carattere transtensivo che tagliano le strutture principali normali e che danno origine a zone di taglio.

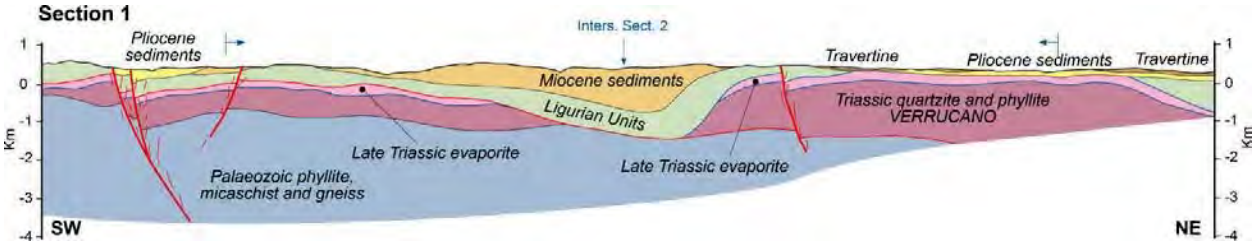

Fig. 5 – Sezione geologica attraverso il P.R. Mensano in direzione SO-NE.

In particolare nel settore sud-occidentale del P.R. Mensano questi lineamenti sono rappresentati dalle strutture normali facenti parte del sistema di Anqua-Montecastelli che sono dissecate dalle strutture di taglio a direzione anti-appenninica che tagliano anche il settore geotermico di Larderello e che si estendono anche verso il settore NO del Permesso.

Il sistema di strutture Anqua-Montecastelli rappresenta i margini strutturali del Bacino di Radicondoli. La faglia di Anqua, mostra un rigetto verticale di quasi 1000m ed è considerata come interessata da attività nel periodo compreso tra il Pliocene-Pleistocene.

[2] *Brogi, A. & Liotta, D. 2008. Highly extended terrains, lateral segmentation of the substratum and basin development: theMiddle–LateMiocene Radicondoli Basin (Inner Northern Apennines, Italy). Tectonics 27, 1–20.*

.

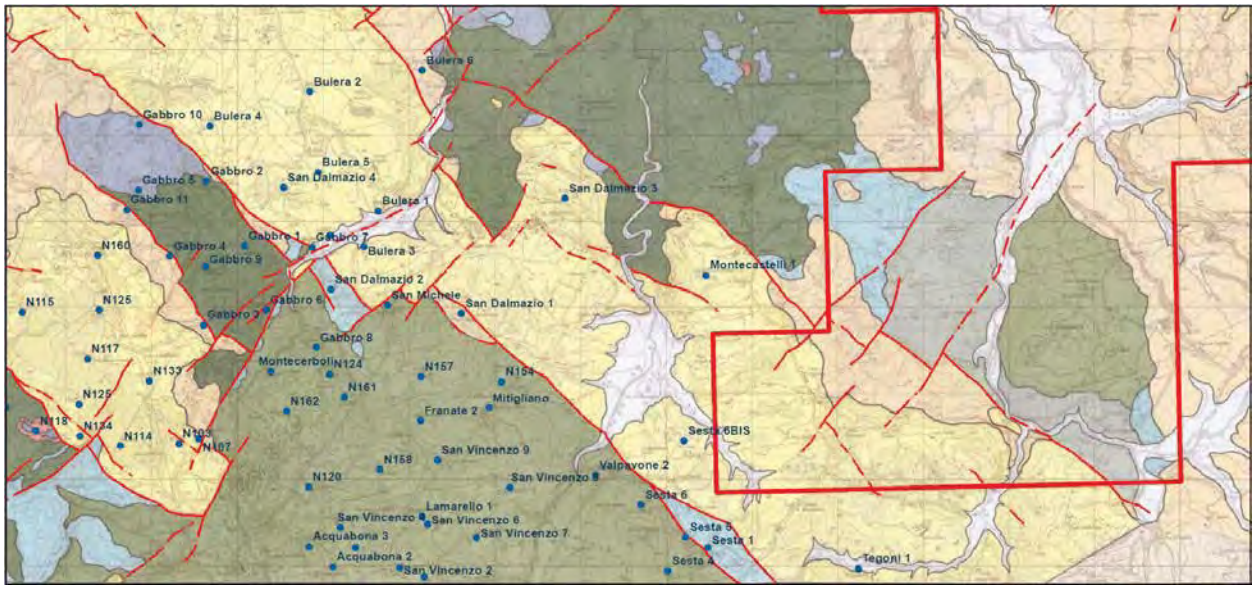

Fig. 6 – Dettaglio dell'area di Anqua-Montecastelli

L'analisi mesostrutturale condotta ha permesso l'identificazione di strutture a cinematica normale con piani subverticali evidenziati da indicatori cinematici di movimento a riempimento calcicito, fratture e strie.

Il Sistema Anqua-Montecastelli è attraversato da una zona di taglio a direzione antiappeninica di età Pliocene-Olocene e che mostra una cinematica di taglio obliquo a componente sia trascorrente sia normale più recente come osservato nell'area di Scapernata dove è chiara la sovrapposizione tra le due tipologie di cinematismo che interessano le fasce di taglio (Fig. 19).

Fig. 7 – Esempio di indicatore cinematico di movimento osservato nell'area di Scapernata.

.

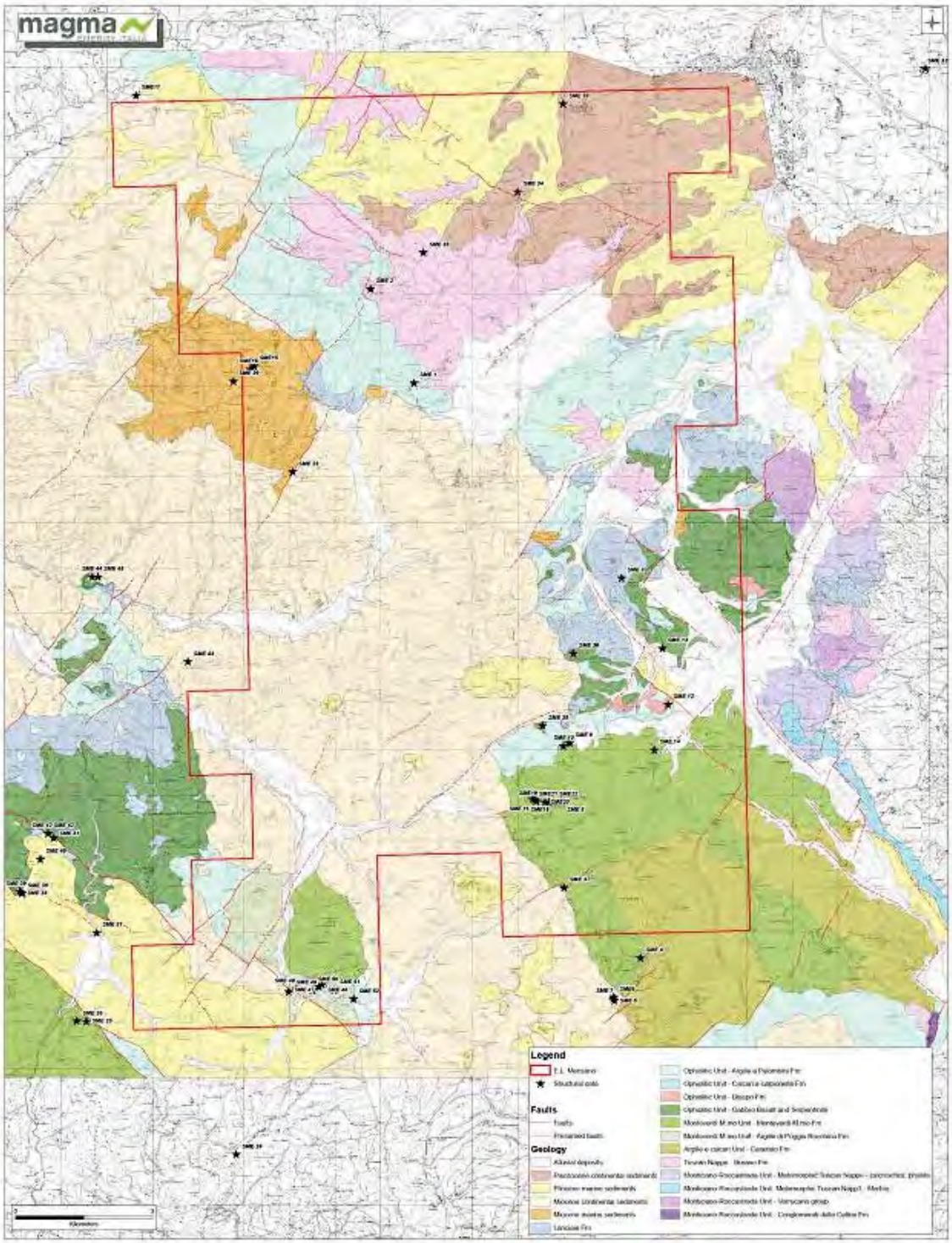

Fig. 8 – Carta geologica del P.R. Mensano con ubicazione delle stazioni di misura strutturale

2. INDAGINI GEOCHIMICHE

Nell'ambito delle attività esplorative svolte da Magma Energy Italia sono state svolte, con la collaborazione dei Dipartimenti di Scienze della Terra delle Università di Siena e di Firenze, due campagne di campionamento geochimico nella primavera e nell'autunno 2012 con l'obiettivo di caratterizzare la composizione chimica dei fluidi delle emergenze di interesse termale nell'area del P.R. Mensano e di correlare i risultati con le caratteristiche geologiche dell'area di studio.

2.1. Dati geochimici

L'attività di campionamento ha previsto la raccolta di campioni di acqua, gas liberi e gas disciolti da 13 siti all'iterno e al di fuori dell'area del Permesso di ricerca.

Le analisi svolte presso le strutture dell'Università di Firenze si sono concentrate sugli ioni maggiori, gli elementi in traccia, i gas disciolti, i gasi liberi gli isotopi stabili dell'Idrogeno e dell'Ossigeno e del Carbonio.

Tab. 1 Composizione chimica media delle acque campionati

	T (°C)	COND (µS/cm^2)	pH	Water Type	$\delta^{18}O$ (‰ vs SMOW)	δD (‰ vs SMOW)
Water samples	14-34	600-3200	2.9-7.7	Ca(Mg)-SO_4(HCO_3)	-8.3;-5.9	-54.5;-40.2

Come si osserva in Tab. 1 le temperature variano da condizioni ipotermali (14°C a Montemiccioli) a termali (34°C a Bagni al Morbo). La salinità varia da 600 (Centopino) to 3200 (Montemiccioli) e il pH è compreso nel range tra 2.0 (Montemiccioli) to 6.7 (Caldanelle).

Le analisi chimiche svolte sui campioni di acqua mostrano a presenza di un mescolamento tra acque di origine relativamente profonda a composizione Ca(Mg)-SO_4 circolanti nelle roce evaporitiche Triassichee acque a composizione Ca-HCO_3 più superficiali derivanti da una circolazione nelle rocce carbonnatiche che sovrastrano le rocce triassiche.

Gli isotopi stabili $\delta^{18}O$ and δD mostrano valori tipici della Toscana Meridionale e confermano un'origine di tipo meteorico delle acque campionate.

La coposizione dei gas disciolti presenta una predominate componente di CO_2 (anche oltre il 90%) tranne per il campione prelevato nel Torrente Scarna dove l'elevato tenore in nitrati (fino al 70%) rivela una probabile contaminazione antropica.

Le analisi relative ai gas N_2-Ar-He confermano l'origine meteorica dei gfluidi campionati

Tab. 2 Composizione chimica dei gas disciolti campionati

	CO_2	N_2	Ar	CH_4	O_2	Ne	He	H_2
Dissolved Gases (%)	8-90	8-72	0.2-1.7	0.02-0.2	0.8-17.3	0.0001-0.0009	0.0007-0.0055	0

La composizione dei gas liberi conferma come la CO_2 sia la componente predominante seppur nei campioni prelevati a Palazzaccio and Palazzo al Piano sia presente una forte

concentrazione di Metano in risposta a probabili reazioni termometamorfiche che interessano le rocce del complesso cristallino profondo

Tab. 3 Composizione chimica dei gas liberi campionati

	CO_2	H_2S	N_2	CH_4	Ar	O_2	Ne	H_2	He
Free Gases (mmol/mol)	580-908	<0.01-3.56	8-163	0.5-236	0.052-4.15	0.114-9.6	0.000001-0.002	0.000005-0.00021	0.011-0.098

L'isotopo del Carbonio ^{13}C analizzato dai campioni di gas campionati evidenzia valori maggiormente negativi (<-12) per i campioni delle Caldane di San Marziale e del Torrente Scarna, suggerendo un'origine di carattere biogenico

Valori tipici di orgine di tipo magmatica ($\delta^{13}C = -7 \div -3$) si riscontrano nei gas liberi di Tignano, Palazzo al Piano e Poggiaccio, e nei gas disciolti di Galleraie Pozzo. Questi valori di $\delta^{13}C$-CO_2 sono in accordo anche con i dati relativi agli isotopi dell'Elio (R/Ra = 1.81) riportati in letteratura (Minissale et al., 1997), supportando un'origine di tali gas legata a processi di degassamento ai livelli del mantello.

In conclusione, sulla base dei risultati ottenuti grazie alla collaborazione con l'Università di Siena e Firenze, le evidenze di interesse geotermiche possono essere suddivise in 4 settori principali:

- Area Nord-Est: sorgenti a temperatura inferiore a 20°C con acque circolanti nelle rocce evaporitiche e carbonatiche che affiorano nella zona
- Area Ovest: Localizzate ma intese emissioni naturali di CO2 proveniente da livelli crostali profondi e che sono associate a strutture tettoniche affini a quelle presenti nell'area di Larderello
- Area Sud-Est: Localizzate manifestazioni con idrocarburi derivanti da risalita di fluidi a seguito di rezioni termometamorfiche delle formazioni ricche in materia organiche presenti nel complesso metamorfico
- Area Ovest: Sorgenti termali e emissioni di gas dove la circolazione dei fluidi è associata a strutture tettoniche che interessano sia i livelli evaporitici triassici dove circolano le acque termali sia i livelli più profondi e che favoriscono la risalita di gas la cui origine è di carattere magmatico.

2.2. Relazione tra manifestazioni geotermali e strutture geologiche

Le manifestazioni geotermali sono strettamente correlate alla presenza di sistemi geotermici attivi (Pavlides & Kilias 1987; Minissale 1991; Altunel & Hancock 1993a, 1993b; Sibson 1996) e alla presenza di strutture tettoniche fragili che grazie alle loro condizioni di permeabilità e pervasività favoriscono la migrazione dei fluidi dai livelli più profondi verso la superficie (Hancock et al. 1999; Cello et al. 2001; Bellani et al. 2004, Caine et al. 1996).

Le manifestazioni geotermali principali presenti nel P.R. Mensano sono quelle di Montemiccioli e Tignano (Fig. 21), associate alla zona di taglio orientata SO-NE, interpretata come il proseguimento verso NE di una delle fasce di taglio principali osservate nell'area di Larderello.

Anche la sorgente di Monteguidi è associata alla presenza di una faglia orientata SO-NE e che favorisce la risalita di acque dai livelli evaporitici del Trias, così come le sorgenti di Onci e Caldane di S.Marziale (Fig. 22).

Le manifestazioni di Palazzo al Piano e Poggiaccio sono associate all'intersezione di strutture appenniniche con una fascia di taglio che interessa il bordo sud-orientale del P.R.

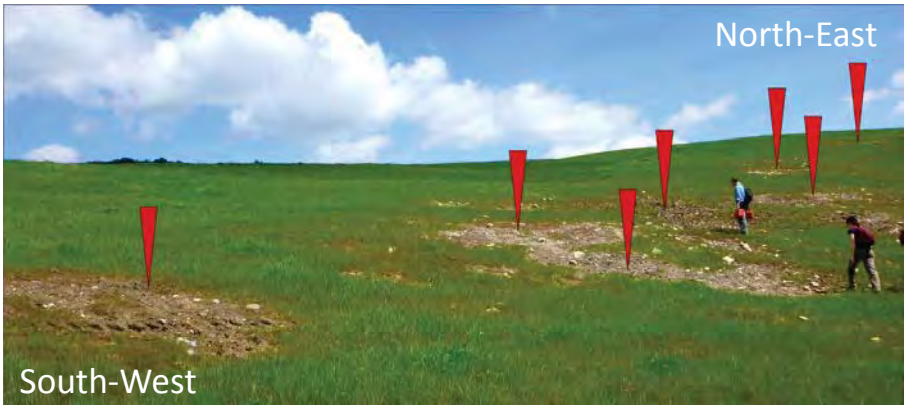

Fig. 9 – Emisioni gassose (CO_2) a Tignano lungo una struttura orientata N°40.

I principali depositi di travertino sono collocati fuori dal permesso di ricerca nella zona di Frosini e delle Gallerarie entrambi allineati lungo faglie Pleistoceniche. Tali depositi sono stati datati con la metodologia Th/U attorno a 12-22ka (Frosini) e 90-130ka (Galleraie).

Mineralizzazioni epitermali di magnesite sono state oggetto di attività estrattiva negli anni '40-50 nella cava di Querceto mentre quelle a stibnite sono state coltivate nella cava delle Cetine di Cotorniano.Queste mineralizzazioni sono assocate ad una attività tettonica Pliocenica che ha interesato un sistema idrotermale con temperature attorno ai 200-220°C come dedotto dall'analisi delle inclusioni fluide.

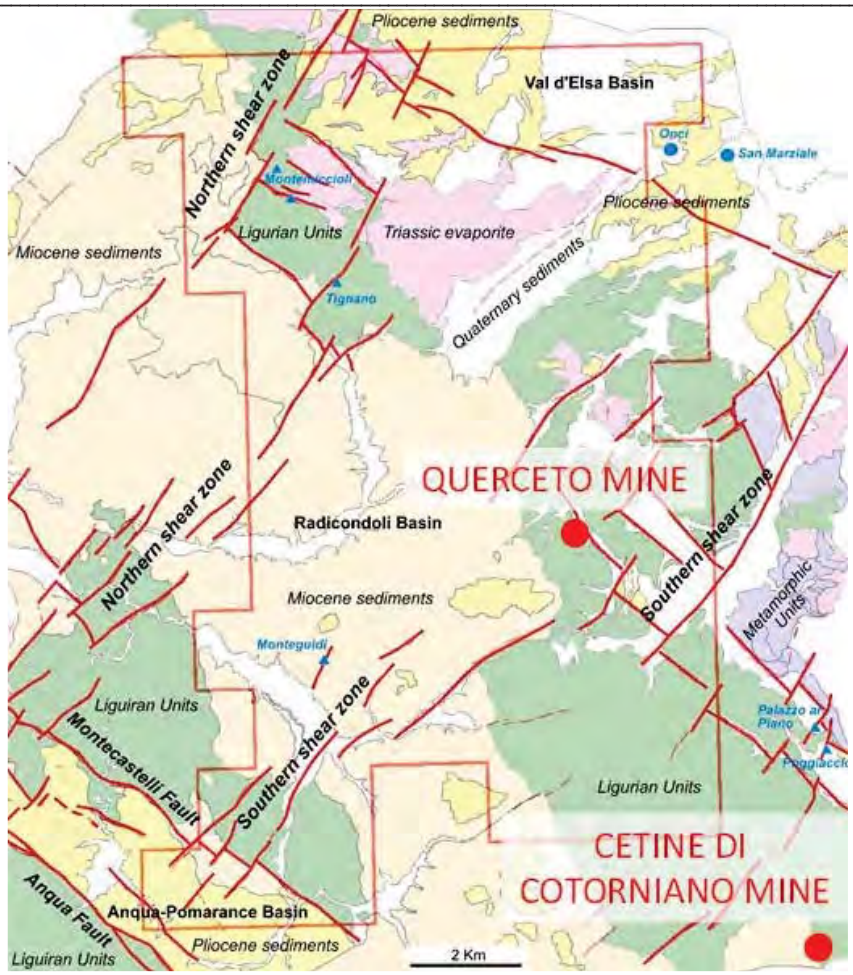

Fig. 10 – Ubicazione delle principali manifestazioni termali e epitermali associate alla strutture geologiche

3. PROSPEZIONI GRAVIMETRICHE

Nel 2012 Magma Energy Italia ha eseguito, in collaborazione con WesternGeco - Integrated EM Center of Excellence di Milano (WG) una campagna di misure gravimetriche (GRAV) nel P.R. Mensano, al fine di: 1) evidenziare eventuali anomalie negative correlabili alla massa intrusiva profonda dell'area di Larderello-Travale; 2) vincolare il modello geologico già ricostrito sulla base dei rilevamenti di superficie, soprattutto per quanto attiene le geometrie delle unità neoautoctone; 3) Identificare e, se possibile, estendere in profondità i lineamenti tettonici evidenziati nei rilevamenti geologici; 4) identificare, se esistenti, elementi anomali nel basamento metamorfico.

La campagna di rilievi GRAV è stata pianificata congiuntamente da Magma Energy Italia e da WesternGeco, sulla base delle informazioni geologiche disponibili e delle esperienze di WG in acquisizioni simili finalizzate all'esplorazione geotermica.

Il piano di lavoro ha compreso:

- L'acquisizione di ~790 punti di misura gravimetrici e GPS-rtk;
- L'uso di gravimetri Scintrex CG-5;
- L'elaborazione dei dati GRAV fino all'anomalia di Bouguer.

3.1. Pianificazione dell'acquisizione

La campagna GRAV è iniziata nel Marzo 2012. Sono stati impiegati 2 equipaggi formati da un operatore, da un assistente e da un autista qualificato.. La squadra di acquisizione, coordinata da un exploration manager e supervisionata da geofisici Magma Energy Italia, è stata guidata da un Party Chief (WG) e da un Senior Operator/Data Processor (WG) presso l'ufficio di campagna.

Vi sono state inoltre delle pause contrattualmente concordate ai fini della sicurezza sul lavoro degli equipaggi (per evitare periodi di lavoro continuativi troppo lunghi), pertanto l'acquisizione si è conclusa nel settembre 2012, con 118 stazioni acquisite. L'ulteriore personale WG coinvolto ha incluso la supervisione da parte di un Operations manager, di un QHSE Manager e di un Senior Geophysicist.

Gli equipaggi GRAV hanno eseguito le misure gravimetriche e topografiche simultaneamente in ogni stazione. Ogni squadra si muoveva con veicoli pick-up 4x4, con gravimetro Scintrex CG5 Autograv e Sistema topografico Trimble, R7/R8 GPS-rtk. Tutti gli strumenti erano facilemente portabili a spalla (max 8 kg/component) per poter accedere a piedi a qualsiasi punto.

E' stato inizialmente pianificata una griglia di tentativo 3D con punti approssimativamente equidistanti, tenendo conto dei limiti dovuti alle asperità morfologiche del territorio. Le squadre GRAV hanno completato le acquisizioni per blocchi, in modo da avere una lunghezza di baseline sempre inferiore a 20 km.

Inizialmente è stato materializzato un reticolo di appoggio gravimetrico agganciato ad una stazione gravimetrica assoluta della rete nazionale, e collegato alla rete geodetica. Dirante l'acquisizione non meno del 5% delle stazioni sono state ripetute in giorni e con percorsi diversi, ai fini di controllo. Le misure GPS-rtk in ogni stazione hanno raggiunto precisione centimetrica.

3.1.1. Permitting

I proprietari dei terreni sono stati contattati direttamente da personale Magma Energy Italia, che ha fornito tutte le informazioni necessarie riguardo alle misure per ottenere l'autorizzazione ad eseguire il lavoro. Sono stati anche organizzati incontri pubblici per informare ed aggiornare le autorità locali sulle attività condotte. Al termine dei Lavori è stato ottenuto il 99.4% di risposte positive da parte dei proprietari (Tab. 1).

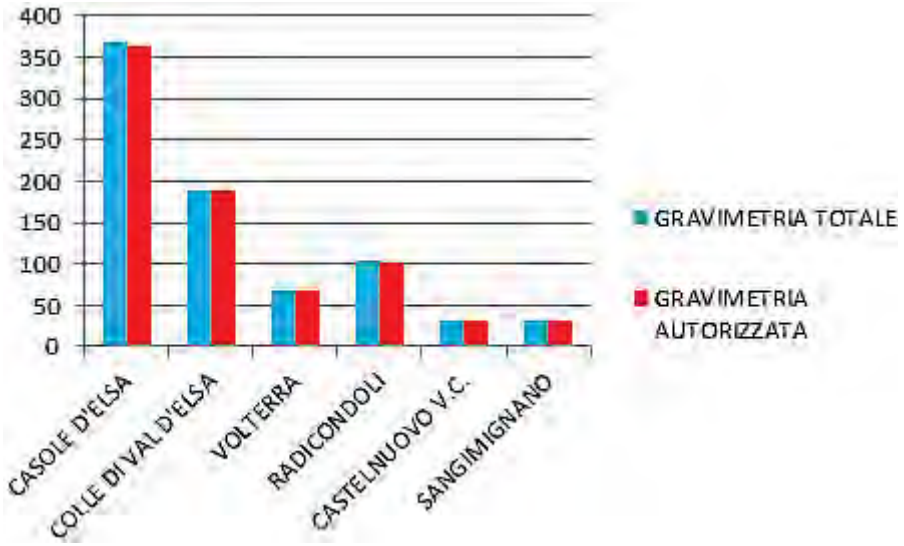

Tab. 1 – Distribuzione delle autorizzazion irichieste ed ottenute per ciascun Comune.

In accordo con la normativa vigente, i Lavori sono stati notificati all'Autorità di Vigilanza della Regione e comunicati alle altre autorità pubbliche.

3.1.2. Base Network

Il valore di gravità assoluta è stato trasferito ad un reticolo di appoggio materializzato sul terreno all'inizio della campagna, mediante un apposito collegamento gravimetrico con la stazione IGSN di Palazzo al Piano. La base network ha permesso la chiusura quotidiana di tutti I loop di misura (Fig. 24).

3.1.3. Acquisizioni

Per ciascuna misura (Fig. 23) sono stati annotati l'ID di stazione, il tempo assoluto, la gravità osservata in mgal. Le correzioni per la marea e la temperatura sono state applicate alla fine di ogni misura.

Fig. 11 - a) Scintrex CG-5. b) Example of gravity measurement. c) Example of GPS measurement.

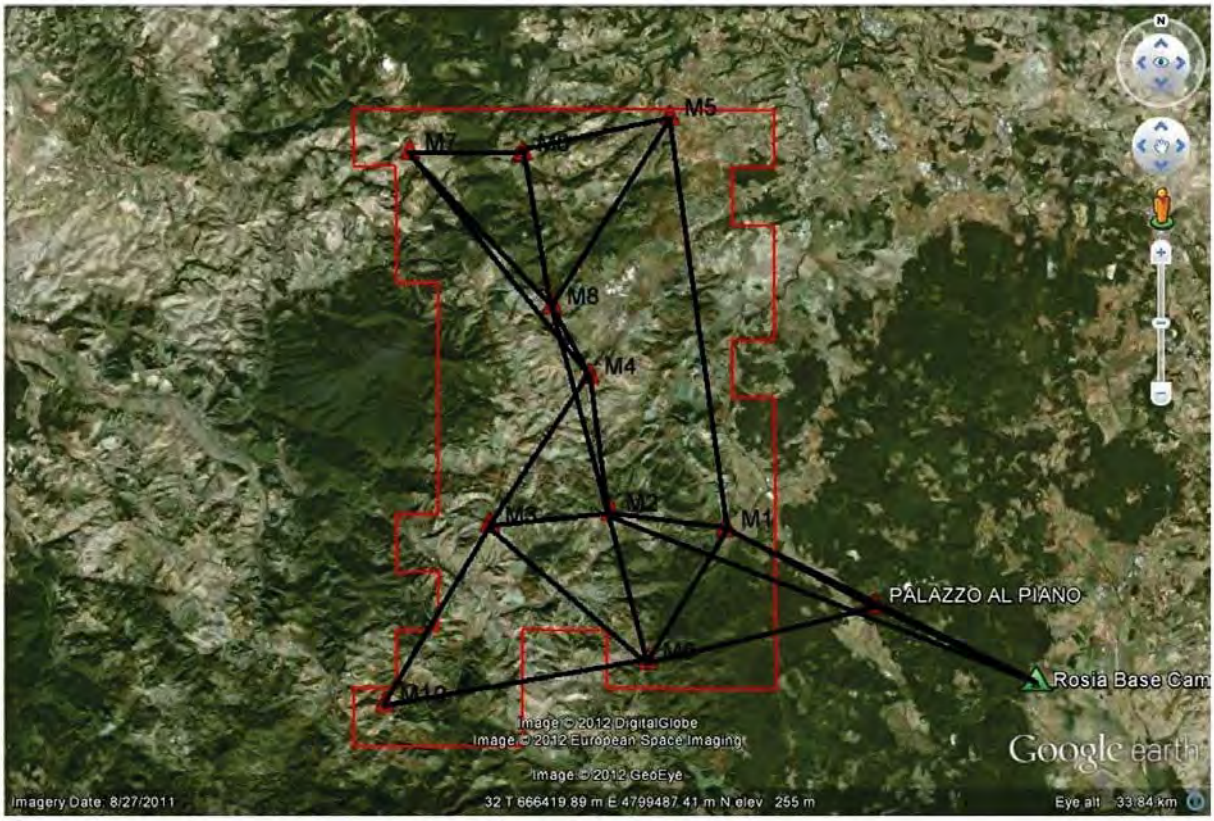

Fig. 12- Gravity Base Network e percorsi di c onnessione alla rete IGNS.

3.1.4. Elaborazione Dati

L'elaborazione e il controllo di qualità dei dati è stato eseguito presso l'ufficio di campagna. I dati gravimetrici sono stati elaborati con gli appositi tool del software WinGLink e hanno compreso il calcolo del reticolo di appoggio, le riduzioni, le correzioni con il DEM del terreno, il calcolo dell'anomalia completa di Bouguer.

Una mappa dei punti di misura acquisiti è mostrata nella Fig. 25.

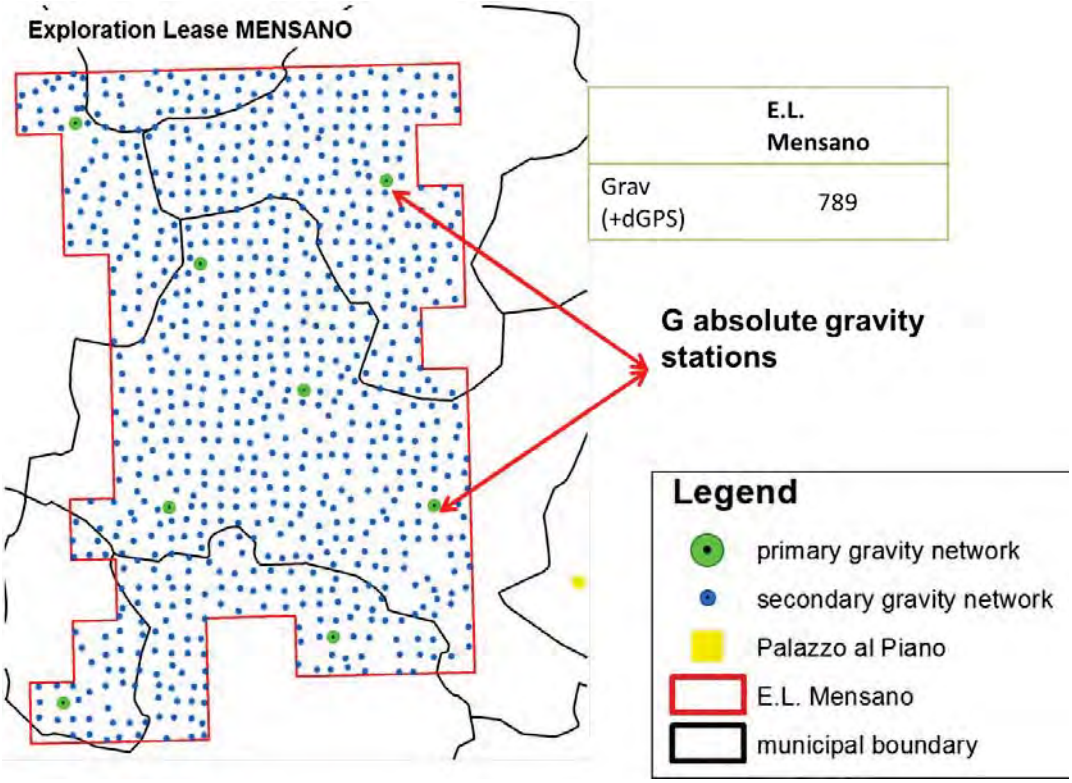

Fig. 13 – Griglia di misurazione gravimetrica nel P.R. Mensano.

3.2. Correzioni

Eseguite preliminarmente le compensazioni ai minimi quadrati dei valori misurati sulla base network, sono state eseguite le compensazioni dell'errore di chiusura su ciascuna rete di misura secondaria.

Le analisi dei dati sono state eseguite con il software WinGlink®. I valori di anomalia di Bouguer sono stati ottenuti mediante un set di correzioni standard (Fig. 26) applicato ai valori osservati, secondo l'equazione:

$$g_{BA} = g_{oss}-(g_{theor} \pm CF \pm CB - CT - CA) ,$$

dove g_{BA} è la Bouguer anomaly, g_{oss} è il valore di gravità osservato, g_{theor} è il valore teorico computato dal geoide GRS 1980, CF è la correzione di Faye computata con il geoide Italgeo 2005, CB è la correzione di Bouguer, CT è la correzione topograficae CA rappresenta un gruppo di correzioni di ordine minore. I valori di g_{BA} sono poi stati ridotti per una densità di riferimento appropriata, identificata con il metodo di Nettleton (1971).

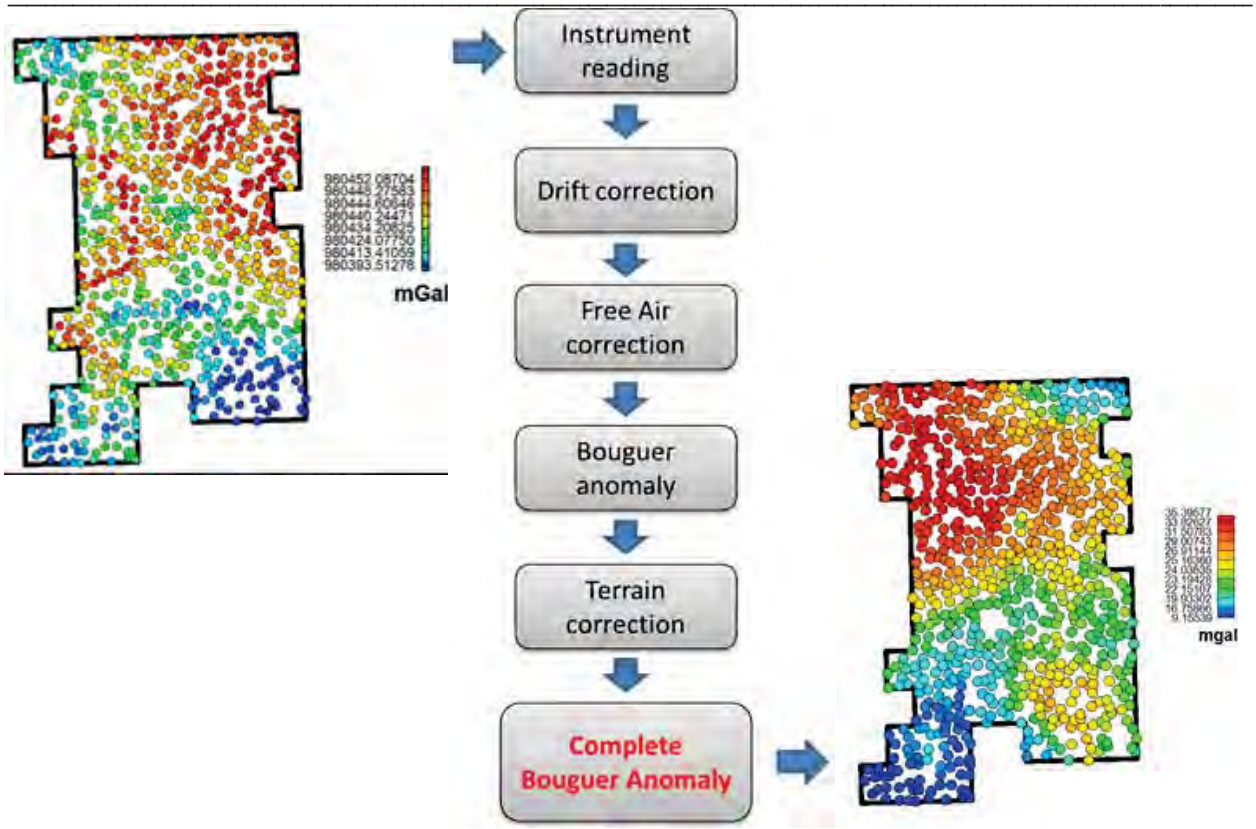

Fig. 14: Flusso di lavoro per ricavare la Complete Bouguer Anomaly dalle letture iniziali.

3.3. Modellazioni

Sono state eseguite modellazioni e inversioni al fine di validare e migliorare la qualità del modello geologico del P.R.Mensano.

L'effetto dei corpi geologici superficiali è ricavabile come residuo di un campo regionale polinomiale del secondo ordine. Il campo residuale risulta caratterizzato da un range di circa 14 mgal. Assegnando densità appropriate ad ogni unità geologica del modello sono state eseguite varie simulazioni di calcolo per ottenere la miglior riproduzione sintetica del campo gravimetrico reale. L'effetto di ciascuna unità geologica è stato computato anche indipendentemente, allo scopo di valutarne l'influenza rispetto alla risposta gravimetrica del modello (Fig. 27).

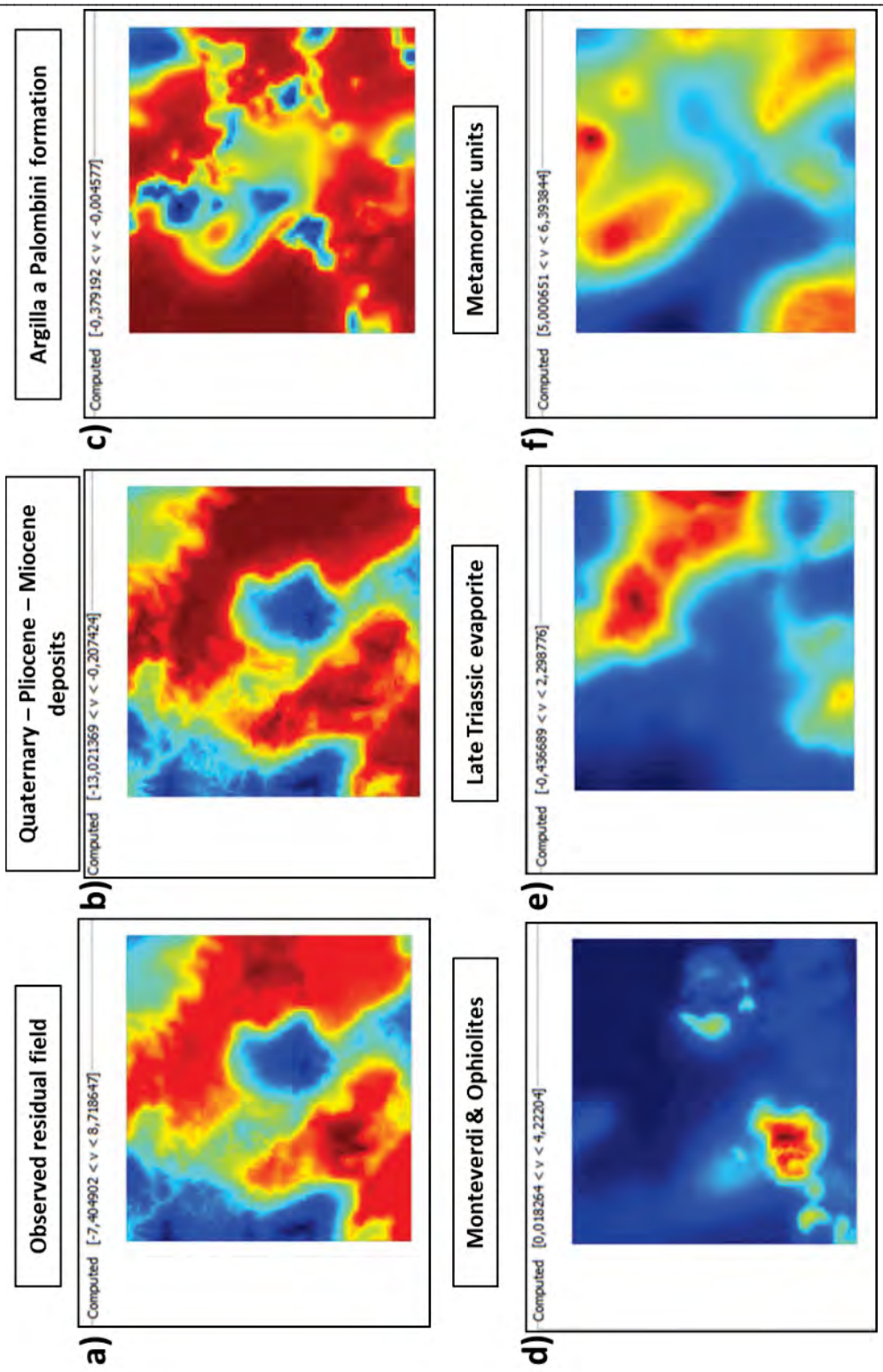

Fig. 15: Campo gravimetrico residuale osservato e risposta gravimetrica delle unità del modello geologico

4. PROSPEZIONI MAGNETOMETRICHE

Assieme alle prospezioni gravimetriche Magma Energy Italia ha eseguito, in collaborazione con WesternGeco - Integrated EM Center of Excellence di Milano (WG) una campagna di misure magnetometriche (MAG) nel P.R. Mensano.

La campagna di rilievi MAG è stata pianificata congiuntamente da Magma Energy Italia e da WesternGeco, sulla base delle informazioni geologiche disponibili e delle esperienze di WG in acquisizioni simili finalizzate all'esplorazione geotermica.

Il piano di lavoro ha compreso:

- L'acquisizione di 783 punti di misura magnetometrici (coincidenti con i punti di misura gravimetrici);
- L'uso di magnetometri GEM GSM-19T;
- L'elaborazione dei dati magnetici.

4.1. Pianificazione dell'acquisizione e permitting

La campagna MAG è stata eseguita dalla stessa squadra che ha acquisito le misure gravimetriche, contestualmente a queste ultime, con la medesima organizzazione di lavoro (vedi par. 3.1) .

4.2. Misure magnetometriche

La campagna di acquisizione magnetometrica ha misurato il campo magnetico terrestre totale in nanoTesla (nT). Il campo osservato è stato corretto rispetto alle variazioni diurne e filtrate dei valori anomaly. Ai dati, preparati per il calcolo del campo residuale, sono stati applicati filtraggi per rimuovere gli effetti superficiali e ridotti al Polo tenendo conto dell'inclinazione e della declinazione del campo magnetico terrestre.

La stazione magnetica di base necessaria per la correzione delle variazioni diurne del campo magnetico è stata collocata in un'area isolata, scelta sulla base del basso rumore sul segnale e della sicurezza del sito. A tale stazione di base è stato assegnato un valore nominale di 40800 nT, prossimo alla media a lungo termine dei valori; tutte le stazioni di campagna sono state riferite a questo valore..

4.3. Elaborazione dei dati

Le elaborazioni dei segnali sono state eseguite con il software Oasis montaj® della Geosoft, adatto ad eseguire le operazioni di correzione, filtraggio e manipolazione dei dati.

La maggior parte dello spettro del segnale risulta essere compresa tra le lunghezze d'onda di circa 4 e 10 km, mentre una componente minore, in buona parte incoerente, risulta compresa tra le lunghezze d'onda di 1 e 4 km.

Il campo TMI è stato quindi ridotto al polo utilizzando i valori di inclinazione e di declinazione del campo magnetico terrestre durante il periodo di acquisizione.

Nel P.R. Mensano le anomalie magnetiche seguono un andamento ben individuabile e i segnali non sono correlati con una distribuzione casuale di corpi ferro- - e ferri-magnetici. Tuttavia, data la grande variabilità naturale delle caratteristiche magnetiche delle varie

formazioni geologiche e non esistendo in letteratura alcuna informazione magnetica relativa all'area, i dati sono stati esaminati da un punto di vista qualitativo.

La mappa del campo magnetico RTP risulta in buon accordo con la mappa gravimetrica residuale, soprattutto nei settori nord e sud-est del P.R., mentre in altri settori vi sono delle apparenti discrepanze.

In particolare, risulta una anomalia magnetica nella parte nord del P.R. correlata alla presenza di unità metamorfiche a profondità relativamente ridotta; altre anomalie rilevate si ritiene che siano da ascrivere alla presenza di elementi ofiolitici sepolti sotto alle unità neoautoctone.

Sono stati inoltre ottenuti dei range dei valori di suscettività per le formazioni del modello geologico. In particolare i depositi sedimentari neogenici e l'unità del Verrucano hanno i valori di suscettività maggiori (circa 0.01). mentre le ofioliti e le evaporiti mostrano valori bassi o negativi di suscettività (0 ÷ -0.0025).

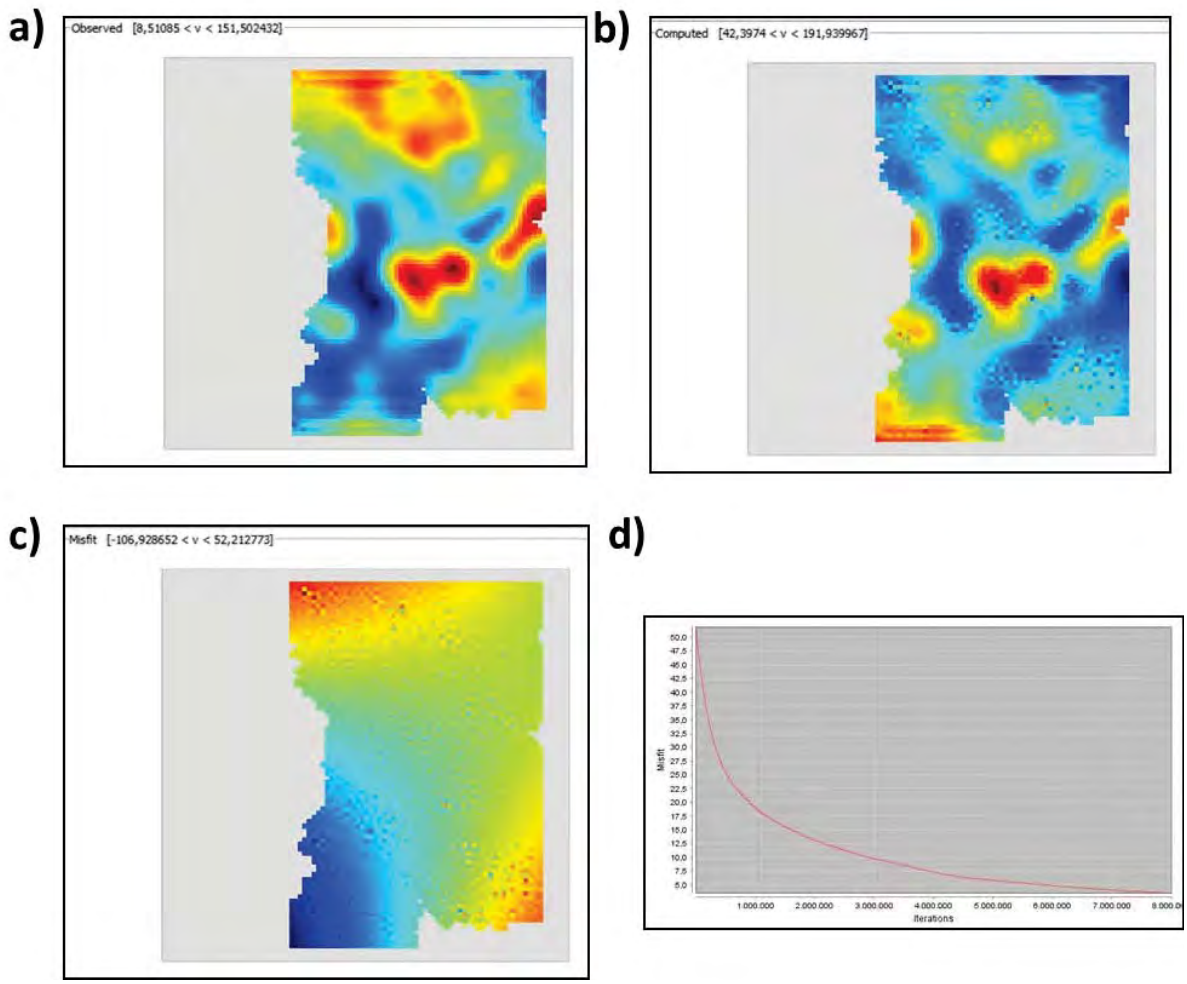

Fig. 16: Risultato dell'inversione tridimensionale dei dati magnetici. a) Campo magnetico osservato; b) Risposta teorica del modello geologico ottimizzato dall'inversione (best-fit model). c) Rappresentazione bidimensionale della discordanza tra il campo osservato e il modello; d) Misfit vs. numero di iterazioni dell'inversioneversus iteration number.

5. PROSPEZIONI MAGNETOTELLURICHE

Nel 2012 Magma Energy Italia ha eseguito, in collaborazione con WesternGeco - Integrated EM Center of Excellence di Milano (WG) una campagna MagnetoTellurica (MT) nel P.R. Mensano, al fine di: 1) ottenere la caratterizzazione ElettroMagnetica (EM) del sottosuolo; 2) vincolare il modello geologico già ricostrito sulla base dei rilevamenti di superficie, soprattutto per quanto attiene le geometrie delle unità geologiche; 3) evidenziare le eventuali anomalie di resistività che potrebbero essere correlate con il serbatoio geotermico.

La campagna di rilievi MT è stata pianificata congiuntamente da Magma Energy Italia e da WesternGeco, sulla base delle informazioni geologiche disponibili e delle esperienze di WG in acquisizioni simili finalizzate all'esplorazione geotermica.

Il piano di lavoro ha compreso:

- Un test MT preliminare con 3 stazioni di prova, per determinare le condizioni di rapporto segnale-rumore e stabilire la localizzazione ottimale per l'installazione della remote reference;
- L'acquisizione di 118 sondaggi MT con strumentazione ADU-07 e bobine MFS-06/07;
- registrazioni notturne normalmente di 14 ore;
- ampiezza di banda di 7 decadi da 10,000Hz a 0.001Hz;
- Elaborazione delle Time Series fino alle curve di resistività apparente e fase (ρ-φ) ed inversione dei dati.

5.1. Pianificazione dell'acquisizione

La campagna MT è iniziata nel Marzo 2012. Sono stati impiegati fino a 3 equipaggi, costituiti da 1 operatore e da 2 assistenti, ciascuno con il compito di montare 3 stazioni al giorno per la registrazione notturna. La squadra di acquisizione, coordinata da un exploration manager e supervisionata da geofisici Magma Energy Italia, è stata guidata da un Party Chief (WG) e da un Senior Operator/Data Processor (WG) presso l'ufficio di campagna. La stazione remota è stata installata permanentemente e gestita dalla squada di appoggio. L'elevato livello di rumore antropico e, in misura minore, guasti casuali, guasti prodotti da animali e sabotaggi da parte di ignoti hanno reso necessario la ripetizione di un certo numero di stazioni. Il tasso effettivo di acquisizione è stato di 6-7 stazioni al giorno. Vi sono state inoltre delle pause contrattualmente concordate ai fini della sicurezza sul lavoro degli equipaggi (per evitare periodi di lavoro continuativi troppo lunghi), pertanto l'acquisizione si è conclusa nel settembre 2012, con 118 stazioni acquisite.

L'ulteriore personale WG coinvolto ha incluso la supervisione da parte di un Operations manager, di un QHSE Manager e di un Senior EM Geophysicist.

5.1.1. Permitting

I proprietari dei terreni sono stati contattati direttamente da personale Magma Energy Italia, che ha fornito tutte le informazioni necessarie riguardo alle misure per ottenere

l'autorizzazione ad eseguire il lavoro. Sono stati anche organizzati incontri pubblici per informare ed aggiornare le autorità locali sulle attività condotte. Al termine dei lavori è stato ottenuto il 95.2% di risposte positive da parte dei proprietari, mentre è stato negato l'accesso a n. 6 siti in tutto (Tab. 2).

MENSANO						Last updated:	01/10/2012
MAGNETOTELLURIC	Required	Approved	Deleted	To be repositioned	Denied	Remaining	Progress
Pts falling in the properties of individual and private roads	78	77	1	0	1	0	98.7%
Pts belonging to farms	46	41	1	0	5	0	89.1%
Total	**124**	**118**	**2**	**0**	**6**	**0**	**95.2%**

Tab. 2 Riepilogo delle autorizzazioni per i siti MT

In accordo con la normativa vigente, i Lavori sono stati notificati all'Autorità di Vigilanza della Regione e comunicati alle altre autorità pubbliche.

5.1.2. Scouting e controllo della strumentazione

Prima dell'esecuzione sono state eseguite delle ricognizioni di dettaglio per identificare le migliori vie di accesso ai siti, i punti di raduno e tutte le possibili sorgenti di rumore EM. Durante i test, per la remote referece è stata scelta una localizzazione quieta e sicura. Inoltre è stata fatta una registrazione notturna di prova di tutti gli strumenti in parallelo, in unico sito, per un controllo di conformità delle registrazioni, in modo da poter rimuovere gli strumenti non perfettamente tarati.

5.2. Metodologia e specifiche tecniche

Ogni equipaggio MT ha gestito tre sistemi di registrazione MT a 5-canali (Fig. 29), che venivano installati durante il giorno, lasciati in acquisizione per tutta la notte (14 ore o più) e recuperati il giorno successivo per una nuova installazione, in modo che ogni equipaggio poteva gestire tre siti di acquizione ogni 24 ore.

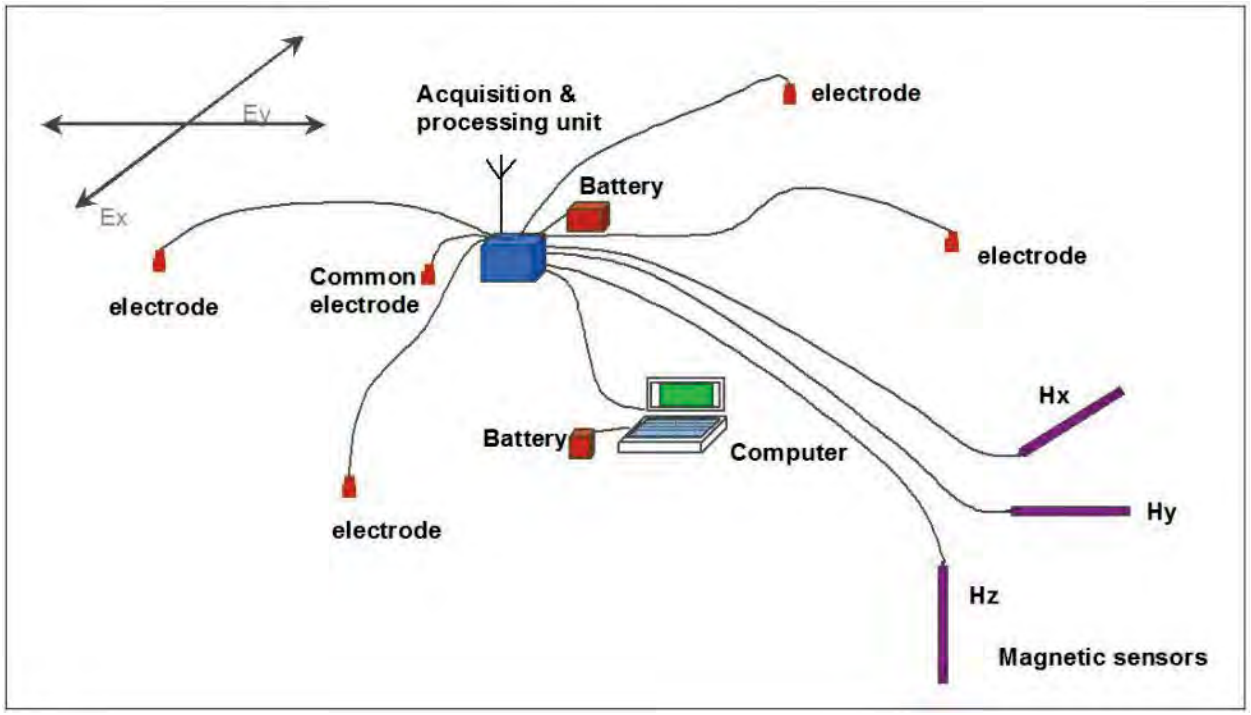

Fig. 17 : diagramma schematico di acquizione MT a 5 canali-channel MT layout diagram (schematic). Il computer è presente solo durante la configurazione del sito e lo scarico dei dati dall'unità di acquisizione. Il sistema pesa in totale 45kg, incluse le batterie a 12V.

5.2.1. Procedura di posa

In sito, l'operatore controlla segni di danneggiamenti da parte di animali o interferenze durante le registrazioni (es. cavi spostati), e scarica i dati su un notebook o su una chiave USB. Le registrazioni vengono controllate per assicurare che le 5 componenti siano state registrate tutte correttamente; solo dopo tale verifica, la strumentazione viene rimossa per il trasporto al sito successivo. I solchi dove sono stati interrati i sensori sono ripristinati con le zolle di terra precedentemente rimosse e accantonate.

Sul nuovo sito, l'operatore controlla il terreno per scegliere la migliore posizione ed orientazione. Più che una ubicazione precisa, è necessario un sito adatto in termini di pendenza e di rumore antropico.

Le componenti del campo magnetico sono misurate mediante bobine ad induzione con forma di un tubo in plastica lungo 85 cm e del diametro di 8 cm, interrate in appositi solchi profondi circa 40 cm. Il campo elettrico viene acquisito mediante dipoli con elettrodi costituiti da cilindri sigillati alti 15 cm e del diametro di 7 cm, collegati con conduttori isolati con PVC. Lo scopo dell'interramento è di minimizzare gli effetti del vento (vibrazioni sui cavi e sulle piante) e di stabilizzare termicamente i sensori. Le installazioni sono fatte in modo da non danneggiare le piante o le loro radici, dalle quali devono essere lontane per problemi di vibrazioni.

5.2.2. Strumentazione

Western Geco ha utilizzato la seguente strumentazione (Tab. 3):

Unit Function	Manufacturer and Model	Units for Field Use Incl R.Ref	Spare Units
MT Recording unit (5 channel, GPS synch)	Metronix ADU-07	13	1
MT Acquisition software	ADU-07 firmware	1	1
MT Magnetic sensors Hx, Hy, Hz coils	Metronix MFS-06/07 broadband induction coils	39	3
MT Electrodes	Wolf non polarizable PbPbCl	56	14
Field computers	Panasonic MF34 (to view ADU if required)	5	1
Other Spare Parts	Spare GPS antenna Spare power supply Spare Coil leads		4 4 5
Miscellaneous	Compasses, eTrex GPS units, levels, all weather notebooks, electrical tape, backpacks, battery chargers, 2 x PC, drives, back-ups, office supplies.		

Tab. 3 Caratteristiche della strumentazione MT

5.2.3. Elaborazione MT

I dati MT di campagna (denominati Time Series), sono stati elaborati utilizzando I codici di Larsen e Chave così come implementati nei codici di calcolo proprietari di WG.

Il codice Larsen usa un sofisticato approccio "robusto" con riferimento remoto, che include un pre-filtraggio per rimuovere il rumore armonico e il de-spiking per rimuovere l'effetto di onde non planari, ove presenti. I files di uscita sono archiviati nel formato geofisico standard SEG EDI. I dati sono stati processati fino alle curve di resistività apparente e fase (ρ-φ) (processing "to .EDI") nel giorno seguente l'acquisizione.

5.3. Acquisizione dati

5.3.1. Acquisizione

Per ciascuna misura sono state annotate sul libretto di campo le informazioni riguardanti le coordinate di stazione, il diagramma di posa, i dipoli, il potenziale e le resistenze di contatto tra i dipoli.

Magma Energy Italia ha quotidianamente eseguito un controllo di qualità dei dati forniti da WG per la loro accettazione. I risultati del QC sono esposti in Fig. 30.

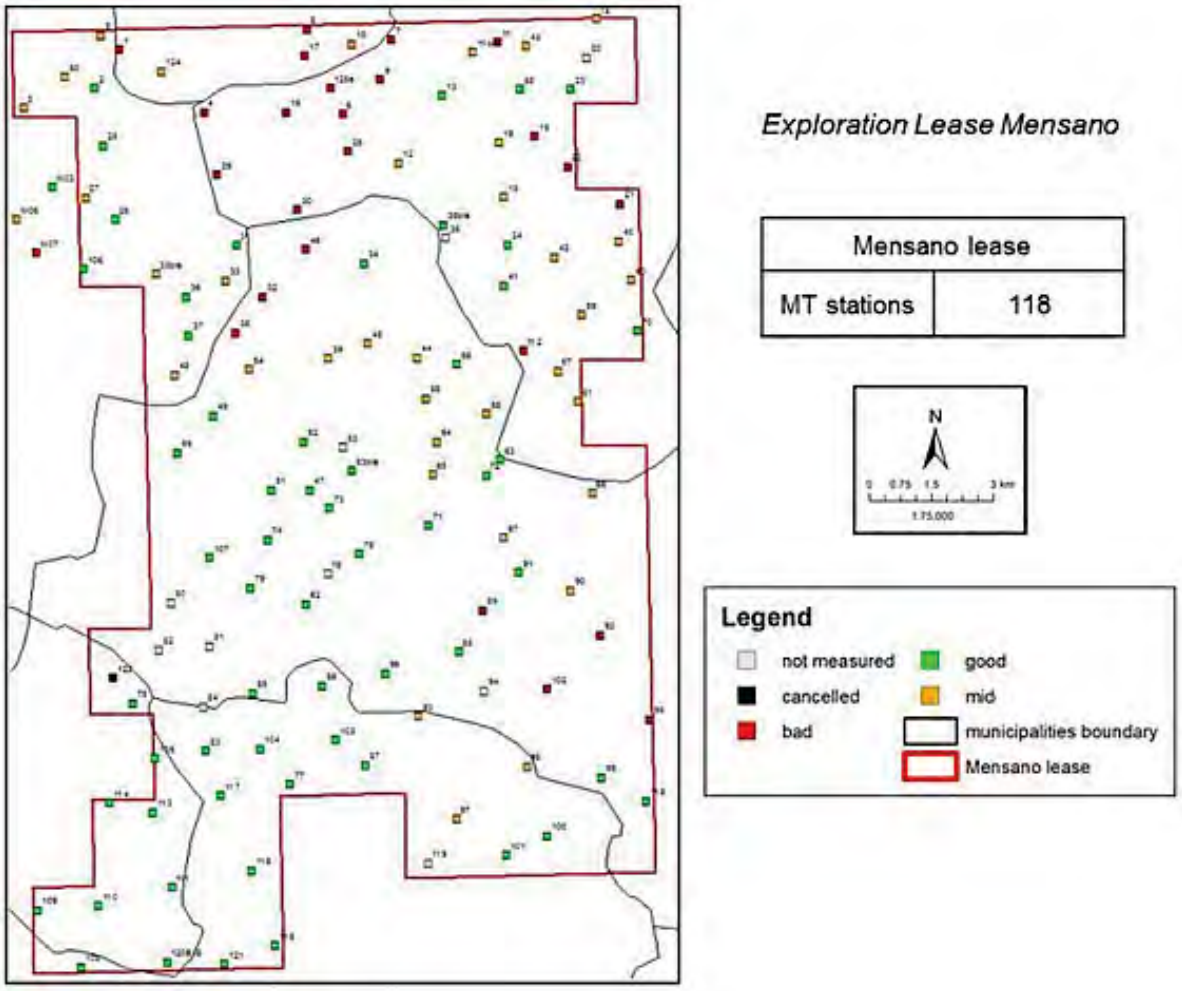

Fig. 18 – Distribuzione e qualità delle stazioni MT nel P.R. Mensano

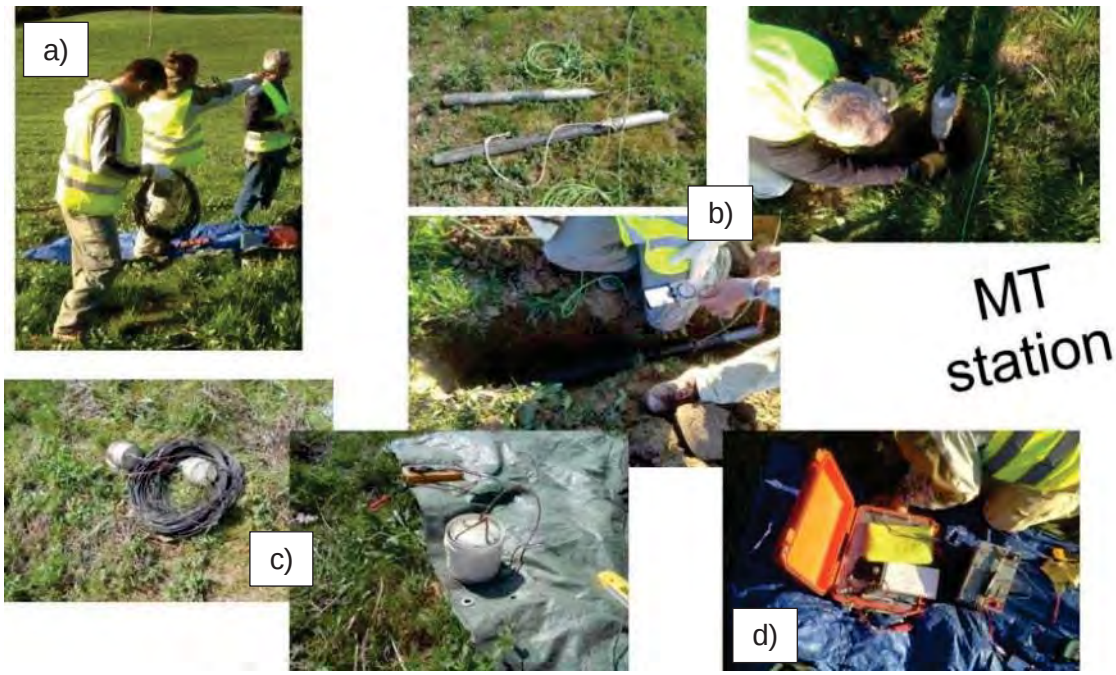

Fig. 19 – squadra MT crew al lavoro (a); bobine a induzione (b); elettrodi (c); unità Metronix ADU-07 (d)

5.3.2. Elaborazione delle Time Series

L'elaborazione delle time series è una procedura molto complessa. Il procedimento scelto è schematizzato nel diagramma di flusso che segue (Fig. 32).

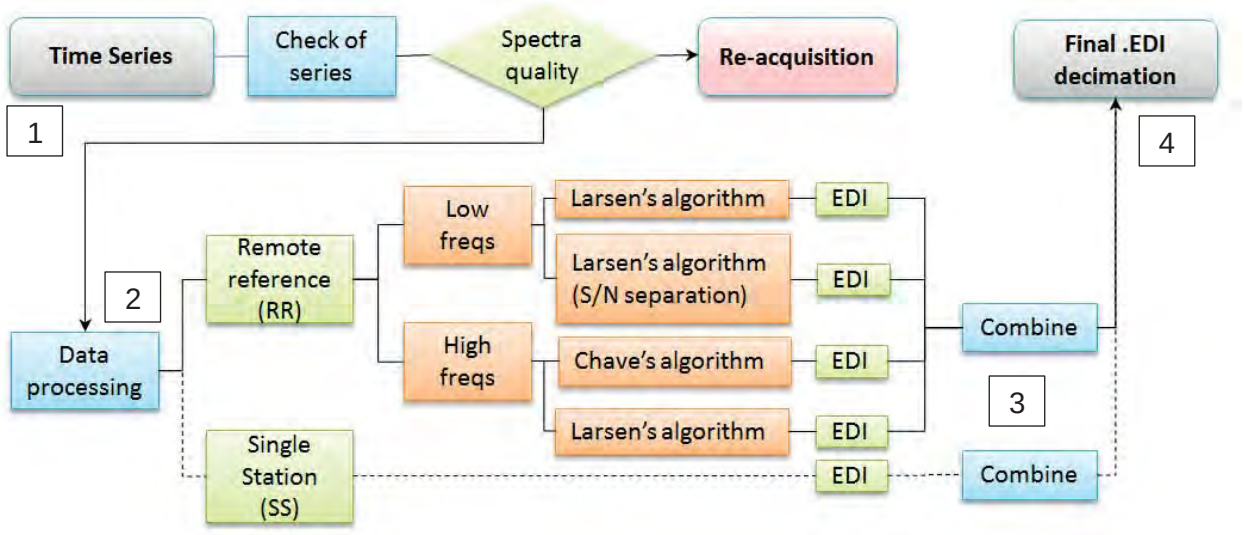

Fig. 20 – Flusso dilavoro della procedura di elaborazione: 1 – analisi delle Time series grezze; 2- data processing; 3- combine; 4- final .edi decimation.

Step1 – Il primo punto è l'analisi delle time series al fine di controllare i segnali sia nel dominio del tempo che della frequenza e identificare eventuali anomalie.

Step2 – Per ogni stazione sono state utilizzate quattro diverse procedure di calcolo, con l'utilizzo della tecnica della remote reference (RR): due codici sui segnali a bassa frequenza e due sui segnali ad alta frequenza, con gli algoritmi di Larsen e Chave. E' stata talvolta utilizzata anche la tecnica in stazione singola (SS). Per ogni banda di frequenza si è ottenuta una curva .edi.

Step 3 e 4 – Per ottenere il profilo MT finale sono state combinate le curve, con apposite procedure di scelta e controllo durante le quali l'operatore ha eliminato le curve rumorose, ottenendo per ogni sito una curva in formato .edi, opportunamente decimata.

5.3.3. Analisi di dimensionalità

E' stata eseguita una analisi dimensionale per controllare la consistenza areale dei sondaggi e ottenere informazioni sul comportamento elettromagnetico in profondità.

Sono stati utilizzati due approcci, mediante la realizzazione di diagrammi di polarizzazione e di mappe di resistività apparente. Inoltre sono stati analizzati i vettori di induzione.

Tutte le analisi sono state eseguite per 6 diversi range di frequenza (1000Hz, 100Hz, 10Hz, 1Hz, 0.1Hz, .01Hz) per indagare a profondità crescenti.

I diagrammi polari sono esposti in Fig. 33. Per ciascuna stazione è stato creado un diagramma polare che mostra una risposta elettromagnetica 1D, 2D or 3D in funzione della frequenza.

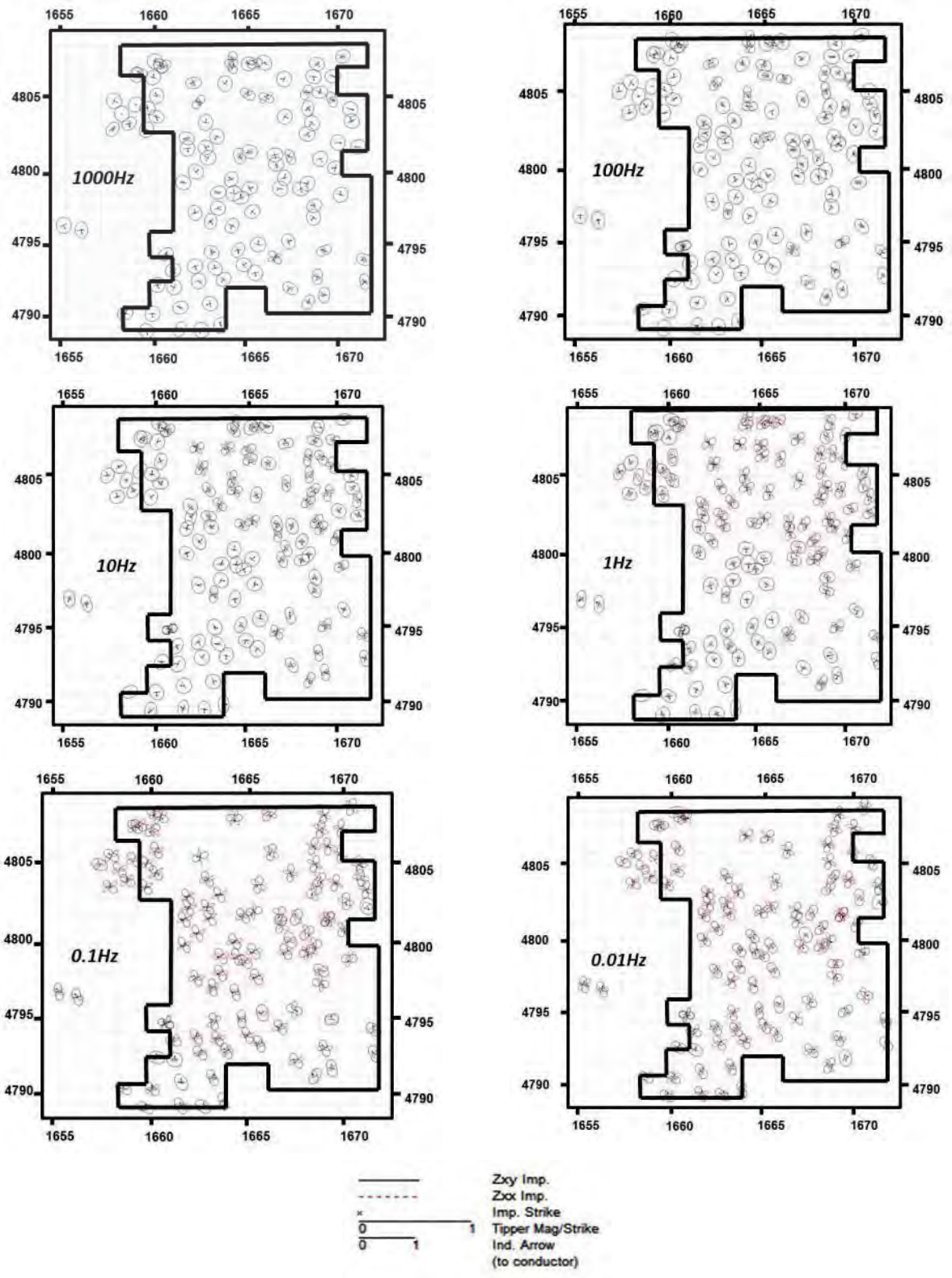

Fig. 21 – Diagrammi di polarizzazione MT a varie frequenze

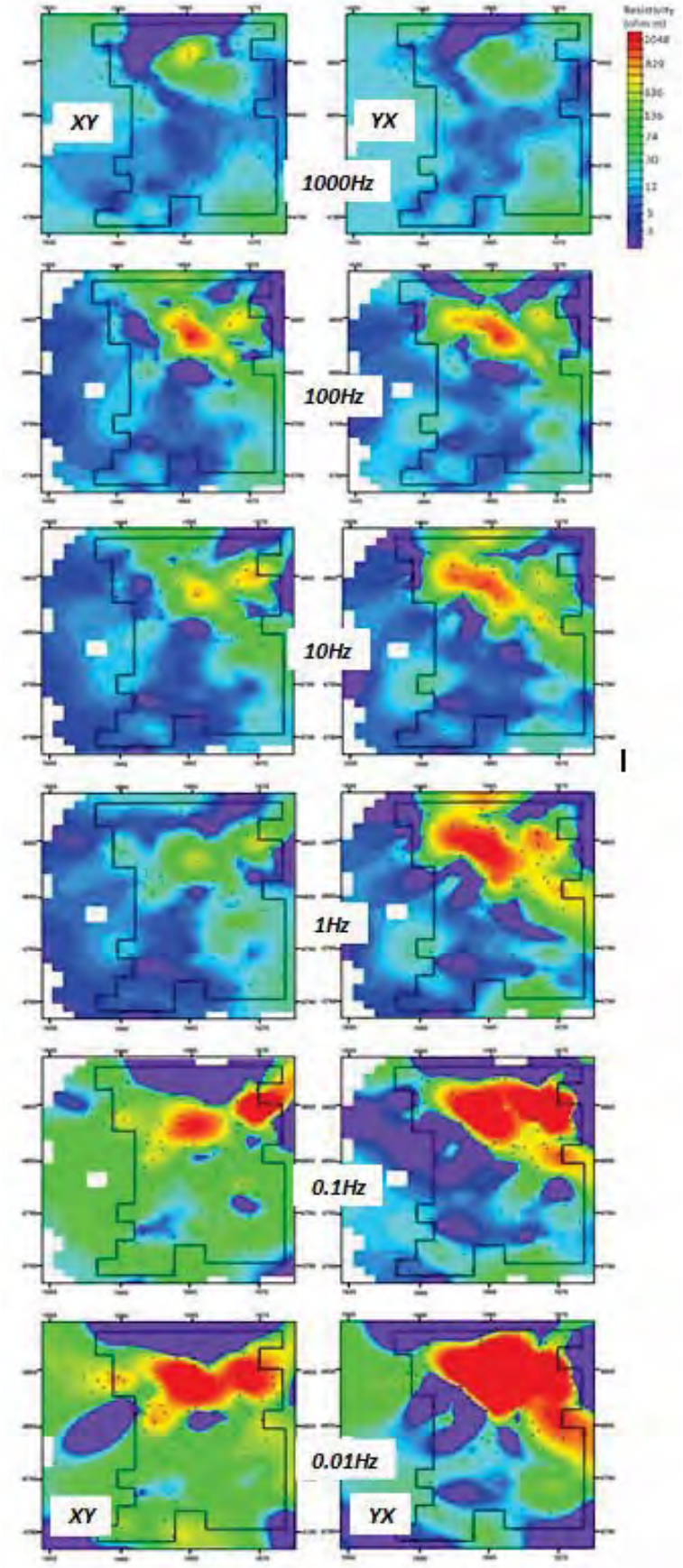

Le mappe di resistività apparente sono mostrate in Fig. 34. Per ogni range di frequenza sono visibili i valori di resistività nelle componenti XY e YX, che consentono di rilevare anomalie in funzione della frequenza e quindi della profondità.

5.3.4. Inversioni

Nelle inversioni monodimensionali le due componenti del tensore sono combinate e possono essere opportunamente modellate.

E' stato utilizzato il softwareWinGlink®, che permette di realizzare sia le trasformate di Bostick che due algoritmi di inversione sia di tipo "Occam" che a strati, per ottenere la miglior simulazione delle curve di resistività apparente e fase.

Sono state quindi ricostruite, mediante opportune interpolazioni, le mappe di resistività in funzione della profondità (Fig. 35).

In base all'analisi di dimensionalità sono poi stati scelti numerosi profili, sia ortogonali che paralleli al principale strike elettromagnetico, realizzando sezioni EM mediante opportune interpolazioni.

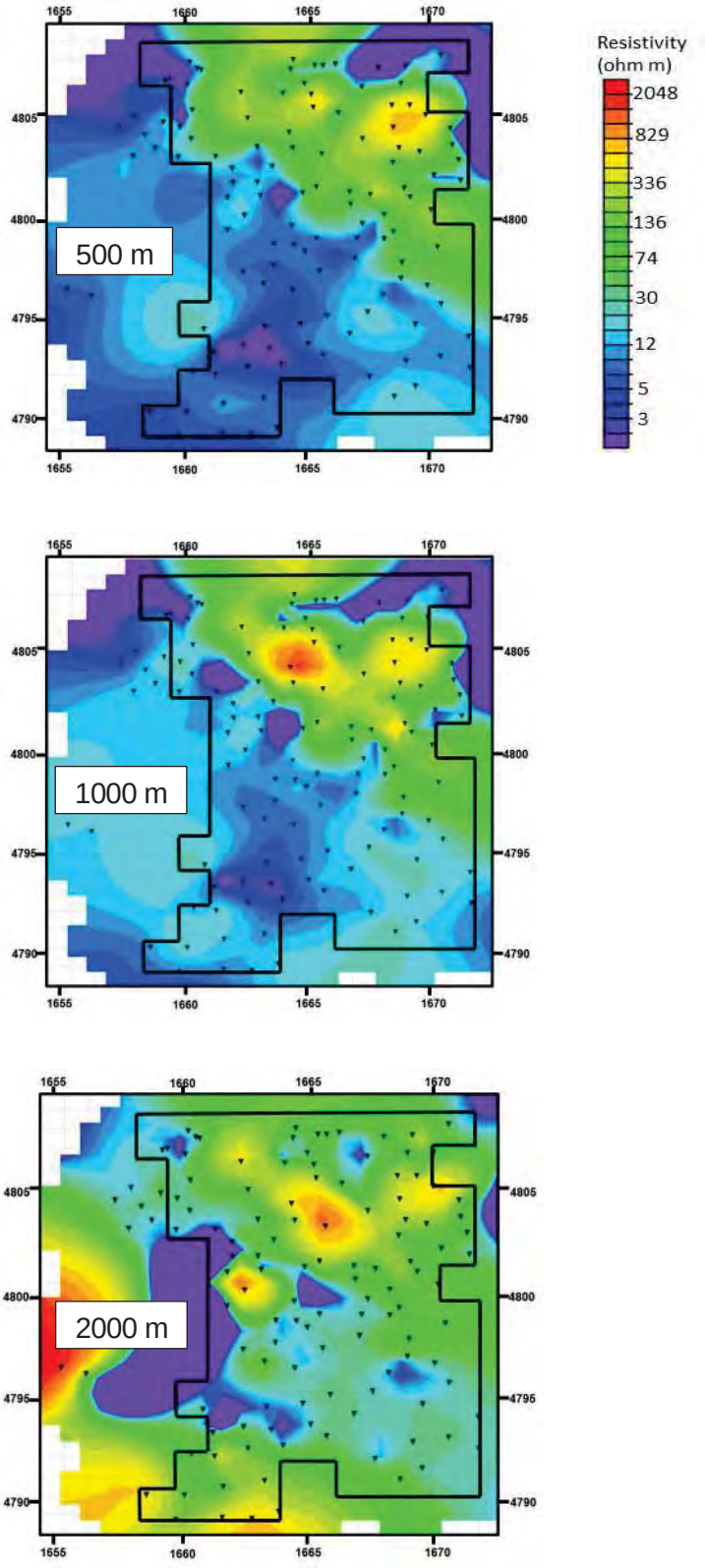

Fig. 23– Mappe di resistività a varie profondità elaborate da trasformate di Bostick.

SISMICA

Mem. Soc. Geol. It.,
19 (1978), 477-484, 4 ff.

CONTRIBUTION TO THE STUDY OF THE DEEP LITHOSPHERIC PROFILES: "DEEP" REFLECTING HORIZONS IN LARDERELLO-TRAVALE GEOTHERMAL FIELD

F. BATINI (*), P. D. BURGASSI (*), G. M. CAMELI (**), R. NICOLICH (***), P. SQUARCI (****)

ABSTRACT

One of the objectives in the exploration of steam fields that have been exploited for long periods is that of individuating deep horizons with the characteristics required of 'reservoirs'.

Various studies are now under way in Larderello-Travale area with this objective in mind (see also GIANELLI *et al.*, this Congress).

The seismic reflection survey is one of the geophysical prospectings that is providing new data on deep structures. The main results obtained so far are:

a) the presence of discontinuous seismic events in correspondence to the top of the present productive horizons;

b) the presence throughout the study area of a reflecting horizon at two-waytime varying from 1.8 to 2.5 sec in Larderello area and from 2.5 to 3.6 sec in Travale area;

c) the presence at the top of this horizon of gentle anti-Apenninic folds and sub-vertical faults in correspondence to the margins of the Neogenic grabens.

INTRODUCTION

Our knowledge of reservoir pressure distribution in exploited fields (CELATI *et al.*, 1976) has shown that vapour-dominated systems exist to a depth of at least 2 km and that the pressure increases with depth.

Based on this data ENEL drilled some wells in Larderello to a depth of about 3 km in an attempt at individuating eventual productive horizons below those in exploitation at present. However, the results were of little commercial interest because of the low permeability of the formations crossed by the wells.

Recently a series of stratigraphic and structural studies (PUXEDDU *et al.*, 1977; BAGNOLI *et al.*, 1978; GIANELLI *et al.*, 1978, this volume) and geophysical surveys, especially seismic reflection (BERNARDI *et al.*, 1976) have begun, in order to define the objective of deep exploration.

The problem is not only that of finding new sources of geothermal fluids but also, on the theoretical side, that of formulating a reliable geothermal field "model".

Deep structural data could be used in future in evaluating the geothermal resources at depths below those considered so far (3000 m) (CATALDI *et al.*, 1977; CATALDI & SQUARCI, 1978) and in dealing with the problem of hot, dry rocks and of reinjecting the effluents from the geothermal power stations.

The most suitable of all the geophysical methods experimented in the Italian geothermal areas, for provinding data on deep structures, is the seismic reflection survey (BERNARDI *et al.*, 1976). In special circumstances this method can also give information on the structures connected with the shallowest geothermal reservoirs. It is used for this purpose in the exploration of the marginal areas of Larderello field and in the new geothermal area of Travale-Radicondoli for defining the trend of the top of the shallowest geothermal reservoir outside the densely drilled areas.

The first seismic reflection profile was made on the eastern margin of Larderello field, in Serrazzano zone, to test the method responses in an area with a complex stratigraphy and tectonics and thick flysch formations in the upper part of the series. The experiment was a success (BERNARDI *et al.*, 1976) the data showing that structural information can be obtained for the top of the potential reservoir and that there are deep reflections far below the top of the phyllitic-quartzitic metamorphic formations. Considering the success of this experiment a programme was drawn up for exploring all the area covered by Larderello and Travale fields, to a total of 190 km (Fig. 1).

(*) Gruppo Minerario, ENEL, Larderello, Italy.
(**) Centro Ricerca Geotermica, ENEL, Pisa, Italy.
(***) Osservatorio Geofisico Sperimentale Trieste, Italy.
(****) Istituto Internazionale Ricerche Geotermiche, CNR, Pisa, Italy.

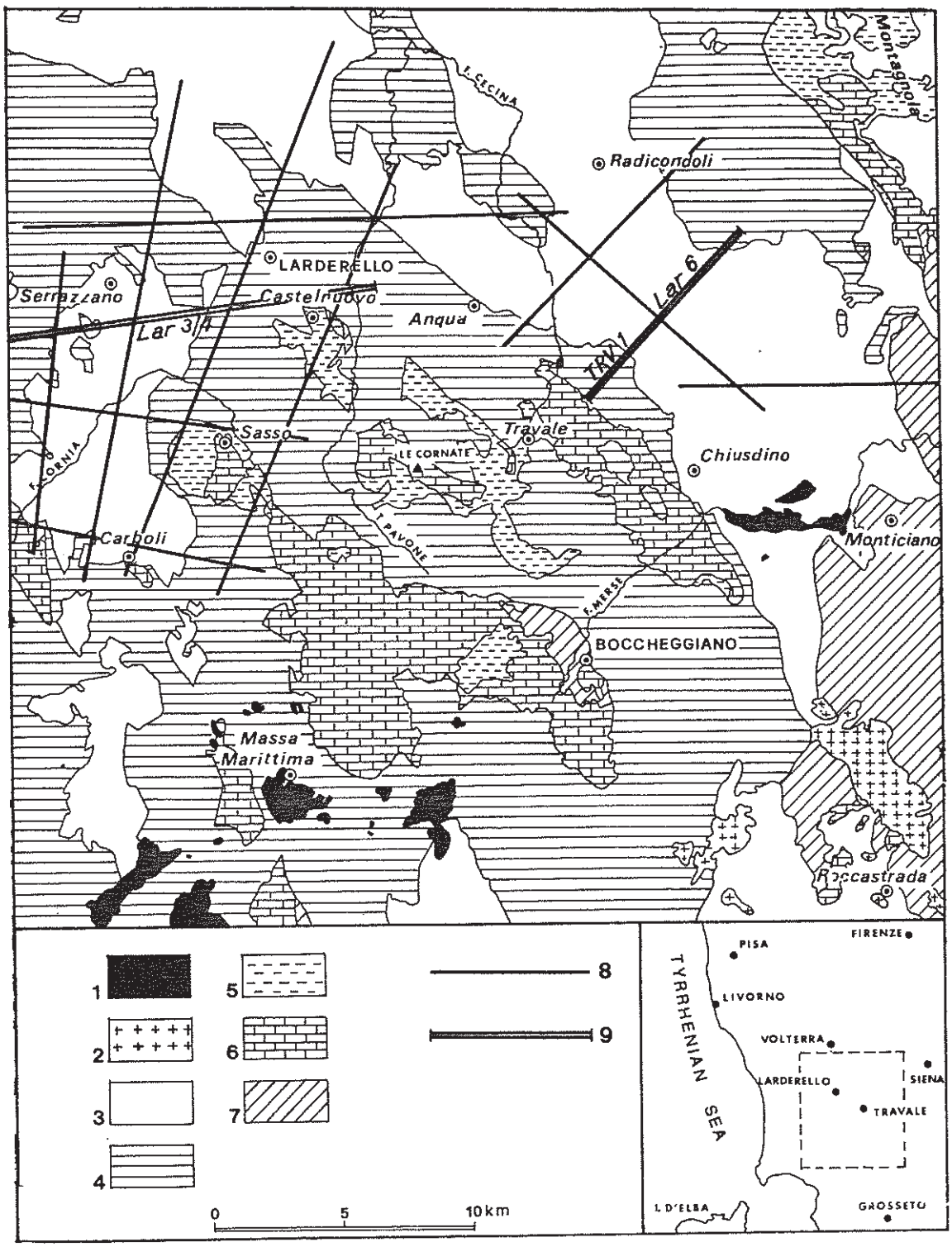

Fig. 1 - Geological sketch map of the geothermal area with location of the seismic profiles. - 1: travertine (Quaternary) 2: Roccastrada rhyolite (2.3 m.y.) 3: Neogenic deposits (Upper Miocene-Pliocene) 4: Ligurid nappes (Eocene-Upper Jurassic): mainly shale 5: Tuscan Nappe (Oligocene-Upper Cretaceous): shale and sandstone 6: Tuscan Nappe: Jurassic limestone and Burano formation (Upper Trias) 7: Upper Triassic-Paleozoic quartzites and phyllites 8: location of seismic profiles 9: location of interpreted seismic profiles.

GEOLOGICAL OUTLINE

The general sequence of lithostratigraphic units in Larderello-Travale area to 3000 m depth can be summarized as follows (GIANELLI *et al.*, 1978, this Congress, and related bibliography), from the bottom up:

1) *"Tuscan crystalline formations"* ("basement"): made up of generally pre-Carboniferous (pre-Sudetian) formations. The following groups have been individuated by GIANELLI *et al.*, this Congress (Fig. 2, D): plagioclase garnet-bearing micaschists in the deepest part; above these phyllitic quartzites, quartzites and phyllites associated with metagraywackes, chloritoschists, calceschists and graphitic phyllites (Boccheggiano group of BAGNOLI *et al.*, 1978). In Anqua and Travale-Radicondoli zone these lithotypes are intercalated with dolomitic marbles and crystalline anhydrites. The uppermost part of the "basement" generally consists of interstratified quartzites and phyllites that can be compared to the Buti group partly attributed to the Silurian (BAGNOLI *et al.*, 1978).

A close analogy has recently been revealed between the Tuscan Paleozoic formations and those of Sardinia (CARMIGNANI *et al.*, 1977; GIANELLI & PUXEDDU, 1978, this volume).

Therefore stratigraphic and structural conditions similar to those of Sardinia may possibly exist even in the underground of this geothermal region.

2) *Tectonic wedge zone:* overthrust wedges (to a maximum total thickness of 1400 m) can be found in Larderello-Castelnuovo and Serrazzano areas, above the "basement". These wedges are made up of both the Tuscan crystalline formations and the Triassic terrigenous ("Verrucano") and Mesozoic carbonate formations. The possibility cannot be excluded that the original "cover" exists, above the basement, in some restricted areas, where it comprises terrigenous trangressive formations of the Triassic Verrucano.

3) *Tuscan nappe:* in the rare situations in which it is complete this nappe consists of the well-known Triassic-Oligocenic sequence, with Mesozoic carbonate formations in the basal part and mainly terrigenous formations in the Cretaceous-Oligocenic upper part (shales and sandstones). This tectonic unit is often made up of incomplete sequences or of the anhydritic Burano formation of the Upper Triassic only. The latter formation, with associated breccia of dolostones and anhydrites, forms the base of the unit. In some places the Tuscan Nappe is completely missing.

4) *Ligurid Nappes:* these are made up of Cretaceous-Eocenic flysch facies formations and ophiolites. These units may lie over any of the previously described units and sometimes over the oldest rocks of the "basement".

5) *Neoautochthon:* it consists of lacustrine, marine and lagoonal sediments of the Upper Miocene (Messinian) and marine sediments of the Pliocene. This group of mainly clayey formations unconformably covers the preceding units and generally fills the graben.

SEQUENCE OF TECTONIC PHASES

The main tectonic phases affecting the area are: the Hercynian (BAGNOLI *et al.*, 1978) for the basement, although older phases cannot be excluded for its deepest parts; the Alpine, mainly Tortonian, with its compressional and distensive phases which controlled the emplacement and folding of the Tuscan (Tuscan Nappe and wedges) and Ligurid units. Finally, the distensive phase, beginning in the Messinian, which gave rise to the main horst and graben structures existing in the area.

THE SEISMIC SURVEY

The seismic reflection survey was planned in 1976 (lines LAR-1 to LAR-7, to a total of about 70 km) and in 1978 (lines LAR-8 to LAR-15: about 116 km). The O.G.S. (Trieste) and the C.G.G. (Paris) shot and processed the data respectively.

The field acquisition techniques were very similar throughout the survey:

— station spacing: 50 m;

— shot: split in boreholes averaging 20 m depth and dynamite charge of 10 kg;

— coverage: 600%;

— recording instruments (T.I.-DFS- 10,000 with 24 traces for the lines SER-1 and TRV-1, T.I.-DFS- III with 48 traces for the lines LAR-1 to LAR-7 and SN-338 for the lines LAR-8 to LAR-15);

— sampling rate: 2 milliseconds.

The data were processed to produce sections such as that shown in Fig. 3. This section includes time variant filtering and predictive t.v. deconvolution, automatic static corrections and migrations.

While computing the field statics some difficulties arose as a consequence of variable topography and heterogeneity of the sedimentary coverage (frequent velocity variations).

The quality of the data appears fair or poor for the shallow reflections that should probably be tied to the known lithologic units, whereas,

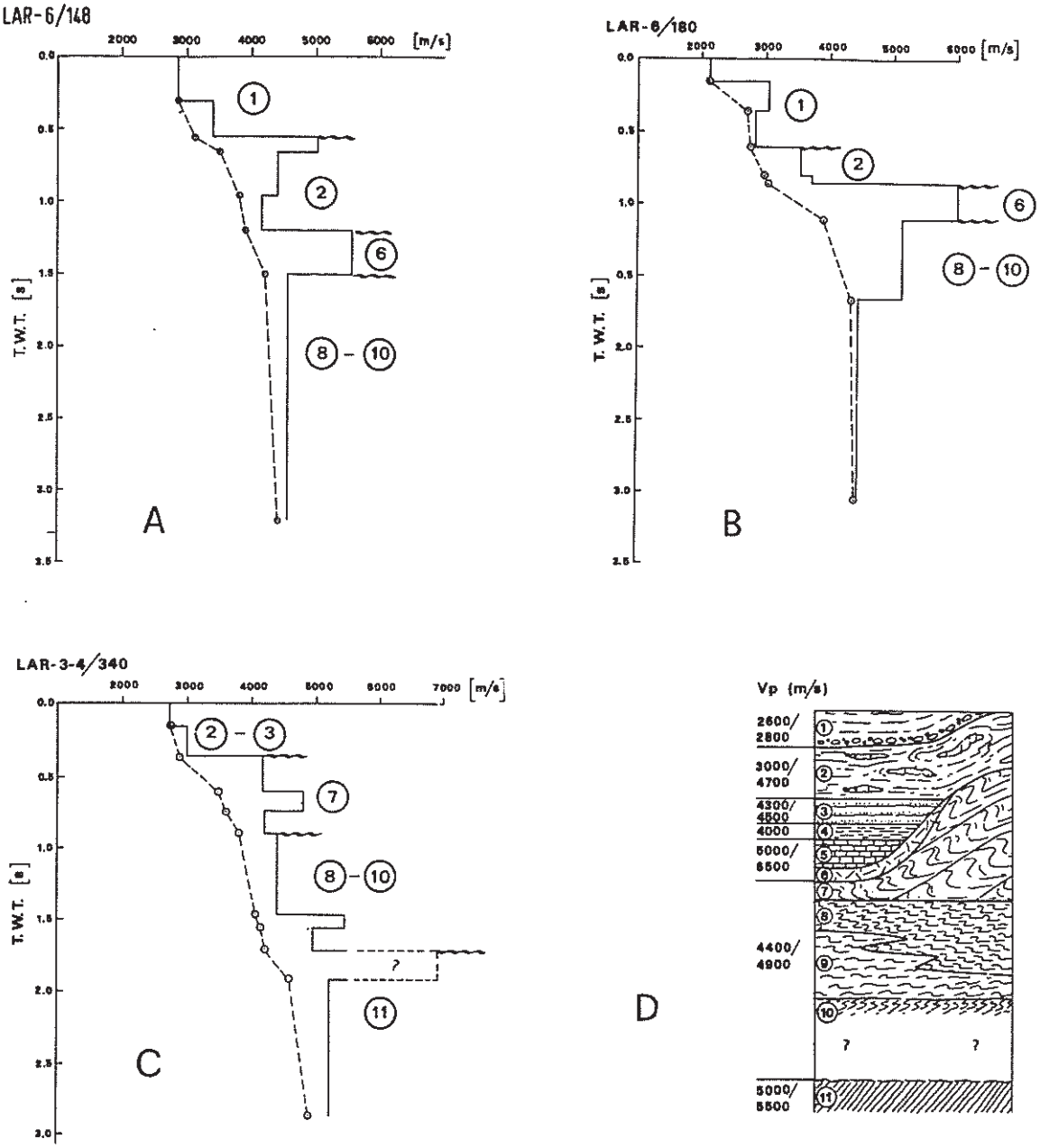

Fig. 2 - Calculated velocity functions and representative stratigraphic column.

A-B-C: velocity function for lines LAR-6, shot point 148 and 180, LAS-3/4, shot point 340. Dashed line - stacking velocity; unbroken line - interval velocity.

D: representative stratigraphic column of Larderello-Travale area with velocity of different formations. 1. Neogenic deposits (mainly clay) (Upper Miocene-Pliocene) 2: Liguridis (mainly shale and ophiolite (Upper Jurassic-Eocene) 3: "macigno" sandstone (Oligocene) 4: "scaglia" shale (Upper Cretaceous-Eocene) 5: limestone (Jurassic) 6: dolomite and anhydrite (Upper Trias) 7: tectonic wedges (mainly quartzite and phyllite) 8: Buti group (mainly quartzite and phyllite) (Silurian) 9: Boccheggiano group (mainly phyllitic quartzite, quartzite and phyllite) (Paleozoic) 10: plagioclase garnet-bearing micaschist (Paleozoic) 11: deep reflecting horizon.

deep within the metamorphic "basement", a higher amplitude reflector indicates, on all the lines, a marked velocity-density change. Its reflection time varies from 1.4 (LAR-8, -12) to 3.8 s (LAR-6, -7) and the very grood penetration of relatively high frequencies allows better resolution than normally encountered at those depths (sometimes more than 7 km).

The primary effect of migration was the spatial relocation of dipping events, together with the collapse of large diffractions, delineation of faults and emphasis of the layered heterogeneous nature of the deep reflecting horizon.

An attempt was made to follow the horizon over all the area and an isochrone map was drawn up to make a structural interpretation. Its main features are as follows:

a) evidence of angular unconformities;

b) presence below the horizon of convergent/divergent dip segments.

Generally speaking similar markers could be produced by gradually higher metamorphic zones, or by a cluster of sills intruded in metamorphic rocks, or by changes in the geochemistry of endogenous rocks.

With regard to the hypothesis of the presence of granite intrusions below the reflecting horizon, such elements are normally detected as zones of low reflector density (see, for example, the Elba plutonic body on line MS-9 in FINETTI *et al.*, 1970). On the other hand, it is hard to believe that all the observed convergent/divergent dip segments are from outside the plane of the section, and in any case the presence of diffractions indicates non-homogeneous media, while the angular unconformities may indicate depositional patterns and/or a tectonic discontinuity.

One of the most useful implements in the lithologic interpretation of seismic reflections is the velocity analysis.

Here the relatively short distance from the source station to the farthest geophone (offsets of only 675 m for SER-1 and TRV-1 and of about 1200 m for the other lines) means that the velocity computations for the deep events are either unrealiable or have significant error bars. The error bars become even greater with depth.

In Fig. 2, A, B, and C three velocity functions (stacking and interval velocities) for lines LAR-6 and LAR-3/4 are given. Interval velocities were computed from the stacking velocities using Dix's equation. The average velocities utilized in the time-depth conversion were obtained from the stacking velocities. In Fig. 4 (LAR-6 and TRV-1) the average velocity was 3960 m/s for T.W.T. down to 3.5 s and 4000 m/s for T.W.T. greater than 3.5 s. For this figure the interpretation was performed on the migrated section even though the shortness of the line should confine a strict interpretation to depths above 3 km, that is, the syncline could be interrupted towards the east by a fault (the eastern limit of the graben).

In Fig. 3 (LAR-3/4) the average velocity utilized was of 3870 m/s.

Figure 2, D shows a representative stratigraphic column, together with the corresponding interval velocities. The velocities were derived from well measurements (including sonic logs) and from seismic data for the deep structures.

CONCLUSIONS

The structural trend of the deep reflecting horizon is characterized by gentle anti-Apenninic folds whereas the structures affecting the Tuscan Nappes and the shallowest parts of the basement generally trend in an Apennine direction. The horizon is, moreover, affected by subvertical faults that in some cases have a very large throw (even more than 1000 m). A typical example of this, on the western margin of Radicondoli graben, is shown in Fig. 4 (see also Fig. 1, lines TRV-1, LAR-6).

The faults either trend in an Apennine (NW-SE) or anti-Apennine (NNE-SSW) direction and appear to be directly connected with the initial phases of formation of the Neogenic basins (Upper Miocene-Messinian) (see Fig. 3, line LAR-3/4, from SP324 to SP308), although the tensional effects cannot be distinguished in all the shallowest horizons.

As far as the geological nature of this horizon is concerned it can be excluded that it represents the roof of a pluton because of the type of reflections, with the presence of angular unconformities, dip reflecting horizons and diffractions and the structural trend of the reflections. The calculated velocities are in contrast with this hypothesis as they appear incapable of reaching 6000 m/s (see Fig. 2, C), even though a velocity lowering may be expected in the presence of high temperatures or overpressured fluids.

The regional-scale petrological and structural studies carried out recently by GIANELLI *et al.* (1978) lead to the exclusion of some hypotheses forwarded in the past on the nature of this horizon (BERNARDI *et al.*, 1976).

At the present stage of our knowledge the hypotheses possible on the reflecting horizon are:

— a contact between units of different gra-

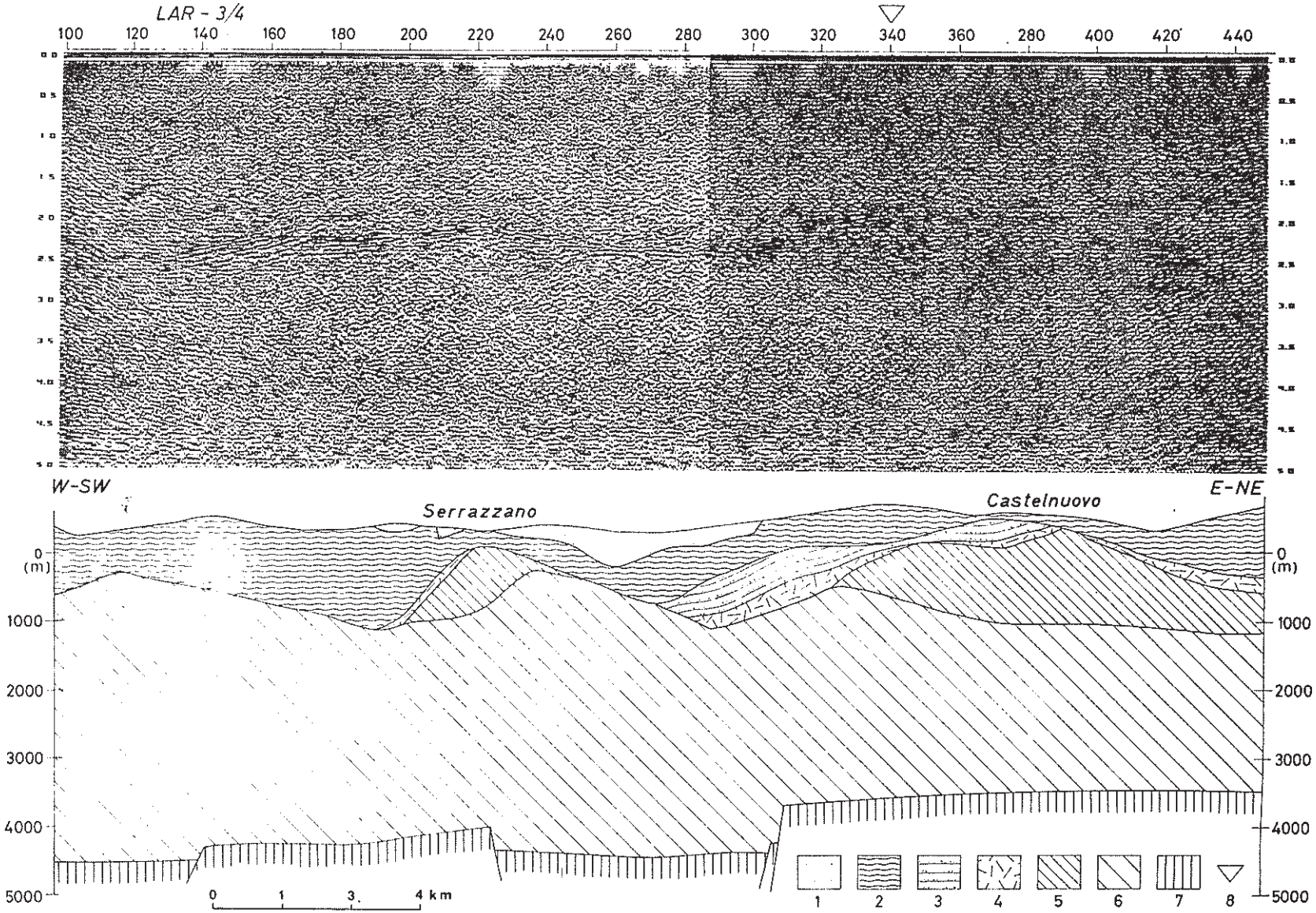

Fig. 3 - Processed seismic line (LAR-3/4) and geological interpretation (Larderello geothermal field). 1: Neogenic deposits 2: Ligurid nappes 3: Tuscan Nappe (sandstone and shale) 4: Tuscan Nappe (Burano formation) 5: tectonic wedges 6: Tuscan crystalline formations 7: deep reflecting horizon 8: location of calculated velocity functions (see Fig. 2, C).

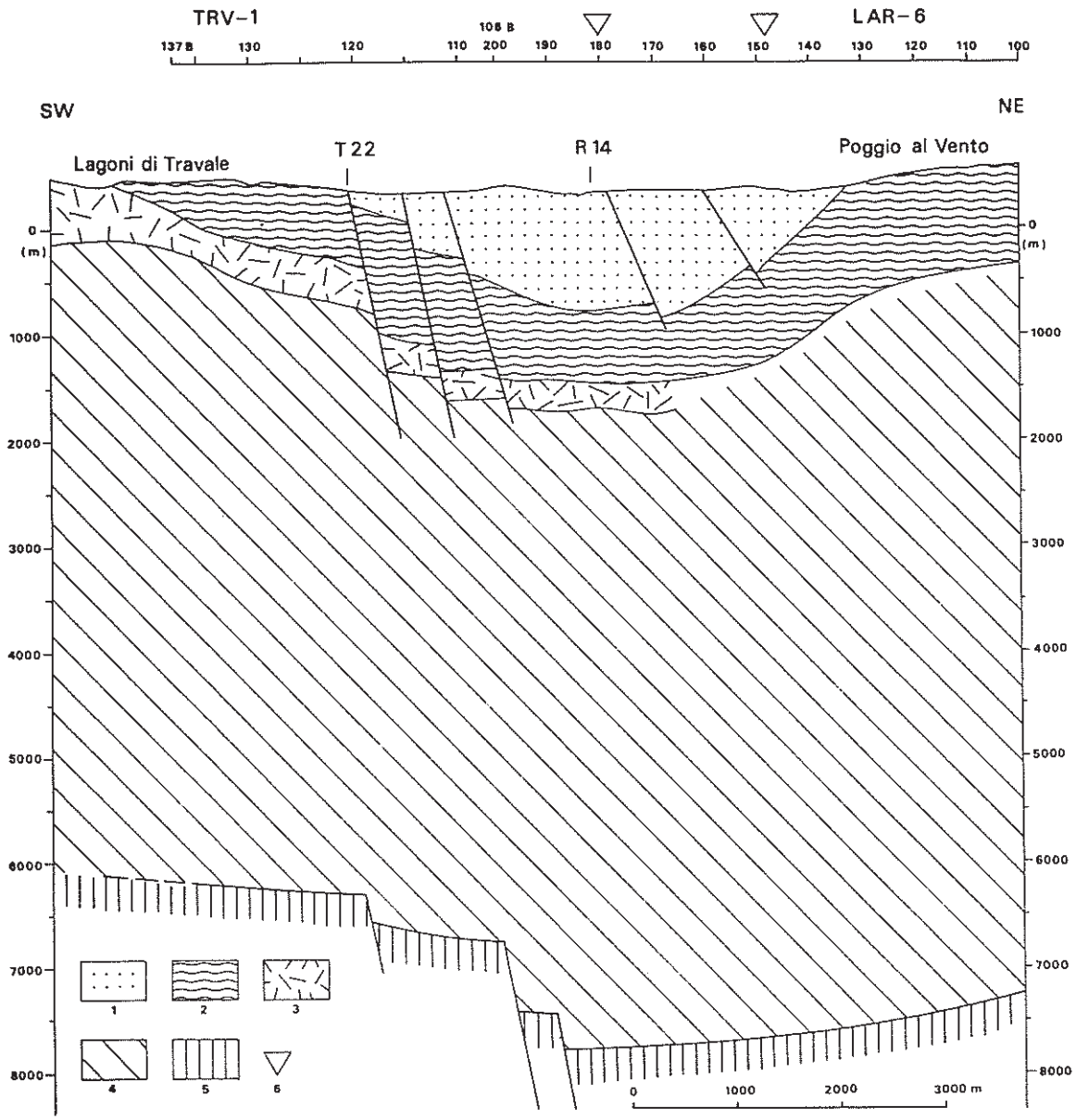

Fig. 4 - Geological interpretation of seismic lines TRV-1 and LAR-6 (Travale geothermal field). 1: Neogenic deposits 2: Ligurid nappes 3: Tuscan Nappe (Burano formation) 4: Tuscan crystalline formations 5: "deep reflecting horizon" 6: location of calculated velocity functions (see Fig. 2, A-B).

des of metamorphism (the lowermost one representing the "actual" regional basement);

— the roof of a Paleozoic carbonate platform;

In this case the analogy between the Paleozoic series of the basement in this area and that of Sardinia lead to the hypothesis that this platform is Cambrian;

— a transgression surface.

In this case, again comparing with Sardinia, the latter might represent the transgression between the Ordovician and Cambrian, tied to the Sardinian phase of the Caledonian orogeny (Cocozza *et al.*, 1976).

Despite the uncertainty still existing on the nature of this horizon, this structural marker is still of great importance when reconstructing a geothermal field model and may also be of considerable significance from the "energy potential" viewpoint.

The tectonic events that have affected this horizon lend support to the hypothesis that within it are zones containing geothermal fluids.

The drilling programme now conducted by ENEL and the processing of the seismic refraction data (D.S.S. programma of the "Progetto Finalizzato Geodinamica", C.N.R.) may solve part of the problems remaining in the interpretation of this horizon.

REFERENCES

BAGNOLI G., GIANELLI G. PUXEDDU M., RAU A., SQUARCI P. & TONGIORGI M. (1978) - *The Tuscan Paleozoic: a critical review.* In "Report on the Tuscan Paleozoic basement" (ed. TONGIORGI M.), Sottoprogetto Energia Geotermica, Progetto Finalizzato Energetica, Internal Report, Pisa. In press.

BERNARDI A., CAMELI G. M., ROMANINI E., SQUARCI P. & STEFANI G. C. (1977) - *Seismic survey in Larderello-first results.* Simposió Internacional sobre Energia Geotermica en America Latina, IILA, Rome, 127-151.

CARMIGNANI L., RAU A., SQUARCI P., TONGIORGI M. & VAI G. B. (1977) - *Le successioni Paleozoiche-Triassiche della Sardegna centrale e dell'Autoctono Apuano: analogie e possibili correlazioni.* G.L.P. 2, suppl. (ed. VAI G. B.), 11-14.

CATALDI R., LAZZAROTTO A., MUFFLER P., SQUARCI P. & STEFANI G. C. (1977) - *Assessment of geothermal potential of Central and Southern Tuscany.* Proc. ENEL-ERDA Workshop, Larderello, Sep. 12-16, 1977, ENEL, 351-412.

CATALDI R. & SQUARCI P. (1978) - *Valutazione del potenziale geotermico in Italia con particolare riguardo alla Toscana centrale e meridionale.* Atti Congresso Assoc. Elettrotecnica Ital., Catanzaro, I. 32, 23-24 Sept. In press.

CELATI R., SQUARCI P., TAFFI L. & STEFANI G. C. (1977) - *Study of water levels in Larderello region geothermal wells for reconstruction of reservoir pressure trend.* Simposio Internacional sobre Energia Geotermica en America Latina, IILA, Rome, 502-526.

COCOZZA T., JACOBACCI A., NARDI R. & SALVADORI I. (1974) - *Schema stratigrafico-strutturale del massiccio sardo-corso e minerogenesi della Sardegna.* Mem. Soc. Geol. it., 13, 85-186.

FINETTI I., MORELLI C. & ZARUDZKI E. (1970) - *Reflection seismic study of the Tyrrhenian Sea.* Boll. Geof. Teor. Appl., 12, 48, 311-346.

GIANELLI G. & PUXEDDU M. (1978) - *Some observations on the genesis of ore deposits and associated evaporites in southern Tuscany.* Soc. Geol. it., 69th Congress, Perugia.

GIANELLI G., PUXEDDU M. & SQUARCI P. (1978) - *Structural setting of the Larderello-Travale geothermal region.* Soc. Geol. it., 69th Congress, Perugia.

PUXEDDU M., SQUARCI P., RAU A., TONGIORGI M. & BURGASSI P. D. (1977) - *Stratigraphic and tectonic study of Larderello-Travale basement rocks and its geothermal implications.* Geothermics, 6, 83-93.

Proceedings World Geothermal Congress 2010
Bali, Indonesia, 25-30 April 2010

3D Seismic Surveys and Deep Target Detection in the Larderello-Travale Geothermal Field (Italy)

Michele Casini[1], Simonetta Ciuffi[1], Adolfo Fiordelisi[1] and Alfredo Mazzotti[2]

[1]Enel Green Power, via Andrea Pisano, 120 – 56122 Pisa (Italy)

[2]Earth Sciences Department-Geophysics, University of Pisa (Italy)

adolfo.fiordelisi@enel.com

Keywords: Italy, Larderello, Travale, 3D seismics, deep exploration, drilling target detection.

ABSTRACT

Deep exploration in the Larderello-Travale area highlighted a single deep geothermal system wider than 400 km^2 and with temperature of about 300°C at a depth of 3000 m. The deep reservoir is hosted in metamorphic/intrusive rocks and is characterized by a highly inhomogeneous permeability. This can increase the mining risk and, as a consequence, the drilling costs. A significant contribution in the detection of potential, productive targets for deep drillings can be provided by a detailed reconstruction of high amplitude seismic markers that, as confirmed by recent 3D seismic surveys, often correspond to fractured levels.

In the framework of a deep exploration project, new 3D surveys were performed in three areas of the Larderello-Travale geothermal system for a total full fold area wider than 100 km^2. Data processing was aimed at preserving the correct signal amplitude and at detailing the subsurface structures. An accurate joint interpretation of well and geophysical data allowed defining the 3D structure and the high amplitude anomalies of a seismic marker that shows a quite good statistical correlation with fractured and productive levels. This marker, known in literature as "H" horizon, is discontinuously present everywhere in the Larderello-Travale system, but can be originated by different or concomitant causes such as lithology changes and/or presence of fractured levels.

More than 10 directional wells have been drilled up to now to reach 3D seismic targets, but for the above said reason their productivity was different. The best results were obtained in the Travale area (3D Montieri-Chiusdino) where the H horizon corresponds to a highly fractured contact metamorphic aureole and where the correlation between well productivity and seismic marker suggests that more than 70% of steam production originates from depth intervals within this horizon.

1. INTRODUCTION

The exploration and exploitation of the Larderello-Travale geothermal system started at the beginning of the last century and initially interested a shallow reservoir, at depth less than 1000m. This is hosted in sedimentary formations (limestone and anhydrite), and has temperatures of about 250°C.

In the middle of 80s, the first deep exploration wells discovered, at depth higher than 3000 m b.s.l., a deeper superheated steam reservoir. This is characterized by temperatures of 300-350°C, (Barelli et al., 1995), pressure of up to 70 bars, and is hosted in metamorphic and intrusive rocks.

Subsequent deep wells confirmed that the deep Larderello and Travale fields belong to the same geothermal system, (Barelli et al. 2000, Bertani et al. 2005). This deep system is roughly delimited by the isotherm of 300°C at a depth of 3000 m, is wide more than 400 km^2 (Figure 1), but its real extension is not yet well defined. Furthermore the deep reservoir, differently from the shallow one, is characterized by a very inhomogeneous permeability distribution and this increases the mining risk and the drilling costs.

Previous studies demonstrated the reliability of seismic surveys in the Larderello-Travale area for locating deep fractured levels (Bertini et al., 2005), which are the productive drilling targets. In particular, a quite good correspondence between fracture systems and high amplitude seismic reflectors was highlighted in the metamorphic basement from a statistical analysis based on seismic 2D lines (Cameli et al., 2000). Furthermore, post-stack and pre-stack attribute analysis performed on 2D seismic data effectively pointed out a seismic anomalous zone with high reflection amplitudes and positive AVO gradients (Mazzotti et al., 2002) in correspondence of fractured levels.

This encouraged the use of 3D seismic surveys to identify potential targets prior to drilling thus reducing the mining risk. After a first test in a small area (Bruciano), three new surveys (see Figure 1) were scheduled in the framework of a new deep exploration program, (Cappetti et al., 2005), that envisaged the drilling of wells down to depths of 3500-4000 m, at the margins of mining licenses already under exploitation.

2. NEW 3D SEISMIC SURVEYS

The new 3D surveys were acquired in the period 2003-2004 with technical solutions aimed to guarantee a theoretic full fold ≥ 1600% for areas of about 34 km^2 at the maximum depth of the potential geothermal targets (4500 m b.s.l). Processing and interpretation were ended in 2005-2006 with the main purpose of providing specific targets for the deep wells to be drilled.

2.1 Acquisition

The acquisition parameters were defined as a compromise between costs and required data quality. Major importance was given to select energy source, bin size and theoretical maximum fold.

On the base of the previous 2D seismic data, explosive was preferred as the energy source. Shot holes 10-12 m deep were drilled and charged with about 3 kg of dynamite. Due to the irregular morphology and to the poor accessibility of all the surveyed areas, many shot holes were drilled by means of eliborne drill units.

A bin size of 25×40 m (50 m receiver group interval and 80 m shot interval) was chosen. The requested fold was achieved employing a source line spacing of 500 m and receiver line spacing of 480 m. The recording stations consisted in linear equispaced arrays of 12 geophones per group. Accessibility problems and environmental constrains caused a partial match between the planned and the real shot hole layout. This caused a heterogeneous coverage distribution but the requested minimum fold of 1600% was ensured in all the surveyed areas (Figure 2).

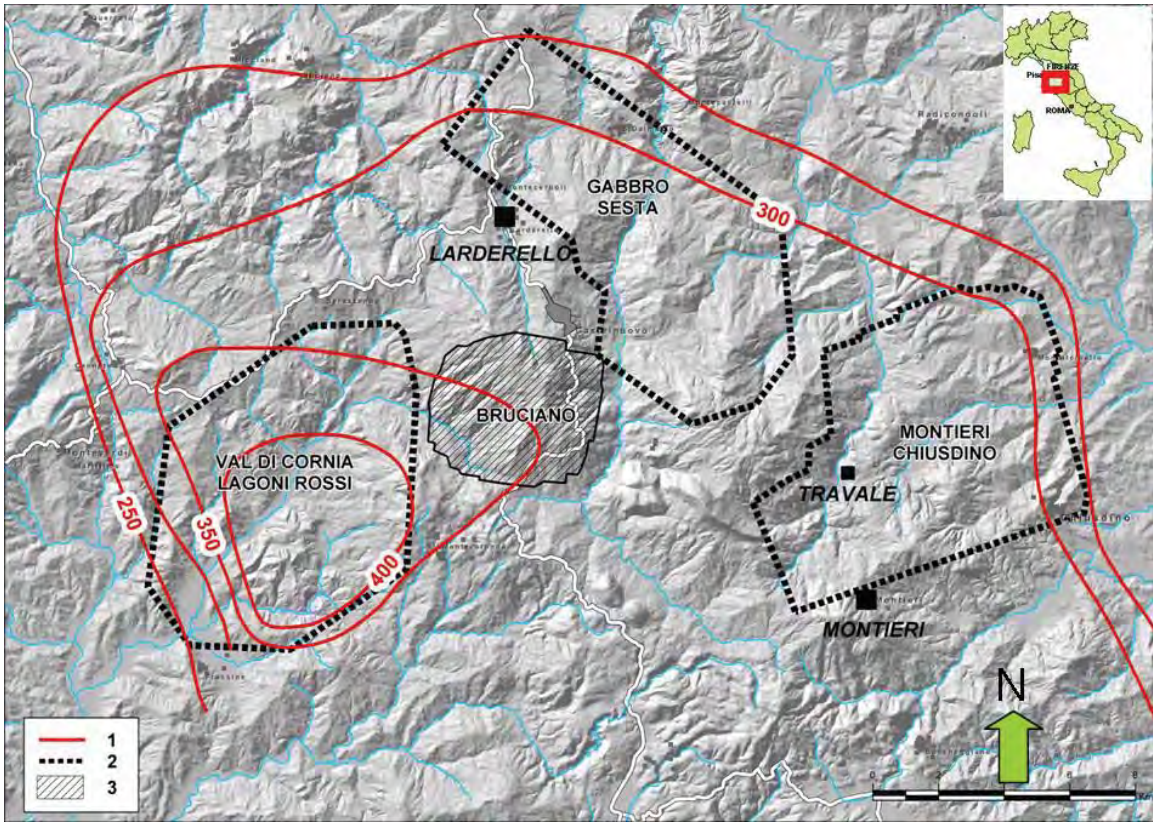

Figure 1: Larderello-Travale area. 1) Isotherms at 3000 m b.s.l.; 2) New 3D seismic surveys; 3) Previous 3D seismic survey.

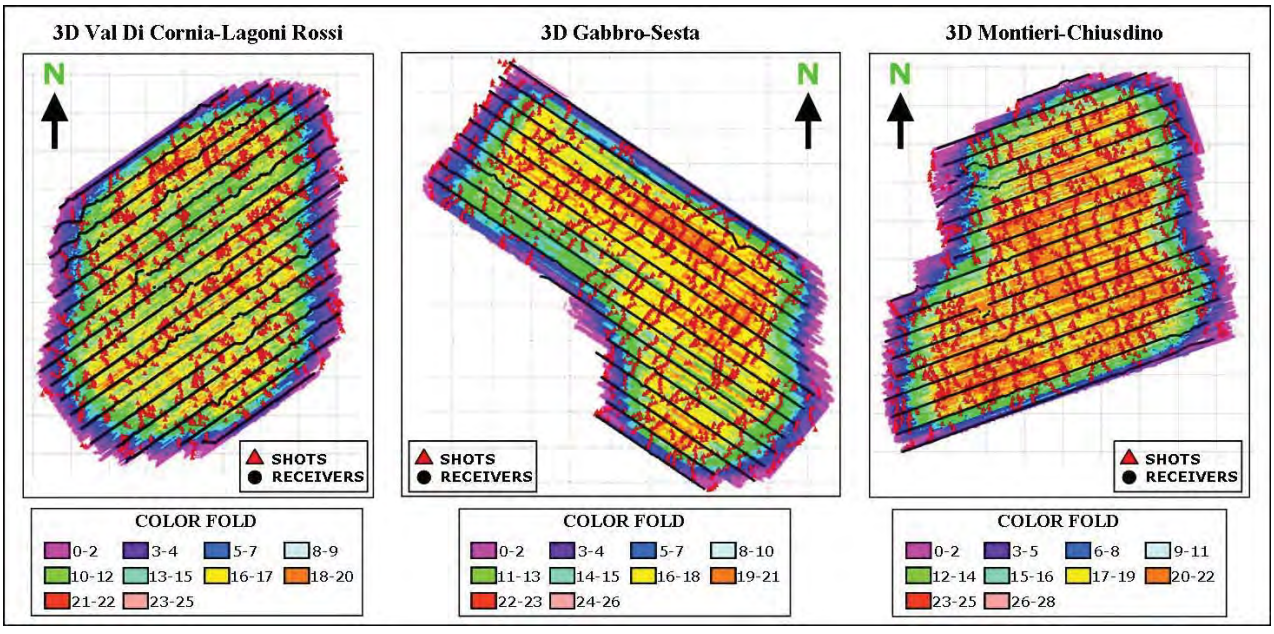

Figure 2: Actual acquisition layout and fold distribution in all the surveyed areas.

2.2 Processing

The same processing sequence was adopted for the three surveys in order to produce homogeneous data and possibly to attempt statistical seismic attribute analysis on the main seismic horizons. To this end, special care was devoted at recovering the true amplitudes of the seismic signals. The complete processing sequence is listed in Table 1.

Table 1: Processing sequence

PROCESSING SEQUENCE
Geometry assignment and bad traces removal
Statistical despiking
Band pass filter (4-8-70-80 Hz)
Refraction statics
Spherical divergence amplitude recovery
Surface consistent amplitude compensation
FX deconvolution in common shot domain
Predictive deconvolution
Velocity analysis
Selection and removal of noisy traces on the carbonate outcrop
Surface consistent residual statics
Refinement of the velocity field
Bin consistent residual statics
NMO and Stack
FXY Deconvolution
Post stack Kirchoff time migration

The whole Larderello-Travale area shows a strong variability in elevations (from 200 to 1000 m a.s.l.) and high lateral variations in the surface velocities. These characteristics requested a particular attention in the computation of statics and residual statics, and in the velocity analysis. The amplitude preserving approach suggested a limited use of multichannel filtering and of any operation which might cause artifacts. Offset dependent geometrical spreading and surface consistent amplitude correction contributed to restore the correct signal amplitude.

Local outcrops of carbonate formations required an additional processing step since they produced a strong energy absorption that affected the data down to the deep seismic markers. The removal of the noisy traces generated by both source and receiver placed on the carbonate outcrops was the adopted solution that improved the lateral continuity of the signals.

Due to the complexity and the high P-wave velocities peculiar to the geological bodies of the investigated areas, only a post stack Kirchoff time migration was applied. The adopted migration velocities were derived from the stacking velocity field after severe smoothing and reduction of the values. However, the final data obtained for the three surveys allowed the identification of the main deep seismic horizons (H and K) already evidenced by previous 2D seismic lines, (Cameli et al. 1994, Fiordelisi et al., 2005), in the whole Larderello - Travale area (Figure 3).

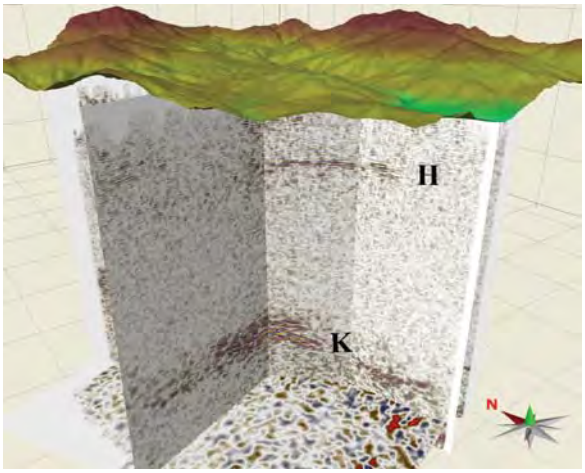

Figure 3: Three-dimensional view of the main seismic markers (H and K) evidenced in one of the 3D seismic volume.

2.3 Interpretation

The integrated interpretation of the 3D seismic with all the geological, geophysical, and well data allowed the update of the geological/structural model for the whole geothermal area and the identification of potential drilling targets. The interpretation was initially addressed to improve the structural reconstruction of the main geological horizons (Figure 4) and in particular the cap rocks formations (Neogene sediments and Liguridi Complex), the top of the Metamorphic basement (represented by phyllites, michaschists and gneiss), and the top of Pliocenic granites.

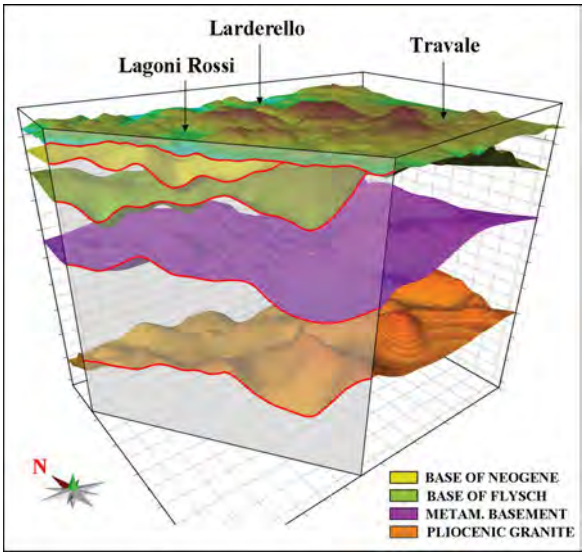

Figure 4: 3D reconstruction of the main geological horizons in the Larderello-Travale area.

The interpretation also allowed a detailed reconstruction of the strongest and deepest seismic markers H and K. The first one is located inside the metamorphic basement at about 0.6-1.4 s TWT. Although present over the entire Larderello-Travale area, it is discontinuous and its meaning can vary depending on different geological settings. On the contrary, the deepest K marker is quite continuous and shows the highest amplitude signals.

In the SE portion of the geothermal system, as testified by the wells, the Pliocene intrusions reach the shallower levels and the H marker is the expression of a contact

metamorphic aureole. In the central area, where the intrusions are supposed to be deeper, the H marker corresponds to levels of skarn/hornfels underlying the presence of thin granites dikes. Finally in the western sector of the field, the H and K markers are almost in vertical continuity and it is difficult to distinguish one from the other. The K marker was never met by drillings and was entirely reconstructed by means of seismic interpretation. This horizon always runs below the top of the old granites (Pliocenic) at about 1.2 - 4s TWT. In a schematic geological model (Figure 5) this horizon was interpreted as a deeper, hotter and more recent (Quaternary) intrusion that embraces the entire Larderello-Travale geothermal field and could also control the temperature distribution with depth (Bertini et al., 2005, Bertini et al., 2006). In particular, the hypothetical 400°C isotherm is supposed to be coincident with the K horizon.

The second phase of the interpretation was aimed at the detection of potential drilling targets and was focused on the H marker. In fact, the high amplitude seismic signals characterizing this horizon can be correlated to fractured levels and hence to promising productive horizons.

For this reason a detailed picking of the H marker, both for the top and for the bottom, was performed to define its 3D structure (Figure 6) and to compute the RMS amplitude map for all the available 3D dataset (Figure 7).

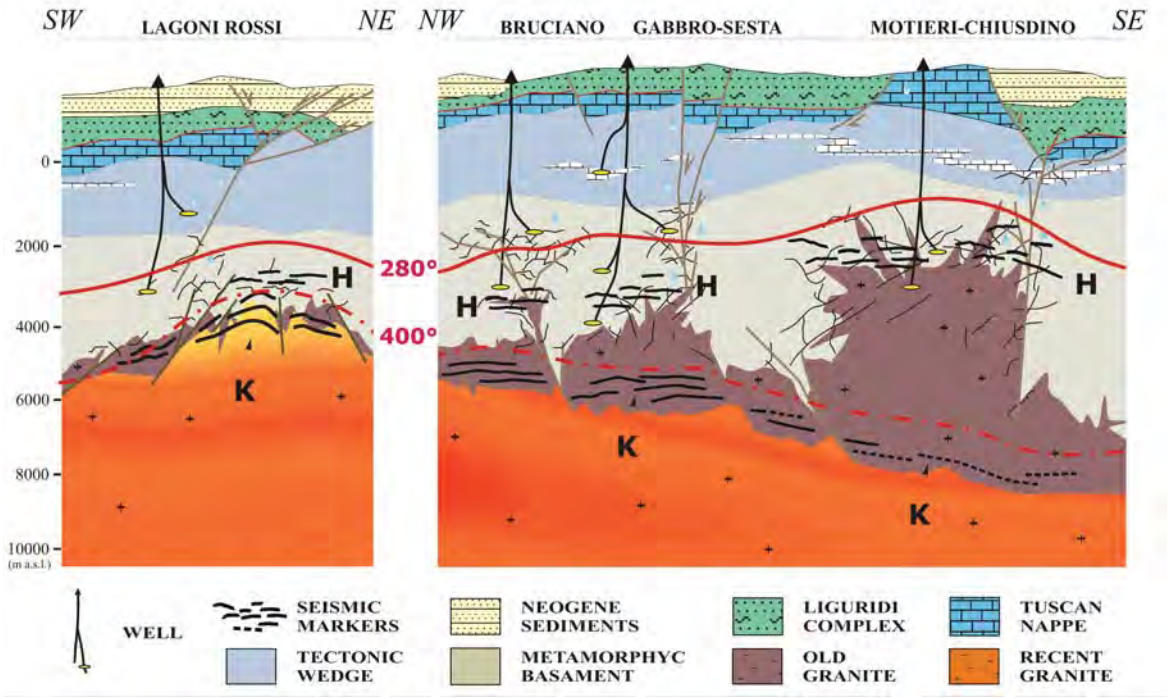

Figure 5: Schematic model of the whole geothermal system.

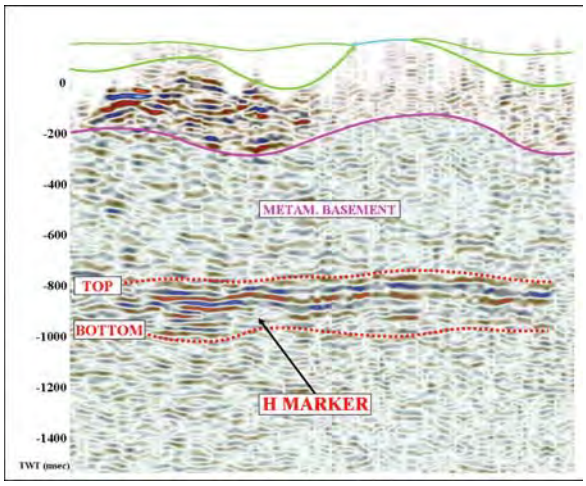

Figure 6: Random line extracted from 3D seismic volume showing the seismic signal corresponding to the H marker within the metamorphic basement.

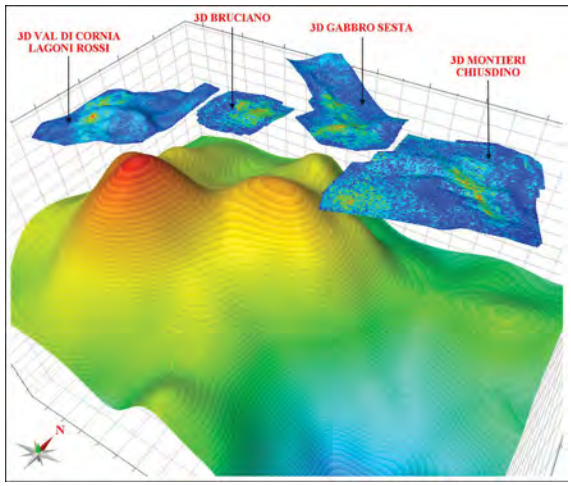

Figure 7: 3D view of the H marker top, with RMS amplitude maps computed for all the seismic surveys, and of the deeper K marker.

The most promising areas, which as above said are characterized by the highest amplitude values, were identified and indicated as potential targets for the deep drillings (Figure 8).

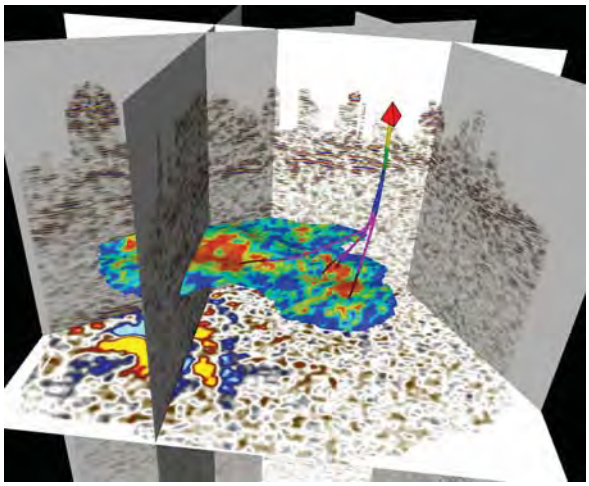

Figure 8: Example of high RMS amplitude values (red color) at the top of the H horizons and deep well profiles.

3. MAIN RESULTS

The experience acquired in more than 30 years of seismic data interpretation in the Larderello area proved that the H marker is often characterized by the coexistence of a high degree of fracturing and of local lithology variations. The meaning of this horizon, as a potential geothermal target, changes according to the geological-structural and thermobaric conditions of the field. In this framework, the emplacement of granites, their age and the geologic context of the host rock play a prominent role.

At the present, the H marker is the main seismic target identified in the Larderello-Travale geothermal system. On the basis of this deep target, ten wells have been drilled in all the 3D seismic areas and confirmed the strong relationship between the seismic reflections of the H horizon and the presence of fractured levels.

The RMS amplitude anomalies were helpful to detect, inside the H marker, more reliable potential targets prior to drilling. Indeed, well data have shown that although a correlation exists between seismic signal characteristics and the presence of fractured levels, there is no certain relationship with the degree of permeability of the fractured rocks. In other words, the productivity of a geothermal target cannot be evaluated on the base of the amplitude of the seismic signal.

From an industrial point of view, the best results were obtained in the Travale area (Montieri-Chiusdino 3D survey), where the H horizon corresponds to a wide contact metamorphic aureole. Well data evidenced the local increase of permeability and fracture occurrence characterizing this marker could be due to dissolution and hydrofracturing processes associated with over-pressured fluids released during the intrusion cooling phase.

In this area all the wells that crossed this seismic reflector were productive. Moreover, the correlation between fractures and seismic markers evidenced that more than 70% of fractured levels occurs within the H horizon (Figure 9).

A good correlation between H marker and fractured levels was verified also in the Gabbro-Sesta and Bruciano 3D surveyed areas (Figure 10). In this central area of the wide Larderello-Travale system the H marker is associated to thin levels of skarn and hornfels that are characterized by local increases of fractures and permeability. A quantitative study on the productivity of the H marker is ongoing for both areas.

In the western area (Val di Cornia – Lagoni Rossi), the lack of deep well data did not allow any direct correlation. In any case, the identification of the H marker as the potential target is affected by several uncertainties arising from the complex structural situation. In fact, the single well that probably reached the seismic horizon was stopped for a near blow-out occurred while drilling (Batini et al., 1983).

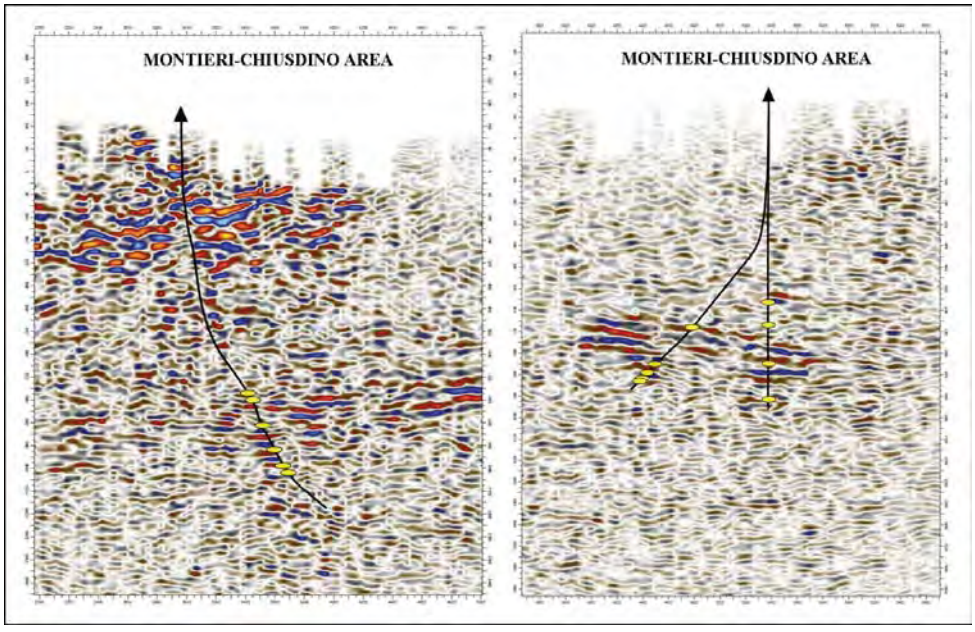

Figure 9: Example of some wells crossing the H marker in the Travale area. In yellow color the productive fractures.

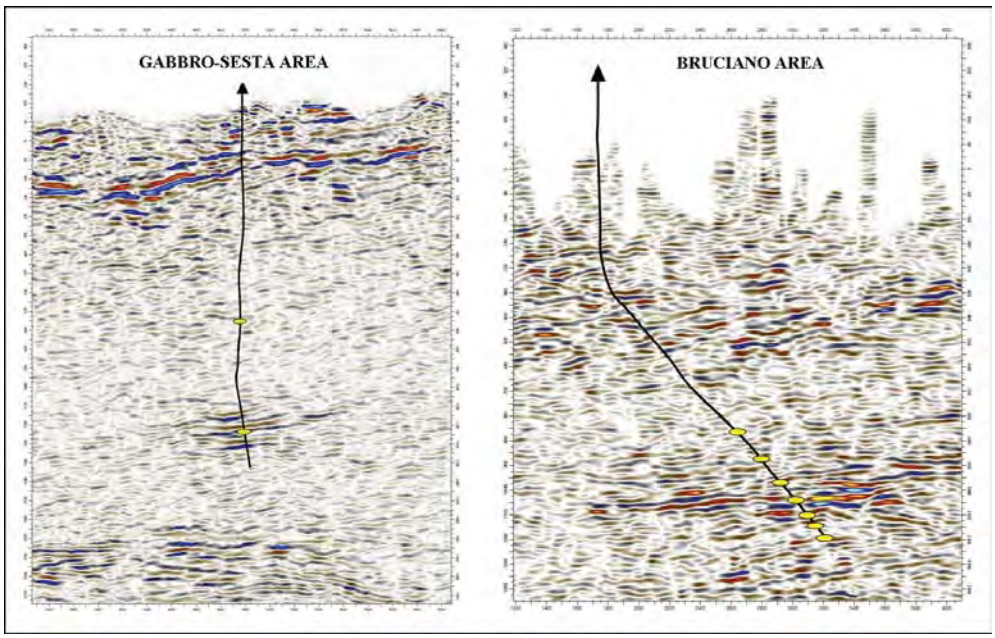

Figure 10: Example of some wells crossing the H marker in the central areas of the geothermal field. In yellow color the productive fractures.

In this area, the deeper K marker reaches its maximum apex (3000 m a.s.l.) and the relevant seismic reflections result to be often in vertical continuity with the above H marker (Figure 11). Thus, it is difficult to distinguish the two horizons and to characterize the seismic target. Furthermore, the thermobaric hostile conditions hypothesized in this area (> 400°C and 300 bars) do not seem to be compatible with the known geothermal reservoir so far exploited. In addition, the safety risks connected to a deep exploration are very prominent.

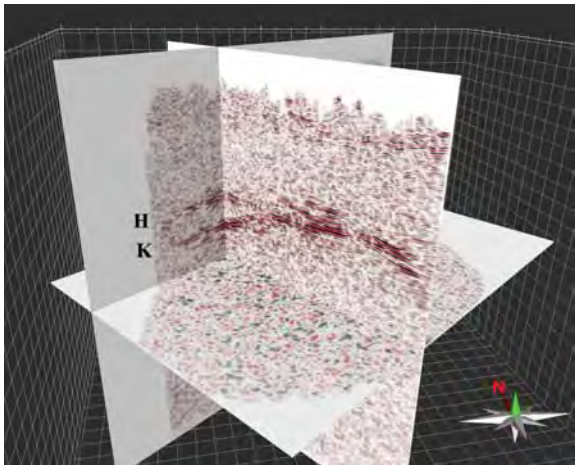

Figure 11: 3D view of the H and K markers in the Val di Cornia – Lagoni Rossi surveyed area.

Therefore, the good correlation between fractured systems, productive levels and seismic markers verified for the central and eastern areas could not be confirmed for the western one.

4. CONCLUSION

The availability of 3D seismic surveys and well data contributed to improve the understanding of the geological and structural context of the whole Larderello-Travale geothermal system.

The interpretation of the seismic volumes evidenced the H marker as the main seismic target identified in the area. It generally corresponds to the metamorphic aureole produced by the Pliocenic granitic intrusions. This marker is very often associated to the presence of fractured and productive levels, and its permeability seems to be related with the granite emplacement.

Amplitude analysis carried out on the H marker signals allowed the identification of drilling targets characterized by the presence of fractured levels. However, the relationship between seismic signal amplitudes and degree of permeability/productivity is more difficult to ascertain and it seems to vary for different areas. The best results have been obtained in the Travale area where more than 70% of steam production originates from depth intervals within this horizon.

REFERENCES

Barelli, A., Cappetti, G. and Stefani, G.: Results of deep drilling in the Larderello-Travale/Radicondoli geothermal area, *Proceedings* World Geothermal Congress, Vol. 2, pp. 1275-1278, Florence, Italy (1995)

Barelli, A., Bertini, G., Buonasorte, G., Cappetti, G., and Fiordelisi, A.: Recent deep exploration results at the margins of the Larderello-Travale geothermal system, *Proceedings* World Geothermal Congress, n. B6-2, (2000).

Batini, F., Bertini G., Bottari A., Burgassi P.D., Cappetti G., Gianelli G. and Puxeddu M.: S.Pompeo 2 deep well: a high-temperature and high-pressure geothermal system. 3rd Int. Sem., Geoth. Update, Eur. Comm., Munich, EUR 8853 EN, 341-353. (1983a).

Batini, F. and Nicolich, R.: The application of seismic reflection methods to geothermal exploration, *U.N. Seminar* on Utilization of geothermal energy for

electric power production and space heating. Florence, Italy (1984).

Bertani, R., Bertini, G., Cappetti, G., Fiordelisi, A., and Marocco B.M.: An update of the Larderello-Travale/Radicondoli deep geothermal system, *Proceedings* World Geothermal Congress, (2005).

Bertini, G., Casini, M., Ciulli, B., Ciuffi S., and Fiordelisi, A.: Data revision and upgrading of the structural model of the Travale Geothermal Field, *Proceedings* World Geothermal Congress, (2005).

Bertini, G., Casini, M., Gianelli, G., and Pandeli, E.: Geological structure of a long-living geothermal system, Larderello, Italy, *Terra Nova*, 00, 1-7 (2006)

Cameli, G.M., Ceccarelli, A., Dini, I. and Mazzotti, A.: Contribution of seismic reflection method to the location of deep fractured levels in the geothermal fields of Southern Tuscany (Italy), *Proceedings* World Geothermal Congress, n. B6-3, (2000).

Cappetti, G., Fiordelisi, A., Casini, M., Ciuffi, S., Mazzotti, A.: A new deep exploration program and preliminary results of a 3D seismic survey in the Larderello-Travale geothermal field (Italy), *Proceedings* World Geothermal Congress, (2005).

Fiordelisi, A., Moffat, J., Ogliani, F., Casini, M., Ciuffi, S., Romi, A.: Revised processing and interpretation of reflection seismic data in the Travale geothermal area (Italy), *Proceedings* World Geothermal Congress, (2005).

Mazzotti, A., Zamboni, E., Stucchi, E., and Ciuffi, S.: Seismic characterization of Geothermal Reservoir: a case study in Western Tuscany, Italy, *64th EAGE Conference and Exhibition*, Extended Abstract, Vol. I. n. C-37 (2002).

Proceedings World Geothermal Congress 2000
Kyushu - Tohoku, Japan, May 28 - June 10, 2000

RECENT DEEP EXPLORATION RESULTS AT THE MARGINS OF THE LARDERELLO TRAVALE GEOTHERMAL SYSTEM

Antonio Barelli, Giovanni Bertini, Giorgio Buonasorte, Guido Cappetti and Adolfo Fiordelisi
ERGA ENEL Group, via Andrea Pisano 121 56122 Pisa Italy

Key Words, Larderello-Travale geothermal field, granitic intrusion, exploration strategy

ABSTRACT

Within the framework of research in the marginal areas of the Larderello–Travale geothermal system, several exploration wells have disclosed an extension of the deep reservoir even below zones of medium or low superficial thermal anomaly.
NE of the Larderello field, Sesta_6bis well crossed a known low temperature (100°C) CO_2 saturated carbonate aquifer, but, at greater depth, in the phyllitic metamorphic basement, a steam reservoir has been discovered at 2400–2800 m. The temperature and pressure are similar to those recorded at the Travale field (300°C and 70 bar).
Two other wells have been drilled in the area south of Travale characterized by large outcrops of permeable carbonate rocks. These constitute the shallow reservoir, bearing fresh meteoric waters, which mask any deeper thermal information. The well Travale Sud_1 crossed several steam productive layers between 2280 and 2890 m in thermometamorphic and granitic rocks. The reservoir temperature and pressure are 300°C and 70 bar. The well Montieri_4 crossed a thick carbonate sequence and then a granitic body from 2000 m to the bottom hole (3700 m), with rather low permeability but with the same temperature and pressure as the deep Travale reservoir. Surprisingly, injection and acidification tests have improved the hydraulic connection with the reservoir.
All the above-mentioned exploration wells have proved to be productive and confirmed the extension of the deep steam-dominated reservoir in marginal areas where the superficial thermal gradient is low.
The deep reservoir is located at a depth of about 3 km inside the metamorphic basement and the granitic body. On the basis of these results, the exploration has been extended and specific development projects have been planned.

1. INTRODUCTION

The deep exploration in the Larderello and Travale geothermal fields revealed the presence of a deeper reservoir at depths ranging from 3000 to 4000 m with a pressure of up to 70 bar and temperatures between 300 and 350 °C (Barelli et al., 1995).
Only one great deep thermal anomaly has been found under the shallow carbonate reservoir and is common to both the Travale and the Larderello geothermal fields (Fig. 1).
The deep reservoir is located inside the metamorphic rocks of the basement, made up of phyllites, micaschists and gneiss.
The metamorphic basement and the overlying calcareous-anhydrite formations constitute a structural high (Bertini et al., 1994) which, although characterized by high density rocks (about 2.7 g/cm^3), falls into a wide negative gravimetric anomaly (Fig.2).
To reproduce this anomaly, 2D gravimetric models require the presence of low density bodies (2.45 g/cm^3), interpreted as granite intrusions at depths ranging between 8 and 12 km (Baldi et al., 1995). This value of density seems to suggest that the granite bodies have temperatures of 800°C and are partially molten (Bottinga and Weill, 1970).
Also of geothermal interest is the seismic marker "K" (Batini and Nicolich, 1984) found at depths between 3 and 7 km and showing a clear correlation with the above-mentioned minimum gravimetric anomaly (see Fig. 2). This marker may indicate a zone of brittle/ductile transition of the rheologic behavior of the rocks because of the temperature (Cameli et al., 1993). Some deep thermal data provide evidence that temperatures of 400–450°C, with lithostatic pressure of about 1 kbar may characterize this marker.
Although characterized by permeable shallow structures and therefore by cold or moderately hot aquifers, the northern and eastern margins of the Larderello-Travale geothermal system are within a great deep thermal anomaly, which may be correlated to the negative gravimetric anomaly and to the structure of the deep seismic marker (K).
The two new areas of Sesta and Chiusdino-Montieri were therefore chosen and over the last five years three wells (Sesta_6bis; Travale Sud_1; and Montieri_4) have been drilled with the aim of extending exploration to the eastern margin of the whole Larderello-Travale geothermal area.
The Sesta area is situated at the eastern border of the Larderello field where the shallow geothermal reservoir is characterized by a moderately hot aquifer (approx. 120°C) with a gas cap.
The Chiusdino–Montieri area, to the south of the Travale field, is characterized by wide outcrops of carbonate-anhydrite rocks, which, on account of their high permeability, may locally represent areas of natural recharging of the geothermal reservoir.

2. DRILLING RESULTS

The location of the exploratory wells must also take into account environmental aspects and acceptability by local administration and inhabitants (we are working in Tuscany).
Preference is given to areas where exploitation is possible and new geothermoelectric power plants can be installed.

2.1 Well Sesta_6bis

The Sesta_6bis well (total depth 3921 m) is located in the western neogenic margin of Radicondoli–Chiusdino, representing the most evident tectonic structure east of the geothermal field of Larderello. This structure is bordered by a system of NW–SE trending faults which also crosses the geothermal field of Travale (Lazzarotto and Mazzanti, 1978).
Preliminary detailed geophysical surveys allowed an accurate location of the well so as to avoid crossing the gas accumulation on top of the shallow geothermal reservoir.
From a geological viewpoint, the Sesta_6bis well crossed 250 m of neogenic sediments and 310 m of flysch facies formations.
At the depth of 560 m, and consistent with the interpretation of geophysical data, the well crossed the tectonic contact

between the cover formations and the underlying Triassic carbonate-anhydrite formations. These are intercalated with phyllites and Triassic-Paleozoic quartzite and constitute the sequence of the Tectonic Wedges (Pandeli et al., 1991).
The well was drilled through these formations, about 1330 m thick, without encountering any significant permeable levels, but a total loss of circulation (TLC) occurred at the depth of 2363 m. A stratigraphic reconstruction below the TLC was performed on the basis of mechanical coring and geophysical logs.
The underlying metamorphic formations met at the depth of 1890 m are made of chlorite–graphitic phyllites with intercalation of limestone (2745-2860 m of depth) and paragneiss. High temperature hornfels are located at bottom hole (3921 m).
The direct contact between phyllites and paragneiss with the absence of micashists is due to a low-angle normal fault towards E-NE (Fig. 3).
Thermometamorphic biotite (400°C) was observed above the fracture at 2363 m, where TLC occurred, but was found to be absent in the underlying cores. The biotite might have resulted from a previous circulation of magmatic fluids, uprising through hydro-fractured systems (Gianelli and Bertini 1993; Gianelli and Ruggeri 1999).
The presence of a subsequent hydrothermal phase, with temperatures higher than 300°C, is indicated by epidote deposits.
The thermal profile of the well (Fig. 4) is characterized by a constant gradient of around 120°C/km down to 2363 m.
Temperatures in the final part of the well were measured according to the fluid temperature recorded at the wellhead during production tests.
The fracture at 2363 m is characterized by injectivity of 5-6 m^3/h/bar and steam pressure of about 50 bar.
Other fractures are present at 3120 m, 3375 m and in the section 3600-3720 m, with injectivity of about 2.5 m^3/h/bar, temperatures of 300°C and steam pressure of about 70 bar.
Extensive production tests have shown that this well may produce about 35 t/h of dry steam with a non-condensable gas content of about 8.5% by weight.

2.2 Well Travale Sud _1

The well Travale Sud_1 (total depth 2897 m) is located approximately 4 Km SE of the Travale exploited area, where wide outcrops of the carbonate-anhydrite formations hosting a cold meteoric aquifer are present.
The well cut these formations, with the thickness of 455 m, and underlying sequence of the Tectonic Wedges, down to 1630 m, made up of Paleozoic phyllites with intercalation of anhydrite. From 1630 m down to a TLC, found at a depth of 2228 m, the metamorphic basement is present. This consists of phyllites, thermometamorphic and carbonate metasomatic rocks (Skarn) with thin veins of granite composition.
The stratigraphic sequence from 2228 m down to bottom hole has been reconstructed by means of mechanical coring, geophysical logs and vertical seismic profile (VSP) which, at a depth of 2400 m, allowed the identification of the top of the thermometamorphic aureole (Andalusite). Geophysical logs (Gamma Ray and VSP) also evidenced an underlying granite intrusion at a depth of 2680 m.
Except for the shallow part, which is affected by the circulation of meteoric waters, the temperature profile of this well is characterized by a conductive gradient between 120 and 150°C/km to the TLC at 2228 m where a temperature of about 300°C has been recorded (see Fig. 4).
Well testing showed that the main productive fracture is at 2420 m with injectivity of 5 m^3/h/bar and reservoir pressure of about 70 bar.
Preliminary production tests have indicated that the Travale Sud_1 well could produce approx. 50 t/h of steam with a wellhead pressure of 30 bar.

2.3 Well Montieri_4.

The Montieri_4 well (total depth 3721 m) is also located near the wide outcrops of the cold shallow reservoir rocks.
After 100 m of shale of the Flysch Nappe the well was drilled through a 1000 m thick sequence of the Tectonic Wedges, consisting of dolomitic limestone and Triassic anhydrite.
The underlying metamorphic basement consists of chlorite–graphite phyllites, presenting thermometamorfic biotite from a depth of approximately 1300 m, and horn fells from about 1900 m.
A granite body, which is highly hydrothermalised in the first 1000 m with formations of chlorite and epidote, extended to a depth of 2000 m.
The thermal profile (see Fig.4) in the first 1000 m, corresponding to the sequence of the Tectonic Wedges, shows a low geothermal gradient consistent with the presence of gypsum and calcite deposits in the fractures, providing evidence of low temperature fluid circulation.
The geothermal gradient in the basement increases up to around 150°C/km and remains unchanged as it crosses the thermometamorphic rocks (horn fells) and the underlying granite intrusion.
Between 2200 and 2740 m the geothermal gradient decreases due to permeability in the granite, indicated by several occurrences of circulation loss and the spread hydrothermal alteration. Fluid inclusions in the chlorite mineralisations provide evidence for the circulation of low salinity hydrothermal fluids (5wt% NaCl) at the temperature of 310–370°C.
Further, but modest, loss of circulation is present down to the depth of 3530 m, where a TLC has occurred.
The main fractures, which were tested during drilling, had initially low of injectivity (0.2-0.7 m^3/h/bar). Several acidification tests (mixtures of HF-HCl) were therefore performed, resulting in a large increase in injectivity. In particular, the fracture at 2880 m is characterized by an injectivity of 5 m^3/h/bar, a reservoir pressure of about 60 bar and temperature of 300°C.
A production test was carried out for some days, and a steam flow rate of about 50 t/h was measured. Unfortunately, the well collapsed close to the production horizons and a repair operation is being planned.

3. CONCLUSIONS

Larderello and Travale have been chosen as exploration areas because of their structure and geothermal features, and also on the basis of environmental evaluations and acceptability, as well as to guarantee the feasibility of the development projects.
The exploration wells Sesta_6bis, Travale Sud_1 and Montieri_4 have confirmed the presence of deep reservoirs with temperatures of 300–330°C and pressures of 50-70 bar.
In particular, the well Sesta_6bis, although drilled where reservoir with low to medium temperatures is found at

shallow depths, has verified the continuity of the deep reservoir between the geothermal fields of Larderello and Travale. The main fracture of the well Sesta_6bis (2370 m) is probably related to a system of hydrofractures of magmatic origin. Therefore, this aquifer probably represents an up-flow of the underlying geothermal reservoir, at a depth of approximately 3100 m.

Both the wells Travale Sud_1 and Montieri_4 have confirmed the presence of deep reservoirs at the southeastern margin of the Travale field, underneath the carbonate-anhydride outcrops containing cold meteoric waters. This provides new opportunities for further exploration south of the Larderello-Travale geothermal field.

The reservoir encountered by the well Travale Sud_1 is found inside a wide contact metamorphic aureole and inside the upper part of a granite intrusion.

The deep reservoir of Montieri_4 is characterized by fractures widely distributed in a granite intrusion. Pressure and temperature are similar to those recorded in the other wells. Acidification operations have considerably increased the permeability of these fractures.

The presence of geothermal reservoirs inside granite intrusions is the main knowledge gained by the wells Montieri_4 and Travale Sud_1.

The positive results of these exploratory wells have allowed the implementation of development projects. Directional wells will be drilled in order to minimize the drilling sites, and, consequently, the environmental impact. Two units, 20 MW each, will be installed in the area and supplied additional wells.

REFERENCES

Baldi, P., Bellani, S., Ceccarelli, A., Fiordelisi, A., Rocchi, G., Squarci, P. and Taffi, L., (1995). Geothermal anomalies and structural features of southern Tuscany (Italy). *Proc. of World Geothermal Congress*, Vol. 2, pp. 1287-1291.

Barelli, A., Cappetti, G. and Stefani, G., (1995). Results of deep drilling in the Larderello-Travale/Radicondoli geothermal area. *Proc. of World Geothermal Congress*, Vol. 2, pp. 1275-1278.

Batini, F. and Nicolich, R., (1984). The application of seismic reflection methods to geothermal exploration. *U.N. Seminar on Utilization of Geothermal Energy for Electric Power Production and Space Heating*, Florence (Italy).

Bertini, G., Elter, F.M. and Talarico, F., (1994). Evidenze di una fase estensionale pre-triassica nel complesso degli gneiss nell'area geotermica di Larderello (Toscana Meridionale). *Studi Geologici Camerti*, Vol. 1994/1, pp. 129-137.

Bottinga, Y. and Weill, D.F., (1970). Densities of liquid silicate systems calculated from partial molar volumes of oxide components. *Am. J. Sci.*, Vol. 269, pp. 169-182.

Cameli, G.M., Dini, I. and Liotta, D., (1993). Upper Crustal structure of the Larderello geothermal field as a feature of post-collisional extensional tectonics (Southern Tuscany, Italy). *Tectonophysics*, Vol. 224, pp. 413-424.

Gianelli, G and Bertini,G. (1993). Natural hydraulic fracturing in the Larderello geothermal field: evidence from well MV_5A. *Boll.Soc. Geol. Ital*. Vol. 112, pp. 507-512

Gianelli, G and Ruggeri, G. (1999). Multi-stage fluid circulation in a Hydraulic fracture breccia of the Larderello geothermal field (Italy). *J. Volcanol. Geotherm. Res.* Vol. 90, pp. 241-261.

Lazzarotto, A. and Mazzanti, R. (1978). Geologia dell'alta Val di Cecina. *Boll. Soc. Geol. It.*, Vol. 95/6, pp. 1365-1487.

Pandeli, E., Bertini, G. and Castellucci, P., (1991). The tectonic wedges complex of the Larderello area (Southern Tuscany, Italy). *Boll. Soc. Geol. It.*, Vol. 110, pp. 621-629.

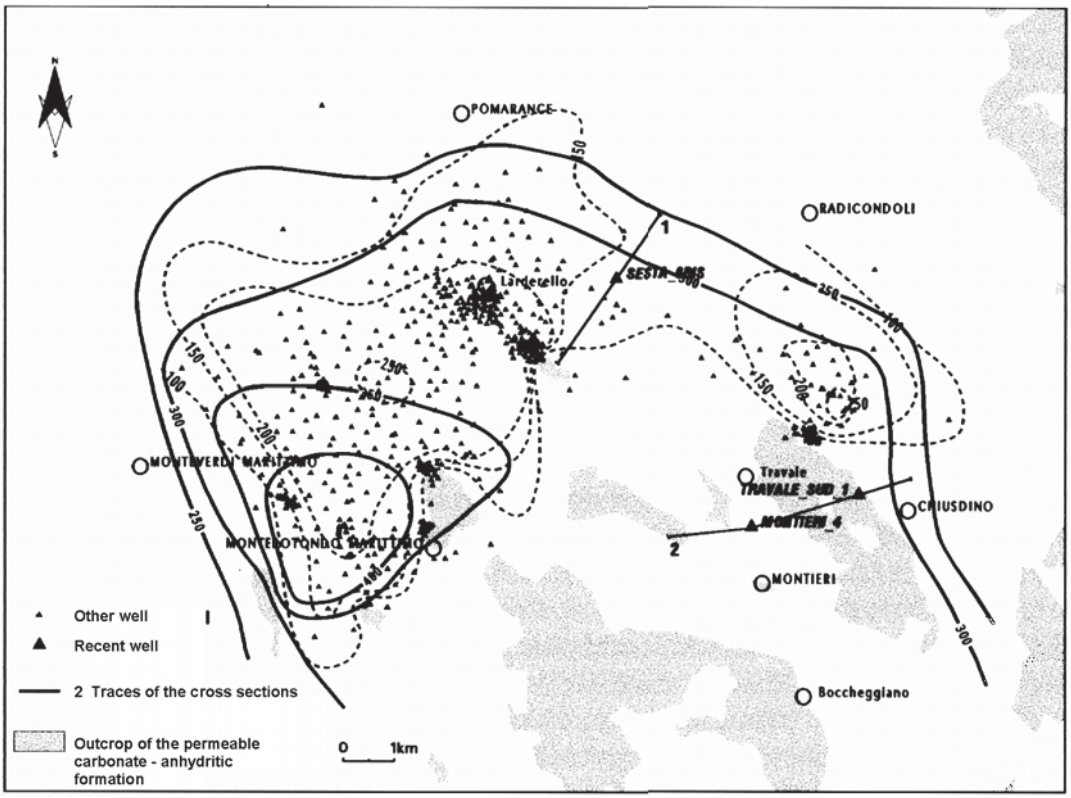

Fig. 1 - Temperature distribution at the reservoir top (dashed line) and at depth of 3000 m b.s.l. (continous line).

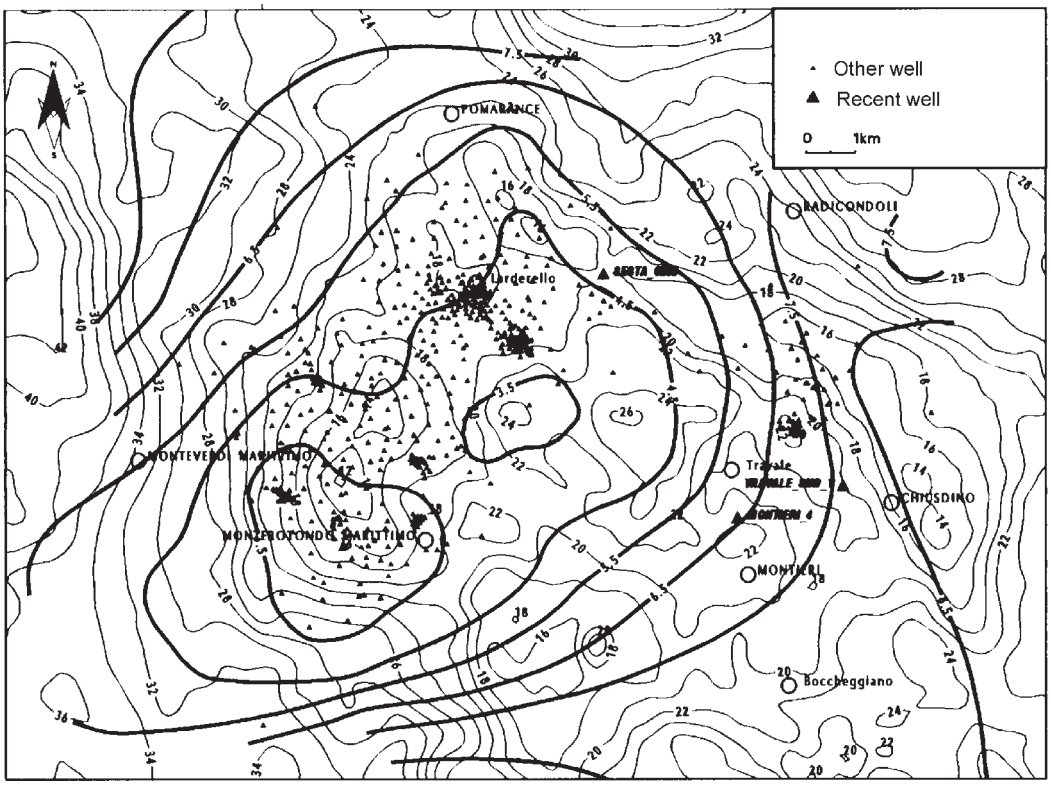

Fig. 2 - Map of the gravimetric Bouguer anomaly (fine line in mgal) and of the top of the seismic marker "K" (bold line in Km b.s.l.).

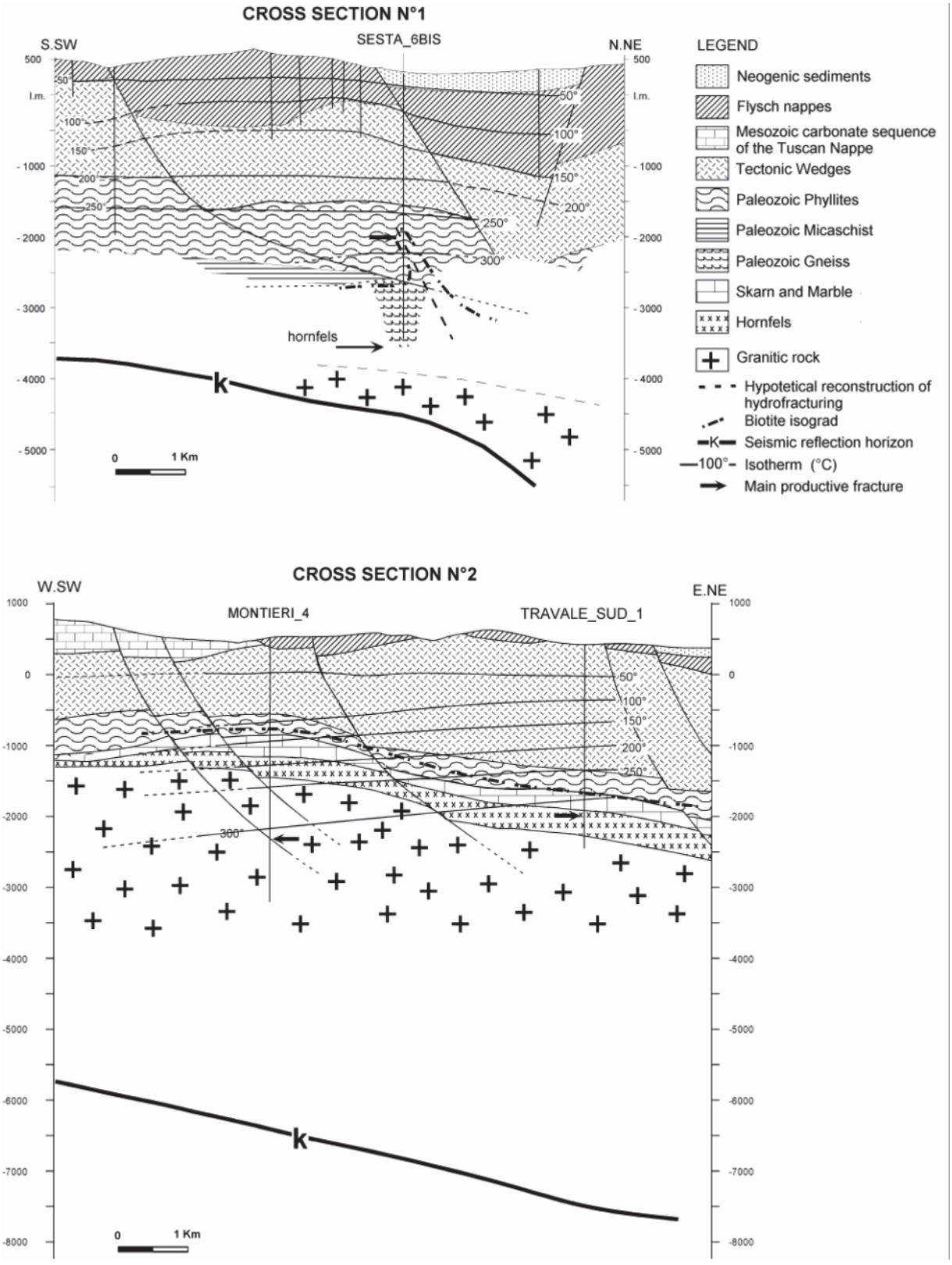

Fig. 3 Schematic geological cross sections through SESTA (N° 1) and MONTIERI - CHIUSDINO (N° 2) exploration areas. (Traces on fig. 1)

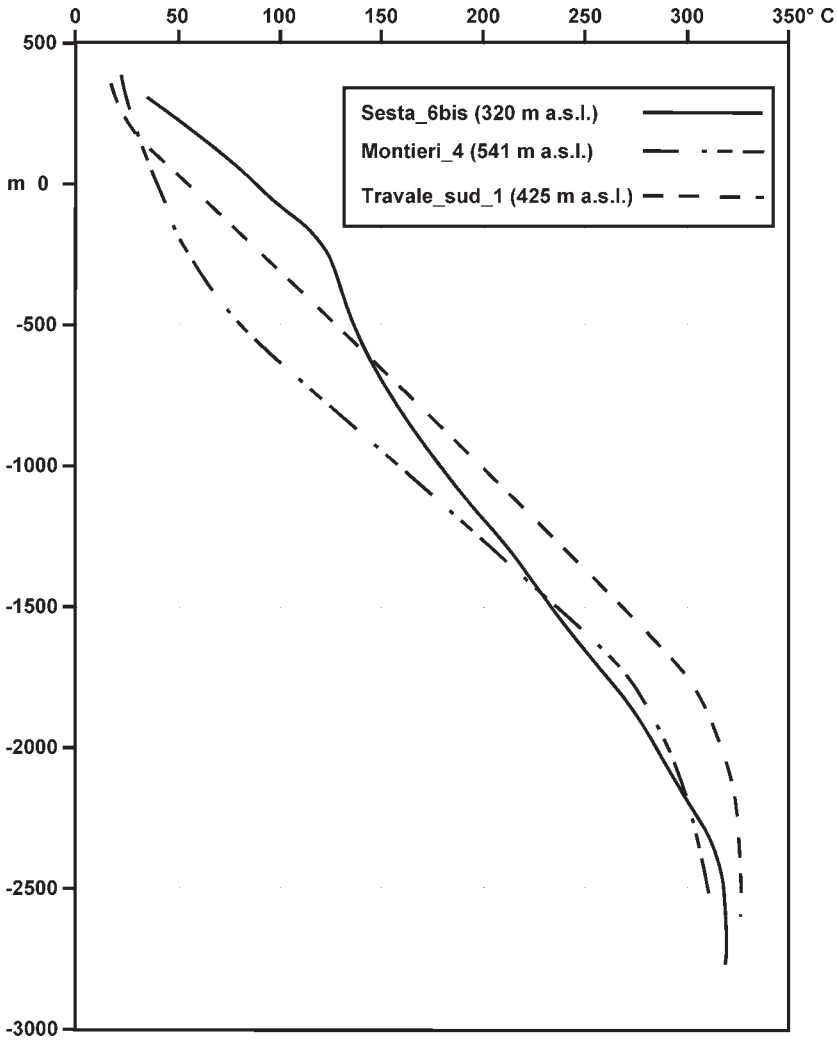

Fig. 4 Temperature versus depth in the exploration geothermal wells.

PROCEEDINGS, Twenty-Seventh Workshop on Geothermal Reservoir Engineering
Stanford University, Stanford, California, January 28-30, 2002
SGP-TR-171

GEOPHYSICAL WELL LOGGING- A CONTRIBUTION TO THE FRACTURES CHARACTERIZATION.

F. Batini, R. Bertani, B. Ciulli, A. Fiordelisi and P. Valenti

Enel Green Power
Pisa, 56100, Italy
e-mail: batini.fausto@enel.it, bertani.ruggero@enel.it,
ciulli.barbara@enel.it, fiordelisi.adolfo@enel.it, valenti.piero@enel.it

ABSTRACT

The need of a proper reconstruction of faults and fracture systems crossed during the well drilling is one of the most important feature for the deep exploration of a geothermal reservoir.
The geophysical well logging have been always utilized for geological and stratigraphic determinations, for the measurement of the main physical characteristics in order to provide calibration parameters for the surface geophysical surveys and for a qualitative localization of fractured and potential productive layers. Recent and specialized techniques and sensors for the detection of geometrical-structural parameters are now widely used.
One of them, the Circumferential Borehole Imaging Log (CBIL), when utilized for potential fractured layers already tagged by other techniques (as acoustic Wave Forms), has been proved as very effective and detailed.
We applied a complete set of this techniques in a deep well of the Larderello-Travale geothermal field, and a detailed analysis and characterization of the fractures was performed. The standard well-testing procedure was also applied, in order to match the results from the different approaches. A satisfactory correspondence was achieved. A preliminary comparison between the geometrical parameters of the fractures and their productivity was also carried out.

INTRODUCTION

In the last 30-35 years the geothermal exploration in Italy has gradually changed its targets.
Up to the mid 70's, the average depth of the geothermal wells was of about 1000 m, with the aim to reach a first and shallow reservoir hosted in a carbonate-anhydrite formation. This reservoir is characterized by a very high permeability due to a wide and diffuse system of fractures.
Subsequently, in order to increase the energy production from geothermal resources, a program of deep exploration started in the Larderello and Travale areas, the oldest Italian geothermal fields.
The average depth of the deep wells generally varies between 3000 and 3500 m, but in some cases a depth of over 4000 m has been reached. The exploration target of these wells is a deep reservoir hosted in a metamorphic basement and/or granitic bodies, where geothermal fluids with a temperature of 300°C and a pressure of 7 MPa can be found (Barelli et al., 2000).
The deep exploration enlarged the edges of the exploitable geothermal field and evidenced that at a depth of 3000 m b.s.l. the geothermal fields of Larderello and Travale belong to the same deep reservoir, with the same temperature and pressure environment (Fig. 1).

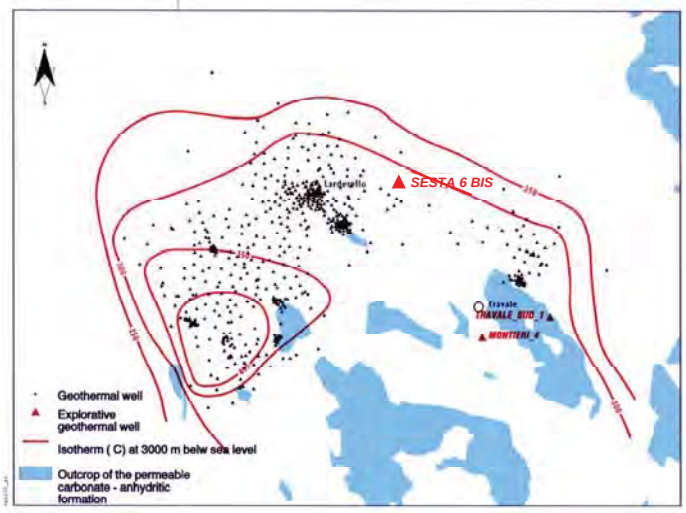

Fig. 1 - Larderello-Travale geothermal field: temperature contour lines at a depth of 3000 m b.s.l.

Differently from the shallow reservoir, in the deep one the fractured systems are not homogeneously distributed, but are confined in very localized levels of depth and are not correlated with specific geological features.
As a consequence of the high cost of the deep drilling, many efforts are in progress in order to find a technical - scientific approach able to reduce the

mining risk by means of the reconstruction of a predictive geo - structural model.
Advanced analysis of seismic reflection data (Cameli et al. 2000) and innovative techniques of well seismic measurements (Batini et al. 1990, 2001) are giving a valid contribution to the detection of deep fractured levels.
The characterization of the fractures in terms of typology and geometric parameters to be correlated to their productive characteristics is extremely important for a complete and detailed delineation of the structural model. In this framework a relevant role is certainly played by updated geophysical well logging techniques.

THE GOAL AND THE APPROACH

The final target is the research and the determination of reliable correlation between rock physic characteristics of the fractures and their nature, attitude and productivity. To this purpose, a fundamental tool of analysis is the acquisition of geophysical, temperature and pressure (T&P) logs in a number of wells as large as possible.

Geophysical Logs

The main geophysical logs usually applied in the deep geothermal exploration in Italy are listed here below together with their diagnostic aim.

- ***Gamma Ray (GR) Spectralog*** - can be performed also in cased holes and allows a detailed stratigraphic reconstruction for the entire depth of the well, even in case of cuttings absence due to Total Loss of Circulation (TLC).
- ***Densilog & Acoustilog*** - contribute to the stratigraphic-structural reconstruction of the well and are essential for the bulk density and seismic wave velocity determination in order to give calibration elements for the interpretation of surface gravimetric and seismic surveys. Furthermore these logs are fundamental to compute the formational elastic parameters and their variations in case of presence of fractures.
- ***Multi-arm Caliper*** – is very useful not only for the imaging of the hole geometry, but also for structural reconstruction by means of break-out analyses.
- ***Borehole Imaging Log*** – allows the 360° mapping of the walls of the hole by analyzing the formational variation of both velocity and resistivity. This is the only, specific tool for the direct fracture analyses in terms of nature and geometric parameters.

Usually, during the field recording phase it is possible to make a preliminary individuation of levels which can be potentially fractured. These are very often associated to:

- sharp decrease of bulk density and P wave velocity (V_P);
- strong attenuation of the wave form (WF);
- intense and very thin cavings in the walls of the hole;
- peaks of GR in case of mineralized fractures.

On the basis of this preliminary individuation, the levels to be investigated with borehole imaging log can be selected. Recently, the Circumferential Borehole Imaging Log (CBIL), based on the digital acoustic imaging technology (McDouglas and Howard, 1989), has became the most commonly used tool in Italy for the fracture investigation of deep geothermal wells. All the processing steps are mainly aimed at pointing out all those variations of the rock physic characteristics that can be related to the presence of fracture systems.
The first processing phase involve the Densilog and Acoustilog (Fig. 2) in order to compute the Acoustic Impedance, the Reflection Coefficient and the Synthetic Seismogram. The last one is particularly useful for a comparison with surface and well seismic profiles data because seismic reflections have been proved to be very often a signature of fractured horizons.
The WF analysis, recorded by means of advanced digital acoustic tool, allows to map the image of the instantaneous amplitude. This shows the WF energy distribution and content evidencing very clearly WF attenuation due to fractures. Furthermore the S wave velocity (V_S) and of the V_P/V_S ratio are also computed from the WF analyses. These parameters are combined with the density values and many elastic properties can be computed (see Fig. 2). Among these elastic parameters the Fracture Toughness Modulus is particularly sensitive to the presence of fractured levels.
The second processing phase (Fig. 3) is aimed at the fracture characterization of both the nature and the structural pattern using data from Multi-arms Caliper and CBIL (orientation-corrected in case of deviated wells).
Rough structural information comes from the break-out analysis of the Multi-arms oriented Caliper that allows the definition of the minimum horizontal stress direction (σ_3) which is orthogonal to the fracture planes considering a vertical direction of the maximum stress (σ_1).
CBIL data allow detailed structural reconstruction. In the CBIL tool an acoustic transducer, continuously spinning on the 360° of the walls of the hole, emits an acoustic pulse directed into the formation and records both the amplitude and the travel-time of the returning wave. The acoustic amplitude is mainly a function of the acoustic impedance of the formation, so that fractures and their nature (open, mineralized, foliation etc.) can be clearly evidenced.
Advanced CBIL processing techniques provide enhanced 360° acoustic amplitude images of the reflected wave. On this images it is possible to

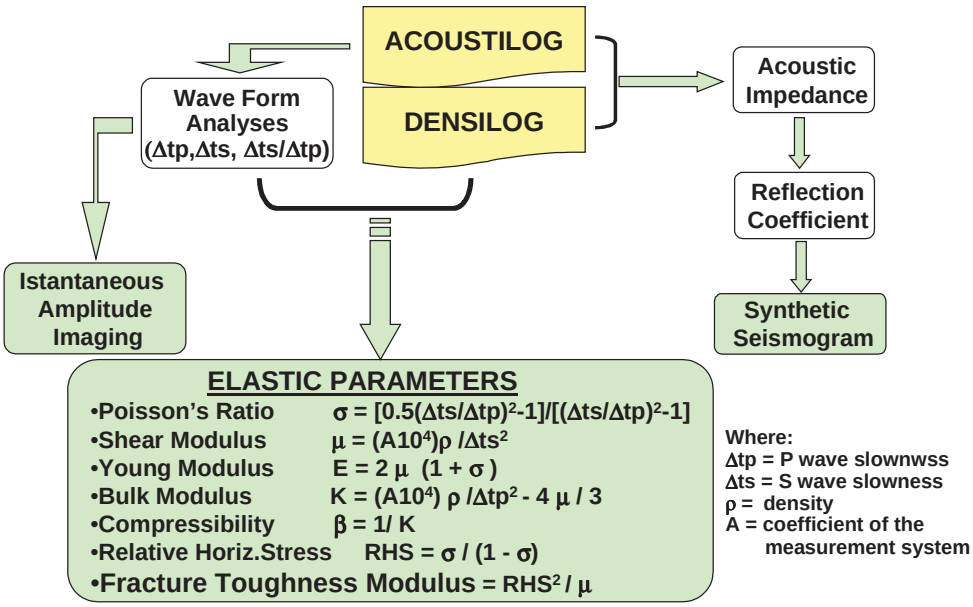

Fig. 2 – Processing Flow Chart of Density and Acoustic Well logging data

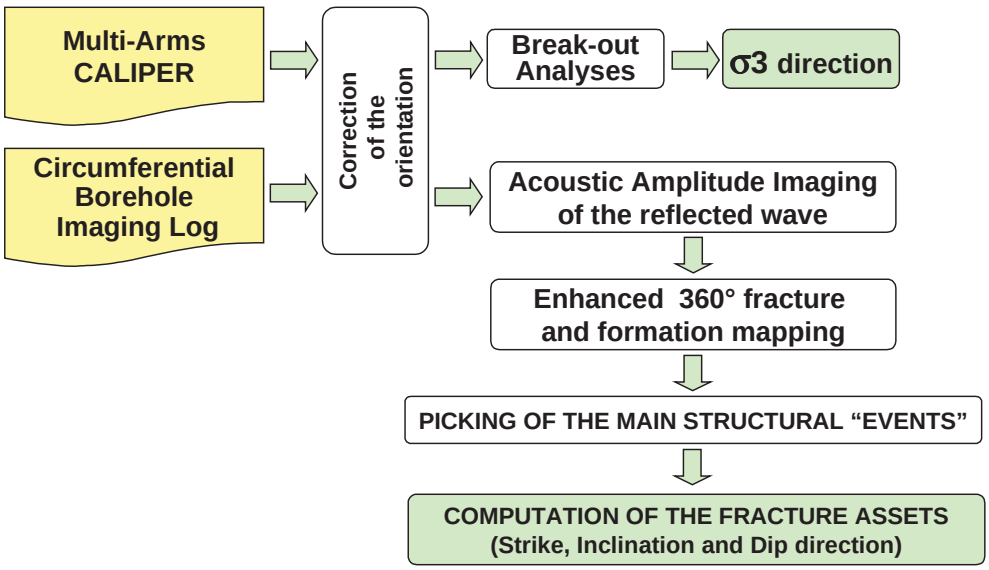

Fig. 3 – Processing Flow Chart for Fracture analyses from Well logging

distinguish different types of fractures as a function both of the acoustic impedance variation degree and of their shape and size.
These "structural events" can be than picked and all the geometric parameters (i.e. strike, inclination and dip direction) computed.

Well Testing

Temperature and pressure log

The most effective physical log measured during drilling, or immediately after well completion is the temperature and pressure one. Enel Green Power laboratories operates in the sector of research and testing using very high tech instrumentation, with a real-time acquisition. In order to operate in the conditions prevailing in the geothermal environment, most of the instrumentation, not commercially available has been especially designed and constructed utilizing innovative technologies. The specific temperature and pressure probe has the following operational limits: 316°C (extreme conditions 400°C) ± 0.2°C and 50 MPa ± 0.3%.
The utilization of T&P log can be a useful tool for the identification of each productive zone in the well and for the direct measurement of the injectivity. The overall injectivity value, measured during an injection test, can be biased by the existence of different fractures inside the well: the correct way of measuring it is to know the individual injection rate for each fracture, and the effective flowing pressure at the different vertical positions. The temperature profile during an injection test will exhibit a change of slope of the thermal gradient where there is a change in the flow rate, i.e. where there is an adsorbing zone: the thermal gradient is proportional to the fluid which passes in the formation.

Drawdown/Injection and interference

The main properties of a reservoir rock are the permeability and the porosity. The first is the rock capability of permitting fluid motion when a pressure difference driving force is applied, the second is given by the total amount of vacuum inside the reservoir, which is the storage of the fluid. The permeability distribution of the reservoir must provide a hydraulic connection throughout all the system; a pressure change in a part of the reservoir (due to exploitation or injection) is propagated in all the system. The propagation velocity of the pressure wave depends on the so-called "hydraulical diffusivity". The well testing is the way for measuring the most important reservoir parameters, as well as the characteristics of the fluid motion (Chierici, 1994)
During the drawdown/injection tests the pressure gauge is placed close to the productive zone, and the pressure change is recorded while the well is operated at constant production/injection rate. From the shape of the curve it is possible to identify the reservoir's unique characteristics: the trasmissivity (the permeability-reservoir height product), the skin factor (the well-reservoir coupling factor), the deviation from the ideal radial flow (storage effects, closed or constant pressure boundaries, linear motion of the fluid along preferential paths).
During an interference test the pressure change a given well is recorded, while a drawdown/injection test of another one is performed (Grant et al, 1982).
This is a very important way for measuring the average characteristics of the reservoir in the volume between the two wells, or for establishing a higher limit of the permeability in the case of negative response.

WELL SESTA 6 BIS A: EXPERIMENTAL DATA

The deviated well Sesta 6 bis A was drilled in the northern area of the Larderello-Travale geothermal field, in the same site of the vertical well Sesta 6 bis (see Fig. 1). The latter had reached productive levels at depth higher than 2400 m, in correspondence of a seismic reflection marker inside the metamorphic basement, but no geophysical logs for fracture characterization had been performed.
In order to investigate and characterize the fractured zones encountered during the drilling of Sesta 6 bis A well, the following set of geophysical logs was performed (Table 1):

Log	Depth Interval (m)	Notes
GR-Spectralog	0 – 3934	0 –2196 in cased hole
Densilog	2195-3934	In open hole
Acoustilog with WF		
4-Arm Caliper		

Table 1: Performed geophysical logs in the well Sesta 6 bis A

A set of six intervals for CBIL investigation were identified by means of the preliminary field fracture detection as follow (Table 2):

Log	Depth Interval (m)
CBIL	2550-2750
	2820-2890
	2915-2975
	3180-3210
	3380-3410
	3740-3780

Table 2: Performed CBIL investigation.

Rock Physic

The standard processing of the geophysical logs contributed to the stratigraphy reconstruction, although the well was drilled for a large depth interval in TLC (from 2600 m to the bottom of the well, 4000 m), and allowed to determine the main rock physical properties for each investigated geological formation. The following table 3 gives an example of geological characterization performed by means of the GR Spectralog, which gives a value of total GR and of its spectral components: Potassium (K), Thorium (TH) and Uranium (U).

Lithology	Depth Interval (m)	GR (GAPI)	K (%)	TH (ppm)	U (ppm)
Neogene Sediments	*0-280*	44.0 ±3.8	1.1 ±0.1	3.9 ±0.6	2.0 ±0.5
Flysch	*280-550*	63.0 ±5.3	1.9 ±0.1	2.8 ±0.77	2.8 ±0.7
Tectonic Wedges	*550–1900)*	48.0 ±7.6	1.92 ±0.1	6.7 ±1.2	2.5 ±0.7
Phyllites	*1900-2220*	93.5 ±12.5	2.38 ±0.6	11.7 ±1.9	3.2 ±1.1
Micaschists	*2220-3800*	109.8 ±35.5	2.40 ±0.9	12.7 ±4.6	4.4 ±1.6
Gneiss	*3800-4000*	N/A	N/A	N/A	N/A

Table 3: Geological characterization from GR Spectralog.

For the micaschists, the investigation by means of many geophysical tools made available further rock physic information (Table 4):

Parameter	Value
V_P	4.87 ± 0.32 (km/s)
V_S	2.81 ± 0.20 (km/s)
V_P/ V_S	1.7 ± 0.1
Density	2.77 ± 0.07 (g/cm^3)
Acoust. Imp.	12.7 ± 1.6 (kmsec^{-1}gcm^{-3})
Young Mod.	53.25 ± 10.2 (GPa)
Poisson Coef.	0.2 ± 0.06
Fract. Toughn.	0.006 (GPa^{-1})

Table 4: Advanced rock physic information for the micaschists interval.

Two core samplings have been analyzed in the TLC interval, in order to have a direct measurement of the relevant rock physics and geological data. In table 5 the petrophysical information from the two cores (the first in the micaschists and the second in the gneiss stratigraphic zones) are presented. The bulk density of 2.6 g/cm^3 can be compared with the previous indirect measurement from geophysical logs of 2.77 g/cm^3 for the micaschists reservoir rock.

Core sample	Depth Interval (m)	Grain density (g/cm^3)	Bulk density (g/cm^3)	Porosity (%)	Heat capacity (J/g°C)
Micaschists	3085-3088	3.0	2.6	1.3	0.67
Gneiss	3830-3833	2.9	2.6	1.6	0.67

Table 5: Core samples petrophysical determinations in the deep TLC drilling zones.

Well testing

During the well drilling (8 May 2000-12 September 2000) many adsorbing zones have been detected, at 818 m and 1618 m; these low productive zones have been covered with the casing. The open hole zone begins at 2202 m.

The first important fractured zone has been highlighted at 2600 m; after acidification and hydraulic stimulation an injection test measured a low injectivity: 1.6 m^3/h/bar. Subsequently, a T&P log has been recorded during another stimulation (with 80 kg/s for 2 ½ hours), followed by another medium-duration injection test (with 8 kg/s). Three adsorbing zones have been identified, but, due to the low overall injectivity, it was decided to deepen the well, until the final depth of 4002 m was reached. The following tests have been performed:

- Build up immediately after drilling;
- A 17 days production test (the well production could be estimated as 4 kg/s at 1.6 MPa well-head pressure);
- Two T&P logs during the production test, with an indication of six productive fractured zones (Fig. 4);
- An interference test (pressure on Sesta 6 bis), showing a linear motion connecting the two wells;
- Final build up after production test.

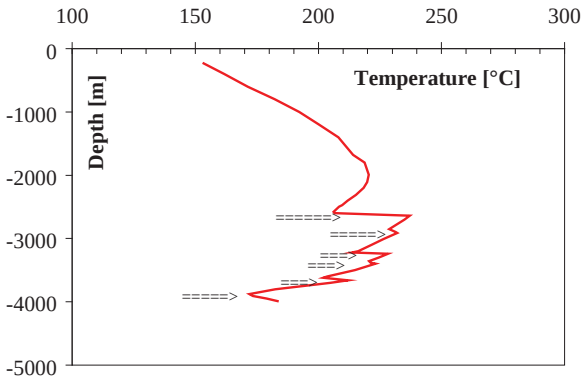

Fig. 4 Temperature dynamic log after production test, showing the fractured zones as change of slope in thermal gradient.

Unfortunately, the drawdown analysis does not give a clear indication of the reservoir characteristics, due to the superposition effects of each production zone.
The final build-up shows a slight tendency toward a radial motion, with a stabilized flow rate of 2.2 kg/s at 1.6 MPa. Assuming 1000 m of reservoir height, the formation permeability can be estimated as 0.7 mD and a negative skin factor of –4.2.

The final list of the fractures is given in Table 6.

Depth (m)	First T&P Flow rate (kg/s)	Second T&P Flow rate (kg/s)
2640	2.08	1.77
2910	1.11	0.14
3240	N/A	0.33
3400	N/A	0.14
3660	N/A	0.33
3880	2.31	1.44
TOTAL	**5.50**	**4.15**

Table 6: Fractures determined by T&P log during production test.

Fracture identification

The geophysical log processing confirmed that the six depth intervals preliminary identified for the CBIL investigation were particularly affected by signatures related to the presence of fractures (Fig. 5).

The CBIL analysis allowed the identification of different kinds of fractures and their geometrical parameters (Fig. 6). These last were processed and mapped for each interval as "pole density of all the fracture planes", using the Wulf's lower hemisphere stereo-graphical projection.
For each interval the pole density distribution, for fractures and faults only (foliations excluded), is shown in Fig. 7 together with the most representative cycle-graphical traces. These are characterized by a prevalent E-W azimuth direction, the dip direction is almost variable, but the inclination shows a tight variation between 65 and 80°.
A comparison with core fracture analysis is possible only for cores extracted from the same metamorphic formation in the vertical well Sesta 6 bis. They are not oriented, so that the only reliable value is an average slope of about 70° measured on few samples of continuous joints.
A comparison between the fractures detected by geophysical logs and well testings is given in table 7 together with a tentative correlation between fracture asset and productivity.
There is quite a correspondence with fractures detected by well testing in four out of six intervals characterized by geophysical fracture signatures.
Excluding the deepest productive zone at 3880 m, not investigated by CBIL, the levels with higher productivity (1.77 and 0.33 kg/s) are associated with sub-vertical fractures (inclination of 70-87°) with a E-W strike direction and Northward dip direction.

Fractured levels from CBIL				**Fractures from Well Testing**	
Depth (m)	*Strike Direction*	*Slope and dip direction*	*Number of Samples*	*Depth (m)*	*Production Flow rate (kg/s)*
2550-2750	E-W	87° N	242	2640	1.77
2820-2890	E-W	84° SE	72	Not detected	
	NNW-SSE	46° E	22		
	N-S	50° W	22		
2915-2975	N-S	27° E	36	2910	0.14
3180-3210	E-W	70° N	18	3240	0.33
3380-3410	WSW-ENE	24° SSE	30	3400	0.14
				3660	0.33
3730-3780	Not definable		few	Not detected	
----------***Bottom Log***----------					
				3880	1.44

Table 7: A comparison between the fractures detected by geophysical logs and well testing.

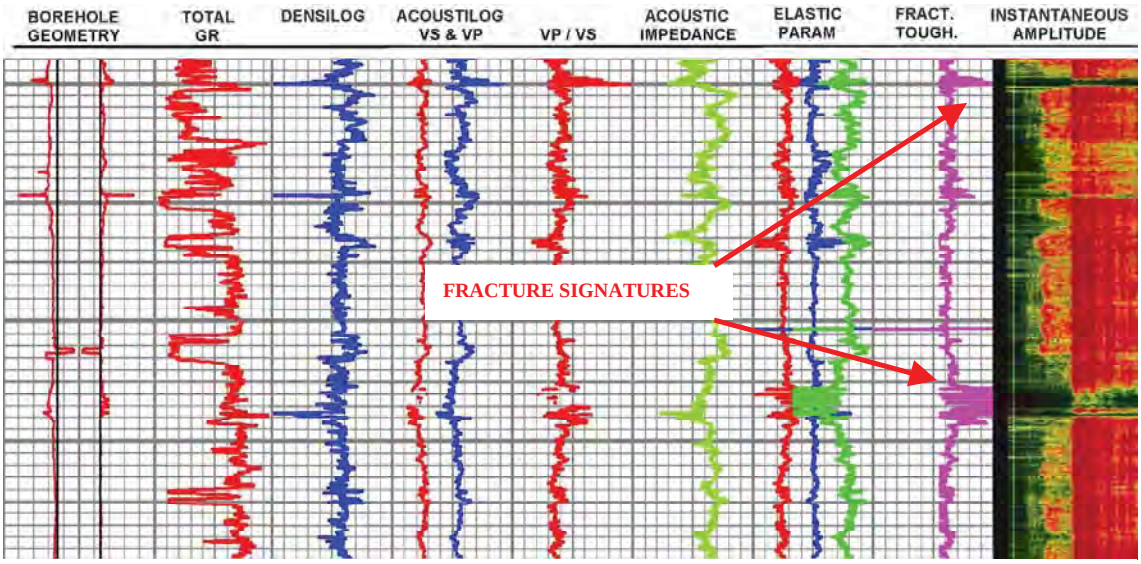

Fig. 5 – Fracture signatures from geophysical logs

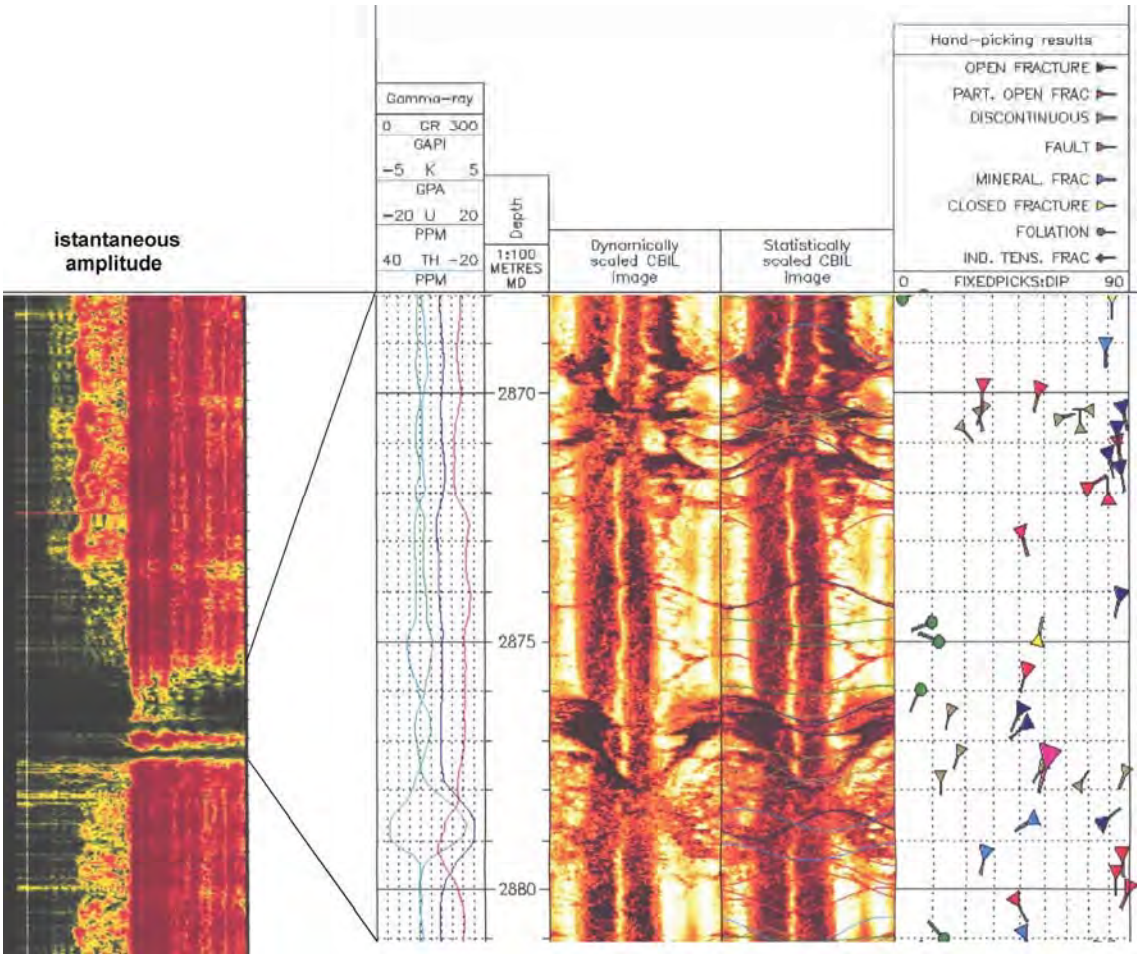

Fig. 6 – Fracture analysis from CBIL

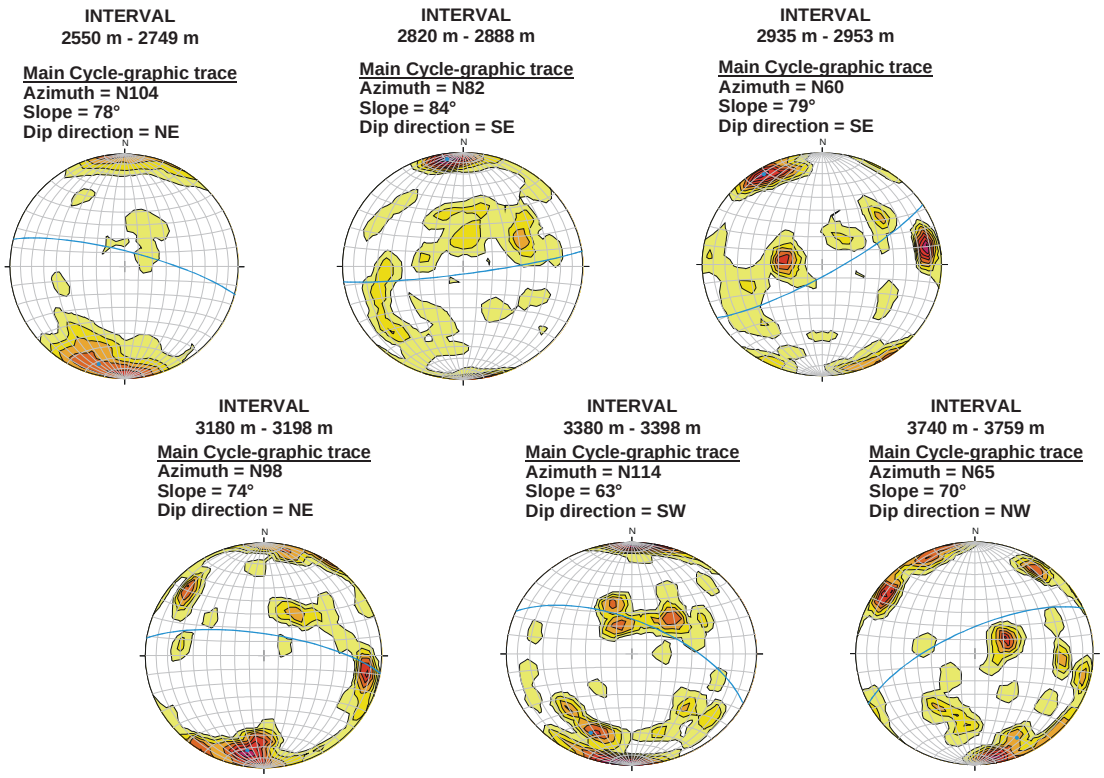

Fig. 7 – Fracture asset mapped as "pole density"

CONCLUSION

In a deep geothermal well of the Larderello-Travale area (Sesta 6 bis A, about 4000 m deep) a complete set of geophysical logs was collected, in order to compare and chaacterize the fractured zones identified with the standard well-testing procedures. In particular, the CBIL method, used in conjunction with other techniques, proved as very effective and detailed for a clear signature of the fractures already tagged by standard well testing procedures.

Unfortunately, one of the most important productive zone (at 3880 m) was not investigated by the geophysical logs. Four of the six intervals characterized by geophysical fracture signatures, have a good correspondence with fractures detected by well testing.

The higher productivity zones (1.77 and 0.33 kg/s, at 2640 m and 3240 m respectively) are in association with sub-vertical fractures (inclination of 70-87°) with a E-W strike direction and Northward dip direction. These results should be considered as preliminary: further experimental verifications will be achieved in the near future.

REFERENCES

Barelli, A., Bertini, G., Buonasorte, G., Cappetti, G. and Fiordelisi, A. (2000), "Recent deep exploration results at the margins of the Larderello-Travale geothermal system", *Proceedings of the World Geothermal Congress 2000 –Japan*, pp 965-970.

Batini, F, Omnes, G. and Renoux, P. (1990), "Delineation of geothermal reservoirs with 3D surface seismic and multi-offset WSP in the Larderello area", *Geothermal Resource Council, Trans.*, **14**, 1381-1386.

Batini, F., Dini, I., Certo, M., Cola, T., Cecconi, F., Soulier, L., Naville, C. and Serbutoviez, S. (2001), "Geothermal reservoir delineation by drillbit seismic while drilling", *Proceedings of the Geothermal Resource Council 2001 –Sam Diego, USA* pp 377-382.

Cameli, G.M., Ceccarelli, A., Dini, I. and Mazzotti, A. (2000), "Contribution of the seismic reflection method to the location of deep fractured levels in the geothermal fields of southern Tuscany (Italy)", *Proceedings of the World Geothermal Congress 2000 – Japan*, pp 1025-1029.

Chierici, G.L. (1994), "Principles of Petroleum Reservoir Engineering", Springler-Verlag, Berlin.

Grant, M.A., Donaldson, I.G. and Bixlet, F. P. (1982), "Geothermal Reservoir Engineering", Academic Press, New York.

McDouglas, J.G. and Howard, M.G. (1989), "Advances in borehole imaging with second generation CBIL (Circumferential Borehole Imaging Log) borehole televiewer instrumentation", *28th Annual Conference Proceedings, Ontario Petroleum Institute Inc., Lamberth, Ontario, Canada*, paper 12.

The deep structure of the Larderello-Travale geothermal field from 3D microearthquake traveltime tomography

T. Vanorio,[1] R. De Matteis,[2] A. Zollo,[3] F. Batini,[4] A. Fiordelisi,[4] and B. Ciulli[4]

Received 7 January 2004; revised 22 February 2004; accepted 15 March 2004; published 8 April 2004.

[1] With the aim of exploring the deep structure of the Larderello-Travale (LT) geothermal field, a high resolution 3-D tomographic inversion of microearthquake traveltimes has been performed. Results show that the deep part of the Larderello-Travale field is characterized by the presence of a structure having a velocity range of 6.0–6.5 km/s and a convex shape deepening towards the northeastern and the southeastern sides of the field. Earthquakes are mostly concentrated on the top of the high velocity structure and below the '*K horizon*' implying a transition of rheological properties at depth. The reported dependence on time of t_s-t_p observed at one station located above an earthquake cluster suggests that the variation in pore fluid pressure might be responsible for the transition of rheological properties along the contact. In such an area, changes in pore fluid pressure might be related to time-dependent hydraulic mechanisms that are very effective in crustal rocks at elevated temperatures. *INDEX TERMS:* 7215 Seismology: Earthquake parameters; 7280 Seismology: Volcano seismology; 8045 Structural Geology: Role of fluids; 8180 Tectonophysics: Tomography; 8424 Volcanology: Hydrothermal systems. **Citation:** Vanorio, T., R. De Matteis, A. Zollo, F. Batini, A. Fiordelisi, and B. Ciulli (2004), The deep structure of the Larderello-Travale geothermal field from 3D microearthquake traveltime tomography, *Geophys. Res. Lett.*, *31*, L07613, doi:10.1029/2004GL019432.

1. Introduction

[2] The LT field, which produces geothermal electricity from hot steam, is emplaced on a structural high within the Northern pre-Apennine belt (Italy). Enel Green Power drilled 195 wells which have provided a fairly good knowledge of the relatively shallow structure (up to ~3.5 km) of the field.

[3] Since the early 1970s production from the shallow reservoirs has declined which, jointly with the growth of energy requirements during the eighty's, forced the exploration into fractured zones in the deeper basement. Of particular interest is a zone known as the '*K horizon*', which is manifested as a discontinuous high-amplitude reflector on seismic reflection lines [*Batini and Nicolich*, 1985; *Brogi et al.*, 2003]. This horizon is regionally located, lying subhorizontally at depths varying beetween 8 and 10 km. In the LT field its depth seems to vary between 3 and 6 km representing the upper boundary of a band of reflections which locally show 'bright spot' features. [*Liotta and Ranalli*, 1999]. Besides being discontinuous, the nature of this horizon is still an open issue: debate is still ongoing as to whether it is either a fractured zone containing supercritical fluids [*Batini et al.*, 1985] or the top of a brittle-ductile transition with the presence of over-pressured fluids [*Brogi et al.*, 2003]. The only direct evidence of an anomalous fluid pressure (~30 MPa) derives from the San Pompeo2 well that might have penetrated this horizon. Deeper parts of the well collapsed while finding fractured rocks at a depth of 2930 m filled with hot fluids trapped beneath phyllites and micaschists [*Batini et al.*, 1985; *Brogi et al.*, 2003].

[4] We show the results of a tomographic inversion of microearthquake traveltimes in the Larderello-Travale field to investigate its deep 3-D velocity structure and the earthquake distribution. Mapping a reliable earthquake distribution at depth, adjunctive information can be achieved that proves useful for the comprehension of the deep structure of this field.

2. The Network and Data Inversion Method

[5] Since 1977 the seismic activity in the field is monitored by a permanent seismic network operated by the Enel Green Power consisting of 26 stations, 3 of which have three-component sensors (Figure 1). We analyzed a dataset consisting of 500 microearthquakes having magnitude $M \geq 1.2$ that have occurred from January 1994 through September 2000. Arrival times measured from digitized seismograms are accurate to about 0.01 s for P- and 0.02 s for S- waves providing a database consisting of ~7,000 P- and ~1,450 S- arrival time readings.

[6] The applied inversion procedure is described by *Benz et al.* [1996] and recently applied to several areas in the word [*Okubo et al.*, 1997; *Villasenor et al.*, 1998]. The method uses the finite differences technique [*Podvin and Lecompte*, 1991] to compute theoretical travel times by solving the Eikonal equation through a complex velocity structure and the least squares LSQR algorithm [*Paige and Saunders*, 1982] for simultaneous inversion of velocity parameters and hypocenter locations. Also, smoothing constraint equations are used to regularize the solution by controlling the degree of model roughness allowed during the inversion procedure.

[7] The 1-D reference velocity model, in Figure 2, has been obtained by a trial and error method based on the minimization of the RMS arrival time residuals. Information from geophysical data and VSP profiles [*Batini et al.*, 1978] have been considered to limit the explored velocity range.

[1]UMR-Géosciences Azur, Université de Nice, Sophia Antipolis, France.
[2]Dipartimento di Studi Geologici e Ambientali, Università del Sannio, Benevento, Italy.
[3]Dipartimento di Scienze Fisiche, Università di Napoli Federico II, Napoli, Italy.
[4]Enel Green Power, Pisa, Italy.

0094-8276/04/2004GL019432$05.00

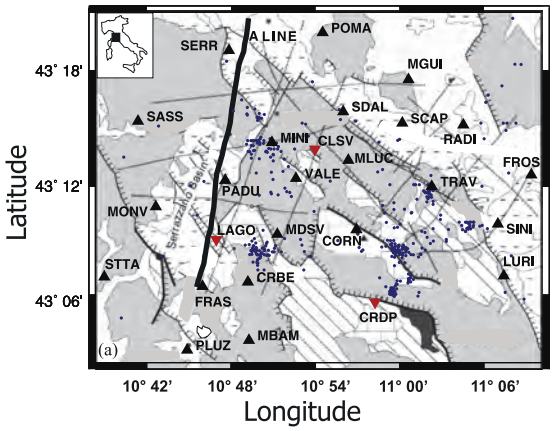

Figure 1. Map of the Larderello-Travale geothermal area showing seismic station (triangles) location (upside-down triangles are for three- component stations), epicenter location (circles) and, the seismic A line (thick line) [modified after *Brogi et al.*, 2003 Reprinted with permission from Elsevier.].

From the initial data set, we selected earthquakes having at least 10 P- phases read, azimuthal gap smaller than 180 and RMS of time residuals smaller than 0.5 s. The selection resulted in 400 events having an average of 18 P- traveltime readings and provided a final dataset consisting of 6,500 P- first arrival times. The distribution of stations/events allowed to investigate a volume of $46 \times 36 \times 16$ km^3 with the top at 1 km above the sea level. The investigated volume has been discretized by using uniform velocity cells having size $1 \times 1 \times 1$ km^3.

3. 3D Images of the Larderello-Travale Structure

[8] Figure 2 shows the map view of the three-dimensional P- velocity structure at four different depths. P- wave arrival time residuals as a function of distance and residual histograms are also shown in Figure 2 both for the initial 1D- (red points and red line, respectively) and for the final 3D- model (blue points and blue line, respectively). After 20 iterations, P- arrival time residuals were reduced by 45% from an initial RMS value of 0.08 s. In order to verify the spatial resolution of the inferred 3D model, a standard checkerboard test has been performed. The result of the test for a checkerboard having cells $2 \times 2 \times 2$ km^3 and velocity of ± 0.15 km s^{-1} is also shown in Figure 2. Test results show that anomalies having a dominant wavelength of 2 km are reasonably well recovered in the whole area up to 7–8 km.

[9] Beneath the LT field, we found evidence of strong vertical and lateral P- wave velocity variations as velocity values span a range between 3.6 and 6.5 km s^{-1} (Figure 2 and Figure 3). Lower velocities (from 3.6 to 5.2 km s^{-1}) are mainly located around the Lago, Miniera, and Padule-Travale areas up to 2 km depth and imply the presence of fractured and steam-bearing formations [*Ito et al.*, 1979]. Instead, a structure having higher velocity (from 5.3 to 6.4 km s^{-1}) which, as depth increases, spreads out over the area, is found at greater depth. This structure deepens from the Lago area towards the NE and SE suggesting a convex shape. The map of Bouguer anomalies in Figure 2 shows a nearly circular low gravity anomaly surrounding higher gravity anomalies. In the same figure, a contour map of the depth to the '*K horizon*', as inferred by the analysis of seismic reflection data [*Barelli et al.*, 2000], is presented as well. The structure is dominated by a large anticline both trending NE-SW with flanks falling off steeply in both directions having two smaller peaks inside the structure at ~3.5 km. Note that the San Pompeo 2 well is located near the western gravity high.

[10] Figure 3 shows the result of three merged cross-sections along the directions reported in Figure 2 and reports the comparison with the '*K horizon*' only where this zone has been clearly detected on seismic profiles [*Brogi et al.*, 2003]. It is worth noting that seismicity mostly lies along the contact between the deeper high velocity structure and the overlying lower velocity zone. Earthquake location and velocity images, reported in this study, have

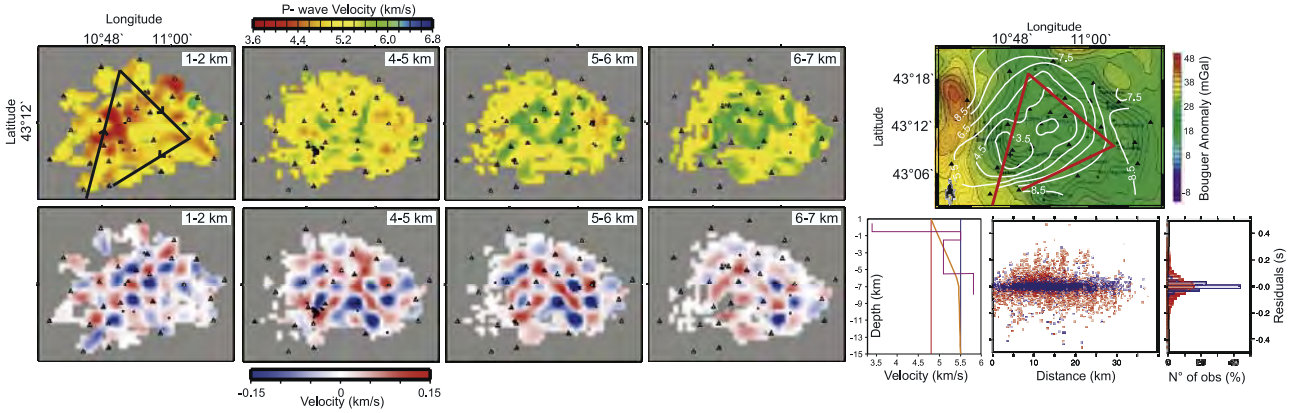

Figure 2. Maps of P- wave velocity and Bouguer gravity anomalies (top) and checkerboard tests (bottom). Each velocity layer is 1 km thick and cells not sampled by any ray are represented in gray. Symbol "+" indicates the location of San Pompeo 2 well. *Bottom left*: The reference 1D P-velocity model used for the 3-D tomografic inversion (orange line). Higher and lower velocity bounds (red and blue lines) obtained by plotting time residuals and VSP data (magenta line). *Bottom right*: P-arrival time residuals as a function of distance and residual histogram referring both to the initial 1D model (red-dots and line) and to the final 3D model (blue- dots and lines).

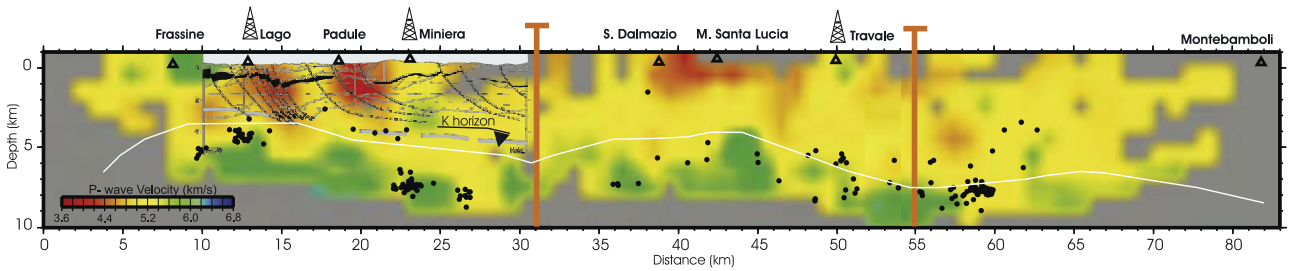

Figure 3. Merged P- velocity cross-sections along the directions shown in Figure 2. Triangles and dots represent station and earthquake locations, respectively. The seismic A *line* whose direction is reported in Figure 1 is also displayed for comparison: the dashed gray line represents the *K horizon* structure as inferred from *Brogi et al.* [2003]. The white solid line delineates the top of the *K horizon* reported in Figure 2 as inferred by *Barelli et al.* [2000].

been obtained by using only P- arrival time data recorded by a dense network. The lack of S- data can generally be a cause for errors in the estimate of earthquake location parameters. In order to verify the reliability of earthquake locations, an *ad hoc* test has been performed: synthetic traveltimes were computed by using the local network geometry, the final- 3-D velocity model and earthquake locations. Events were then re-located in the 3-D velocity model using the synthetic dataset. As a trial starting solution, the locations obtained in different 1-D velocity models were used. The comparison between the test result and the initial earthquake coordinates is shown in Figure 4, demonstrating well constrained solutions can be obtained using only P- data from the dense Larderello network.

4. Discussion and Concluding Remarks

[11] The 3-D tomographic inversion performed in the LT field has imaged a deep high velocity structure. *Elter and Pandeli* [1990] report that below the sedimentary cover, the crystalline basement is subdivided into two tectonic units: the upper unit consists mostly of quartzites, phyllites and micaschists affected by metamorphism while the gneiss complex constitutes the lower unit. The upper unit of the crystalline basement has been reached by the San Pompeo well and correlated to the reflective '*K horizon*' retrieved at this depth by seismic surveying [*Brogi et al.*, 2003]. Also, on the basis of local and anomalous pressure encountered in the San Pompeo well, as well as of temperature data extrapolated from those measured in shallower wells, *Liotta and Ranalli* [1999] postulated that the '*K horizon*' might signify a brittle-ductile transition rather than a lithologic variation if over-pressured fluids are invoked.

[12] Results from this study show that the shape of the high velocity structure follows the '*K horizon*' [*Barelli et al.*, 2000] along all the profile shown in Figure 3 (white line). In particular, the '*K horizon*' [*Barelli et al.*, 2000; *Brogi et al.*, 2003] lies within the lower velocity zone just above both the high velocity structure and the earthquake locations. On this basis, we argue that the deep high velocity structure might correspond either to stronger lithology variations or to less fractured parts of the crystalline basement. In order to verify the possibility that hot fluids might be trapped below the phyllite and micaschist formations, we have investigated a possible signature on velocity.

[13] Using Vp velocity information alone can be ambiguous because a low P-wave velocity can be due both to overpressure and to the presence of gas. *Prasad* [2002] and *Dvorkin et al.* [1999] have shown that the Vp/Vs ratio helps to differentiate between the two cases. We report in Figure 5 the variation of t_s - t_p, which is proportional to both Vp/Vs and hypocentral depth, as a function of time. Data refer to events located in a space of $1 \times 1 \times 1$ km^3, whose center is at 4 km depth, under the vertical direction of the three-component LAGO station. To take into account the spatial offset between events, values of t_s-t_p have been corrected as though they had nucleated from a common origin whose location is in the center of the cluster. Figure 5 shows a *quasi*- cyclic fluctuation of t_s - t_p as a function of time whose order of magnitude is equal to ~0.2 s. The estimate of uncertainties on location of <0.25 km (Figure 4) suggests that such a fluctuation can not be related to errors in location. If this fluctuation was due to mislocalization, it would imply a location error

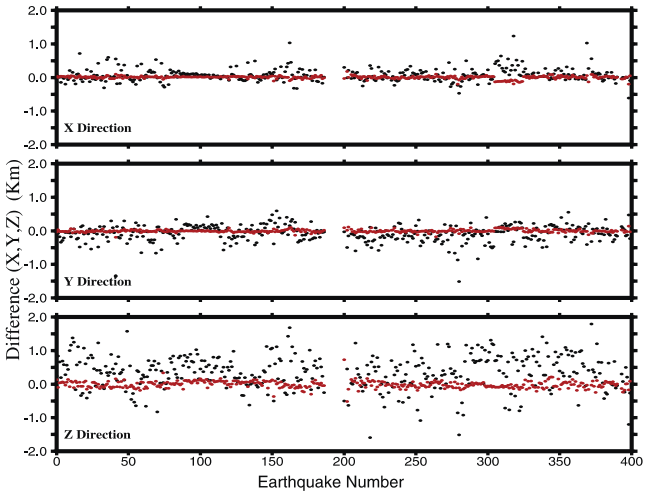

Figure 4. Test results showing the difference, along the *x*, *y*, and *z* directions, between localizations in the final 3D tomographic model and those obtained by inversion of synthetic traveltimes (red dots). Differences before the inversion procedure are also reported for comparison (black dots). The estimated error on localizations results to be <0.25 km.

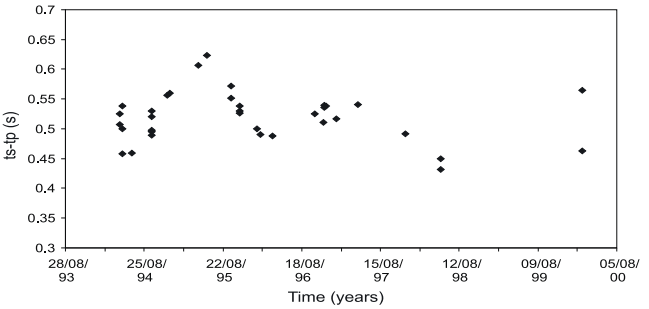

Figure 5. Variation of t_s - t_p as a function of time at the LAGO station.

equal to ~1.5 km. Therefore, we attribute such a fluctuation as being due to a variation of the Vp/Vs ratio which, for a $\Delta(t_s - t_p)$ of 0.2 s, is equal to ±0.3. As reported by *Nur and Walder* [1990], the state of crustal porosity, permeability and, fluid content is transient. This is mostly true in hydrothermal zones where healing and sealing processes responsible for pathway clogging are fast enough [*Smith and Evans*, 1984; *Summers et al.*, 1978]. Through such a mechanism, if permeability is low and its rate of reduction with porosity is relatively fast, the pore pressure of the trapped fluids will rapidly rise to overcome the least principal stress, leading to 1) natural hydrofracturing (increase of t_s - t_p) accompanied by release of fluids, 2) drop in pore pressure accompanied by loss of porosity (i.e., crack closure) due to compaction (decrease of t_s - t_p). Several studies [*Kanamori and Heaton*, 2000; *Hickman et al.*, 1995; *Cheng and Nur*, 1992] show that thermal pressurization may play a relevant role in faulting and earthquake processes. This mechanism is particularly required in the case of sub-horizontal crustal reflectors as they are mechanically very difficult to explain unless high pore pressure is involved [see *Hickman et al.*, 1995, and references therein]. Other weakening processes such as the syntectonic alteration of deformation zones having a weaker mineralogy with strong preferred orientation [*Wintsch et al.*, 1995] as micashists and fluid-assisted deformation mechanisms at hydrothermal conditions [*Blanipied et al.*, 1995] may also play an important role.

[14] By providing a 3-D lateral velocity variation of the Larderello-Travale deep structure, this study will be useful to enhance the seismic reflection data processing that, in complex geological settings, has to deal with the trade-off between the stacking- and rms- velocities [*Lynn and Claerbout*, 1982]. Furthermore, the earthquake location in the 3-D velocity model provided evidence that seismicity is distributed in a range from 4 km to 8 km depth between the deep high velocity structure on the one hand and, the '*K horizon*' on the other. This latter together with the reported t_s - t_p fluctuation suggests that this zone may contain fluids whose pressure changes over time. We postulate that pressure changes are due to time-dependent hydraulic mechanisms.

[15] **Acknowledgments.** We are grateful to H. Benz for having provided the 3-D tomographic code. G. Giberti, F. Lancieri and L. Cantore contributed to the picking of data. This work was performed under the auspicies of the GNV-INGV (FP2000-2003) and Department of Civil Protection. T. Vanorio has been supported by a MC Fellowship of the European Community program (HPMF-CT-2002-01777).

References

Barelli, A., G. Bertini, G. Buonasorte, G. Cappetti, and A. Fiordelisi (2000), Recent deep exploration results at the margins of the Larderello-Travale geothermal system, paper presented at Proceedings of the 2000 World Geothermal Congress, Int. Geother. Assoc., Tohoku, Japan.

Batini, F., and R. Nicolich (1985), P and S reflection seismic profiling and well logging in the Travale geothermal field, *Geothermics*, *14*, 731–747.

Batini, F., P. D. Burgassi, G. M. Cameli, R. Nicolich, and P. Squarci (1978), Contribution to the study of the deep lithospheric profiles: Deep reflecting horizons in Larderello-Travale geothermal field, *Mem. Soc. Geol. Ital.*, *19*, 477–484.

Batini, F., G. Bertini, G. Giannelli, E. Pandeli, M. Puxeddu, and I. Villa (1985), Deep structure, age and evolution of the Larderello-Travale geothermal field, *Trans. Geotherm. Resourc. Counc.*, *9*, 253–259.

Benz, H. M., B. A. Chouet, P. B. Dawson, J. C. Lahr, R. A. Page, and J. A. Hole (1996), Three-dimensional P and S wave velocity structure of Redoubt Volcano, *Alaska, J. Geophys. Res.*, *101*, 8111–8128.

Blanipied, M. L., D. A. Lockner, and J. D. Byerlee (1995), Frictional slip of granite at hydrotheral conditions, *J. Geophys. Res.*, *100*, 13,045–13,064.

Brogi, A., A. Lazzarotto, D. Liotta, and G. Ranalli (2003), Extensional shear zones as imaged by reflection seismic lines: The Larderello geothermal field (central Italy), *Tectonophysics*, *363*, 127–139.

Cheng, Q., and A. Nur (1992), Pore fluid pressure effects in anisotropic rocks: Mechanism of induced seismicity and weak faults, *Pure Appl. Geophys.*, *139*, 463–479.

Dvorkin, J., G. Mavko, and A. Nur (1999), Overpressure detection from compressional- and shear-wave data, *Geophys. Res. Lett.*, *26*, 3417–3420.

Elter, F. M., and E. Pandeli (1990), Alpine and Hercynian orogenic phases in the basement rocks of the northern Apennines (Larderello geothermal field, southern Tuscany, *Italy, Eclogae Geol. Helv.*, *83*, 241–264.

Hickman, S., R. Sibson, and R. Bruhm (Eds.) (1995), Mechanical involvement of fluids in faulting, *J. Geophys. Res.*, *100*, 12,831–13,132.

Ito, H., J. DeVilbiss, and A. Nur (1979), Compressional and shear waves in saturated rock during water-steam transition, *J. Geophys. Res.*, *84*, 4731–4735.

Kanamori, H., and T. H. Heaton (2000), Microscopic and macroscopic physics of earthquakes, in *Geocomplexity and the Physics of Earthquakes*, *Geophys. Monogr. Ser.*, vol. 120, edited by J. B. Rundle, D. L. Turcotte, and W. Klein, pp. 147–163, AGU, Washington, D. C.

Liotta, D., and G. Ranalli (1999), Correlation between seismic reflectivity and reology in extended lithosphere: Southern Tuscany, inner northen Apennines, Italy, *Tectonophysics*, *315*, 109–122.

Lynn, W. S., and J. F. Claerbout (1982), Velocity estimation in laterally varying media, *Geophysics*, *47*, 884–897.

Nur, A., and J. Walder (1990), Time-dependent hydraulics of the Earth's crust, in *The Role of Fluids in Crustal Processes*, pp. 113–127, Natl. Acad. Press, Washington, D. C.

Okubo, P. G., H. M. Benz, and B. A. Chouet (1997), Imaging the crustal magma sources beneath Mauna Loa and Kilauea volcanoes, Hawaii, *Geology*, *25*, 867–870.

Paige, C. C., and M. A. Saunders (1982), LSQR: An algorithm for sparse linear equations and sparse least squares Trans, *Math. Software*, *8*, 43–71.

Podvin, P., and I. Lecompte (1991), Finite difference computation of traveltimes in very contrasted velocity models: A massively parallel approach and its associated tools, *Geophys. J. Int.*, *105*, 271–284.

Prasad, M. (2002), Acoustic measurements in sands at low effective pressure: Overpressure detection in sands, *Geophysics*, *67*, 405–412.

Smith, D. L., and B. Evans (1984), Diffusional crack healing in quartz, *J. Geophys. Res.*, *89*, 4125–4135.

Summers, R., K. Winkler, and J. Byerlee (1978), Permeability changes during the flow of water through westerly granite at temperatures of 100°–400°C, *J. Geophys. Res.*, *83*, 339–344.

Villasenor, A., H. M. Benz, L. Filippi, G. De Luca, R. Scarpa, G. Patane, and S. Vinciguerra (1998), Three-dimensional P wave velocity structure of Mt. Etna, Italy, *Geophys. Res. Lett.*, *25*, 1975–1978.

Wintsch, R. P., R. Christoffersen, and A. K. Kronenberg (1995), Fluid-rock reaction weakening of faut zones, *J. Geophys. Res.*, *100*, 13,021–13,032.

R. De Matteis, Dipartimento di Studi Geologici e Ambientali, Università del Sannio, Benevento, Italy.

F. Batini, B. Ciulli, and A. Fiordelisi, Enel Green Power, Via Andrea Pisano, 120, I-56122 Pisa, Italy.

T. Vanorio, UMR-Geosciences Azur, Université de Nice, Sophia Antipolis, 250 Rue Albert Einstein, F-06560 Valbonne, France. (vanorio@geoazur.unice.it)

A. Zollo, Dipartimento di Scienze Fisiche, Università di Napoli Federico II, I-80125 Napoli, Italy.

Geothermics, Vol. 14, No. 5/6, pp. 731 – 747, 1985.
Printed in Great Britain.

0375 – 6505/85 $3.00 + 0.00
Pergamon Press Ltd.

P AND S REFLECTION SEISMIC PROFILING AND WELL LOGGING IN THE TRAVALE GEOTHERMAL FIELD

F. BATINI* and R. NICOLICH†

**ENEL, Unità Nazionale Geotermica, Piazza Bartolo da Sassoferrato, Pisa, Italy and †University of Trieste, Trieste, Italy*

Abstract—Two high resolution seismic reflection profiles, obtained with vibrators as sources of P and of horizontally polarized SH waves, were recorded and elaborated. In the well CH-3, 2704 m deep and located close to the profiles, several geophysical logs were carried out: temperature, SP and induction, density, natural radioactivity, and sonic logs with P and S wave velocity measurements. These data enabled the calculation of the elasticity moduli and of the mechanical properties of the rocks affected. The sonic log results were subsequently calibrated by means of a vertical seismic profile which permitted the computation of synthetic seismograms and a VSP log for comparison with the seismic sections and correlation between S and P seismic reflectors. The structural maps obtained from data interpretation describe with sufficient detail the fracture trend of the Travale field.

By comparing V_s and V_p velocities for the different geological units, as defined by the interpretation, the change in the $\alpha = V_p/V_s$ ratio and in the Poisson coefficient has been tentatively utilized to correlate the seismic data with material properties.

The influence of lithology on the elastic constants is discussed, as well as the influence of the saturating fluids and of the degree of saturation. The different attenuation of the P and S waves, depending on the above-mentioned characteristics, demonstrates the possibilities offered by seismic methods in the evaluation of the potential of geothermal reservoirs.

INTRODUCTION

Laboratory measurements and theoretical studies have demonstrated that P and S wave velocities depend on lithological changes and the type and amount of saturating fluids in porous media under particular saturation, pressure and temperature conditions.

The V_p/V_s ratio was tentatively measured in geothermal fields by utilizing reflection profiling (Goupillard and Cherry, 1977) and passive seismological data (Ferrucci and Hirn, 1984).

We employed track-mounted vibrators for P and horizontally polarized SH wave generation along two high-resolution reflection profiles. At the same time, sonic logs, vertical seismic profiles and other geophysical data were collected in well CH-3, depth 2704 m, drilled by ENEL in the same area and completed by the time of the field data acquisition.

The aim of the study is to improve interpretation methodologies in geothermal areas, especially for the recognition of the structures of the metamorphic-crystalline basement by means of seismic methods with high geometrical resolution and good penetration (4 – 5 km). The determination and evaluation of the potential of geothermal reservoirs and of the nature of their fluid content will reduce drilling risks and optimize the cost/benefit ratio of any deep drilling programme in spite of the high costs of the seismic exploration.

Seismic techniques in high enthalpy geothermal field investigation were extensively applied in the Larderello, Travale and Mt. Amiata areas, with about 280 km of seismic lines acquired with dynamite or vibrating sources (Batini *et al.*, 1978; Batini and Nicolich, 1984).

Correlation of the seismic data with the geological structures is particularly difficult because of the complexity of the metamorphic-crystalline basement and of the sedimentary cover, which is also highly tectonized or chaotic.

Nevertheless, the results obtained in the Tuscan geothermal area are very interesting, particularly for the inventory of promising deep reservoirs inside the basement, while the possibility of

the upward migration of these fluids through fractures and permeable units has been verified by drilled wells (Batini *et al.*, 1983).

REFLECTION SEISMIC SURVEY

Two seismic reflection profiles (TR-1 and TR-2) about 9 km in length were recorded (Fig. 1) with the following objectives:

- acquisition of detailed structural information on the carbonate geothermal reservoir,
- description of fracturing trends,
- differentiation of the structures and geothermal properties of the Paleozoic metamorphic units.

The survey area is very uneven, with elevations varying between 330 and 460 m, and is covered with thick vegetation. Roads or tracks allowing the passage of vehicles are very scarce and are not straight. Moreover, the size and weight of the shear wave vibrators discouraged the creation of new tracks because of excessive cost and potential irreversible damage to the environment.

The vibrator positions were restricted to roads or preexisting tracks and the "slalom line" technique (Trade Mark of Compagnie Général de Géophysique) was employed.

The field crew was equipped with a 48-channel SN-338 B digital recording system with all the auxiliary instruments for Vibroseis (T.M. Continental Oil) operations. The horizontal geophones were set up to record SH waves and buried to avoid interference from wind noise. The coverage was 2400%.

The seismic array configuration is represented in Fig. 2 and Table 1 gives some acquisition and elaboration parameters.

Wiggle-variable area sections were presented after the application of standard processing sequences with coherence optimization, wave equation migration and true amplitude presentation with both polarities. Different vertical scales were utilized in order to facilitate the correlation between the P and S sections. The data quality was not very good, mainly because of the tectonic complexity at the edge of the Radicondoli – Chiusdino basin (Batini *et al.*, 1985) with an intricate pattern of vertical faults.

Further complications occur along the very sinuous profile TR-2 because the slalom line technique cannot eliminate all the lateral anomalous events.

The true amplitude sections could help very little in data evaluation because of high transmission losses inside the Neogenic formations, which strongly attenuate frequencies higher than 70 Hz and thus limit the possibility of acquiring high-resolution data with good penetration. Nevertheless it is possible to observe different attenuation phenomena for P and S waves inside the reservoir and the Paleozoic basement.

The critical process of associating reflection events on the P and S wave (Common Depth Point) sections with common geologic interfaces is still problematic and an accurate comparison was possible only after well measurements in CH-3 and analysis of the stratigraphies in neighbouring wells.

WELL MEASUREMENTS

Geophysical data were collected in well CH-3 inside the carbonate reservoir and the Paleozoic basement. The objectives were: inventory of fractured zones, determination of the petrophysical characteristics of the rocks, computation of correct velocity function for depth reduction of the seismic data, computation of a synthetic seismogram and analysis of the variations of the elastic moduli of rocks bearing fractures and different pore fluids.

Unfortunately the well was not productive and the measurements had also to be restricted to

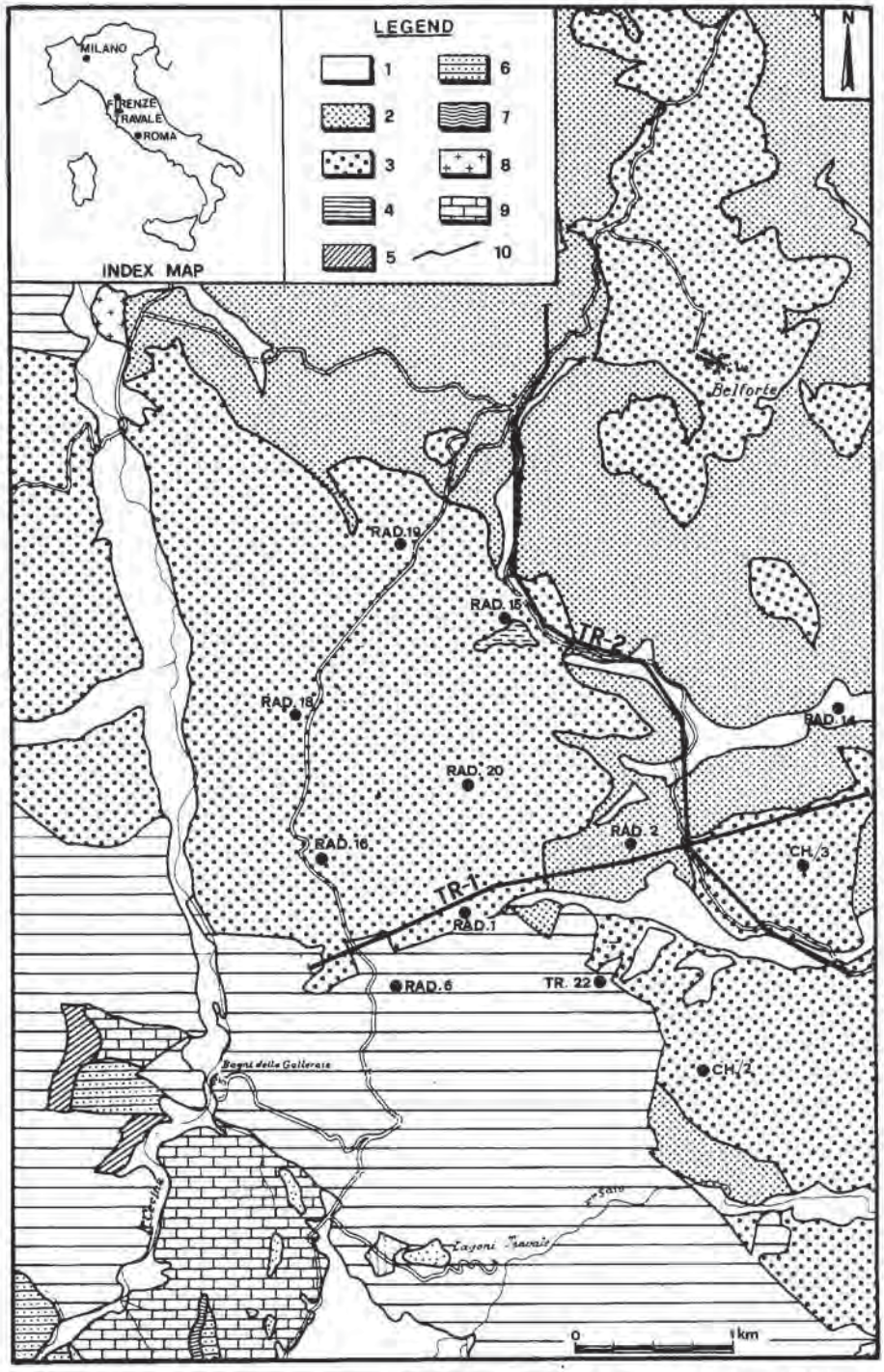

Fig. 1. Seismic profiles TR-1 and TR-2 and the geologic sketch map: (1) alluvium, (2) Pliocene, (3) Miocene, (4) flysch, (5) Eocene, (6) sandstone (Macigno), (7) Cretaceous – Eocene (Tuscan wedges), (8) massive limestones (Lower Lias), (9) dolomite (Norian – Rhaetian), (10) seismic profiles; RAD 20 well.

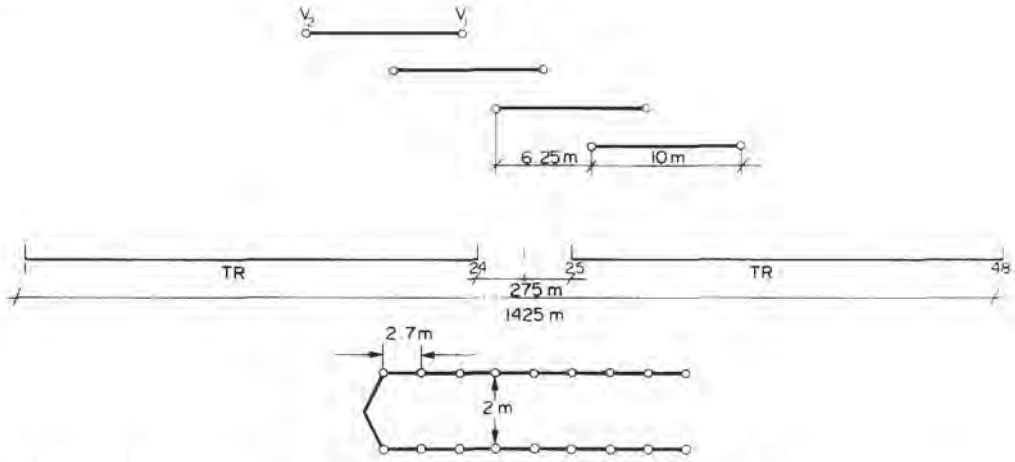

Fig. 2. High-resolution reflection seismic data acquisition: vibration pattern, spread configuration, geophones array. V_1, V_2 = vibrators, TR = traces.

Table 1. Acquisition and elaboration parameters

Profile	Vibrators	Sweep No.	Vibr. point		Recording		Processing	
			length (s)	frequency (Hz)	sampl. rate (ms)	length (s)	sampl. rate (ms)	length (s)
TR-1 (P)	2	16	26	14 – 125	2	30	2	4
TR-1 (S)	2	16	24	7 – 63	2	30	4	6
TR-2 (P)	2	16	26	14 – 70	2	30	4	4
TR-2 (S)	2	32	24	7 – 40	2	30	4	6

the 1750 m (top of the carbonate reservoir) and 2500 m interval, depending on the temperature range of the downhole tools.

The following logs were recorded: temperature, SP and induction, density, sonic with the recording of the complete waveform, and natural-γ. Data processing provided the following additional data:

— energy spectra for P and S waves and S-sonic log from processing of the complete waveforms,
— log of the porosity variations and of the elastic moduli, that is, a complete set of the mechanical properties of the rocks crossed and, therefore, of their lithological variations.

These data, referred to the most significative depth interval, are represented in Fig. 3.

From the log data we can distinguish the alternation of anhydrites and dolomites inside the carbonate reservoir. The contact between the Triassic carbonates and the Paleozoic basement at 2015 m is also well defined. It appears to be a tectonic contact with wedges of anhydrites inside the fractured and mineralized metamorphic formations (depth interval 2015 – 2090 m).

The high schistosity of the phyllites and the intercalations of quartzites in the Paleozoic formations are revealed by strong variations of density and of the natural-γ radioactivity.

The inventory of fractured zones was obtained from the trend of different parameters in correspondence to sharp attenuations of the S-waves. These intervals are, however, very small or of limited importance.

The V_p against V_s values measured in the anhydrites interval range between 1.8 and 1.9, which represents the average of the values for dolomites and pure limestones measured *in situ*

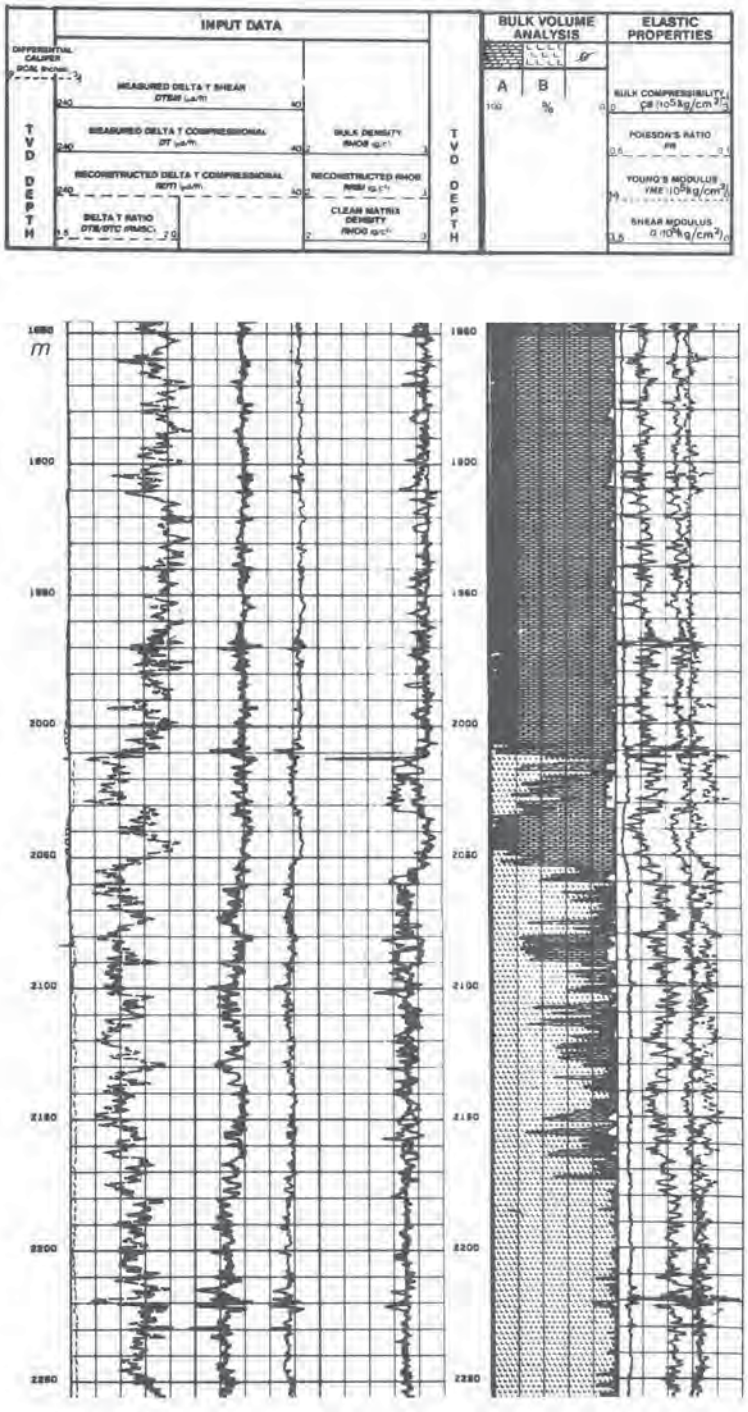

Fig. 3. CH-3 well log data: P-sonic, S-sonic, V_p/V_s ratio, density, lithology with porosity information, compressibility, Young's modulus, shear modulus and Poisson coefficients. Depth interval 1850 – 2250 m. A = carbonate reservoir, B = metamorphic basement.

and on samples (Pickett, 1963). The same (V_p, V_s) clustering inside the Paleozoic formations is limited between 1.7 and 1.8.

It must be noted that very low porosities (0 – 3%) were found in well CH-3. Therefore, velocities and V_p/V_s ratio seem to be related mainly to lithological changes.

The elastic properties of the basement and of the Triassic anhydrites are characterized by different Poisson coefficients ($\mu = 0.30$ for anhydrites; $\mu = 0.26$ for the basement) and of shear moduli ($G = 2.8 \times 10^5$ kg/cm^2 for the anhydrites; $G = 2.1$ for the basement). However, the frequency distribution of both μ and G inside the basement shows some dispersion of the values because of lithological variations (alternation of metamorphic rocks and anhydrites in the depth range 2060 – 2180 m) and fracturation phenomena. The smallest values are observed where the presence of fractures is presumed to be a consequence of a differential decrease of V_p with respect to V_s.

Table 2 lists the average petrophysical characteristics of the rocks involved in the measurements.

Table 2. Average physical and elastic parameters measured in well CH-3

Parameters			Anhydrites	Metamorphic rocks
Specific electric resistivity	R	ohm·m	600	300
Natural-radioactivity	G.R.	A.P.I.	10	130
Density	ρ	g/cm^3	2.9	2.7
P-wave velocity	V_p	km/s	5.8	4.9
S-wave velocity	V_s	km/s	3.1	2.8
V_p/V_s ratio	α	—	1.9	1.7
Poisson coeff.	μ	—	0.30	0.26
Young's modulus	E	10^5 kg/cm^2	7.0	5.0
Shear modulus	G	10^5 kg/cm^2	2.8	2.1
Compressibility	C	10^5 kg/cm^2	2.0	3.0

THE VERTICAL SEISMIC PROFILE AND COMPARISONS BETWEEN THE REFLECTION SEISMIC AND WELL LOGS

In well CH-3 a vertical seismic profile (VSP) was recorded by a logging tool with three-component geophones (Geolock, T.M. of C.G.G.). The measurements, performed at different depth levels spaced 20 – 30 m from 300 to 2240 m and utilizing P and S vibrators as seismic sources, allowed us to define interval P and S velocities (Fig. 4). A synthetic seismogram, with different wavelets and with displays of multiples according to different reflection coefficients from the surface, was computed.

Further processing of the VSP records, with recovery of the up-going waves from the reflecting horizons and cancellation of multiples and dipping events, gave two VSP logs and two pseudo-impedance logs for both P and S waves. Figures 5 and 6 show the comparison between P and S seismic sections and the synthetic seismograms, VSP logs, pseudo-impedance logs and acoustic impedance logs.

INTERPRETATION OF SEISMIC PROFILES

The logs from well CH-3 were utilized to check the seismic events. Extrapolation of the data through the seismic sections enabled us to make correlations with stratigraphies of neighbouring wells and assess an average interval velocity for the different formations to be used in the preparation of the isobath maps. Figures 7 – 10 show the migrated P and S seismic lines with the interpretation and Fig. 11 shows the depth section for profile TR-1.

Quite good reflections are evident in the P sections (Figs 7 and 9) which correspond to the

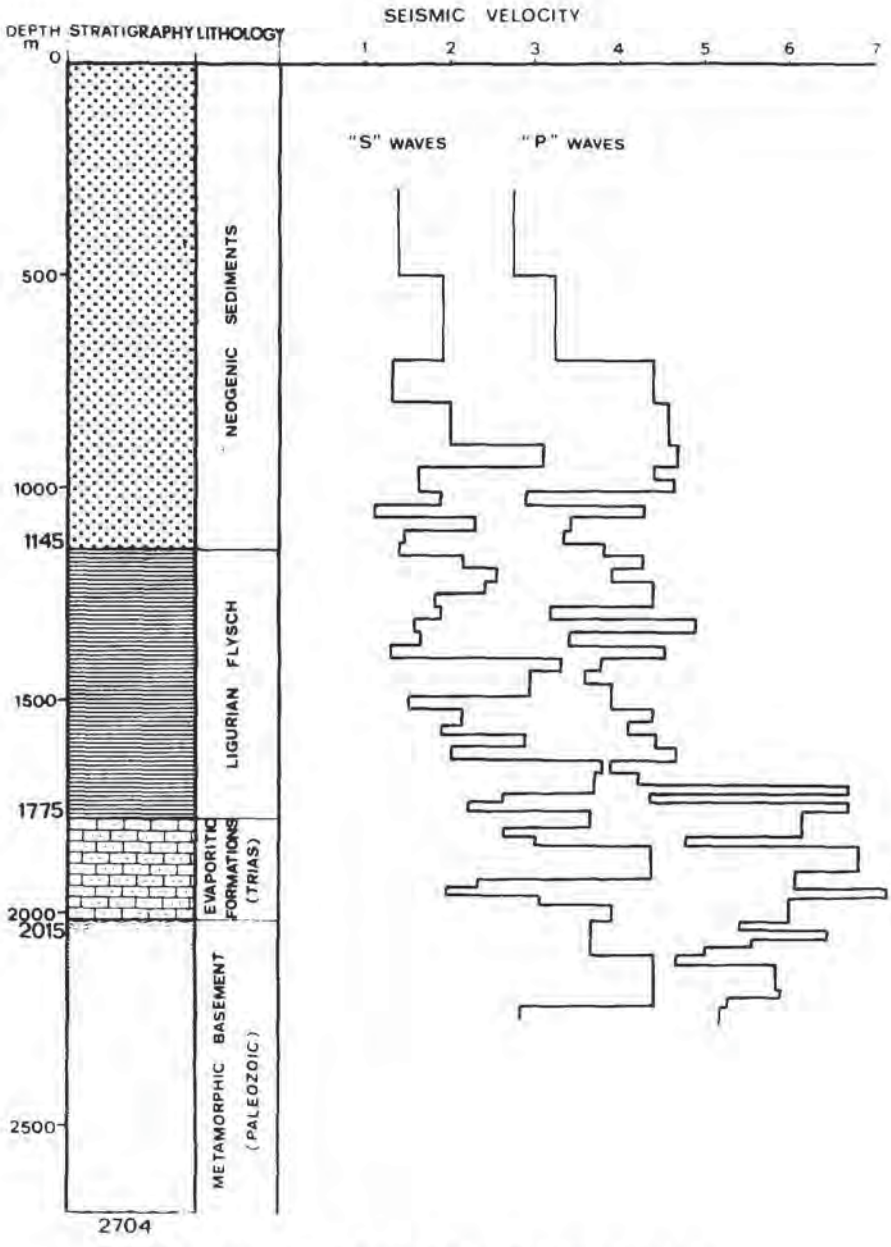

Fig. 4. CH-3 well stratigraphy and P and S interval velocity.

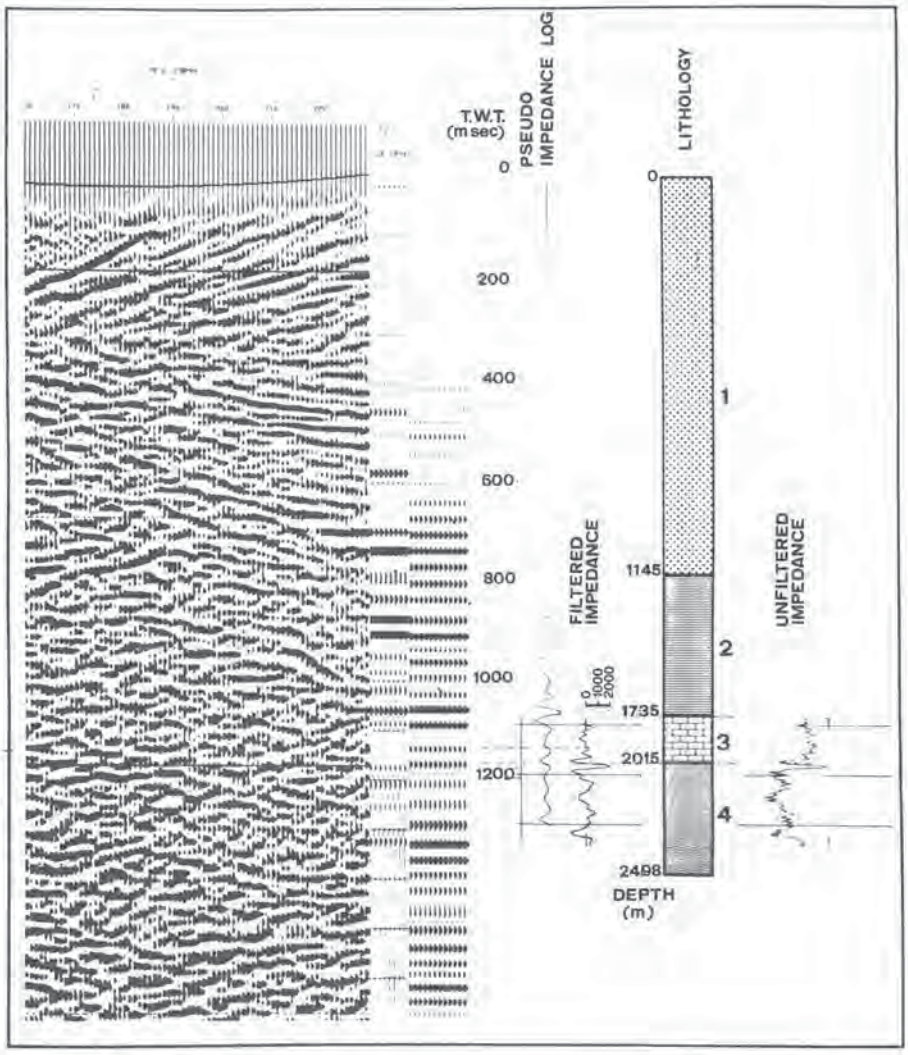

Fig. 5. Association of the seismic reflection data from the profile TR-1P with the synthetic seismogram, the VSP (vertical seismic profile) log P-waves, the pseudo-impedance log and the impedance log.

Neogenic formations representing the Messinian – Pliocenic evolution of the graben. The Ligurian nappes show a poor continuity in the reflections from their boundaries; they appear chaotic, but with some continuous reflectors in the lower part of the formation where some lithological differentiations must be located. Definition of the reservoir interval is also complicated by the presence of different units of the Tuscan nappes. At the top of the basement the reflections are very variable or poor, but inside the basement bunches of high amplitude reflections are present.

The S waves are highly scattered in the Neogenic formations and in the upper part of the Ligurian nappes. Inside the reservoir and at the top of the basement the S reflections seem to be

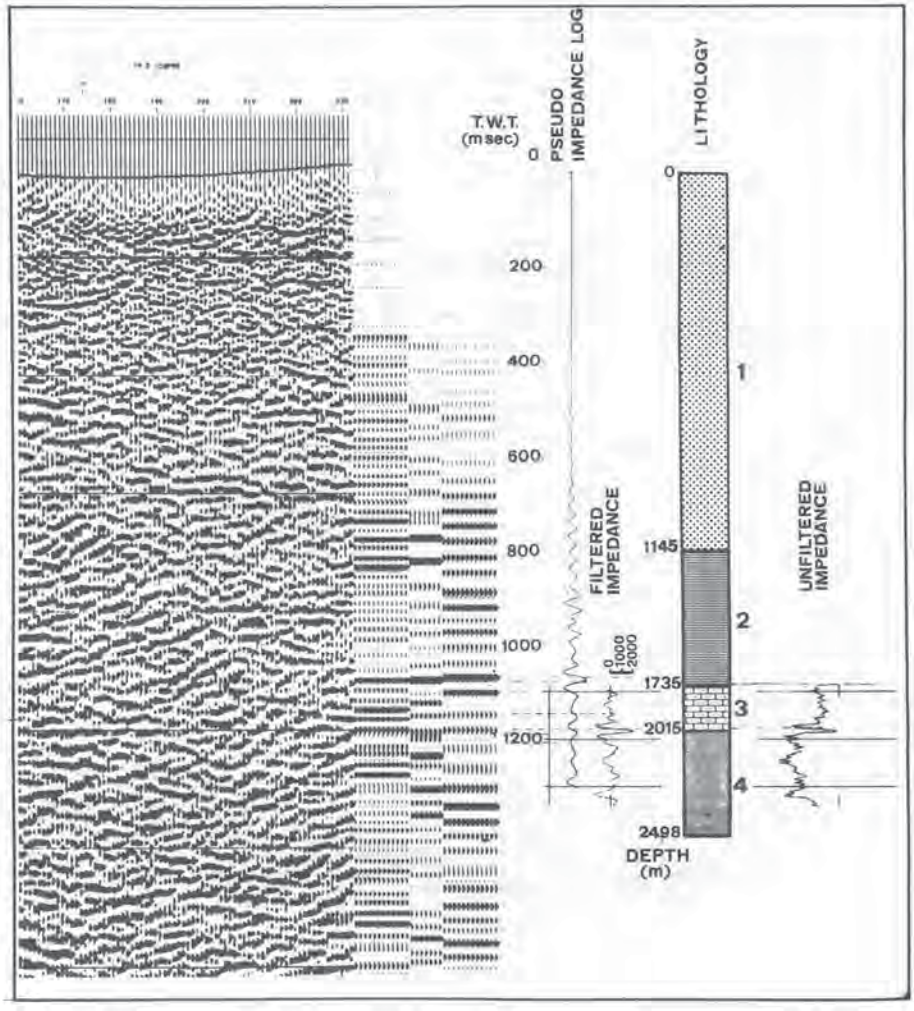

Fig. 6. Same as Fig. 5 with TR-1S and log S-waves.

connected to lithologic variations or fluid content and poorly related with the general tectonic setting.

The isobaths of the top of the basement are presented in Fig. 12. This map utilizes all the seismic data available, together with those collected in the wells drilled by ENEL in the area studied.

Further velocity analysis, performed on reflection data after interpretation of the final processed sections, allowed us to compute the average interval velocities, the ratio $\alpha = V_p/V_s$ and the Poisson coefficient μ for the different formations with particular regard to the reservoir. The average values for the Neogenic sediments are $\alpha = 2.080$, $\mu = 0.349$; and for the Ligurian nappes $\alpha = 1.880$, $\mu = 0.302$.

Figures 13 and 14 display the values for V_p, V_s and α inside the reservoir along the seismic line TR-1 and TR-2.

The interpretation should be continued, using the results obtained by many authors from measurements on samples and *in situ*. The ratio α is influenced by lithology (Pickett, 1963;

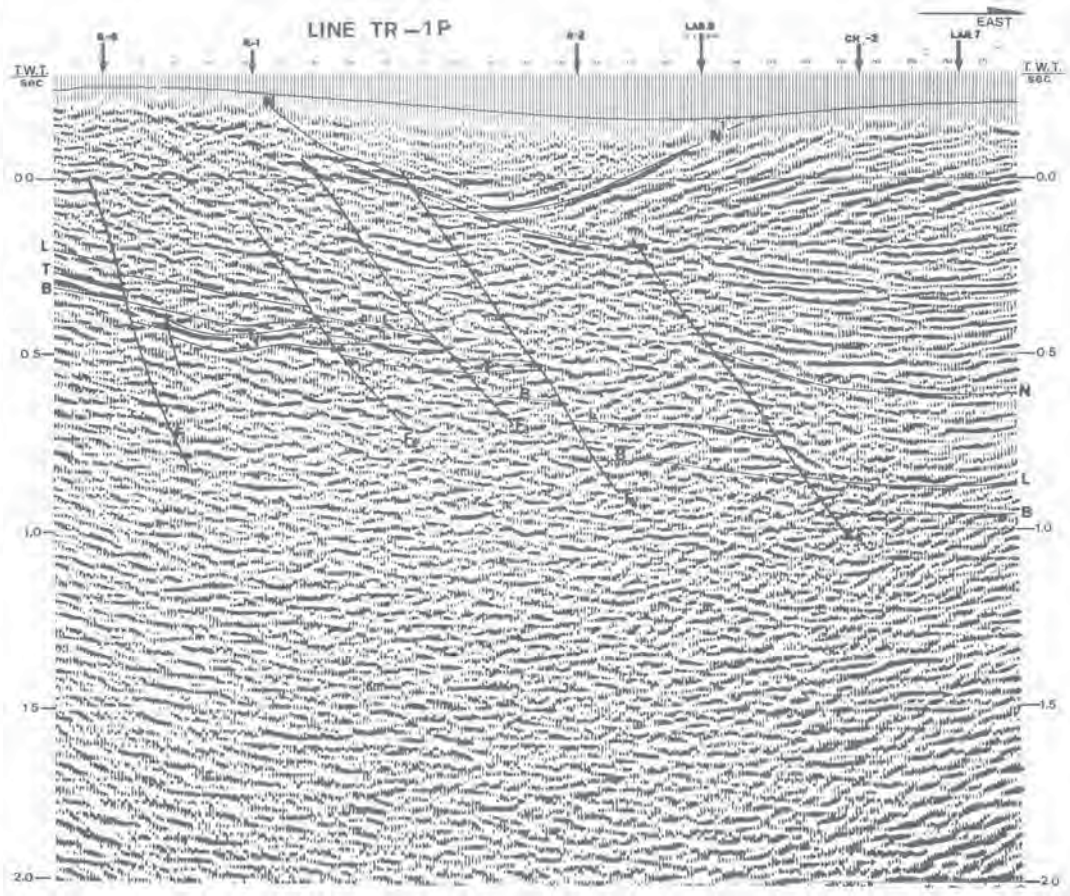

Fig. 7. Profile TR-1P, migrated section, with the interpretation overimpressed: horizon N' = base of Pliocene, N = base of Neogene, L = base of Ligurian nappes, T = base of Macigno formation, T_1 = base of Tuscan wedges, B = top of metamorphic basement; F_1, F_2 . . . = faults.

Tatham, 1982), but porosity also affects α (Biot, 1956; Domenico, 1974, 1977; Gardner *et al.*, 1968; Leslie and Mons, 1982). Moreover, fracture porosity lowers both V_p and V_s (Gardner *et al.*, 1968) but the form and orientation of the fractures also affect the α ratio in different ways (Tatham, 1982). The number of microfractures is directly connected to the increase in temperature (Gregory, 1977).

Winkler and Nur (1982) and Kustler and Toksöz (1974) studied the influence of the pore fluids and saturation degree, while Johnston and Toksöz (1980) clarified the importance of differential pressures.

Reflectivity changes (A_p and A_s amplitudes) are also evident when water or steam are present: the attenuation ratio Q_p/Q_s is greater than 1 in partially saturated rocks, but lower than 1 in dry or fully saturated rocks (Winkler and Nur, 1982; Johnston and Toksöz, 1980; Mochizuki, 1982).

CONCLUSIONS

The seismic data clearly reveal the trends of the macrofactures. The Apenninic trend (Fig. 12) is indicated by the major faults F_1 and F_5 or F_7. The latter represents the system of faults

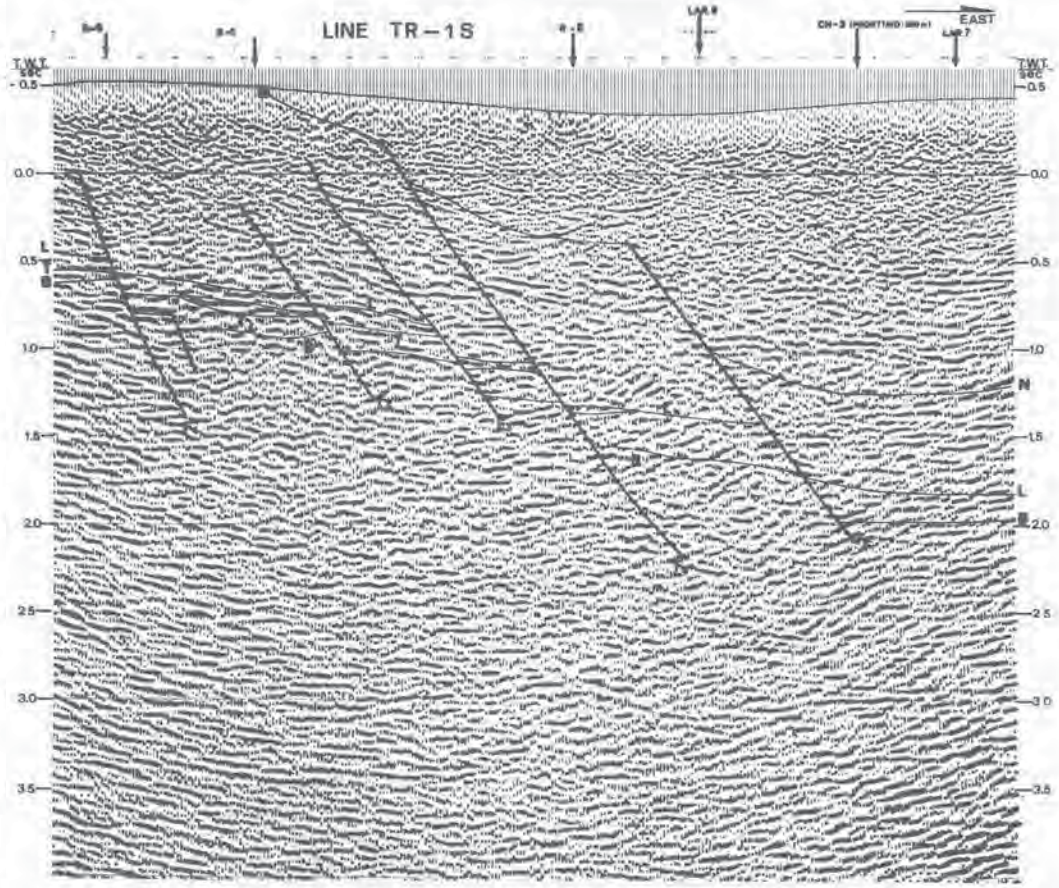

Fig. 8. Profile TR-1S, migrated section, with the interpretation overimpressed: horizon N = base of Neogene, L = base of Ligurian nappes, T = base of Macigno formation, T_t = base of Tuscan wedges, B = top of metamorphic basement.

bordering the Neogene basin towards the east. The anti-Apenninic trend is represented by fault F_6, with possible components of horizontal lateral movements. F_6 separates the Travale field from the new zone explored in the last few years, while F_5 seems to limit the productive zones towards the east. However, the geothermal potential of the reservoir inside the boundaries of the macrofractures is conditioned by the fracturation degree. These conditions and the nature of fluid content may affect the V_p and V_s velocities.

According to the sonic data collected in well CH-3, lithology seems to be responsible for the main velocity changes. Nevertheless, an increase of α was found to correspond to the gas – water interface indicated at a depth of 1920 m inside the reservoir by shut-in pressure data. This interface is also evidenced by the pseudo-impedance log and by the seismic reflection data. Clear changes of α are evident in the basement where some fractures are present. Inside the sedimentary cover an increase of α could indicate the presence of water, while a decrease of α could be related to the presence of gas. In Fig. 13 the sharp increase of V_s (CDP 95-112) could be related to a gas zone with low porosity and permeability, as verified by a dry well (R-11) and by lower temperature values (Batini *et al.*, 1985). In the CDP (Common Depth Point) intervals 19 – 50 and 130 – 140, increased α values are related to the presence of a liquid phase in the

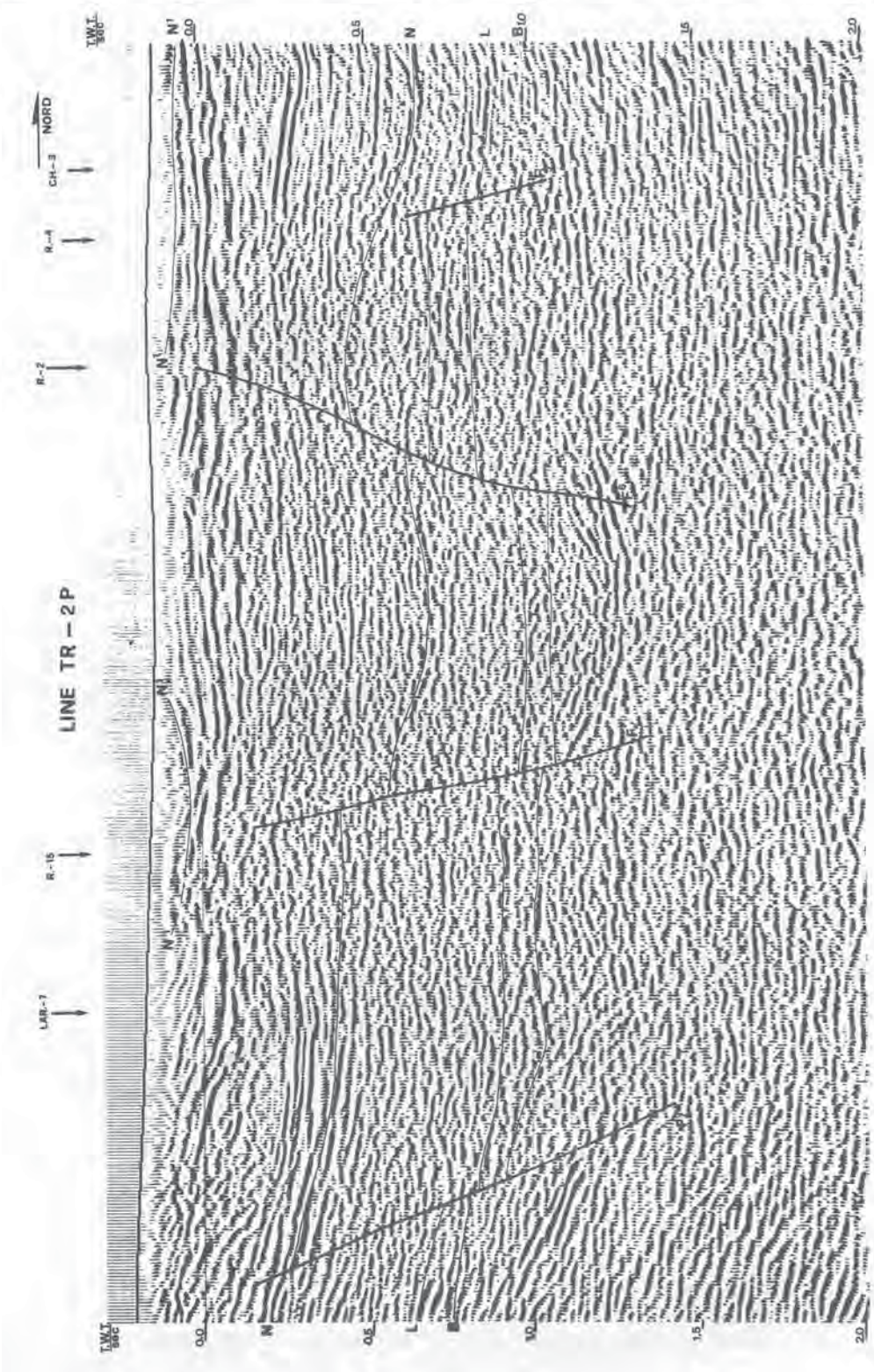

Fig. 4. Profile TR-2P, migrated section, with the interpretation overimpressed: horizon N' = base of Pliocene, N = base of Neogene, L = base of Ligurian nappes, B = top of metamorphic basement.

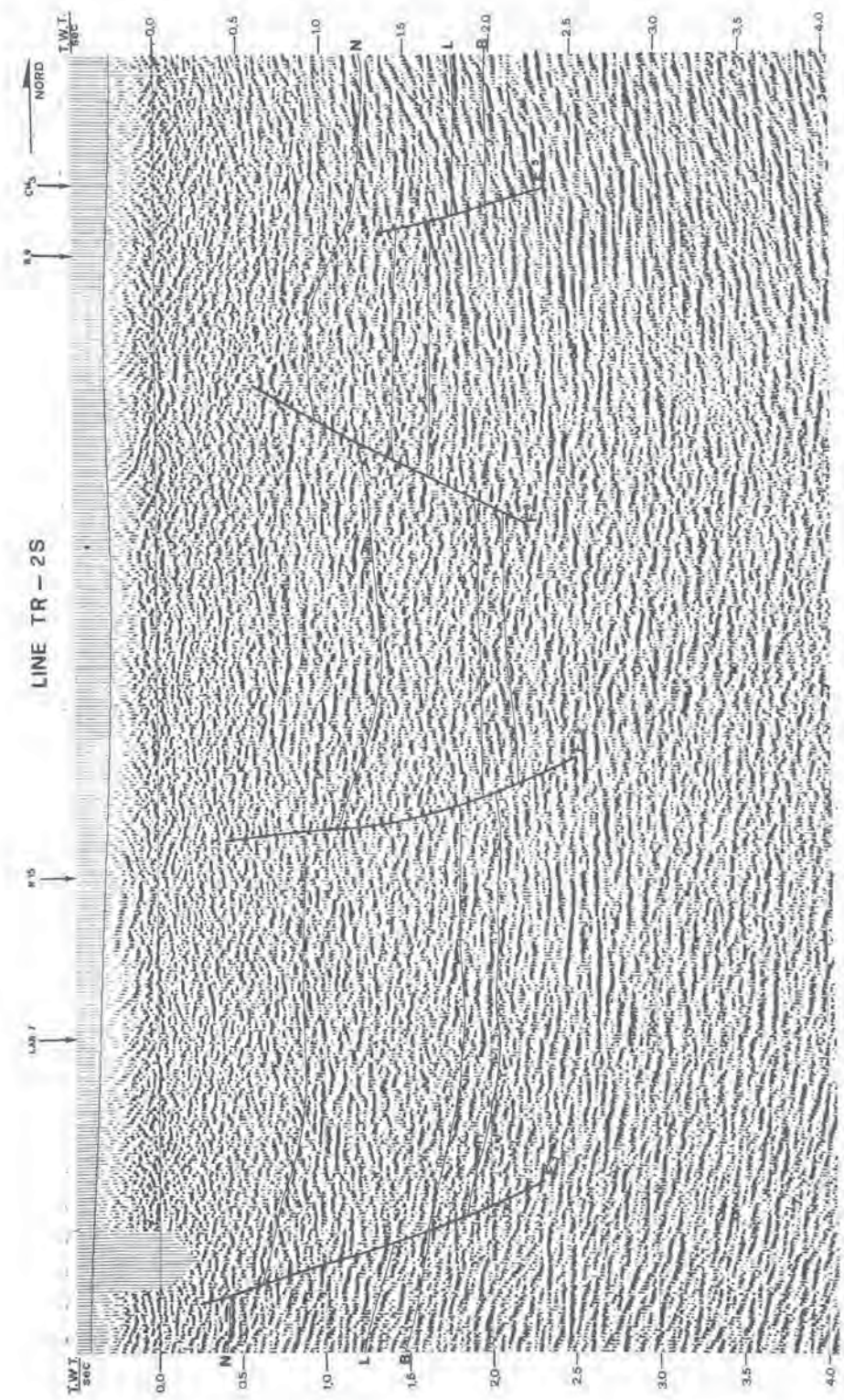

Fig. 10. Profile TR-2S, migrated section, with the interpretation overimpressed: horizon N = base of Neogene, L = base of Ligurian nappes, B = top of metamorphic basement.

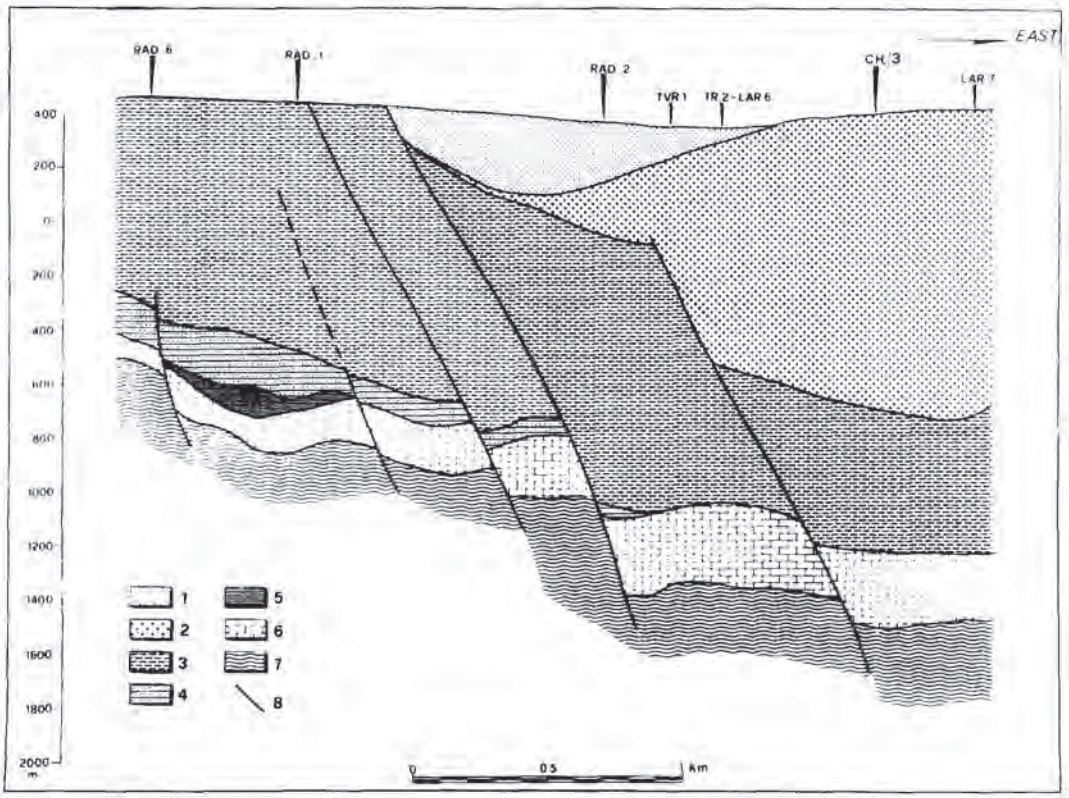

Fig. 11. Profile TR-1P, depth section: (1) Pliocene, (2) Upper Miocene, (3) Ligurian nappes (flysch), (4) sandstone (Macigno), (5) Tuscan wedges, (6) Burano anhydrites, (7) metamorphic basement, (8) vertical discontinuities.

reservoir (wells R-6 and R-2). Figure 14 shows variations of the α ratio which are evident in the area of well R-4 (gas – steam), and particularly near well R-15 (high water saturation).

Analysis of the reflectivity data reveals high A_p values and low A_s values in the reservoir and in the basement, where partially saturated rocks or sharp variation of the differential pressures are assumed (profile TR-1, CDP 1 – 80; profile TR-20, CDP 70 – 110, 250 – 300 and 380 – 394). As high A_p and high A_s are found to correspond to abrupt lithological changes, high A_s and low A_p seem to be linked to the presence of gas or steam. The amplitude anomalies revealed by the seismic data can, therefore, be related to the geothermal potential of the carbonate reservoir exploited at present and of eventual fluid traps inside highly fractured layers of the metamorphic basement.

The recorded P and S data support the conceptual model for the Travale geothermal field; that is, upward migration of fluids through macrofractures or vertical faults and their horizontal spreading in the shallower permeable layers.

Acknowledgements—The acquisition and processing of seismic data and well logging were performed by the subcontractors Compagnie Générale de Géophysique and Schlumberger respectively. We wish to thank ENEL, Italy, for permission to use geological and geophysical data and technical assistance.

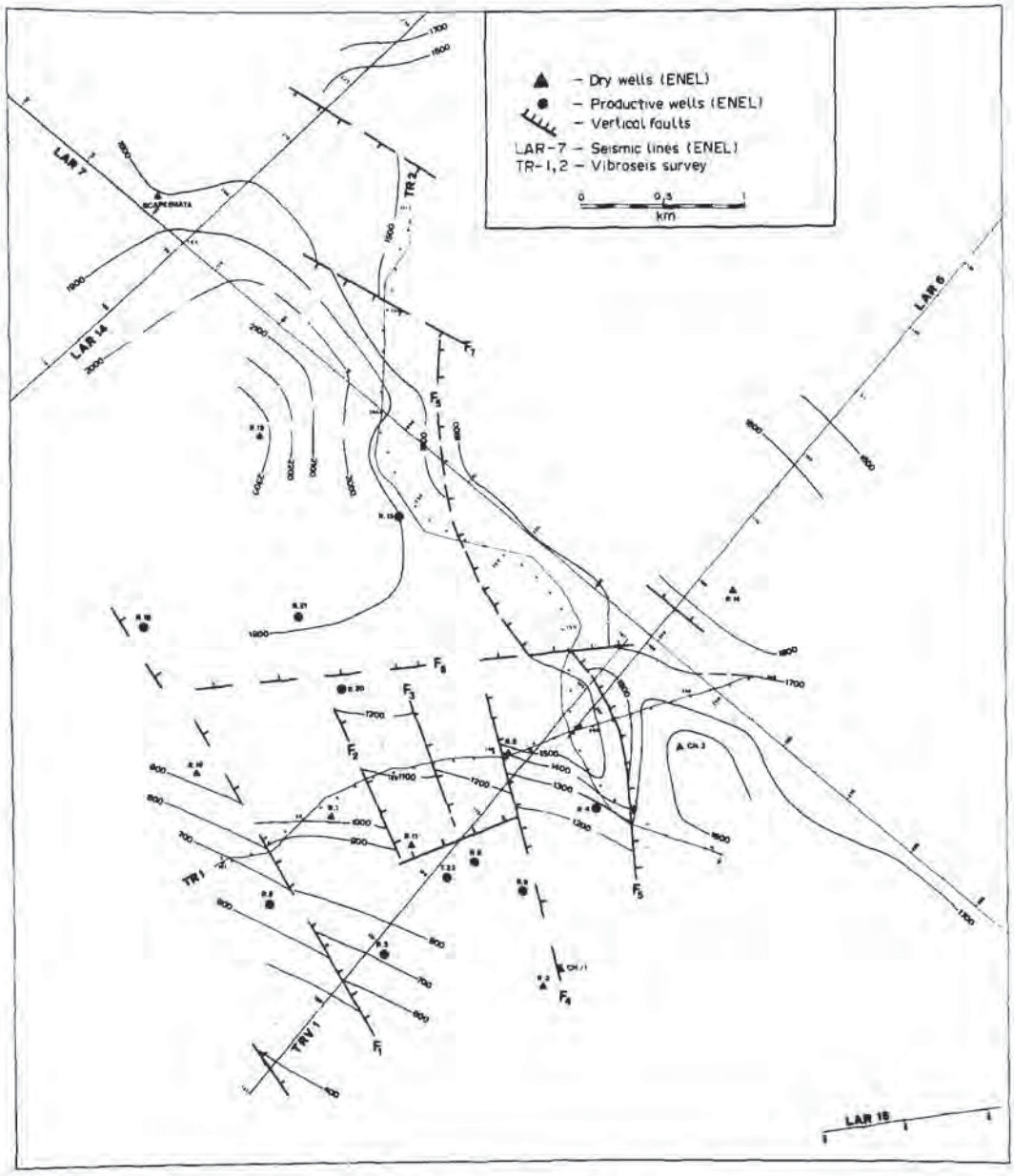

Fig. 12. Isobaths of the top of metamorphic basement.

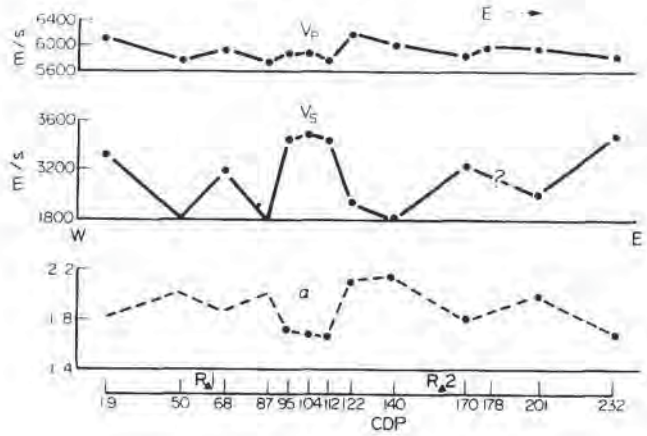

Fig. 13. Profile TR-1: distribution of the average values of V_p, V_s and α in the carbonate reservoir.

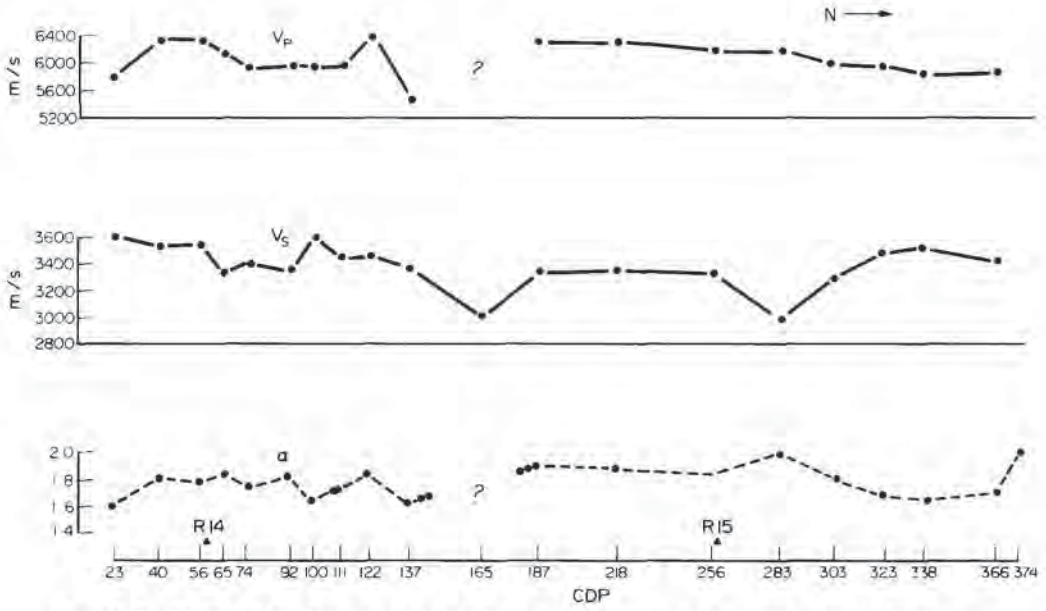

Fig. 14. Profile TR-2: distribution of the average values of V_p/V_s and α in the carbonate reservoir.

REFERENCES

Batini, F. and Nicolich, R. (1984) The application of seismic reflection methods to geothermal exploration. *Seminar on Utilisation of Geothermal Energy for Electric Power Production and Space Heating*. Florence, May 1984. United Nations, Geneva, Economic Commission for Europe.

Batini, F., Castellucci, P. and Neri, G. (1985) The Travale geothermal field. *Geothermics* **14**, 623 – 636.

Batini, F., Burgassi, P. D., Cameli, G. M., Nicolich, R. and Squarci, P. (1978) Contribution to the study of the deep lithospheric profiles: "deep" reflecting horizons in Larderello – Travale geothermal field. *Mem. Soc. Geol. Ital.* **19**, 477 – 484.

Batini, F., Bertini, G., Bottai, A., Burgassi, P. D., Cappetti, G., Gianelli, G. and Puxeddu, M. (1983) S. Pompeo 2 deep well: a high temperature and high pressure geothermal system. *Third EEC Int. Seminar European Geothermal Update*, 29 November – 1 December, Munich.

Biot, M. A. (1956) Theory of propagation of elastic waves in a fluid saturated porous solid. *J. acoust. Soc. Am.* **28**, 168 – 191.

Domenico, S. N. (1974) Effects of water saturation on seismic reflectivity of sand reservoirs encased in shales. *Geophysics* **39**, No. 12.

Domenico, S. N. (1977) Elastic properties of unconsolidated porous sand reservoirs. *Geophysics* **42**, No. 12.

Ferrucci, F. and Hirn, A. (1984) P and differential arrival times at a dense array: a marker of the Travale field from local earthquakes. *Third EEC Int. Seminar European Geothermal Update*, 29 November – 1 December, Munich, 1983, EUR 8853 EN.

Gardner, G. H. G., Gardner, L. W. and Gregory, A. R. (1968) Formation velocity and density. Diagnostic basis for stratigraphic traps. *38th Congress Soc. Exploration Geophysicists*, Denver, U.S.A.

Goupillard, P. L. and Cherry, J. T. (1977) Utilisation of seismic exploration technology for high resolution mapping of a geothermal reservoir. Energy Research and Development Administration, SAN/1249-1, Washington, U.S.A.

Gregory, A. R. (1977) Aspect of rock physics from laboratory and log data that are important to seismic interpretation. In: *"Seismic" Stratigraphy—Application to Hydrocarbon Exploration* (Edited by Payton, C. E.), pp. 15 – 46. AAPG Publ.

Johnston, D. H. and Toksöz, M. N. (1980) Ultrasonic P and S wave attenuation in dry and saturated rocks under pressure. *J. geophys. Res.* **86**, 925 – 936.

Kustler, G. T. and Toksöz, M. N. (1974) Velocity and attenuation of seismic waves in two-phase media: Part II. Experimental results. *Geophysics* **39**, No. 5.

Leslie, H. D. and Mons, F. (1982) Sonic waveform analysis. *SPWLA Twenty-third Annual Logging Symp.* 6 – 9 July 1982.

Mochizuki, S. (1982) Attenuation in partially saturated rocks. *J. geophys. Res.* **87**, 8598 – 8604.

Pickett, G. R. (1963) Acoustic character logs and their application in formation evaluation. *J. Petrol. Technol.*

Tatham, R. H. (1982) V_p/V_s and lithology. *Geophysics* **47**, 336 – 344.

Winkler, K. W. and Nur, A. (1982) Seismic attenuation: effects of pore fluids and frictional sliding. *Geophysics* **47**, 1 – 15.

Available online at www.sciencedirect.com
SCIENCE DIRECT®
Journal of volcanology and geothermal research
ELSEVIER
Journal of Volcanology and Geothermal Research 132 (2004) 15–29
www.elsevier.com/locate/jvolgeores

Heat flow, deep temperatures and extensional structures in the Larderello Geothermal Field (Italy): constraints on geothermal fluid flow

S. Bellani [a], A. Brogi [b,*], A. Lazzarotto [b], D. Liotta [c], G. Ranalli [d]

[a] *Istituto di Geoscienze e Georisorse, CNR, Via Moruzzi 1, 56124 Pisa, Italy*
[b] *Dipartimento di Scienze della Terra, Universita' di Siena, Via Laterina 8, 53100 Siena, Italy*
[c] *Dipartimento di Geologia e Geofisica, Universita' di Bari, Via Orabona 4, 70125 Bari, Italy*
[d] *Department of Earth Sciences and Ottawa–Carleton Geoscience Centre, Carleton University, Ottawa, Canada K1S 5B6*

Received 9 April 2003; accepted 24 November 2003

Abstract

The Larderello geothermal field is located in the inner Northern Apennines (southern Tuscany), an area which has been affected by extensional tectonics since the Early–Middle Miocene. The structure of the Larderello field is characterised by NW-trending, NE-dipping Pliocene to Present normal faults. Their geometry down to depths of 4–5 km is constrained by field, borehole, and reflection seismic data. An association between extensional structures and heat flow maxima (up to 1000 mW/m^2) is recognisable from detailed surface heat flow mapping. In order to investigate the relationships among extensional structures and heat flow, subsurface isotherms were traced, subject to borehole control, along variously oriented geological cross-sections. The isotherms show vertical displacements associated with the recent normal faults and related deformation zones, which reach the brittle/ductile transition. Estimates of the relative importance of convective and conductive components of heat flow suggest that fluid circulation is particularly important in correspondence with the normal faults, accounting for the correlation between isotherm perturbations and extensional structures. In this view, extensional shear zones are interpreted as the main structural pathways for the flow of hot geothermal fluids.

Keywords: crustal extension; heat flow; shear zones; fluid flow; Larderello geothermal field

1. Introduction

Continental extensional tectonic environments with high heat flow are often affected by geothermal systems, independently from the geodynamic context in which they are located (see e.g. Muffler and Duffield, 1995; Barbier, 2002). Important examples are the geothermal areas of Yellowstone (Eaton et al., 1975, Morgan et al., 1977; Lucchitta, 1990), of northern California (Younker et al., 1982), of the Pannonic Basin (Ravnik et al., 1995), and of the Rhine Graben (Werner and Kahle, 1980; Brun et al., 1992). An extensional tectonic setting also characterises southern Tus-

* Corresponding author. Fax: +39-05-7723-3938.
E-mail address: brogiandrea@unisi.it (A. Brogi).

0377-0273/03/$ – see front matter © 2003 Elsevier B.V. All rights reserved.
doi:10.1016/S0377-0273(03)00418-9

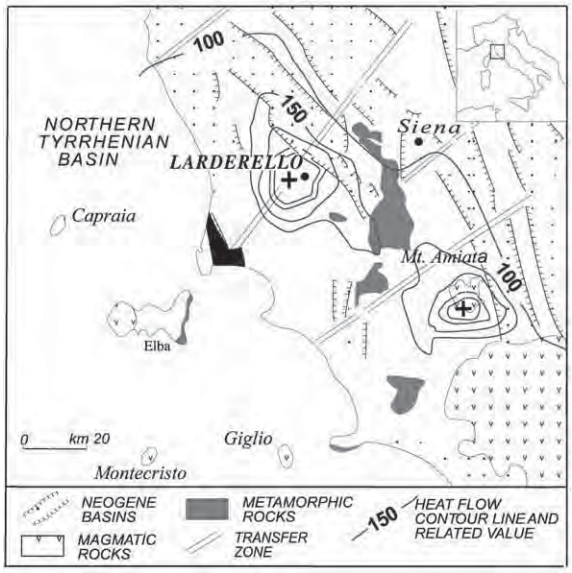

Fig. 1. Structural sketch map of southern Tuscany with regional heat flow contour lines (equidistance: 50 mW/m^2). The plus signs show the Larderello and Monte Amiata geothermal fields where heat flow reaches 1000 mW/m^2 and 600 mW/m^2, respectively (redrawn from Baldi et al., 1995).

cany, where the Larderello geothermal field is located (Fig. 1). The region is part of the inner Northern Apennines, which have been affected by post-collisional extensional tectonics since the Early–Middle Miocene (Carmignani et al., 1994; Rossetti et al., 1999). Extension was accompanied by widespread Late Miocene–Quaternary magmatism deriving from mixing of crustal and mantle sources (Serri et al., 1993). Since the Middle Pliocene, southern Tuscany has been affected by rapid surface uplift (Dallmeyer and Liotta, 1998), in contrast with the coeval thermal subsidence affecting the nearby northern Tyrrhenian Basin (Bartole, 1995 and references therein).

An anomalous high value of heat flow characterises a large part of southern Tuscany. This region can be encompassed on a map by the 100 mW/m^2 contour line (Fig. 1), i.e. a value almost double the continental average (cf. Sclater and Christie, 1980). Inside this wide region, two areas, corresponding to the Larderello and Mt. Amiata geothermal fields, reach values of up to 1000 mW/m^2 (Larderello) and 600 mW/m^2 (Mt. Amiata). Both fields are exploited for the production of geothermal energy.

This paper focuses on the Larderello geothermal field, where the large amount of available geophysical and geological data makes the area suitable as a natural laboratory to investigate the relationships between extensional structures, deep isotherms, fluid circulation, and heat flow. We combine a new compilation of surface heat flow data, surface and borehole geology, several seismic reflection lines, and borehole-controlled subsurface isotherms to investigate whether normal faults and associated deformation zones (which we term extensional shear zones) are correlated with perturbations of the thermal regime. These perturbations are in all likelihood transient in nature, but provide information on the factors affecting fluid circulation in the geothermal field. The evidence leads us to hypothesise that the shear zones act as preferred pathways for fluid circulation, and that the latter is locally important in generating temperature gradient anomalies superimposed to the high background geotherm of the area, due to the transient effects of lithosphere extension and crustal magmatic intrusion.

2. Geological framework

After the convergent and collisional stages which determined the structural emplacement of the Northern Apennines tectonic units (Late Cretaceous–Early Miocene), the region was affected by extensional tectonics (Miocene–Present; e.g. Jolivet et al., 1994; Carmignani et al., 1995). Collisional and extensional processes are expressed in the structure of the Larderello geothermal field. A geological map of the area is shown in Fig. 2. Five regional tectono–stratigraphic elements have been recognised (Fig. 3):

(1) Miocene–Pliocene and Quaternary sediments, filling extensional tectonic depressions and unconformably overlying the substratum.

(2) The Ligurian Complex, which includes the Ligurian Complex s.s. and the Subligurian Complex. These consist of remnants of Jurassic oceanic crust and its related Jurassic–Cretaceous sedimentary cover, and Cretaceous–Oligocene flysch,

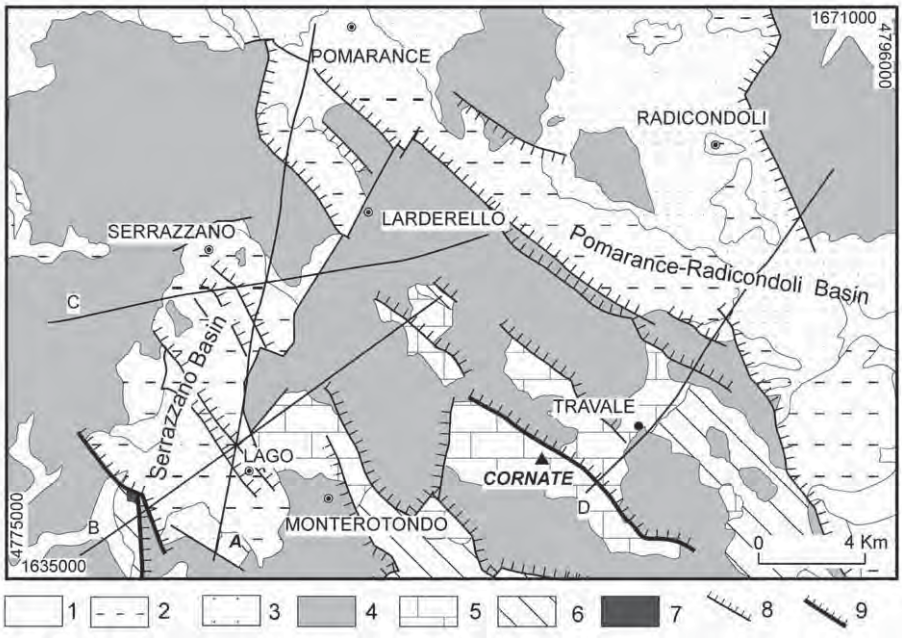

Fig. 2. Geological sketch map of the Larderello area. Key: (1) Quaternary continental sediments; (2) Pliocene marine sediments; (3) Miocene continental, brackish and marine sediments; (4) Ligurian Complex (Jurassic–Oligocene); (5) Tuscan Complex (Late Trias–Early Miocene sedimentary sequence); (6) Tuscan Complex (Late Triassic evaporite); (7) Palaeozoic phyllite; (8) normal faults; (9) normal faults mineralised by mixed sulphides of hydrothermal origin, linked to the Pliocene–Quaternary Tuscan magmatism (Arisi Rota et al., 1971). Lines A–D denote the geological sections shown in Figs. 6 and 7.

respectively. The Ligurian Complex was thrust eastward over the Tuscan Complex during Late Oligocene–Early Miocene.

(3) The Tuscan Complex, including sedimentary rocks ranging from Late Triassic evaporites to Late Oligocene–Early Miocene turbidites.

(4) Below the Tuscan Complex, the substratum is known mainly through drilling of geothermal wells penetrating the crust down to a depth of about 3.5 km. It is made up of two units (Bertini et al., 1991), i.e. the upper Monticiano–Roccastrada Unit (MR U), and

(5) the lower Gneiss Complex (see Fig. 3 for more details).

In the Larderello area, boreholes encounter felsic dykes and granitoids at different depths, with cooling ages ranging between 3.80 and 2.25 Ma (Gianelli and Laurenzi, 2001). Magmatic fluids from these granitoids are considered to be the agents of the hydrothermal mineralisation characterising many deep borehole samples (Gianelli, 1994).

Two geothermal reservoirs in the Larderello field are industrially exploited: a shallow one (about 700–1000 m below ground level on average) located at the base of the sedimentary cover in the cataclastic level mainly corresponding to the Late Triassic evaporites, and a deep one, located in fractured metamorphic rocks at depths ranging between 2000 and 4500 m. The fluids stored in these reservoirs originate from mixing among dominant meteoric waters, products of water–rock interaction, and fluids from deep magmas (D'Amore and Bolognesi, 1994).

Information on deeper structural levels is derived from seismic reflection lines. The profiles show a clear distinction between a poorly reflective uppermost crust and a highly reflective mid–lower crust (Cameli et al., 1993). The top of the reflective crust is marked by a high-amplitude discontinuous reflector with local bright spot features, named K-horizon (Batini et al., 1978; Batini and Nicolich, 1985). The K-horizon in the Larderello area ranges in depth from about 3 to

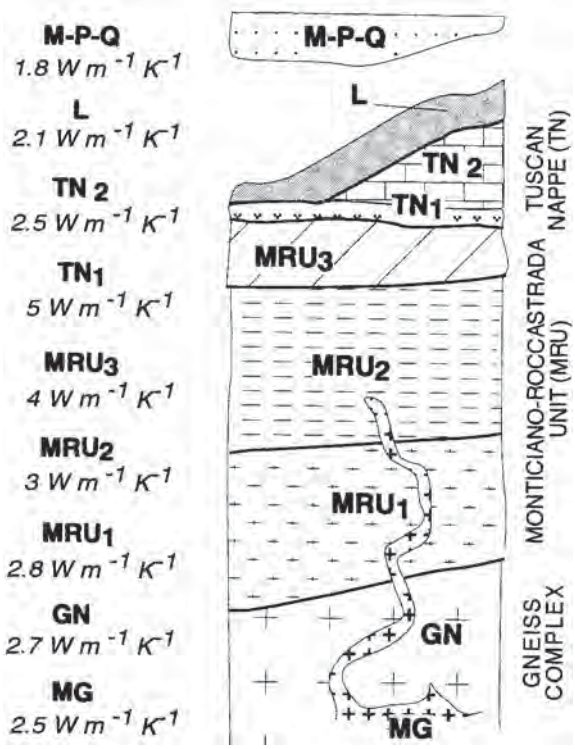

Fig. 3. Tectono–stratigraphic units of the Larderello area: MPQ, Miocene, Pliocene and Quaternary sediments; L, Ligurian Complex Tuscan Nappe (TN): TN_2, Early Miocene–Rhetic sequence; TN_1, Late Triassic evaporites; Monticiano–Roccastrada Unit (MRU): MRU_3, Mesozoic–Palaeozoic Group, made up of dolostones and limestones (Late Triassic), quartz meta-conglomerates, quartzites and phyllites (Verrucano Group, Middle–Early Triassic), sandstones, phyllites (Middle–Late Carboniferous-Early Permian); MRU_2, Phyllitic–Quartzitic Group; MRU_1, Palaeozoic Micaschist Group; GN, Gneiss Complex; MG, magmatic intrusions. Thermal conductivity values for each tectono–stratigraphic unit are listed on the left (data from Baldi et al., 1994a; Della Vedova et al., 2001).

6 km (Cameli et al., 1998 and references therein). Temperature borehole data, hypocentral distributions of micro-earthquakes, and rheological considerations suggest that the K-horizon marks the upper boundary of an active shear zone at the top of the brittle/ductile transition (Cameli et al., 1993; 1998; Liotta and Ranalli, 1999). The origin of the reflectivity at the K-horizon and immediately below has been discussed by several authors. It is generally agreed that localised high fluid pressures can explain the observed high contrast in acoustic impedance (see e.g. Gianelli et al., 1997; Liotta and Ranalli, 1999; Brogi et al., 2003).

3. Larderello extensional structures

Post-collisional extensional tectonics intensely affected the inner zone of the Northern Apennines, resulting in the present crustal and lithospheric thickness of about 22 and 30 km, respectively (see review by Liotta et al., 1998).

In the Larderello area, three extensional tectonic events are recognisable. The first and second occurred in Miocene times, and resulted in the juxtaposition of the Ligurian Complex on the Triassic evaporites, on the Verrucano Group and on the Phyllitic–Quartzitic Group along low angle normal faults (Baldi et al., 1994b; Dallmeyer and Liotta, 1998). The latest extensional event (Pliocene–Present) is typified by high-angle normal faults, generally NW–SE striking and NE-dipping, which dissect Early–Middle Pliocene and Early Pleistocene sediments. At depth, these faults coalesce in wider extensional shear zones which tend to flatten with increasing depth (Fig. 4). Three such extensional shear zones are recognisable in the Larderello area (Fig. 5A). Intersections between the shear zones and the top of the brittle–ductile transition are correlated with loss of the K-horizon reflectivity. It has been hypothesised that the loss of seismic reflectivity is connected to fluid migration from the K-horizon to shallower levels along the shear zone (Brogi et al., 2003).

4. Heat flow

Fig. 5B shows the surface heat flow map of the Larderello area, compiled on the basis of data from hundreds of shallow temperature gradient measurements and deep exploration geothermal wells (cf. Cataldi et al., 1995; Della Vedova et al., 2001 with references therein). Thermal borehole data have been carefully selected, using only wells drilled for temperature gradient determination in the impervious cover formations or deep

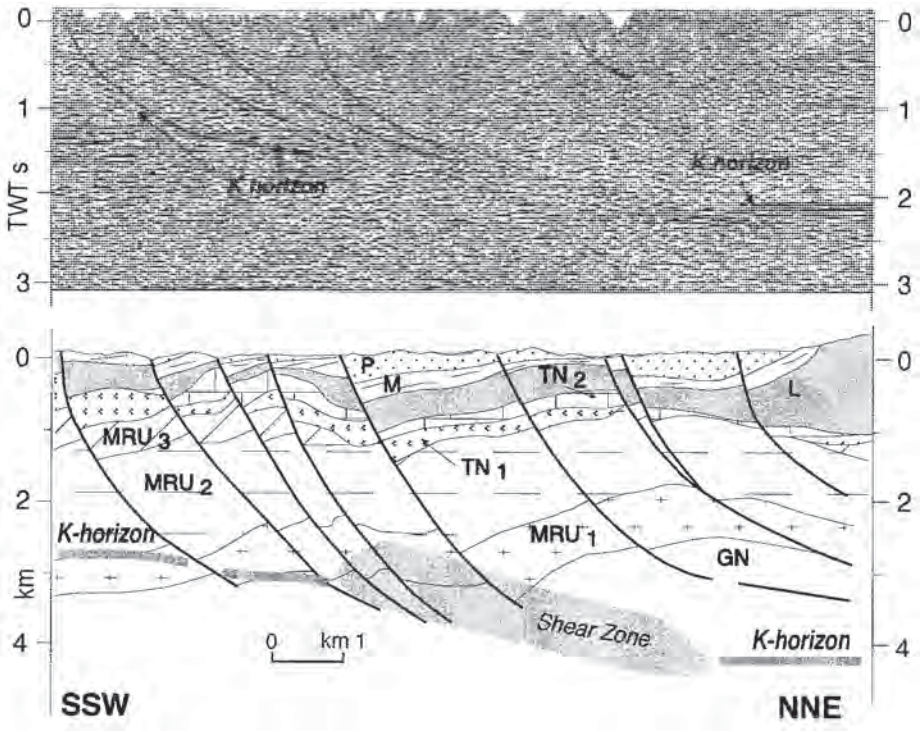

Fig. 4. (Top) Part of the unmigrated seismic reflection line A (for location see Fig. 2). Datum plane is 200 m above sea level. Normal faults and the K-horizon are highlighted. (Bottom) Geological interpretation. Symbols as in Fig. 3 (modified from Brogi et al., 2003).

geothermal wells unaffected by fluid flow, to minimise the effect of fluid movements on the temperature gradients. Thermal conductivity data have been obtained from core samples when available, or from estimates based on lithology (Baldi et al., 1994a; Angenheister, 1982). Data from deep core samples have been corrected for in-situ temperatures according to Somerton (1992). Typical room temperature thermal conductivities for the various units are shown in Fig. 3.

A first-order feature of the heat flow map is a SW–NE elongated anomaly encompassed by the 200 mW/m^2 contour line. This is superimposed on a general NW–SE trending heat flow anomaly affecting central Italy, as shown by regional heat flow maps (Mongelli et al., 1998). Within the area enclosed by the 200 mW/m^2 contour, the map shows two large relative maxima (up to 1000 mW/m^2). The western maximum, centered in the Lago locality, is located in the Serrazzano extensional basin; the eastern one is in the Larderello area. These maxima appear to be correlated with the occurrence of Pliocene–Present normal faults. A third large anomaly (>500 mW/m^2) is located ESE of Larderello near Travale.

5. Extensional structures and geothermal anomalies

Extensional structures, location of the shear zones at depth, and surface heat flow in the Larderello area are shown in Fig. 5A,B. In the Serrazzano Basin, the pattern of the local heat flow maxima shows a correlation with the trend of the normal faults and deep shear zones. A similar feature typifies also the Larderello area, suggesting a relation between surface heat flow pattern and the trend of geological structures. In the Travale area, the maximum of the surface heat flow contour lines is centred in the southernmost part of the normal faults bordering the Pomarance Basin.

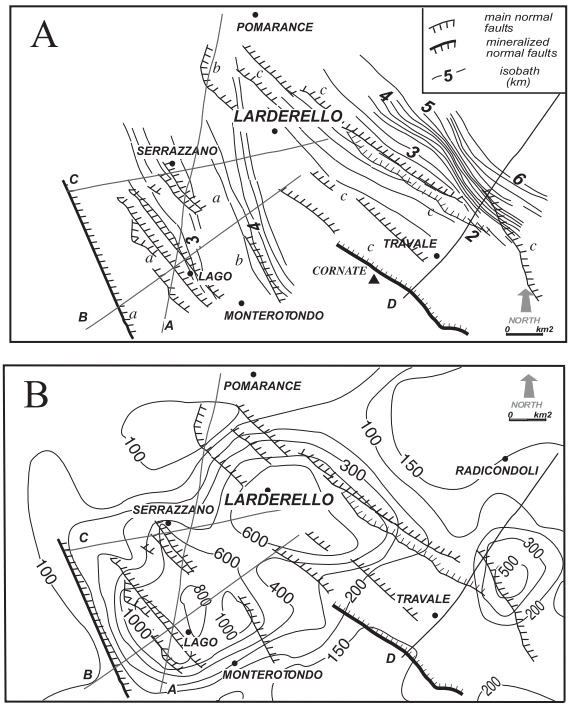

Fig. 5. (A) Isobaths of the three main extensional shear zones (from W to E: Serrazzano–Lago, Larderello–Monterotondo and Pomarance–Travale shear zones). Symbols (a), (b), and (c) denote normal faults related to the western, central and eastern shear zones, respectively (modified from Brogi et al., 2003). (B) Normal faults and heat flow contours (mW/m^2) in the Larderello geothermal field (thermal raw data from Baldi et al., 1995, reanalysed, digitised, and redrawn).

To investigate the relationship between geothermal anomalies and extensional structures, we constructed geological sections (Figs. 6 and 7; location in Fig. 2) through the extensional shear zones and the surface heat flow maxima. The sections integrate field and borehole data with interpretation of reflection seismic lines. The sections are then compared with the pattern of upper crustal isotherms, drawn on the basis of temperature borehole measurements. In Figs. 6 and 7, we have traced isotherms only where we considered the borehole control sufficiently good on the basis of location and number of data points.

5.1. Line A

This section (Fig. 6, Line A) crosses in an approximately N–S direction the Serrazzano and Pomarance Pliocene Basin, passing through the Lago geothermal anomaly, where the highest heat flow of the Larderello geothermal field is recorded. NE-dipping listric normal faults related to the latest extensional event characterise the structural setting. The geometry of these faults is well constrained by borehole and field data from the surface down to about 2.5 km. Their continuation down to the top of the brittle–ductile transition is defined by reflection seismic data (Cameli et al., 1993; Brogi et al., 2003) which indicate coalescence of the faults into brittle shear zones and associated loss of continuity in the K-horizon (see also Fig. 4).

The heat flow profile shows a wide maximum (>800 mW/m^2) in the southernmost part of the section. This value decreases northwards to about 150 mW/m^2. This trend is reflected in the underground temperature distribution, as marked by the 200°C isotherm, which deepens northwards from less than 1 km to about 2 km of depth. The isotherm pattern shows perturbations in correspondence with the normal fault system defining the southwestern shear zone.

5.2. Line B

This section (Fig. 6, Line B) makes a large angle with line A (see Fig. 2), crossing in a SW–NE direction the two heat flow maxima which characterise the southern part of the Serrazzano Basin. The geological structures along this section are well known from field, borehole, and seismic data (Lazzarotto and Mazzanti, 1978; Batini et al., 1978).

The heat flow trend shows a wide maximum in the central part of the section, in correlation with a similarly wide culmination of the isotherms. As in the previous section, the isotherm pattern suggests thermal perturbations associated to the normal fault system of the Serrazzano Basin.

5.3. Line C

This section (Fig. 7, Line C) trends WSW–ENE, crossing the northern part of the Serrazzano Basin and the Larderello geothermal anomaly.

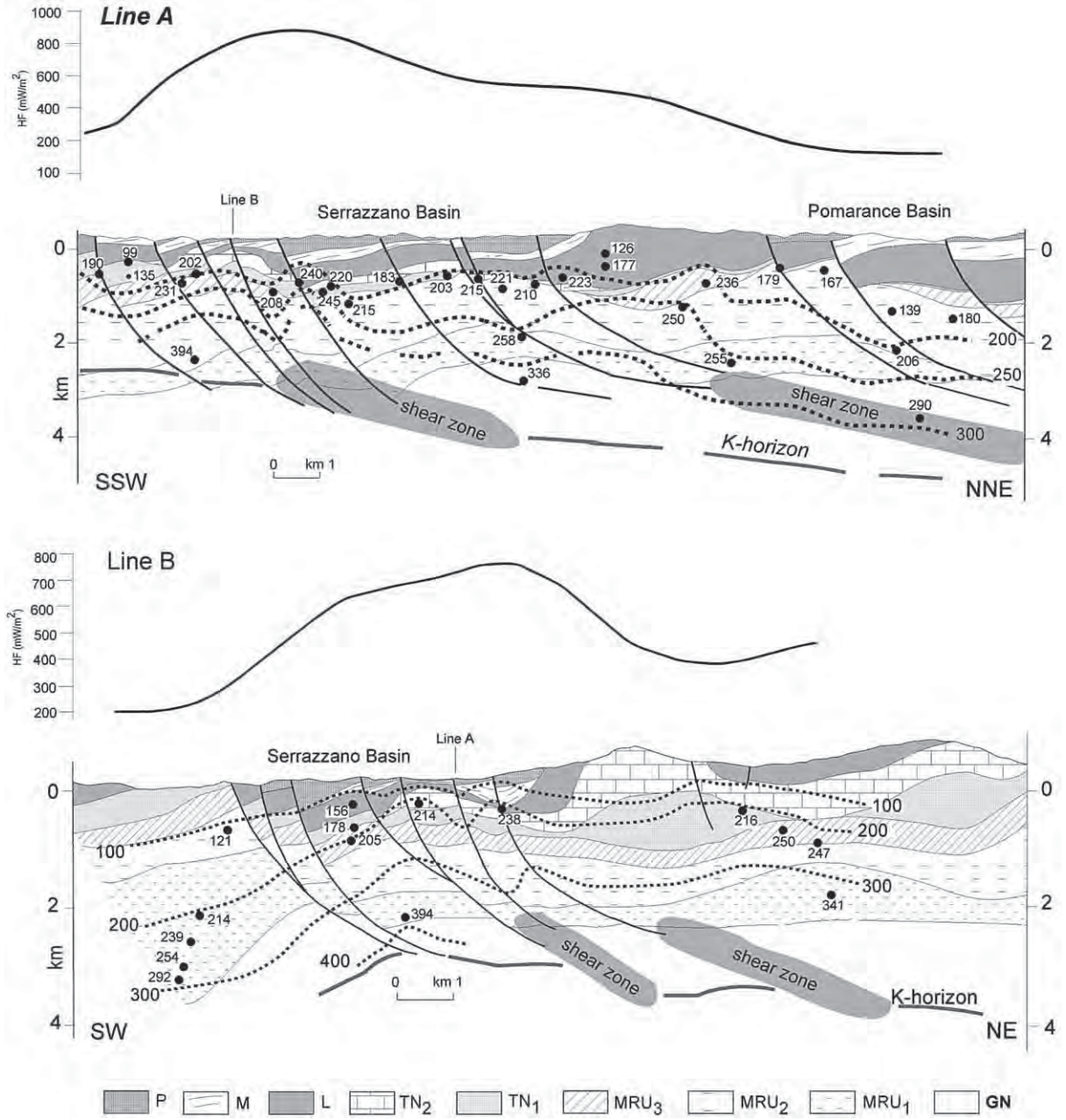

Fig. 6. Geological cross sections, isotherms, and surface heat flow along lines A and B (locations given in Fig. 2). Symbols as in Fig. 3; black circles represent temperature measurements in °C. Isotherms subject to the weakest control are denoted by a broken dashed line in both sections. The downward displacement of 300°C isotherm on line B is controlled by the intersection with Line A.

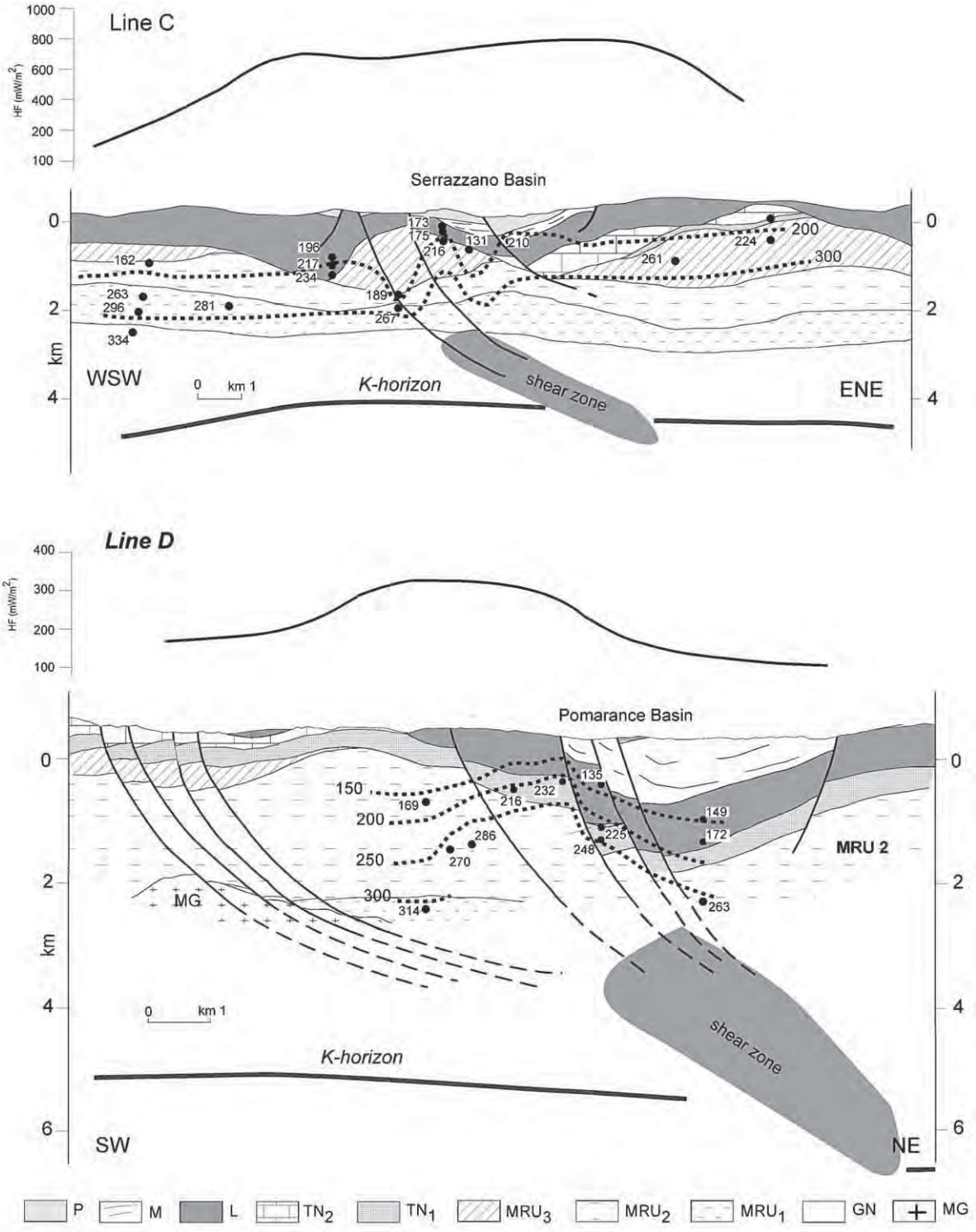
Line C
HF (mW/m²)
1000
800
600
400
200
100
Serrazzano Basin
0
2
4
km
WSW
ENE
0 km 1
K-horizon
shear zone
173
175
216
131
210
224
200
300
196
217
234
162
261
263
296
281
189
267
334
Line D
HF (mW/m²)
400
300
200
100
Pomarance Basin
0
2
4
6
km
SW
NE
0 km 1
K-horizon
shear zone
MRU 2
MG
150
169
200
232
216
135
149
172
225
248
250
286
270
300
314
263
P
M
L
TN2
TN1
MRU3
MRU2
MRU1
GN
MG

Surface heat flow is very high along the whole section, ranging from 250 to 600 mW/m^2. The perturbing effect of the normal fault system affecting the western border of the Serrazzano Basin on the deep temperatures is evident. The isotherms, approximately flat or gently rising eastwards along most of the section, show perturbations in correspondence of the faults.

5.4. Line D

Fig. 7, Line D shows this section, which crosses in a SW–NE direction the structures along the western border of the Pomarance Basin, where the Travale geothermal anomaly is located. Surface heat flow shows a clear culmination of about 400 mW/m^2 roughly coincident with the thermal maximum. Although few thermal data are available, an increase in temperature in correspondence of the normal faults bordering the Basin can be recognised. Activity of these faults has been dated as Quaternary on the basis of the age of deformed sediments (Baldi et al., 1994b).

6. Discussion

Significant thermal effects can develop during extensional tectonics if the extensional strain rate of the lithosperic mantle is rapid. The concomitant displacement of isotherms results in softening of the lithospere, surface uplift, and possibly partial melting (Kusznir and Park, 1987; Ranalli and Murphy, 1987; Lister et al., 1991). In the latter case, migration of magmatic melts from depth to mid-upper crustal levels represents the most efficient mechanism of heat transfer.

Since Middle Pliocene, southern Tuscany has been affected by surface uplift, whereas the Northern Tyrrhenian Sea has been affected by subsidence (see e.g. Zitellini et al., 1986). Several models have been proposed to account for these features (e.g. among others, Locardi, 1982; Lavecchia, 1988; Patacca et al., 1990) In any case, the occurrence of recent magmatism in southern Tuscany (see e.g. Serri et al., 1993) and in the Larderello area (Gianelli and Laurenzi, 2001) suggests that heat transfer was enhanced by migration of magmatic melts. Regionally, the effects of extension and magmatic intrusion are sufficient to explain the general features of the Larderello geothermal field, which shows a background heat flow of the order of 200 mW/m^2 (Mongelli et al., 1998). However, hydrothermal activity is dependent upon the interaction among heat sources, circulation of fluids, and permeable pathways (Curewitz and Karson, 1997). Here, we wish to assess in a preliminary way the role of fluid circulation on the more local thermal anomalies associated with the extensional shear zones.

Isotopic (Minissale et al., 2000; Magro et al., 2003 for a review) and fluid inclusions studies have shown that several types of fluids are involved in the geothermal activity of the Larderello area. Data from fluid inclusions (Cathelineau et al., 1994; Ruggieri and Gianelli, 1999, and references therein) have documented two stages of hydrothermal activity (Manzella et al., 1998). An early stage of fluid inclusions, characterised by magmatic and metamorphic fluids, is related to the emplacement of granitoids and to the accompanying reheating of basement metamorphic rocks; a late stage of trapped fluids, typified by meteoric waters with different composition and salinity, is the result of water–rock interaction, fluid boiling, vapour condensation and mixing. These fluids have evolved to present-day conditions, essentially characterised by superheated and vapour-dominated geothermal fluids.

Areas with high fracture density are generally associated with high values of permeability. Permeabilities of about 10^{-15} m^2 and of 10^{-14} to 10^{-15} m^2 have been estimated for the Larderello deeper and shallower reservoirs, respectively (Calore et al., 1981; Bertani and Cappetti, 1995). These values should represent lower limits for permeability in the extensional shear zones. Permeability shows a typical distribution in fault zones

Fig. 7. Geological cross sections, isotherms, and surface heat flow along lines C and D (locations given in Fig. 2). Symbols as in Fig. 3; see Fig. 6 for isotherms symbols.

and related fracture damage zones (Caine et al., 1996; Evans et al., 1997). Other factors (mainly lithology and confining pressure) being equal, permeability increases from the wallrock to the damage zone and decreases from the damage zone to the core of the fault, where fine-grained gouge is usually present (Seront et al., 1998; Wibberley and Shinamoto, 2003).

In the Larderello geothermal field, the thicknesses of fractured deformation bands associated with the extensional shear zones are estimated to be of the order of a few hundred metres (Brogi et al., 2003). To account for this volumetric feature, a mesh of fractures (Sibson, 1996) is supposed to be present. Depending on the angle with the main fault, single fractures can develop with different kinematics. However, extensional fractures should be pervasive in the deformation zone, and act as efficient conduits to promote circulation of fluids. In areas characterised by geothermal fluid flow, fractures and veins can be filled very rapidly by hydrothermal precipitation. Therefore, voids in shear zones must be maintained by the dynamics of faults, resulting in the re-opening of previous fractures or in the generation of new ones if sufficiently large stress concentrations are present (Barton et al., 1995). The Larderello superheated, steam dominated fluids, should have the capacity to decrease the amount of stress required for the maintenance of permeability and fluid flow (Sib-

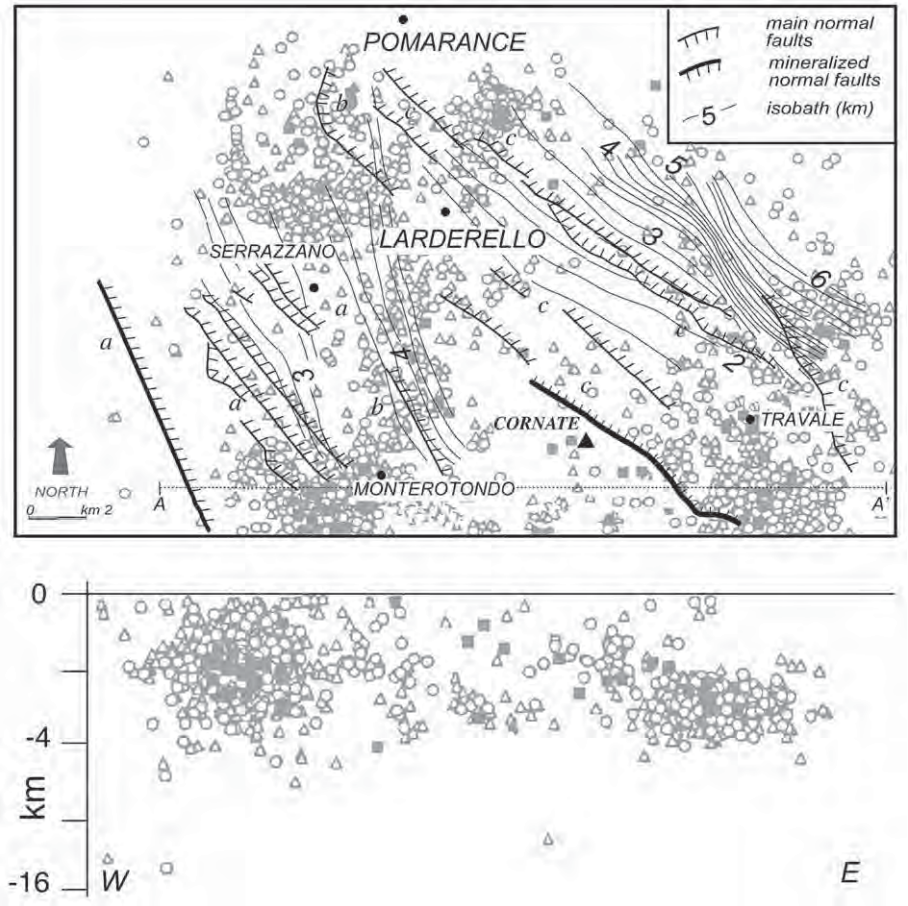

Fig. 8. (Top) Normal faults and related shear zones in the Larderello geothermal area compared with 1977–1993 micro-earthquake locations (magnitude, M, in the range 0–2.5). (Bottom) Hypocentres distribution along vertical cross-section A–A′ (dotted line on map). Symbols: triangles, $0 < M < 1$; circles, $1 < M < 2$; squares, $M > 2$ (seismic data from Batini et al., 1995).

son, 1996). The micro-earthquake distribution (see Fig. 8) confirms that the upper crust is kinematically active, although seismic activity is volumetrically pervasive rather than clearly associated with extensional shear zones.

The perturbation of isotherms in correspondence of the normal faults strongly suggests a correlation between the faults (and associated deformation zones) and fluid circulation. In principle, a large fault displacement (Ehlers and Chapman, 1999) and a displacement rate faster than the rate of isotherm re-equilibrium (Ter Voorde and Bertotti, 1994) can displace isotherms across a fault. However, fault displacements are small in the Larderello area, and appear insufficient to cause thermal variations between hangingwall and footwall. On the other hand, the locally predominant focussing of fluid circulation by convection can account for the isotherm perturbation in the shear zones. This hypothesis is also consistent with the fact that the pattern varies along strike, and consequently cannot be accounted simply in terms of isotherm displacement on the two sides of the faults.

In order to assess the relative importance of convective heat transfer in the Larderello area in general, and in the shear zones in particular, we have estimated the Péclet number, which gives the ratio of convective to conductive components of heat flow in a permeable system (cf. e.g. Clauser and Villinger, 1990):

$$Pe = (\rho c v H)/\lambda$$

where ρ, c, and v are density, specific heat, and Darcy velocity of the fluid, respectively; H is the characteristic thickness of the layer, and λ is the rock thermal conductivity. If $Pe > 1$ the system is dominated by convection. Using $\rho = 600$ kg/m^3 (density of supercritical water at $T \approx 400$°C, $P \approx 100$ MPa), $c = 2$ kJ/(kg°C) (specific heat of steam), $H = 5$ km, and $\lambda = 2.5$ W/(m K) (typical rock thermal conductivity), it follows that $Pe > 1$ if the Darcy velocity is $v \geq 4 \times 10^{-10}$ m/s ≈ 1 cm/a as an order of magnitude.

There is no direct information on Darcy velocities in the Larderello field. However, if the force potential driving the flow is approximately the same, an order-of-magnitude change in permeability will result in an equivalent change in velocity, since these two quantities are linearly related (cf. Scheidegger, 1960 for a thorough discussion of Darcy's law). Within a given system (see e.g. Clauser and Villinger, 1990 for the Rhinegraben), Darcy velocities $v > 1$ cm/a are usually associated with permeabilities $k > 10^{-14}$ m^2, as likely to be found in fault deformation zones, and within the limits of those measured in the Larderello field. Consequently, the Péclet number shows qualitatively that the Larderello field is convection-dominated, with enhanced fluid flow in high-permeabilty extensional shear zones. Since a complete hydrodynamic analysis of the field is lacking, these considerations are only of indicative value. However, on the basis of information available at present, the highly likely conclusion is that the Péclet number is supercritical and higher in correspondence of the high-permeability extensional shear zones, where consequently fluid circulation is the predominant localised factor in heat transfer within the system.

A similar conclusion can be reached from an estimation of the Nusselt number, giving the ratio of total to conductive heat transfer (cf. e.g. Haenel et al., 1988):

$$Nu = (QH)/(\lambda \Delta T A)$$

where Q is the total heat loss of the system, A the area and ΔT the temperature difference (from top to bottom) in the conductive regime, assumed to be 435°C (average surface temperature 15 C° and K-horizon temperature 450°C; Liotta and Ranalli, 1999), λ is taken as before, and H is the depth to the K-horizon. To have free (natural) convection in the system, $Nu > 1$. The Nusselt number can in principle be estimated from the ratio of total to conductive heat flow. However, this estimation is complicated by the fact that in the Larderello field the background conductive heat flow is the sum of two transients only approximately known, resulting from regional extension and more recent (< 5 Ma) magmatic intrusions. Furthermore, there is a problem with averaging the short-wavelength thermal perturbations associated with the extensional shear zones. As an example, if the local background heat flow is taken as 200 mW/m^2, most of the Larderello field has

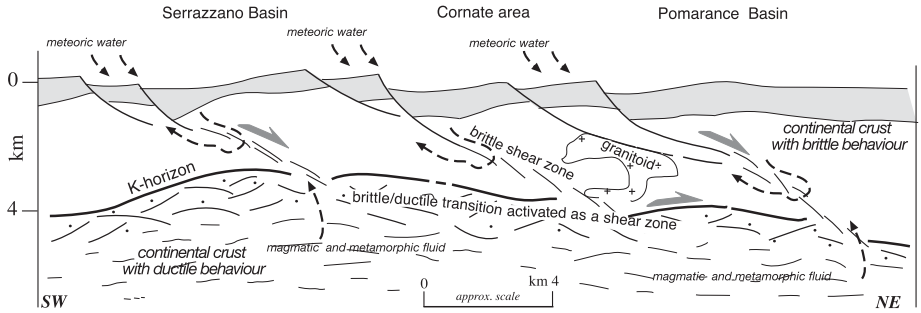

Fig. 9. Geological interpretation of the Larderello geothermal area. The extensional shear zones and the top of the brittle–ductile transition are shown (thick arrows indicate the sense of shear). The shear zones act as hydraulic channels where geothermal fluid circulation is enhanced (dashed arrows). Light grey: sedimentary cover.

$Nu > 2$, with values up to 3–4 in correspondence of some shear zones (see Fig. 5B). This confirms the result that heat transfer in the field has an important convective component, particularly in correspondence with normal faults and associated deformation zones.

Normal fault systems and their related fractures deformation zones can act as hydraulic channels (Curewitz and Karson, 1997 with references therein; Imbach, 1997; Furuya et al., 2000). If this is the case at Larderello, the perturbation of the isotherms can be interpreted on the basis of fluid movements in these structural pathways superimposed on a longer-wavelength thermal anomaly. According to this interpretation, the upward displacement of isotherms in the Serrazzano and Larderello shear zones (Figs. 6 and 7) is caused by the localised heat advection caused by hot geothermal fluids along the shear zones in the uppermost 5 km of crust (Fig. 9). This advective component is locally important and can substantially exceed the background heat flow.

Downward flow of meteoric waters depends on system characteristics such as regional topography, lithology and hydraulic head variations. It is possible, however, that extensional shear zones may have a locally enhancing role also in the downward movement of fluids. The transfer of these waters from the shallower to the deeper reservoir is probably channelled along the extensional shear zones, which cross the shallower reservoir and sole out at the brittle/ductile transition below the deeper reservoir. This channelling can account for the downward displacement of the isotherms.

7. Conclusions

The integration of field, borehole, heat flow, and seismic reflection data is a powerful tool to investigate the deep circulation of geothermal fluids.

In the Larderello geothermal field, upper crustal isotherms are perturbed in correspondence with normal faults. We have interpreted this as a consequence of the movement of fluids in localised deformation zones, corresponding to the three main shear zones identified in the area (refer to Fig. 9). These act as preferential pathways for the flow of mixed meteoric and deep fluids of magmatic and metamorphic origin. Circulation is favoured by the kinematic activity of the brittle shear zones and by the pressure of the geothermal fluids itself. In this framework, the extensional shear zones represent conduits to the Larderello deep reservoir. Fluids migrating along these pathways can be trapped in the more superficial reservoir, represented by the Triassic evaporitic level. Also the precipitation of geothermal minerals, determining the partial occlusion of fractures in the deformation zones, can contribute to the increase of fluid pressure and, consequently, to the growth of the permeable zone.

Acknowledgements

The ENEL–Green Power Agency allowed us to consult their geological and geophysical archive. MURST 2000 grants (to A.L.) sustained this re-

search. The research of G.R. on lithosphere dynamics is also supported by NSERC (Natural Sciences and Engineering Research Council of Canada). Thanks are due to M. Fernandez and to an anonymous reviewer whose constructive comments helped to improve the paper.

References

Angenheister, G. (Ed.), 1982. Numerical Data and Functional Relationships in Science and Technology, vol. 1. Physical Properties of Rocks. Springer, Berlin, 373 pp.

Arisi Rota, F., Brondi, A., Dessau, G., Franzini, M., MonteAmiata, S.p.A., Del Sele, S.M., Stea, B., Vighi, L., 1971. I Giacimenti minerari. Rend. Soc. Ital. Mineral. Petrol. 27, 357–544.

Baldi, P., Bellani, S., Ceccarelli, A., Fiordelisi, A., Squarci, P., Taffi, L., 1994a. Nuovi dati geotermici nelle aree a Sud-Est ed a Sud del campo geotermico di Travale (Toscana). Atti del 13° Convegno GNGTS, C.N.R, Roma, pp. 211–221.

Baldi, P., Bellani, S., Ceccarelli, A., Fiordelisi, A., Squarci, P., Taffi L., 1995. Geothermal anomalies and structural features of southern Tuscany. World Geothermal Congress Proceedings, Florence, pp. 1287–1291.

Baldi, P., Bertini, G., Cameli, G.M., Decandia, F.A., Dini, I., Lazzarotto, A., Liotta, D., 1994b. La tettonica distensiva post-collisionale nell'area geotermica di Larderello (Toscana meridionale). Studi Geol. Camerti 1, 183–193.

Barbier, E., 2002. Geothermal energy and current status: An overview. Renew. Sustainable Energy Rev. 6, 3–65.

Bartole, R., 1995. The North Tyrrhenian–Northern Apennines post-collisional system: Constraints for a geodynamic model. Terranova 1, 7–30.

Barton, C.A., Zobach, M.D., Moos, D., 1995. Fluid flow along potentially active faults in crystalline rock. Geology 23, 683–686.

Batini, F., Burgassi, P.D., Cameli, G.M., Nicolich, R., Squarci, P., 1978. Contribution to the study of the deep lithospheric profiles: Deep reflecting horizons in Larderello–Travale Geothermal field. Mem. Soc. Geol. Ital. 19, 477–484.

Batini, F., Nicolich, R., 1985. P and S reflection seismic profiling and well logging in the Travale geothermal field. Geothermics 14, 731–747.

Batini, F., Fiordelisi, A., Graziano, F., Nafi Toksöz, M., 1995. Earthquake and tomography in the Larderello geothermal area: Geothermal anomalies and structural features of southern Tuscany. World Geothermal Congress Proceedings, Florence, pp. 817–820.

Bertani, R., Cappetti, G., 1995. Numerical simulation of the Monteverdi zone western border of the Larderello geothermal field. World Geothermal Congress Proceedings, Florence, pp. 1735–1740.

Bertini, G., Cameli, G.M., Costantini, A., Decandia, F.A., Di Filippo, M., Dini, I., Elter, F.M., Lazzarotto, A., Liotta, D., Pandeli, E., Sandrelli, F., Toro, B., 1991. Struttura geologica fra i monti di Campiglia e Rapolano Terme (Toscana meridionale): Stato attuale delle conoscenze e problematiche. Studi Geol. Camerti 1, 155–178.

Brogi, A., Lazzarotto, A., Liotta, D., Ranalli, G., 2003. Extensional shear zones as imaged by reflection seismic lines: The Larderello geothermal field (central Italy). Tectonophysics 363, 127–139.

Brun, J.P., Gutscher, M.A., and DEKORP-ECORS teams, 1992. Deep crustal structure of the Rhine Graben from DEKORS-ECORS seismic reflection data: A summary. Tectonophysics 208, 139–147.

Caine, J.S., Evans, I.P., Forster, C.B., 1996. Fault zone architecture and permeability structure. Geology 24, 1025–1028.

Calore, C., Celati, R., Gianelli, G., Norton, D., Squarci, P., 1981. Studi sull'origine del sistema geotermico di Larderello. Atti del Convegno Energia Geotermica: Prospettive Aperte dalle Ricerche, CNR, Roma, pp. 218–225.

Cameli, G.M., Dini, I., Liotta, D., 1993. Upper crustal structure of the Larderello geothermal field as a feature of post-collisional extensional tectonics (Southern Tuscany, Italy). Tectonophysics 224, 413–423.

Cameli, G.M., Dini, I., Liotta, D., 1998. Brittle/ductile boundary from seismic reflection lines of southern Tuscany (Northern Apennines, Italy). Mem. Soc. Geol. Ital. 52, 153–163.

Carmignani, L., Decandia, F.A., Disperati, L., Fantozzi, P.L., Lazzarotto, A., Liotta, D., Oggiano, G., 1995. Relationships between the Sardinia–Corsica–Provençal Domain and the Northern Apennines. Terranova 7, 128–137.

Carmignani, L., Decandia, F.A., Fantozzi, P.L., Lazzarotto, A., Liotta, D., Meccheri, M., 1994. Tertiary extensional tectonics in Tuscany (Northern Apennines, Italy). Tectonophysics 238, 295–315.

Cataldi, R., Mongelli, F., Squarci, P., Taffi, L., Zito, G., Calore, C., 1995. Geothermal ranking of Italian territory. Geothermics 24, 115–129.

Cathelineau, M., Marignac, C., Boiron, M.C., Gianelli, G., Puxeddu, M., 1994. Evidence for Li-richbrines and early magmatic fluid-rock interaction in the Lrderello geothermal system. Geochim. Cosmochim. Acta 58, 1083–1099.

Clauser, C., Villinger, H., 1990. Analysis of conductive and convective heat transfer in a sedimentary basin, demonstrated for the Rheingraben. Geophys. J. Int. 100, 393–414.

Curewitz, D., Karson, J.A., 1997. Structural setting of hydrothermal overflow: Fracture permebility maintained by fault propagation and interaction. J. Volcanol. Geotherm. Res. 79, 149–168.

D'Amore, F., Bolognesi, L., 1994. Isotopic evidence for a magmatic contribution to fluids of the geothermal systems of Larderello, Italy and the Geysers, California. Geothermics 23, 21–32.

Dallmeyer, R.D., Liotta, D., 1998. Extension, uplift of rocks and cooling ages in thinned crustal provinces: the Lardarello

Geothermal Area (Inner Northern Apennines, Italy). Geol. Mag. 135 (2), 193–202.

Della Vedova, B., Bellani, S., Pellis, G., Squarci, P., 2001. Deep temperatures and surface heat flow distribution. In: Vai G.B., Martini, I.P. (Eds.), Anatomy of an Orogen: The Apennines and Adjacent Mediterranean Basins. Kluwer Academic Publishers, Amsterdam, pp. 65–76.

Eaton, G.P., Christiansen, R.L., Iyer, H.M., Pitt, A.M., Mabey, D.R., Blank, H.R., Zietz, I., Gettings, M.E., 1975. Magma beneath Yellowstone National Park. Science 188, 787–796.

Ehlers, T.A., Chapman, D.S., 1999. Normal fault thermal regimes: Conductive and hydrothermal heat transfer surrounding the Wasatch fault, Utah. Tectonophysics 312, 217–234.

Evans, J.P., Forster, C.B., Goddard, J.V., 1997. Permeability of fault-related rocks, and implications for hydraulic structure of fault zones. J. Struct. Geol. 19, 1393–1404.

Furuya, S., Aoki, M., Gotoh, H., Takenaka, T., 2000. Takigami geothermal system, northeastern Kyushu, Japan. Geothermics 29, 191–211.

Gianelli, G., 1994. Ipotesi di un modello di crosta superiore per le aree geotermiche toscane. Studi Geol. Camerti 1, 195–200.

Gianelli, G., Laurenzi, M.A., 2001. Age and cooling rate of the geothermal system of Larderello. Geotherm. Res. Counc. Trans. 25, 731–735.

Gianelli, G., Manzella, A., Puxeddu, M., 1997. Crustal models of the geothermal areas of Southern Tuscany. Tectonophysics 281, 221–239.

Haenel, R., Rybach, L., Stegena, L. (Eds.), 1988. Handbook of Terrestrial Heat-Flow Density Determination. Kluwer, Dordrecht, 486 pp.

Imbach, T., 1997. Deep groundwater circulation in the tectonically active area of Bursa, Northwest Anatolia, Turkey. Geothermics 26, 251–278.

Jolivet, L., Daniel, J.M., Truffert, C., Goffé, B., 1994. Exhumation of deep crustal metamorphic rocks and crustal extension in arc and back-arc regions. Lithos 33, 3–30.

Kusznir, N.J., Park, R.G., 1987. The extensional strength of the continental lithosphere: Its dependence on geothermal gradient, and crustal composition and thickness. In: Coward, M.P., et al. (Eds.), Continental Extensional Tectonics. Geol. Soc. Spec. Publ. 28, London, pp. 35–52.

Lazzarotto, A., Mazzanti, R., 1978. Geologia dell' alta Val di Cecina. Boll. Soc. Geol. Ital. 95, 1365–1487.

Lavecchia, G., 1988. The Tyrrhenian–Appennines system: Structural setting and seismotectogenesis. Tectonophysics 147, 263–296.

Liotta, D., Cernobori, L., Nicolich, R., 1998. Restricted rifting and its coexistence with compressional structures: Results from the CROP 3 traverse (Northern Apennines, Italy). Terra Nova 10, 16–20.

Liotta, D., Ranalli, G., 1999. Correlation between seismic reflectivity and rheology in extended lithosphere: Southern Tuscany, inner northern Apennines, Italy. Tectonophysics 315, 109–122.

Lister, G.S., Etheridge, M.A., Symonds, P.A., 1991. Detachment models for the formation of passive continental margins. Tectonics 10, 1038–1064.

Locardi, E., 1982. Individuazione dei strutture sismogenetiche dall' esame della evoluzione vulcano–tettonica dell' Appennino e del Tirreno. Mem. Soc. Geol. Ital. 24, 569–595.

Lucchitta, I., 1990. Role of heat and detachment in continental extension as viewed from the eastern Basin and Range Province in Arizona. Tectonophysics 174, 77–114.

Magro, G., Ruggieri, G., Gianelli, G., Bellani, S., Scandiffio, G. 2003. Helium isotopes in paleofluids and present-day fluids in the Larderello geothermal field: Constraints on the heat source. J. Geophys. Res. 108 (B1), ECV3, 1–12.

Manzella, A., Ruggieri, G., Gianelli, G., Puxeddu, M., 1998. Plutonic–geothermal systems of Southern Tuscany: A review of the crustal model. Mem. Soc. Geol. Ital. 52, 283–294.

Minissale, A., Magro, G., Martinelli, G., Vaselli, O., Tassi, G.F., 2000. Fluid geochemical transect in the Northern Apennines (central-northern Italy): Fluid genesis and migration and tectonic implications. Tectonophysics 319, 199–222.

Mongelli, F., Palumbo, F., Puxeddu, M., Villa, I.M., Zito, G., 1998. Interpretation of the geothermal anomaly of Larderello, Italy. Mem. Soc. Geol. Ital. 52, 305–318.

Morgan, P., Blackwell, D.D., Spafford, R.E., 1977. Heat flow measurements in Yellowstone Lake and thermal structure of the Yellowstone caldera. J. Geophys. Res. 82, 3719–3732.

Muffler, L.J., Duffield, W.A., 1995. The role of volcanic geology in the exploration for the geothermal energy. World Geotherm. Congr. Proc., Florence 2, 657–662.

Patacca, E., Sartori, R., Scandone, P., 1990. Tyrrhenian basin and Apenninic arcs: Kinematic relations since late Tortonian times. Mem. Soc. Geol. Ital. 45, 425–451.

Ranalli, G., Murphy, D.C., 1987. Rheological stratification of the lithosphere. Tectonophysics 133, 281–295.

Ravnik, D., Rajver, D., Polijak, M., Zivcic, M., 1995. Overview of the geothermal field of Slovenia in the area between the Alps, the Dinarides and the Pannonian basin. Tectonophysics 250, 135–149.

Rossetti, F., Faccenna, C., Jolivet, L., Funiciello, R., Tecce, F.., Brunét, C., 1999. Syn- versus post-orogenic extension: The case study of Giglio Island (Northern Tyrrhenian Sea, Italy). Tectonophysics 304, 71–93.

Ruggieri, G., Gianelli, G., 1999. Multi-stage fluid circulation in a hydraulic fracture breccia of the Larderello geothermal field (Italy). J. Volcanol. Geotherm. Res. 90, 241–261.

Scheidegger, A.E., 1960. The Physics of Flow through Porous Media. Macmillan, New York.

Sclater, J.G., Christie, P.A.F., 1980. Continental stretching: An explanation of the Post-Mid-Cretaceous subsidence of the Central North Sea Basin. J. Geophys. Res. 85, 3711–3739.

Seront, B., Wong, T.F., Caine, J.S., Forster, C.B., Bruhn, R.L., 1998. Laboratory characterization of hydromechanical properties of a seismogenic normal fault system. J. Struct. Geol. 20, 865–881.

Serri, G., Innocenti, F., Manetti, P., 1993. Geochemical and

petrological evidence of the subduction of delaminated Adriatic continental lithosphere in the genesis of the Neogene–Quaternary magmatism of central Italy. Tectonophysics 223, 117–147.

Sibson, R.H., 1996. Structural permeability of fluid-driven fault-fracture meshes. J. Struct. Geol. 18, 1031–1042.

Somerton, W.H., 1992. Thermal Properties and Temperature-Related Behaviour of Rock–Fluid Systems. Development in Petroleum Science 37, Elsevier, Amsterdam, 257 pp.

Ter Voorde, M., Bertotti, G., 1994. Thermal effects of normal faulting during rifted basin formation, 1. A finite difference model. Tectonophysics 240, 133–144.

Werner, D., Kahle, H.G., 1980. A geophysical study of the Rhinegraben, kinematics and geothermics. Geophys. J. R. Astron. Soc. 62, 617–629.

Wibberley, C.A.J., Shinamoto, T., 2003. Internal structure and permeability of major strike-slip fault zones: The Median Tectonic Line in Mie Prefecture, Southwest Japan. J. Struct. Geol. 25, 59–78.

Younker, L.W., Kasameyer, P.W., Tewhey, J.D., 1982. Geological, geophysical, and thermal characteristics of the Salton Sea Geothermal field, California. J. Volcanol. Geotherm. Res. 12, 221–258.

Zitellini, N., Trincardi, F., Marani, M., Fabbri, A., 1986. Neogene tectonics of the Northern Tyrrenhian sea. G. Geol. 48, 25–40.

Proceedings World Geothermal Congress 2010
Bali, Indonesia, 25-29 April 2010

Numerical Modeling for the Larderello-Travale Geothermal System (Italy)

Antonio Barelli, Maurizio Cei, Ferdinando Lovari and Paolo Romagnoli

via Andrea Pisano, 120 – 56100 Pisa

antonio.barelli@enel.com

Keywords: Numerical modeling, TOUGH2, Larderello, Travale, Italy

ABSTRACT

The Larderello-Travale field was simulated via the three-dimensional numerical model TOUGH2.

This work was mainly aimed at investigating:

- The superheated steam production mechanism;
- The interactions between the geothermal field and the surrounding deep aquifers including their long distance pressure draw-down;
- The field sustainability.

The simulated area is 5000km^2, abundantly covering the geothermal fields of Larderello and Travale, whose area totals "only" 300km^2. This choice was made to evaluate the pressure draw-down induced in the faraway aquifers by production exploitation.

To fulfill the work aims, no constant pressure boundaries (i.e. mass sources) were introduced.

The depth of the domain was set to 7000 m according to a seismic reflection horizon which is believed to represent the reservoir bottom. This bottom is impermeable, but allows the natural heat flow to take place. The reservoir top is modeled as an impermeable layer of rock that acts as a cover. The only interactions with the environment are natural manifestations and some well known shallow aquifers where the cover is absent.

The natural state was successfully simulated assuming a natural manifestation flow-rate of some 10% of the present extraction rate.The rock permeability was tuned to match the initial pressures and temperatures.

The history of the industrial exploitation was then introduced and the resulting pressure distribution was compared with the actually recorded data achieving satisfactory results.

The production mechanism resulted to be not only the steam expansion in the superheated reservoir core, but also and mainly the liquid evaporation in the steam-water contiguous zones.

The field production results to be sustainable at least for the next 100 years.

1. WORK AIMS

The numerical modeling of the Larderello-Travale geothermal system (Figure 1) represents a challenging task, because of both the unhomogeneous permeability and the different field production histories.

Although the producing area is 300km^2 (Bertani et al., 2005), a simulated area of 4900km^2 (70×70km) was chosen so as to include the whole geothermal system and also the surrounding aquifers. This was done to investigate the possible interaction between them.

Another important scope was to explain how a superheated and depressurized geothermal system, with negligible meteoric water recharge, could produce such an enormous amount of steam.

Forecasting the future evolution of field production was an important work aim too.

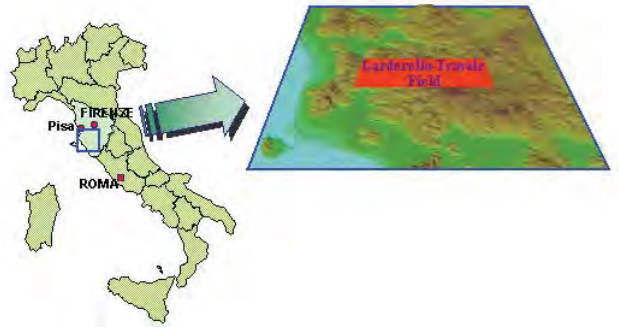

Figure 1: Larderello-Travale field location.

2. HISTORICAL FIELD EXPLORATION

2.1 Larderello field

At Larderello first wells were drilled in 1926, tapping the shallow carbonate formations (Barelli et al., 2000; Batini et al., 2003). Between 1926 and 1940, 136 wells were drilled over an area of 4km^2 with a high success ratio (82%).

In the following ten years, the exploitation area was doubled with another 69 wells. All these wells tapped the steam carbonate reservoir with a maximum pressure of 32bar (Bertani et al., 2005). From the 1950s to 1980s the drilled area was further extended to about 100km^2.

In the early 1980s, a deep exploration program began with some 3500m wells, which encountered productive layers in the metamorphic basement. This reservoir was characterized by an average pressure of 40bar and 300-350°C temperature (Barelli et al., 1995b). At present the total Larderello production is about 3300t/h.

2.2 Travale field

The geothermal exploitation of the Travale field began in the early 1950s when some 20 wells were drilled to the depth of a few hundred meters near the natural manifestations, in a water-dominated system (Barelli et al., 1995a; Batini et al., 2003). Production caused the surface manifestations to disappear and triggered the inflow of meteoric water causing these wells to be soon watered out.

In the 1970s, the exploration was extended northward aiming at a deeper and hotter reservoir, named “Horst”. The permeable rocks were met at a depth of 500-1000m in carbonate formations with a pressure of 60bar and a temperature of 280°C (Barelli et al., 1995a). These formations hosted a steam-dominated system. This reservoir and the previous water-dominated one are somehow interconnected.

At the beginning of the 1980s, the exploitation was extended further northwards to a deeper layer (1300-2000m), named “Graben” (Barelli et al., 1995a). This reservoir had an initial reservoir pressure of about 60bar and experienced a continuous flow-rate decline without substantial changes in steam quality and gas content.

After 1992, some 4000m deep wells were drilled in an extended area, investigating a deeper reservoir hosted in the metamorphic basement and in the granite intrusions. The abundant reservoir fluid was superheated steam with an initial pressure of 70bar, in vaporstatic equilibrium with the previously discovered reservoirs (Barelli et al., 1995b). The temperature has been about 300°C-350°C.

The good results of the deep exploration allowed for an increase of steam production up to 1000t/h.

3. NUMERICAL MODELLING OF LARDERELLO-TRAVALE GEOTHERMAL FIELD

Larderello-Travale field was simulated via the three-dimensional numerical simulator TOUGH2, which is a general-purpose code for multi-dimensional fluid and heat flows of multiphase, multicomponent fluid mixtures in porous and fractured media (Pruess et al., 1999)

The simulated area covers about 5000km^2 in southern Tuscany. This area has been chosen substantially larger than the producing geothermal area (Figure 2) in order to obtain results independent from the assumed boundary conditions.

3.1 Larderello-Travale Conceptual Model

Larderello-Travale geothermal system is a superheated dominated one. The main hydrogeological features are: a clayey-shaley cap rock (from 0m to 500m), a fractured carbonatic formation (from 500m to 1000m), a metamorphic basement (from 1000 to 3000m) and granite intrusion.

At depths greater than 3000m, Larderello and Travale are part of a one only geothermal system root at 300-350°C (Barelli et al., 1995b). However, during model tuning, a low permeable sect has been inserted between Larderello and Travale areas to simulate the peculiar pressure response to exploitation.

The boundaries between the high-permeability reservoir core and the low-permeability deep surroundings geothermal aquifers (aquicludes) have been identified with the 250°C isotherm, which is believed to be the minimum possible reservoir temperature.

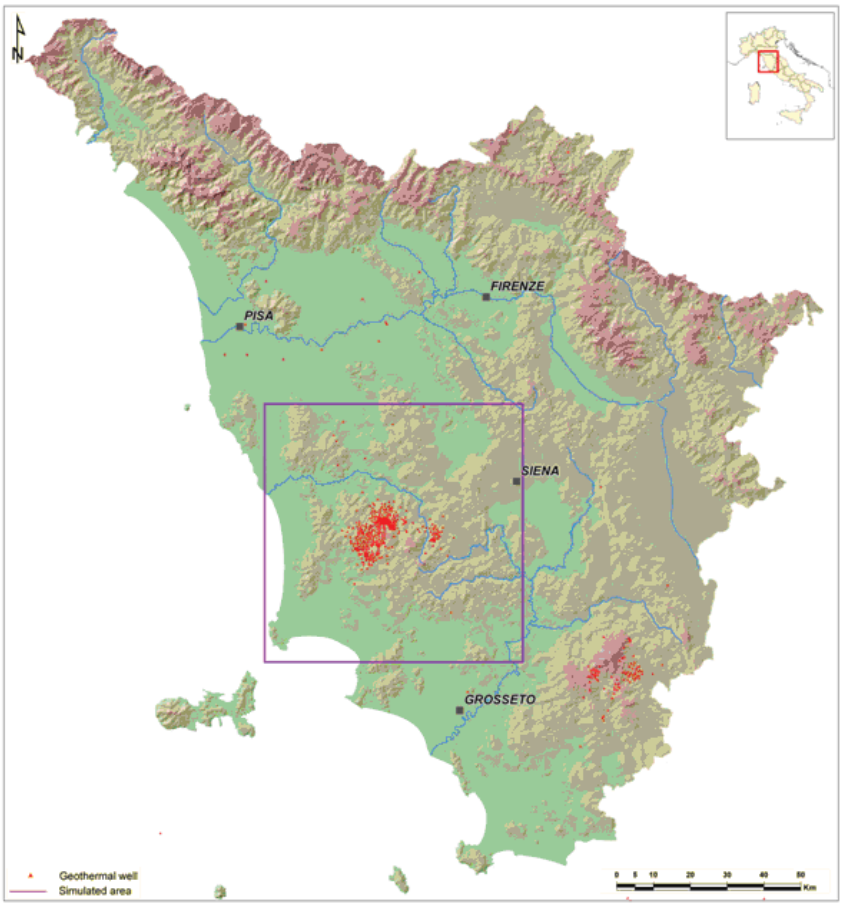

Figure 2: Larderello-Travale simulation domain.

The recharge of the superheated reservoir core may occur through these aquicludes. A two-phase zone is envisaged between the superheated reservoir and the water-dominated boundaries. In this way, the natural liquid water, which is present in the deep aquicludes, can recharge the reservoir in response to the pressure drop induced by exploitation.

3.2 Geological schematizations for the Larderello-Travale field

In this numerical modeling some geological features have been used as an input. The field geology is described in a companion paper (Arias et al., 2010, in press). The geological schematization used in this paper is described below:

- COVER – The reservoir cover is made of Neogene sediments in flysh facies. Cover thickness vary from 200m in the central part of the reservoir to 1000m in the external zones. Its permeability is practically null;
- INTERMEDIATE LAYER – Due to the lack of fractures in the field periphery, the rocks are not very permeable in the uppermost part of the potential reservoir as a whole. These volumes have been given a low permeability value. The boundary between these unproductive layers and the actual reservoir has been identified with the first fractured layer encountered by drillings. Where this information is lacking, the 250°C isotherm was adopted.
- GEOTHERMAL RESERVOIR – Different values of permeability have been used according to well testing results. The reservoir bottom is identified by the K-horizon and it is impermeable;
- K HORIZON – K horizon is believed to be the reservoir bottom, because it could be associated to the 400°C isotherm which could hinder fracturation. K horizon depth varies between 3000-4000m in the western zone and 8000-10000m in the Travale area (Bertini et a.l, 2006). To allow heat flow, but avoid the mass flow from the bottom, the K horizon has been modeled with fixed temperature cells, associated with no permeability rocks;
- LATERAL BOUNDARIES – Outside the geothermal reservoir, low permeability zones have been introduced. Its permeability and porosity have been calculated using the peripheral wells draw-down.

In total, 16 rock types have been used in this simulation.

3.3 Interactions with the environment

The only interactions between the geothermal reservoir and the environment are the natural manifestations and some well-known shallow aquifers where the cover is absent.

As for the natural manifestations, three permeable blocks were introduced to allow for their flow rate. Their productivity index (PI) has been chosen to match the estimated historical production.

As for the shallow aquifer interactions, some cells with imposed constant pressure have been introduced where are reservoir outcrops (Barelli et al., 1995b; Ceccarelli et al., 1987).

3.4 Domain and Simulation Grid

The simulation grid is made of about 10000 cells, subdivided into 16 vertical layers. The simulation area is 4900 km2 (70×70 km) and total vertical thickness is nearly 7500 m (from +500 m a.s.l. to -7000 m a.s.l.).

Each horizontal layer is formed by 25×25 cells with different sizes. A greater details is necessary in the inner simulation domain where cell size is 2×2 km. In the bordering area, 8×8 km cell size has been adopted (Figure 3). The cell thickness varies with depth; the deeper cells are some thousand meters thick, while the shallow ones are only 200 m (Figure 4).

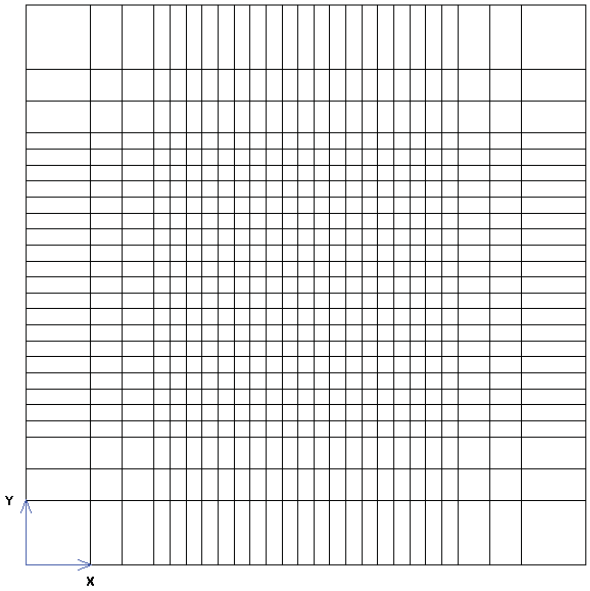

Figure 3: Simulation horizontal layer.

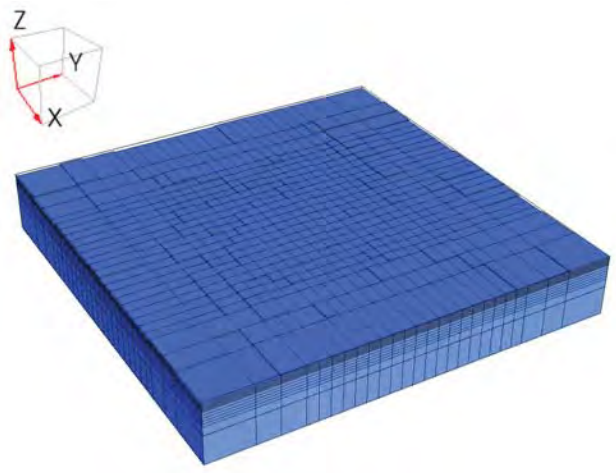

Figure 4: 3D simulation grid.

3.5 Boundary Conditions

To simulate Larderello-Travale geothermal field, no-mass sources have been introduced as boundary conditions. Consequently, all the borders have been set as no-flow boundaries. However, the distance from the producing area is so large that this choice has little impact on the results. The results of the natural-state simulation have been used as the initial condition for production history simulation.

At the top and bottom of the simulation grid, boundary conditions have been imposed as fixed temperatures.

As for the bottom cells, where the reservoir is present, temperatures vary between 250 °C and 320 °C, according to

temperature distribution data. Outside the producing reservoir, the bottom temperature is defined by a natural gradient.

4. NATURAL STATE SIMULATION

Model tuning in the natural state was based on comparison between simulated and actual temperature and pressure distributions. Simulated temperature, pressure and steam quality distributions have been obtained by modeling Larderello-Travale natural state, while the actual data come from static temperature and pressure well profiles.

During model tuning, rock parameters such as porosity and permeability were changed to optimize the simulation. These three-dimensional distributions were subsequently used to simulate field production history and to evaluate the future system evolution.

In order to simulate the natural state, the thermal evolution of Larderello-Travale system has been reconstructed from the time of the magmatic intrusion to historical times. In the initial condition of this propedeutic simulation ($3.5\text{-}0.5\times10^6$ years), temperature and pressure gradients were respectively the average earth temperature gradient and hydrostatic pressure. The whole reservoir volume was initially filled with liquid water (Figure 5).

The magmatic intrusion prompted reservoir temperatures to increase and pressure began to decrease because of the onset of natural manifestations. Initially the vaporization process took place initially at the reservoir top (Figure 6), and then spread all over the reservoir volume (Figure 7).

During this phase (Figure 6), the two main reservoirs (Larderello and Travale) differentiated from the surrounding aquicludes. These latter underwent a lesser temperature increase and, in general, were also depressurized to a lesser degree. The extent of such phenomena was an inverse function of the distance from the reservoir.

Natural manifestations produced a complete reservoir vaporization (Celati et al., 1975) prior to the beginning of the industrial exploitation (early 1900s).

To check the reliability of the natural state simulation, the simulated and observed temperature and pressure horizontal distributions have been mapped at different depths, yielding satisfactory results. The comparison between simulated vertical temperature profiles and well data has been made subdividing the Larderello area (Figure 8) into four zones (Monteverdi, Larderello, Val di Cornia and Selva) and the Travale area (Figure 9) into two zones (Travale and Montieri) on the basis of their thermal characteristics.

Natural state three dimensional distributions of temperature, pressure and steam quality are shown in Figure 10, Figure 11 and Figure 12. For a better visualization of these figures, vertical dimension (z axis) is exaggerated by a factor of 5.

Total natural manifestation flow rate resulted to be 120t/h, in accordance with the order of magnitude estimated on the basis of boric acid production at the beginning of the 20th century, while the natural state inflow from the three well-known aquifers resulted to be some 30t/h. The remaining 90t/h were supplied by evaporation of liquid water which was present in deep confining aquicludes. The relevant heat flow which was needed for water vaporization was supplied by the magmatic body through the bottom boundary.

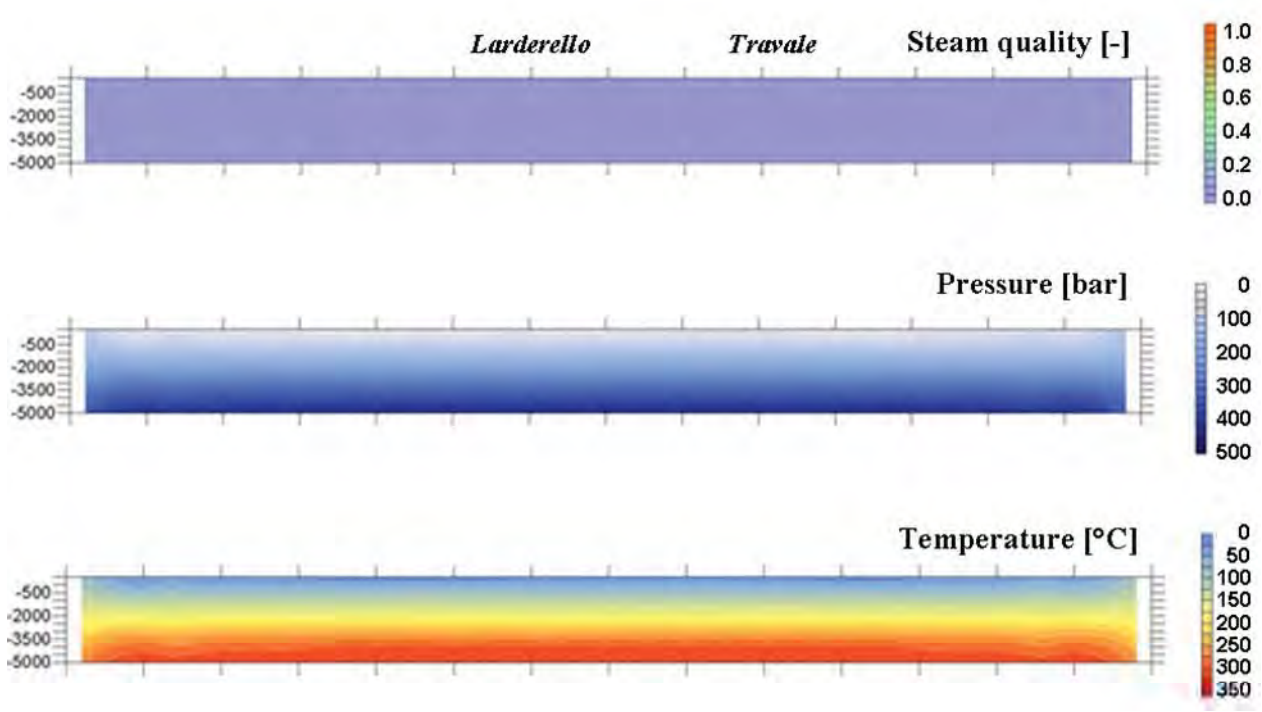

Figure 5: Steam quality, pressure and temperature distributions before the intrusion of the magmatic body.

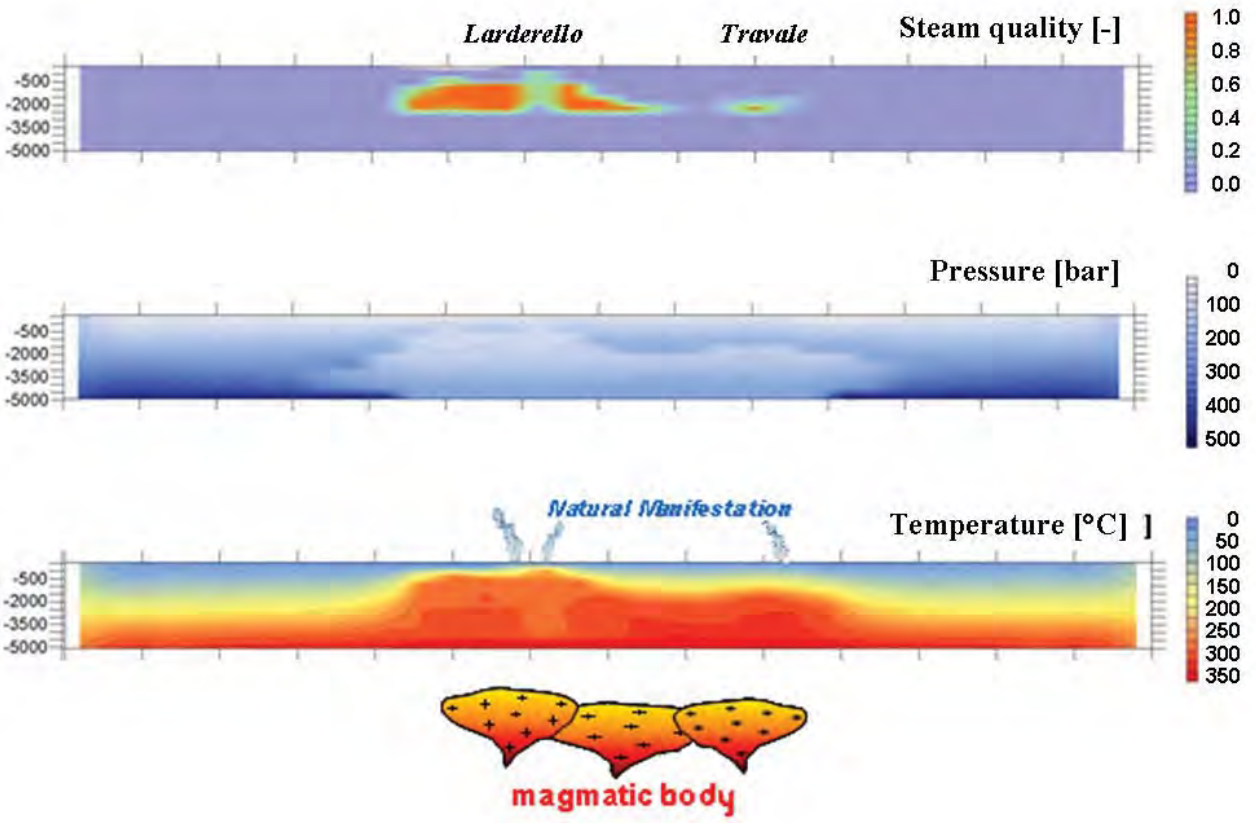

Figure 6: Steam quality, pressure and temperature distributions after the intrusion of the magmatic body.

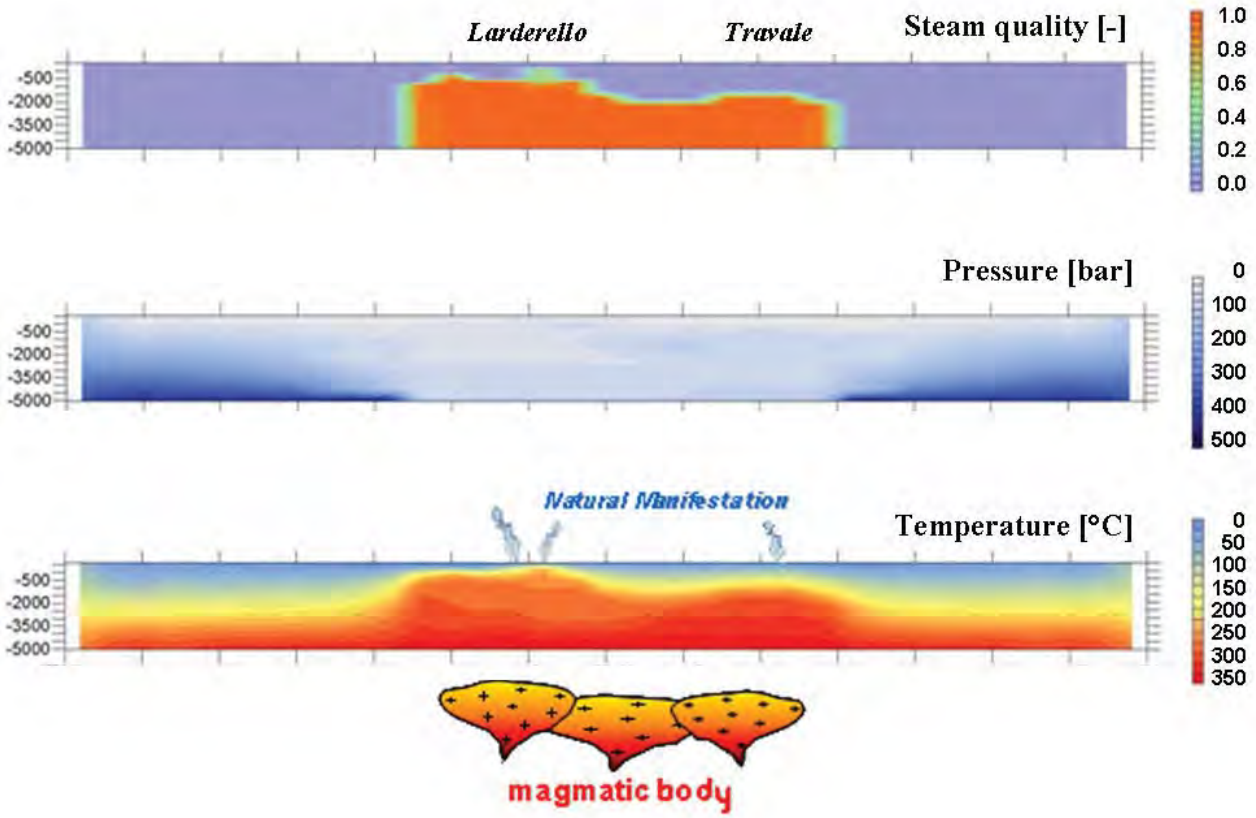

Figure 7: Steam quality, pressure and temperature distributions at natural state.

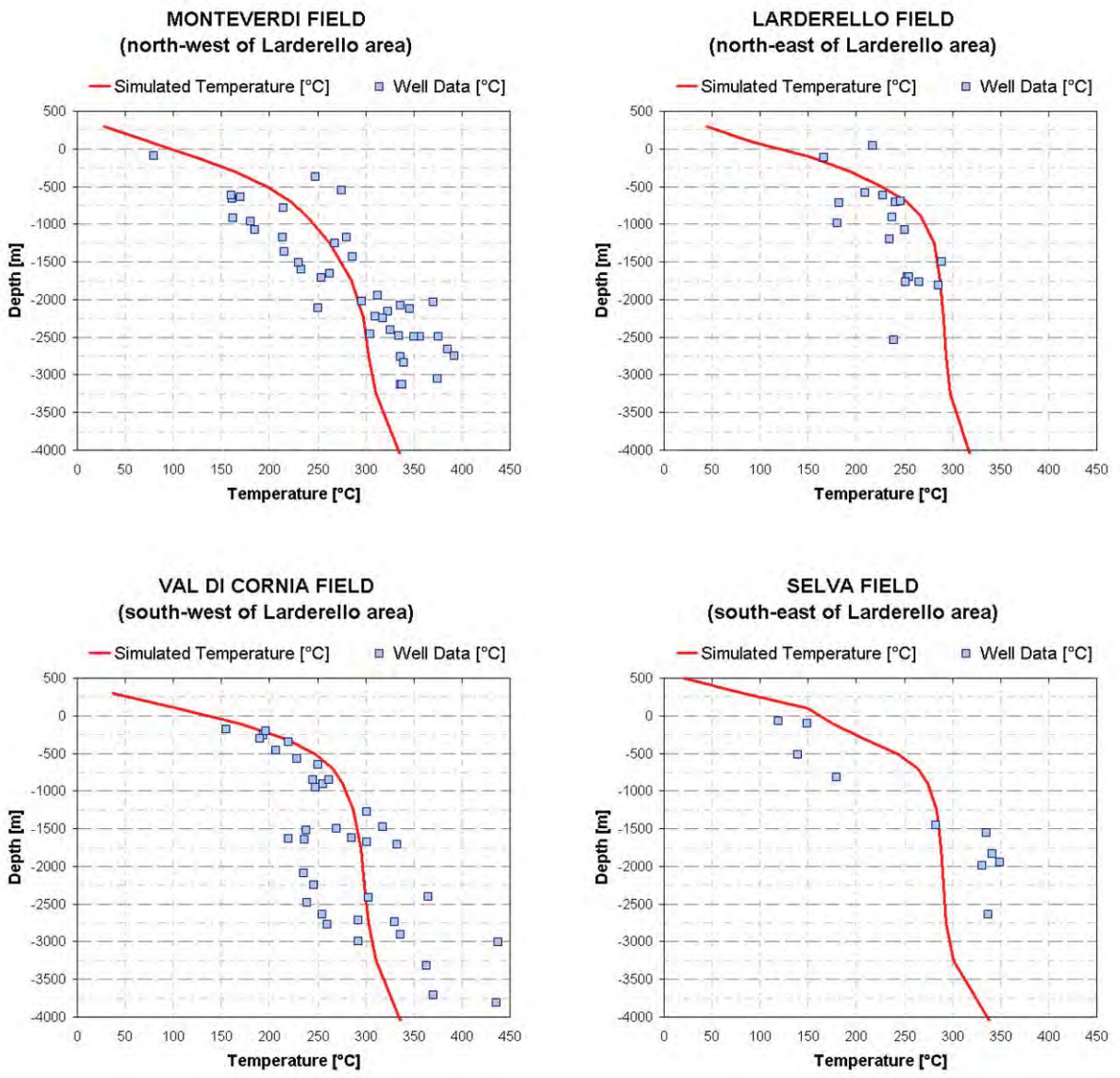

Figure 8: Simulated and observed temperature vertical profiles for Larderello area.

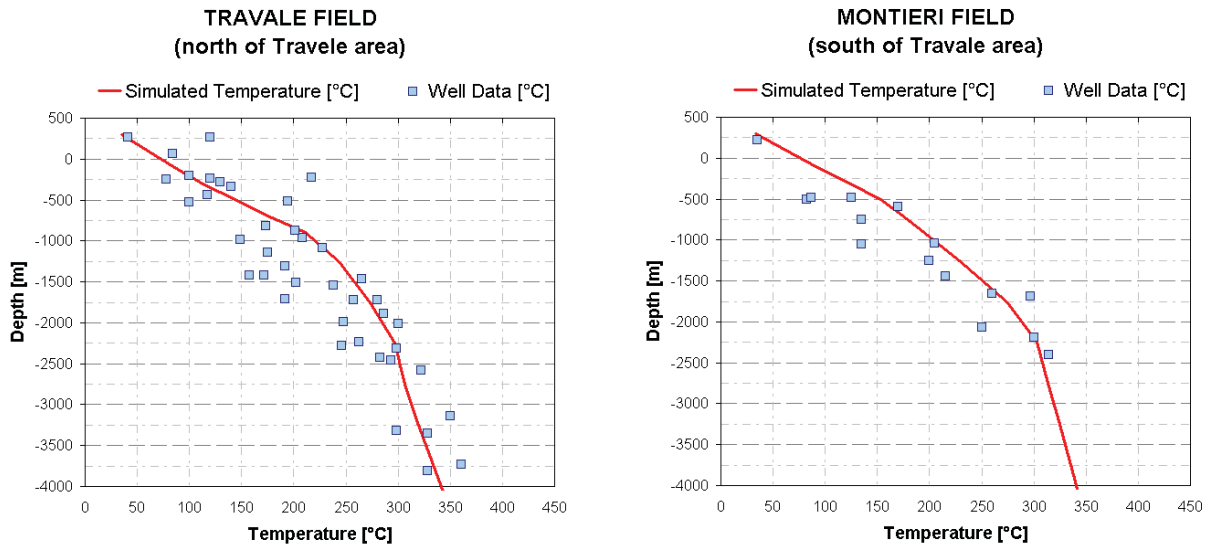

Figure 9: Simulated and observed temperature vertical profiles Travale area.

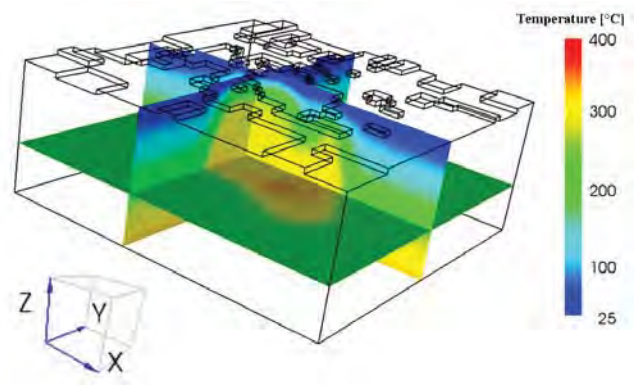

Figure 10: Temperature 3D distribution for natural state (vertical dimension is exaggerated by factor of 5).

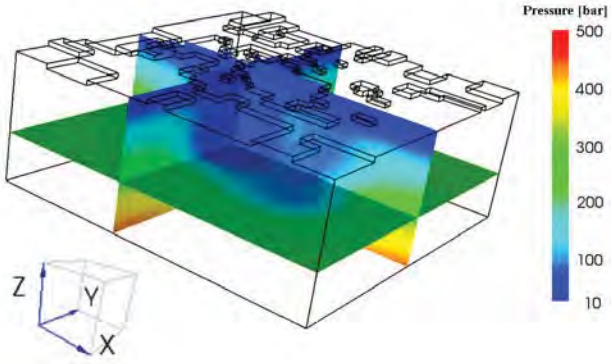

Figure 11: Pressure 3D distribution for natural state (vertical dimension is exaggerated by factor of 5).

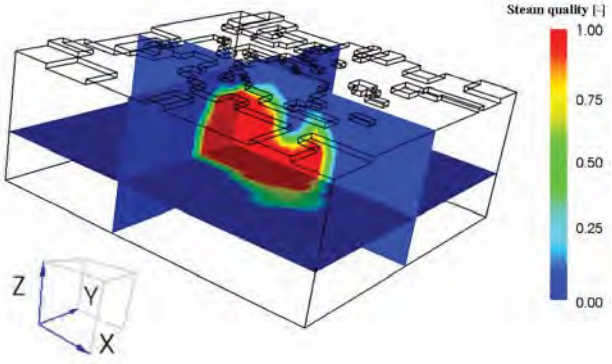

Figure 12: Steam quality 3D distribution for natural state (vertical dimension is exaggerated by factor of 5).

5. PRODUCTION HISTORY SIMULATION

Once a satisfactory match for the natural state was achieved, the industrial production was simulated.

The main objectives of this simulation were to develop a numerical model which could simulate the observed data for about 80 years of production and reiniection (from 1927 to 2008) and to analyze the reservoir behavior during industrial exploitation. Once a plausible numerical model of the Larderello-Travale system has been developed, it was used to envisage future development scenarios and to assess their sustainability. For sake of simplicity the productive wells (more than 100) have been grouped in some equivalent ones (about 20 wells) according to their location.

The simulated decline in field pressure was compared with the data (Figure 13). To improve the match, slight variations of rock parameters were introduced.

Fairly good results have been obtained both for shallow reservoir pressure histories and for deeper ones, with the only exception of the deep Travale area, where the simulated pressure resulted a little higher than the historical data. This is probably due to the fact that the data were relevant to wellhead, whilst the simulated ones were relevant to the actual depth. The difference is due to the weight of the steam/gas column which, in this case, is not negligible.

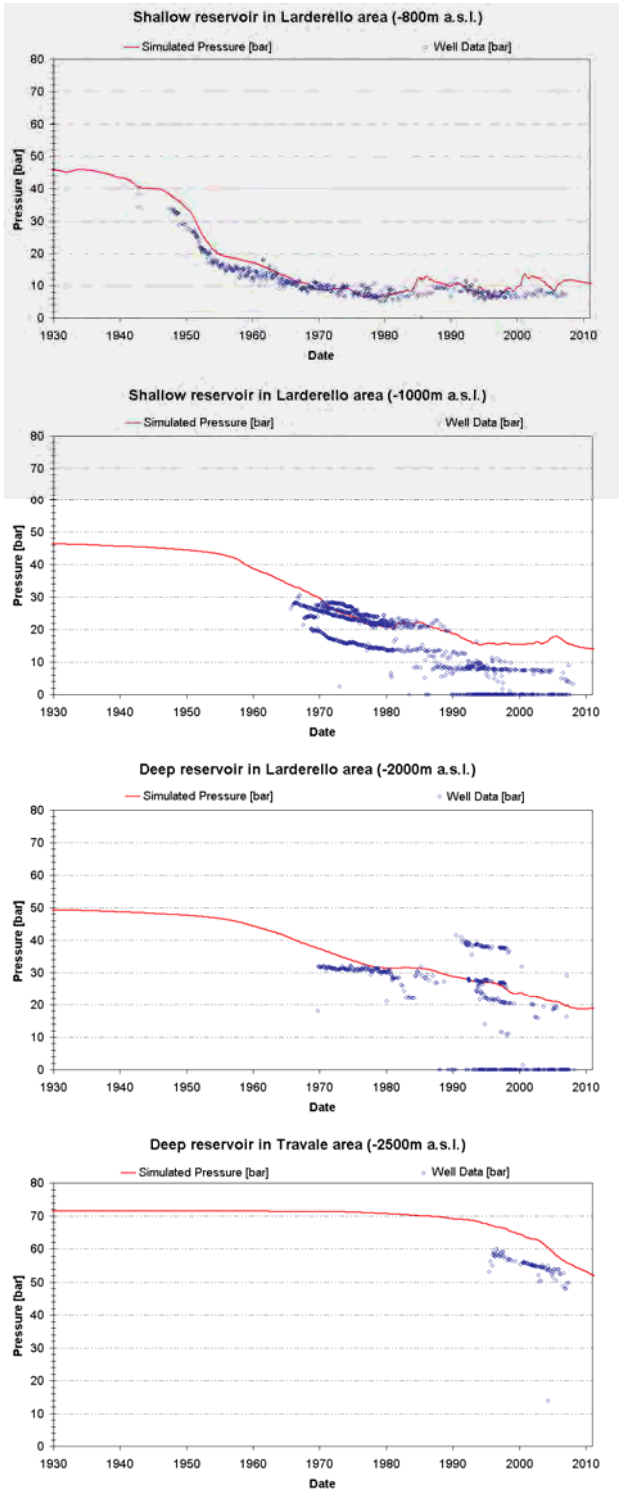

Figure 13: Well pressure evolution with time.

6.1 General results and future field performance

The most important achievements resulting from production history match are:

- No significant temperature variations are evident during industrial exploitation in the reservoir core (Cappetti et al., 1995). Natural state and present temperatures at -3000m depth are very close (Figure 14). Only two-phase cells display a sizeable temperature loss because they are placed at the boundary between steam reservoir and water aquicludes. In these zones, steam is generated at the expenses of the rock sensible heat. This observation gives an insight into the production mechanism. At the reservoir top, where reiniection takes place, temperatures locally decrease substantially. In these spots too, steam is generated by means of the heat supplied by rocks.

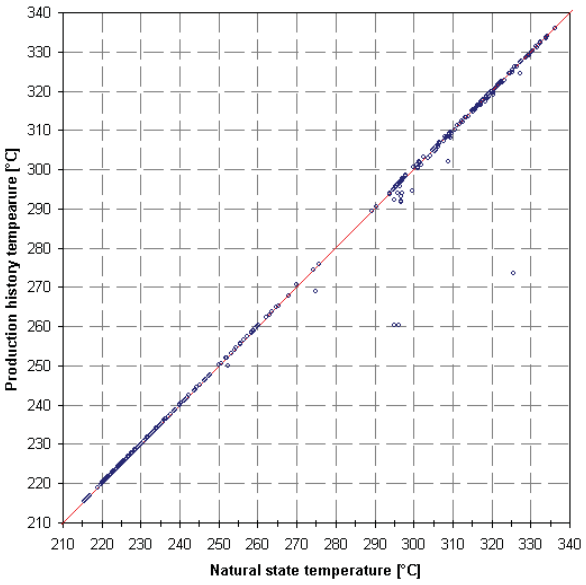

Figure 14: Temperature comparison between natural state and production history at -3000m depth.

- A pressure draw-down takes place in the central part of the reservoir, while the pressure of the surroundings deep aquicludes pressure is only very slightly affected: only a small pressure decrease can be noticed at the interface between the steam dominated reservoir and the surrounding aquicludes. This pressure decrease causes the evaporation of liquid water in the nearness of the steam dominated reservoir. Natural state and present pressures for each cell at -3000m depth are shown in Figure 15.

- Our simulation demonstrated that the geothermal production does not need the contribution of the potable aquifers which are not involved in the recharge mechanism. They are also separated from the geothermal system by a thick impermeable layer of cap rock.

- The reservoir is fed only by three well-known aquifers in correspondence of local outcrops of carbonate formations at a depth of some 500m. Their total flow resulted around 300t/h, less than 10% of total production flow rate.

- Natural discharge of geothermal fluid through fumarolic areas became less and less important with time (Figure 16) because of the reduction in reservoir pressures during exploitation.

- The good results, achieved by the simulation of natural state and the production history, have allowed a confident prediction of the future exploitation. Current production resulted to be sustainable for at least 100 years.

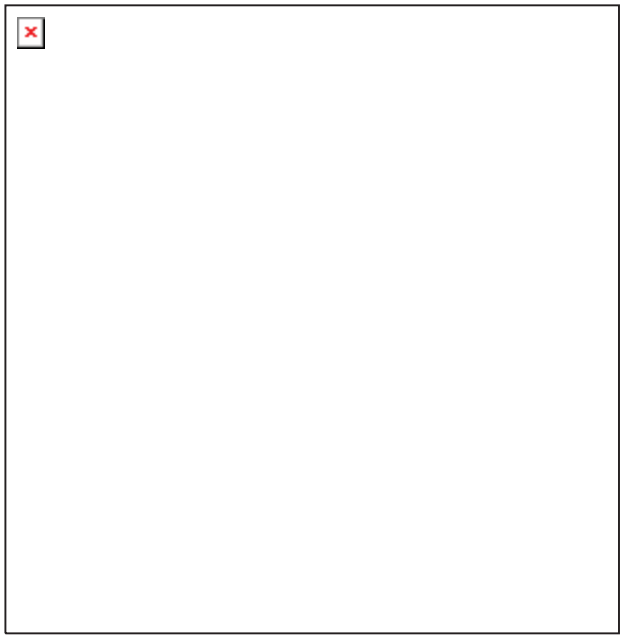

Figure 15: Pressure comparison between natural state and production history at -3000m depth.

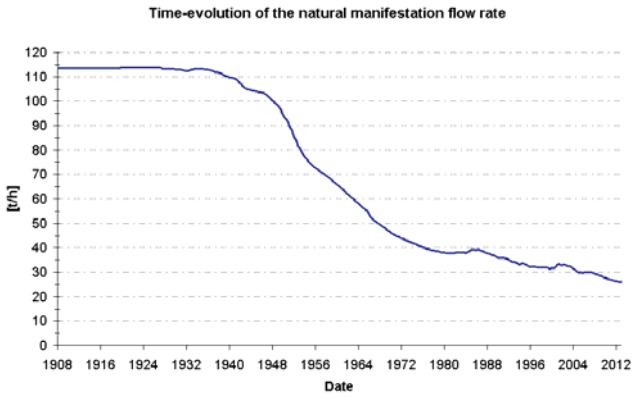

Figure 16: Natural manifestation flow rate with time during industrial exploitation.

6. CONCLUSIONS

A successful simulation of the field evolution from the emplacement of the magmatic body to present (3 million years) has been carried out.

Temperature and pressure distributions in the simulated natural state fit reasonable well with data.

Fairly good results have been obtained from the comparison between the simulated and observed pressure evolution at different reservoir depths during the industrial exploitation. Horizontal temperature distributions obtained by production history simulation have shown that no significant temperature variations are apparent during industrial exploitation. On the contrary, pressure draw-down is sustained in the central part of the reservoir.

The pressure of the surrounding deep aquicludes are not generally affected by production, but a slight pressure decrease can be noticed at the interface between the steam dominated reservoir and the surrounding aquicludes. This is caused by the evaporation of liquid water in the nearness of the steam dominated reservoir. This steam generation supplies most of the system recharge explaining the enormous productive capacity of the geothermal system.

This numerical simulation has allowed understanding the geothermal processes that are at the basis of the continuous steam production in the Larderello-Travale system.

The good simulation results have allowed the prediction of future evolution. Field exploitation resulted sustainable for at least 100 years.

REFERENCES

Arias, A., Dini, I., Casini, M., Fiordalisi, A., Perticone, I., and Dell'Aiuto, P.: Geoscientific feature update of the Larderello-Travale geothermal system (Italy), for a regional numerical modeling *Proceedings*, World Geothermal Congress, Bali, Indonesia (2010), in press.

Barelli, A., Bertani, R., Cappetti, G., and Ceccarelli, A.: An update on Travale – Radicondoli geothermal field, *Proceedings*, World Geothermal Congress, Florence, Italy (1995a).

Barelli, A., Cappetti, G., and Stefani, G.: Results of deep drilling in the Larderello-Travale/Radicondoli geothermal area, *Proceedings*, World Geothermal Congress, Florence, Italy (1995b).

Barelli, A., Bertini, G., Buonasorte, G., Cappetti, G., and Fiordelisi, A.: Recent deep exploration results at the margins of the Larderello-Travale geothermal system, *Proceedings*, World Geothermal Congress, Kyushu-Tohoku, Japan, (2000).

Batini, F., Bertini, G., Gianelli, G., Pandeli, E., and Puxeddu, M.: Deep structure of the Larderello field: contribution from recent geophysical and geological data, *Soc. Geol. Ital. Mem.*, **25**, (1983), 219–235.

Batini, F., Brogi, A., Lazzarotto, A., Liotta, D., and Pandeli, E.: Geological features of the Larderello-Travale and Mt. Amiata geothermal areas (southern Tuscany, Italy), *Episodes*, **26**, (2003), 239-244.

Bertani, R.: World Geothermal power generation in the period 2001-2005, *Geothermics*, **34**, (2005), 651-690.

Bertani, R., Bertini, G., Cappetti, G., Fiordelisi, A., and Marocco, B.M.: An update of the Larderello-Travale/Radicondoli deep geothermal system. *Proceedings*, World Geothermal Congress, Antalya, Turkey (2005).

Bertani, R.: World Geothermal Generation in 2007, *Proceedings*, European Geothermal Congress, Unterhaching, Germany, (2007).

Bertini, G., Casini, M.. Gianelli, G., and Pandeli E.: Geological structure of a long-living geothermal system, Larderello, Italy, *Terra Nova*, **18**, (2006), 163-169.

Bjornsson, G., Hjartarson, A., Bodvarasson, GS., and Steingrimsson B.: Development of 3-D geothermal reservoir model for the greater hengill volcano in sw-iceland, *Proceedings*, Tough Symposium 2003, Lawrence Berkeley National Laboratory, Berkeley, California (2003).

Bodvarsson, G.S., Lippmann, M.J., and Pruess K.: Modeling of Geothermal Systems. Geothermal Resources Council. - Vol. 23, n.4, pp. 144-160. (1994).

Buonasorte, G., Cataldi, R., and Passaleva, G.: Geothermal development in Italy: from Present to Future, *Proceedings*, European Geothermal Congress, Unterhaching, Germany (2007).

Cappetti, G., and Stefani, G.: Strategies for sustaining production at Larderello, *Transactions*, Geothermal Resources Council, Salt Lake City, U.S.A., (1994).

Cappetti, G., Parisi, L., Ridolfi, A., and Stefani, G.: Fifteen years of reinjection in the Larderello-Valle Secolo area: analysis of the production data. *Proceedings*, World Geothermal Congress, Florence, Italy (1995).

Cappetti, G., Fiordelisi, A., Casini, M., Ciuffi, S., and Mazzotti, A.: A new deep exploration program and preliminary results of a 3D seismic survey in the Larderello-Travale geothermal field (Italy), *Proceedings*, World Geothermal Congress, Antalya, Turkey (2005).

Ceccarelli, A., Celati, R., Grassi, S., Minissale, A., and Ridolfi, A.: The southern boundary of Larderello Geothermal field, *Geothermics*, **16**, (1987), 505-515.

Celati, R., Squarci, P., Taffi, L., and Stefani, G.C.: Analysis of water levels and reservoir pressure measurement in geothermal wells, *Proceedings*, 2nd U. N. Symposium on the Development and Use of Geothermal Resources, San Francisco, CA (1975).

Celati, R., Cappetti, G., Calore, C., Grassi, S., and D'Amore, F.: Water recharge in Larderello geothermal field, *Geothermics*, **20**, (1991), 119-133.

Fiordelisi, A., Moffat, J., Ogliani, F., Casini, M., Ciuffi, S., and Romi, A.: Revised Processing and Interpretation of Reflection Seismic Data in the Travale Geothermal Area (Italy), *Proceedings*, World Geothermal Congress, Antalya, Turkey (2005).

Pruess, K.: TOUGH2-A general purpose numerical simulator for multiphase fluid and heat flow, Lawrence Berkeley Laboratory report LBL-29400 .(1991).

Pruess, K., Oldenburg, C., and Moridis, G.: TOUGH2-User's Guide, Version 2.0, Lawrence Berkeley Laboratory report LBNL-43134 (1999).

Int J Earth Sci (Geol Rundsch)
DOI 10.1007/s00531-007-0249-0

ORIGINAL PAPER

Thermal modelling of the Larderello geothermal field (Tuscany, Italy)

Bruno Della Vedova · Claudio Vecellio · Stefano Bellani · Umberta Tinivella

Received: 27 February 2007 / Accepted: 6 September 2007

Abstract We present a 3-D thermal model of the Larderello geothermal field (Tuscany) to evaluate (1) the extent and contribution of the heat transfer mechanisms (conduction vs. convection) at the intermediate-upper crust levels, (2) the variability of the heat and mass fluxes entering from below and (3) the crucial role of the formation permeability. The model, composed by three main layers, considers the upper 10 km of the crust to better constrain the simulations with experimental data from borehole, fluid inclusion studies and hypocentral distributions. Several sets of simulations were carried out with different bottom boundary temperatures and different formation permeabilities for the two deeper layers. The results indicate that the present temperature (*T*) and pressure distributions in the Larderello field require deep reservoir rocks with higher permeability than the overlying capping units and underlying intermediate crust. Permeability values of 1 mDarcy for the reservoir rocks are enough to allow fluid convection, if the temperature at 10 km depth is as high as 500 ± 50°C. The presence of localized zones with formation permeability 50–100 times higher than the surrounding rocks strongly favours the migration of overpressurized fluids, which episodically break through the overburden, feeding the presently exploited geothermal fields.

Keywords Larderello geothermal field · Convective heat transfer · Fluid over-pressure · K-horizon · 3-D thermal modelling

B. Della Vedova (✉) · C. Vecellio
Dipartimento di Ingegneria Civile e Ambientale,
Università di Trieste, Via Valerio 10, 34127 Trieste, Italy
e-mail: dellavedova@units.it

S. Bellani
Istituto di Geoscienze e Georisorse, CNR,
Via Moruzzi 1, 56124 Pisa, Italy

U. Tinivella
Istituto Nazionale di Oceanografia e Geofisica Sperimentale,
OGS, Borgo Grotta Gigante 42/C, 34010 Sgonico (Trieste), Italy

Introduction

The lithospheric extension and the upper mantle doming of the Tuscan-Tyrrhenian domain are among the most remarkable and active tectonic processes within the entire Alpine-Mediterranean deformation area. They have been active since Miocene times (Carmignani et al. 1994; Brunet et al. 2000) and are likely sustained by mass and heat fluxes from the upper mantle, as suggested by the intense tectonic and volcanic activity, associated to extremely high and variable surface heat flux anomalies (Della Vedova et al. 2001). All these processes document a predominant heat transfer mechanism by vertical mass flow, which accumulates large amount of geothermal resources at accessible depths in the upper crust.

Despite intensive exploration and exploitation drilling programs, carried out in Tuscany, the nature, physical properties and heat transfer mechanisms of the intermediate and lower crust and of the upper mantle are still debated. The reconstruction of the temperature distribution with depth (*T*-*z*) in this area is crucial for the understanding of the nature and physical properties of the lithospheric units, as well as for the comprehension of the rheology and future evolution of the extended areas.

To understand the crustal structures and their relationship in the geothermal fields of Southern Tuscany, three seismic lines (CROP 18A, 18B, and CROP 03, Fig. 1) were

acquired on land in the frame of the CROsta Profonda (CROP) project (Scrocca et al. 2003). Along with wide-angle reflection and refraction deep seismic soundings (DSS data; Giese et al. 1981), the CROP seismic lines give information about the crustal structure of the geothermal province. These seismic reflection profiles cross specifically the Larderello and Monte Amiata geothermal fields. They have been recently reprocessed in order to better characterize the crustal and upper mantle structures of the Tuscan geothermal area. The results (Accaino et al. 2005, 2006; Tinivella et al. 2005) show a remarkable definition of the geometry of the "K-horizon" (the main marker of this region as defined by Batini et al. 1978), a second deeper and more continuous similar horizon (here after called K_2 horizon), sub-vertical mantle intrusions, strong reflectors in the lower crust and a discontinuous crust/mantle transition characterized by strong anisotropy in the seismic velocity (10–20%; Accaino et al. 2006). Accurate analyses of the seismic attributes suggest the presence of over-pressurized fluids below the K-horizon, down to about 10 km (Accaino et al. 2005). Fluid inclusion studies on rock samples coming from the Larderello geothermal field (Dini et al. 2005) allowed to discriminate the nature and thermodynamic characteristics of early fluid inclusions, as distinct from the late inclusions.

In this paper, we use the available geophysical data to constrain a set of preliminary convective thermal models, to be compared with the experimental borehole data and with the estimates of temperature (T) and fluid pressures from fluid inclusions and deep seismic data. The main objectives were to evaluate (1) the heat transfer mechanisms at the intermediate-upper crust levels, (2) the variability of the heat and mass fluxes entering from below and (3) the crucial role of the formation permeability.

The thermal convection in porous/fractured media, including the temperature and pressure effects on thermodynamic and transport properties, was specifically discussed by Straus and Schubert (1977).

Regional geologic setting

The Tuscan geothermal area is located in the inner side of the Northern Apennines (Fig. 1), where post-collisional extensional tectonics has been active since the Early Middle Miocene (Carmignani et al. 1994; Brunet et al. 2000), accompanied by a widespread Late Miocene-Quaternary magmatism (Serri et al. 1993) showing a progressive migration of the younger magmatic events in the E-ENE direction. The regional extension affecting the entire Western Mediterranean since Early–Middle Miocene, including the inner Northern Apennines (i.e., southern Tuscany), was coeval with the compression developing at the outer Apennines front, on the Adriatic side. The lithospheric extension was accompanied by mantle softening, crustal underplating and dike intrusion into the thinned continental crust.

The geologic and tectonic setting of southern Tuscany has been studied by several authors, including Decandia et al. (1998), Liotta et al. (1998), Brogi et al. (2003, 2005), and references therein.

The Larderello geothermal field in southern Tuscany produces superheated steam and fluids with a clear upper mantle isotopic signature (Magro et al. 2003); it is generally considered as a single, large hydrothermal system recharged by meteoric waters and heated from deep magmatic sources intruded into the thinned continental crust (Baldi et al. 1993). Although extrusive rocks are not outcropping in the Larderello area, felsic dikes and granitic bodies, encountered in boreholes at different depths, clearly indicate that magmas derive from mixing of mantle and crustal sources (Serri et al. 1993).

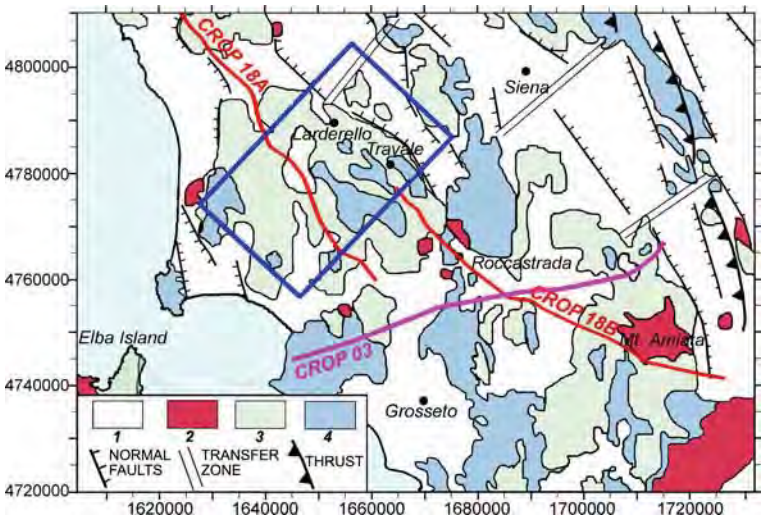

Fig. 1 Simplified geological map of the Tuscan geothermal area (modified after Carmignani et al. 2004; Decandia et al. 1998). (1) Neoautochtonous sediments (Lower Miocene-Pliocene); (2) Igneous rocks (Pliocene-Quaternary); (3) Allochtonous flysch *facies* units (Cretaceous-Eocene); (4) Potential reservoir formations (Tuscan Nappe, Tectonic Slices, Metamorphic Units: Precambrian–Late Triassic). Location of the main tectonic features are shown. CROP profiles and the position of the 3-D numerical model are indicated

From late Miocene to late Pliocene, N–S to NW–SE trending normal faults were active in southern Tuscany, bordering several extensional basins (Pascucci et al. 1999) in a non-rotational setting (Mattei et al. 1996). The continuity of adjacent basins throughout southern Tuscany is interrupted by NE–SW strike-slip faults (Fig. 1). The Larderello field is characterised by normal faults with Apenninic direction (NW-trending, NE-dipping). Their geometry down to depths of 4/5 km is constrained by field, borehole, and seismic reflection data (Liotta and Ranalli 1999). Normal faulting within the Apennines and its peri-Thyrrenian foundered thrust belt leads to increasing vertical permeability, connectivity and fluid mixing in progressively larger and interconnected sectors of the stretched crust (Ghisetti and Vezzani 2002).

Seismic surveys detected a regional high-amplitude discontinuous reflector with local "bright spot" features ("K-horizon"), which marks the top of the reflective crust (Brogi et al. 2003 and references therein). It is largely accepted that the reflectivity of this horizon is related to fluids entrapped in fractured levels. The negative gravity anomaly in the area (Nicolich and Marson 1994) also accounts for the presence of over-pressurized fluids (Accaino et al. 2005), which induces a density decrease in the country rocks.

The K-horizon tops at about 3 km depth in correspondence of the Larderello and Mt. Amiata geothermal fields, deepening towards the peripheral areas. Accaino et al. (2005) and Tinivella et al. (2005) recognized a second highly reflective and more continuous horizon, beneath the K-horizon, named "K_2", that might hence be considered as a regional sub-horizontal surface (at a depth of 8–9 km) likely more isothermal than the above K-horizon and already within the ductile zone (T in excess of 450°C).

Geophysical data and crustal structures

The crustal structure of the Tuscan area is defined on the basis of the Deep Seismic Sounding (DSS) data (Giese et al. 1981; Nicolich 1989), body (Piromallo and Morelli 1998; Spakman 1990) and surface wave velocity tomography (Panza et al. 2003). DSS data define the top of the lower crust, at a depth from 12 to 16 km, on the basis of its V_p velocity of 6.8–7.3 km s^{-1}. The crust-mantle boundary, imaged at 22–25 km depth (Locardi and Nicolich 2005; Nicolich 1989) is laminated and characterized by an anomalously low upper mantle velocity of 7.5–7.8 km s^{-1}, likely corresponding to the culmination of the soft mantle upwelling beneath the geothermal province. The surface expression of this deeply rooted thermal process affects the whole Tuscan area (Della Vedova et al. 1991, 2001) and suggests a predominant heat transfer mechanism by upward mass flow, as shown in the thermal gradient map of Fig. 2.

Bouguer gravity anomalies, when computed with a reduction density of 2,670 kg m^{-3}, evidence an excess of mass in the lower crust of the geothermal province, which is isostatically under-compensated (Velicogna et al. 1996; Marson et al. 1998). In addition, the Geoid elevation shows a steep gradient moving from western Tuscany towards Umbria-Marche regions (Barzaghi et al. 2002), confirming a strong lateral change in mass distribution at the depth of

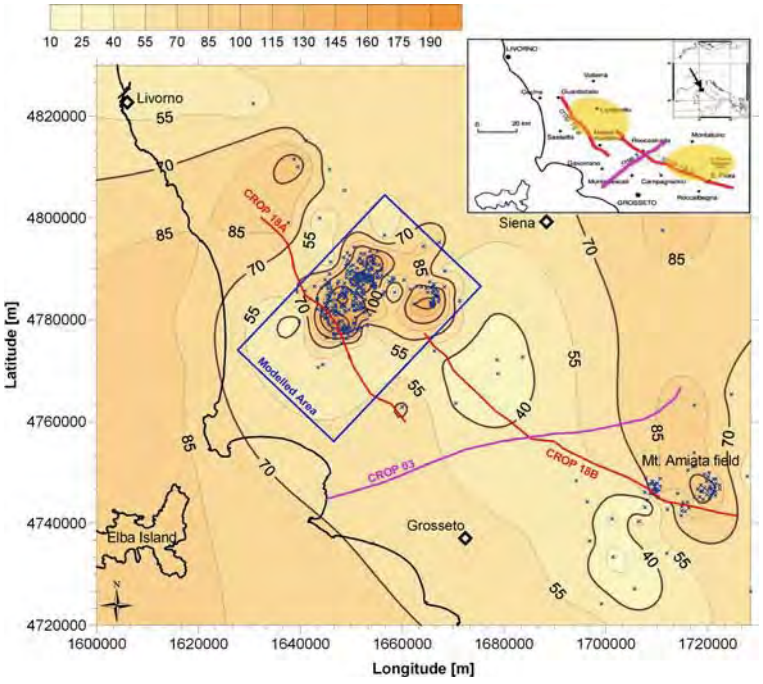

Fig. 2 Simplified map of the vertical geothermal gradient in the Tuscan area (mK m^{-1}). Location of CROP profiles and geothermal wells (*crosses*) is shown. The *box* indicates the extension of the 3-D numerical model. Location of the Larderello and Monte Amiata fields is shown in the *inset* map

the crust-mantle boundary. On the other hand, when the Bouguer anomaly (Fig. 3) is computed with a reduction density of 2,400 kg m^{-3}, it shows a clear *deficit* of mass in the upper crust (Nicolich and Marson 1994; Baldi et al. 1995; Tinivella et al. 2005).

The emplacement of plutons (Acocella and Rossetti 2002), requires roof uplift of the crustal units to accomodate the ascent of granitic magmas; indeed, the Pliocene deposits of the Tuscan geothermal district experienced more than 600 m of regional uplift (Marinelli et al. 1993).

The seismic results of the CROP 18A transect (Fig. 4) through the Larderello field (Accaino et al. 2005) significantly improved the knowledge on the stretched continental crust underlying the Tuscan area. It is characterized by: a complex and structured upper part, an intermediate less (or poorly) reflective crust and a highly reflective mid-lower crust, often bottomed by a laminated crust-mantle boundary at 22–24 km depth. The K-horizon reaches minimum depths of about 3–6 km in the geothermal areas, whereas it deepens to greater depths moving outwards. The character of the high-amplitude reflectors within the middle and lower crust (K_2 horizon and others deeper) is sometimes stronger than the signature of the well-known shallower K-horizon. The amplitude of these deep reflectors drops off in the proximity of the Larderello and Monte Amiata geothermal fields, where, instead, the K-horizon above is well imaged. Non-conventional analysis (such as AVO; Accaino et al. 2005) on the seismic data suggests that the upper remarkable K-horizon beneath the Larderello and Monte Amiata geothermal fields can be associated with fluid over-pressure conditions. The K_2 horizon, instead, is a deeper and a more regional reflecting interval, compatible with a lithologic change. However, the shape and depth of this structure, as well as the associated micro-earthquakes hypocenters down to 8 km depth (Vanorio et al. 2004), suggest that the K_2 horizon might be a reasonable image of the brittle-ductile transition.

The reflectivity associated with lithologic changes beneath K_2 can be explained by the presence of mantle intrusions into the extended deep continental crust. The intrusion of mantle-derived magmas has been studied in depth in the Ivrea-Verbano zone by Sinigoi et al. (2003). The heat input at the base of the crust induces crustal erosion and underplating which triggers partial melting of lower crust granulite *facies*. The upward migration of melts increases the density of the depleted restitic rocks, which could provide a laminated seismic image, because of repeated episodes of dikes/sills intrusion. A sharp distinction between denser materials and lighter melts/rocks explains the presence of alternating impedance and observed reflectivity.

The rising of the partial melting front from the lower crust affects the overlying crustal rocks (anatexis), with production of granitic melts quickly migrating to higher crustal levels. Fluid over-pressure occurs in reservoir rocks when capped by impermeable layers; the strong reflective K-horizon marks the transition between the deep reservoir and the cap rocks.

Possible diffused intrusions, likely distributed laterally (sills) and at depth, are likely present below the

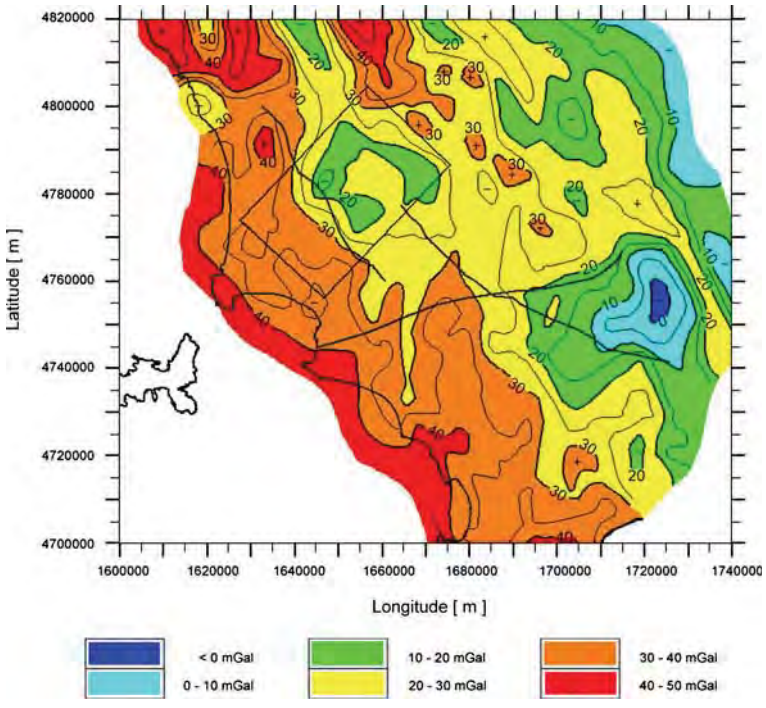

Fig. 3 Bouguer gravity anomalies (in mGal) of the Tuscan geothermal area (modified after Baldi et al. 1995). Location of CROP profiles and 3-D numerical model is shown

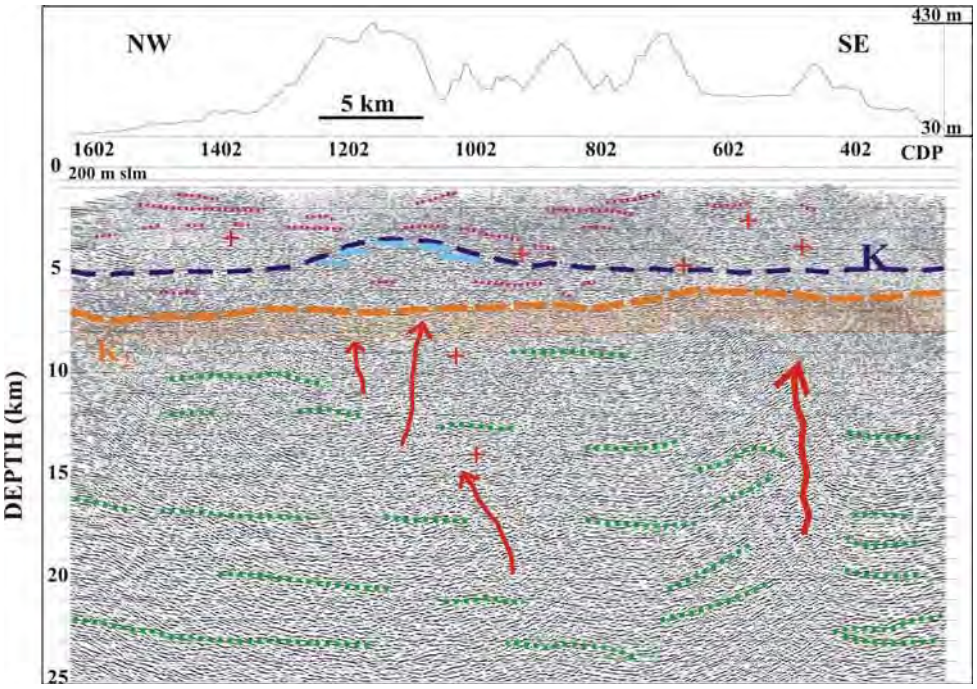

Fig. 4 Interpreted post-stack depth migrated CROP 18A across the Larderello field, showing K horizons, evidence of fluid traps (*blue spots*), vertical conduits (*arrows*), magmatic intrusions (*crosses*) and deep reflections (*dotted lines*). Modified after Accaino et al. (2005, 2006)

culmination of the K-horizon in correspondence of the Larderello field and also at the SE end of line 18-A (Fig. 4). The seismic analysis (Accaino et al. 2006) of the CROP 03 line, though external to the studied area (Fig. 1), confirmed that the lithosphere of the Tuscan geothermal province is affected by significant velocity and density changes, with geothermal fluids rising from great depths. From the theoretical modelling, the porosity in the over-pressurized zones seems to have a value of the order of 5%, with a consequent decrease in density, which could partly explain the observed negative Bouguer anomalies (Nicolich and Marson 1994).

Thermal state of the area and isotopic constraints on the deep fluids

The lithospheric extension of the Tuscan region is clearly associated to intense heat flow anomalies, as imaged by surface heat flux measurements (Bellani et al. 2004), suggesting a predominant heat transfer mechanism by vertical mass flow. Groundwater flow and geothermal fluid circulation in the shallow levels of the crust are here important in generating very intense and laterally variable local heat flux anomalies (with values up to 1 W m^{-2}). This high frequency component is superimposed on the regionally high background heat flux (150–200 mW m^{-2}) of the Tuscany-Latium area (Mongelli et al. 1989; Bellani and Della Vedova 2004), which reflects the transient effects of the recent lithospheric extension and associated intrusion of mantle derived magmas and fluids into the crust.

Temperature distribution in the Larderello area is well known down to depths of 4–4.5 km, thanks to the extensive drilling for geothermal exploration and exploitation. The thermal field shows a pronounced heterogeneity, with strong lateral T changes; at about 5 km depth we observe up to 200°C T difference, over lateral distances of a few tens of km (Della Vedova et al. 2001; Bellani et al. 2004). This means that the whole area is still far from steady state conditions, though the geothermal activity dates back to at least 3.8 Ma (Gianelli and Laurenzi 2001). The progressive migration of the magmatic activity to the NE and the present geothermal activity of the Tuscan district likely require episodic input events of mass and energy, through the extensional brittle structures.

Two geothermal reservoir systems are industrially exploited in the Larderello field:

- the shallow reservoir system (at about 700–1,000 m depth), located in cataclastic rocks (evaporites) at the base of the sedimentary cover,
- the deep reservoir system, located in the fractured metamorphic basement (schists, phyllites, micaschists and gneisses) at depths ranging between 2,000 and 4,500 m.

The geothermal steam from permeable horizons within the metamorphic basement is characterised by temperatures well above 300°C and up to more than 400°C (Barelli et al. 2000).

Larderello is the preferential escape area in Tuscany for mantle-derived fluids, as indicated by the good agreement among relative maxima of He isotopic ratio R/R_a, where R_a

represents its typical air value, positive heat flow anomalies and relative minima of the Bouguer gravity map (Magro et al. 2003).

The existence of relatively high R/R_a values in the Tuscan magmatic province is therefore, consistent with heat input at the base of the crust, anatexis of the overlying crustal rocks, production of granitic melts and their migration/intrusion into higher crustal levels.

At the brittle-ductile transition, the formation permeability decreases sharply (Bailey 1990; Fournier 1991), creating an impervious boundary (Kennedy and Van Soest 2006; Kennedy et al. 1997). ^{3}He enriched fluids rising through vertical conduits homogenize with crustal derived fluids, enriched in radiogenic ^{4}He, fill the permeable formations and spread horizontally, as a function of lateral permeability. The coexisting presence at the surface of both thermal and ^{3}He positive anomalies, indicates that both energy and mass fluxes traverse the crust and issue at surface, producing in Larderello the strongest "mantle signature" (up to R/R_a values of 3, as compared to average crustal values around 0.02) among the volcanic areas of central Italy. The deep extensional structures (Acocella and Rossetti 2002; Vanorio et al. 2004; Accaino et al. 2005) beneath southern Tuscany are supposed to connect hydraulically the upper mantle with the intermediate/upper crust (Brogi et al. 2003; Bellani et al. 2005).

Thermal and fluid dynamic modelling

On the basis of the CROP seismic data, integrated with existing geological and geophysical results, we set up a simplified 3-D thermal model to qualitatively evaluate the extent and relative importance of the main heat transfer mechanisms (conduction vs. convection), their space and time variability and the crucial role of the formation permeability (k) at the intermediate-upper crustal levels. The simulated T-z distribution could then be compared with the experimental borehole data and with the estimates of T and fluid pressures from fluid inclusions and deep seismic data.

The model domain includes the whole Larderello geothermal field, extending over an area of 42 × 26 km (see Fig. 1) and with a vertical thickness of 10 km, in order to include both K horizons. It is oriented according to the regional tectonic setting, with its short side along strike with the Apenninic orientation. It is composed by three main layers: the top layer represents heterogeneous rocks and terrains (mainly sedimentary rocks) above the upper K-horizon, the second layer represents the geological formations (intrusive and metamorphic rocks) in between the two K horizons (locally interested by over-pressurized fluids) and the third layer represents the crystalline basement between K_2 and the model bottom. We deliberately chose to limit the total depth of the model to 10 km (about twice as much the maximum depth reached by boreholes in the Tuscan geothermal area), in order to control and validate the SHEMAT (see Appendix 1) numerical results with the geological and geophysical observations collected in the upper crust. The mesh is 1 × 1 × 0.3 km (Fig. 5) and it considers (for a selected set of simulations) a single one extensional fault, with Apenninic direction, bordering the NE side of the Larderello field (Fig. 1). The reason for including a single regional deep fault was twofold: firstly to locally simulate the fault contribution to the vertical heat transfer mechanism, connecting the deep heat source (corresponding to the basement rocks) to the over-pressurized reservoirs located between the K horizons, and secondly to study the topologic relationship between the location of the fault and the development and position of the upward and downward rims of the hydrothermal circulation cells (Kühn et al. 2006a).

The boundary conditions include a constant T (20°C) and a constant hydraulic head (0.1 MPa) at the upper boundary of the model, located at +350 m a.s.l. Zero horizontal gradients of T and hydraulic head were set on the lateral faces (adiabatic and impermeable boundaries) and

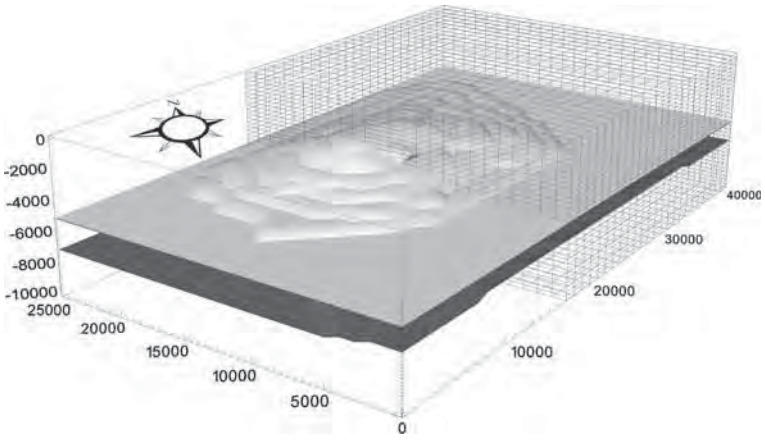

Fig. 5 3-D grid (42 × 26 × 10 km) of the Larderello numerical model (see location in Figs. 1, 2, 3). View point is from *S*. the geometry of K-(*upper*) and K_2 (*lower*) horizons is shown. The mesh ends in correspondence of the CROP 18A section

Table 1 Summary of the boundary conditions for all model simulations

Boundary	Temperature	Head
Top	T = cost. = 20°C	h = cost.
Bottom	T = cost.(400–600°C)	$\nabla \times h = 0$
Lateral	$\nabla \times T = 0$	$\nabla \times h = 0$

constant T and impermeability condition ($dh/dz = 0$) at the bottom boundary. The industrial exploitation of the geothermal fields (steam extraction and water re-injection) was not considered, because of the long time of the simulations (8–12 Ma). The boundary conditions are summarized in Table 1.

Initial values for the thermal properties were assigned according to Bellani and Della Vedova (2004) and Toulokian et al. (1981). The initial conditions include both the geothermal gradient and the gradient of the fluid pressures (when advection/convection is involved). We set an initial linear T gradient between the upper and the lower boundary. The hydraulic gradient of the fluids was assumed hydrostatic. The T and pressure effects on fluid density were considered during the simulations.

Our thermal modelling included initial sensitivity studies using variations in the assumed material properties of model components, the most important being the hydrogeologic parameters (such as porosity, permeability and hydraulic head) and the thermal parameters (such as the thermal conductivity and the bottom T condition).

Table 2 shows the results of the sensitivity analyses on the computed T distribution, upon changes of the formation thermal conductivity λ of the three main units: changing λ by 20% in the reservoir and basement units (where convection prevails) causes a negligible variation in the T distribution with depth, vice versa, changing λ by the same amount in the cap rock formations (where conduction prevails) causes a significant change in the T distribution. The latter change is of the same magnitude as that produced by a λ variation of 20% in all three units.

The results of the sensitivity analysis on the assumed formation porosity (Table 3) are in agreement with those of Kühn et al. (2006b). For porosity values changing between 0.01 and 0.20 there is very little influence on the T distribution and flow field pattern (the convective cells remain practically identical), and with the only difference being the simulation time to steady state.

Table 2 Sensitivity analysis of the changes (%) on the average computed T gradient caused by changes (%) in the average formation thermal conductivity (λ) of the various units

Domains interested by λ change	λ change (%)	T gradient change (%)
All three units	+20	–9.5
Reservoir and basement units	+20	+0.6
Cap rock unit	+20	–9.0

The criteria for deciding the reliability of model results is how well the models match a composite target function, defined by different sets of experimental data, such as: borehole data (T measurements, geological and geochemical data, fluid inclusion studies) and regional geological and geophysical data (described in the previous chapters).

Because of the inherent uncertainty of many model parameters (e.g., subsurface geometry and properties of the host rocks) and of the initial and boundary conditions (e.g., bottom T), a large number of model calculations were run in order to study the range of possible solutions. In this study emphasis was placed on the basal heat flux input (bottom T) and on the formation permeability contrast among the three main layers.

We computed more than one hundred models, considering different geometries and boundary conditions and also including the presence of a major regional fault hydraulically connecting the heat input, through the base of the model, with the geothermal reservoirs beneath the upper K-horizon. The latter case was simulated using different contrasts in formation permeability, between the fault and the surrounding rocks. We discuss here the most significant results of the numerical modelling.

Table 3 Thermal and hydraulic properties of the modelled materials: effective porosity (n_e), formation permeability (k) heat capacity (C) and thermal conductivity (λ)

	Cap rock	Reservoir	Basement	Deep fault	Water
n_e (/)	0.15	0.05	0.03	0.10	/
k (m^2)	10^{-17}	5×10^{-15}–5×10^{-16}	5×10^{-16}–5×10^{-17}	10^{-13}–10^{-14}	/
C [MJ/(m^3 K)]	2.18	2.18	2.18	2.18	4.186
λ [W/(m K)]	2.5	2.9	2.9	2.9	0.65

C and λ values are matrix values, referred to room T and pressure conditions

Crustal stratigraphy and properties of rocks

The upper 10 km of the crust were simply subdivided in the following three main units (Figs. 4, 5), characterized by specific thermal and hydraulic properties (Tables 3, 4):

- *Sedimentary cap rocks.* This layer (3–5 km thick) represents the heterogeneous geological sequences above the upper K-horizon. It is mainly composed by sedimentary rocks (Paleozoic to Present), with limited amount of igneous and metamorphic rocks. The upper boundary of this layer was approximated by the average elevation of about +350 m, characterized by a constant hydraulic head (to avoid the complications of the unsaturated zone). Its bottom is described by the depth to the K-horizon (Accaino et al. 2005, 2006). The permeability of this unit was assumed to be quite low ($k = 10^{-17}$ m^2) in all models (Table 3) to suppress regional groundwater movement and convective flow, as suggested by the experimental geotherms, which indicate a heat transfer mechanism mainly provided by conduction. This condition is obviously not completely true, because there are several leakage zones in the cap rock, feeding the exploited shallow geothermal reservoirs. Our numerical grid is too coarse ($1 \times 1 \times 0.3$ km) to consider these local features and, therefore, the assumed porosity and formation permeability cannot be directly compared with those obtained from experimental flow and pressure well tests in the exploited geothermal wells.
- *Geological sequences between the K horizons.* This layer (1–4 km thick) mainly represents a sequence of metamorphic and intrusive rocks. The upper boundary corresponds to the K-horizon, which was reconstructed as a dome, on the basis of the seismic data. This discontinuity represents a significant change in porosity and fluid content of the formation, locally characterized by over pressured fluids (Accaino et al. 2005). This layer represents the major and regional deep reservoir system in the Tuscan area, likely fed by deep fluid and mass injections, through the complex and numerous deformation zones (faults, vertical conduits, shear zones).
- *Basement rocks.* This layer (3–4 km thick) mainly represents crystalline basement rocks, locally intruded by dikes and sills, bounded between K_2 and the model total depth (10 km). The hydraulic properties (k and n_e) of this unit are unknown, therefore they were numerically estimated a posteriori in an iterative way, matching a composite target function, defined on the basis of the T data in the above 3–4 km, the earthquake hypocentral distribution (Vanorio et al. 2004) and the Curie T depth (Della Vedova et al. 1991).

Results and discussion

Selected results of 3-D simulations are presented in Figs. 6, 7, 8 and 9. In these examples we evaluate the T distribution and the fluid flow vectors along the plane including part of the CROP 18A section (Figs. 6, 7) and along a fault plane sub-parallel to the CROP 18A and located to the NE (Fig. 8). Figure 9 is a constant depth view of the same model as in Fig. 6.

The most relevant thermal differences among the various models are produced by changing the permeability value of the "basement layer" and by the change in the bottom T condition. These parameters are the real variables of the problem. The presence of the vertical fault (Fig. 8) adds a further complication to the model, useful to evaluate the extent, time scale and the effects of the presence of a vertical preferential fluid pathway on the T(z) distribution.

The simulation time to steady state was variable, depending upon the assumed parameters, from a few Ma (about 5) for the high permeability models (including the fault models), to 10–12 Ma for the low permeability ones. The maximum values of the average linear velocities range

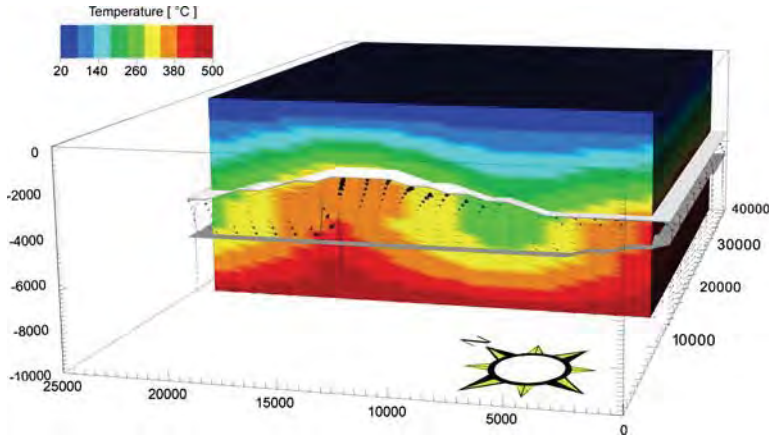

Fig. 6 3-D model results computed with model 500_d parameters (Table 4), simulation time 12 Ma. The SW face shows the CROP 18A section. *Different colours* indicate T values; the size of the *arrows* is proportional to the average linear fluid velocity vectors. Max average linear velocity: 0.1 m a^{-1}. See text for more explanation

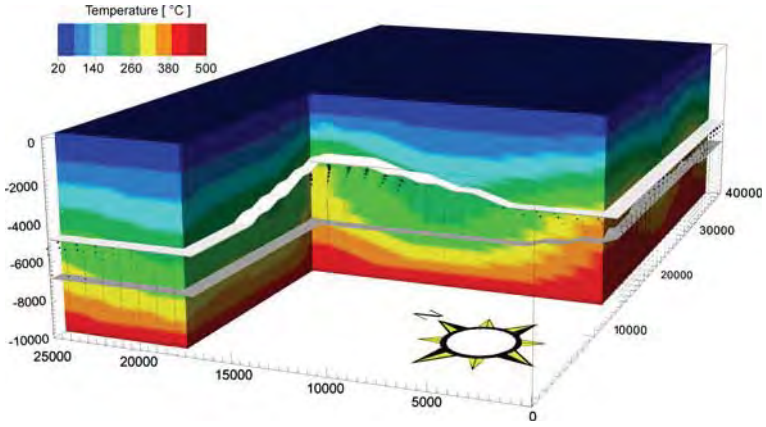

Fig. 7 3-D model results computed with model 450_d parameters (Table 4), simulation time 12 Ma. Part of CROP 18A section is shown to allow the 3-D view of the geometries and *T* distribution. The *different colours* indicate *T* values; the size of the *arrows* is proportional to the average linear fluid velocity vectors. Max average linear velocity: <0.1 m a^{-1}. See text for more explanation

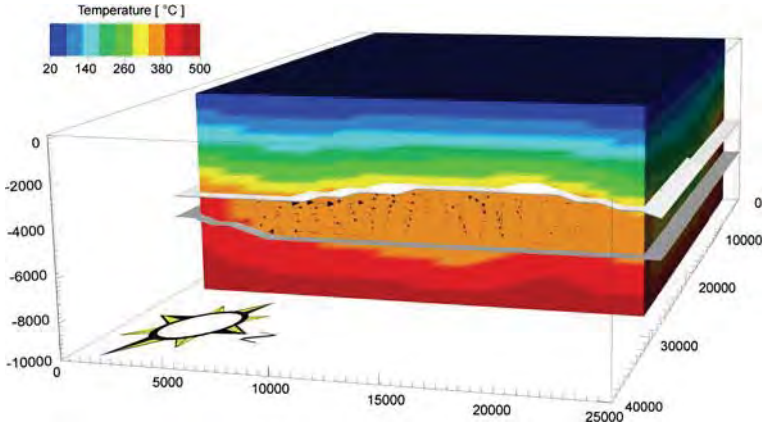

Fig. 8 3-D model results computed with model 500_d parameters (Table 4), including the fault zone to the NE end of the box (Fig. 1). The fault plane is seen from NE, fault permeability $k = 10^{-13}$ m^2, simulation time 8 Ma. The *different colours* indicate *T* values; the size of the *arrows* is proportional to the average linear fluid velocity vectors. Max average linear velocity: 0.5 m a^{-1}. See text for more explanation

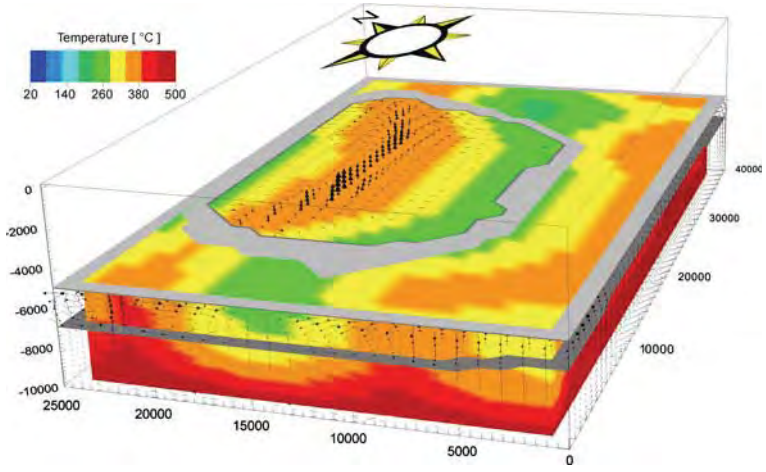

Fig. 9 3-D model results at 5 km constant depth, computed with model 500_d parameters (Table 4), simulation time 12 Ma. View from *S*. The intersection with the K-horizon is artificially enlarged (gray closed band). The size of the arrows is proportional to the average linear fluid velocity vectors. Max average linear velocity: 0.1 m a^{-1}. See text for more explanation

from 1.5×10^{-8} (about 0.5 m a^{-1}) to 3.1×10^{-9} m s^{-1} (0.1 m a^{-1}) for the high and low permeability reservoirs, respectively.

Parameters calibration

The formation permeability *k* and the thermal conductivity λ (Table 3) were, particularly, subject to calibration, by minimizing the residual between computed and observed *T*-*z* data.

The estimate of the rock and fluid parameters strongly depends on the assumed petrogenetic model. Using variations in the assumed material properties we conducted sensitivity studies on the propagation of uncertainties in the input parameters, downstream to the thermal modelling results. For this purpose, we created several sets of models to calibrate the formation permeability and the bottom *T*.

Table 4 Index map of the formation permeability (k) for the model subscripts a, b, c, d, with a bottom T of 500°C

Model ID	Formation permeability (k)					
	Cap rock unit		Reservoir unit		Basement unit	
	m^2	mDarcy	m^2	mDarcy	m^2	mDarcy
500_a	10^{-17}	0.01	5×10^{-15}	5	5×10^{-16}	0.5
500_b	10^{-17}	0.01	5×10^{-16}	0.5	5×10^{-16}	0.5
500_c	10^{-17}	0.01	5×10^{-15}	5	5×10^{-17}	0.05
500_d	10^{-17}	0.01	5×10^{-16}	0.5	5×10^{-17}	0.05

Table 4 summarizes the formation permeability assumptions for one set of these models, with bottom T of 500°C.

Further sets of models were run using the formation permeability contrasts of Table 4, but assuming a different bottom T boundary condition, every 50°C, from 400 to 600°C. The reason for choosing 400°C as the lower T limit is because it cannot be cooler than the T observed in the Carboli 11 well (437°C at 3,343 m depth, see well location in Fig. 13), on the other hand the upper T limit (600°C) approximately corresponds to the Curie T, estimated at about 10 km depth.

In all simulations the computed T was monitored against the target function, at two reference sites: RS1 in the centre of the Larderello geothermal field and RS2, located 10–12 km to the east, in between the Larderello and Travale fields (Fig. 13). The experimental T-z distribution in the areas surrounding RS1 (within a square box approximately 10 × 10 km) and RS2 (within a square box approximately 5 × 5 km) have been used for comparison with the computed geotherms $T(z)$, as shown in Figs. 10, 11 and 12. By minimizing the residuals between computed and observed T-z data we estimated the best average values for the bottom T and for the permeability contrast between the two deeper layers (Table 4). Among all the simulations (Figs. 10–12), the ones with 500 ± 50°C bottom T condition provided the best matching with the observations.

We also checked the simulations with respect to two different scenarios, i.e.,: considering an average constant permeability of the reservoir rocks between K-and K_2 horizons (Figs. 6, 7), and assuming a localized vertical fault zone with NW–SE direction, bordering to the NE the Larderello field (Fig. 8). Therefore, there will be two

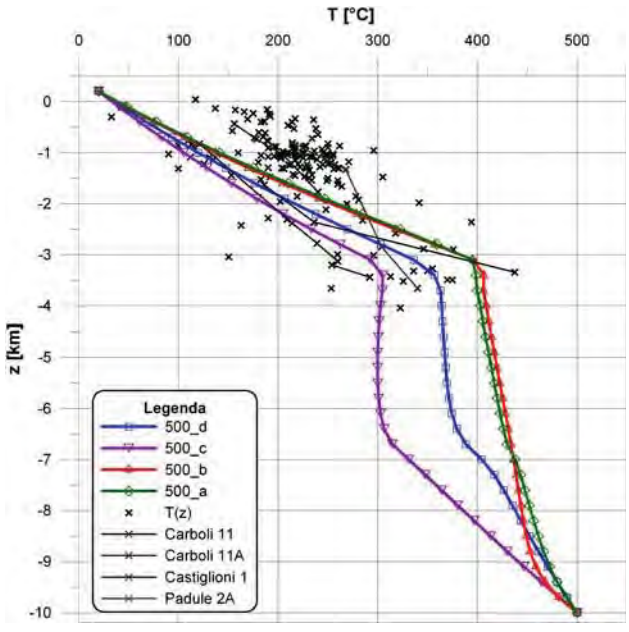

Fig. 10 Computed geotherms $T(z)$ versus bottom hole experimental T-z and a few selected multipoint geotherms single wells in the RS1 target area (position in Fig. 13). The four geotherms from the surface down to 10 km depth where computed with the model parameters as in Table 4. Bottom T = 500°C

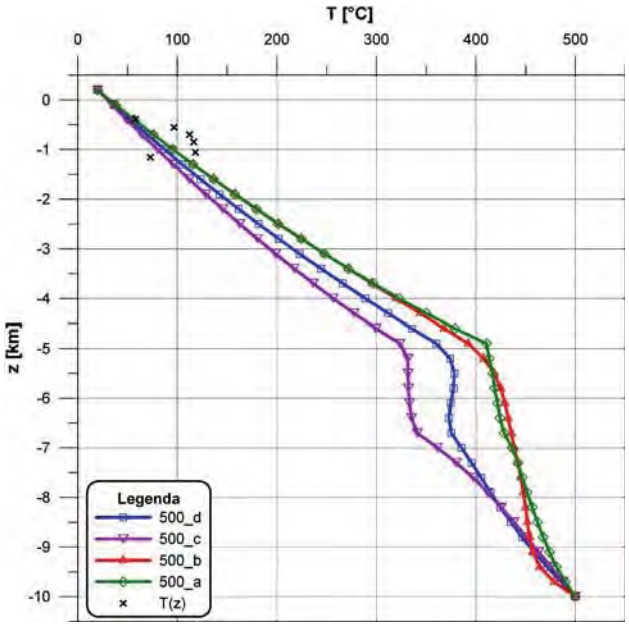

Fig. 11 Computed geotherms $T(z)$ versus a few experimental T-z, off the Larderello field (see RS2 position in Fig. 13). The four geotherms from the surface down to 10 km depth were computed with the model parameters as in Table 4. Bottom T = 500°C

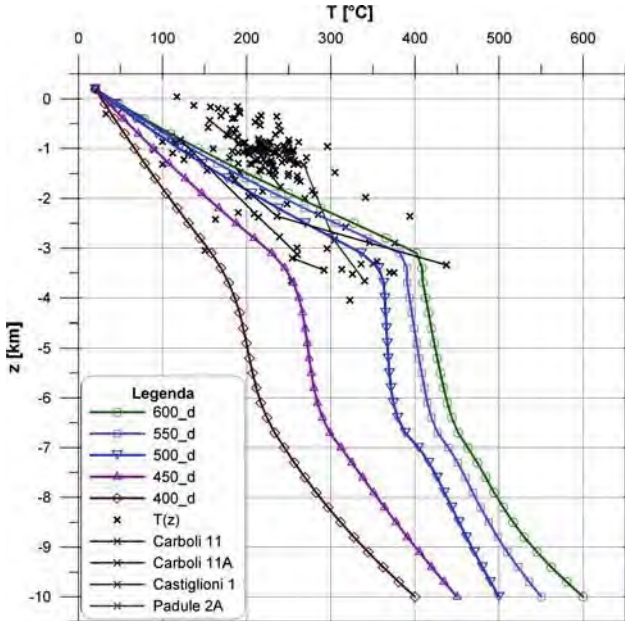

Fig. 12 Computed geotherms versus both experimental *T*-*z* and a few selected measured geotherms within the RS1 area (position in Fig. 13) in the Larderello geothermal field, simulated with variable bottom *T* conditions (every 50°C, from 400 to 600°C). The five geotherms from the surface down to 10 km depth were computed with the model parameters 500_d, as in Table 4

further sets of simulations to compare with each reference site.

The difference between the observed geothermal gradient at 1,000 m depth and the computed gradient at the same depth was also produced (Fig. 13), to evaluate the 3-D distribution of the geothermal field.

Additional data for model calibration come were provided by interpreted CROP profiles (presence of over pressured fluids), geochemistry data (He isotopes and isotope ratios), fluid inclusion data (trapping *T*) and gravity data (lateral heterogeneity in mass distribution at selected depths).

Simulations without considering the presence of the fault

The conditions for the simulations shown in Fig. 6 (Model 500_d) and Fig. 7 (Model 450_d) are very similar, differing in the bottom *T* condition only. The 3-D *T* and velocity fields show as the *T* and pressure structures of the Larderello field are driven by geometry, formation permeability, permeability contrasts among the main layers, and by heat input from below. It is possible to recognize two clear large convective cells in the reservoir between K horizons, along the CROP 18A section, oriented from NW (left hand side) to SE, and a third smaller cell to the SE end (Fig. 6). The size of the velocity vectors is proportional to the average linear velocity. The vertical plane through the culmination of the K-horizon (orthogonal to the page) corresponds to the deep "aquifer divider", being the *locus* of an upward diverging flow of two large adjacent convective cells. The descending rim of the SE

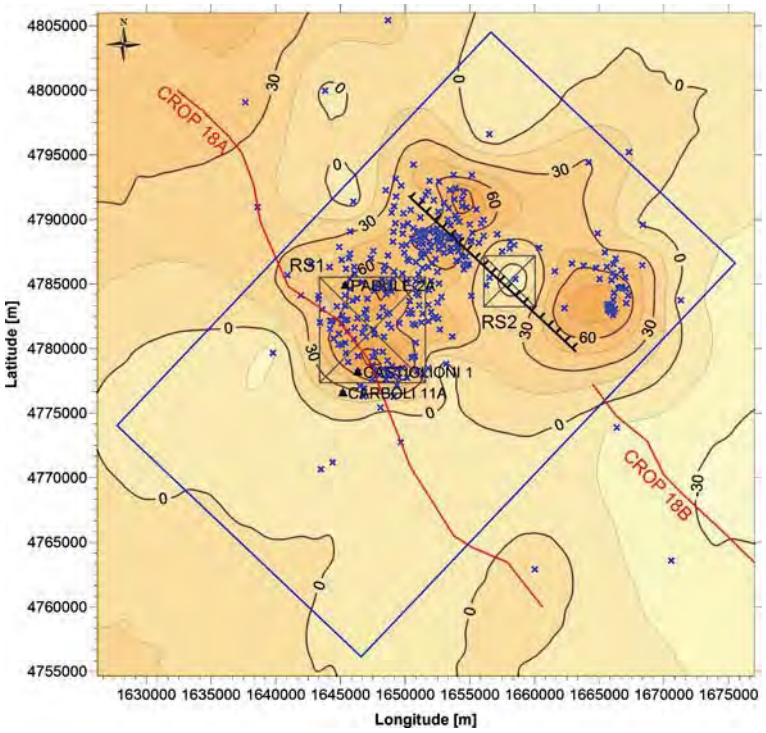

Fig. 13 Smoothed *T* gradient residuals (*T* experimental–*T* computed) in the upper 1 km of sediment. The simulation parameters for the computed *T* gradient are those of model 500_d (Table 4), with fault permeability $k = 10^{-13}$ m^2. Location of selected wells with observed geotherms (Figs. 10, 12) is shown (*black triangles*). *Blue crosses* are geothermal boreholes with single *T* measurements. Target sites (RS1 and RS2) and the fault location are also indicated

convective cell contributes to the cooling (green colour) within the reservoir. The simulated T for the upward fluid circulation is of the order of 400°C (Fig. 6), for a bottom T condition of 500°C, and of the order of 300°C, for a bottom T condition of 450°C (Fig. 7). The former values allow a better matching between simulated and measured T, at about 3–4 km depth in the Larderello field (Fig. 10.) The lateral extent of the anomalous T in the reservoir rocks, sustained by the ascending geothermal fluids, is of the order of 7–8 km, for the conditions simulated in Fig. 6, and it corresponds to the area interested by overpressurized fluids on the interpreted seismic section of CROP 18A (Fig. 4). Moreover, this distance is of the same order of magnitude of the lateral extension (about 10 km) of the observed thermal gradient anomaly (Fig. 2) and of the $^{3}He/^{4}He$ isotopic anomaly at the surface (Magro et al. 2003). Furthermore, the conditions simulated in Fig. 7 do not match either the observed T values at 3–4 km depth (Fig. 10), or the wavelength of the observed positive geothermal gradient anomaly (Fig. 2). The comparison between the two simulations shows as the bottom boundary T condition is extremely critical with respect to the simulated T and fluid velocity fields in the 3-D domain, although the convective cells have the same position, extent and circulation sense.

Given the low assumed permeability for the upper cap rock layer, the fluid velocity and T field in the model domain is driven by the permeability contrast between basement layer and reservoir layer and by the bottom T condition.

The horizontal section of 500_d model (Fig. 9) intersects the K-horizon at 5 km depth, allowing to reconstruct the space distribution of the convective cells. Three main convective cells extending in a sinuous way all along the longitudinal side of the model (with a NE–SW direction) can be recognized: the two adjacent ones interesting the Larderello field contribute to an upward converging flow, sustaining a strong advective vertical heat transfer (orange), whereas the two cells to the SE sustain a downward flow, characterized by a negative T anomaly (green). The geometry and boundary conditions of the models strongly influence the solutions close to the borders; nonetheless the central part of the simulated domain provides results in good agreement with the available observations within the calibration target sites (RS1 and RS2 in Fig. 13). The computed 1-D geotherms for the Larderello field are compared in Fig. 10 with the available experimental measurements, assuming a bottom T value condition of 500°C and four different permeability contrast (as shown in Table 4). The T measurements and thermal gradients measured within the upper layer are not adequately described by model simulations, both as absolute T values and as thermal gradients. There are two main reasons for this: first, because we wanted to extract the low frequency signature of the main regional geotherms (suggesting a prevailing heat transfer by conduction), thus avoiding the local effects due to lithology and structural heterogeneities, second, because the formation permeability of the cap rock is qualitatively bimodal: very high in correspondence of the localized fresh fractures and faults and very low in correspondence of the bulky rock.

To understand the meaning of the four different geotherms (labelled 500_a, 500_b, 500_c, and 500_d, according to the formation permeability values listed in Table 4 below the K-horizon depth (Fig. 10), it is useful to analyze them in three steps: first comparing 500_a with 500_c geotherms, then comparing 500_b with 550_d and finally cross-correlating the two groups together. However, it should be noticed that the simulated geotherms represent the $T(z)$ distribution in a vertical column of cells with a base area of 1×1 km, whereas the experimental data refer to larger target areas of 10×10 km (RS1) and 5×5 km (RS2), respectively.

The first group compares the simulation results between two models with the same formation permeability in the reservoir (5 mDarcy) and in the cap rock (0.01 mDarcy) layers, respectively, differing by the permeability of the basement layer only. The two geotherms are very different, with the 500_c geotherm strongly two-legged below the K-horizon. Thus the formation permeability of the basement layer appears to be the most critical parameter in controlling the mass and energy transport toward the upper levels, and, as a consequence, the T distribution within the modelled domain.

The other two models (500_b and 500_d) have the same formation permeability in the reservoir layer (0.5 mDarcy), but these values are one order of magnitude lower with respect to the first two models. The 500_b model has a single homogeneous deep unit (reservoir + basement) with the same formation permeability. The two geotherms are much closer, but show an analogous behaviour as the previous ones. Also in this case, the permeability of the bottom basement layer drives the mass and energy flow entering the domain from the bottom boundary.

The above comparisons suggest that the shape of the geotherms (almost linear versus two-legged) in the two deeper layers is controlled by the formation permeability of the basement layer, with almost linear geotherms in the case of high permeability of the bottom layer. In this case, the change in formation permeability of the reservoir rocks produces slight changes between the 500_a and 500_b geotherms. Because of the T boundary condition and the homogeneous permeability of the 500_b model, the average thermal gradient between 3.5 and 9 km is almost constant (apart from the lower boundary condition).

On the other hand, when the formation permeability of the bottom layer is very low (models 500_c and 500_d), the two-legged geotherms could spread over a larger domain of the *T*-*z* space, as a function of the formation permeability of the above reservoir rocks. If the hydraulic resistance of the reservoir is lower, then the total mass and energy fluxes through it is higher, with higher *T* gradients in the basement unit and very low *T* gradients in the reservoir unit; vice versa, if the hydraulic resistance of the reservoir is higher (model 500_d), then the *T* gradients in the basement unit are lower and the *T* gradients in the reservoir unit are higher, with respect to the corresponding gradients of the 500_c model. The highest *T* value, measured at about 3.2 km depth in the Carboli 11 well (Barelli et al. 2000) is anomalously high, corresponding to simulated *T* at depths greater than about 6 km. This measurement was conservatively assumed to correspond to vertical mass/heat input from greater depths. The lateral *T* variability at about 3.5 km depth beneath the Larderello field is enormous, ranging between 250 and 440°C (average of about 350°C), suggesting that the field is still far from thermal equilibrium.

Figure 11 shows the same geotherms as in Fig. 10, but for the NE marginal area of the Larderello geothermal field (RS2 in Fig. 13). In this case the comparison between simulations and experimental data is not very informative, because of the lack of deep information in areas less interesting from the exploitation point of view. Nonetheless, the interpretation of these geotherms is expected to follow the same line of reasoning as for the geotherms in Fig. 10.

The geotherm 500_d in Fig. 10 was assumed to correspond to an average *T* distribution with depth for the field, therefore the formation permeability values used for that simulation (Table 4) were chosen to run several simulations with changing bottom *T* boundary condition, with the aim of evaluating its effect on the computed geotherms (Fig. 12). We assumed five different bottom *T* values, every 50°C, in the *T* interval from 400 to 600°C and compared the resulting geotherms with available *T*-*z* measurements. The geotherms better constraining the observations require a bottom *T* of at least 500 ± 50°C.

The comparison between observed and computed *T*-gradients (using model 500_d with fault) in the upper 1 km is shown in Fig. 13 as residuals map. Computed and observed anomalies are in reasonable good agreement for the regional field, whereas, at shorter wavelength, there are three main discrepancies, with differences up to 60 mK m^{-1}. These large residuals correspond to the local high intensity thermal gradient anomalies, generated by the shallow exploited reservoirs, which were not included in our simulations. The location of wells with a single *T* value (blue crosses) and with multiple *T* measurements (black triangles) are also shown (see also Figs. 10–12).

Simulations with the presence of the fault

The extensional fault zone with Apenninic direction (Fig. 1) was simulated as a vertical prism, completely internal to the model domain, in order both to avoid singularities at the boundaries and to consider the likely ductile behaviour of the rocks from the K_2 horizon down to the model bottom. Therefore, the fault extends from about 7 km depth up to the K-horizon (located at about 4.6 km depth), or even higher (2.2 km depth into the cap rock) in other simulations. The fault is 1 km thick and characterized by a formation permeability ranging from 10 to 100 mDarcy.

The simulation results show how the depth to the top of the fault zone is critical for the development, or absence of the shallow geothermal reservoirs. The thermal gradients away from the fault, and particularly above its top, might be very high, depending upon the permeability contrast between the fault and the country rock (with a very low formation permeability) and upon the depth to the fault bottom. Assuming the fault top at 2.2 km, the computed thermal gradients largely exceed the experimental *T* gradients in the upper 1 km layer, thus indicating that the fault presence and geometry and/or the assumed formation permeability for the fault are not appropriate. Depths to the fault top greater than 4 km produce *T* distributions closer to the measured *T* data.

The upward fluid flow through fractures and the associated heat transfer mechanism are likely more adequate in other areas of the Larderello field, where the fractures network operates at a more localized and dense pattern, to sustain the shallow geothermal reservoirs. The simulation with the fault zone interesting the reservoir rocks only (corresponding to a vertical high permeability zone of 100 mDarcy connecting the two K horizons), computed with the formation permeability as the 500_d model (Table 4), shows the development of several convective cells in the fault zone volume (Fig. 8). The figure shows the fault zone plane, which has a direction sub-parallel to the CROP 18A profile. The velocity vectors of Figs. 6 and 8 have the same scale, allowing the comparison of the velocity field in a homogeneous layer (Fig. 6), with the same field in a fault plane (Fig. 8). In the latter case, the mass and heat transfer from the basement rocks to the top of the reservoir (K-horizon) is substantially enhanced, inducing a higher heat flux through the overlying cap rocks.

The *T* and pressure perturbations in the reservoir, away from the fault, are strongly dependent upon the specific geometry and properties chosen for each simulation. Using for the fault zone a formation permeability of 100 mDarcy and the other parameters as in model 500_d (Table 4), the lateral effects on the *T* field within the reservoir, measured at the RS1 and RS2 target sites, are quite different,

depending upon the lateral distance and permeability contrast between the fault zone and the country rocks. However, the comparison between models with and without the fault shows somehow comparable results. The thermal effects in the cap rock layer, because of the presence of a fault confined below the K-horizon, are significant near the fault top, but they fade away rapidly, because of the low permeability of this layer.

Conclusions

Geological and geophysical data were integrated into a simple 3-D conceptual model, considering heat and mass fluxes from below the K_2 horizon, in order to investigate heat transfer mechanism and the rule of both formation permeability and bottom *T* boundary conditions.

The comparison between observed and computed *T* data was used to highlight the possible variability of the bottom *T* and formation permeability of the two deeper units.

The results indicate the crucial role of the hydraulic resistance contrast within the deeper layers and of the bottom *T* on the upward heat transfer rate.

A few scenarios are coherent with the regional framework:

- predominant thermal convection between K horizons (high *k* with limited over-pressure) and hydraulically resistant bottom layer (models 500_a, 500_c);
- limited thermal convection between K horizons (low *k*, i.e., over-pressure) and high *k* values below (i.e., more efficient mass flux from the lower crust an upper mantle, models: 500_b, 500_d);
- general "cap rock" behaviour of the formations above K-horizon (apart from local heterogeneities, such as the shallow reservoirs).

The simulations results represent almost steady-state conditions and do not consider neither any change with time of the bottom *T* boundary condition, nor any episodic dike/fluid intrusion into the upper crust layers, as it should be expected, considering the available petrologic (Villa and Puxeddu 1994; Gianelli and Laurenzi 2001) and fluid inclusion data (Magro et al. 2003). Not being able to dimension space, time, mass and heat input of these intrusion events, we conceptually simulated the effects of a single fault disturbance in the above-discussed models, as an analogue to the input of extra heat into the model. The reliability of these models is, therefore, qualitative and generally considered valid for the comprehension of heat transfer mechanisms, at regional scale, but it cannot be used for local scale features.

The borehole $T(z)$ data, integrated with hypocentral distribution, fluid inclusions studies, isotope geochemistry and Curie *T* depth suggest a bottom *T* of 500 ± 50°C at about 10 km depth (Dini et al. 2005). The rule of *P-T* conditions in high enthalpy geothermal fields is more critical than the geological framework and inherited structural features, although locally tectonics may be important.

The overall evaluation of the model results suggests as the major source of uncertainty pertains to the poorly constrained parameters of heat input and permeability of the reservoir and basement rocks, such as: the space distribution and age of the dike intrusions, their depth of emplacement, the residence time of magma before eruption and the permeability change with time.

Acknowledgments We are grateful to several colleagues and friends for constructive criticism and discussion. We thank Prof. Izzy Kutasov and an anonymous reviewer for their constructive criticism and precious comments. This work was partly supported by COFIN-MIUR 2006 funding to the first authors.

Appendix 1

The numerical modelling was performed using the commercial code SHEMAT 7.1 (Clauser 2003) considering various boundary conditions, inner geometries and formation permeabilities.

SHEMAT 7.1 code (Clauser 2003) was used to carry out the simulations of coupled heat and fluid fluxes. The solute transport was not simulated, although we assumed a purely speculative average density of the fluid of 1,100 kg m^{-3} (at room *T*). The 3-D regional conductive-convective model was realized by means of unsteady forward simulations, under the assumptions of impervious and isothermal top and bottom boundaries, lateral adiabatic faces and variable internal physical properties.

Solving the non stationary problem consists of finding the *T*, pressure and fluid velocity fields within the model domain, assuming appropriate initial and boundary conditions.

The code SHEMAT was used to simulate both the solid-state heat conduction and the conductive-convective flow of pore fluids. Non-stationary equations of non-isothermal hydrodynamics, accounting for phase transition, were used to carry out the three dimensional modelling of the convective flow. The most important assumptions were:

- flow conforms to Darcy's law;
- effects of the capillary pressure are neglected;
- both phases (solid matrix, liquid) are considered to be in local thermal equilibrium;
- fluid flow does not affect the solid matrix.

The problem is described by a system of mass and energy conservation equations in Cartesian coordinates for

convective two-phase flow through a porous medium (Faust and Mercer 1979):

$$\nabla \cdot \left(\underline{\lambda} \nabla T - \rho_f c_f T \vec{v} \right) = \frac{\partial T}{\partial t} \left[n \rho_f c_f + (1 - n) \rho_m c_m \right] \tag{1}$$

$$\underbrace{\rho_f g (\alpha + n \beta)}_{S_S} \frac{\partial h_0}{\partial t} = \nabla \cdot \left[\underbrace{\frac{\rho_f g \underline{k}}{\mu}}_{\underline{K}} (\nabla h_0 + \rho_r \nabla z) \right] \tag{2}$$

where

α rock compressibility (Pa^{-1});
β fluid compressibility (Pa^{-1});
c specific heat capacity (J kg^{-1} K^{-1});
g gravitational acceleration (m s^{-2});
h hydraulic potential, head (m);
$\underline{\lambda}$ tensor of thermal conductivity (W m^{-1} K^{-1});
$\underline{k}$ tensor of permeability (m^2);
$\underline{K}$ tensor of hydraulic conductivity (m s^{-1});
n porosity (/);
ρ density (kg m^{-3});
S_S specific storage coefficient (m^{-1});
T temperature (K);
t time (s);
$\vec{v}$ Darcy (filtration) velocity; specific discharge (m s^{-1}).

Subscripts

f liquid;
m matrix;
0 reference condition.

SHEMAT assumes the properties of water as a function of fluid pressure and T for pressure greater than saturation pressure or T lower than critical T, limited to pressure and T below 100 MPa and 1,000°C, respectively (Meyer et al. 1979). SHEMAT accounts for the T dependence of rock thermal conductivity according to Zoth and Hänel (1988). Examples of the application of the SHEMAT code may be found in Clauser (2003).

References

Accaino F, Tinivella U, Rossi G, Nicolich R (2005) Geofluid evidence from analysis of deep crustal seismic data (Southern Tuscany, Italy). J Volcanol Geotherm Res 148:46–59

Accaino F, Nicolich R, Tinivella U (2006) Highlighting the crustal structure of the southern Tuscany by reprocessing the CROP 03 profile. Boll Geof Teor Appl 47(3):425–445

Acocella V, Rossetti F (2002) The role of extensional tectonics at different crustal levels on granite ascent and emplacement: an example from Tuscany (Italy). Tectonophysics 354:71–83

Bailey RC (1990) Trapping of aqueous fluids in the deep crust. Geophys Res Lett 17:1129–1132

Baldi P, Bellani S, Ceccarelli A, Fiordelisi A, Squarci P, Taffi L (1995) Geothermal anomalies and structural features of southern Tuscany. In: proc world geothermal congress, Florence, Italy vol 2, pp 693–696

Baldi P, Bertini G, Ceccarelli A (1993) Geothermal fields of central Italy. Res Geol 16:69–81

Barelli A, Bertini G, Buonasorte G, Cappetti G, Fiordelisi A (2000) Recent deep exploration results at the margins of the Larderello-Travale geothermal system. In: proc World Geothermal Congress, Kyushu-Tohoku, Japan, pp 965–970

Barzaghi R, Betti B, Borghi A, Sona G, Tornatore V (2002) The Italian quasi-geoid ITALGEO99. Boll Geodesia Scienze Affini 1:33–51

Batini F, Burgassi PD, Cameli GM, Nicolich R, Squarci P (1978) Contribution to the study of the deep lithospheric profiles: deep reflecting horizons in Larderello-Travale geothermal field. Mem Soc Geol It 19:477–484

Bellani S, Della Vedova B (2004) 2-D thermal modelling across the geothermal fields of Tuscany, Italy. Eos Trans, AGU, 85 (47) Fall Meeting, Abstract T43B–1326

Bellani S, Brogi A, Lazzarotto A, Liotta D, Ranalli G (2004) Heat flow, deep temperatures and extensional structures in the Larderello Geothermal Field (Italy): constraints on geothermal fluid flow. J Volcanol Geotherm Res 132:15–29

Bellani S, Magro G, Brogi A, Lazzarotto A, Liotta D (2005) Insights into the Larderello geothermal field: structural setting and distribution of thermal and ^{3}He anomaly. In: proc World Geothermal Congress, Antalya, Turkey, pp 1–4

Brogi A, Lazzarotto A, Liotta D, Ranalli G (2003) Extensional shear zones as imaged by reflection seismic lines: The Larderello geothermal field (central Italy). Tectonophysics 363:127–139

Brogi A, Lazzarotto A, Liotta D, Ranalli D, CROP–18 Working Group (2005) Crustal structures in the geothermal areas of southern Tuscany (Italy): insights from CROP-18 deep seismic reflections lines. J Volcanol Geotherm Res 148:60–80

Brunet C, Monié P, Jolivet L, Cadet JP (2000) Migration of compression and extension in the Tyrrhenian Sea, insights from 40Ar/39Ar ages on micas along a transect from Corsica to Tuscany. Tectonophysics 321:127–155

Carmignani L, Decandia FA, Fantozzi PL, Lazzarotto A, Liotta D, Meccheri M (1994) Tertiary extensional tectonics in Tuscany (Northern Apennines, Italy). Tectonophysics 238:295–315

Carmignani L, Lazzarotto A, Brogi A, Conti P, Cornamusini G, Costantini A, Meccheri M, Sandrelli P (2004) Carta geologica della Toscana. Regione Toscana, Direzione Generale delle Politiche Territoriali e Ambientali, Servizio Geologico

Clauser C (2003) Numerical simulation of reactive flow in hot aquifers. SHEMAT and Processing SHEMAT. Springer, Berlin, pp 1–333

Decandia FA, Lazzarotto A, Liotta D, Cernobori L, Nicolich R (1998) The Crop 03 traverse: insights on post-collisional evolution of northern Apennines. Mem Soc Geol It 52:427–439

Della Vedova B, Marson I, Panza GF, Suhadolc P (1991) Upper mantle properties of the Tuscan-Tyrrhenian area: a key for understanding the recent tectonic evolution of the Italian region. Tectonophysics 195:311–318

Della Vedova B, Bellani S, Pellis G, Squarci P (2001) Deep temperatures and surface heat flow distribution. In: Vai GB, Martini IP (eds) Anatomy of an orogen: the Apennines and adjacent Mediterranean basins. Kluwer, Dordrecht, pp 65–76

Dini A, Gianelli G, Puxeddu M, Ruggieri G (2005) Origin and evolution of Pliocene-Pleistocene granites from the Larderello geothermal field (Tuscan Magmatic Province, Italy). Lithos 81:1–31

Faust CR, Mercer JW (1979) Geothermal reservoir simulation 1. Mathematical models for liquid and vapor-dominated hydrothermal systems. Water Resour Res 15(1):23–30

Fournier RO (1991) The transition from hydrostatic to greater than hydrostatic fluid pressures in presently active continental hydrothermal systems in crystalline rock. Geophys Res Lett 18:955–958

Ghisetti F, Vezzani L (2002) Normal faulting, transcrustal permeability and seismogenesis in the Apennines (Italy). Tectonophysics 348:155–168

Gianelli G, Laurenzi MA (2001) Age and cooling rate of the geothermal system of Larderello. Geotherm Res Counc Trans 25:731–735

Giese P, Wigger P, Morelli C, Nicolich R (1981) Seismische studien zur bestimmung der krustenstruktur-anomalien der Toskana. Commission European Communities, EUR, pp 1–108

Kennedy BM, Kharaka YK, Evans WC, Ellwood A, DePaolo DJ, Thordsen J, Ambats G, Mariner RH (1997) Mantle fluids in the San Andreas fault system, California. Science 278:1278–1281

Kennedy BM, Van Soest MC (2006) A helium isotope perspective on the Dixie Valley, Nevada hydrothermal system. Geothermics 35–1:26–43

Kühn M, Zeeb C, Gessner K (2006a) 2D or not 2D: are two dimensions enough to accurately model convective fluid flow through faults and surrounding host rocks? In: proc computational methods in water resources—XVI, Copenaghen, Denmark, pp 1–8

Kühn M, Dobert F, Gessner K (2006b) Numerical investigation of the effect of heterogeneous permeability distributions on free convection in the hydrothermal system at Mount Isa, Australia. Earth Planet Sci Lett 244:655–671

Liotta D, Ranalli G (1999) Correlation between seismic reflectivity and rheology in extended lithosphere: Southern Tuscany, inner northern Apennines, Italy. Tectonophysics 315:109–122

Liotta D, Cernobori L, Nicolich R (1998) Restricted rifting and its consistence with compressional structures: Results From Crop-3 Traverse (Northern Apennines, Italy). Terra Nova 10(1):16–20

Locardi E, Nicolich R (2005) Crust-mantle structures and Neogene-Quaternary magmatism in Italy Boll Geof Teor Appl 46(2–3):169–180

Magro G, Ruggieri G, Gianelli G, Bellani S, Scandiffio G (2003) Helium isotopes in paleofluids and present-day fluids of the Larderello geothermal field: constraints on the heat source. J Geophys Res 108-B1:1–12

Marinelli G, Barberi F, Cioni R (1993) Sollevamenti Neogenici ed intrusioni acide della Toscana e del Lazio settentrionale. Mem Soc Geol It 49:279–288

Marson I, Cernobori L, Nicolich R, Stoka M, Liotta D, Palmieri F, Velicogna I (1998) CROP03 profile: a geophysical analysis of data and results. Mem Soc Geol It 52:123–137

Mattei M, Kissel C, Funiciello R (1996) No tectonic rotation of the Tuscan Tyrrhenian margin (Italy) since late Messinian. J Geophys Res 101:2835–2845

Meyer CA, McClintock RB, Silvestri GJ, Spencer RC (1979) ASME steam table—thermodynamic and transport properties of steam. American Society of Mechanical Engineers, New York

Mongelli F, Puxeddu M, Zito G (1989) Anomalie residue del flusso di calore nella fascia tosco-laziale: interpretazione della anomalia di Larderello. In: proc VIII Conference "Gruppo Nazionale Geofisica della Terra Solida", Rome, pp 1147–1170

Nicolich R (1989) Crustal structures from seismic studies in the frame of the European Geotraverse (southern segment) and CROP projects. In: Boriani A, Bonafede M, Piccardo GB, Vai GB (eds). The lithosphere in Italy: advances in earth science research. Accademia Nazionale dei Lincei, Roma pp 41–61

Nicolich R, Marson I (1994) Caratteri geofisici delle strutture crostali nella Provincia Geotermica Toscana. Studi Geologici Camerti 1:163–168

Panza GF, Pontevivo A, Chimera G, Raykova R, Aoudia A (2003) The lithosphere-asthenosphere: Italy and surroundings. Episodes 26:169–174

Pascucci V, Merlini S, Martini IP (1999) Seismic stratigraphy of the Miocene–Pleistocene sedimentary basins of the northern Tyrrhenian sea and western Tuscany (Italy). Basin Res 11:337–356

Piromallo C, Morelli A (1998) P-wave propagation heterogeneity and earthquake location in the Mediterranean region. Geophys J Int 135:232–254

Scrocca D, Doglioni C, Innocenti F, Manetti P, Mazzotti A, Bertelli L, Burbi L, D'Offizi S (eds) (2003) CROP ATLAS—Seismic Reflection Profiles of the Italian Crust. Memorie Descrittive della Carta Geologica d'Italia, vol LXII, Dipartimento Difesa del Suolo, APAT, Roma, pp 1–194

Serri G, Innocenti F, Manetti P (1993) Geochemical and petrological evidence of the subduction and delaminated Adriatic continental lithosphere in the genesis of Neogene–Quaternary magmatism of central Italy. Tectonophysics 223:117–147

Sinigoi S, Quick JE, Peressini G, Mayer A (2003) An example of the Apulian lower crust: the Ivrea-Verbano zone.Transalp conference ext. abs. of oral and poster presentations. Mem Sci Geol 54:101–104

Spakman W (1990) Tomographic images of the upper mantle below central Europe and the Mediterranean. Terra Nova 2:542–553

Straus JM , Schubert G (1977) Thermal convection of water in a porous media: effects of temperature- and pressure-dependent thermodynamics and transport properties. J Geopys Res 82:325–333

Tinivella U, Accaino F, Rossi G, Nicolich R (2005) Petrophysical analysis of CROP-18 crustal seismic data. Boll Soc Geol It 3:205–211

Toulokian YS, Judd WR, Roy RF (eds) (1981) Physical properties of rocks and minerals. MacGrow Hill/CINDAS data series on material properties vol II-2 Purdue Research Foundation, pp 1:549

Vanorio T, De Matteis R, Zollo A, Batini F, Fiordelisi A, Ciulli B (2004) The deep structure of the Larderello-Travale geothermal field from 3D microearthquake traveltime tomography. Geophys Res Lett 31: L07613, DOI: 10.1029/2004GL019432

Velicogna I, Marson I, Suhadolc P (1996) Morfologia della Moho da gravità, topografia ed isostasia. In: proc XIV conference "Gruppo Nazionale Geofisica della Terra Solida" Roma vol 1, pp 405–418

Villa I, Puxeddu M (1994) Geocronology of the Larderello geothermal field: New data and the ''closure temperature'' issue. Contrib Mineral Petrol 115:415–426

Zoth G, Hänel R (1988) Appendix. In: Hänel R, Rybach L, Stegena L (eds) Handbook of terrestrial heat flow density determination. Kluwer, Dordrecht, pp 447–468

Proceedings World Geothermal Congress 2015
Melbourne, Australia, 19-25 April 2015

Simulation of Flow and Heat Transport in a High-Enthalpy Reservoir in Tuscany, Italy

Anozie Ebigbo[1], Jan Niederau[1], Martin Thorwart[2], Marko Riedel[3], Catherine Alexandrakis[3], Gabriele Marquart[1], Renate Pechnig[4], Ivano Dini[5], Ruggero Bertani[5]

[1] Institute for Applied Geophysics and Geothermal Energy, RWTH Aachen University, Aachen, Germany
[2] Department for Applied Geophysics, Institute for Geosciences, Christian-Albrechts-University, Kiel, Germany
[3] Institute of Geophysics and Geoinformatics, TU Bergakademie Freiberg, Freiberg, Germany
[4] Geophysica Beratungsgesellschaft mbH, Aachen, Germany
[5] Enel Green Power, via Andrea Pisano, 120, 56122 Pisa (Italy)

aebigbo@eonerc.rwth-aachen.de

Keywords: reservoir modelling, numerical simulations, uncertainty estimation, OED, exploration guidelines

ABSTRACT

The choice of injection/extraction or exploratory borehole positions and depths in geothermal fields of high enthalpy is a key issue in ensuring the success of the exploitation of such fields. These have to be chosen based on a very limited amount of information, making a proper handling of uncertainties inevitable.

The area of interest in this study spans an area of 22 km × 15 km, encompasses a largely unexploited geothermal field in southern Tuscany, Italy, and is characterized by geothermal gradients of over 100°C/km. Even though a relatively large amount of data from seismic profiles, boreholes, and laboratory measurements is available, the geological model, which comprises two target horizons in fractured metamorphic and sedimentary rocks as well as several faults, suffers from a large amount of uncertainty. For example, rock permeability distribution and fault location/type are crucial for the proper description of advective heat transport.

This work: 1) establishes a realistic reservoir model based on various interpretations of reflection seismic data and petrophysical core and cutting studies; 2) reproduces temperature measurements at various depths in a numerical simulation; 3) determines promising locations for production boreholes within the reservoir.

1. INTRODUCTION

Tuscany can be considered the birthplace of geothermal power generation. Thermal anomalies cause temperature gradients to exceed 100 °C/km locally, reaching maximum values of up to 300 °C/km (Della Vedova, 2008; Romagnoli, 2010). Situated in the hinterland of the northern Apennines, the Mt. Amiata region is an important geothermal resource in Italy. Operating geothermal fields in the region generate around 60 MW of electrical energy (Dini, 2010), exploiting the high heat flow of up to 100 mW/m².

An area (22 km × 15 km) within this region has been chosen by Enel Green Power, Italy for geothermal exploitation. The area is characterized by a high thermal gradient, presumably due to the presence of a young granite pluton at a depth ranging between about 4.5 km and 6 km. The variations in depth of this heat source cause strong differences in thermal gradient within the area. Fluid flow through the heterogeneously fractured sedimentary and metamorphic rocks further complicates and distorts the distribution of temperature. Such heterogeneity heavily influences the productivity and longevity of geothermal production installations, making the right positioning of boreholes crucial. With limited geophysical data, a high degree of uncertainty makes the choice of borehole positions difficult. Flow and heat-transport simulations, as presented in this study, can make a significant contribution at reducing uncertainty and improving the understanding of dominant processes and mechanisms.

The study presented here is part of the work program of the interdisciplinary MeProRisk ("Novel Methods for Exploration, Development, and Exploitation of Geothermal Reservoirs - a Toolbox for Prognosis and Risk Assessment") group and has been performed in a collaborative way involving working groups from universities and commercial firms. The MeProRisk approach combines interpretations of geological and geophysical field and borehole log data, with laboratory data and hydrothermal numerical simulations. In a companion paper to the WGC 2015 (Rabbel et al., 2015) the interpretation of seismic and gravity data from the area under investigation is discussed.

2. GEOLOGICAL BACKGROUND

The collision of the African (Adriatic microplate) and European plate gave rise to major fold-and-thrust belts such as the northern Apennines. This orogen consists of various thrust-related lithologies, ranging from marine and continental sediments to metamorphites. Compression due to continent-plate collision gave rise to an eastward stacking of these tectonic units (Brogi, 2008b). They comprise: a) Quaternary and Neogene sediments, accumulated in young graben systems and unconformably overlying pre-Neogene units; b) Ligurian and Subligurian units, which consist of remnants of the oceanic crust and its marine to pelagic sedimentary cover; c) Tuscan Nappe units, represented by continental margin deposits (Triassic to Miocene) of the Adria paleomargin, comprising basal evaporites, overlain by carbonate and pelagic-turbiditic successions (Batini et al, 2003; Brogi 2008a and references therein). The compressional regime transitioned into an extensional stress regime, as is indicated by two generations of normal faults (low- and high-angle normal faults) throughout the inner zone of the northern Apennines. The units in the area under consideration in this work, which is in southern Tuscany, are situated in this inner zone and, hence, affected by these tectonic phases, i.e. compression followed by extension.

Integrated studies in the inner zone of the northern Apennines yielded the hypothesis that, during the extensional phase, the Tuscan Nappe units were affected by mega-boudinage (e.g. Brogi, 2006, 2008b); see Fig. 1. The resulting mega-boudins (also called

extensional horses) are "isolated" patches of Tuscan Nappe successions separated from other strata by low-angle normal faults (LANFs), whereas high-angle normal and transtensional faults reflect the youngest stage of extension and displace previously developed structures (Brogi, 2008c). While this hypothesis explains geologic field data, it primarily considers the sedimentary complex above a detachment horizon. During deformation, shear strain was accumulated in incompetent units, e.g. the basal evaporitic layer of the Tuscan Nappes: the Burano formation. It served as a detachment during the tectonic evolution of the target area and separates the upper sedimentary complex from the deeper Tuscan metamorphic complex. During the compressional tectonic setting, units belonging to the metamorphic complex were affected by high-pressure/low-temperature (HP/LT) metamorphism. The metamorphic complex consists of the Monticiano-Roccastrada unit (MRU) which is usually divided into three sub-units (MRU1–3). From top to bottom, these are: The Verrucano unit (MRU1, Triassic), comprising metasandstones and metaconglomerates; a phyllite succession (MRU2, Carboniferous), which consists of graphitic phyllites and metasandstones; a micashist group (MRU3). The MRU1 as well as a deeper gneiss complex known from other geothermal areas in Tuscany are not encountered in boreholes close to the study area, but found as xenoliths in Quaternary lavas in the area (van Bergen, 1983).

As deformation affected both sedimentary cover and metamorphic complex (Fig. 1), the occurrence of duplex structures and thrust-related repetitions of units do also occur in the metamorphic units, e.g. the MRU2 units (Brogi, 2008b). Brogi (2008) considers deformation in the metamorphic complex and its lateral segmentation during the extensional phases as connected to a migration of the brittle-ductile transition to greater depths.

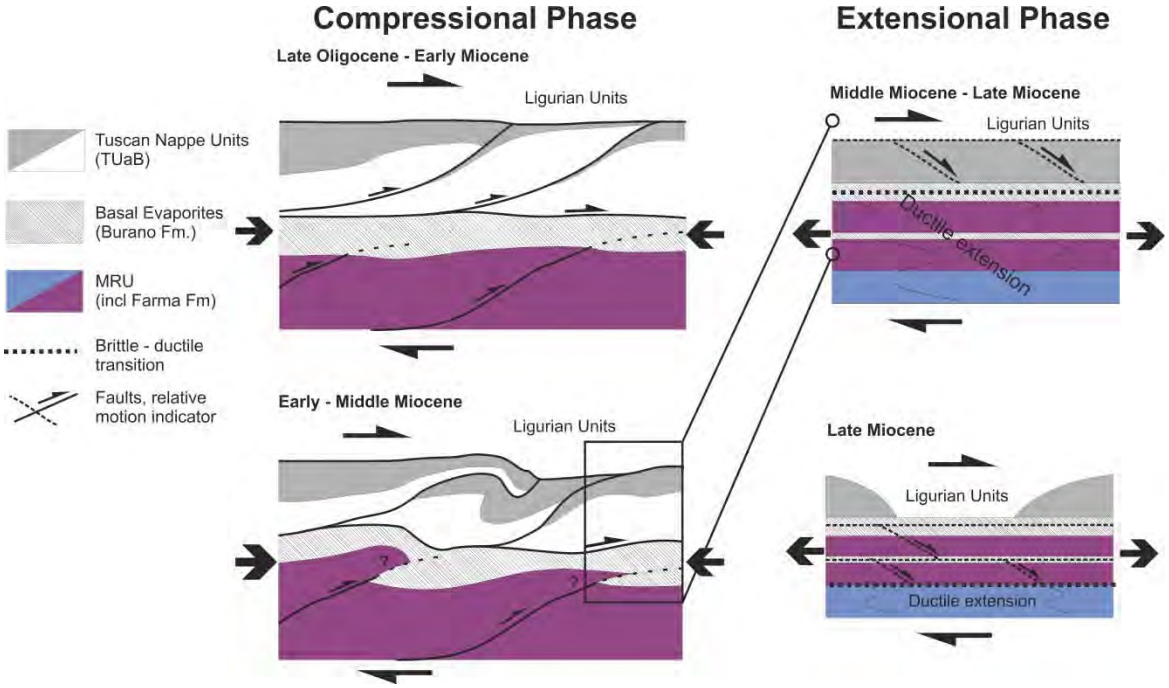

Figure 1: Schematic illustration of the possible evolution of compressional and extensional structures which affected the sedimentary and metamorphic complexes. During the compressional stage, eastward stacking of Ligurian units onto the Tuscan Nappe units and MRU occurred with a contemporaneous development of duplex structures. During middle to late Miocene, the stress regime transitioned from compressive to primarily tensile, causing the segmentation of units by step-wise low angle normal faults above the brittle-ductile transition and ductile extension beneath it (modified from Brogi, 2006; 2008b).

Accepting the described mega-boudinage of the Tuscan Nappe units of the sedimentary complex, several implications for the structural interpretation of the subsurface of our study area can be deduced:

1) During the compressional tectonic setting, an eastward stacking of the sedimentary units (Ligurian down to Tuscan Nappe units) is contemporaneous to eastward thrusting and the generation of duplex structures within the Monticiano-Roccastrada units (Brogi, 2008b; Carmignani et al., 2001, and references therein).

2) Shear strain was concentrated in more plastic layers, resulting in detachment horizons such as the phyllite succession in the MRU or the basal evaporites of the Tuscan Nappe units (Burano Formation). As a consequence, the Burano formation and MRU3/MRU2 formed repeating sequences with more competent units. Alternation of Burano formation and Phyllite sequences was found in some deep boreholes outside the sudy area.

3) During the extensional tectonic setting, lateral segmentation of the sedimentary cover by means of boudinage and the development of LANFs led to the generation of extensional horses, i.e. isolated patches of Tuscan Nappe units. Ligurian units fill the arising accumulation space by segmentation.

4) Segmentation of the sedimentary complex predates segmentation of the metamorphic complex and connected crustal thinning due to migration of the brittle-ductile transition to greater depths. As a consequence, it is assumed that extension in the MRU

transitioned from ductile extension to an extensional duplex system (Brogi 2008b), i.e. the duplex structures formed during compression are separated by LANFs during subsequent extension.

5) Due to high strain rates, the lateral thickness of the Burano formation is highly variable.

In our structural model, those key features are represented by: (1) stacking of the Burano formation (basal evaporites) and palaeozoic phyllites (referred to as the Farma formation) deduced from seismic interpretation; (2) Modeling the Tuscan units above Burano (TUaB) as extensional horses, i.e. mega-boudins bound by LANFs; (3) Implementation of high-angle normal faults as structural elements, displacing older strata.

The structural model (Fig. 2) was developed using an implicit modeling approach (Lajaunie, 1997) implemented in the software 3D GeoModeller. Structural interpretation of five seismic sections in the study area and geological data from the surface constitute the main sources of input data for our geometrical model. Three strong reflectors in the seismic sections were attributed to the tops of the Burano formation and the K horizon. This horizon (Fig. 2) is a prominent feature in geothermal areas in Tuscany, whose nature is still a major point of discussion (reflector of the top of recent granitoid intrusion, shear zone at the top of the brittle-ductile transition, or a horizon/part of carapace penetrated by supercritical fluids) (Batini, 2003; Bertani, 2005; Bertini 2006; Romagnoli, 2010)..Even though the nature of the K horizon is not clear, experience from operating geothermal fields (e.g. Larderello and Travale) suggest that the K horizon corresponds to an isotherm of between 400 °C and 450 °C. This is a crucial assumption for our numerical model.

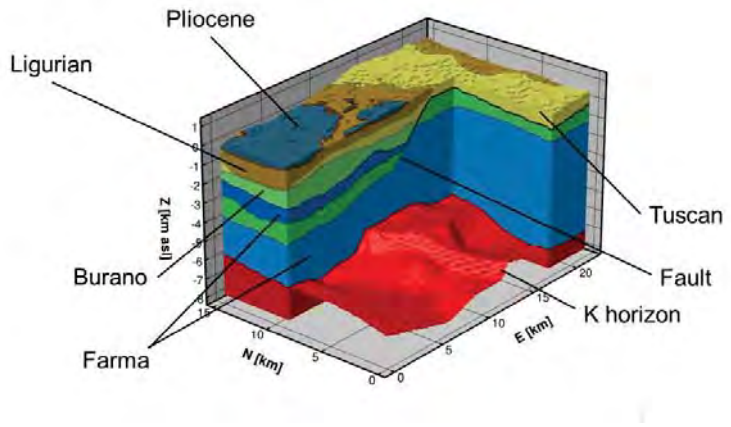

Figure 2: Geological model of the area of interest. Ligurian units fill accumulation space between separated patches of the Tuscan Nappe unit. Since there are no clear demarcations in seismic sections, the MRU was not divided into its subgroups and will henceforth be referred to as the Farma formation. Stacking of the MRU and Burano formations is inferred in the western side of the model.

In addition to the five seismic sections, accessible input data for our models comprise:

- A gravity survey over the whole model area;
- Magnetotelluric measurements;
- Temperature data and geophysical logs from 3 boreholes;
- Core and cutting material for laboratory measurements on thermal conductivity, density, and matrix porosity (only on core).

This integrated database not only provides the geometric input for the structural model, but also the possibility of calibration and the definition of rock properties which are assigned to the corresponding units in the numerical model (Table 1).

3. HYDROTHERMAL SIMULATIONS

The structural model shown in Fig. 2, of dimensions 22 km × 15 km × 9 km in *E* (East), *N* (North), and *z* (depth) directions, respectively, has been discretized in a hexagonal grid with block is of dimension 250 m × 250 m × 100 m. Based on this model we performed flow and transport simulation with the code SHEMAT-Suite, a simulator based on the finite-difference scheme and capable of modeling steady-state and transient hydro-geothermal reservoirs.

Two coupled equations (flow, Eq. (1), and heat transport, Eq. (2)) are solved iteratively in steady state to obtain hydraulic head h [m] and temperature T [°C].

$$\nabla \cdot \left[\frac{\rho_w g \mathbf{K}}{\mu_w} \left(\nabla h + \rho_r \nabla z \right) \right] = 0 \tag{1}$$

Here, **K** is permeability [m²], h is the hydraulic head [m], z is the vertical coordinate in space [m] (positive upward), ρ_w is water density [kg/m³], μ_w is the dynamic viscosity of water [kg/(m s)], g is gravity [m/s²] and $\rho_r = (\rho_W - \rho_0)/\rho_0$ accounts for the difference between water density and a reference density (at atmospheric conditions).

$$\nabla \cdot \left(\rho_{\mathrm{w}} h_{\mathrm{w}} \mathbf{v} - \lambda_{\mathrm{e}} \nabla T \right) = H \tag{2}$$

where h_w is the specific enthalpy of the fluid [J/(m³ K)], **v** is the Darcy flux [m/s], λ_e is the tensor of effective thermal conductivity [W/(m K)] and H the radiogenic heat production [W/m³]. The simulator comprises several constitutive relationships which relate fluid and rock properties to temperature and pressure. In particular, the physical properties of supercritical water (i.e. density, enthalpy, viscosity, and thermal conductivity) are calculated using the correlations provided by the International Association for the Properties of Water and Steam (Wagner, et al., 2000). It should be noted that the physical conditions that prevail in the reservoir do not allow for the existence of two-phase (water/steam) conditions. For further information on the simulator SHEMAT-Suite, see Rath, et al. (2006).

Table 1 lists rock properties of the various geological units in the simulation model. These properties are obtained from a petrophysical analysis of rock cores and cuttings from boreholes in the area and well-logging data. The values highlighted in grey are estimated from literature, whereas those in bold face are adjusted to fit the available borehole temperature data. Note that thermal conductivity decreases with temperature (Zoth & Haenel, 1988). Rock permeability is primarily caused by fractures which have been assumed to lead to an isotropic, depth-dependent permeability (Manning & Ingebritsen, 1999); the dependence on depth being as a result of fracture sealing due to the overburden. Hence, the permeability K is expressed as an exponential function of overburden thickness z_b, a maximum permeability K_0, and a scaling factor d.

$$K = K_0 e^{-z_b / d} \tag{3}$$

The value of the scaling factor is unknown. It has, in combination with the maximum permeability, been fit to the temperature measurements as 1000 m. However, since very little information is available on the values of K_0 and d, a large amount of uncertainty persists in the model, making a detailed study of the influence of these parameters on uncertainty essential in future work.

Table 1: Simulation parameters

Parameter/property	Farma	Burano	TUaB[c]	Ligurian	Pliocene
Matrix thermal conductivity [W/(m K)][a]	4.10	4.73	4.10	2.54	1.30
Heat production rate [μW/m^3]	1.42	0.16	0.32	0.14	0.14
Porosity	0.03	0.02	0.10	0.1	0.1
Permeability [10^{-15} m^2][b]	**0.60**	**10.0**	**1.00**	0.1	0.1

[a] Value at surface. Thermal conductivity is decreases with temperature.
[b] Maximum value for given unit within domain. Permeability is depth-dependent.
[c] TUaB: Tuscan units above Burano.

3.1 Boundary Conditions

At the top of the domain, i.e. at the land surface, the temperature is dependent on air temperature, and thus topography. The values are determined using a set of shallow-well temperature measurements with temperatures ranging from 22 °C to 41 °C at depths between 147 m and 200 m below the ground surface. The hydraulic head at the land surface is set to be equal to the elevation of the land surface (topography).

As mentioned in Section 2, the K horizon is assumed to represent a 450 °C temperature isotherm, thus providing a boundary condition at the bottom of the domain. There is no flow across the K horizon.

In order to obtain lateral boundary conditions for temperature, a steady-state simulation is run with no-flow lateral boundaries (top and bottom boundaries are as described above), producing a temperature distribution which accounts for conductive and convective heat flow. The results of this simulation are stored and used as the lateral boundary conditions for temperature. The hydraulic head at the lateral boundaries are chosen to be equal to the land-surface elevation.

3.2 Simulation Results

The steady-state temperature distribution in the model domain in Fig. 3 depicts the general conductive flow of heat from the 450 °C isotherm at the K horizon to the surface and the deviation thereof as a result of advective heat transport due to the regional groundwater flow and free convection. As such, the distribution of temperature is primarily influenced by the depth of the K horizon in that area and the direction and magnitude of fluid velocities.

Lateral flow through the domain occurs mainly in the Burano formation due to their relatively high permeability. The general direction of flow is from NE to SSW. This can be seen in Fig. 4 which depicts the Darcy flow at a depth 1 km below sea level.

A comparison of simulation results with available borehole measurements (exclusively in the eastern part of the domain) shows a good fit at depths down to approximately 1.5 km below msl (see Fig. 5). The change in temperature gradient with depth in Borehole°2 (of Fig. 5), which occurs in the highly permeable Burano formation, is also represented. At greater depths, temperatures are underestimated. This is most probably due to the presence of a zone or zones of increased permeability (due to an increased

fracture density) in the Farma formation which, for lack of adequate data, has not been incorporated in the model yet. The temperature distribution particularly in Borehole 2 shows an area with a steeper temperature gradient which could be due to increased convection in that area. A reinterpretation of seismic profiles in which one correlates areas of high reflectivity with high fracture density could help account for this phenomenon in the model.

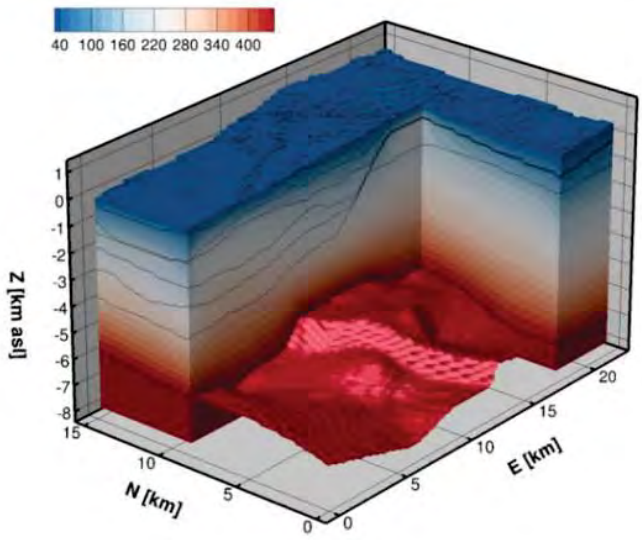

Figure 3: Steady-state temperature distribution in °C in the simulation domain. The K horizon is shown as an isosurface near the bottom.

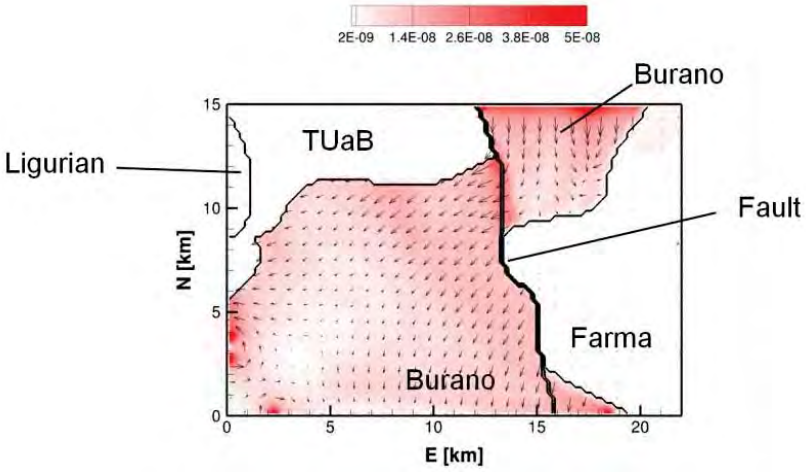

Figure 4: Magnitude (in color) and direction (arrows) of the Darcy-flow vector 1 km below mean sea level (in m/s). Due to the permeabilities of the units, flow occurs mainly within the Burano formation.

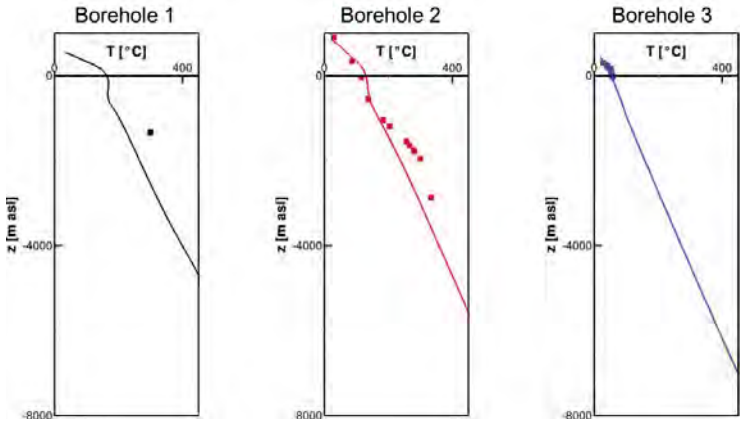

Figure 5: Comparison of temperature profiles from simulation (lines) with borehole measurements (symbols).

3.3 Discussion of Results

These steady-state simulations provide a useful tool with which one can study the thermal regime and identify promising areas for geothermal production. In Fig. 6, 250 °C and 200 °C isotherms within the model domain are shown and overlaid with a permeability color map. The highest temperatures are achieved where the heat source (K horizon) is shallowest, i.e. in the northeast and where the strata of permeable rocks are thickest, i.e. in the northwestern part. A thick geothermal reservoir (in this case composed of the Tuscan units – Burano and TUaB) produce larger amounts of convection, transporting hot water to shallower regions. Hence, further exploration and/or exploitation of the reservoir would most likely be successful in the northern part of the reservoir. That notwithstanding, there are several sources of uncertainty, the adequate quantification of which is a prerequisite for accurate predictions regarding the selection of suitable sites for geothermal exploitation. Uncertainties stem mainly from the lack of precise information with respect to rock-permeability distribution as well as location and shape of the heat source. Further, the geological interpretation of seismic profiles and logging data from boreholes to obtain a geological model (e.g., as shown in Fig. 2) leaves room for different interpretation. Some of the choices in interpretation of geophysical data may have significant consequences for the flow and heat-transport processes and ultimately on the simulation results.

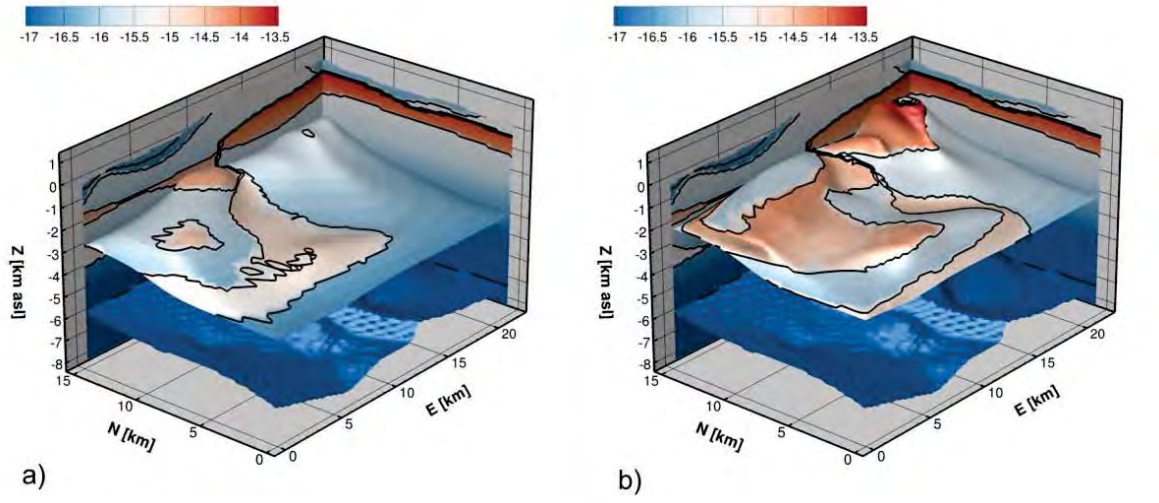

Figure 6: 250 °C (a) and 200 °C (b) isothermal surface. Logarithm of permeability (in m²) is shown in color. Black lines demarcate rock unit boundaries.

4. CONCLUSIONS

The largely unexploited, high-enthalpy geothermal reservoir in southern Tuscany presented here is characterized by relatively large variations in temperature gradients presumably due to the varying shape and depth of the young granitic intrusion (heat source) and the heterogeneous flow field. A successful geothermal exploitation relies on the proper choice of borehole positions. Due to the limited amount of geophysical data, a high degree of uncertainty makes this a difficult task. Flow and heat-transport simulations help in understanding dominant processes and in the handling of uncertainty.

A realistic reservoir model based on interpretations of reflection seismic data and petrophyscial core and cutting measurements is established and is the basis of the simulation model. It comprises a metamorphic basement and basal evaporites overlain by Tuscan Nappe and Ligurian units. The simulation model reproduces temperature measurements at various depths. The temperature distribution predicted in the simulations provides crucial information on rock strata of high permability and fluid flow direction, and on locations where high temperature gradients can be expected at shallow depths. Considering the model results the most appropriate region for geothermal exploitation is in the northern part of the study area.

The temperature data hints at possible zones of high permeability within the metamorphic basement not captured by the simulation model. A reinterpretation of seismic reflection data with the aim of identifying areas of high fracture density could aid in accounting for such zones.

The handling of uncertainty as introduced, e.g. by interpretation of geophysical data or heterogeneous parameter distributions (particularly permeability and thermal conductivity) will be tackled by the use of various stochastic approaches such as inverse modeling, Monte Carlo simulations, and the application of the “optimal-experimental-design” approach.

ACKNOWLEDGEMENT

This study is part of the MeProRisk-II project and is funded by the Federal Ministry of Environment (BMU) under the grant 0325389.

REFERENCES

Batini, F., Brogi, A., Lazzarotto, A., Liotta, D., and Pandeli, E. : Geological features of Larderello-Travale and Mt. Amiata geothermal areas (southern Tuscany, Italy). *Episodes*, *26*(3), (2003), 239-244.

Bertani, R., Bertini, G., Cappetti, G., Fiordelisi, A., and Marocco, B. M.: An update of the Larderello-Travale/Radicondoli deep geothermal system. In *Proceedings* (2005), pp. 24-29.

Bertini, G., Casini, M., Gianelli, G., and Pandeli, E.: Geological structure of a long-living geothermal system, Larderello, Italy. *Terra Nova*, *18*(3), (2006), 163-169.

Brogi, A.: Neogene extension in the Northern Apennines (Italy): insights from the southern part of the Mt. Amiata geothermal area. *Geodinamica Acta*, *19*(1), (2006), 33-50.

Brogi, A.:The Triassic and Palaeozoic successions drilled in the Bagnore geothermal field and Poggio Nibbio area (Monte Amiata, Northern Apennines, Italy). *Bollettino Società Geologica Italiana*, *3*, (2008a), 599-613.

Brogi, A.: Kinematics and geometry of Miocene low-angle detachments and exhumation of the metamorphic units in the hinterland of the Northern Apennines (Italy). *Journal of Structural Geology*, *30*(1), 2-20 (2008b).

Brogi, A.: The structure of the Monte Amiata volcano-geothermal area (Northern Apennines, Italy): Neogene-Quaternary compression versus extension. *International Journal of Earth Sciences*, *97*(4), (2008c), 677-703.

Carmignani, L., Decandia, F. A., Disperati, L., Fantozzi, P. L., Kligfield, R., Lazzarotto, A., Liotta, D., and Meccheri, M. : Inner Northern Apennines. In *anatomy of an Orogen: the Apennines and adjacent Mediterranean Basins*, (pp. 197-213). Springer Netherlands (2001).

Della Vedova, B., Vecellio, C., Bellani, S., and Tinivella, U.: Thermal modelling of the Larderello geothermal field (Tuscany, Italy). *International Journal of Earth Sciences*, *97*(2), (2008), 317-332.

Lajaunie, C., Courrioux, G., & Manuel, L.: Foliation fields and 3D cartography in geology: principles of a method based on potential interpolation. *Mathematical Geology*, *29*(4), (1997), 571-584.

Rabbel, W., Thorwart, M., Behrendt, R., Holzrichter, N., Niederau, J., Ebigbo, A., Marquart, G., Dini, I., and Ciuffi, S.:A Stochastic Assessment of Geothermal Potential Based on Seismic and Potential Field Analysis and Hydro-thermal Forward Modeling – an Example from Tuscany (Italy), Proceedings World Geothermal Congress 2015 Melbourne, Australia, 19-25 April 2015.

Rath, V., Wolf, A., and Bücker, M.: Joint three-dimensional inversion of coupled groundwater flow and heat transfer based on automatic differentiation: sensitivity calculation, verficiation, and synthetic examples. *Geophysical Journal International, 167*, (2006), pp. 453-466.

Romagnoli, P., Arias, A., Barelli, A., Cei, M., and Casini, M.: An updated numerical model of the Larderello–Travale geothermal system, Italy. *Geothermics*, *39*(4), (2010), 292-313.

van Bergen, M. J.: Polyphase metamorphic sedimentary xenoliths from Mt. Amiata volcanics (Central Italy); evidence for a partially disrupted contact aureole. *Geologische Rundschau*, *72*(2), (1983), 637-662.

Wagner, W., Cooper, J. R., Dittmann, A., Kijima, J., Kretzschmar, H.-J., Kruse, A., et al.: The IAPWS Industrial Formulation 1997 for the Thermodynamic Properties of Water and Steam. *Journal of Eng. For Gas Turbines and Power, 122*, (2000) pp. 150-182.

Zoth, G., and Haenel, R.: Thermal conductivity. In R. Haenel, L. Rybach, & L. Stegena, *Handbook of terestrial heat-flow density determination.* Norwell, Mass.: Kluwer Acad. (1988).

Wang, C.T., and Horne, R.N.: Boiling Flow in a Horizontal Fracture, *Geothermics*, **29**, 759-772. (1999).

Geothermics 39 (2010) 292–313

Contents lists available at ScienceDirect

Geothermics

journal homepage: www.elsevier.com/locate/geothermics

An updated numerical model of the Larderello–Travale geothermal system, Italy

Paolo Romagnoli, Alessia Arias*, Antonio Barelli, Maurizio Cei, Michele Casini

Enel Green Power S.p.A., Via A. Pisano 120, 56122 Pisa, Italy

ARTICLE INFO

Article history:
Received 10 June 2010
Accepted 13 September 2010
Available online 29 October 2010

Keywords:
Geothermal
Larderello
Travale
Modeling
TOUGH2
Italy

ABSTRACT

Larderello–Travale is one of the few geothermal systems in the world that is characterized by a reservoir pressure much lower than hydrostatic. This is a consequence of its natural evolution from an initial liquid-dominated to the current steam-dominated system. Beneath a nearly impermeable cover, the geothermal reservoir consists of carbonate-anhydrite formations and, at greater depth, by metamorphic rocks. The shallow reservoir has temperatures in the range of 220–250 °C, and pressures of about 20 bar at a depth of 1000 m, while the deep metamorphic reservoir has temperatures of 300–350 °C, and pressures of about 70 bar at a depth of 3000 m. The 3D numerical code "TOUGH2" has been used to conduct a regional modeling study to investigate the production mechanism of superheated steam, the interactions between the geothermal field and the surrounding deep aquifers, and the field sustainability. All the available geoscientific data collected in about one century of exploration and exploitation have been used to provide the necessary input parameters for the model, which covers an area (4900 km^2) about 10 times wider than the Larderello–Travale geothermal field (400 km^2). The numerical model explains the origin of the steam extracted in about one century of exploitation and shows that, at the current level, the production is sustainable at least for the next 100 years.

1. Introduction

The generation of electricity from geothermal resources in Italy started at the beginning of the 20th century in the Larderello and Travale geothermal fields (Barelli et al., 1995a,c, 2000; Batini et al., 2003) with the exploitation of a shallow reservoir at a depth of 500–1500 m which consists of carbonate-anhydrite formations of Mesozoic age. Since the mid-1980s, drilling technology improvements enabled geothermal fluid production from a deeper reservoir, which is hosted in metamorphic rocks at depths greater than 3000 m.

Pressure, temperature, and composition of the geothermal fluids are almost constant over the exploited area, supporting the hypothesis of a single, very large fractured geothermal system (Bertini et al., 2006). The deep Larderello–Travale reservoir has temperatures in the range of 300–350 °C and pressures of 40–70 bar. It is one of the few examples of superheated steam system on earth with about 50 °C of superheating (Bertani, 2005). At present, the installed capacity in the entire Larderello–Travale geothermal area is 722 MWe, that is 89% of the total (810.5 MWe) installed capacity in Italy (Cappetti et al., 2010).

To forecast the future evolution of the field and its production sustainability, a numerical modeling effort has been carried out covering an area of 70 km × 70 km (Fig. 1). This large areal extent requires the availability of a large amount of data to determine the various system parameters. The poor quality of available information particularly for the shallow aquifers, a varied field exploitation history, and complexities arising from anisotropic distribution of permeability, make the numerical modeling of the Larderello–Travale geothermal system an extremely difficult task. Further challenges arise in explaining how a superheated and depressurized geothermal system, with negligible recharge from local meteoric waters could produce such an enormous amount of steam.

To develop a detailed model of the Larderello–Travale system, all the geoscientific data collected up to the end of 2009, were considered and analyzed (Arias et al., 2010). In this way, reliable input parameters were generated for the numerical model with the goal of producing a macro-description of the geothermal system (Barelli et al., 2010). The final objective of the model is the evaluation of the possible interactions between the geothermal field, during its exploitation, and the hydrologic basins in the area.

For this reason, the numerical model must take into account both the geothermal system and the regional hydrology. Although the producing area is only 400 km^2, an area of 4900 km^2 was chosen for the simulation to include both the geothermal system and the surrounding aquifers.

* Corresponding author at: Enel Green Power S.p.A., Renewable Energies Division, Via A. Pisano 120, 56122 Pisa, Italy. Tel.: +39 050 6185866; fax: +39 050 6185504.
E-mail address: alessia.arias@enel.com (A. Arias).

0375-6505/$ – see front matter © 2010 Elsevier Ltd. All rights reserved.
doi:10.1016/j.geothermics.2010.09.010

Nomenclature

G_D	steam discharge from deep circulation (t/h)
G_L	steam discharge from local recharge (t/h)
G_T	total rate of steam discharge (t/h)
A	gas/steam ratio in the total discharge
B	gas/steam ratio in the fluid of deep origin
V_{steam}	available volume for the steam storage (m^3)
V_{res}	reservoir volume (m^3)
M_{steam}	steam mass (t)

Greek symbols

ϕ	reservoir porosity
$\rho_{(T;P)}$	steam density (kg/m^3)

2. Historical field exploration

Exploration and exploitation of the Larderello field started at the beginning of the 20th century, and were later extended to the Travale field in the 1950s. Initial drilling work in both fields only reached a shallow carbonate-anhydrite reservoir. But a deep exploration program, that was carried out in Larderello during the 1980s and in Travale in the 1990s, found an exploitable steam-dominated system in the metamorphic basement at a depth of about 2.5–4 km. Data from the deep reservoir revealed that Larderello and Travale fields belong to the same geothermal system (Fig. 2). At present, the total steam production from the Larderello–Travale geothermal system is over 4700 t/h.

2.1. Larderello field

The first well was drilled in Larderello in 1926, tapping the shallow carbonate formations (Barelli et al., 2000; Batini et al., 2003). Between 1926 and 1940, 136 wells were drilled over an area of 4 km^2 with a high success rate of 82%. In the following 10 years, the exploitation area was doubled with another 69 wells. All these wells tapped the carbonate reservoir with a maximum pressure of 32 bar and a temperature of 220–230 °C (Bertani et al., 2005). From the 1950s to 1980s, the drilled area was further extended to about 100 km^2.

The boundaries of the shallow reservoir were reached by exploitation in the 1970s, and two innovative strategies were successfully developed to sustain production namely, injection of condensate from geothermal power plants, and steam extraction from new deep productive horizons.

Injection started in 1979 as an experimental strategy in the central part of the Larderello field ("Valle Secolo") which was considered the most favorable area in terms of reservoir permeability and superheated conditions (Barelli et al., 1995b; Cappetti et al., 1995). As a consequence of the re-evaporation of injected water, steam production increased in the "Valle Secolo" area, reaching a steady production level of about 1500 t/h. Furthermore, the gas/steam ratio decreased, improving the power plant specific consumption (i.e., steam requirements per MW), and the reservoir pressure was recovered without any substantial temperature change in the produced fluid (Barelli et al., 1995b). Currently, more than 1500 t/h of water are injected into the Larderello system.

In the early 1980s, a deep exploration program began with wells reaching some 3500 m which encountered productive layers in the metamorphic basement. This reservoir contained superheated steam with an average pressure of 40 bar and temperature of 300–350 °C (Barelli et al., 1995c). As a result of injection, and expansion of the drilled area both vertically and laterally, fluid production increased in the Larderello field and is now about 3700 t/h.

2.2. Travale field

The geothermal exploitation of the Travale field began in the early 1950s, when 20 wells were drilled near the natural manifestations to a depth of a few hundred meters and penetrated a water-dominated Mesozoic carbonate reservoir that is different from that in the Larderello area (Barelli et al., 1995a; Batini et al., 2003). Production caused the surface manifestations to disappear and triggered the inflow of meteoric water that quickly flooded the wells.

In the 1970s, the exploration was extended northward, targeting a deeper and hotter reservoir, named "Horst". Permeable rocks were encountered at a depth of 500–1000 m in the Mesozoic carbonate formation (see above) with a pressure of 60 bar and a temperature of 280 °C (Barelli et al., 1995a). This reservoir hosts a saturated steam-dominated system that is in pressure equilibrium with the previously discovered water-dominated one.

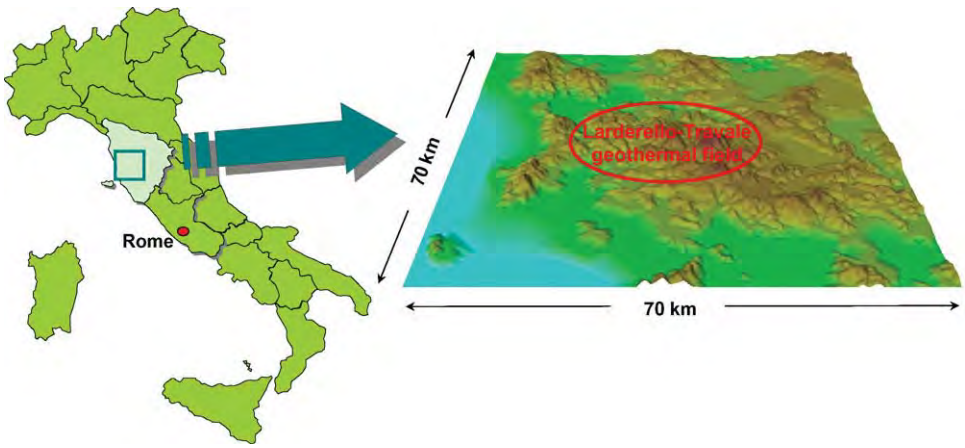

Fig. 1. Location of the 70 km × 70 km numerical modeling area (Tuscany Region, Italy).

At the beginning of the 1980s, production was extended deeper (1300–2000 m) and northward in the same 60 bar "Horst" reservoir that, in this case, is named "Graben" (Barelli et al., 1995a). A continuous flow-rate decline without substantial changes in the steam quality and gas content was observed as a result of the exploitation of this deeper layer.

After 1992, about 30 deep wells were drilled up to depths of 4000 m in a wider area to investigate a deeper reservoir hosted in the metamorphic basement and in the granite intrusions. This reservoir contained superheated steam in vapor-static equilibrium with all the previously discovered shallower reservoirs (Barelli et al., 1995c), had a temperature of about 300–350 °C and had an initial pressure of 70 bar. The success of the deep exploration program increased the steam production up to 1000 t/h. An injection strategy has not been adopted for the Travale area because of its high pressure (50–60 bar).

3. Geologic outline

Extensive geologic data from the 4900 km^2 area chosen for the Larderello–Travale numerical simulation have been collected, reanalyzed, and interpreted. In the following, the stratigraphic-structural setting, the hydrogeologic, and the physical characteristics of the area are described with particular attention to the outlines of the geothermal system. An evaluation of the local recharge of the system is also presented.

3.1. Stratigraphic-structural setting

The present-day geologic setting is the result of compressive and extensional geodynamic processes that began 30 Ma ago (Oligocene) with the Alpine-Apennine orogenesis (Carminati and Doglioni, 2004). From Lower Miocene, the extensional tectonic regime resulted in the formation of NW–SE tectonic basins, crustal thinning with consequent upwelling of magma bodies and increased heat flow. The geothermal gradient in the Larderello–Travale system is greater than 100 °C/km and reaches maximum values of 300 °C/km (Baldi et al., 1995).

The most recent outcrops correspond to the Quaternary marine and continental deposits on the coastal plain and in the alluvial valley, while the oldest ones are represented by the metamorphic rocks of the Paleozoic Basement (Bertini et al., 2006). The presence of travertine beds and volcanic rocks is suggestive of hydrothermal circulation, and recent magmatic activity, likely connected to the geothermal phenomena. The main and most widespread outcrops in the Larderello–Travale area are:

- *Neoautochthonous complex*: Clays, with minor sands, conglomerates and detrital limestones;
- *Ligurian/sub-Ligurian complex*: Jurassic-Eocene clayey-marly units in flysch facies; and
- *Tuscan Nappe complex*: Triassic-Lower Miocene arenaceous and clayey-marly formations, calcareous-siliceous rocks, dolostone and anhydrites.

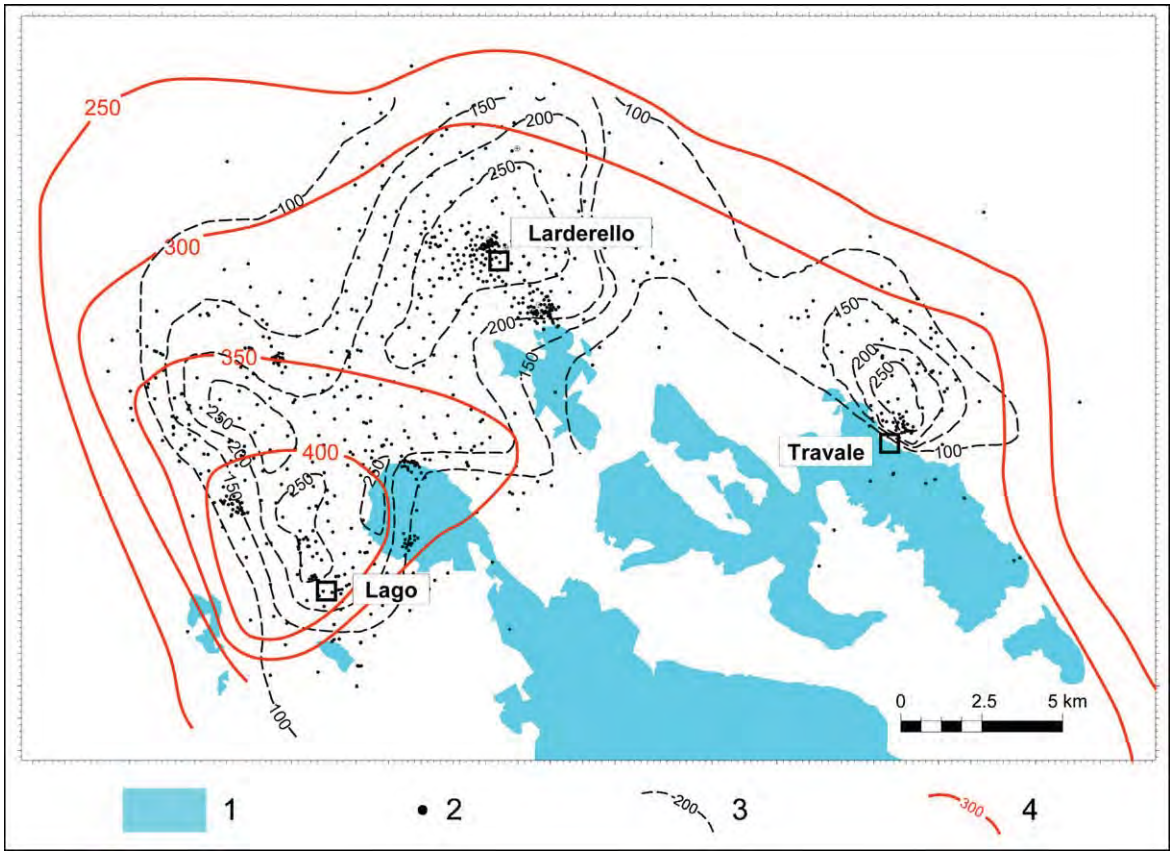

Fig. 2. Temperature distribution in the Larderello–Travale geothermal field. (1) Outcrops of permeable formations; (2) geothermal wells; (3) temperature at the top of the shallow reservoir; (4) temperature at 3000 m b.s.l. Figure modified from Cappetti et al. (2005).

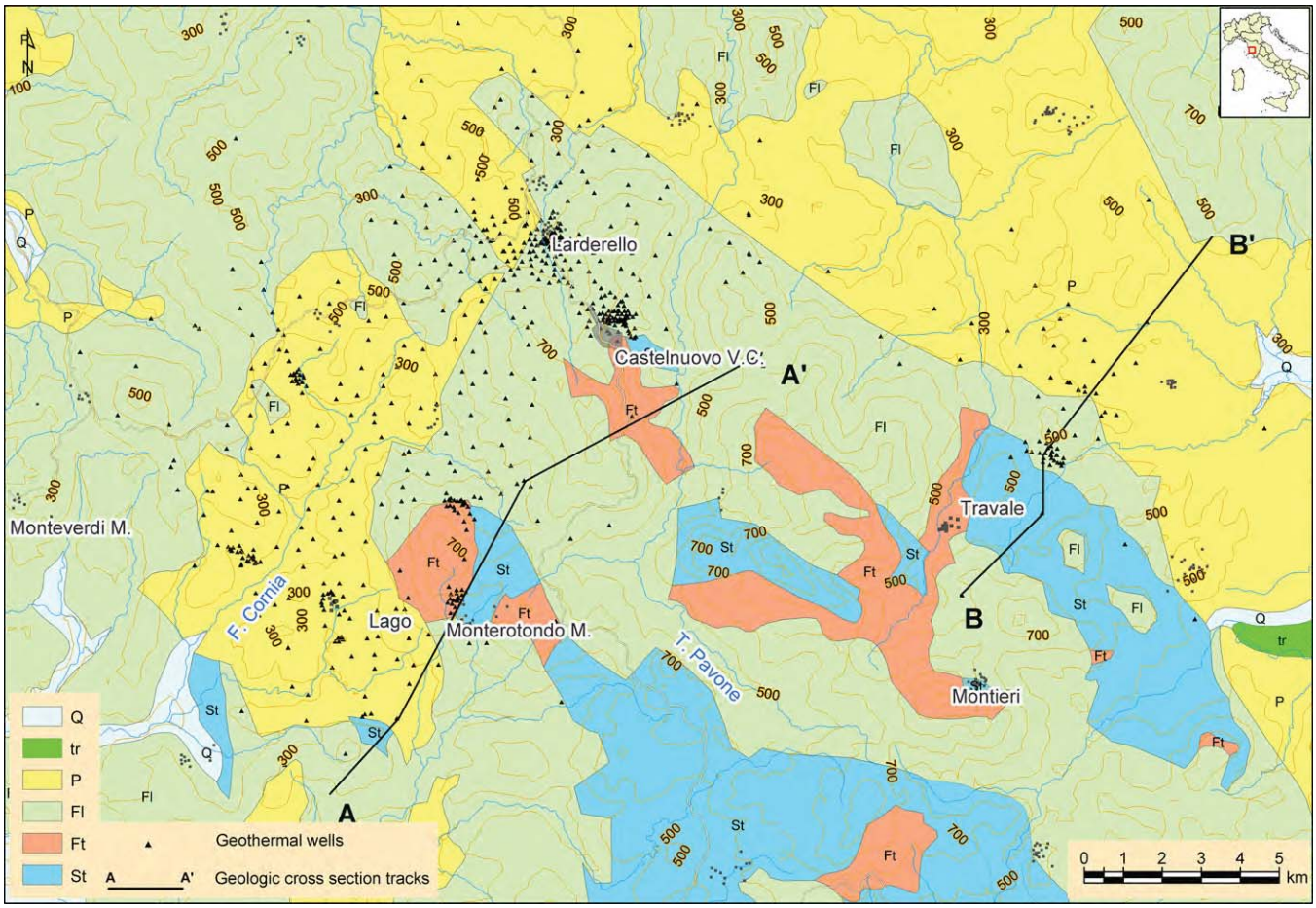

Fig. 3. Schematic geology of the Larderello–Travale geothermal area simplified from Giannini et al. (1971). Q: Quaternary deposits; tr: Plio-Quaternary Travertines; P: Neoautochthonous terrigenous deposits (Lower Pliocene–Upper Miocene); Fl: Ligurian and sub-Ligurian Flysch complex (Jurassic – Eocene); Ft: terrigenous formations of Tuscan Units (Upper Cretaceous–Lower Miocene); St: mainly carbonate formations of Tuscan Units (Upper Trias – Malm).

A reconstruction of the geological setting at depth (Figs. 3 and 4) has been carried out using data from deep wells and geophysical surveys (Bertini et al., 2006).

3.2. Hydrogeologic outline

Larderello–Travale is one of the few steam-dominated geothermal systems in the world and has a sub-hydrostatic pressure gradient. The thermal and structural setting of the system allowed its natural evolution from an initially liquid state to its current superheated steam condition. The liquid phase is presently confined to a few local structures (Fig. 5) that, for the presence of permeable outcrops, facilitate the seepage of meteoric waters into the reservoir (Barelli et al., 1995c). The depressurization of the reservoir occurred prior to industrial exploitation of the geothermal resource as verified by the first drilling data in the area (Celati et al., 1975). A strong pressure disequilibrium should have existed between the steam-dominated reservoir (with 60–70 bar at 4000 m depth) and the regional peripheral aquifers (with hydrostatic pressure of 300–400 bar at 3000–4000 m depth). This requires the presence of a very low permeability boundary in order to limit the interactions among the geothermal system and peripheral aquifers, and consequently allow the existence of the system itself.

From a hydrogeologic point of view, the field is characterized by nearly impermeable formations (Neoautochthonous and Flysch Units) having a thickness of up to 1000 m which act as a caprock for the geothermal system (Fig. 6) hosted in the Mesozoic carbonate-anhydrite formations (shallow reservoir) and in the Paleozoic metamorphic basement (deep reservoir).

The formations constituting the caprock locally exhibit permeable lithologies that host shallow aquifers of limited areal extent. These permeable lithotypes are mainly represented by valley alluvia, detrital limestones in the Neoautochthonous formations, carbonate levels in the Flysch and the underlying "*Macigno*" sandstones. The latter two formations are turbidite sequences that generally exhibit low permeability, and are usually separated from the underlying geothermal reservoir by clayey-marly lithotypes (so-called "*Scaglia Toscana*"). Only in an area near Castelnuovo V.C., the "Macigno" formation is in direct contact with the steam reservoir and can supply a minimum recharge to the system (Calore et al., 1982).

In any case, the aquifers hosted in the overlying formations are underlain by impermeable rocks that prevent interactions with the geothermal system. These aquifers can feed a number of seasonal thermal springs (i.e., Bagno al Morbo, La Perla, Terme del Bagnolo, Bagni San Michele in Fig. 5) which are heated by thermal conduction (Duchi et al., 1992) and are characterized by low salinity values (TDS generally <1000 mg/kg).

The reservoir formations crop out in the southern part of the field along a ridge with a NW Apennine direction. The infiltration of meteoric water to a deeper level is made possible by the carbonate-anhydrite outcrops that represent zones of interference

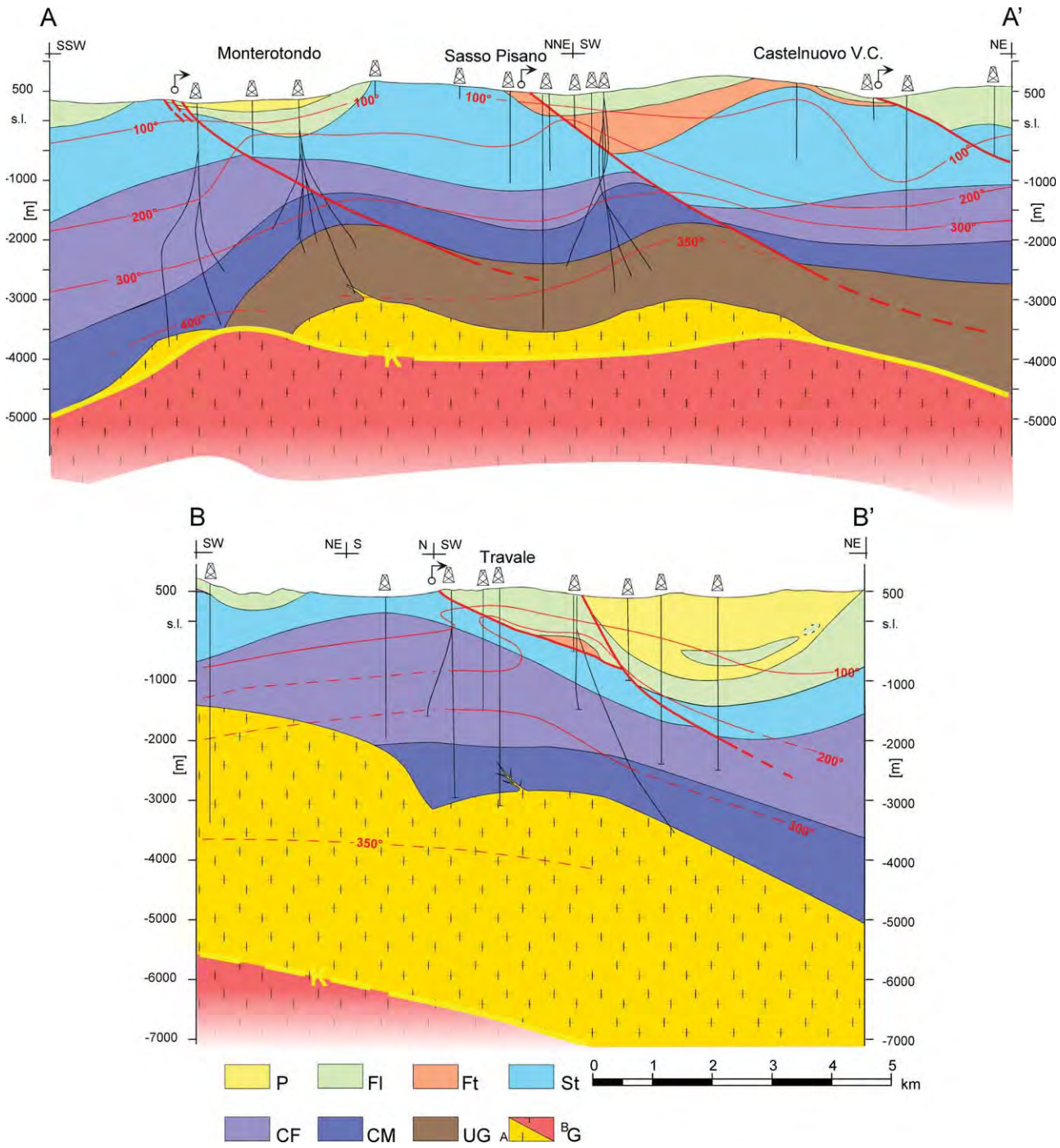

Fig. 4. Geologic cross-sections of the Larderello–Travale geothermal area. See Fig. 3 for locations of cross-sections. P: Neoautochthonous terrigenous deposits (Lower Pliocene–Upper Miocene); Fl: Ligurian and sub-Ligurian Flysch Complex (Jurassic – Eocene); Ft: terrigenous formations of Tuscan Units (Upper Cretaceous–Lower Miocene); St: predominantly carbonate formations of Tuscan Units (Upper Trias – Malm); CF: Phyllites and Quartzites complex (Upper Cambrian – Ordovician); CM: Micaschist complex (Precambrian – Lower Paleozoic); UG: Gneiss Unit (Precambrian – Lower Paleozoic); G: Granite A. Pliocene; B. Quaternary (?).

with the shallow geothermal reservoir. A few wells have encountered water rather than steam (see Fig. 6) and hence these areas have been considered as the boundaries of the shallow geothermal field (Ceccarelli et al., 1987).

The carbonate outcrops feed a deep circulation system that supplies the springs at the south-eastern boundaries of the carbonate ridges. These springs (i.e., Vene di Ciciano, Venelle, Aronna) display high flow rates with medium to low temperatures (around 25 °C). A mixing between the incoming water and the geothermal steam occurs at the northwestern end of the ridges (Fig. 7). This inflow represents the so-called local recharge of the geothermal system and the phenomenon is sometimes evidenced by thermal inversion in a few wells at the field boundaries. Otherwise, the shallow aquifers are perched and separated from the steam reservoir, as verified by some deep wells that have penetrated these aquifers (see Fig. 6), and by the horizontal temperature distribution at the top of the shallow geothermal reservoir. In fact, a strong horizontal thermal gradient, caused

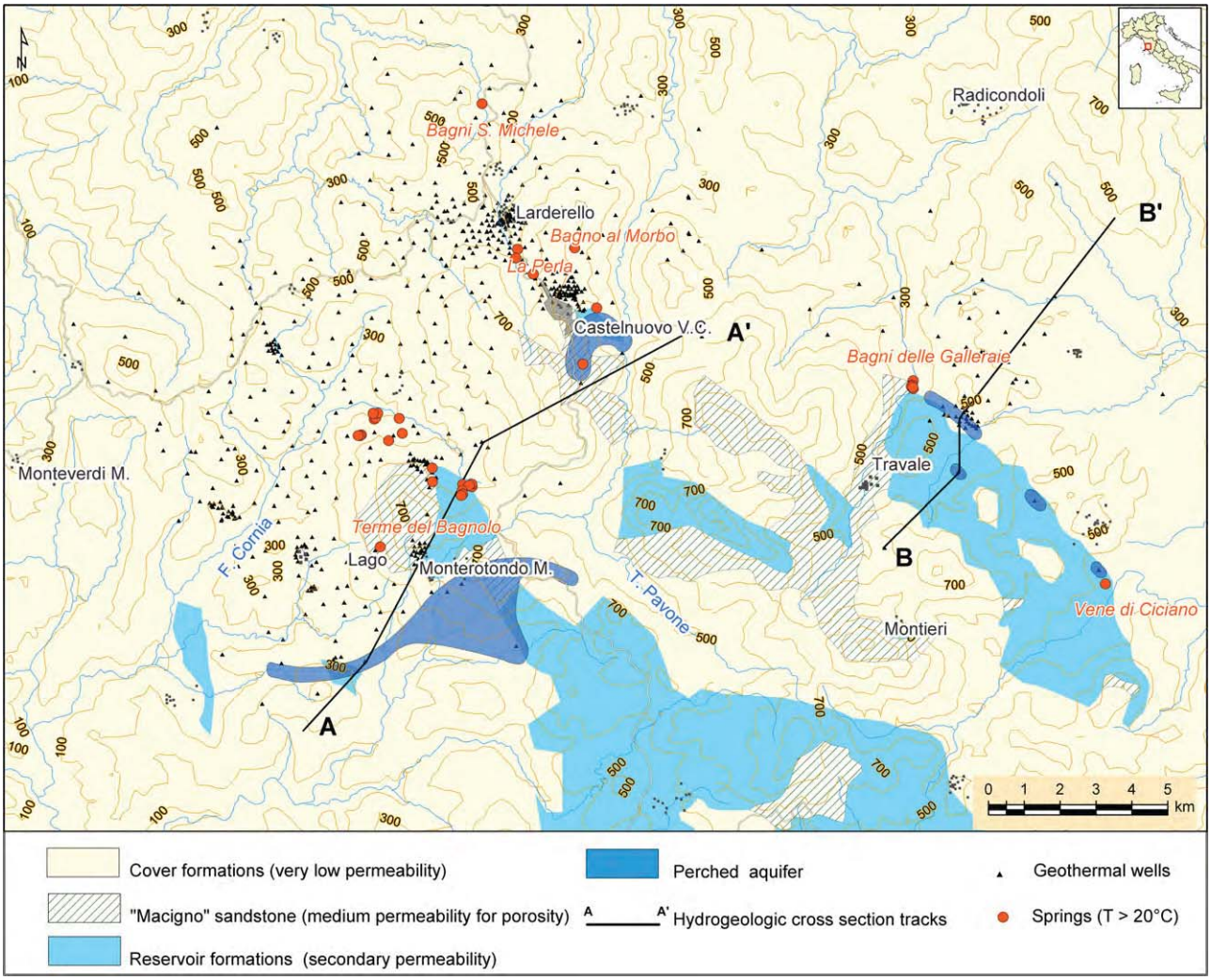

Fig. 5. Hydrogeologic map of the Larderello–Travale area.

by the interference of cold water inflow, occurs only in outcrops of the shallow reservoir. The contribution of the shallow aquifers constitutes only a part of the total natural recharge in the Larderello–Travale system, and has been preliminary estimated, from gas/steam ratio analyses, to be 390–580 t/h (i.e., $3.3–5.0 \times 10^6$ m^3/year).

Deep drilling shows no thermal influence on the deep metamorphic system due to the above-mentioned permeable outcrops. This is supported by the thermal anomaly being open in the south (see Fig. 2) where these outcrops are widely present.

Two main perched aquifers with piezometric levels of 160 m (base aquifer) and 330 m a.s.l. have been identified within the carbonate formation of the Tuscan Units that can locally feed the geothermal reservoir. These large aquifers are characterized by high permeability, very small piezometric horizontal gradients (typical of karst aquifers), medium–low temperatures (20–25 °C), and a southward outflow (see Fig. 7).

The primary porosity of the geothermal reservoir rocks is very low (1–5%) and homogeneous (Cataldi et al., 1978), while a highly variable fracturing results in a wide range of possible secondary permeability values (Bertani and Cappetti, 1995). Generally, the shallow reservoir is characterized by a homogenously distributed fracture system that can be denser in structural highs. The metamorphic basement however exhibits a large permeability variation due to the nonhomogeneous and localized fracturing (Fig. 8).

3.3. Geologic and physical characteristics of the model

The geoscientific features used as inputs for the numerical model are described below and are shown graphically in Fig. 9. The caprock for the geothermal system consists of the low permeability formations of Flysch Units and Neoautochthonous clayey deposits. Its thickness varies from 200 to 400 m in the central part of the modeled reservoir to about 1000 m in the boundary zones, and its permeability has been chosen to be negligibly small (10^{-21} m^2).

In order to distinguish the caprock from the reservoir, both stratigraphic and production well data were analyzed. From a geological perspective the top of the reservoir corresponds to the base of the Flysch (Fig. 10), while from a production point of view it is determined by the first fractured layer encountered in the exploited area. Outside the geothermal system, the reservoir top was assumed to coincide with the 250 °C isotherm which is the average temperature value at the reservoir top. The drilling data indicate a substantial

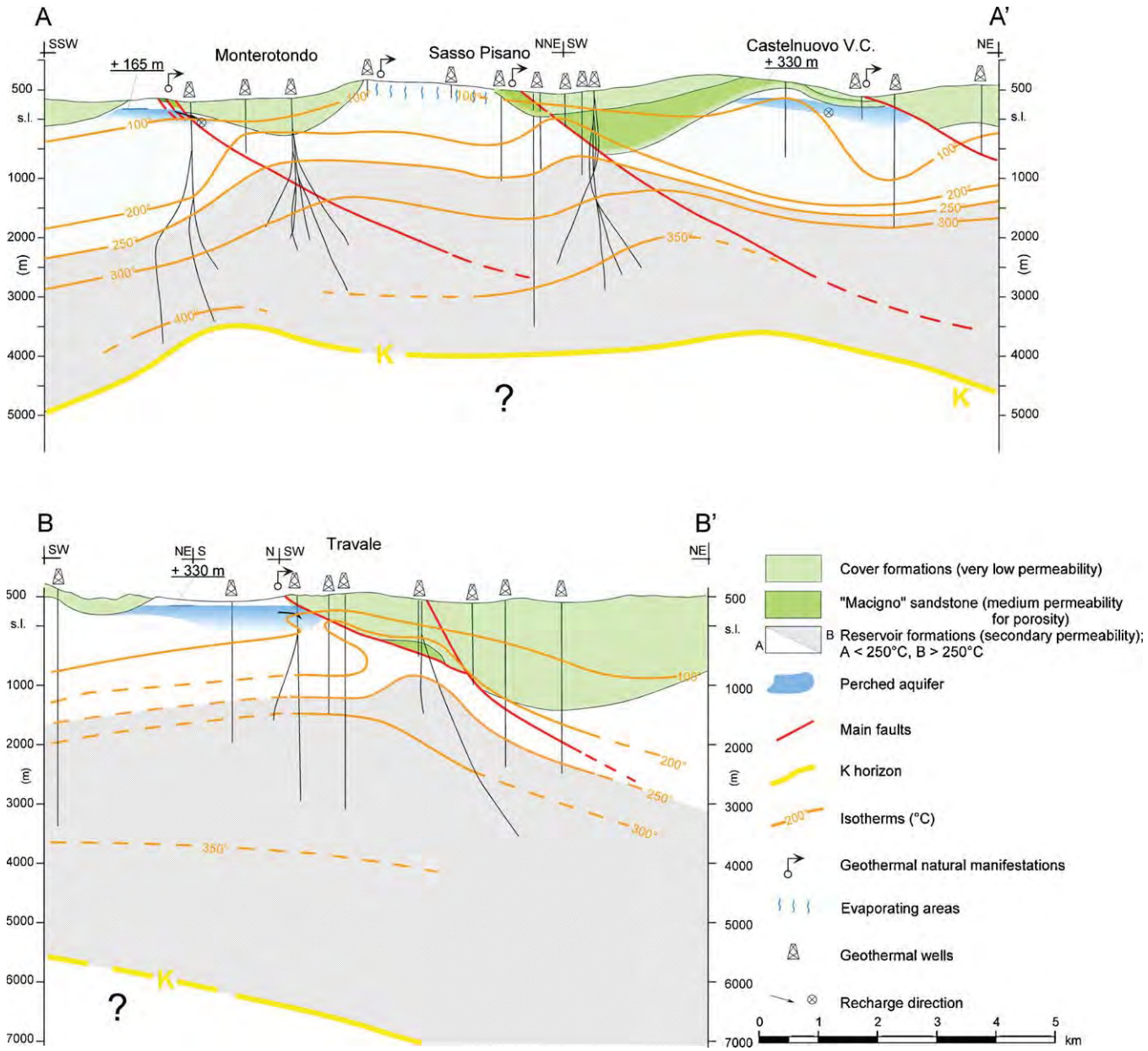

Fig. 6. Hydrogeologic cross-sections of the Larderello–Travale area. See Fig. 5 for locations of cross-sections.

coincidence of the first fractured/productive levels with the depth of the 250 °C isotherm in the central part of the field (Fig. 11).

The boundary between the potential reservoir (the geological formation that can host a reservoir) and the productive formation is considered as the reservoir top in the numerical simulation, thus distinguishing two different bodies:

- an *intermediate layer* in the uppermost part of the potential reservoir, characterized by unfractured low permeability rocks (3×10^{-20} m^2) with a maximum porosity value of 2%, and
- the *productive geothermal reservoir* with permeabilities ranging from 10^{-13} to 10^{-15} m^2, porosity from 2% to 4%, and temperature in the range of 250–320 °C.

As mentioned previously, the Larderello and Travale are part of the same 300–350 °C geothermal system at depths greater than 3000 m. Nevertheless, a low permeability (10^{-16} m^2) section was inserted in the numerical model between Larderello and Travale areas, to simulate the different pressure response of the two fields as evidenced by exploitation (see Fig. 9).

Reflection seismic data (Batini et al., 1983; Brogi et al., 2005; Gianelli et al., 1997) highlighted the presence of an intense and continuous reflector inside the Palaeozoic crystalline basement, the so-called K-horizon (Fig. 12). Its nature is still a subject of debate (brittle/ductile transition, recent granitoid intrusions, carapace permeated by supercritical fluids, etc.) and its depth varies between 3–4 km in the western zone and 8–10 km in the Travale geothermal area (Bertini et al., 2006). The K-horizon is associated with the 400 °C isotherm and is considered the *base of the reservoir*

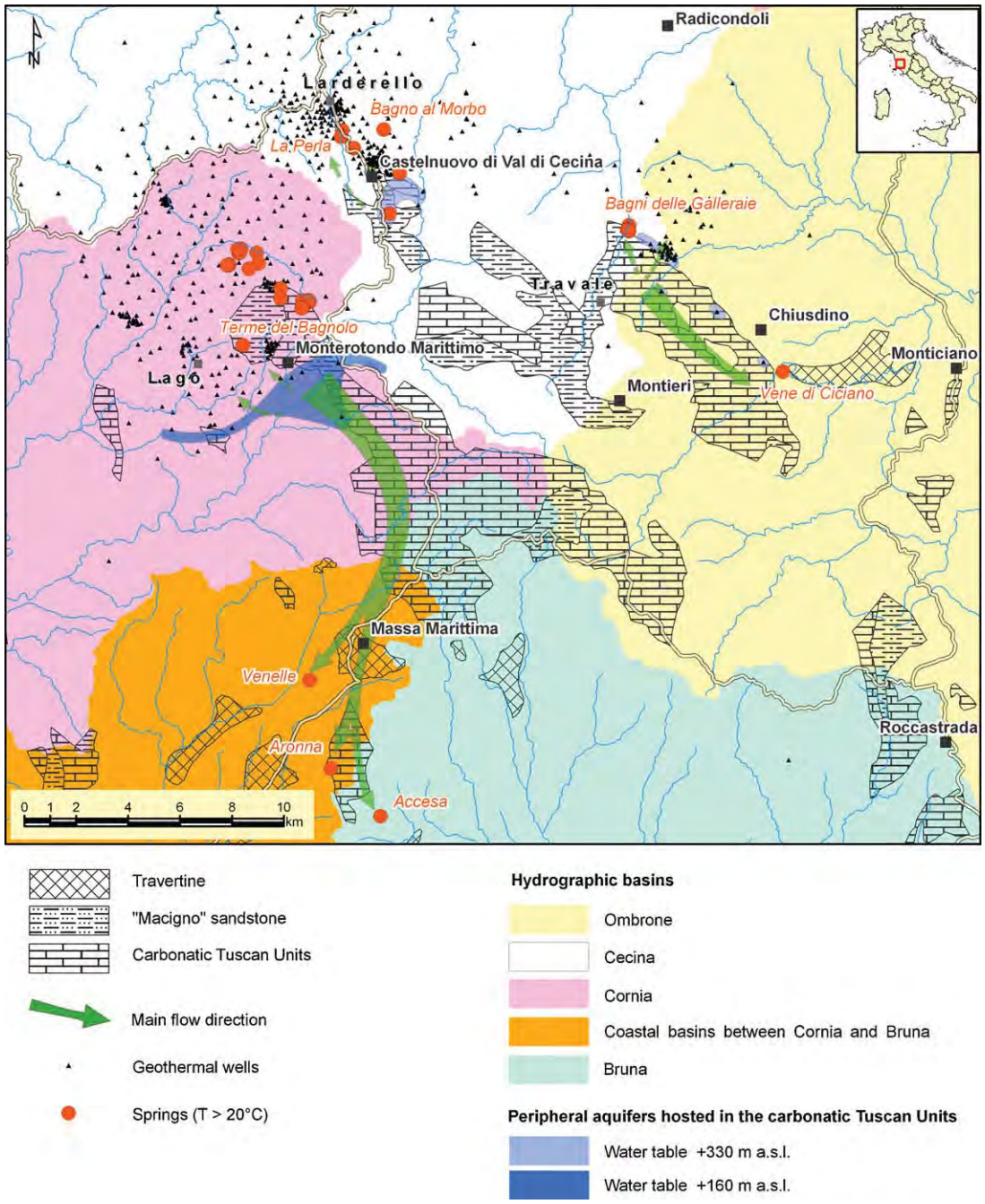

Fig. 7. Interpreted hydrogeologic map of the Larderello–Travale area.

in the numerical model (i.e., it is believed to be the lower boundary of the exploitable geothermal system). At this temperature, the rock ductility should be sufficiently high to prevent natural fracturing. Due to numerical modeling constraints, the shape of this seismic marker was simplified and was set at a depth of 4000 m in the Lago area, and at 7000 m in the Travale one. In order to allow for heat flow but no mass flow from the bottom, the K-horizon was modeled by using impermeable ($k = 0$) and constant temperature cells.

The *lateral boundaries* of the geothermal reservoir are treated in the model as low permeability zones (1.5×10^{-18} m^2) in order to hydraulically separate the surrounding deep aquifers from the steam dominated reservoir. The permeability of these boundaries was estimated from the peripheral well data.

In the numerical model, the caprock is nearly impermeable, but some cells are considered permeable in order to simulate the interaction zones between the geothermal reservoir and the environment. As previously mentioned, the only interactions are the natural manifestations and some perched aquifers. The natural manifestations were modeled by inserting three virtual wells, one for each of the three main zones of outflow, and their productivity index (PI) was chosen to match the estimated historical production. In order to connect these virtual wells to the reservoir, three permeable blocks were introduced in the model. As for the perched

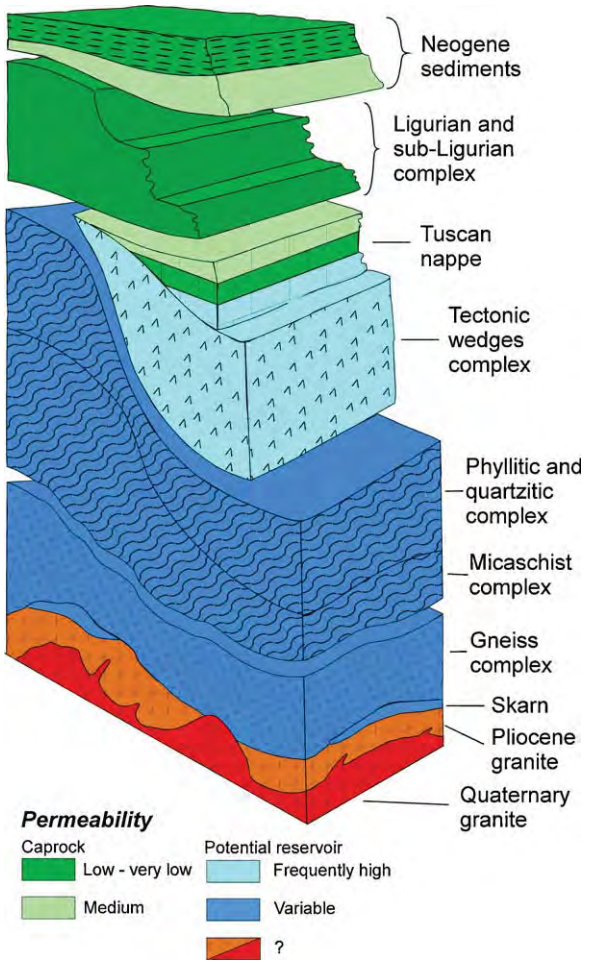

Fig. 8. Structural-stratigraphic and hydrogeologic sketch of the geothermal area (Arias et al., 2010).

aquifer, a number of cells with constant pressure were introduced to simulate the reservoir outcrops (Barelli et al., 1995c; Ceccarelli et al., 1987).

The numerical model has sixteen rock types, twelve for the reservoir, two for the impermeable caprock, and two others for the lateral boundaries where the regional aquifer is hosted. The petrophysical parameters are summarized in Table 1 for the main rock types used in the model.

3.4. Evaluation of the geothermal system local recharge

Prior to industrial exploitation, the geothermal system was recharged by deep regional inflows with long circulation times. The progressive increase of steam production from wells located near the carbonate outcrops (shallow reservoir), triggered a local influx of water (Fig. 13). The local recharge results in a lowering of the non-condensable gas content, and at times in the production of a two phase fluid. In fact, the steam from local recharge is gas free because of the short circulation times (less than 50–70 years based on isotopes; internal unpublished data). The variation with time of the steam extraction rate and of the gas/steam ratio allows the evaluation of local recharge. This is done using a mixing model between the superheated steam derived from deep circulation (primary steam) and that from local recharge (Fig. 14). The total steam production and the gas/steam ratio were analyzed for the so-called "Horst" sector of the Travale area, for the "Castelnuovo V.C." and "Valle Secolo" sectors of the Larderello area, and for the "Monterotondo" and "Lago" sectors of the Val di Cornia area (Fig. 15).

The evaluation of the primary steam fraction is based on a mass balance and can be performed only for geothermal wells not affected by water injection and with a constant production rate. The wells that showed production decline and lowering of the steam gas content were not considered in this evaluation.

Assuming that the gas content in steam from local recharge is negligible, and defining:

$$G_T = G_L + G_D \tag{1}$$

where G_T is the total steam discharge rate, G_D the steam from deep circulation (primary steam), and G_L the steam from local recharge , there follows:

$$G_T \times A = G_D \times B \quad \text{and} \quad G_D = \frac{G_T \times A}{B} \tag{2}$$

Here A is the gas/steam ratio in the total discharge and B the gas/steam ratio in the fluid of deep origin. Substituting for G_D from Eq. (2) into Eq. (1), results in:

$$G_L = G_T - \frac{G_T \times A}{B} \quad \text{and} \quad G_L = G_T\left(1 - \frac{A}{B}\right)$$

Assuming the gas content of the primary steam (B) remains unchanged from its original value of 10.7% by weight (based on data from the early wells), steam flow derived from local recharge was computed, taking into account the lowering of the non-condensable gas content from the beginning of the industrial exploitation up to present time. This analysis was applied to those areas of the Larderello–Travale system most affected by the mixing between primary steam and local recharge fluids (shallow carbonate reservoir):

- *Travale area* ("Horst" reservoir)
- *Larderello area* ("Castelnuovo V.C." and "Valle Secolo")
- *Val di Cornia area* ("Monterotondo" and "Lago")

The mixing model input parameters and the results of the computation for each sector are summarized in Table 2. Since these recharge values are based on indirect evaluation, higher local recharge values (+10–40%) have been tentatively adopted for comparison with the results of the numerical model where water inflow is simulated using constant pressure grid blocks. The total steam production from local recharge is in the range of 390–580 t/h ($3.3–5.0 \times 10^6$ m^3/year) and Table 3 shows the recharge values for each of the three areas (Travale, Laderello, Val di Cornia).

Table 1
Petrophysical parameters for main the rock types.

Rock types	Permeability (m^2)	Porosity (%)	Thermal Conductivity (W/m °C)
Reservoir (12 rock types)	10^{-16} to 10^{-13}	2–5	2
Caprock (2 rock types)	0–10^{-20}	0.1–2	2
Lateral aquifers (2 rock types)	10^{-18} to 10^{-16}	2	2

4. Numerical modeling

The Larderello–Travale system was simulated using the numerical simulator TOUGH2, a general-purpose code for modeling multi-dimensional, multiphase/multi-component flow and heat transport in porous and fractured media (Pruess et al., 1999).

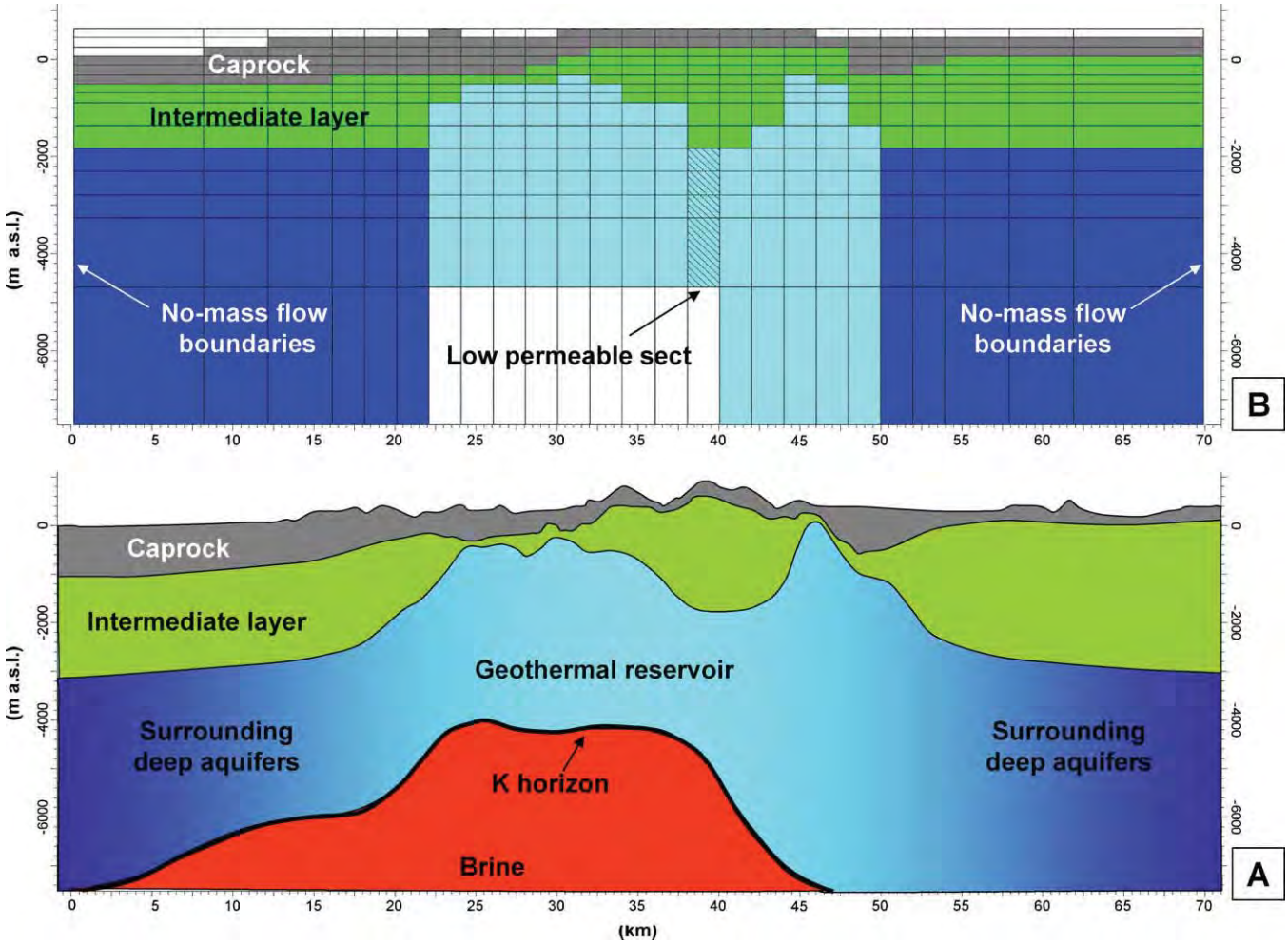

Fig. 9. Comparison of geology (A) and numerical model (B) on a W–E cross-sections.

The modeling was performed using the "equation of state" module (EOS1) for pure water. All water properties (density, specific enthalpy, viscosity, and saturated vapor pressure) are supplied by the International Formulation Committee steam equation tables (1967). While Corey curves were adopted for the relative permeability, capillarity, adsorption, and double porosity were not considered.

Although the Larderello–Travale geothermal system at depths greater than 3000 m is a single superheated steam-dominated system with temperature of 300–350 °C, a low permeability section is inserted between the Larderello and Travale areas (see Fig. 9) to simulate the pressure response to production. Furthermore, the lateral boundaries between the high-permeability reservoir core and the surrounding low-permeability deep regional aquifers are assumed to be at 250 °C which is believed to be the minimum reservoir temperature.

4.1. Conceptual model and natural geothermal system evolution

The numerical simulation is based on a conceptual model for the Larderello–Travale system that explains the origin of the steam produced over a century. The permeable portion of the geothermal system could not have contained the total amount of superheated steam extracted since the beginning of the exploitation. The main features of the conceptual model can be summarized as follows:

- a clayey-shaley caprock (from 0 to 500 m)
- a fractured carbonate reservoir (from 500 to 1000 m)
- a metamorphic reservoir (from 1000 to 4000–5000 m)
- a granitic intrusion as the heat source of the system

Before the emplacement of granitic intrusions, temperature, and pressure, distributions at depth are assumed to be given by the average geothermal gradient and the hydrostatic pressure gradient. Initially, the entire reservoir volume was liquid saturated (Fig. 16). Subsequent to granitic intrusions (3.0–0.5 Ma), the temperature gradually increased in the reservoir and the pressure started to decrease due to the onset of natural manifestations (Celati et al., 1975) that were triggered by the fluid evaporation process. The steam-dominated zone initially developed at the top of the reservoir and then spread all over the reservoir volume (Fig. 17). Complete vaporization of the reservoir water, resulted in a superheated and depressurized system long time before the start of exploitation (Fig. 18).

The main reservoir recharge, particularly during exploitation, comes from the surrounding low permeability regional aquifers in response to pressure drop. A two-phase zone

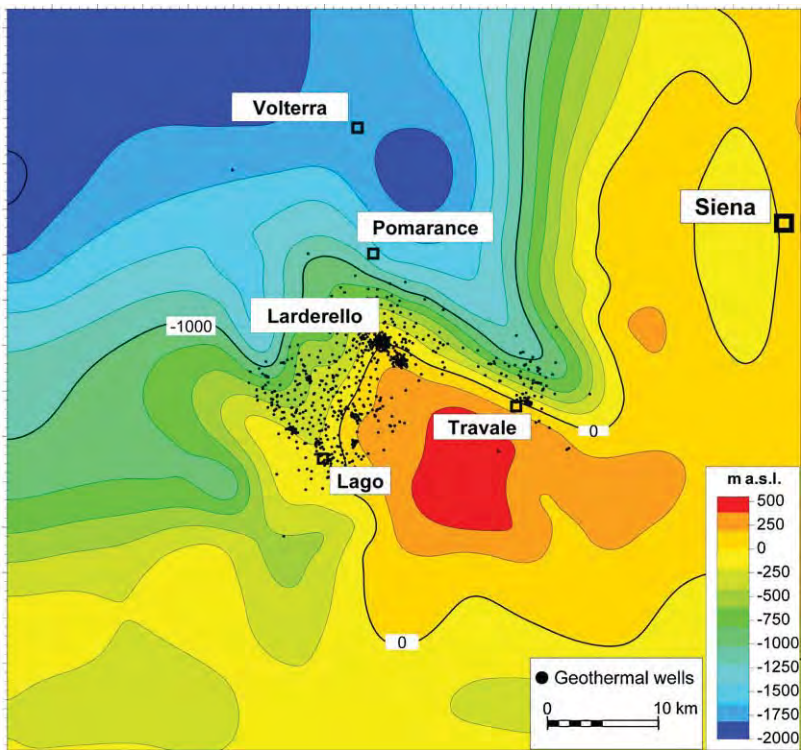

Fig. 10. Map of the Flysch formations base (m a.s.l.).

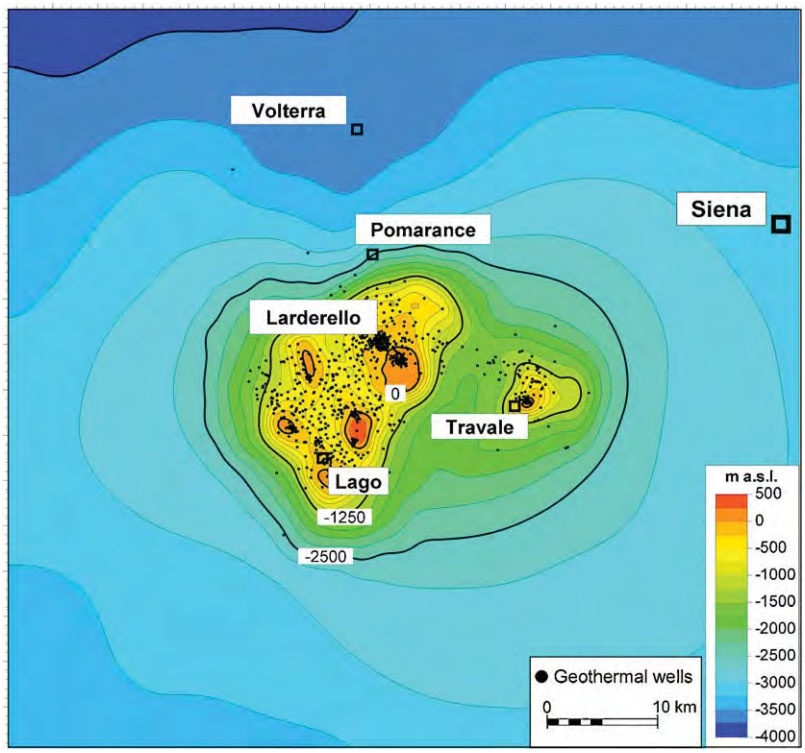

Fig. 11. Map of the top of productive reservoir (m a.s.l.).

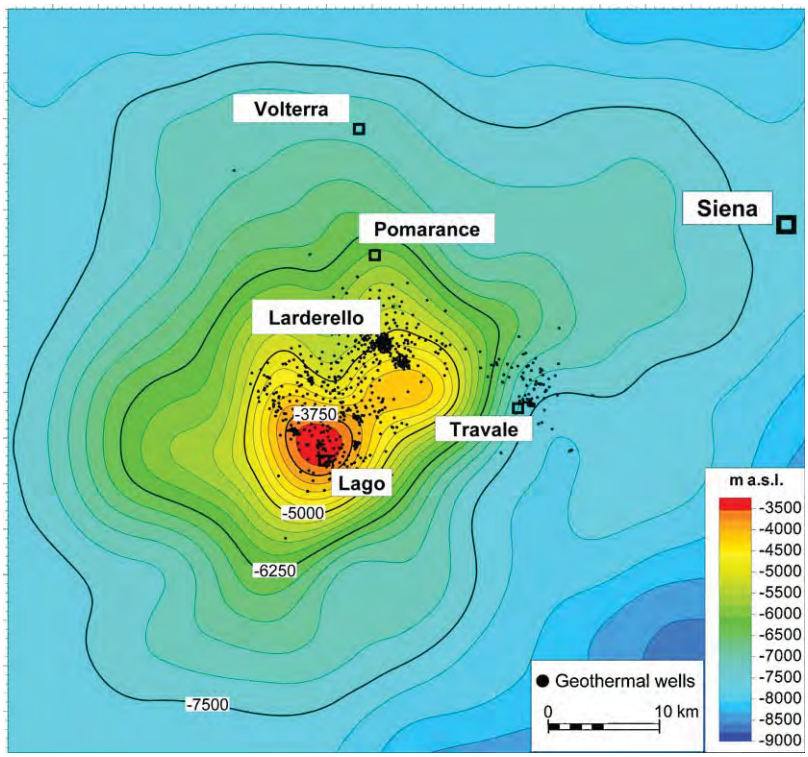

Fig. 12. Map of the seismic K-horizon (m a.s.l.).

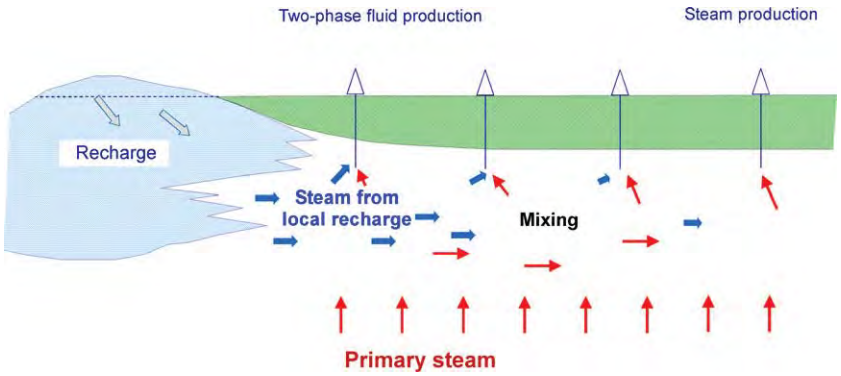

Fig. 13. Schematic cross-section of the interference between the local recharge and the deep primary steam.

is likely to exist near the boundaries between the superheated reservoir and the regional aquifers. Only this type of recharge can explain the large amount of steam extracted over a century of exploitation, i.e., 1.8×10^9 t. It is also possible to evaluate the maximum amount of steam that could be contained in the geothermal system. Since the Larderello–Travale system has an area of about 400 km^2 and an average thickness of about 2 km, the total reservoir volume (V_{res}) is 800 km^3. Assuming a porosity (ϕ) of about 2%, the available volume for the steam storage in the reservoir (V_{steam}) is:

$$V_{steam} = V_{res} \cdot \phi = 16\,\text{km}^3.$$

Thus, the maximum steam amount (M_{steam}) which could be contained in the Larderello–Travale geothermal system is:

$$M_{steam} = V_{steam} \cdot \rho_{(300\,^\circ\text{C};\ 50\,\text{bar})}$$

$$= 16\,\text{km}^3 \cdot 22.075\,\frac{\text{kg}}{\text{m}^3} = 0.35 \times 10^9\,\text{t}$$

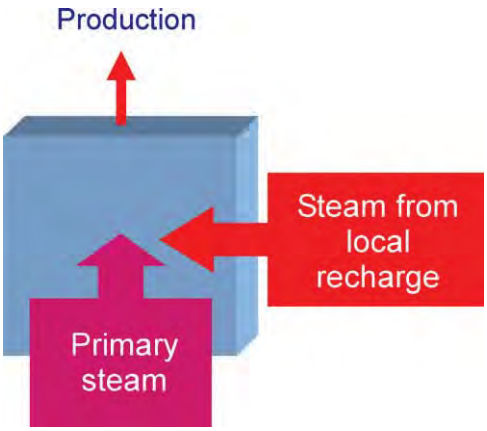

Fig. 14. Mixing recharge model.

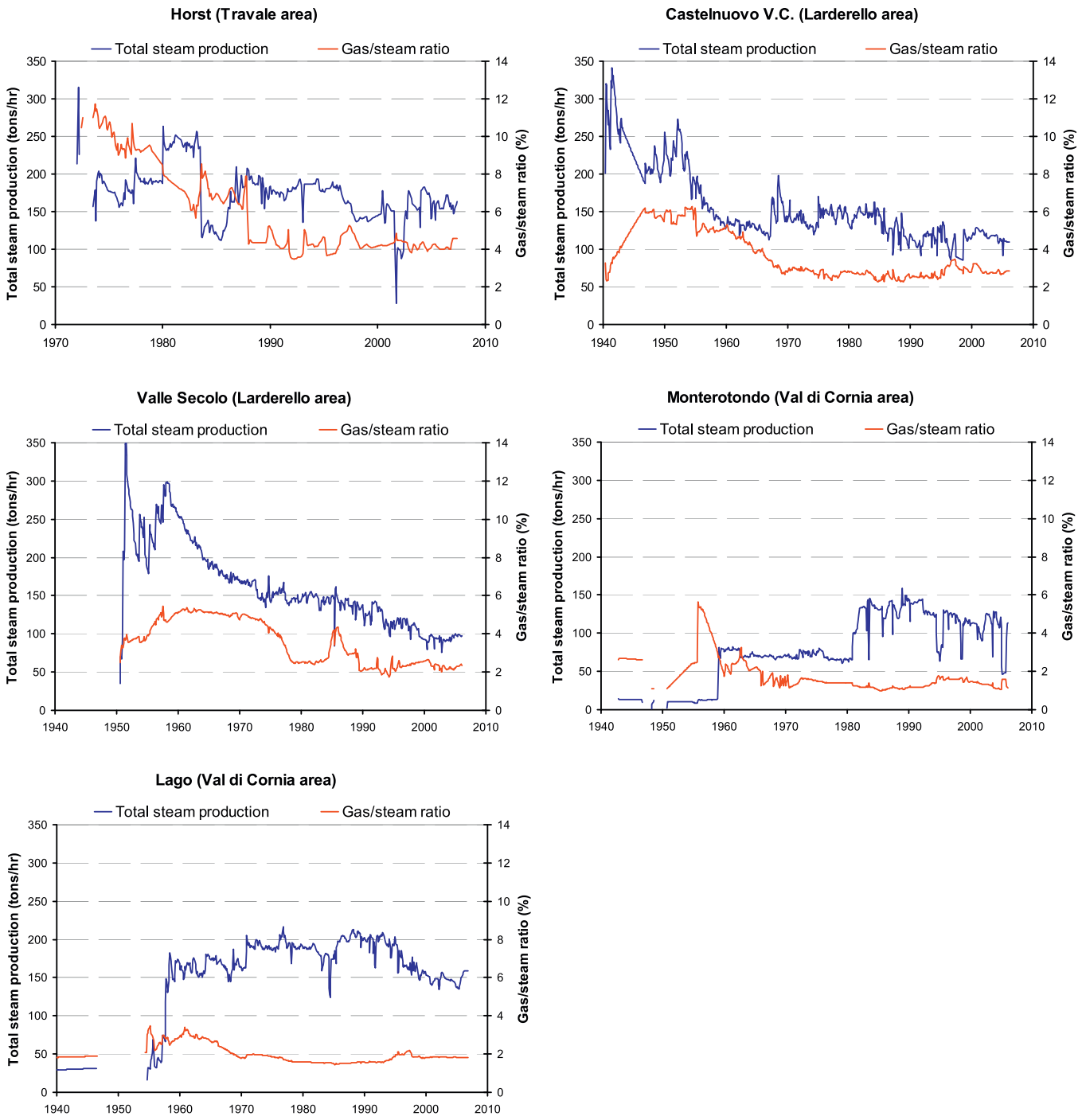

Fig. 15. Production history for the different areas of Larderello–Travale geothermal field.

where $\rho_{(300\,^{\circ}C;50\,bar)}$ is the steam density evaluated at a temperature of 300 °C and a pressure of 50 bar, which is the average pressure and temperature in the reservoir. The total steam extracted to date is more than five times the storage capacity of the Larderello–Travale geothermal system. Even the assumption of an equivalent porosity of 10% to account for the amount of adsorbed water, cannot explain the amount of the steam extracted from Larderello–Travale geothermal system. The continuous evaporation of water in the boundary zone, between the superheated reservoir and the surrounding regional water-dominated aquifers, recharges the reservoir at a rate that certainly is much higher than the shallow local recharge (390–580 t/h).

4.2. Simulation grid and boundary condition

The simulation domain has an area of 4900 km^2 (70 km × 70 km) and a maximum total vertical thickness of nearly 7500 m (from 500 m a.s.l. to 7000 m b.s.l.). The depth to the bottom of the reservoir (K-horizon in Fig. 9) varies between 4000 m in the western zone and about 7000 m in the Travale area. The numerical grid is subdivided into 16 layers and consists of about 10,000

Table 2
Input data and results of the mixing model for the local recharge zones.

Local recharge zone	Original gas/steam ratio B (%)	Present gas/steam ratio A (%)	Total steam capacity G_T (t/h)	Computed recharge (t/h)
Horst (Travale area)	10.70	4.60	160	91
Castelnuovo V.C. (Larderello area)	6.00	2.95	110	56
Valle Secolo (Larderello area)	5.00	2.40	100	52
Monterotondo (Val di Cornia area)	2.85	1.18	110	64
Lago (Val di Cornia area)	3.00	1.80	160	64

cells; each horizontal layer consists of 625 (25×25) cells with variable sizes (Fig. 19). A cell size of 2 km × 2 km is used in the central part where greater detail is necessary. Along the domain boundary, a 8 km × 8 km cell size has been adopted. The layer thickness varies with depth from a maximum of a few thousand meters (deep layers) to only 200 m (shallow layers).

To demonstrate the field sustainability, a no-mass flow condition (see Fig. 9) is imposed over all the domain boundaries. The large distance between the grid boundaries and the producing area guarantees that the field behavior is not affected by the assumed boundary conditions.

Temperatures and pressures are assumed to be time invariant in the cells at the top and bottom of the simulation grid. A fixed temperature of 15 °C and atmospheric pressure were set for cells along the upper boundary. The temperatures varied between 350 °C and 400 °C for cells in the bottom layer inside the producing reservoir. The TOUGH EOS1 is not applicable at temperatures above the critical point of water. Temperatures above the critical point are associated with impermeable blocks along the bottom boundary that act as heat sources without allowing mass flow. Outside the producing area, the temperatures in the bottom boundary cells were set to values calculated according to the average earth thermal gradient.

The only interactions between the geothermal reservoir and the external environment are the natural geothermal manifestations and the inflow of cold water from shallow aquifers, where the caprock is absent (see Section 3.4). The natural manifestations were modeled by three virtual wells with a productivity index (PI) chosen to match the historical flow rate. The PI was estimated from the production data of the chemical industry (boric acid extraction) that began in the early 19th century.

As for the interaction with the shallow aquifer, fixed pressure cells were used where the reservoir outcrops are present. The fixed pressure cells are connected via permeable blocks to the geothermal reservoir. The permeability values for these blocks were chosen to match the results of the mixing model (see Table 2).

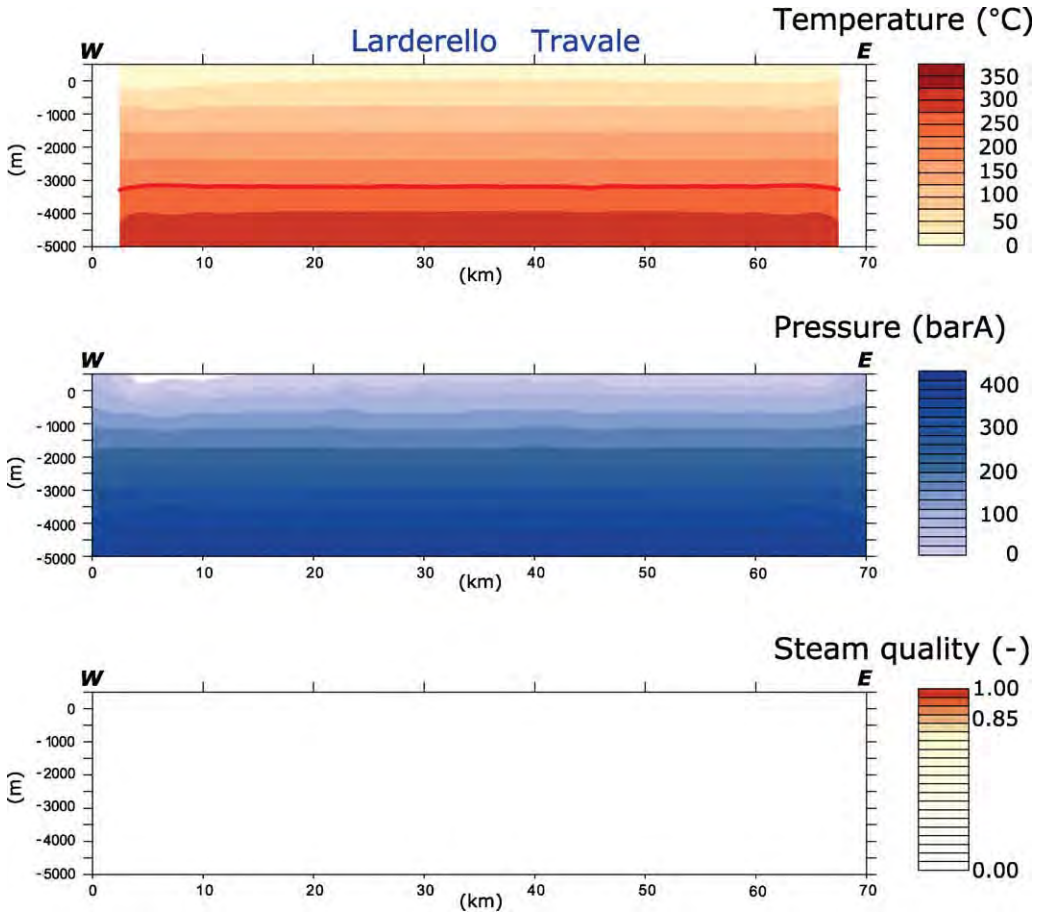

Fig. 16. Temperature, pressure and steam quality distribution along a W–E section before the emplacement of magmatic bodies (~3.0 Ma).

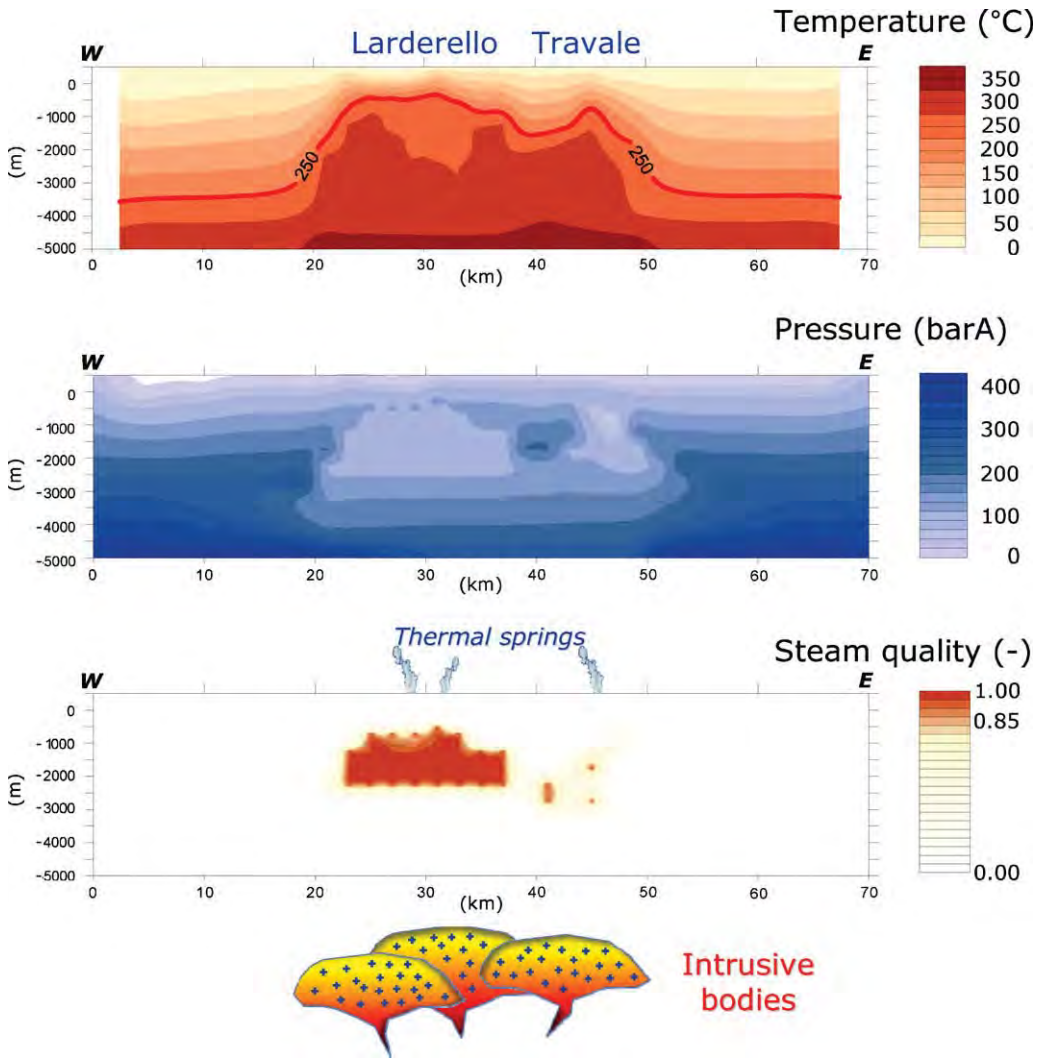

Fig. 17. Temperature, pressure and steam quality distribution along a W–E section after the emplacement of magmatic bodies (3.0–0.5 Ma).

Table 3
Local recharge values adopted for a comparison with the numerical model.

Local recharge area	Total recharge (t/h)
Travale area	90–130
Larderello area	150–210
Val di Cornia area	150–240

5. Natural state simulation

During simulation of the natural state that covers a period of about 3 Ma, the permeability and porosity values were tuned to match the temperature distribution at depth. To verify the reliability of the natural state simulation, the areal distributions of the simulated values of temperature, pressure, and steam quality were compared with the measurements at different depths. Satisfactory agreement was found, particularly for the temperature (Fig. 20). Additionally, simulated well temperature profiles were compared with observed data from the early wells. To this end, the Larderello area (Fig. 21) was subdivided into four zones (Monteverdi, Larderello, Val di Cornia, and Selva) and the Travale area (Fig. 22) into two zones (Travale and Montieri) on the basis of their thermal characteristics.

The total natural manifestations flow rate was calculated to be 120 t/h. This is the same order of magnitude as the estimate based on boric acid production at the beginning of the 20th century. The natural state inflow from the shallow aquifers in the three areas previously considered (Larderello, Travale and Val di Cornia) was computed to be 300 t/h. The evaporation of the surrounding deep aquifer (regional) has been considered in the numerical modeling which guarantees the recharge of the geothermal. The computed natural state simulation was used as the initial condition for production history simulation.

6. Production history simulation and system sustainability

Once a satisfactory match for the natural state was achieved, the same three-dimensional distributions of permeability and porosity, obtained during the natural state simulation, were used to simulate field production history and to predict the future sys-

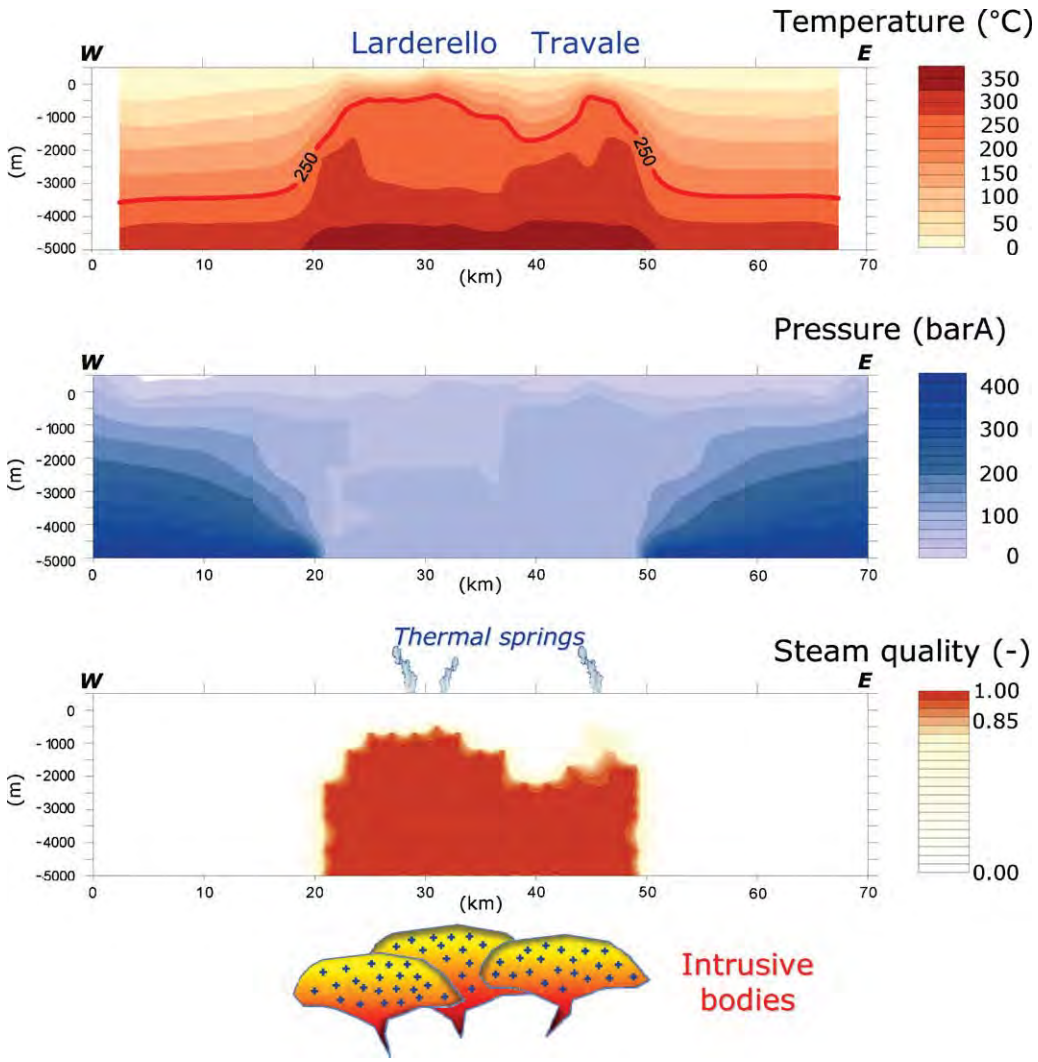

Fig. 18. Temperature, pressure and steam quality distribution along a W–E section before the exploitation of the system (1900).

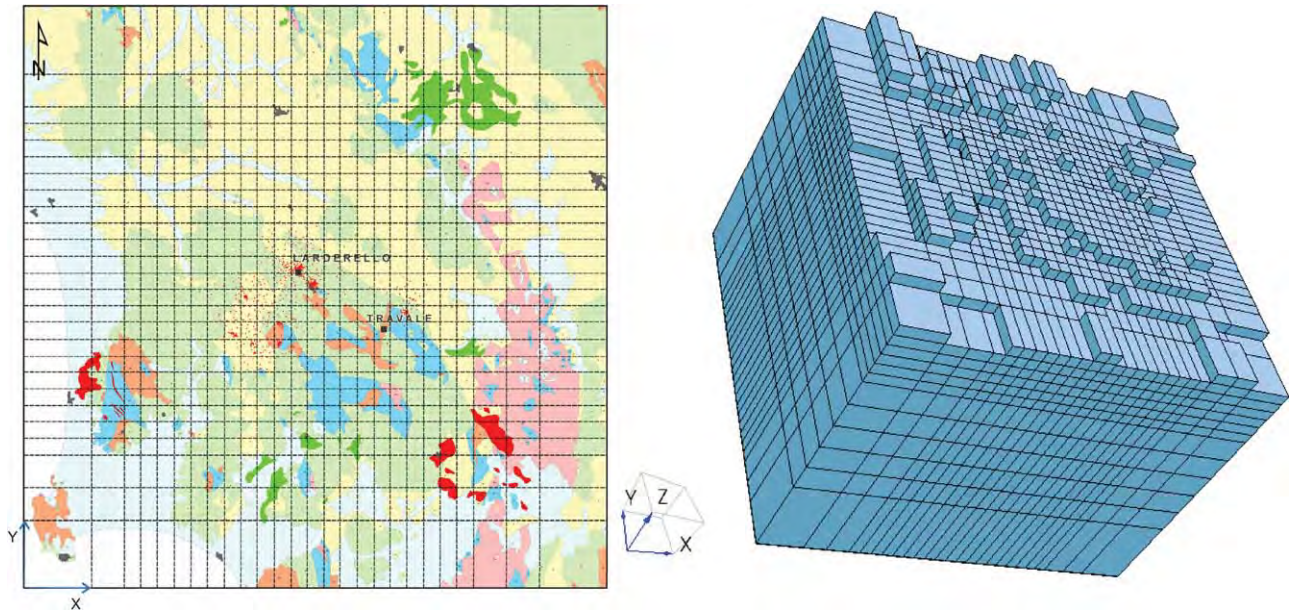

Fig. 19. 2D horizontal and 3D simulation grids.

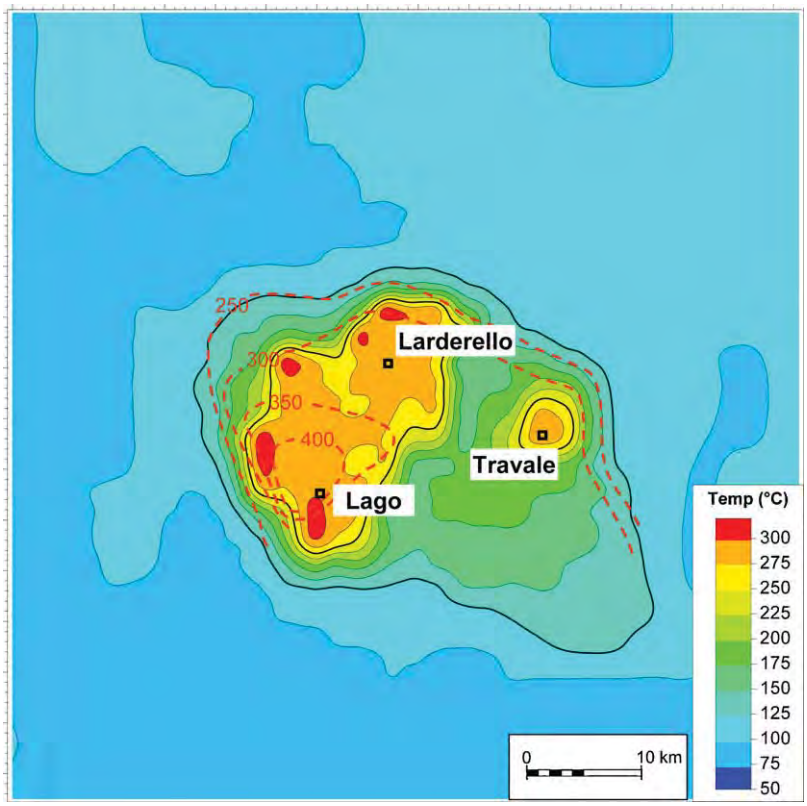

Fig. 20. Observed (dashed lines) and simulated temperature distribution (continuous lines) at 3000 m b.s.l.

tem evolution. The exploitation history was modeled using the production and injection data (1927–2009) collected in more than 700 wells grouped into 20 "virtual" wells accordingly to their location and depth. The system evolution due to production was simulated by comparing the computed pressure decline with the observed pressures obtained from static wellhead measurements (Fig. 23). Fairly good agreement was obtained both for shallow and deep reservoir pressure histories, with the only exception being the shallow Travale reservoir ("Graben") where the simulated pressure is higher than the historical data. This difference is probably due to local permeability variations that cannot be estimated in the framework of a current regional modeling.

The horizontal distributions of the simulated temperature, pressure and steam quality were compared with measurements at different depths, yielding satisfactory results. To quantify the effects of exploitation, the simulation results for temperature and pressure corresponding to the natural state and the present state are compared in Figs. 24 and 25, respectively. Each dot in the graphs represents one of the 625 cells at 3000 m b.s.l. There is only a slight reduction in pressure in cells located inside the reservoir. A pressure draw-down takes place in the central part of the reservoir, while the pressure of the surrounding deep aquifers is only slightly affected. A small pressure decrease can be noticed at the interface between the steam dominated reservoir and the surrounding aquifers. This small pressure decrease causes the evaporation of liquid water near the steam/water interface. No significant temperature variations are evident during exploitation in the reservoir (Cappetti et al., 1995). Only two-phase cells display a sizeable temperature decline because these cells are placed at the boundary between steam reservoir and water aquifers.

Our simulation demonstrates that the contribution of the shallow aquifers, which are separated from the geothermal system by a thick impermeable caprock, is not necessary for sustainable geothermal production. The contribution of the perched aquifers is only local, as they partially feed the geothermal reservoir at small outcrops of carbonate formations. The total local inflow is around 300 t/h, less than 10% of the total production flow rate (Fig. 26). The discharge of the geothermal fluids through natural manifestations decreases with time (Fig. 27) as the reservoir pressure is reduced during exploitation.

In conclusion, the numerical modeling illustrates that only very few changes from the natural state of the geothermal system have been induced by the exploitation (Fig. 28). Good agreement between the measurements and the simulated results for the natural state and the production history allows a confident prediction of the reservoir response to future exploitation. Results show current production from the Travale–Larderello geothermal system is sustainable for at least 100 years.

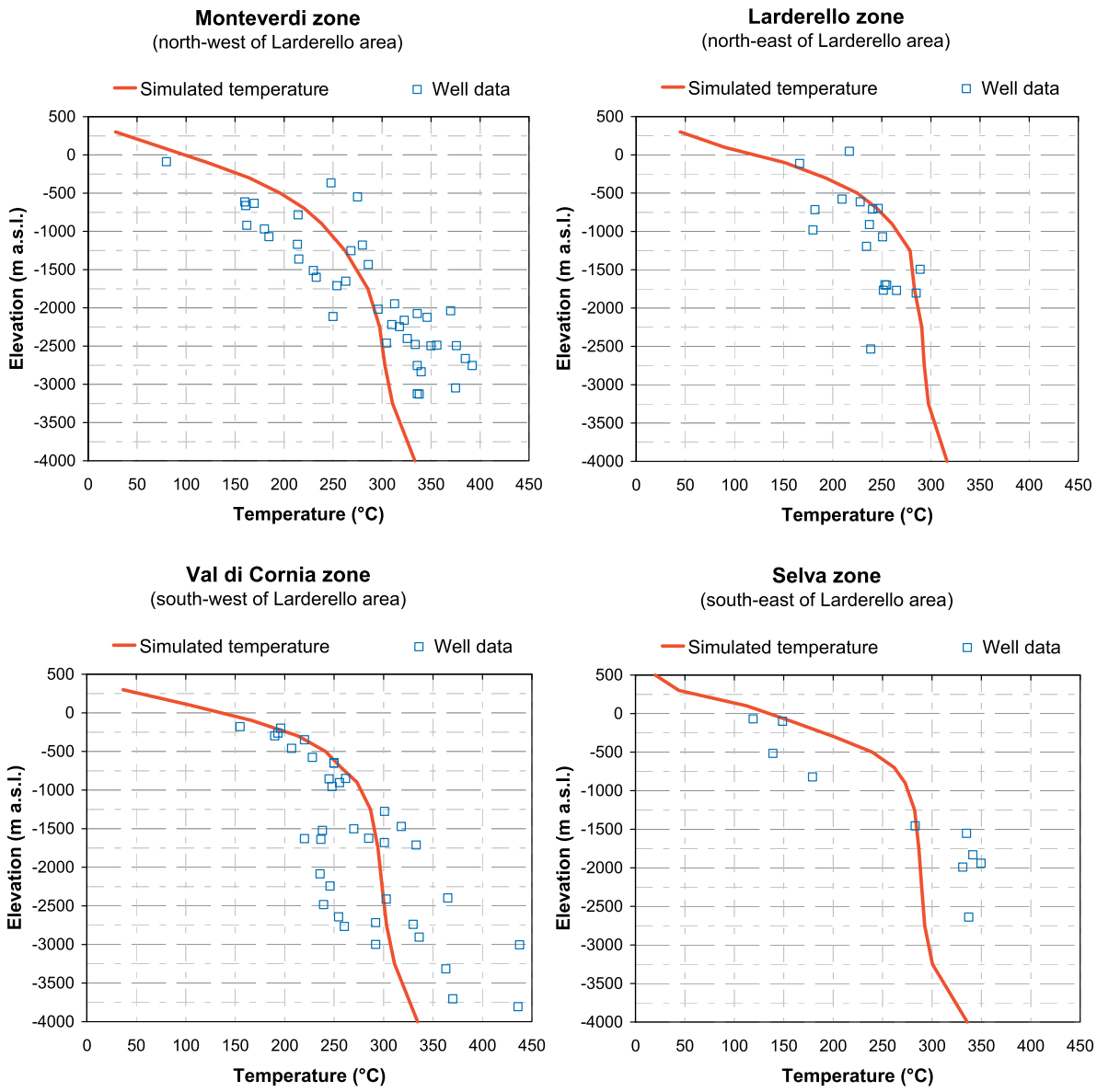

Fig. 21. Observed and simulated well temperature profiles in the Larderello area.

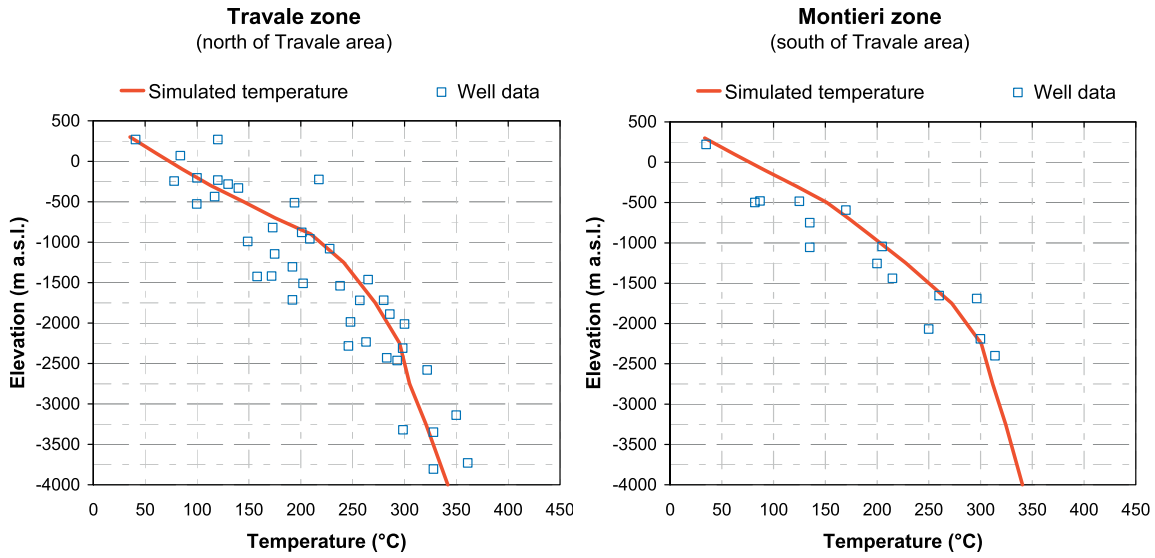

Fig. 22. Observed and simulated well temperature profiles in the Travale area.

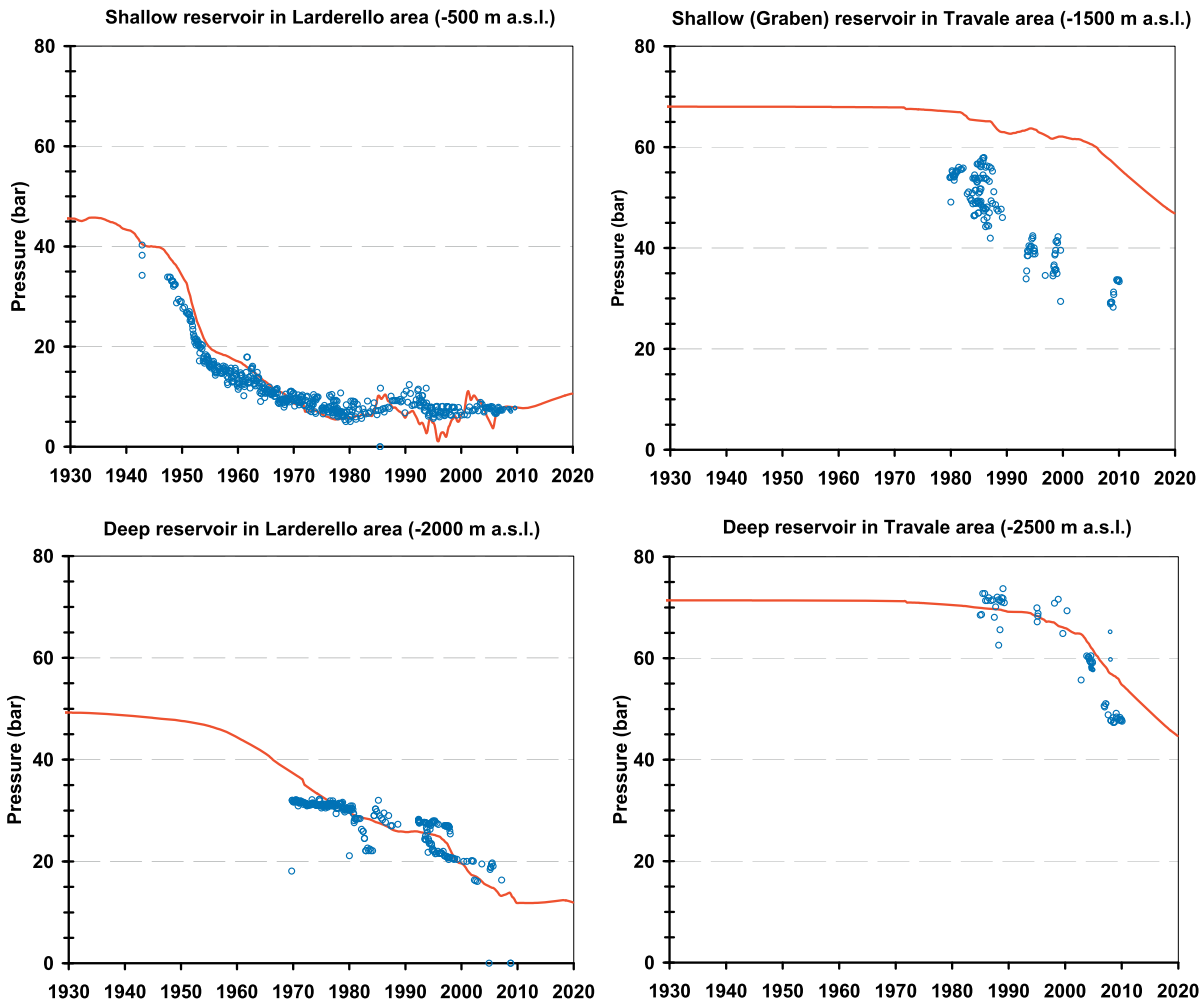

Fig. 23. Observed and simulated pressure decline in the Larderello and Travale reservoirs.

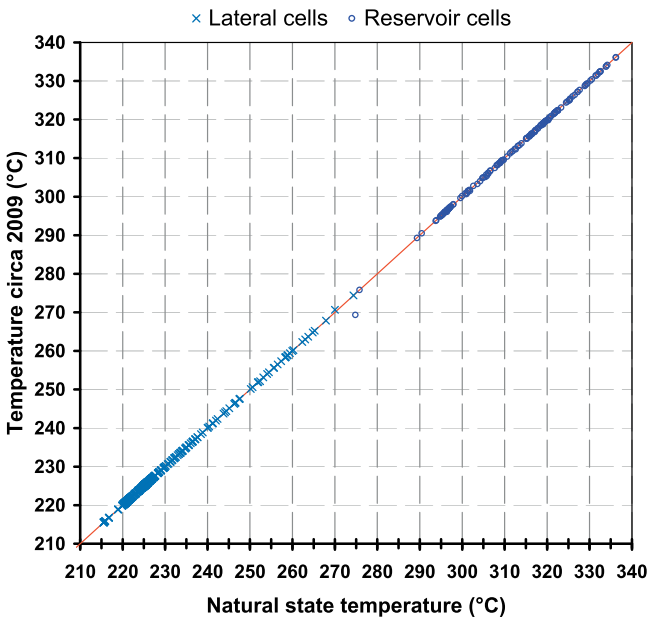

Fig. 24. Comparison between natural and present state temperature at 3000 m b.s.l.

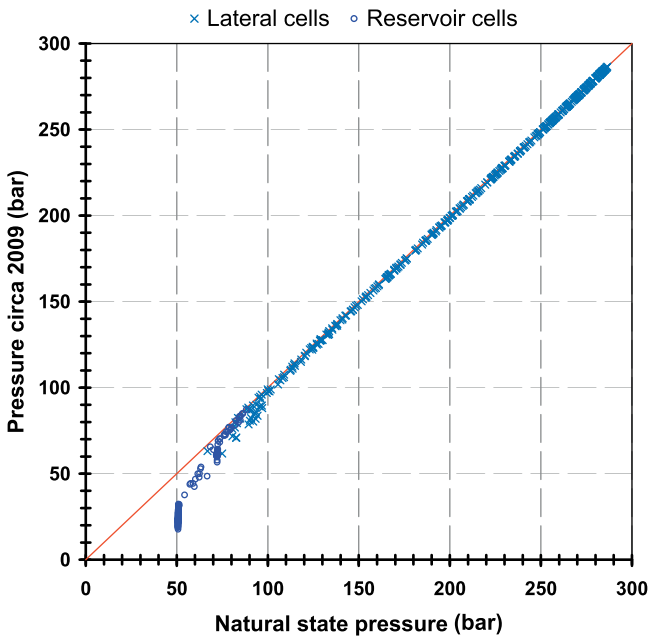

Fig. 25. Comparison between natural and present state pressure at 3000 m b.s.l.

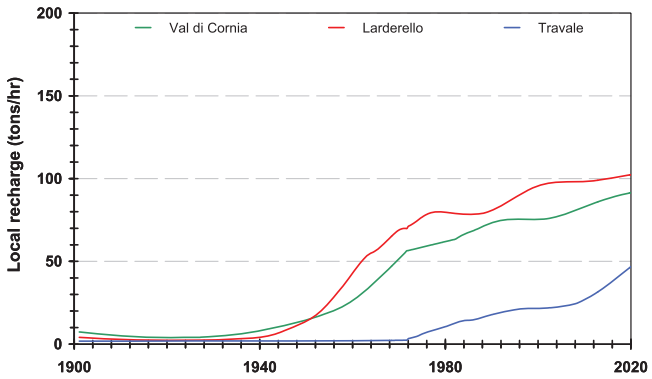

Fig. 26. Simulated system recharge from local influx.

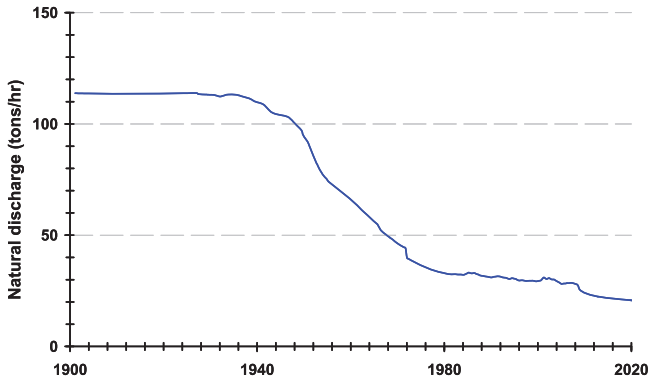

Fig. 27. Simulated total discharges from natural manifestations.

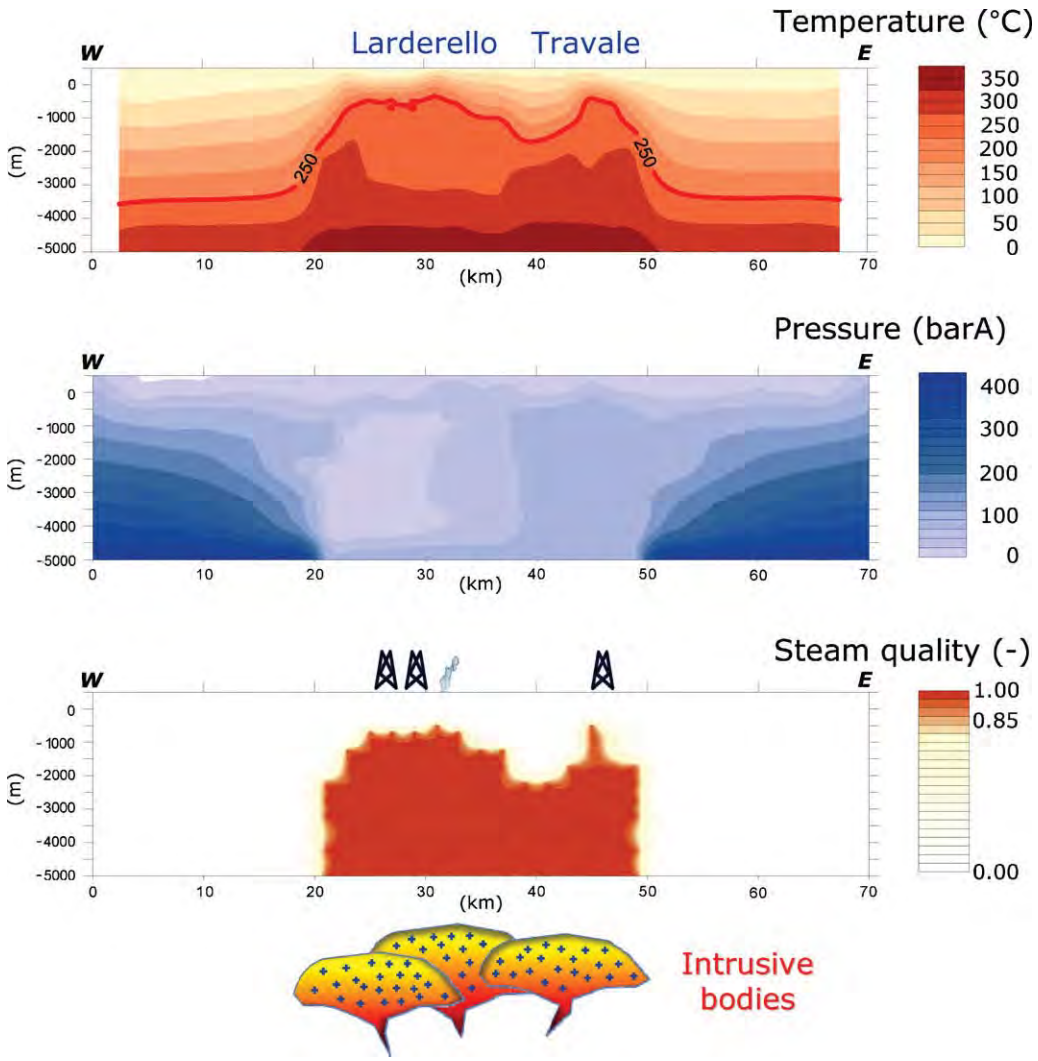

Fig. 28. Simulated temperature, pressure and steam quality distribution along a W–E section at the end of 2009.

7. Conclusions

Based on an updated analysis of all the available geoscientific data from the surface surveys and wells, a numerical model of the Larderello–Travale geothermal system has been developed. The main elements of this model can be summarized as followed:

- A low-permeability caprock consisting of Neogene and Flysch formations, and with thickness ranging from about 200 to 1000 m, overlies the geothermal reservoir.
- The productive geothermal reservoir comprises both carbonate-anhydrite and metamorphic formations. In the central part of the field the reservoir top was inferred from the first fractured level encountered in the wells, while in the peripheral areas, where well data are lacking, it was assumed to be coincident with the 250 °C isotherm which is the temperature at the top of the reservoir.
- The bottom of the geothermal system is taken to be coincident with the K-seismic horizon, since it could correspond to the 400 °C isotherm. A ductile/brittle transition at about 400 °C implies the lack of fracture permeability at greater depths. The depth of K-horizon varies from 8–10 km in the eastern sector of the geothermal system to 3–4 km in the western sector.

All of the above-mentioned elements, as well as the average formation density, porosity, and permeability values have been defined for an area of about 5000 km^2 centered around the geothermal system. Then, a simulation of the field evolution has been carried out for a time interval of about 3 Ma, starting from the emplacement of the magma bodies up to the present. The main results of the numerical modeling are:

- Computed temperature and pressure distributions for the natural state are in fairly good agreement with the observed values. The pressure evolution at different reservoir depths during the exploitation displays satisfactory agreement with the simulation results.
- No significant temperature variations are observed during exploitation, while pressure draw-down is observed in the central part of the geothermal system.
- Generally, the pressure in the surrounding deep aquifers is not affected by production; only a slight pressure decrease, caused by the evaporation of liquid water, is noticed at the interface with the steam dominated reservoir.
- The steam generated by evaporation in the surrounding deep aquifers provides most of the system recharge and explains the enormous productive capacity of the geothermal system; the recharge from local shallow inflows accounts for less than 10% of the total production flow rate.
- A conceptual model, that explains the origin of the steam extracted in almost 100 years of exploitation of the Larderello–Travale system, is for the first time supported by a numerical model. The conceptual model assumes the presence of a two-phase zone along the lateral boundaries between the geothermal reservoir and the surrounding regional water dominated aquifers. The vaporization of the water takes place in response to pressure drop and guarantees the main recharge of the reservoir.
- The numerical model was used to predict the future evolution of the Larderello–Travale geothermal system; the current level of production is sustainable for at least another 100 years. The regional dimensions of the model may limit the accuracy of predictions on a local scale, and more work is needed to refine the model for localized applications.

Current plans include, up-dating the model in the next 3–4 years. If the produced steam flow rate increases significantly, the CO_2 role can be evaluated by using EOS2 equations in the model.

Acknowledgements

We are grateful to our ex-colleague Adolfo Fiordelisi for his contributions, technical suggestions, and moral support in the preparation of the paper. We would also like to thank the ArcGis team (Paolo Dell'Aiuto and Loris Rossi) for the geologic and hydrogeologic images that appear in this paper.

References

Arias, A., Dini, I., Casini, M., Fiordelisi, A., Perticone, I., Dell'Aiuto, P., 2010. Geoscientific feature update of the Larderello–Travale geothermal system (Italy), for a regional numerical modelling. In: Proceedings World Geothermal Congress 2010, Bali, Indonesia, p. 11.

Baldi, P., Bellani, S., Ceccarelli, A., Fiordelisi, A., Rocchi, G., Squarci, P., Taffi, L., 1995. Geothermal anomalies and structural features of southern Tuscany (Italy). In: Proceedings World Geothermal Congress 1995, Florence, Italy, pp. 1287–1291.

Barelli, A., Bertani, R., Cappetti, G., Ceccarelli, A., 1995a. An update on Travale – Radicondoli geothermal field. In: Proceedings World Geothermal Congress 1995, Florence, Italy, pp. 1581–1586.

Barelli, A., Cappetti, G., Stefani, G., 1995b. Optimum exploitation strategy at Larderello-Valle Secolo. In: Proceedings World Geothermal Congress 1995, Florence, Italy, pp. 1779–1783.

Barelli, A., Cappetti, G., Stefani, G., 1995c. Results of deep drilling in the Larderello–Travale/Radicondoli geothermal area. In: Proceedings World Geothermal Congress 1995, Florence, Italy, pp. 1275–1278.

Barelli, A., Bertini, G., Buonasorte, G., Cappetti, G., Fiordelisi, A., 2000. Recent deep exploration results at the margins of the Larderello–Travale geothermal system. In: Proceedings World Geothermal Congress 2000, Kyushu-Tohoku, Japan, pp. 965–970.

Barelli, A., Cei, M., Lovari, F., Romagnoli, P., 2010. Numerical modeling for the Larderello–Travale Geothermal System (Italy). In: Proceedings World Geothermal Congress 2010, Bali, Indonesia, p. 9.

Batini, F., Bertini, G., Gianelli, G., Pandeli, E., Puxeddu, M., 1983. Deep structure of the Larderello field: contribution from recent geophysical and geological data. Memorie della Societa Geologica Italiana 25, 219–235.

Batini, F., Brogi, A., Lazzarotto, A., Liotta, D., Pandeli, E., 2003. Geological features of the Larderello–Travale and Mt. Amiata geothermal areas (southern Tuscany, Italy). Episodes 26, 239–244.

Bertani, R., Cappetti, G., 1995. Numerical simulation of the Monteverdi zone (western border of the Larderello geothermal field). In: Proceedings World Geothermal Congress 1995, Florence, Italy, pp. 1735–1740.

Bertani, R., Bertini, G., Cappetti, G., Fiordelisi, A., Marocco, B.M., 2005. An update of the Larderello–Travale/Radicondoli deep geothermal system. In: Proceedings World Geothermal Congress 2005, Antalya, Turkey, p. 6.

Bertani, R., 2005. World Geothermal power generation in the period 2001–2005. Geothermics 34, 651–690.

Bertini, G., Casini, M., Gianelli, G., Pandeli, E., 2006. Geological Structure of a Long-living Geothermal System, vol. 18. Terra Nova, Larderello, Italy, pp. 163–169.

Brogi, A., Lazzarotto, A., Liotta, D., 2005. Results of the CROP 18 project. Bollettino della Societa Geologica Italiana 3, 236, Special Issue.

Calore, C., Celati, R., D'Amore, F., Noto, P., 1982. Geochemical evidence of natural recharge in Larderello and Castelnuovo areas. In: Proceedings 8th Workshop Geothermal Reservoir Engineering, Stanford University, Stanford, CA, USA, pp. 323–328.

Cappetti, G., Fiordelisi, A., Casini, M., Ciuffi, S., Mazzotti, A., 2005. A new deep exploration program and preliminary results of a 3D seismic survey in the Larderello–Travale geothermal field (Italy). In: Proceedings World Geothermal Congress 2005, Antalya, Turkey, p. 8.

Cappetti, G., Parisi, L., Ridolfi, A., Stefani, G., 1995. Fifteen years of reinjection in the Larderello-Valle Secolo area: analysis of the production data. In: Proceedings World Geothermal Congress 1995, Florence, Italy, pp. 1997–2000.

Cappetti, G., Romagnoli, P., Sabatelli, F., 2010. Geothermal power generation in Italy 2005–2009 update report. In: Proceedings World Geothermal Congress 2010, Bali, Indonesia, p. 8.

Carminati, E., Doglioni, C., 2004. Europe – Mediterranean Tectonics. Encyclopedia of Geology. Elsevier, pp. 135–146.

Cataldi, R., Lazzarotto, A., Muffler, P., Squarci, P., Stefani, G., 1978. Assessment of geothermal potential of central and southern Tuscany. Geothermics 7, 91–131.

Ceccarelli, A., Celati, R., Grassi, S., Minissale, A., Ridolfi, A., 1987. The southern boundary of Larderello Geothermal field. Geothermics 16, 505–515.

Celati, R., Squarci, P., Taffi, L., Stefani, G.C., 1975. Analysis of water levels and reservoir pressure measurement in geothermal wells. In: Proceedings 2nd U.N. Symposium on the Development and Use of Geothermal Resources, San Francisco, CA, USA, pp. 1583–1590.

Duchi, V., Minissale, A., Manganelli, M., 1992. Chemical composition of natural deep and shallow hydrothermal fluids in the Larderello geothermal field. Journal of Volcanology and Geothermal Research 49, 313–328.

Gianelli, G., Manzella, A., Puxeddu, M., 1997. Crustal models of the geothermal areas of southern Tuscany (Italy). Tectonophysics 281, 221–239.
Giannini, F., Lazzarotto, A., Signorini, R., 1971. Carta geologica della Toscana Meridionale, scale 1:200.000, Annex of "La Toscana meridionale, fondamenti geologico-minerari per una prospettiva di valorizzazione delle risorse naturali". Rendiconti della Società Italiana di Mineralogia e Petrologia, XXVII.
Pruess, K., Oldenburg, C., Moridis, G., 1999. TOUGH2-User's Guide, Version 2.0, Report LBNL-43134. Lawrence Berkeley Laboratory, Berkeley, CA, USA, p. 198.

RETE GEOTERMICA TOSCANA

C/O TOSCOGEO S.R.L.
VIA ERNESTO ROSSI N° 9 - 52100, AREZZO
TEL. 0575 32641 - FAX. 0575 326464

TOSCOGEO
geothermal energy
Società del gruppo GRAZIELLA green power

magma ENERGY ITALIA

Permesso di ricerca di fluidi geotermici finalizzato alla sperimentazione di impianto pilota "Castelnuovo" (Regione Toscana)

MODELLISTICA DI SERBATOIO

ADDENDUM AL PROGRAMMA DEI LAVORI REV. 1 –OTTOBRE 2015

PREPARATO DA:
magma ENERGY ITALIA

Distribuzione: M.I.S.E.

Rev.	*Data*	*Oggetto*	*Autore*	*Emissione*
02				
01				
00	19.11.2015	Emissione	Magma Energy	F.Batini

INDICE

1. La modellistica di serbatoio

Con un lavoro svolto congiuntamente tra Magma Energy Italia e Schlumberger-Geothermex è stato costruito e calibrato sulla base dei dati esistenti un modello geotermico di serbatoio per l'area di Castelnuovo, sul quale sono state svolte simulazioni volte a valutare la fattibilità di un impianto geotermoelettrico binario. Questa attività è stata eseguita grazie al simulatore TETRAD (ADA International Consulting Ltd.), ampiamente utilizzato per l'analisi termofluidodinamica 3D multifase e multicomponente di serbatoi geotermici e petroliferi (Menzies e Pham 1995, Butler *et al.* 2000) Esso modella flussi di calore e massa attraverso mezzi porosi e fratturati, nell'ultimo caso le fratture possono essere specificate attraverso l'opzione "dual porosity".

Nei modelli a doppia porosità ogni blocco di base è ulteriormente suddiviso in una frattura e un blocco di matrice. Le fratture sono interconnesse tra loro, mentre il blocco di matrice è connesso alla frattura adiacente. In base a tale disposizione, i fluidi geotermici si muovono principalmente attraverso la rete di fratture interconnesse, mentre la matrice agisce come stoccaggio di fluido. Le equazioni differenziali di conservazione della massa e dell'energia vengono discretizzate nella loro forma integrale con uno schema alle differenze finite, mentre i flussi sono espressi attraverso la legge di Darcy nella versione multifase e multicomponente.

2. Il modello iniziale

Per lo sviluppo del modello di serbatoio Geothermex ha fatto riferimento a informazioni geofisiche e petrofisiche presenti nella letteratura scientifica, ai dati pubblicati sui pozzi esistenti nel campo confinante di Larderello e al modello geologico del serbatoio realizzato da Magma Energy Italia.

Il modello geologico è il risultato dell'integrazione dei rilievi di campagna con i dati geofisici dell'analisi magnetometrica, magnetotellurica e gravimetrica condotti da Magma Energy e relativi al dominio spaziale di calcolo considerato.

Per la calibrazione del modello Geothermex si è servita delle isoterme estrapolate da Magma Energy su dati pubblici relativi a misure di temperatura da pozzetti di gradiente e da pozzi profondi esistenti dell'area geotermica "tradizionale".

Il modello sviluppato da Geothermex copre un'area di 9,5 x 13 km; l'ampiezza della superficie oggetto della simulazione è stata scelta per rappresentare il quadro geologico generale e per ridurre l'impatto dei possibili effetti di bordo sui risultati del modello. Il modello geometrico si estende in direzione verticale fino a una profondità massima di circa 7000 m, ed è suddiviso in 18 strati di vario spessore .Ogni strato del modello è suddiviso a sua volta in 28x21 celle. La suddivisione è stata realizzata in modo tale da avere una discretizzazione più dettagliata del reservoir principale e della zona di produzione, dove le celle hanno dimensioni di 200m x 200m x 300m. La griglia di base si compone di 10594 celle, ma il numero è incrementato dall'utilizzo della formulazione dual porosity fino a un valore complessivo di 21168 blocchi, dando origine a un modello elaborato che richiede sforzi computazionali notevoli per ogni simulazione. La base del modello è definita dal top dell'orizzonte K ottenuto da articoli e da dati sismici pubblicati relativamente alla zona di interesse.

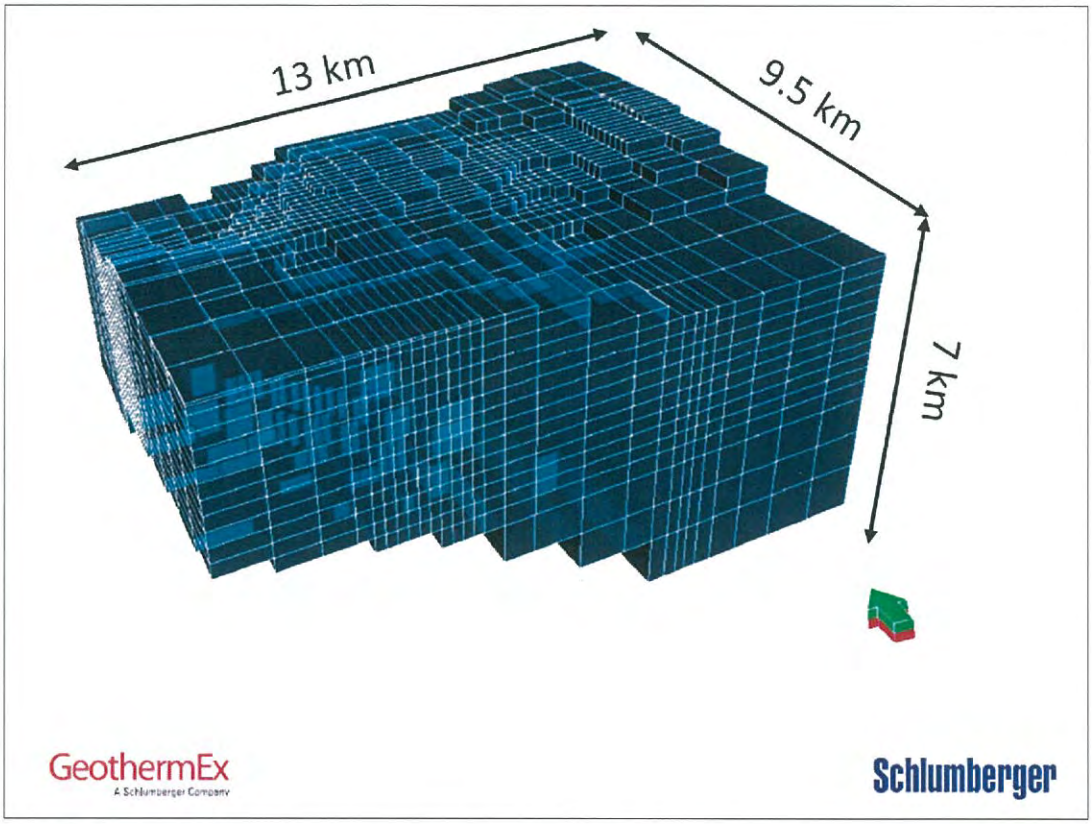

Fig. 1 - Vista prospettica del modello tridimensionale e della griglia di simulazione numerica

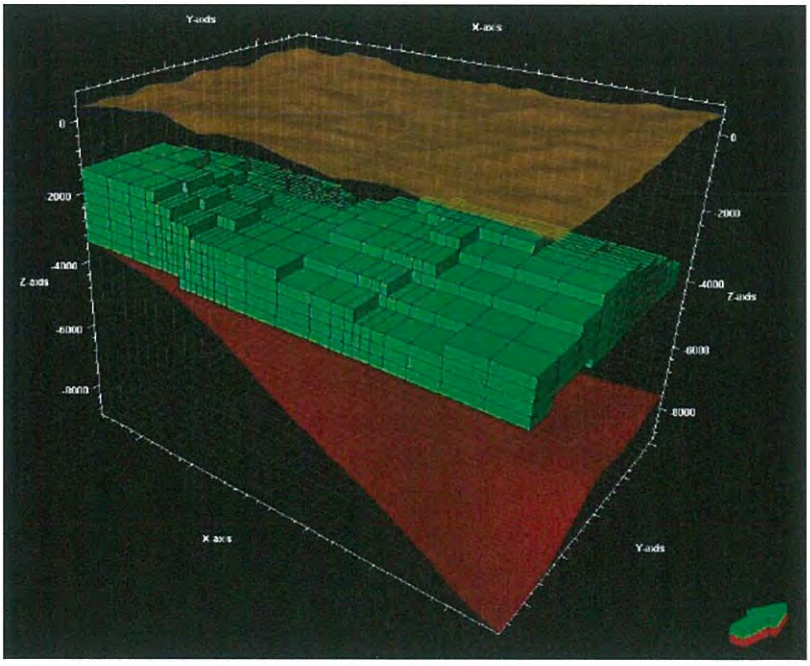

Fig. 2 - In verde le celle che rappresentano l'orizzonte produttivo. Come riferimenti sono indicate la superficie e il top dell'orizzonte K

3. Il modello imperturbato

Una volta definito il layout della griglia di simulazione, la prima parte della simulazione è stata incentrata sulla riproduzione delle condizioni termodinamiche del modello imperturbato, che rappresenta il punto di partenza per le simulazioni successive.

Le principali fasi per la realizzazione del modello iniziale imperturbato sono state le seguenti:

1. Matching della distribuzione delle temperature iniziali, ottenute dall'interpolazione di dati dei pozzi geotermici esistenti nelle zone circostanti l'area di studio;
2. Matching della distribuzione delle pressioni, ottenute attraverso l'interpolazione di dati dei pozzi geotermici esistenti nelle zone circostanti l'area di studio;
3. Perturbazione del campo indisturbato con l'introduzione della storia produttiva dei pozzi circostanti;
4. Ricostruzione della saturazione in gas incondensabili in serbatoio.

Le condizioni al contorno del modello sono state definite come segue:

- Diffusione del calore per conduzione;
- Ricarica del fluido geotermico dalla base del modello (150 t/h a 350°C)
- Dual-Porosity;
- Permeabilità fratture: 18 mD;
- Permeabilità matrice: 0,01mD;
- Porosità: 3%

Mediante simulazioni eseguite su scala temporale di 200.000 anni il modello imperturbato raggiunge condizioni stazionarie, tali da garantire che l'evoluzione della pressione e della temperatura in serbatoio siano trascurabili rispetto ai cambiamenti indotti dalla coltivazione (decine di anni).

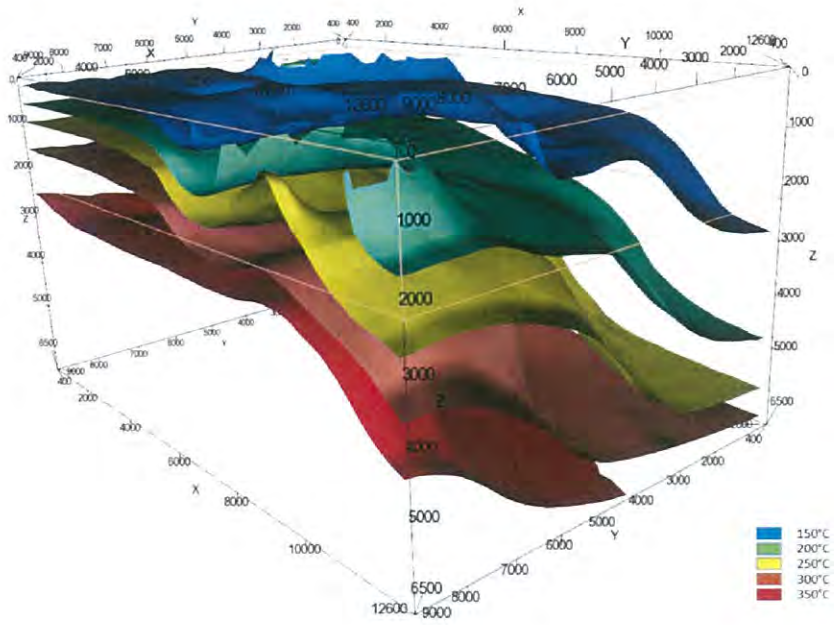

Fig. 3 – Distribuzione iniziale di temperatura

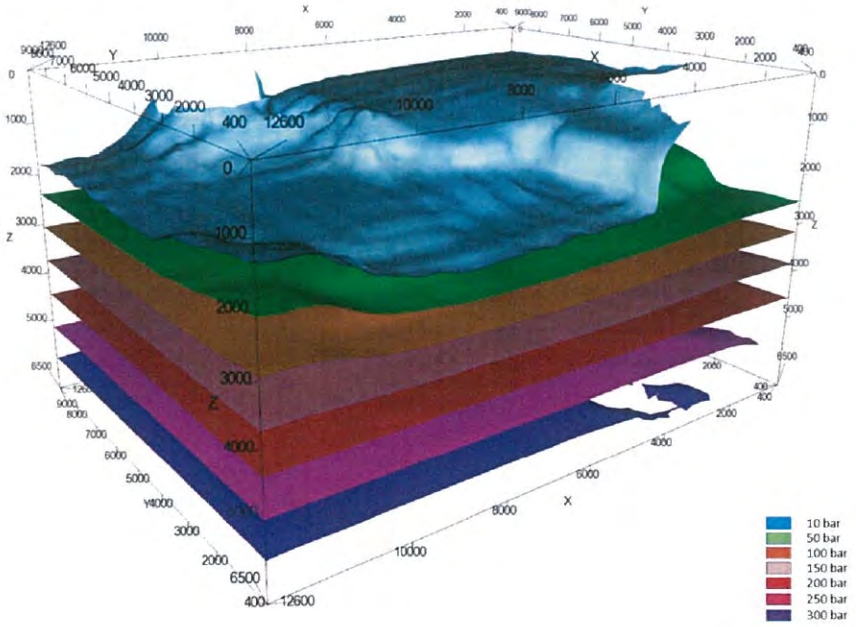

Fig. 4 – Distribuzione iniziale di pressione

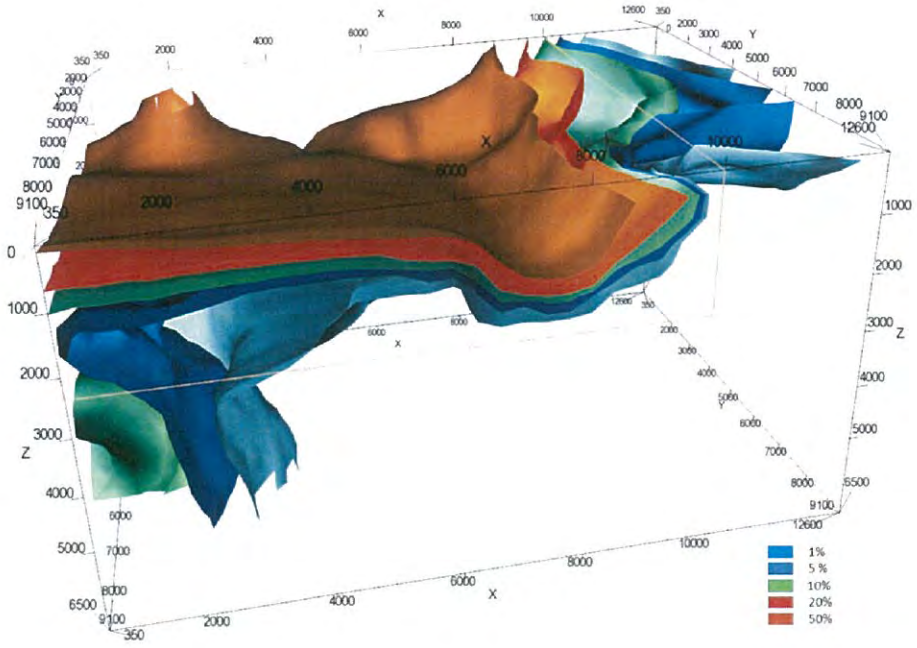

Fig. 5 – Distribuzione iniziale della saturazione in Gas Incondensabili (NCGs)

4. Simulazioni di coltivazione

Il risultato dello stato stazionario rappresenta il punto di partenza per un'analisi più specifica del serbatoio, valutando la risposta del sistema alla coltivazione in termini di abbassamento della temperatura e della pressione su un periodo di 30 anni, che coincide con la vita utile di un impianto geotermico.

Al modello sono stati pertanto aggiunti i pozzi di estrazione e reiniezione previsti dal progetto, per valutare la sostenibilità dello stesso.

Per la simulazione della coltivazione del campo si sono considerati due pozzi di estrazione e un pozzo per la reiniezione totale del fluido. Al fine di simulare i pozzi di estrazione sono state considerate come vincoli le seguenti condizioni a boccapozzo: pressione minima = 15 bar; portata totale del campo pozzi = 70 t/h. Per il pozzo di reiniezione è stato considerato di reimmettere la stessa portata estratta ad una temperatura di 90 °C.

Il progetto pilota prevede di reimmettere il condensato insieme ai gas incondensabili presenti nel fluido geotermico e il modello di coltivazione simula il comportamento e la propagazione dei gas nel serbatoio.

Tutti i pozzi sono posizionati nella stessa postazione di perforazione (Fig. 6). Il primo produttore (CAS-P1) è ipotizzato verticale; il secondo produttore CAS-P2 è ipotizzato deviato verso sud ovest, con uno scostamento dalla verticale a fondo pozzo di 800 m; Il pozzo di reiniezione è deviato a nord-ovest e ha uno scostamento di 1000 m dalla verticale. I pozzi saranno in Open Hole tra 2200 e circa 3500 m, profondità che interseca la zona dove è maggiore la probabilità di incontrare le fratture produttive nella formazione metamorfica.

Le simulazioni hanno evidenziato come, mantenendo una distanza di almeno 1000 m tra il pozzo di reiniezione e i pozzi di produzione, non si verifichino sui produttori interferenze significative sia per le variazioni di pressione e temperatura che in termini di aumento di concentrazione dei gas incondensabili. Pertanto con tale geometria il sistema di reiniezione totale non comporta ritorno di gas ai pozzi di produzione, né influenza negativamente la capacità produttiva dei pozzi estrattori.

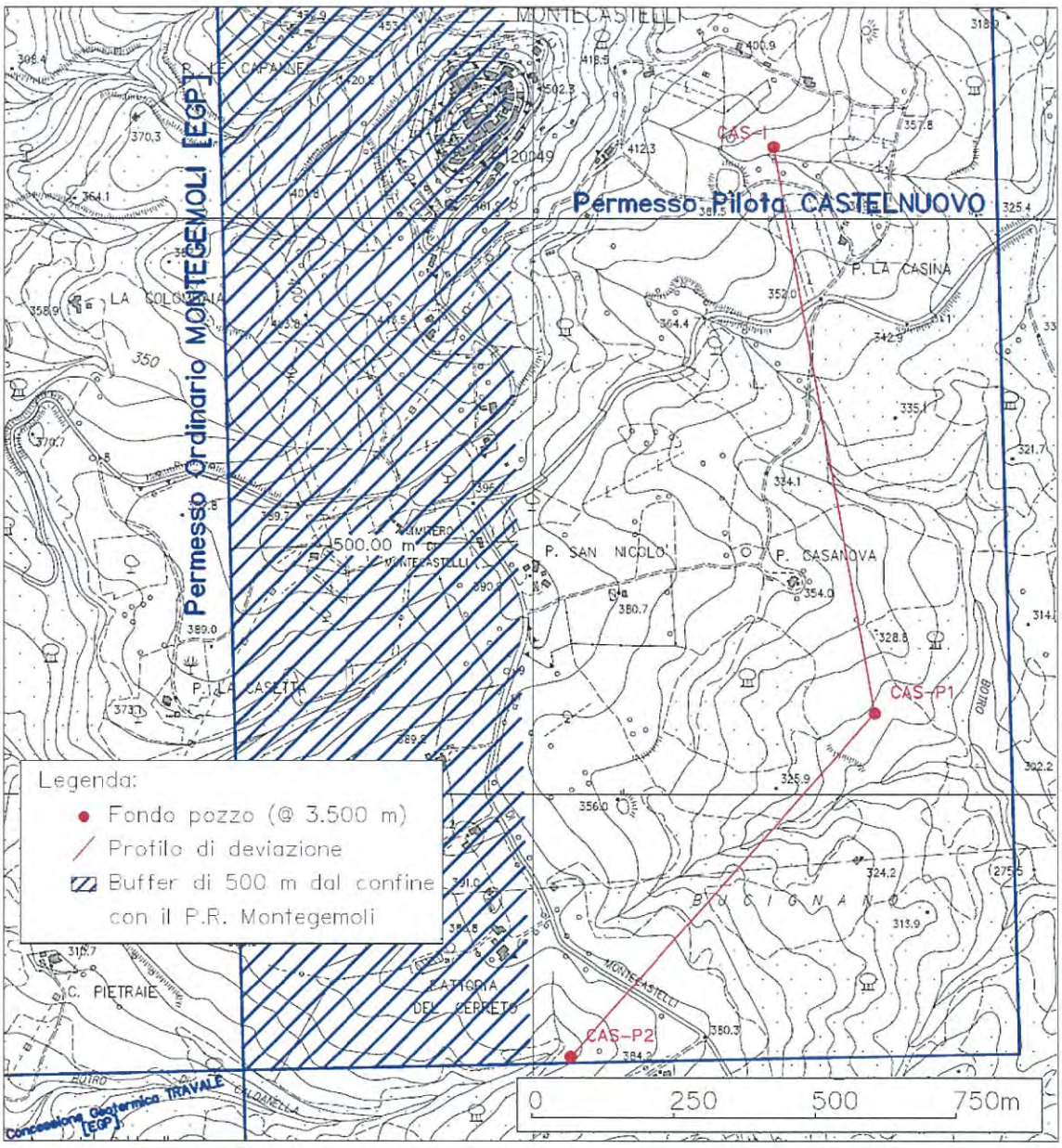

Fig. 6 - Localizzazione del fondo pozzo per i pozzi del permesso pilota "Castelnuovo". Si precisa che il limite sud del permesso confina con il Permesso di Ricerca "Mensano" di cui è titolare Magma Energy Italia, che ha già assentito alla deroga sulla distanza di rispetto.

5. Risultati delle simulazioni di produzione e reiniezione

Le simulazioni eseguite sul modello dimostrano come il serbatoio sia in grado di sostenere l'estrazione e la reiniezione di 70 t/h di fluido geotermico, in condizioni tali da sostenere la piena operatività dell'impianto per tutta la sua vita utile, garantendo livelli di temperatura e pressione superiori a quelli minimi di progetto.

I risultati delle simulazioni a 30 anni evidenziano una variazione finale di temperatura ai produttori non superiore a –8°C (Fig. 7) e una variazione di pressione inferiore a –6 bar (Fig. 8).

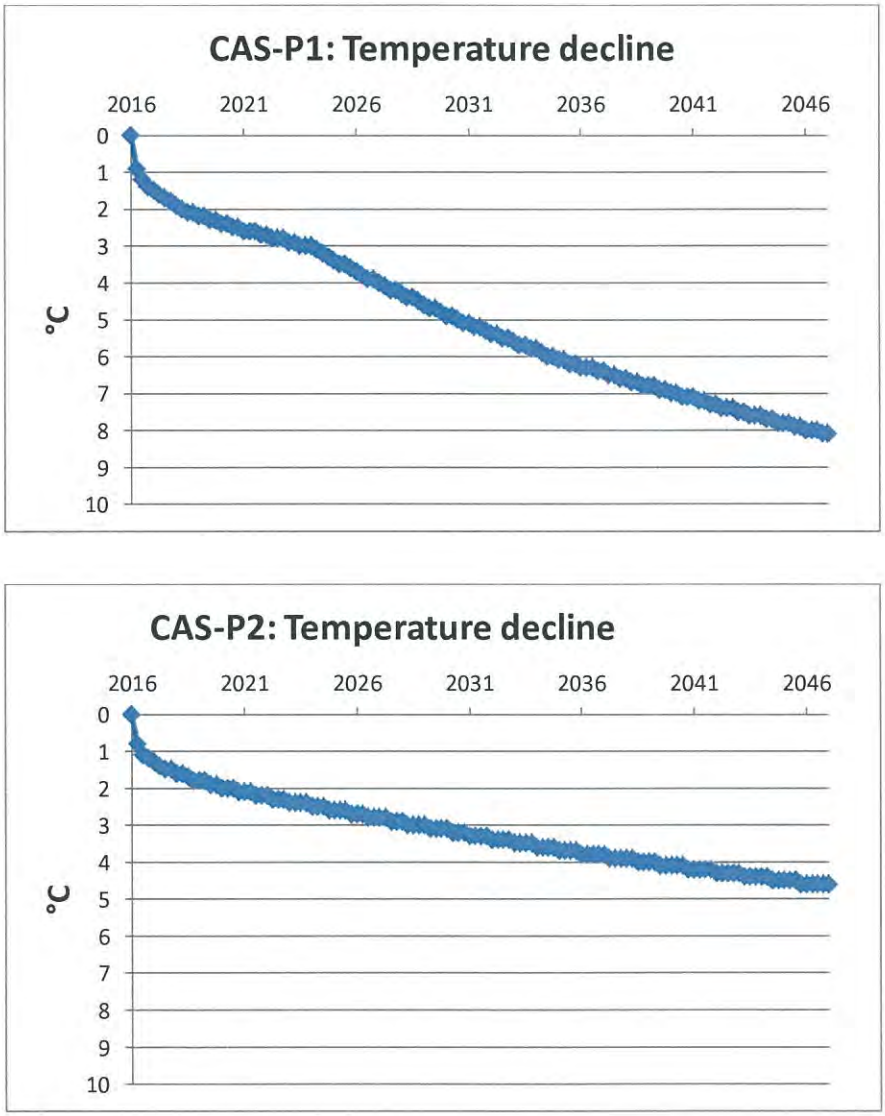

Fig. 7 – Variazione di temperatura in serbatoio nei due pozzi di produzione

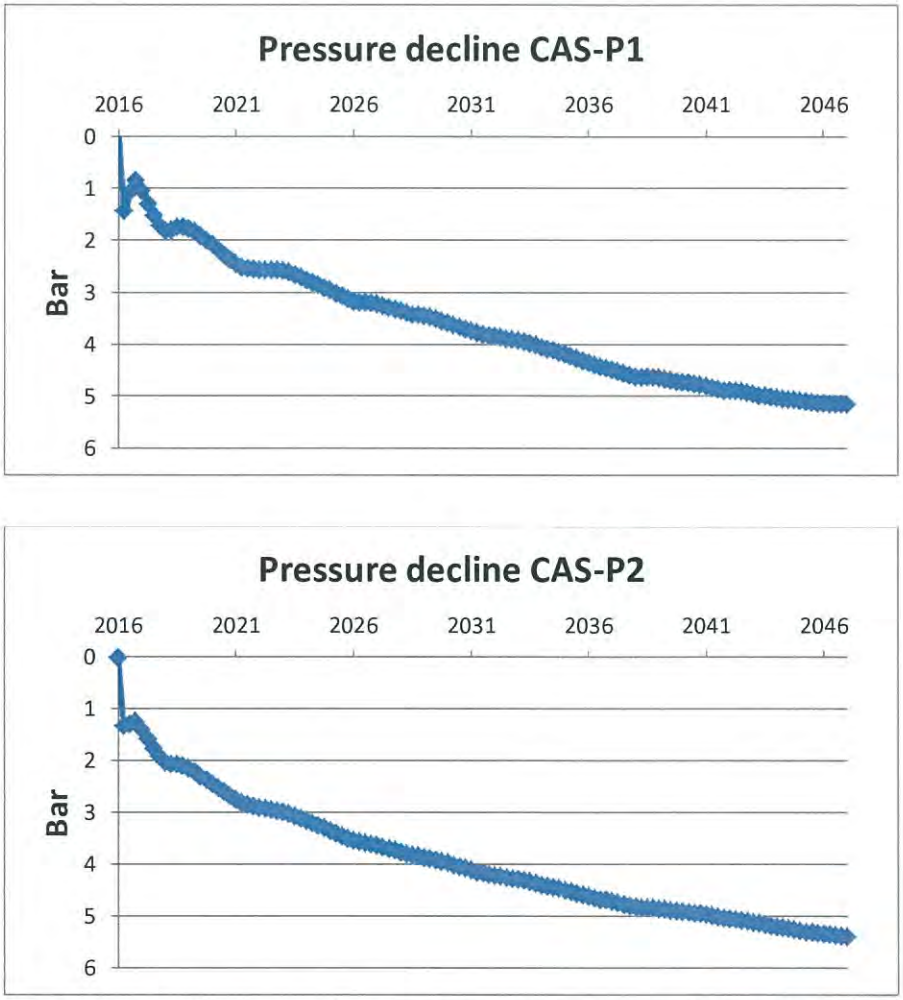

Fig. 8 - Variazione di pressione nelle celle del serbatoio attraversate dai pozzi di produzione

Le simulazioni hanno fornito anche l'andamento della variazione del campo di pressione in serbatoio nel tempo. I due pozzi di produzione si trovano ad una distanza alla quale la variazione di pressione risultante non genera una interferenza reciproca tale da alterare la capacità produttiva richiesta ai singoli pozzi.

Dalle simulazioni appare (Fig. 9, Fig. 11, Fig. 12) come la reiniezione non comporti alcun effetto di disturbo sui pozzi produttivi, né per quanto riguarda l'eventuale propogazione di un "fronte freddo" dal reiniettore ai produttori, né per un' eventuale propagazione del *plume* dei gas incondensabili reiniettati; in particolare, questi ultimi rimangono confinati nella zona del pozzo reiniettore senza raggiungere i pozzi produttori e quindi senza influenzare la composizione del fluido estratto.

Il pozzo di reiniezione ha un effetto in serbatoio opposto, in termini di pressione, a quello dei pozzi di produzione, in quanto l'ingresso di fluidi in serbatoio non può avvenire se questi non hanno una pressione più elevata della pressione di strato, generando quindi una variazione di pressione che viene dissipata nel serbatoio in funzione delle sue

caratteristiche di trasmissività. La simulazione di serbatoio ha permesso di calcolare tale variazione di pressione, ottenuta per un periodo di reiniezione di 30 anni; questa si attesta attorno a +15 bar, con un raggio di influenza di circa 200 m attorno al pozzo (Fig. 10, Fig. 12). In relazione alla distanza dai pozzi di produzione, a 1000 m dal reiniettore risulta un contributo alla variazione di pressione dell'ordine di +1bar, quindi non significativa.

La temperatura nell'immediato intorno del pozzo di reiniezione si abbassa, in 30 anni di esercizio, da 244°C a 177°C. Il fronte corrispondente ad una variazione termica di –10°C indotta nel serbatoio rimane confinato in un raggio di circa 300 m attorno al reiniettore e non raggiunge mai i pozzi di produzione.

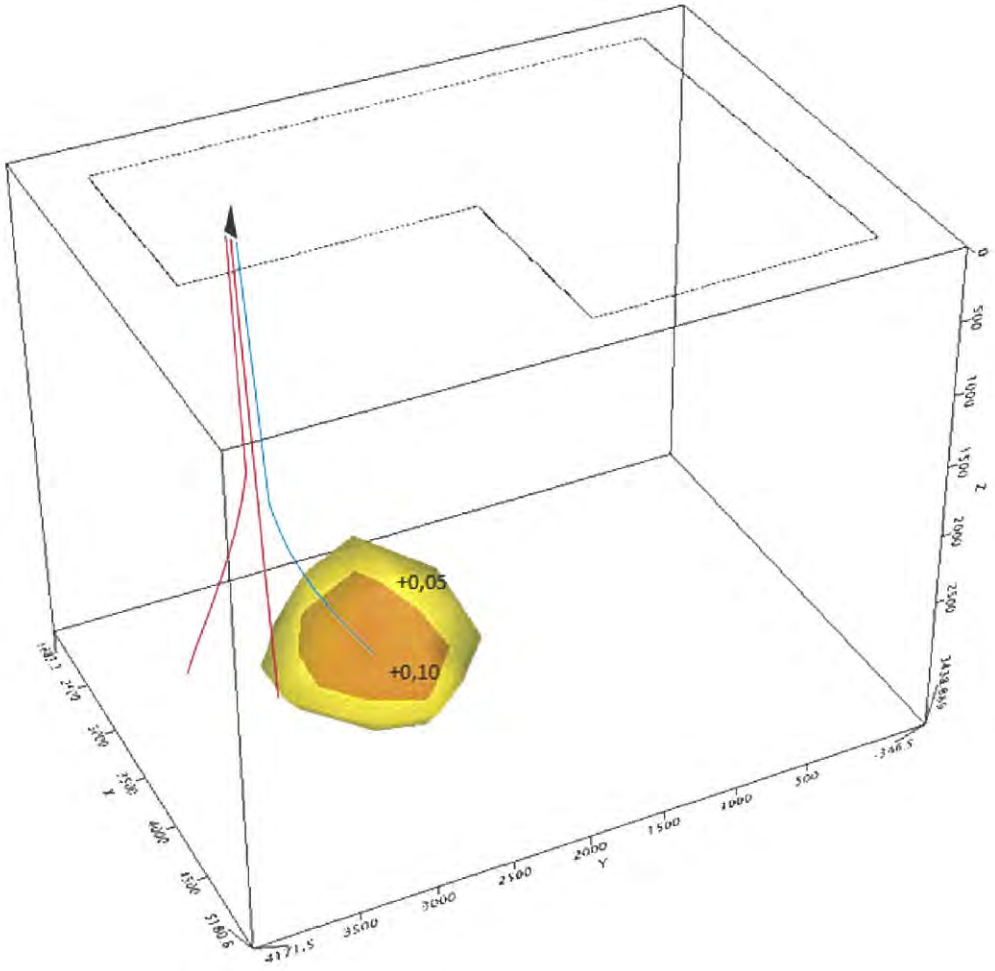

Fig. 9 - Propagazione del plume di NGC nell'intorno del reiniettore CAS-I (differenza nella frazione di massa post e pre sfruttamento). Simulazione a 30 anni.

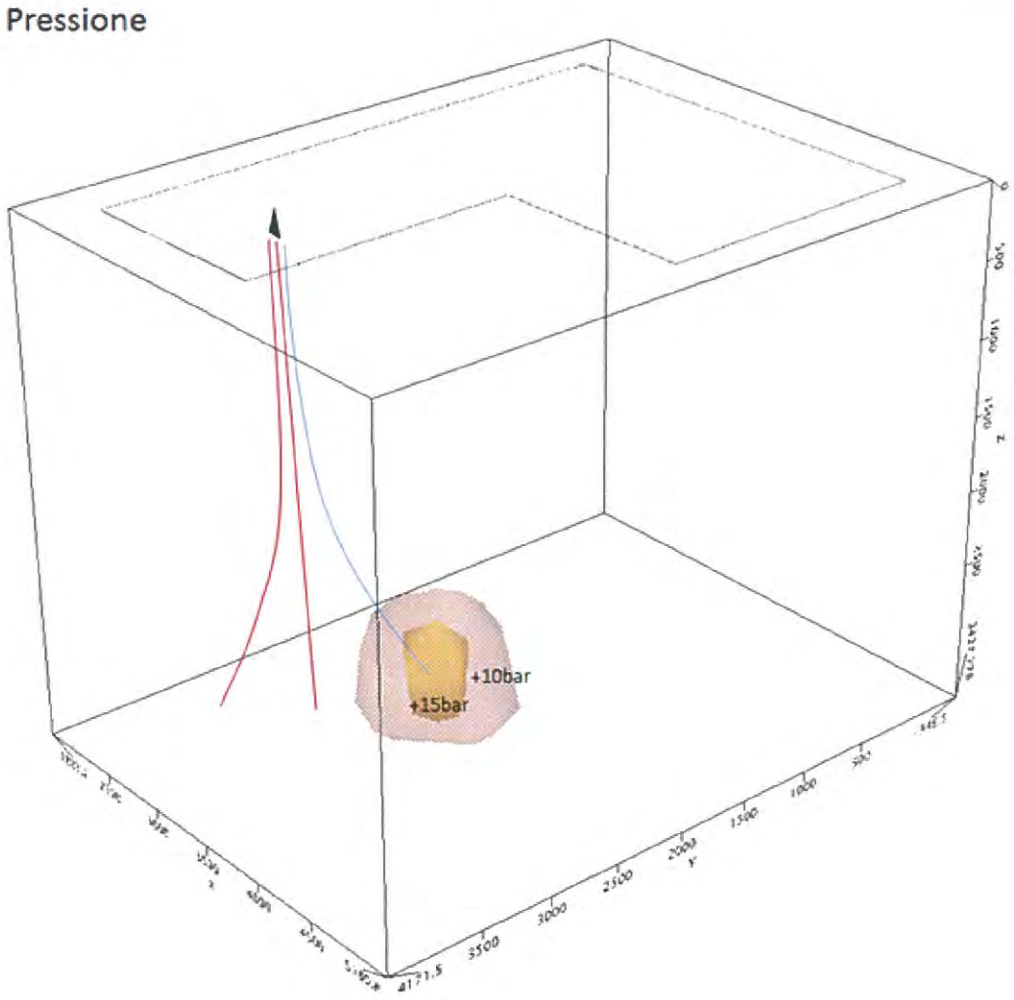

Fig. 10 Perturbazione del campo di pressione al reiniettore CAS-I. Simulazione a 30 anni.

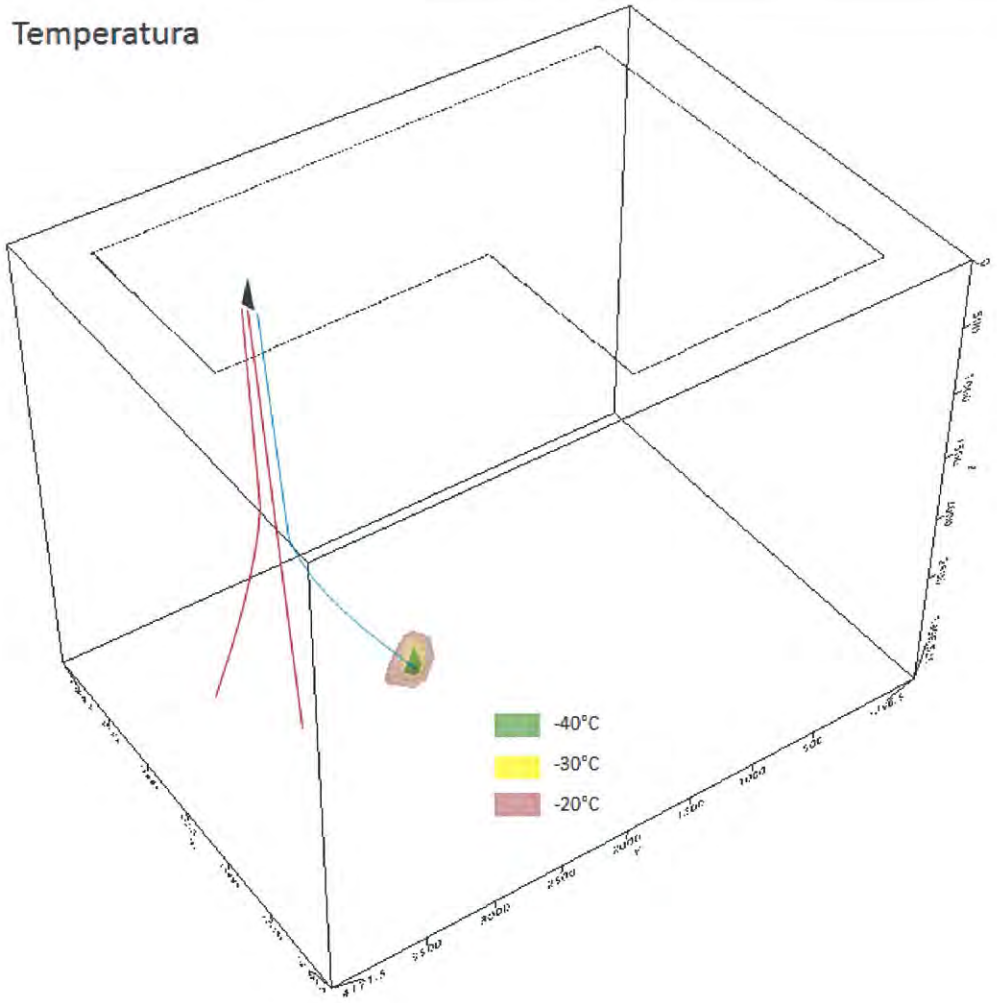

Fig. 11 - Perturbazione termica indotta dal CAS-I. Simulazione a 30 anni.

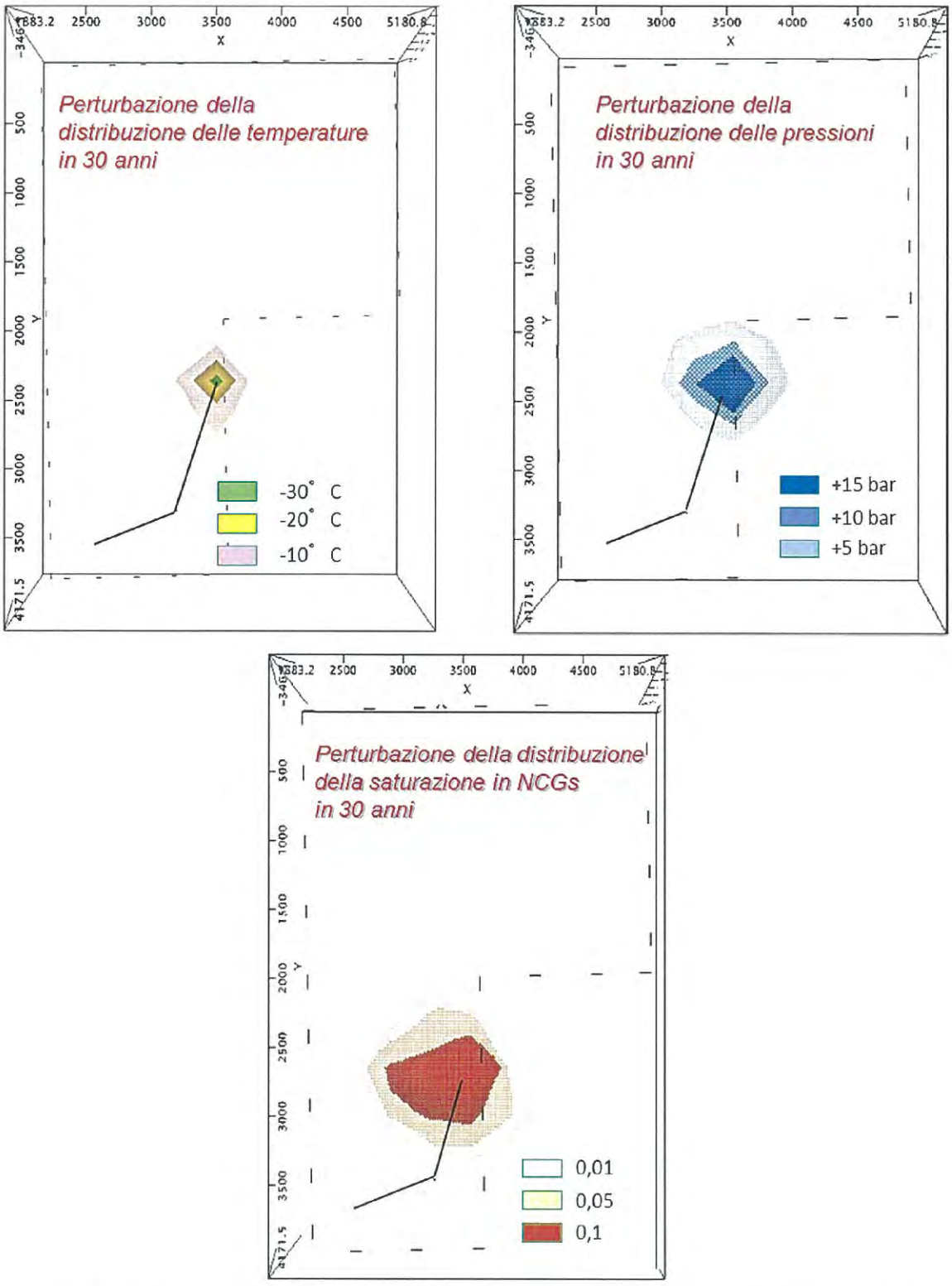

Fig. 12 - Perturbazione termica, di pressione e di saturazione in NCG indotta dal CAS-I, vista sul piano di –3000 m in serbatoio. Simulazione a 30 anni.

6. Sistema di reiniezione totale (condensato e NCGs)

A differenza delle operazioni svolte sinora nelle aree geotermiche Toscane, dove viene reiniettata soltanto la frazione condensata dei fluidi estratti, uno degli obiettivi del progetto pilota Castelnuovo è la reiniezione di tutto il fluido estratto dal serbatoio, previa condensazione, nonché dei gas incondensabili.

Nell'ottica di minimizzare il numero dei pozzi, è stata analizzata la fattibilità di uno schema di reiniezione che prevede l'utilizzo di un unico pozzo di reiniezione, nel quale i due fluidi (condensato e gas incondensabili) vengono immessi attraverso due tubazioni concentriche calate in pozzo e fluiscono parallelamente e separati fino ad una certa profondità alla quale si miscelano e scendono in un'unica corrente.

Allo scopo è stata realizzata una simulazione numerica del pozzo reiniettore in collaborazione con Schlumberger-Geothermex, utilizzando il software modellazione di flussi dinamici multifase OLGA®, in grado di modellare l'iniezione di gas incondensabili (prevalentemente anidride carbonica, al 98%) nella corrente liquida. In particolare è stata usata la versione di OLGA "Compositional Tracking", con la quale le proprietà dei fluidi sono calcolate usando la composizione chimica locale istantanea. L'analisi è stata condotta valutando l'impatto di alcune variabili sul sistema, tra cui la profondità di mixing per le due correnti fluide. Sono state valutate le pressioni necessarie a bocca-pozzo per l'iniezione dei fluidi per profondità di mixing comprese tra 0 m e 1250 m MD (Measured Depth).

L'iniezione in serbatoio di una miscela fluida è ipotizzata in corrispondenza di una singola frattura (o livello di assorbimento) ad una profondità di 3000 m TVD. A questo livello è stata assunta una temperatura del serbatoio pari a 250°C e una pressione statica pari a 85 bar.a. Il gradiente di temperatura circostante è stato assunto variabile linearmente da 20°C a 0 m TVD fino a 250°C a 3000 m.

La pressione di iniezione necessaria all'ingresso in frattura è superiore alla pressione statica del serbatoio, in funzione delle condizioni di iniettività. Questa resistenza all'iniezione è stata considerata simulando alcune iniettività di serbatoio, come rappresentate nella Tabella 1:

Tabella 1 – Scenari di iniettività considerati

		kg/Pa-s
Low Estimate for injectivity (ton/hr/bar)	0.36	1.000E-06
Nearby Measured Injectivity (ton/hr/bar)	1.78	4.944E-06
High Estimate for injectivity (ton/hr/bar)	8.90	2.472E-05

B[kg/Pa-s] = B [ton/hr-bar] *(1000/(3600*1.0e+05))

La composizione del flusso di gas incondensabili è stata assunta come segue (Tabella 2):

Tabella 2 – Composizione dei NCG

CO2	97.50%	
H2S	2%	
Other	0.50%	% of "Other"
NH3	0.0451%	9.03%
Ar	0.0003%	0.06%
N2	0.0340%	6.79%
CH4	0.1925%	38.50%
H2	0.2281%	45.62%

In generale si assiste a una maggiore spesa energetica per la compressione del gas abbassando il punto di mixing in pozzo e, al contrario, un aumento della potenza richiesta per comprimere il condensato se il punto si alza verso la superficie. Nell'intervallo di profondità che risulta più favorevole per unire le due correnti è possibile reiniettare il condensato a pressione pressochè atmosferica e i gas a pressioni inferiori a 60 bar a boccapozzo.

Dai risultati del modello (vedi par. 6.1), la reiniezione attraverso un solo pozzo appare sempre fattibile, avendo l'accortezza di gestire le fasi transitorie in modo opportuno, ad esempio durante le operazioni messa in esercizio dell'impianto è consigliabile avviare l'iniezione del condensato prima di quella dei gas, in modo da consentire all'acqua di raggiungere una velocità tale da trasportare i gas verso il basso e consentire il loro ingresso in serbatoio. In nessuno degli scenari simulati si è assistito ad un ritorno dei gas in superficie, né ad un accumulo sotto il punto di mixing.

6.1. Simulazione della reiniezione in pozzo

Il gruppo di modellazione di Schlumberger Integrated Solutions (SIS), sotto il coordinamento di GeothermEx, ha modellato con successo il sistema di iniezione proposto per l'impianto geotermico pilota "Castelnuovo". Il modello del sistema, che è stato sviluppato utilizzando il software di simulazione OLGA, è stato in grado di modellare con accuratezza l'iniezione in pozzo di Gas Non Condensabili (NCGs), costituiti principalmente da CO_2, nel flusso dell'acqua di iniezione, inclusi gli effetti termici e la tendenza alla risalita del fluido bifase.

I risultati complessivi delle analisi di modellazione hanno demostrato che il sistema di iniezione su un solo pozzo rappresenta un approccio fattibile per lo smaltimento di acque di condensa e di NCG.

Lo studio di fattibilità ha inoltre riscontrato che la miscela acqua-NCG può essere iniettata in tutte le condizioni esaminate, incluse quelle a minore iniettività, a condizione che vi sia una sufficiente pressione di iniezione sulla linea di iniezione dell'acqua e dei gas.

La configurazione di progetto più efficiente si ha quando la linea di iniezione viene installata tra 250 e 500 m di profondità. In queste condizioni, assumendo un pozzo con iniettività di 1.78 t/h/bar (ossia un valore relativamente basso), la pressione di iniezione delle condense è prossima a quella atmosferica, mentre la pressione richiesta per l'iniezione dei NCG non supera 43 bar.a, nella configurazione ipotizzata per il pozzo. Con una linea di iniezione installata tra 250 e 500 m di profondità, l'energia richiesta per il sistema di iniezione durante l'iniezione continua della miscela in pozzo viene minimizzata.

Oltre a minimizzare i consumi energetici necessari, mantenere la linea di iniezione a quote relativamente superficiali riduce le difficoltà di avviamento e di interruzione delle operazioni nel pozzo di iniezione dovute alla riduzione della massima pressione di iniezione del gas nel sistema. Durante questo processo di revisione della fattibilità è stato riscontrato che molte problematiche possono essere evitate semplicemente eseguendo delle procedure adeguate.

Ad esempio, durante le operazioni di interruzione controllata dell'iniezione, è consigliabile interrompere l'iniezione dei gas prima di interrompere l'iniezione delle condense. Pertanto si deve permettere di iniettare almeno 10 volte il volume del pozzo mediante la linea delle condense per far defluire la miscela acqua-NCG all'interno del serbatoio. Similarmente, durante le operazioni di avviamento è raccomandato di iniziare iniettando solamente condense per almeno 10 volte il volume del foro prima di iniziare l'iniezione di NCG, in

modo che l'acqua di iniezione abbia un flusso con velocità sufficiente da trascinare verso il basso i gas non condensabili e quindi trasportarli in serbatoio.

Una modellazione integrale dell'avviamento e dell'interruzione del sistema potrebbe essere svolta in modo da conoscere meglio e gestire una eventuale brusca interruzione di emergenza, ma questa analisi dovrebbe includere molteplici elementi che in questa fase non sono ancora ben noti (pompe di iniezione, tubazioni, separatori, condensatori etc.). Nel complesso, lo studio di fattibilità ha confermato la consistenza del modello concettuale che vede l'utilizzo di un unico pozzo per la reiniezione sia dei NCG che delle acque di condensa; il prossimo passo sarà quello di progettare un adeguato completamento del pozzo per implementare questo sistema di iniezione.

6.2. **Scenari analizzati**

Per lo studio di simulazione del sistema di iniezione proposto sono stati analizzati 12 diversi scenari di iniezione per comprendere appieno come il sistema potrebbe comportarsi sotto vari scenari di design

La variabile primaria oggetto di indagine è stata la profondità alla quale il gas non condensabile (NCG) potrebbe essere iniettato nel flusso di condensato che fluisce verso il basso. Le profondità indagate variavano da 0 m di profondità misurata (MD) a - 1250 (MD).

La variabile secondaria indagata è stata l'iniettività, nell'ottica di capire quale impatto essa avrebbe avuto sulla scelta della profondità di iniezione appropriata per i NCG. L'iniettività media assegnata è stata 1,78 t/h/bar, sulla base del valore misurato sul primo livello di assorbimento nel pozzo più vicino. Da questo è stato ricavato e utilizzato come valore più grande un valore 5 volte maggiore (8,9 t/h/bar), mentre per il valore minore è stato considerato 1/5 dell'iniettività media (0,36 t/h/bar, che costituisce un valore estremamente basso). Tale gamma di valori di iniettività è stata scelta al fine di riprodurre in maniera adeguata i valori attesi a completamento del pozzo.

Dopo la costruzione del modello e una volta definiti i parametri da esaminare, la modellazione si è sviluppata valutando l'impatto che la profondità di iniezione e l'iniettività avrebbero sulla capacità del sistema di smaltire la miscela NCG-acqua analizzando 12 scenari diversi.

I risultati cruciali di tutti i 12 scenari di simulazione sono stati rappresentati nelle figure dalla 1 alla 12, nelle quali è rappresentato l'andamento del profilo di pressione in funzione della profondità misurata del pozzo. La linea viola rappresenta il profilo di pressione della miscela acqua-NCG nel pozzo al di sotto del punto di miscelamento, mentre la linea rossa e blu rappresentano rispettivamente il profilo di pressione per i gas e per il condensato. (Nota: la linea rossa e blu non sono rappresentate in Figura 1 poiché la miscela si forma appena prima di entrare nel pozzo di reiniezione)

Le tabelle 4 e 5 presentano una sintesi dei valori di pressione a testa pozzo sia per il liquido che per i gas NCG per ogni scenario indicato nelle figure da 1 a 12.

La tabella 4 presenta la pressione richiesta per i gas per poterli iniettare nella flusso di condensato geotermico che fluisce verso il basso. Dove presenti, le celle rosse rappresentano i valori di pressione a testa pozzo superiori a 60 bar e quindi meno favorevoli alla realizzazione pratica della reinieizone, mentre le celle gialle e verdi indicano valori di pressione inferiori e quindi condizioni favorevoli per la reiniezione.

La tabella 5 presenta la pressione a testa pozzo per la reiniezione del condensato, distinguendo i valori di pressione di iniezione superiori 9.6 bara e quindi sfavorevoli e colorate in rosso, e i valori inferiori a 9,6 bara, favorevoli, colorati di verde.

Esaminando le tabelle le è possibile trarre le seguenti conclusioni dagli scenari valutati:

- Qualora si verificassero condizioni di iniettività molto bassa (0,36 ton/h/bar) il sistema di reinieizione richiederà notevole pressione di iniezione sia per il condensato che per i NCG, rendendo poco vantaggiosa l'applicazione commerciale del sistema a causa degli eccesivi costi di pompaggio.
- I vantaggi che derivano da un'alta iniettività non sono così significativi come gli svantaggi che comporta un basso valore di iniettività. L'aumento di iniettività riduce leggermente la pressione necessaria per i gas a testa pozzo, ma poiché il fluido iniettato è un gas, la pressione non diminuisce in modo significativo come avverrebbe nel caso si operasse esclusivamente con un fluido allo stato liquido. Sulla linea del condensato la maggiore iniettività non si riflette con benefici tecnici. Infatti la pressione a boccapozzo rimane sotto la pressione atmosferica a 0,4 bara (quando l'iniezione dei NCG avviene sotto 500 m)
- Al diminuire della profondità di miscelamento, anche la pressione di iniezione dei gas incondensabili decresce. Nel caso estremo di realizzare il mixing in superficie la pressione di iniezione degli incondensabili si riduce a 22 bara.
- Sulla linea del condensato, se la profondità di mixing diminuisce, si riduce la densità nella parte alta della colonna di miscela gas-liquido. Questo comporta un incremento della pressione del condensato a valori maggiori di quella atmosferica. Questo richiederebbe l'impiego di una pompa. Riducendo eccessivamente la profondità cui i fluidi si uniscono si assisterebbe ad un incremento della pressione ottimale per la reiniezione del liquido.

Tabella 3 – Pressione di iniezione dei Gas non condensabili richiesta a boccapozzo, per ogni scenario

		NCG Line Injection Pressure (Bar-a)					
		Mixing Depth (m-MD)					
		0	250	500	750	990	1250
Low Estimate for injectivity (ton/hr/bar)	0.36	---	---	---	99.0	107.2	112.7
Nearby Measured Injectivity (ton/hr/bar)	1.78	22.0	33.1	42.7	52.4	58.4	63.3
High Estimate for injectivity (ton/hr/bar)	8.90	---	---	---	47.4	52.9	53.7

Tabella 4 – Pressione di iniezione delle condense richiesta a boccapozzo, per ogni scenario

		Brine Line Injection Pressure (Bar-a)					
		Mixing Depth (m-MD)					
		0	250	500	750	990	1250
Low Estimate for injectivity (ton/hr/bar)	0.36	---	---	---	43.0	39.4	39.2
Nearby Measured Injectivity (ton/hr/bar)	1.78	22.0	6.3	0.4	0.4	0.4	0.4
High Estimate for injectivity (ton/hr/bar)	8.90	---	---	---	0.4	0.4	0.4

7. Conclusioni

Dalle simulazioni eseguite sul modello di serbatoio risultano:

- la sostenibilità del progetto per i 30 anni di vita utile dell'impianto;
- l'assenza di significative interazioni termodinamiche tra la zona produttiva e quella di reiniezione, in termini di propagazione del fronte termico;
- l'assenza di interazioni tra la zona produttiva e quella di reiniezione, riguardo alla propagazione in serbatoio del plume di gas incondensabili (modellati come CO_2 in quanto composti al 98% da anidride carbonica);
- una variazione massima di pressione, in 30 anni, inferiore a –6 bar presso i pozzi di produzione;
- una variazione massima di temperatura per i produttori in 30 anni, che si attesta intorno a –8 °C.

Dalle simulazioni eseguite per dimostrare la fattibilità della reimmisione totale dei fluidi (miscela NCG e condensato liquido) in un unico pozzo, sono stati ottenuti i seguenti risultati:

- I risultati della modellazione hanno dimostrato che applicando una sufficiente pressione di iniezione sulla fase gassosa, iniettando la fase liquida per caduta (eccetto che nell'ipotesi di una iniettività del pozzo estremamente bassa) non si verificherà un flusso controcorrente in risalita durante le operazioni di iniezione in condizioni stazionarie;
- Il tubing di iniezione dei NCG può essere collocato ad una profondità anche inferiore a quella inizialmente assunta per lo studio (990 metri) assicurando comunque l'adeguata reinieizione in serbatoio dei gas. Riducendo la profondità del tubing di reiniezione dei gas la pressione di iniezione può essere ridotta, riducendo in tal modo il costo delle operazioni. Per ridurre la quantità di energia richiesta al il sistema di reiniezione, la profondità di mixing più favorevole è situata tra 250 e 500 m, in base alla configurazione dello schema proposto, alle ipotizzate condizioni del serbatoio, e alle condizione di pressioni di iniezione desiderate.

8. Grafici delle simulazioni di reiniezione in pozzo

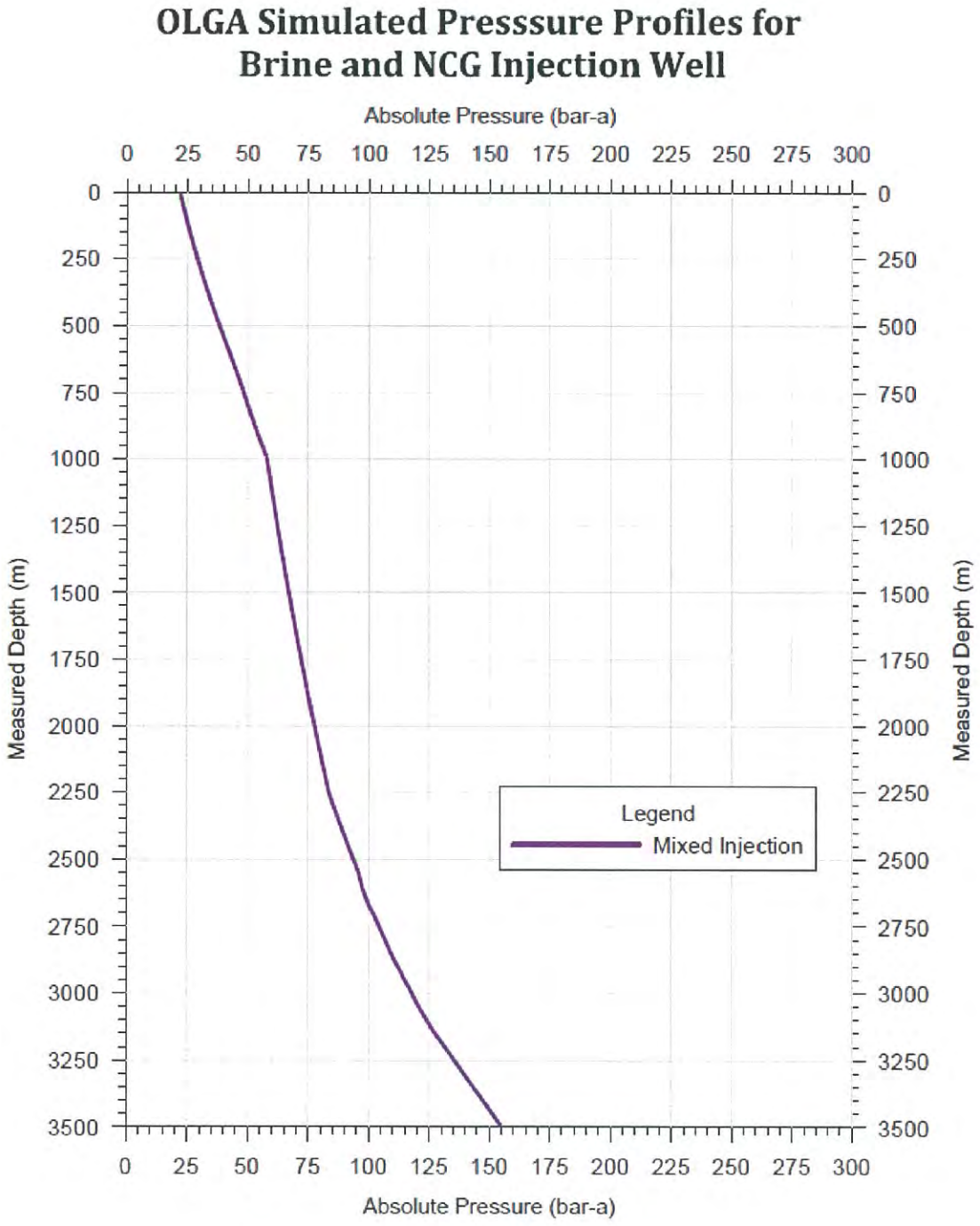

Fig. 13 - Iniettività = 1.78 t/h/bar; Profondità di iniezione = 0 m

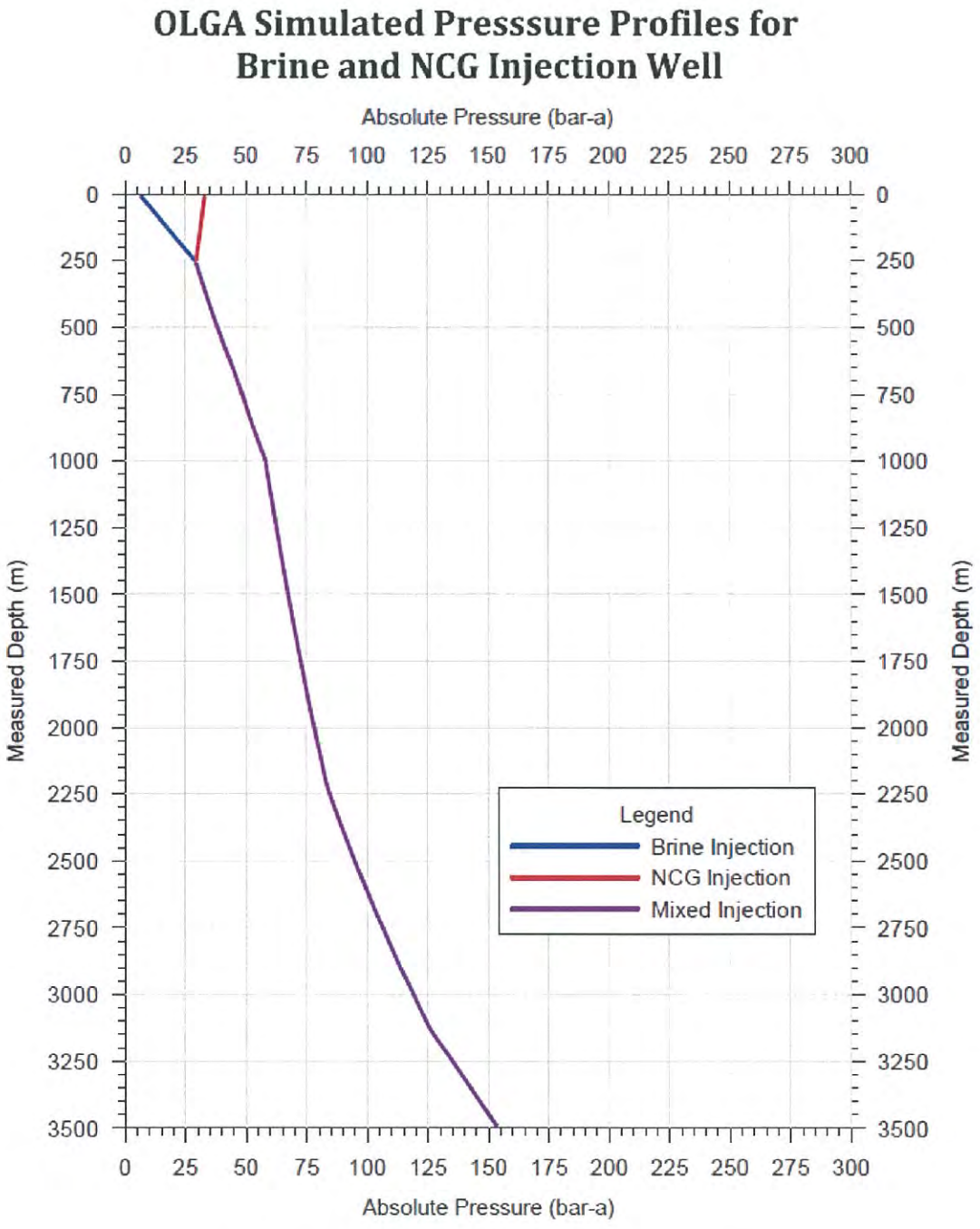

Fig. 14 - Iniettività = 1.78 t/h/bar; Profondità di iniezione = 250 m

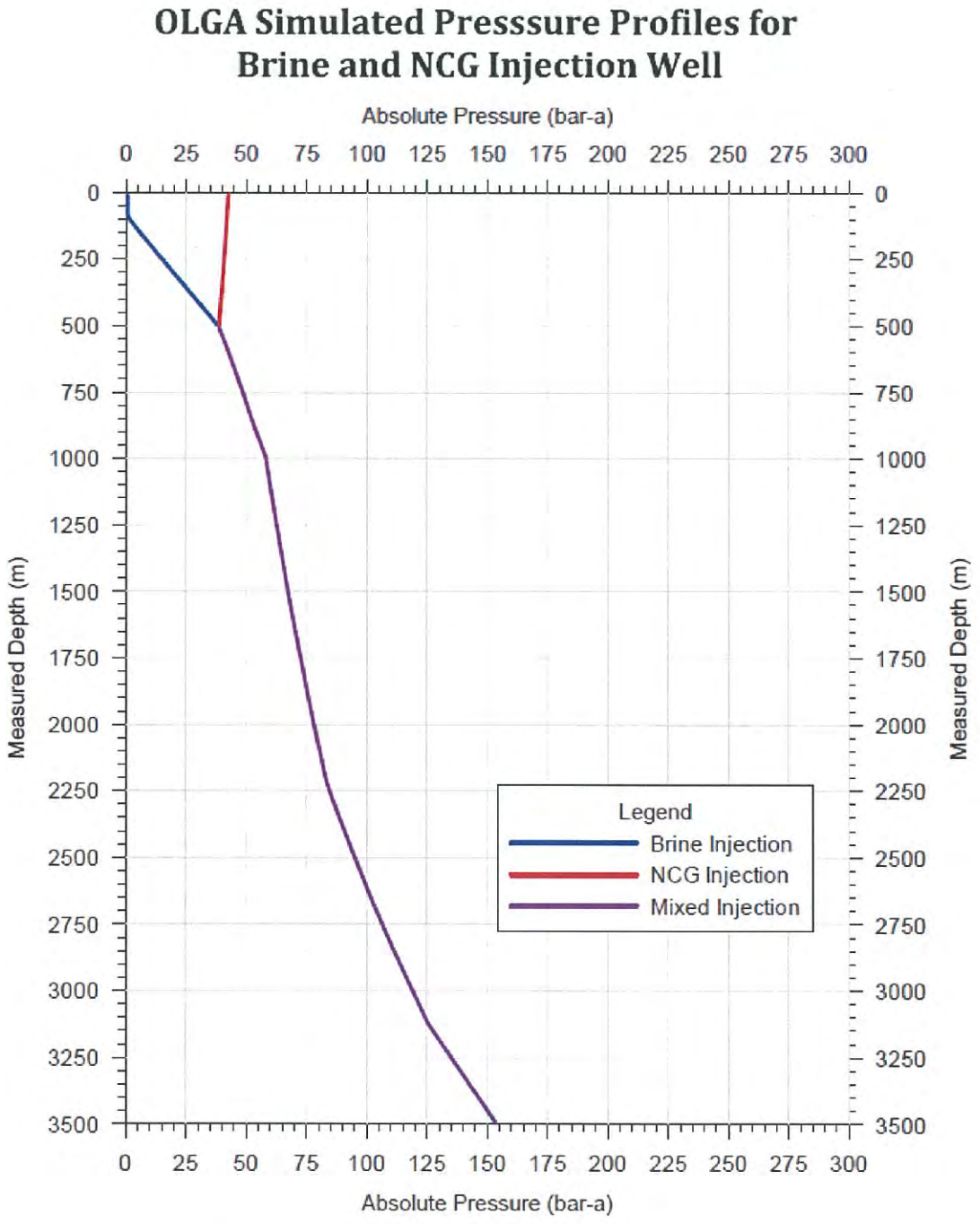

Fig. 15 - Iniettività = 1.78 t/h/bar; Profondità di iniezione = 500 m

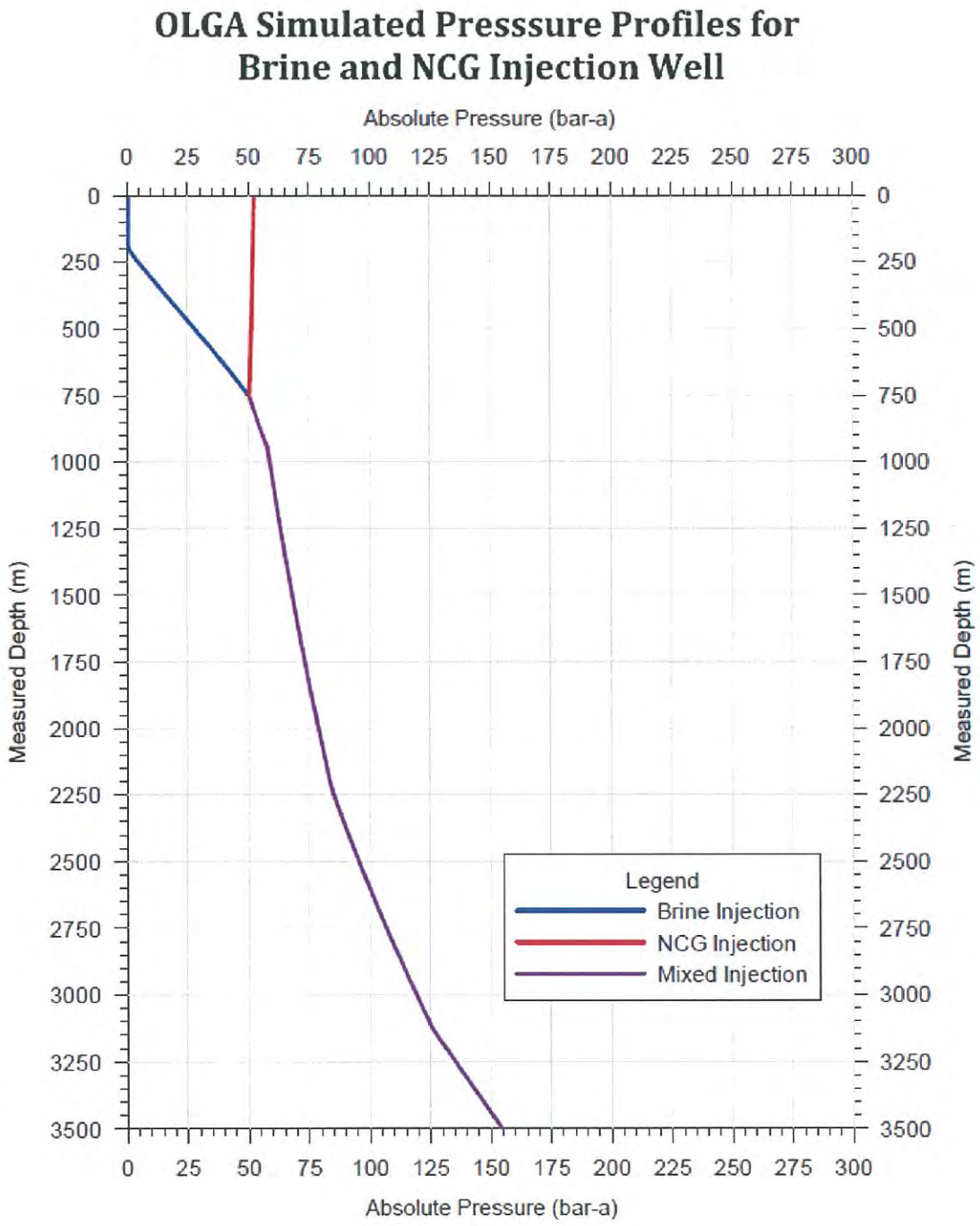

Fig. 16 - Iniettività = 1.78 t/h/bar; Profondità di iniezione = 750 m

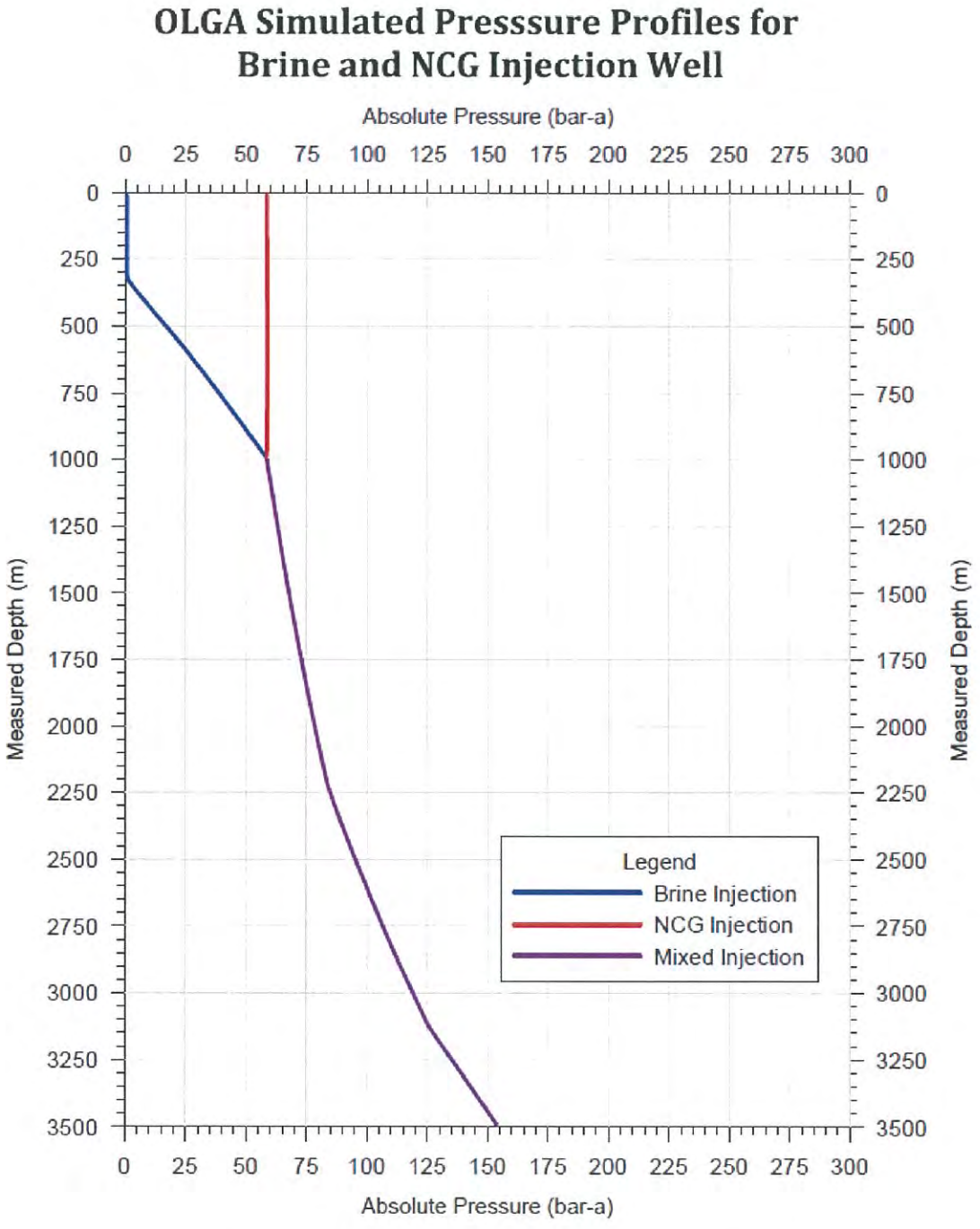

Fig. 17 - Iniettività = 1.78 t/h/bar; Profondità di iniezione = 990 m

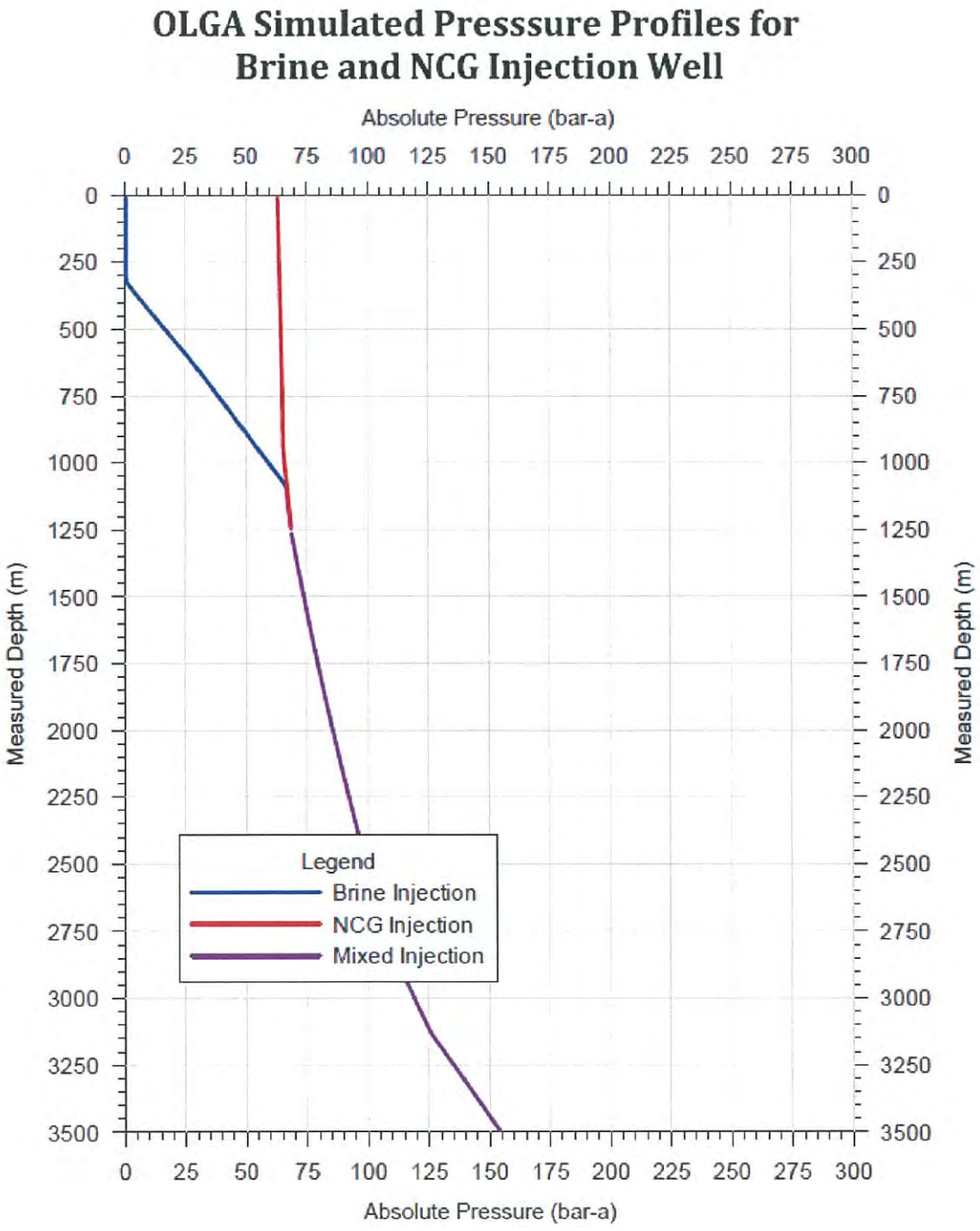

Fig. 18 - Iniettività = 1.78 t/h/bar; Profondità di iniezione = 1250 m

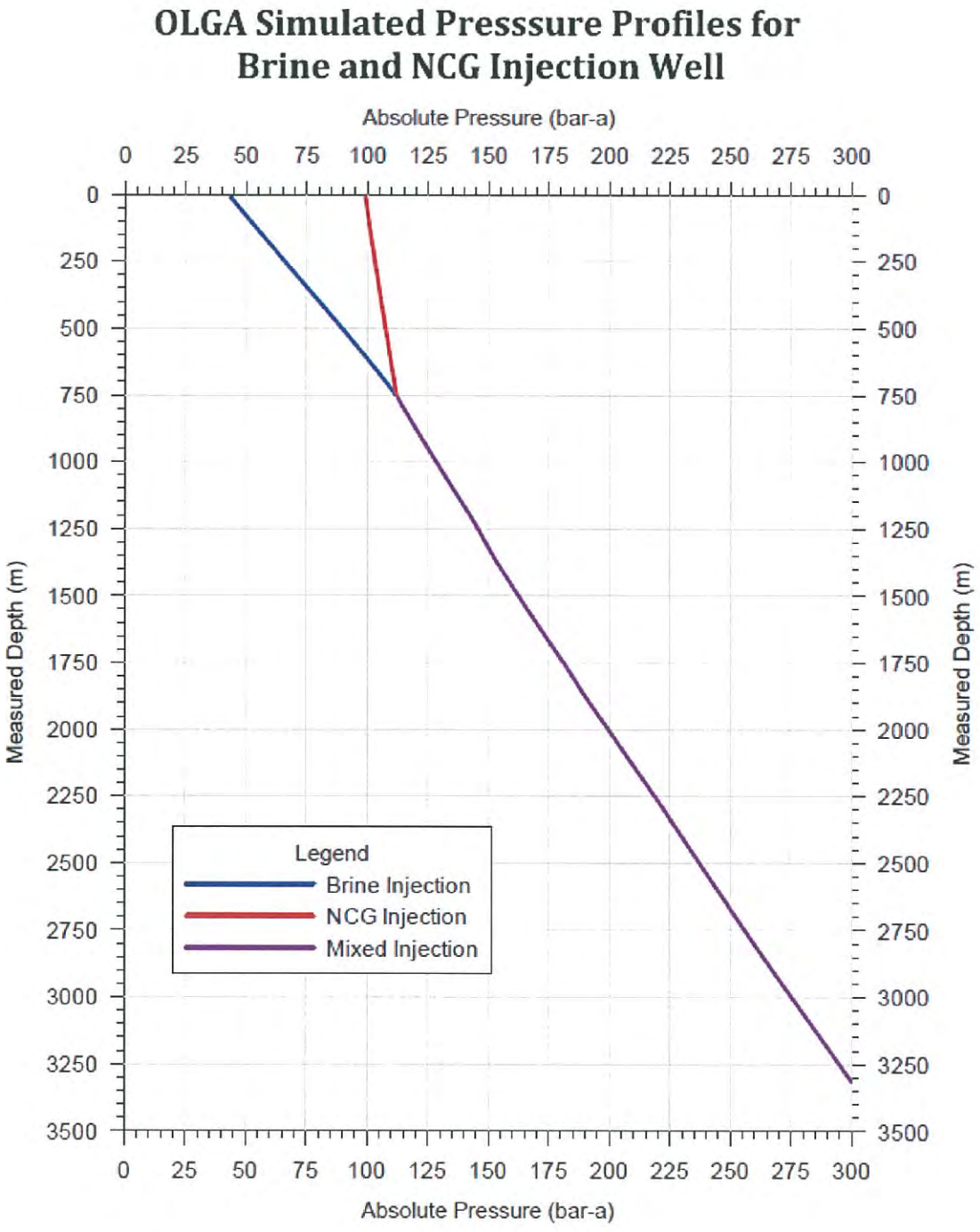

Fig. 19 - Iniettività = 0.36 t/h/bar; Profondità di iniezione = 750 m

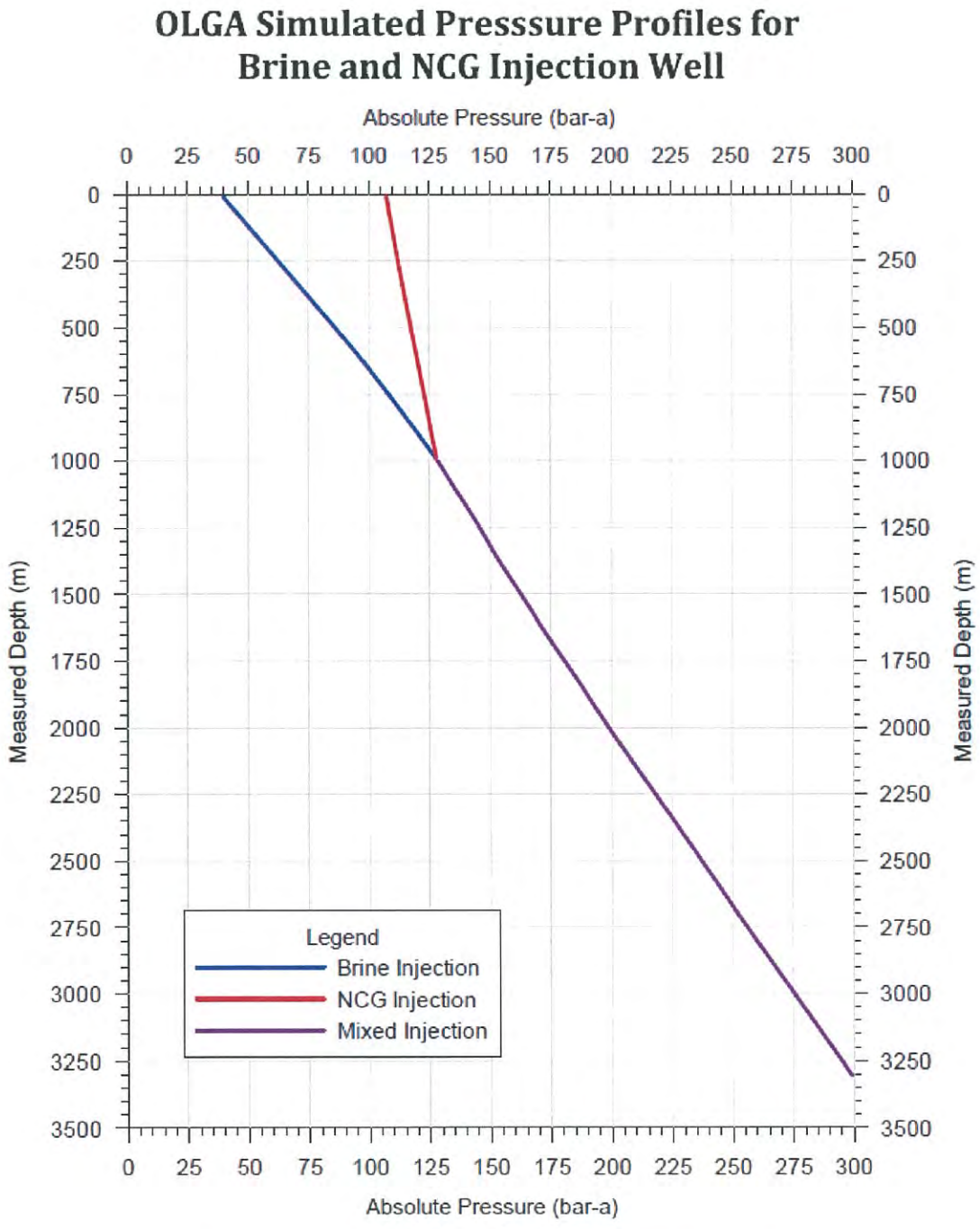

Fig. 20 - Iniettività = 0.36 t/h/bar; Profondità di iniezione = 990 m

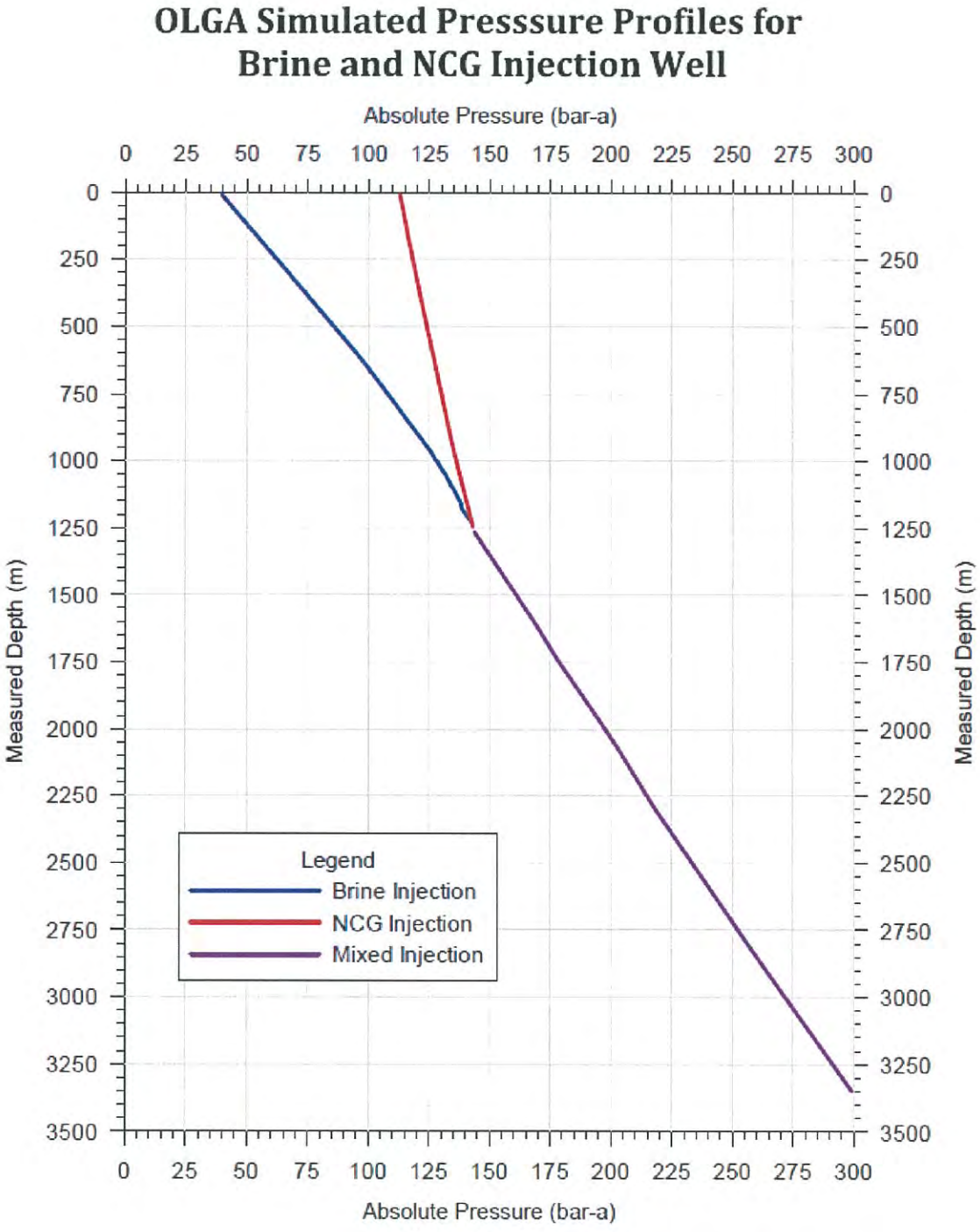

Fig. 21 - Iniettività = 0.36 t/h/bar; Profondità di iniezione = 1250 m

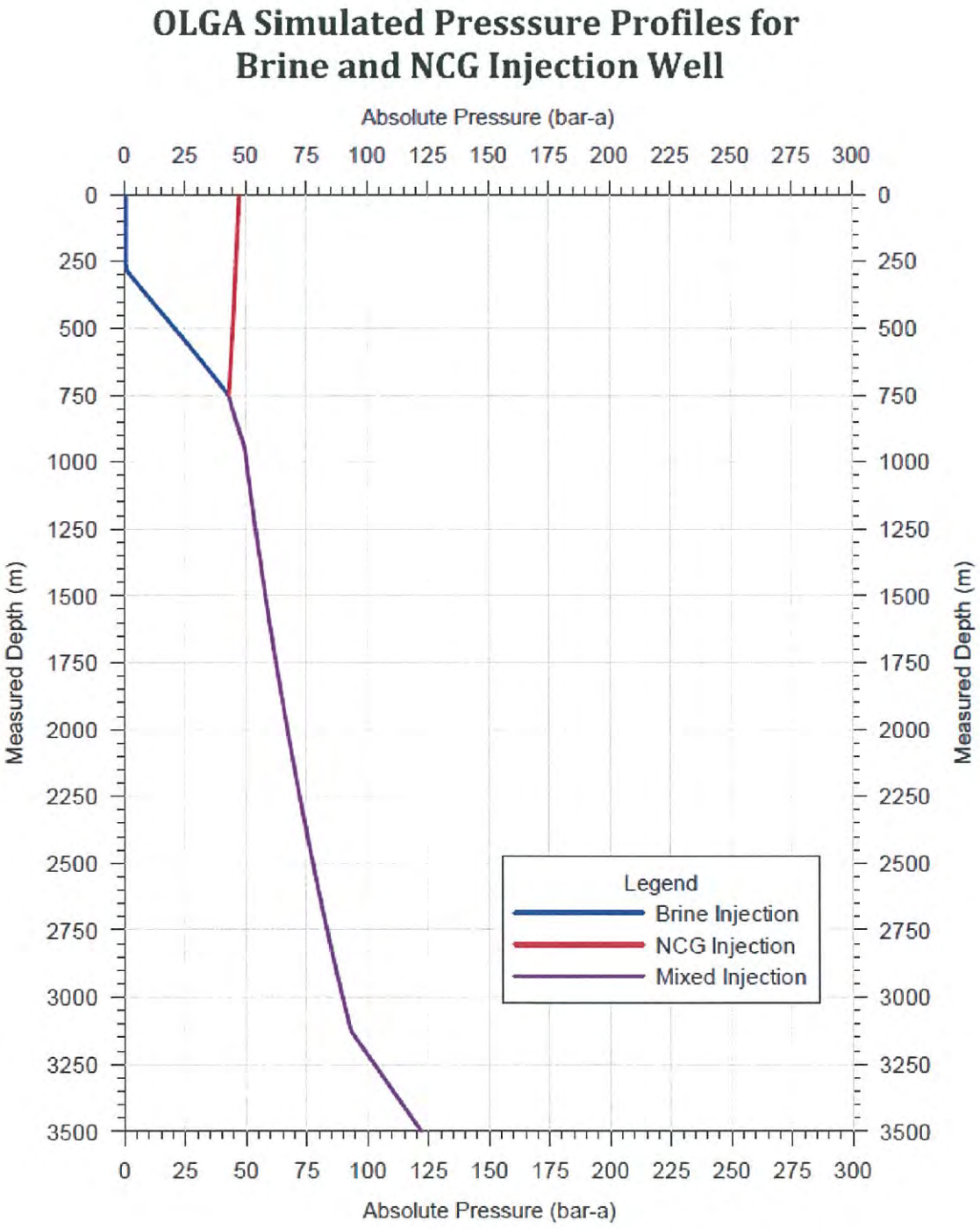

Fig. 22 - Iniettività = 8.90 t/h/bar; Profondità di iniezione = 750 m

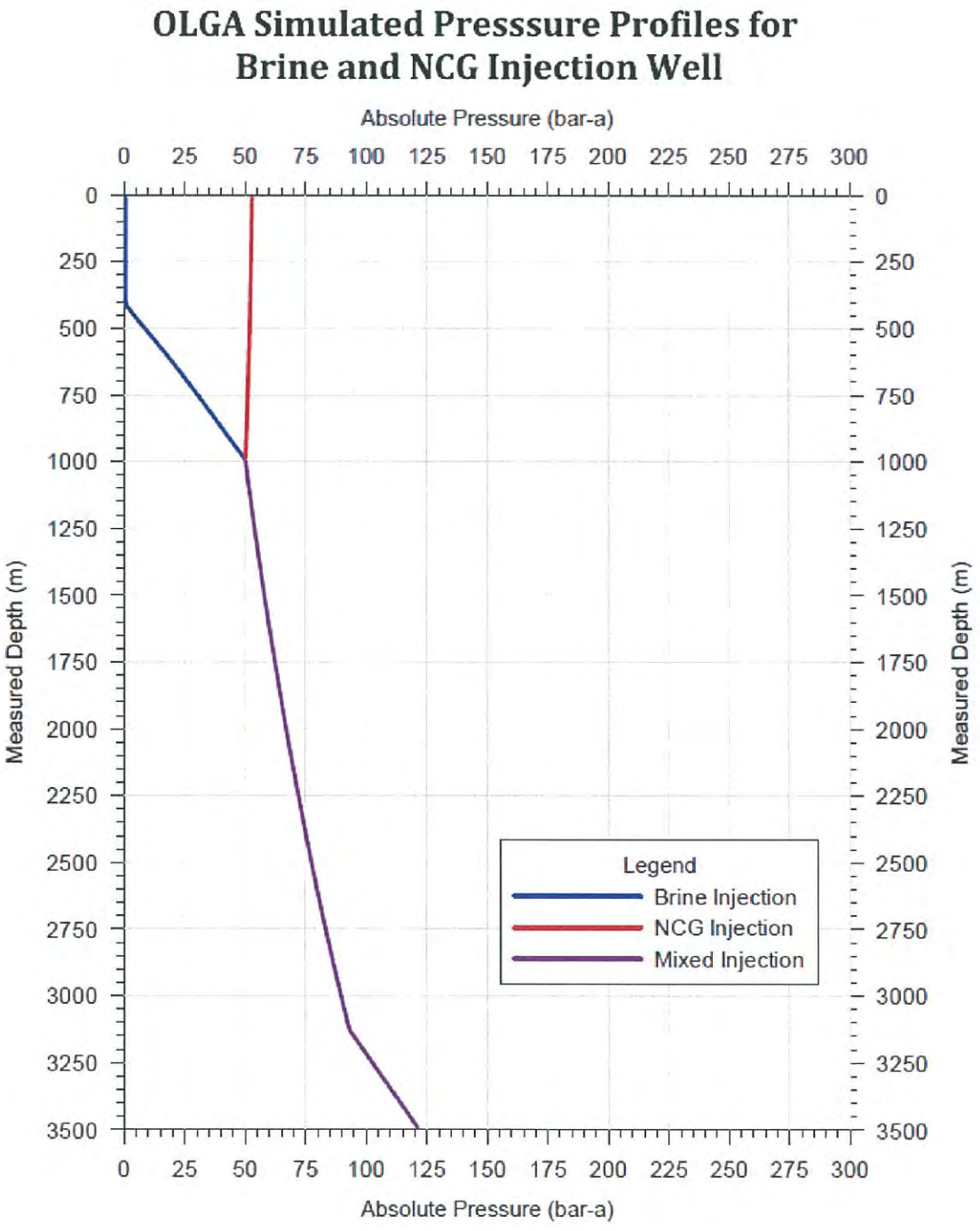

Fig. 23 - Iniettività = 8.90 t/h/bar; Profondità di iniezione = 990 m

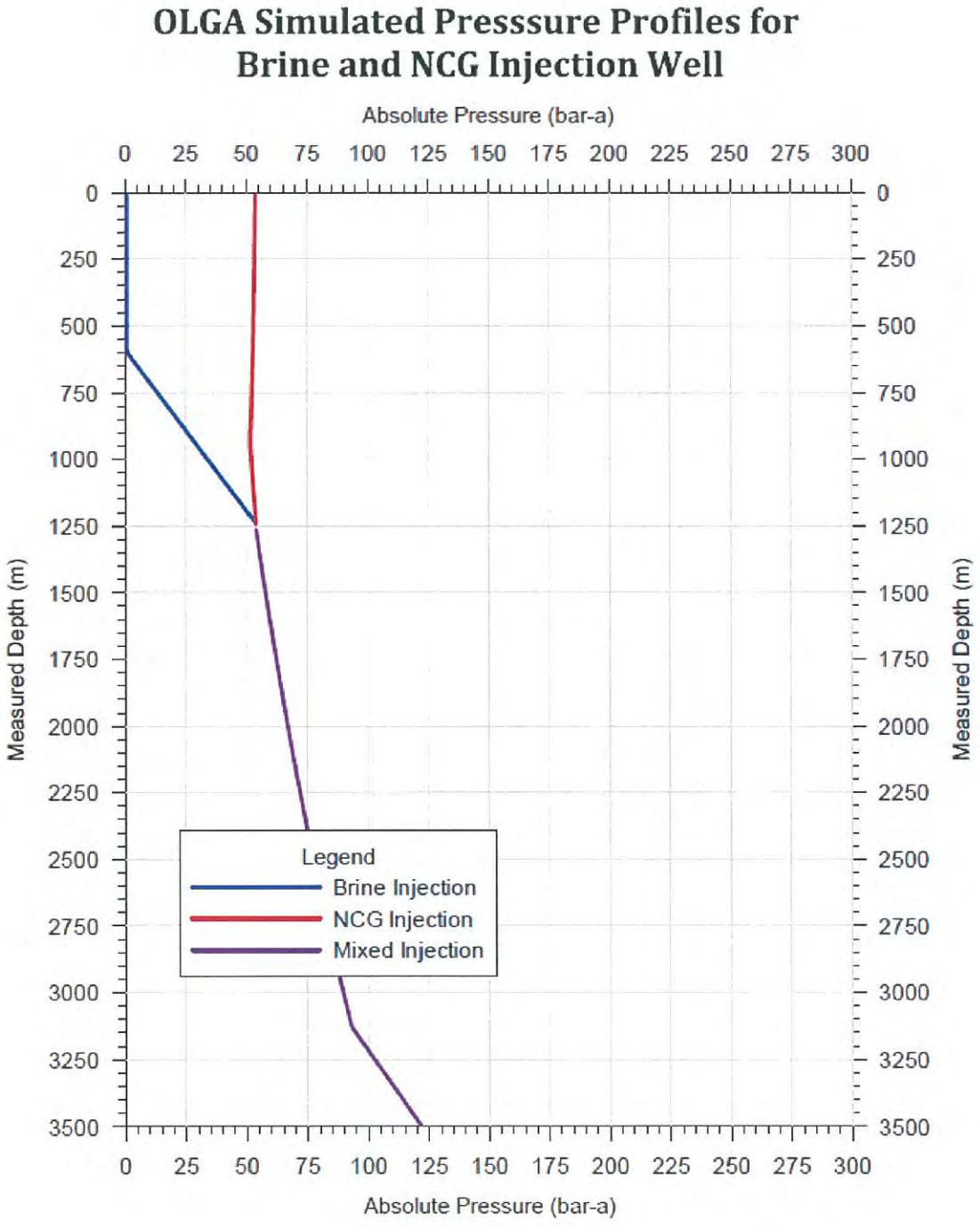

Fig. 24 - Iniettività = 8.90 t/h/bar; Profondità di iniezione = 1250 m

Spett.le **Ministero dello Sviluppo Economico**
Direzione Generale per le Risorse Minerarie ed Energetiche
Divisione VI - Titoli minerari di idrocarburi, geotermia, cave e miniere, BUIG, cartografia e statistiche
Via Molise, 2
00187 Roma
Alla c.a. Ing. Marcello Saralli
dgrme.div06@pec.mise.gov.it

Oggetto: **Istanza di rilascio del permesso di ricerca di fluidi geotermici finalizzato alla sperimentazione di impianti pilota denominato "Castelnuovo"- Regione Toscana (Provv. Pisa e Siena)**
Vs. Comunicazione Prot. n. 0029423 del 18/11/2015 trasmessa solo a mezzo Posta Elettronica Certificata

Ad integrazione del Programma dei Lavori Rev. Ottobre 2015 inviato in allegato alla nostra PEC del 20/10/2015 ed acquisito agli atti di codesta Amministrazione con prot. 25532 e facendo seguito alle comunicazioni di cui alla Vostra PEC in oggetto, in previsione della prossima seduta della CIRM trasmettiamo in allegato la seguente documentazione:

1. Aggiornamento del Costo degli Investimenti a seguito della proposta ottimizzazione progettuale
2. Addendum al Programma dei Lavori Rev. Ottobre 2015

Rimaniamo a disposizione per eventuali richieste di informazioni e/o chiarimenti ed in attesa di ricevere le Vostre valutazioni sulla diversa soluzione progettuale

Con osservanza,

Tosco Geo S.r.l.

Arezzo, 20 novembre 2015